ASTRONOMICAL INSTITUTE
SLOVAK ACADEMY OF SCIENCES

PROCEEDINGS OF THE WORKSHOP

BINARY AND MULTIPLE STARS IN THE ERA OF BIG SKY SURVEYS

September 9 – 13, 2024, Litomyšl, Czech Republic

CONTRIBUTIONS OF THE ASTRONOMICAL OBSERVATORY SKALNATÉ PLESO

• VOLUME LV •

Number 3



April 2025

Editorial Board

Editor-in-Chief
Augustín Skopal, *Tatranská Lomnica, The Slovak Republic*

Managing Editor
Richard Komžík, *Tatranská Lomnica, The Slovak Republic*

Editors
Zoltán Garai, *Tatranská Lomnica, The Slovak Republic*
Oleksandra Ivanova, *Tatranská Lomnica, The Slovak Republic*
Július Koza, *Tatranská Lomnica, The Slovak Republic*
Aleš Kučera, *Tatranská Lomnica, The Slovak Republic*
Luboš Neslušan, *Tatranská Lomnica, The Slovak Republic*
Vladimír Porubčan, *Bratislava, The Slovak Republic*
Theodor Pribulla, *Tatranská Lomnica, The Slovak Republic*

Advisory Board
Bernhard Fleck, *Greenbelt, USA*
Arnold Hanslmeier, *Graz, Austria*
Marian Karlický, *Ondřejov, The Czech Republic*
Jan Vondrák, *Prague, The Czech Republic*

©
Astronomical Institute of the Slovak Academy of Sciences
2025

ISSN: 1336–0337 (on-line version)

CODEN: CAOPF8

Editorial Office: Astronomical Institute of the Slovak Academy of Sciences
SK - 059 60 Tatranská Lomnica, The Slovak Republic

CONTENTS

List of participants 11
Preface 19

Session A: Importance of binaries

A01: H.M.J. Boffin, D. Jones: **The importance of binary stars** . . . 21
A03: A. Gallenne: **Accurate determination of binary star masses and distances using optical long-baseline interferometry** . 37

Session B: Interacting binary stars

B01: U. Munari: **Symbiotic Novae** 47
B02: M. Otulakowska-Hypka: **High-angular-resolution studies of symbiotic novae** 67
B04: G. Rauw: **X-raying the wind interactions of massive binaries.** What we have learned from 25 years of observations 75
B07: S. Rosu: **Apsidal motion in massive binaries: or how to sound stellar interiors** 81
BP02: R. Canbay: **Distribution of cataclysmic variables in our Galaxy and their position in the HR diagram in the Gaia era** 91
BP04: F. Kaczmarek, M. Otulakowska-Hypka, F. Millour, N. Nardetto, C. Paladini, A. Mérand, C.A. Hummel, J. Mikołajewska, B. Lopez, F. Patat, M. Wittkowski, A. Meilland, A. Domiciano de Souza: **Insights from mid-infrared interferometric observations of the symbiotic nova RS Ophiuchi** 98
BP08: E.P. Pavlenko, K.A. Antonyuk, S.Yu. Shugarov, O.I. Antonyuk, N.V. Pit: **ER UMa: a dwarf nova that continues to amaze** 103
BP09: S.Yu. Shugarov, P.Yu. Golysheva, S. Dallaporta, U. Munari: **Long term *UBVRI* photometric and spectral monitoring of nova KT Eri during 2009-2023** 108
BP10: M. Tomova: **A look into the behaviour of BF Cygni after 2009** 112
BP11: E.B. Yorulmaz, İ. Özavcı, E. Bahar, H.V. Şenavcı, G.A.J. Hussain, O. Kochukhov: **Doppler imaging of the contact binary DU Boo** 117

Session C: Pulsations in binaries and active binaries

C01: S.J. Murphy: **Pulsations in binary stars – a short review** . . 122

C02: B. Pilecki: **Cepheids in spectroscopic binary systems - current status and recent discoveries** 141
C03: P. Karczmarek: **Binary Cepheids: Insights from a simulation-based approach** 152
C04: J. Southworth: **SWIPE: Stars WIth Pulsations and Eclipses** 165
C07: A. Liakos: **A catalogue of δ Sct pulsators in binary systems in 2024** 172
C10: Zs. Kővári: **Magnetic activity in close binary systems** 182
CP03: A. Miszuda: **Pulsational characteristics of mass accreting stars in close binary systems** 196

Session D: Binary star evolution

D03: D. Jones: **Post-common-envelope planetary nebulae** 200
D04: Z. Li, Y. Zhang, H. Chen, H. Ge, D. Jiang, J. Li, X. Chen, Z. Han: **A new route to massive helium-rich hot subdwarfs** 211
D06: P. Kroupa: **Are binary-star populations regionally different?** 217
DP01: V. Bakış, Z. Eker, F. Soydugan, S. Bilir: **Interrelated Main-Sequence MLR, MRR, MTR Relations from Planet Hosting Stars** 234
DP02: J.P. Sánchez Arias, M. Cabezas, J. Vos: **The impact of a variable angular momentum loss on long-period sdB binaries** 238

Session E: Multiple systems

E01: A. Tokovinin: **Populations of hierarchical stellar systems** . . 243
E02: P. Zasche: **Doubly eclipsing systems: Divide et impera** . . . 255
E07: R.A. Matson, R. Gore, S.B. Howell, D.R. Ciardi: **Demographics of M dwarf binary exoplanet hosts discovered by TESS** . . . 263
E10: E. Kıran, V. Bakış, Ö.L. Değirmenci: **Spectroscopic and photometric study of a possible multiple system: V684 Mon** . . 270
E12: A. Moharana, K.G. Hełminiak, T. Pawar, G. Pawar: **Formation of compact hierarchical triples** 280
EP01: F. Akar, Ö. Başẗurk, E.M. Esmer, E. Sertkan, B. Güler, M.B. Bayram: **Orbital analysis of additional bodies around eclipsing binaries HT Vir and MR Del** 286
EP07: H.V. Şenavcı, D. Bohlender, E. Bahar, S. Gu, İ. Özavcı, M. Yılmaz, E.B. Yorulmaz, O. Latković, A. Čeki: **Discovery of a third body around semi-detached binary V527 Dra through eclipse timing and radial velocity variations** 295
EP08: E. Sertkan, Ö. Başẗurk, E.M. Esmer, F. Akar, B. Güler: **A catalog of exoplanets around post-common envelope eclipsing binaries: CuPS-ETV** 301

EP10: M. Wolf, L. Šmecler, H. Kučáková, T. Hynek, P. Zasche, K. Hornoch, R.F. Auer: **Period changes in low-mass eclipsing binaries:.** V1828 Aql, NSVS 2676703, and NSVS 6507557 307

Session F: Modelling

F01: A. Prša: **The present and the future of modeling eclipsing binary systems** 313
F05: P. Hadrava: **Fourier disentangling of spectra in observational surveys** 325
F06: P. Németh, J. Vos, M. Cabezas: **Enhanced spectral disentangling techniques for long-period hot subdwarf binaries** 340
F07: K. Masuda, T. Hirano, M. Tomoyoshi: **Weighing single-lined spectroscopic binaries using tidal RVs: the case of V723 Mon** 346
FP01: E. Bahar, İ. Özavcı, E.B. Yorulmaz, G.A.J. Hussain, H.V. Şenavcı: **Surface mapping of the young solar-like star V1358 Ori with the updated SpotDIPy code** 352
FP03: B. Keskin, Ö. Baştürk: **Eclipsing binary classification with machine learning techniques** 357
FP04: M. Niaei, Ö. Baştürk: **octans: Observed calculated diagram and light curves** 362
FP05: S. Overall, J. Southworth: **EBOP MAVEN.** A machine learning model for predicting eclipsing binary light curve fitting parameters 366
FP06: Š. Parimucha, P. Gajdoš, Y. Markus, V. Kudak: **Prediction of photometric parameters of overcontact eclipsing binaries using deep-learning model** 370
FP07: Š. Parimucha, Y. Markus, P. Gajdoš, V. Kudak: **Classification of light curves of eclipsing binaries using deep-learning models** 374
FP08: G. Szász: **New "pseudo-rotating" model atmospheres** . . . 377
FP09: O. Vozyakova, Š. Parimucha, M. Kamenec: **IGEBC - Interactive Gaia Eclipsing Binary Catalog** 382
FP10: S. Zola, G. Stachowski, K. Jarosik, K. Kasprzak, W. Waniak: **On accuracy of eclipsing binary system parameters determination from light curve modeling** 385

Session G: Observations

G01: M. Abdul-Masih: **Observations of massive contact binaries in the local universe** 390
G02: T. Merle, G. Traven, M. Van der Swaelmen, S. Van Eck, A. Jorissen, J. Desuter, M. Dorsch, G. Van de Steene: **Spectroscopic binaries in *Gaia*-ESO, *Gaia* and 4MOST surveys** 405

G03: D. Sebastian, A.H.M.J. Triaud, P.F.L. Maxted, M. Brogi: **Accurate dynamical masses from binaries with extreme brightness ratios** 412
G06: Y. Guo, C. Liu, L. Wang, J. Wang, B. Zhang, K. Ji, Z. Han, X. Chen: **The multiplicity properties of early-type stars from LAMOST DR8** 421
G08: C. Navarrete, A. Recio-Blanco, P. de Laverny, A. Escorza: **Physical stellar properties of red giant ellipsoidal binaries in Gaia DR3** 425
G10: R.S. Rathour, R. Smolec, G. Hajdu, P. Karczmarek, V. Hocdé, O. Ziółkowska, I. Soszyński, A. Udalski: **Non-evolutionary effects on period change in Magellanic Cepheids** 431
G12: K.G. Hełminiak, A. Moharana, T.B. Pawar, G. Pawar: **Adding TESS to CRÉME.** Light curves and masses of 300+ eclipsing binaries 438
G15: H. Willems: **Determining the physical parameters of eclipsing binaries from the B-Type Binaries Characterization programme (BBC) with PHOEBE** 444
GP02: C.I. Eze, G. Handler, F. Kahraman Aliçavuş, T. Pawar, A. Miszuda: **Characterizing the variability of a sample of massive stars in eclipsing binaries** 452
GP04: P. Gajdoš, Š. Parimucha: **Spectroscopic monitoring of eclipsing binaries at Ondřejov observatory** 462
GP05: B. Güler, Ö. Baştürk, E.M. Esmer, E. Sertkan, F. Akar: **ObserPy: A tool for efficient observation planning in astronomy** . . 466
GP07: L. Iliev, A. Miroshnichenko: **Spectral variations of Be/shell star Pleione connected with its 218^{d} binary period** 470
GP08: R. Jaros, A. Niedzielski, A. Wolszczan, E. Villaver: **BD+48 873b - a brown dwarf companion candidate** 474
GP09: L. Lantzi, P.-E. Christopoulou: **The first orbital period investigation of low mass ratio systems from Catalina Sky Survey** 478
GP11: B.D. Mason, R.A. Matson: **The double star catalogs of the USNO** 481
GP12: R.A. Matson, B.D. Mason, S. Stepanoff: **Kinematic solutions in the Washington Double Star catalog: adding 169,000 orbits to the Visual Orbit catalog** 484
GP14: P. Németh, O. Maryeva, E.S.G. de Almeida, J.P. Sánchez Arias, M. Kraus, J. Vos, J. Kubát, M. Vučković, B. Doležalová: **Revisiting the unique qWR – B7V composite binary HD 45166** . . . 487
GP15: A. Niedzielski, A. Wolszczan, R. Jaros, B. Deka-Szymankiewicz: **Binary stars in Pennsylvania-Toruń Planet Search** 490

GP17: İ. Özavcı, E. Bahar, M. Yılmaz, H.V. Şenavcı, E.B. Yorulmaz: **The first light curve analysis of marginally eclipsed binary KZ Vir using TESS data** 493
GP18: B. Özkardeş, H. Bakış: **New spectroscopic observations of the semidetached binary V375 Cas** 498
GP21: J. Southworth, P.F.L. Maxted: **The PLATO Multiple Star Working Group (MSWG)** 502
GP22: S. Taşdemir, D.C. Çınar: **A detailed analysis of close binary OCs** 506
GP23: F. Tezcan, Ö. Baştürk, C. Yeşilyaprak, S. Aliş: **Direct imaging potential of outer companions of eclipsing binary stars with 4-meter telescope of the Eastern Anatolia Observatory (DAG)** 512
GP28: M. Yılmaz, İ. Özavcı, E. Bahar, H.V. Şenavcı, B.S. Azizoglu: **Photometric and spectroscopic analysis of the eccentric eclipsing binary BD+72 780** 517

The Contributions of the Astronomical Observatory Skalnaté Pleso
are available in the full version
in the frame of ADS Abstract Service
and can be downloaded in a usual way from the URL address:

https://ui.adsabs.harvard.edu/

as well as from the website of
the Astronomical Institute of the Slovak Academy of Sciences
on the URL address:

https://www.astro.sk/caosp/caosp.php

The journal is covered/indexed by:

Web of Science (WoS)
WoS Core Collection: Science Citation Index Expanded

SCOPUS

Index Copernicus International

PROCEEDINGS OF THE INTERNATIONAL CONFERENCE

Edited by

Theodor Pribulla, Miloslav Zejda

BINARY AND MULTIPLE STARS IN THE ERA OF BIG SKY SURVEYS

September 9 – 13, 2024, Litomyšl, Czech Republic

Dept. of Theoretical Physics and Astrophysics, Faculty of Science, Masaryk University, Brno, Czech Republic
Astronomical Institute, Charles University, Prague, Czech Republic
Astronomical Institute, Academy of Sciences of the Czech Republic, Ondřejov, Czech Republic
Astronomical Institute of Slovak Academy of Sciences, Slovak Republic
Town of Litomyšl

https://kopal2024.physics.muni.cz/

Scientific Organizing Committee

Theodor Pribulla, chair (Slovakia)
Volkan Bakış (Türkiye)
Tamás Borkovits (Hungary)
Edwin Budding (New Zealand)
Eleftheria P. Christopoulou (Greece)
Szilárd Csizmadia (Germany)
Kosmas Gazeas (Greece)
Kelly Hambleton (U.S.A.)
Krzysztof Hełminiak (Poland)
Ondřej Pejcha (Czech Republic)
Grzegorz Pietrzyński (Poland)
John Southworth (U.K.)
Christopher A. Tout (U.K.)
Petr Zasche (Czech Republic)
Staszek Zola (Poland)

Local Organizing Committee

Miloslav Zejda (co-chair)
Jan Janík (co-chair)
Richard Komžík
Michaela Severová
Ilona Suchá
Pavel Suchan
Gabriel Szász

LIST OF PARTICIPANTS

Abdul-Masih, Michael	Instituto de Astrofisica de Canarias, Spain
Akar, Furkan	Ankara University, Astronomy & Space Sciences Department, Ankara, Türkiye
Bahar, Engin	Ankara University, Astronomy & Space Sciences Department, Ankara, Türkiye
Bakış, Volkan	Akdeniz University, Space Sciences and Technologies Department, Antalya, Türkiye
Başẗurk, Özgür	Ankara University, Astronomy and Space Sciences Department, Ankara, Türkiye
Boffin, Henri M.J.	European Southern Obseratory, Germany
Bókon, András	ELTE Eötvös Loránd University, Gothard Astrophysical Observatory, Szombathely, Hungary
Borkovits, Tamás	Baja Astronomical Observatory of Szeged University and HUN-REN-SZTE Stellar Astrophysics Research Group, Hungary
Brož, Miroslav	Faculty of Mathematics and Physics, Charles University, Czech Republic
Budaj, Ján	Astronomical Institute, Slovak Academy of Sciences, Tatranská Lomnica, Slovakia
Canbay, Remziye	Istanbul University, Institute of Graduate Studies in Science, Programme of Astronomy and Space Sciences, Türkiye
Cehula, Jakub	Faculty of Mathematics and Physics, Charles University, Czech Republic
Christopoulou, Eleftheria P.	Department of Physics, University of Patras, Greece
Çınar, Deniz Cennet	Institute of Graduate Studies in Science, Istanbul University, Istanbul, Türkiye
Csizmadia, Szilárd	German Aerospace Center (DLR), Germany
Czavalinga, Donát R.	HUN-REN-SZTE Stellar Astrophysics Research Group, Baja, Hungary
da Rocha, Danilo F.	Observatório Nacional, Brazil
Dodd, Jonathan	University of Leeds, U.K.
Dróżdż, Marek	University of the National Education Commission, Kraków, Poland
Espinoza Arancibia, Felipe	Nicolaus Copernicus Astronomical Center, Warsaw, Poland
Eze, Christian I.	Nicolaus Copernicus Astronomical Center, Warsaw, Poland

Forgács-Dajka, Emese	HUN-REN-SZTE Stellar Astrophysics Research Group, Eötvös Loránd University, Institute of Physics and Astronomy, Department of Astronomy, Hungary
Frank, Megan	University of Wyoming, U.S.A.
Gajdoš, Pavol	Astronomical Institute of the Czech Academy of Sciences, Czech Republic
Gallenne, Alexandre	Universidad de Tarapacá, Casilla 7D, Arica, Chile
Gazeas, Kosmas	National and Kapodistrian University of Athens, Greece
Graczyk, Dariusz	Nicolaus Copernicus Astronomical Center, Polish Academy of Sciences, Toruń, Poland
Green, Matthew	Max Planck Institute for Astronomy, Heidelberg, Germany
Grygar, Jiří	Institute of Physics, Czech Academy of Sciences, Czech Republic
Güler, Barış	Ankara University, Türkiye
Guo, Zhao	KU Leuven, Belgium
Guo, Yanjun	Yunnan Observatories, Chinese Academy of Sciences, China
Hadrava, Petr	Astronomical Institute of Czech Academy of Sciences, Czech Republic
Hambálek, Ľubomír	Astronomical Institute, Slovak Academy of Sciences, Tatranská Lomnica, Slovakia
He, Yuji	National Astronomical Observatory, Chinese Academy of Sciences, China
Hełminiak, Krzysztof	Nicolaus Copernicus Astronomical Center of the Polish Academy of Sciences, Poland
Hoogeveen, Geert	KNVWS-WVS, Netherlands
Hřibová, Magdaléna	Masaryk University, Faculty of Science, Department of Theoretical Physics and Astrophysics, Brno, Czech Republic
Iliev, Lubomir	Institute of Astronomy and National Astronomical Observatory, Bulgarian Academy of Sciences, Bulgaria
Janík, Jan	Masaryk University, Faculty of Science, Department of Theoretical Physics and Astrophysics, Brno, Czech Republic
Jaros Robert	Nicolaus Copernicus University in Toruń, Poland
Jones, David	Instituto de Astrofisica de Canarias, Spain
Kaczmarek, Fabian	Adam Mickiewicz University in Poznań, Poland
Kahraman Alicavus, Filiz	Çanakkale Onsekiz Mart University, Türkiye
Kalari, Venu	Gemini Observatory/NSF's NOIRLab, Chile

Karczmarek, Paulina	Departamento de Astronomía, Universidad de Concepción, Chile
Keskin, Bedri	Ankara University, Graduate School of Natural & Applied Sciences, Astronomy & Space Sciences Department, Ankara, Türkiye
Kıran, Evrim	Atatürk University, Türkiye
Klement, Robert	European Southern Observatory, Chile
Kolář, Jakub	Masaryk University, Faculty of Science, Department of Theoretical Physics and Astrophysics, Brno, Czech Republic
Kővári, Zsolt	Konkoly Observatory, HUN-REN Research Centre for Astronomy and Earth Sciences, Hungary
Kroupa, Pavel	Astronomical Institute, MFF, Charles University, Czech Republic; HISKP, University of Bonn, Germany
Krushevska, Viktoriia	Astronomical Institute, Slovak Academy of Sciences, Tatranská Lomnica, Slovakia
Krynski, Pawel	Université Libre de Bruxelles, Institut d'Astronomie et Astrophysique, Belgium
Kučáková, Hana	Research Centre for Theoretical Physics and Astrophysics, Institute of Physics, Silesian University in Opava, Czech Republic
Kundra, Emil	Astronomical Institute, Slovak Academy of Sciences, Tatranská Lomnica, Slovakia
Kurfürst, Petr	Masaryk University, Faculty of Science, Department of Theoretical Physics and Astrophysics, Brno, Czech Republic
Lantzi, Louiza	University of Patras, Greece
Li, Jiangdan	Yunnan Observatories, Chinese Academy od Sciences, China
Li, Zhenwei	Yunnan Observatories, Chinese Academy of Sciences, China
Liakos, Alexios	National Observatory of Athens, Institute for Astronomy, Astrophysics, Space Applications and Remote Sensing, Greece
Maliuk, Andrii	Astronomical Institute, Slovak Academy of Sciences, Tatranská Lomnica, Slovakia
Markus, Yana	Institute of Physics, Faculty of Science, Pavol Jozef Šafárik University in Košice, Slovakia
Marsakova, Vladyslava	Richelieu Scientific Lyceum, Odesa, Ukraine
Mártonfi, Pavol	Institute of Physics, Faculty of Science, Pavol Jozef Šafárik University in Košice, Slovakia
Mason, Brian	U.S. Naval Observatory, United States

Masuda, Kento	Department of Earth and Space Science, Graduate School of Science, Osaka University, Japan
Matson, Rachel	U.S. Naval Observatory, United States
Merle, Thibault	Université Libre de Bruxelles, Observatoire Royal de Belgique, Belgium
Mikulášek, Zdeněk	Masaryk University, Faculty of Science, Department of Theoretical Physics and Astrophysics, Brno, Czech Republic
Miszuda, Amadeusz	Nicolaus Copernicus Astronomical Center, Poland
Mitnyan, Tibor	HUN-REN-SZTE Stellar Astrophysics Research Group, Baja Astronomical Observatory of University of Szeged, Baja, Hungary
Moe, Maxwell	University of Wyoming, United States
Moharana, Ayush	Nicolaus Copernicus Astronomical Center, Polish Academy of Sciences, Poland
Munari, Ulisse	INAF National Institute of Astrophysics, Italy
Murphy, Simon	University of Southern Queensland, Australia
Navarrete, Camila	Observatoire de la Côte d'Azur, France
Németh, Peter	Astronomical Institute of the Czech Academy of Sciences, Astroserver.org, Czech Republic
Niaei, Mohammad	Ankara University, Türkiye
Niedzielski, Andrzej T.	Institute of Astronomy, Nicolaus Copernicus University in Torun, Poland
Ogloza, Waldemar	Mt.Suhora Observatory, Univeristy of the National Education Comission, Kraków, Poland
Ohlídal, Prokop	Masaryk University, Faculty of Science, Department of Theoretical Physics and Astrophysics, Brno, Czech Republic
Oláh, Katalin	Konkoly Observatory, Hungary
Ordóñez, Toro J.	Institute of Radio Astronomy and Astrophysics, National Autonomous University of Mexico, Mexico
Otulakowska Hypka, Magdalena	Adam Mickiewicz University in Poznań, Poland
Overall, Stephen	Keele University, U.K.
Özavcı, İbrahim	Ankara University, Department of Astronomy and Space Sciences, Türkiye
Özkardes, Burcu	Çanakkale Onsekiz Mart University, Türkiye
Parimucha, Štefan	Institute of Physics, University of P.J. Šafárik in Košice, Slovakia
Pavlenko, Elena	Crimean astrophysical observatory, Ukraine
Pawar, Ganesh N.	Nicolaus Copernicus Astronomical Center, Polish Academy of Sciences, Toruń, Poland

Pejcha, Ondřej	Institute of Theoretical Physics, Faculty of Mathematics and Physics, Charles University, Czech Republic
Pešta, Milan	Institute of Theoretical Physics, Faculty of Mathematics and Physics, Charles University, Czech Republic
Pilecki, Bogumił	Centrum Astronomiczne im. M. Kopernika PAN, Poland
Pribulla, Theodor	Astronomical Institute, Slovak Academy of Sciences, Tatranská Lomnica, Slovakia
Prša, Andrej	Villanova University, Department of Astrophysics and Planetary Science, Villanova, United States
Rain, Maria J.	European Southern Observatory, Germany
Ramezani, Tahereh	Masaryk University, Faculty of Science, Department of Theoretical Physics and Astrophysics, Brno, Czech Republic
Ranaivomanana, Tahina P.	Radboud University, KU Leuven, Netherlands
Ratajczak, Milena	Astronomical Observatory, University of Warsaw, Poland
Rathour, Rajeev S.	Nicolaus Copernicus Astronomical Centre, PAN, Warsaw, Poland
Rauw, Gregor	Space Technology & Astrophysical Research (STAR) Institute, Liege University, Belgium
Rosu, Sophie	KTH Royal Institute of Technology, The Oskar Klein Centre, Stockholm, Sweden
Sairam, Lalitha	University of Cambridge, United Kingdom
Sanchez Arias, Julieta P.	Astronomical Institute of the Czech Academy of Sciences, Czech Republic
Schaffenroth, Veronika	Thüringer Landessternwarte Tautenburg, Germany
Sebastian, Daniel	University of Birmingham, United Kingdom
Semenko, Eugene	National Astronomical Research Institute of Thailand (NARIT), Thailand
Şenavcı, Hakan V.	Ankara University, Faculty of Science, Department of Astronomy and Space Sciences, Türkiye
Serebriakova, Nadya	KU Leuven, Belgium
Sertkan, Ezgi	Ankara University, Türkiye
Shugarov, Sergey	Astronomical Institute, Slovak Academy of Sciences, Tatranská Lomnica, Slovakia
Skopal, Augustin	Astronomical Institute, Slovak Academy of Sciences, Tatranská Lomnica, Slovakia
Smečka, Ondřej	Masaryk University, Faculty of Science, Department of Theoretical Physics and Astrophysics, Brno, Czech Republic
Southworth, John	Keele University, United Kingdom

Stachowski, Greg	Jagiellonian University Astronomical Observatory, Poland
Stevens, Dan	University of Minnesota, Duluth, United States
Szász, Gabriel	Masaryk University, Faculty of Science, Department of Theoretical Physics and Astrophysics, Brno, Czech Republic
Sztakovič, Ján	University of Szeged, Eszterházy Károly Catholic University, Hungary
Taormina, Mónica	Centrum Astronomiczne im. Mikołaja Kopernika PAN, Poland
Taşdemir, Seval	Istanbul University, Institute of Graduate Studies in Science, Programme of Astronomy and Space Sciences, Türkiye
Tezcan, Fatma	Atatürk University, Science Faculty, Department of Astronomy and Space Sciences, Erzurum, Türkiye
Tkachenko, Andrew	Institute of Astronomy, KU Leuven, Belgium
Tokovinin, Andrei	Cerro Tololo Interamerican Observatory, NSF's NOIRLab, Chile
Tomova, Mima	Institute of Astronomy and NAO, Bulgarian Academy of Sciences, Bulgaria
Tout, Christopher A.	University of Cambridge, United Kingdom
Uzundag, Murat	KU Leuven, Belgium
Vaňko, Martin	Astronomical Institute, Slovak Academy of Sciences, Tatranská Lomnica, Slovakia
Volvach, Alexandr	Radio Astronomy and Geodynamic Department CrAO, Ukraine
Werner, Norbert	Masaryk University, Faculty of Science, Department of Theoretical Physics and Astrophysics, Brno, Czech Republic
Wielgórski, Piotr	Nicolaus Copernicus Astronomical Center of the Polish Academy of Sciences, Poland
Willems, Henry	Max-Planck Institute for Astronomy, Heidelberg, Germany
Wolf, Marek	Astronomical Institute, Charles University Prague, Czech Republic
Xia, Caiyun	Masaryk University, Faculty of Science, Department of Theoretical Physics and Astrophysics, Brno, Czech Republic
Xiong, Jianping	Yunnan Observatories, Chinese Academy of Sciences, China
Yang, Mingkuan	National Astronomical Observatories of China, China
Yilmaz, Mesut	Ankara University, Kreiken Observatory, Türkiye

Yontan, Talar	Istanbul University, Astronomy and Space Sciences, Türkiye
Yorulmaz, Eda B.	Ankara University, Department of Astronomy and Space Sciences, Türkiye
Zasche, Petr	Charles University, Faculty of Mathematics and Physics, Astronomical Institute, Praha, Czech Republic
Zavrtálek, Jay	Gymnázium Matyáše Lercha, Czech Republic
Zejda, Miloslav	Masaryk University, Faculty of Science, Department of Theoretical Physics and Astrophysics, Brno, Czech Republic
Zola, Staszek	Astronomical Observatory, Jagiellonian University, Poland

PREFACE

This issue is fully dedicated to about seventy papers presented at the international conference Binary and Multiple Stars in the Era of Big Sky Surveys, which took place in September 2024 in the picturesque Czech historical town of Litomyšl, the birthplace of the composer Bedřich Smetana and the equally famous astrophysicist and mathematician Zdeněk Kopal. The five-day conference of the IAU symposia level, held by Department of Theoretical Physics and Astrophysics, Faculty of Science, Masaryk University in Brno; Astronomical Institute, Charles University, Prague; Astronomical Institute, Academy of Sciences of the Czech Republic, Ondřejov; and Town of Litomyšl from Czech Republic, and Astronomical Institute of Slovak Academy of Sciences, Slovak Republic, was attended by 143 astronomers from 25 countries on all continents except Africa and Antarctica. There were 130 oral talks on the conference program, 21 of which were invited (with e.g., H. Boffin, M. Brož, J. Budaj, P. Hadrava, D. Jones, U. Munari, A. Prša, A. Tkachenko, A. Skopal, A. Tokovinin, N. Werner, as speakers), and 28 posters, presented in a special Poster Session.

The chief leitmotif of the conference was the life of binary stars and multiple star systems, followed by modern instruments of big sky surveys. Most stars in our Universe live in binary and multiple systems. Understanding these objects is critical for practically all fields of astrophysics. A companion's presence significantly alters a star's evolution, resulting in many unusual objects, including type Ia supernovae, symbiotic stars, classical novae, or post-common-envelope

systems. Observations of the binary stars enable us to determine stars' masses, radii, and luminosities directly. These are necessary inputs for all models of stellar structure and evolution. Binary and multiple systems affect all galactic environments, including stellar associations and open and globular clusters.

The field of binary systems significantly benefits from numerous all-sky surveys and satellite missions, which are primarily focused on exoplanets or pulsating stars. The unprecedented precision of the satellite data revolutionized research of binary stars. Numerous fine effects are routinely observed and must be considered in the modeling. The continuous satellite photometry led to the detection of long-period eclipsing binaries and multiply-eclipsing multiple systems. The study of binaries also benefits from a simultaneous analysis of different types of observations, including radial velocities, line profiles, multi-color photometry, astrometry, or polarimetry. Despite substantial progress in the field, there are still many open questions. Those include the formation of close binaries and multiple systems, the common-envelope evolution, the magnetic dynamo, and activity in binary stars or stellar mergers.

The conference was the third of the specialized astrophysical conferences from 2004, 2014, and 2024, commemorating the legacy of the outstanding Czech astrophysicist, Zdeněk Kopal. Theodor Pribulla was the chairman of the SOC for the last (2024) conference. Together with Miloslav Zejda they are also the editors of this proceedings. The conference was very successful and inspiring, and in the final discussion, most participants expressed their wish to meet in the same format, but preferably in five years or sooner.

Zdeněk Mikulášek, Masaryk University in Brno, Czech Republic

Contrib. Astron. Obs. Skalnaté Pleso **55/3**, 21 – 36, (2025)
https://doi.org/10.31577/caosp.2025.55.3.21

The importance of binary stars

H.M.J. Boffin[1] **and D. Jones**[2,3,4]

[1] *ESO, Karl-Schwarzschild-str. 2, 85748 Garching, Germany (E-mail: hboffin@eso.org)*

[2] *Instituto de Astrofísica de Canarias, 38205 La Laguna, Tenerife, Spain (E-mail: djones@iac.es)*

[3] *Departamento de Astrofísica, Universidad de La Laguna, E-38206 La Laguna, Tenerife, Spain*

[4] *Nordic Optical Telescope, Rambla José Ana Fernández Pérez 7, 38711, Breña Baja, Spain*

Received: November 27, 2024; Accepted: January 08, 2025

Abstract. Stars are mostly found in binary and multiple systems, as at least 50% of all solar-like stars have companions — a fraction that goes up to 100% for the most massive stars. Moreover, a large fraction of them will interact in some way or another over the course of their lives. Such interactions can, and often will, alter the structure and evolution of both components in the system. This will, in turn, lead to the production of exotic objects whose existence cannot be explained by standard single star evolution models, including gravitational wave progenitors, blue stragglers, symbiotic and barium stars, novae, and supernovae. More generally, binary stars prove crucial in many aspects, ranging from cultural ones, to constraining models of stellar evolution, star formation, and even, possibly, of gravity itself. They also provide a quasi-model independent way to determine stellar masses, radii, and luminosities. We here provide a brief summary of the importance of binary stars.

Key words: binaries: general – binaries: close – Stars: formation – Gravitation

1. Binary stars are ubiquitous

The Sun is a single star – which is likely one of the reasons we are here (see Sec. 4) – but a large number of stars, and the majority of solar-like and massive stars, are members of binary systems (Whitworth & Lomax, 2015; Fuhrmann et al., 2017; Merle, 2024), with the mass ratio distribution depending on the primary mass (Boffin et al., 1993; Boffin & Pourbaix, 2019; Boffin & Trimble, 2020). Looking at the night sky, its brightest star, Sirius, is a binary. Discovered by Bessel (1844), it is reported in a paper of which we cannot resist quoting the first sentence as it is still most relevant when discussing binary stars:

> The subject which I wish to communicate to you, seems to me so important for the whole of practical astronomy, that I think it worthy of having your attention directed to it.

The companion of Sirius, discovered via astrometry, turned out to be a white dwarf (WD), and Sirius is now the prototype of its own class of systems (Liebert et al., 2013; Bond et al., 2017). Such systems, containing a main-sequence star and a WD, can also be used to infer the ages of the main-sequence stars (Fouesneau et al., 2019; Zhang et al., 2023a).

In our close vicinity, we also find binary stars. Thus, Alpha Centauri is a binary system of solar-like stars, located just 4.3 light-years from the Sun, and appearing as a visual binary with an orbital period of about 80 years (Heintz, 1982; Pourbaix & Boffin, 2016). In fact, it is likely that Alpha Centauri forms with the closest star to the Sun, Proxima Centauri, a triple system! Another of the closest systems to be Sun, located only 2 parsecs away, is the binary brown dwarf that forms Luhman 16 (Luhman, 2013; Boffin et al., 2014; Bedin et al., 2017, 2024). Finally, another famous multiple is the couple Mizar and Alcor in the Big Dipper (Fig. 1), known as *jumyouboshi* (or "lifespan star") in Japan because it is thought that if you cannot distinguish both stars with your naked eyes, you will die within a year. Astronomy can be deadly! We now know that Alcor and Mizar are themselves binaries, while each components of Mizar is another binary (Mamajek et al., 2010). Thus, we have here nice examples of binaries on various scales and discovered by various techniques. A rather similar bright system of six stars in three binary systems is given by Castor, the second brightest star in the constellation Gemini.

2. Binary stars constrain stellar models

As shown by the Alcor & Mizar example, binary stars span a wide range of separations. At one extreme, we have the binary star HM Cancri, which has the shortest orbit of all the known AM CVn systems. These are composed of a WD accreting from another WD or Helium star. As such, they have all short orbital periods, with the one of HM Cancri being 321 seconds (Israel et al., 2002; Roelofs et al., 2010). This system is a nice laboratory as Munday et al. (2023) show that mass transfer is counteracting gravitational-wave dominated orbital decay and that it is one of the brightest verification binaries for the Laser Interferometer Space Antenna spacecraft. On the other extreme, we have common proper motion pairs, which are weakly gravitationally bound with orbital periods of up to several millions of years.

One of the principal uses of binary stars is to obtain accurate radius, masses, and luminosities of stars. This will then be very useful to constrain stellar evolution models. The best systems for this are double-eclipsing binaries with spectroscopic and photometric orbits, as in this case, one can obtain all the parameters, in an almost model-independent way. Some of the most recent examples can be



Figure 1. Starry Night Over the Rhone by Vincent Van Gogh, showing the Big Dipper and the binary system Mizar and Alcor. Oil on canvas, Musée d'Orsay, Paris.

found in the series of papers by J.-L. Halbwachs and colleagues (for example, Halbwachs et al., 2020) and those by John Southworth in `The Observatory`. In Southworth (2024), he determines the masses and radii of the component solar-like stars of the binary system V454 Aurigae with amazing precision[1], finding masses of 1.034 ± 0.006 $M_\odot$ and 1.161 ± 0.008 $M_\odot$, and radii of 0.979 ± 0.003 $R_\odot$ and 1.211 ± 0.003 $R_\odot$. If these values are also as accurate, then they are wonderful tests of theoretical models, although it would be useful to determine the abundance of elements in the system with great accuracy as well for even more constraints. More such systems are listed in the Detached Eclipsing Binary Catalogue[2], while another interesting example that could serve as a test for magnetic stellar evolution models can be found in Hinse et al. (2024). This can also be done with wide binaries, especially those that contain a WD and a MS star (Fouesneau et al., 2019; Rebassa-Mansergas et al., 2021; Moss et al.,

[1]The values in his Table III are in fact even more precise that what is written in the abstract and is quoted here.

[2]`https://www.astro.keele.ac.uk/jkt/debcat/`

2022).

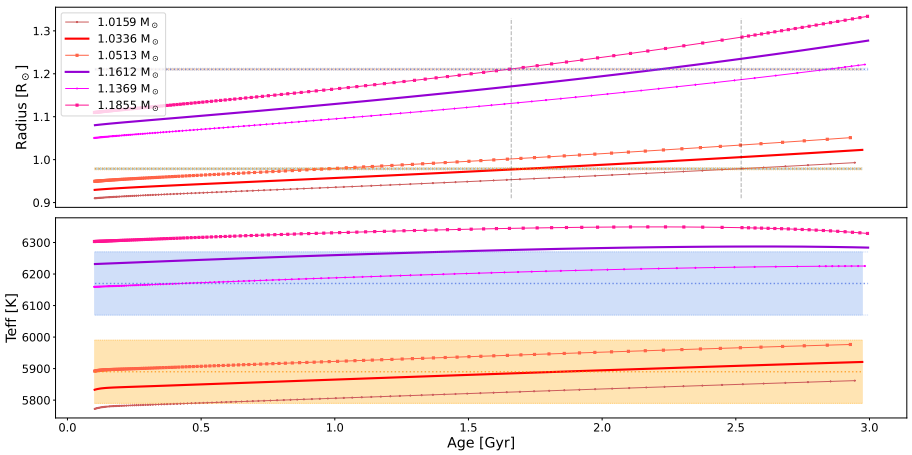


Figure 2. Comparison between MIST models for solar metallicity stars of masses corresponding to the components of V454 Aurigae and the parameters determined by Southworth (2024). The top panel shows the radius as a function of age, while the bottom panel concerns the effective temperature as a function of age. In each panel, the lower set of curves correspond to the less massive component, the upper ones to the more massive one. The determined values of the radii are so precise that the allowed range appears like horizontal lines, while for the temperatures, the uncertainty is greater and the possible ranges are shown with the shaded areas.

The data on V454 Aurigae can in principle be used to infer, in a model-independent way, the ages of the stars, assuming both components are coeval – a reasonable assumption – and thus test stellar models. Figure 2 shows a comparison between the precise radii and less precise temperatures of both components in V454 Aurigae with MIST[3] stellar evolution models, assuming solar metallicity and masses in the range determined by Southworth (2024). As can be seen, the precise radius allows us in principle to determine the most plausible interval of ages (1.66 to 2.33 Gyr), while the agreement is not so good for the temperature of the stars, especially as far as the most massive component is concerned. The quality of the data we can now achieve will likely also allow us to constrain the assumptions used by different stellar evolution models. In Fig. 3, we compare the evolution of the radius and the temperature as a function of age for a Sun, using both MIST and PARSEC[4] evolutionary tracks. The difference is remarkable and probably due to different calibrations. When the components

[3] https://waps.cfa.harvard.edu/MIST/
[4] http://stev.oapd.inaf.it/PARSEC/

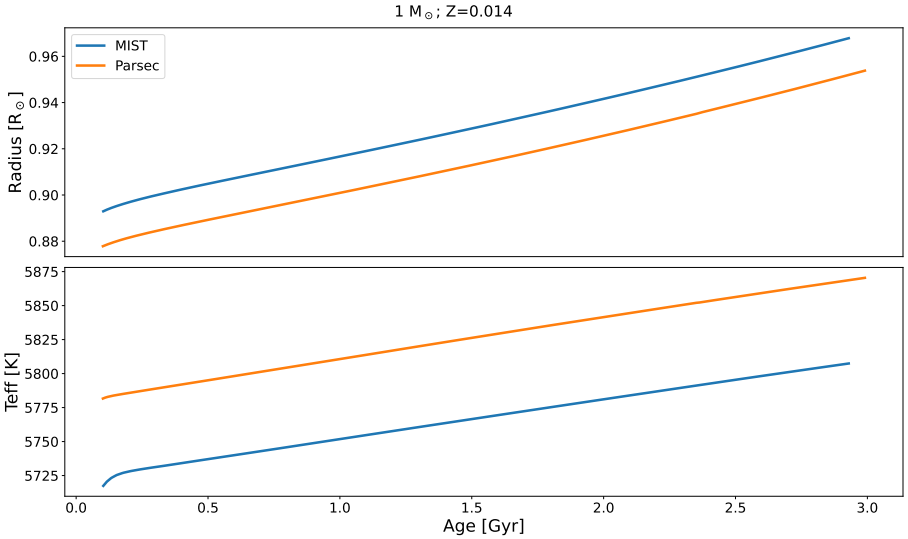


Figure 3. Comparison between MIST and PARSEC evolutionary tracks for a solar mass star of Z=0.014. The panels show the same as in Fig. 2: top is the radius as a function of age; bottom is the effective temperature.

of the binary system are pulsating, one can then combine asteroseismology with mass estimates, thereby constraining ages. This is detailed in the contribution of Simon Murphy in this volume.

In the previous paragraph, we mentioned that the high-quality data provide constraints in a model-independent way. This is not fully correct. Indeed, the analysis of light curves at the precision done in such examples will depend to some extent on the limb-darkening law – in this case, a Power-2 one – and the coefficients used in the law. These are in fact derived from models (Claret & Southworth, 2023)! Thus, it is important to ensure self-consistency when doing such an analysis.

One can also constrain the mass-luminosity relation using binaries and compare with models, as done for example in Mann et al. (2019) or in Hwang et al. (2024), where the latter paper also highlights differences between MIST and PARSEC tracks. Similarly, binary stars containing a white dwarf can be used to constrain models as far as the initial-final mass of white dwarfs are concerned (Hollands et al., 2024), although one needs to be careful that the white dwarfs are not the result of mergers in case the binary was initially a triple system (Heintz et al., 2022, 2024). A thorough discussion of the impact of binary stars on stellar evolution can be found in the book edited by Beccari & Boffin (2019).

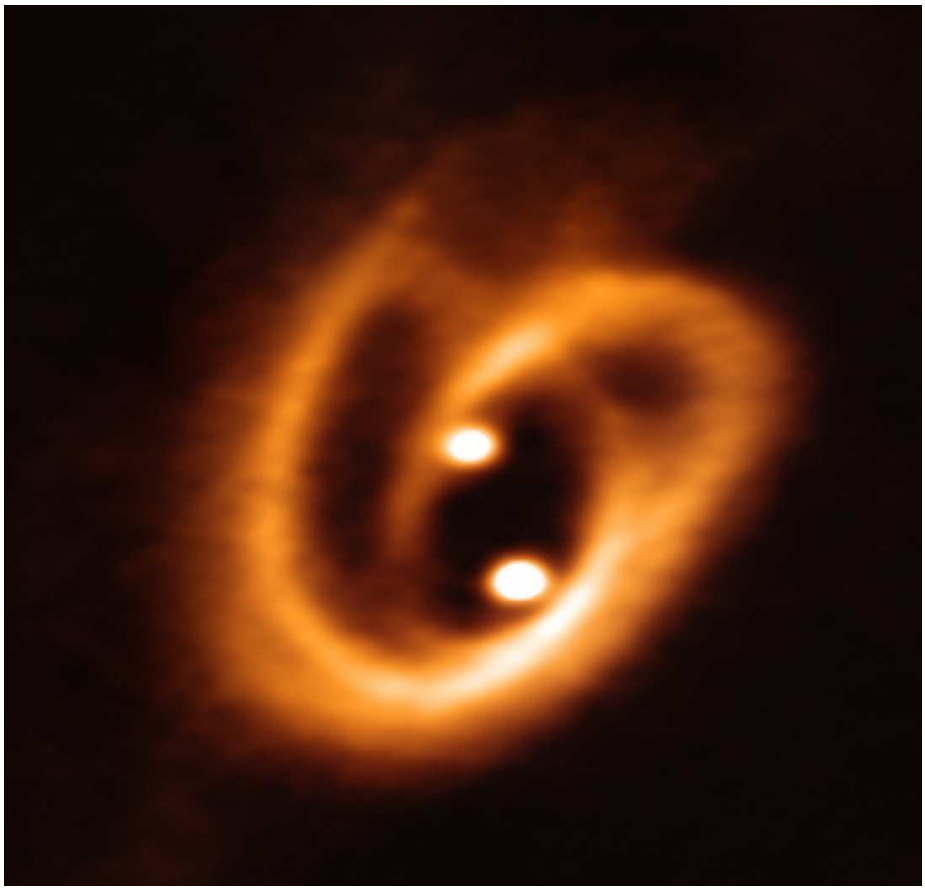


Figure 4. Some stars form as binaries, as shown in this rendering based on ALMA data. Credit: ALMA (ESO/NAOJ/NRAO), Alves et al. (2019)

3. Binary stars constraint theories

Many stars form as binaries (Fig. 4) or multiple stars. Thus, binaries can also tell us a lot about the formation of stars. Recent work has shown that the fraction of binaries is anti-correlated with metallicity at short separation: metal-poor stars appear to present a multiplicity fraction a factor of 2-3 higher than metal-rich stars (Badenes et al., 2018). In addition, Mazzola et al. (2020) found another anti-correlation, even steeper than the one with metallicity, this time between the α-elements and binarity. Other parameters such as mass or age seem to have a smaller impact on the close binary fraction. They interpret this as due to the α-elements being trapped in dust and ices, and this is thus another indication

that stars form via disc fragmentation.

Binary stars can also be used to test gravity theories. The discovery of binary pulsars and how their orbital period decays was a remarkable confirmation of General Relativity (Hulse & Taylor, 1975; Taylor & Weisberg, 1982; Freire & Wex, 2024). More recently, this was also illustrated with the discovery of gravitational waves emitted by the in-spiralling of binary neutron stars or binary black holes (Abbott et al., 2016, 2017, 2023). The recent discovery of BH3 in unreleased Gaia data – the third example of a quiescent black hole (BH) in a binary system – is quite interesting as, with an estimated mass of 33 $M_\odot$, it appears to be the most massive BH in the Milky Way and is therefore similar to those discovered from their gravitational wave emissions (Gaia Collaboration et al., 2024). It appears to have a metallicity of −2.56, indicating that massive BHs are the remnants of metal-poor stars and are likely formed through dynamical exchanges in clusters (Rastello et al., 2023; Tanikawa et al., 2024; Marín Pina et al., 2024), although alternative theories exist (Iorio et al., 2024).

Extremely wide binary stars, with weak gravitational interaction between both components, are in principle a good test of gravitation theories. Indeed, if their separation is larger than roughly 10,000 au, then the MOND theory of gravitation predicts higher orbital velocities than those expected with Newtonian dynamics (Hernandez et al., 2012). Many studies have been done in recent years, following the Gaia data releases, including Pittordis & Sutherland (2019); Hernandez (2023); Chae (2023, 2024b); Banik et al. (2024); Chae (2024a); Cookson (2024) and Hernandez & Kroupa (2024). However, such measurements prove difficult as the external field effect predicted by MOND is less severe in the Galactic plane, where most such binary stars can be studied, than in the Halo. Moreover, one needs to have all three components of the relative velocities and should correct for projection effects (El-Badry, 2019, 2024). For now, therefore, it seems like the results are still inconclusive. It is clear, however, that they could have a tremendous impact.

4. Binary stars affect planets

The first effect of binaries on exoplanet discoveries is the need to be cautious when we seem to detect a planetary transit. Binary stars are one of the possible contaminants, as a background eclipsing system could mimic a planetary transit.

More importantly, binary stars may affect the existence of exoplanets. Planets in binary systems can either follow a S-orbits, that is, orbit one of the components ("circumprimary or circumsecondary orbits"), or P-orbits, in which case, they orbit both stars ("circumbinary planets"). P-orbits are generally rather far from the stars and thus harder to detect and perhaps less interesting as they are likely not in the habitable zone (Simonetti et al., 2020). Relatively few circumbi-

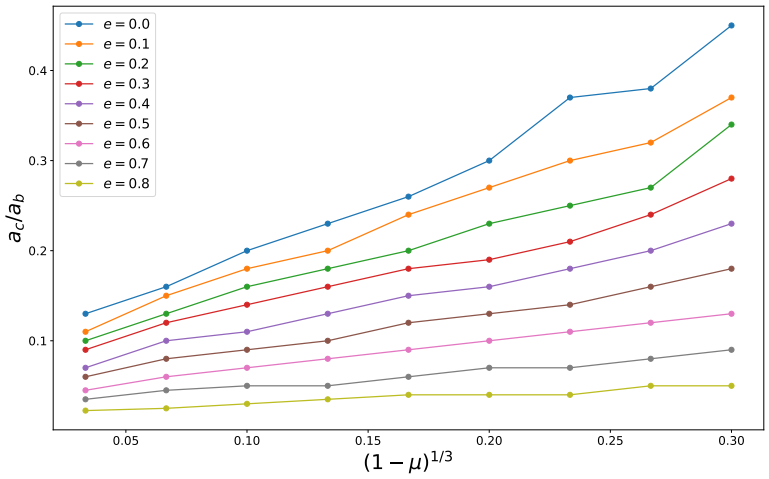


Figure 5. The relation between the ratio of the critical semi-major axis, a_c, for stable S-orbits in a binary system to the binary separation, a_b, as a function of $(1-\mu)^{1/3}$, where μ is the mass fraction of the secondary component in the binary system, $\mu = m_2/(m_1+m_2)$. Figure based on the results from Holman & Wiegert (1999).

nary planets are known[5], especially as some mechanisms during the pre-main sequence may remove such planets (Fleming et al., 2018). An interesting system is NN Ser. Composed of a WD and a M-type companion in a 0.13-day orbit, it has been followed extensively and shows clear deviations of its eclipse timing. This led Beuermann et al. (2010) and then Marsh et al. (2014) to infer the presence of possibly two planets around the close binary. More recently, Özdönmez et al. (2023) could only confirm the signal of one planet, with an orbital period of 19.5 years. Whether such planet exists and how it formed – is it primordial or was it formed after the common envelope evolution from the ejected material? – are still hotly debated questions.

In the case of S-orbits, they would only be stable if they are within 0.13 to 0.45 the binary orbital separation, depending on the mass ratio, and for a circular orbit. For a very eccentric orbit, these values are 0.022 and 0.05 only (Fig. 5, Holman & Wiegert, 1999) – see also Jang-Condell (2015) and Quarles et al. (2020). Thus, it is no surprise that Wang et al. (2014) "find that compared to single star systems, planets in multiple-star systems occur 4.5 ± 3.2, 2.6 ± 1.0, and 1.7 ± 0.5 times less frequently when a stellar companion is present

[5] https://exoplanet.eu/planets_binary_circum/ lists 27 such planets only, compared to 230 S-type planets.

at a distance of 10, 100, and 1000 au, respectively." More recently, Moe & Kratter (2021) find that "binaries with a < 1 au fully suppress S-type planets, binaries with a $= 10$ au host close planets at $15^{+17}_{-12}\%$ the occurrence rate of single stars, and wide binaries with a > 200 au have a negligible effect on close planet formation". They also found that about 40% of solar-type primaries in magnitude-limited samples do not host close planets due to suppression by close stellar companions, confirming a previous result by Kraus et al. (2016). This is likely due to the role of stellar companions in disrupting the protoplanetary disk (Duchêne, 2010) within the first 1-2 Myr of disc evolution (Kraus et al., 2012; Barenfeld et al., 2019), providing support to the disc fragmentation scenario (see also Tokovinin & Moe, 2020). Binarity seems, however, to play a positive role in the existence of very massive short-period giant planets and brown dwarfs (Eggenberger et al., 2004; Fontanive et al., 2019; Childs & Martin, 2021). It also drives larger eccentricities of the planets (Eggenberger et al., 2004; González-Payo et al., 2024). Finally, it is also noteworthy that the orbits of transiting planets often align with the orbital planes of their stellar companions (Dupuy et al., 2022; Christian et al., 2022, 2024; Behmard et al., 2022; Lester et al., 2023; Zhang et al., 2023b).

5. Binary stars and the cosmic distance scale

Another extremely debated question is the so-called H_0 tension, which relies on accurately measuring the distance to the most distant objects. Such measurements are based on the cosmic distance ladder, in which different kinds of astrophysical objects probe different scales. Eclipsing binary systems offer the most accurate way to measure the distance to the Large Magellanic Cloud, the first step on the ladder. An accuracy of 5% is now feasible to a distance of around 3 Mpc, and so such measurements are also done in the Small Magellanic Cloud, and in the Andromeda and Triangulum galaxies (Pietrzyński et al., 2019).

Apart from eclipsing binaries, the first rungs on the ladder are based on cepheids. However, as these variable stars originated from stars with intermediate masses, the majority are likely to be members of binary systems (Pilecki et al., 2024). If not taken into account, this can have a drastic effect on the calibration and thus on the derived distances. Indeed, cepheids in binary systems seem to be overluminous compared to models (Evans et al., 2024) and such binaries are now thought to be cause of the scatter in the period-luminosity relation (Gallenne et al., 2018).

Finally, on the other end of the cosmic distance ladder are Type Ia supernovae, which are generally assumed to be syandard candles. Given that it is still unclear what is the origin of such events – although all scenarios assume a binary model – it is a rather amazing act of faith to rely on them for such an important endeavour; an act that clearly illustrates the importance of binary stars!

Acknowledgements. DJ acknowledges support from the Agencia Estatal de Investigación del Ministerio de Ciencia, Innovación y Universidades (MCIU/AEI) and the European Regional Development Fund (ERDF) with reference PID-2022-136653NA-I00 (DOI:10.13039/501100011033). DJ also acknowledges support from the Agencia Estatal de Investigación del Ministerio de Ciencia, Innovación y Universidades (MCIU/AEI) and the the European Union NextGenerationEU/PRTR with reference CNS2023-143910 (DOI:10.13039/501100011033).

References

Abbott, B. P., Abbott, R., Abbott, T. D., et al., Observation of Gravitational Waves from a Binary Black Hole Merger. 2016, *Physical Review Letters*, **116**, 061102, DOI:10.1103/PhysRevLett.116.061102

Abbott, B. P., Abbott, R., Abbott, T. D., et al., GW170817: Observation of Gravitational Waves from a Binary Neutron Star Inspiral. 2017, *Physical Review Letters*, **119**, 161101, DOI:10.1103/PhysRevLett.119.161101

Abbott, R., Abbott, T. D., Acernese, F., et al., Population of Merging Compact Binaries Inferred Using Gravitational Waves through GWTC-3. 2023, *Physical Review X*, **13**, 011048, DOI:10.1103/PhysRevX.13.011048

Alves, F. O., Caselli, P., Girart, J. M., et al., Gas flow and accretion via spiral streamers and circumstellar disks in a young binary protostar. 2019, *Science*, **366**, 90, DOI:10.1126/science.aaw3491

Badenes, C., Mazzola, C., Thompson, T. A., et al., Stellar Multiplicity Meets Stellar Evolution and Metallicity: The APOGEE View. 2018, *Astrophysical Journal*, **854**, 147, DOI:10.3847/1538-4357/aaa765

Banik, I., Pittordis, C., Sutherland, W., et al., Strong constraints on the gravitational law from Gaia DR3 wide binaries. 2024, *Monthly Notices of the RAS*, **527**, 4573, DOI:10.1093/mnras/stad3393

Barenfeld, S. A., Carpenter, J. M., Sargent, A. I., et al., The Effect of Binarity on Circumstellar Disk Evolution. 2019, *Astrophysical Journal*, **878**, 45, DOI:10.3847/1538-4357/ab1e50

Beccari, G. & Boffin, H. M. J. 2019, *The Impact of Binary Stars on Stellar Evolution*, Cambridge Astrophysics (Cambridge University Press)

Bedin, L. R., Dietrich, J., Burgasser, A. J., et al., HST astrometry of the closest brown dwarfs-II. Improved parameters and constraints on a third body. 2024, *Astronomische Nachrichten*, **345**, e20230158, DOI:10.1002/asna.20230158

Bedin, L. R., Pourbaix, D., Apai, D., et al., Hubble Space Telescope astrometry of the closest brown dwarf binary system - I. Overview and improved orbit. 2017, *Monthly Notices of the RAS*, **470**, 1140, DOI:10.1093/mnras/stx1177

Behmard, A., Dai, F., & Howard, A. W., Stellar Companions to TESS Objects of Interest: A Test of Planet-Companion Alignment. 2022, *Astronomical Journal*, **163**, 160, DOI:10.3847/1538-3881/ac53a7

Bessel, F. W., On the variations of the proper motions of Procyon and Sirius. 1844, *Monthly Notices of the RAS*, **6**, 136, DOI:10.1093/mnras/6.11.136

Beuermann, K., Hessman, F. V., Dreizler, S., et al., Two planets orbiting the recently formed post-common envelope binary NN Serpentis. 2010, *Astronomy and Astrophysics*, **521**, L60, DOI:10.1051/0004-6361/201015472

Boffin, H. M. J., Cerf, N., & Paulus, G., Statistical analysis of a sample of spectroscopic binaries containing late-type giants. 1993, *Astronomy and Astrophysics*, **271**, 125

Boffin, H. M. J. & Pourbaix, D., The mass-ratio distribution of spectroscopic binaries along the main sequence. 2019, *Mem. Societa Astronomica Italiana*, **90**, 359

Boffin, H. M. J., Pourbaix, D., Mužić, K., et al., Possible astrometric discovery of a substellar companion to the closest binary brown dwarf system WISE J104915.57-531906.1. 2014, *Astronomy and Astrophysics*, **561**, L4, DOI:10.1051/0004-6361/201322975

Boffin, H. M. J. & Trimble, V., My companion is bigger than your companion! 2020, *The Observatory*, **140**, 1, DOI:10.48550/arXiv.1910.07793

Bond, H. E., Schaefer, G. H., Gilliland, R. L., et al., The Sirius System and Its Astrophysical Puzzles: Hubble Space Telescope and Ground-based Astrometry. 2017, *Astrophysical Journal*, **840**, 70, DOI:10.3847/1538-4357/aa6af8

Chae, K.-H., Breakdown of the Newton-Einstein Standard Gravity at Low Acceleration in Internal Dynamics of Wide Binary Stars. 2023, *Astrophysical Journal*, **952**, 128, DOI:10.3847/1538-4357/ace101

Chae, K.-H., Measurements of the Low-acceleration Gravitational Anomaly from the Normalized Velocity Profile of Gaia Wide Binary Stars and Statistical Testing of Newtonian and Milgromian Theories. 2024a, *Astrophysical Journal*, **972**, 186, DOI:10.3847/1538-4357/ad61e9

Chae, K.-H., Robust Evidence for the Breakdown of Standard Gravity at Low Acceleration from Statistically Pure Binaries Free of Hidden Companions. 2024b, *Astrophysical Journal*, **960**, 114, DOI:10.3847/1538-4357/ad0ed5

Childs, A. C. & Martin, R. G., Terrestrial planet formation in a circumbinary disc around a coplanar binary. 2021, *Monthly Notices of the RAS*, **507**, 3461, DOI:10.1093/mnras/stab2419

Christian, S., Vanderburg, A., Becker, J., et al., Wide Binary Orbits are Preferentially Aligned with the Orbits of Small Planets, but Probably Not Hot Jupiters. 2024, *arXiv e-prints*, arXiv:2405.10379, DOI:10.48550/arXiv.2405.10379

Christian, S., Vanderburg, A., Becker, J., et al., A Possible Alignment Between the Orbits of Planetary Systems and their Visual Binary Companions. 2022, *Astronomical Journal*, **163**, 207, DOI:10.3847/1538-3881/ac517f

Claret, A. & Southworth, J., Power-2 limb-darkening coefficients for the uvby, UBVRIJHK, SDSS ugriz, Gaia, Kepler, TESS, and CHEOPS photometric systems. II. PHOENIX spherically symmetric stellar atmosphere models. 2023, *Astronomy and Astrophysics*, **674**, A63, DOI:10.1051/0004-6361/202346478

Cookson, S. A., Influence of selection criteria on the interpretation of rotational behaviour of wide-binary star systems. 2024, *Monthly Notices of the RAS*, **533**, 110, DOI:10.1093/mnras/stae1820

Duchêne, G., Planet Formation in Binary Systems: A Separation-Dependent Mechanism? 2010, *Astrophysical Journal, Letters*, **709**, L114, DOI:10.1088/2041-8205/709/2/L114

Dupuy, T. J., Kraus, A. L., Kratter, K. M., et al., Orbital architectures of planet-hosting binaries - II. Low mutual inclinations between planetary and stellar orbits. 2022, *Monthly Notices of the RAS*, **512**, 648, DOI:10.1093/mnras/stac306

Eggenberger, A., Udry, S., & Mayor, M., Statistical properties of exoplanets. III. Planet properties and stellar multiplicity. 2004, *Astronomy and Astrophysics*, **417**, 353, DOI:10.1051/0004-6361:20034164

El-Badry, K., The geometric challenge of testing gravity with wide binaries. 2019, *Monthly Notices of the RAS*, **482**, 5018, DOI:10.1093/mnras/sty3109

El-Badry, K., Gaia's binary star renaissance. 2024, *New Astronomy Review*, **98**, 101694, DOI:10.1016/j.newar.2024.101694

Evans, N. R., Schaefer, G. H., Gallenne, A., et al., The Orbit and Dynamical Mass of Polaris: Observations with the CHARA Array. 2024, *Astrophysical Journal*, **971**, 190, DOI:10.3847/1538-4357/ad5e7a

Fleming, D. P., Barnes, R., Graham, D. E., Luger, R., & Quinn, T. R., On the Lack of Circumbinary Planets Orbiting Isolated Binary Stars. 2018, *Astrophysical Journal*, **858**, 86, DOI:10.3847/1538-4357/aabd38

Fontanive, C., Rice, K., Bonavita, M., et al., A high binary fraction for the most massive close-in giant planets and brown dwarf desert members. 2019, *Monthly Notices of the RAS*, **485**, 4967, DOI:10.1093/mnras/stz671

Fouesneau, M., Rix, H.-W., von Hippel, T., Hogg, D. W., & Tian, H., Precise Ages of Field Stars from White Dwarf Companions. 2019, *Astrophysical Journal*, **870**, 9, DOI:10.3847/1538-4357/aaee74

Freire, P. C. C. & Wex, N., Gravity experiments with radio pulsars. 2024, *Living Reviews in Relativity*, **27**, 5, DOI:10.1007/s41114-024-00051-y

Fuhrmann, K., Chini, R., Kaderhandt, L., & Chen, Z., Multiplicity among Solar-type Stars. 2017, *Astrophysical Journal*, **836**, 139, DOI:10.3847/1538-4357/836/1/139

Gaia Collaboration, Panuzzo, P., Mazeh, T., et al., Discovery of a dormant 33 solar-mass black hole in pre-release Gaia astrometry. 2024, *Astronomy and Astrophysics*, **686**, L2, DOI:10.1051/0004-6361/202449763

Gallenne, A., Kervella, P., Evans, N. R., et al., A Geometrical 1% Distance to the Short-period Binary Cepheid V1334 Cygni. 2018, *Astrophysical Journal*, **867**, 121, DOI:10.3847/1538-4357/aae373

González-Payo, J., Caballero, J. A., Gorgas, J., et al., Multiplicity of stars with planets in the solar neighbourhood. 2024, *Astronomy and Astrophysics*, **689**, A302, DOI:10.1051/0004-6361/202450048

Halbwachs, J. L., Kiefer, F., Lebreton, Y., et al., Masses of the components of SB2 binaries observed with Gaia - V. Accurate SB2 orbits for 10 binaries and masses of the components of 5 binaries. 2020, *Monthly Notices of the RAS*, **496**, 1355, DOI:10.1093/mnras/staa1571

Heintz, T. M., Hermes, J. J., El-Badry, K., et al., Testing White Dwarf Age Estimates Using Wide Double White Dwarf Binaries from Gaia EDR3. 2022, *Astrophysical Journal*, **934**, 148, DOI:10.3847/1538-4357/ac78d9

Heintz, T. M., Hermes, J. J., Tremblay, P. E., et al., A Test of Spectroscopic Age Estimates of White Dwarfs Using Wide WD+WD Binaries. 2024, *Astrophysical Journal*, **969**, 68, DOI:10.3847/1538-4357/ad479b

Heintz, W. D., On the orbital and radial motions of alpha Centauri. 1982, *The Observatory*, **102**, 42

Hernandez, X., Internal kinematics of Gaia DR3 wide binaries: anomalous behaviour in the low acceleration regime. 2023, *Monthly Notices of the RAS*, **525**, 1401, DOI:10.1093/mnras/stad2306

Hernandez, X., Jiménez, M. A., & Allen, C., Wide binaries as a critical test of classical gravity. 2012, *European Physical Journal C*, **72**, 1884, DOI:10.1140/epjc/s10052-012-1884-6

Hernandez, X. & Kroupa, P., A recent confirmation of the wide binary gravitational anomaly. 2024, *arXiv e-prints*, arXiv:2410.17178, DOI:10.48550/arXiv.2410.17178

Hinse, T. C., Baştürk, Ö., Southworth, J., et al., Absolute dimensions of solar-type eclipsing binaries. NY Hya: A test for magnetic stellar evolution models. 2024, *Astronomy and Astrophysics*, **687**, A116, DOI:10.1051/0004-6361/202244066

Hollands, M. A., Littlefair, S. P., & Parsons, S. G., Measuring the initial-final mass relation using wide double white dwarf binaries from Gaia DR3. 2024, *Monthly Notices of the RAS*, **527**, 9061, DOI:10.1093/mnras/stad3729

Holman, M. J. & Wiegert, P. A., Long-Term Stability of Planets in Binary Systems. 1999, *Astronomical Journal*, **117**, 621, DOI:10.1086/300695

Hulse, R. A. & Taylor, J. H., Discovery of a pulsar in a binary system. 1975, *Astrophysical Journal, Letters*, **195**, L51, DOI:10.1086/181708

Hwang, H.-C., Ting, Y.-S., Cheng, S., & Speagle, J. S., Dynamical masses across the Hertzsprung-Russell diagram. 2024, *Monthly Notices of the RAS*, **528**, 4272, DOI:10.1093/mnras/stae297

Iorio, G., Torniamenti, S., Mapelli, M., et al., The boring history of Gaia BH3 from isolated binary evolution. 2024, *Astronomy and Astrophysics*, **690**, A144, DOI:10.1051/0004-6361/202450531

Israel, G. L., Hummel, W., Covino, S., et al., RX J0806.3+1527: A double degenerate binary with the shortest known orbital period (321s). 2002, *Astronomy and Astrophysics*, **386**, L13, DOI:10.1051/0004-6361:20020314

Jang-Condell, H., On the Likelihood of Planet Formation in Close Binaries. 2015, *Astrophysical Journal*, **799**, 147, DOI:10.1088/0004-637X/799/2/147

Kraus, A. L., Ireland, M. J., Hillenbrand, L. A., & Martinache, F., The Role of Multiplicity in Disk Evolution and Planet Formation. 2012, *Astrophysical Journal*, **745**, 19, DOI:10.1088/0004-637X/745/1/19

Kraus, A. L., Ireland, M. J., Huber, D., Mann, A. W., & Dupuy, T. J., The Impact of Stellar Multiplicity on Planetary Systems. I. The Ruinous Influence of Close Binary Companions. 2016, *Astronomical Journal*, **152**, 8, DOI:10.3847/0004-6256/152/1/8

Lester, K. V., Howell, S. B., Matson, R. A., et al., Visual Orbits and Alignments of Planet-hosting Binary Systems. 2023, *Astronomical Journal*, **166**, 166, DOI:10.3847/1538-3881/acf563

Liebert, J., Fontaine, G., Young, P. A., Williams, K. A., & Arnett, D., The Age and Stellar Parameters of the Procyon Binary System. 2013, *Astrophysical Journal*, **769**, 7, DOI:10.1088/0004-637X/769/1/7

Luhman, K. L., Discovery of a Binary Brown Dwarf at 2 pc from the Sun. 2013, *Astrophysical Journal, Letters*, **767**, L1, DOI:10.1088/2041-8205/767/1/L1

Mamajek, E. E., Kenworthy, M. A., Hinz, P. M., & Meyer, M. R., Discovery of a Faint Companion to Alcor Using MMT/AO 5 μm Imaging. 2010, *Astronomical Journal*, **139**, 919, DOI:10.1088/0004-6256/139/3/919

Mann, A. W., Dupuy, T., Kraus, A. L., et al., How to Constrain Your M Dwarf. II. The Mass-Luminosity-Metallicity Relation from 0.075 to 0.70 Solar Masses. 2019, *Astrophysical Journal*, **871**, 63, DOI:10.3847/1538-4357/aaf3bc

Marín Pina, D., Rastello, S., Gieles, M., et al., Dynamical formation of Gaia BH3 in the progenitor globular cluster of the ED-2 stream. 2024, *Astronomy and Astrophysics*, **688**, L2, DOI:10.1051/0004-6361/202450460

Marsh, T. R., Parsons, S. G., Bours, M. C. P., et al., The planets around NN Serpentis: still there. 2014, *Monthly Notices of the RAS*, **437**, 475, DOI:10.1093/mnras/stt1903

Mazzola, C. N., Badenes, C., Moe, M., et al., The close binary fraction as a function of stellar parameters in APOGEE: a strong anticorrelation with α abundances. 2020, *Monthly Notices of the RAS*, **499**, 1607, DOI:10.1093/mnras/staa2859

Merle, T., Dancing with the Stars: a Review on Stellar Multiplicity. 2024, *Bulletin de la Societe Royale des Sciences de Liege*, **93**, 170, DOI:10.25518/0037-9565.11641

Moe, M. & Kratter, K. M., Impact of binary stars on planet statistics - I. Planet occurrence rates and trends with stellar mass. 2021, *Monthly Notices of the RAS*, **507**, 3593, DOI:10.1093/mnras/stab2328

Moss, A., von Hippel, T., Robinson, E., et al., Improving White Dwarfs as Chronometers with Gaia Parallaxes and Spectroscopic Metallicities. 2022, *Astrophysical Journal*, **929**, 26, DOI:10.3847/1538-4357/ac5ac0

Munday, J., Marsh, T. R., Hollands, M., et al., Two decades of optical timing of the shortest-period binary star system HM Cancri. 2023, *Monthly Notices of the RAS*, **518**, 5123, DOI:10.1093/mnras/stac3385

Özdönmez, A., Er, H., & Nasiroglu, I., Investigation on the orbital period variations of NN Ser: implications for the hypothetical planets, the Applegate mechanism, and the orbital stability. 2023, *Monthly Notices of the RAS*, **526**, 4725, DOI:10.1093/mnras/stad3086

Pietrzyński, G., Graczyk, D., Gallenne, A., et al., A distance to the Large Magellanic Cloud that is precise to one per cent. 2019, *Nature*, **567**, 200, DOI:10.1038/s41586-019-0999-4

Pilecki, B., Thompson, I. B., Espinoza-Arancibia, F., et al., Cepheids with giant companions. II. Spectroscopic confirmation of nine new double-lined binary systems composed of two Cepheids. 2024, *Astronomy and Astrophysics*, **686**, A263, DOI:10.1051/0004-6361/202349138

Pittordis, C. & Sutherland, W., Testing modified gravity with wide binaries in Gaia DR2. 2019, *Monthly Notices of the RAS*, **488**, 4740, DOI:10.1093/mnras/stz1898

Pourbaix, D. & Boffin, H. M. J., Parallax and masses of α Centauri revisited. 2016, *Astronomy and Astrophysics*, **586**, A90, DOI:10.1051/0004-6361/201527859

Quarles, B., Li, G., Kostov, V., & Haghighipour, N., Orbital Stability of Circumstellar Planets in Binary Systems. 2020, *Astronomical Journal*, **159**, 80, DOI:10.3847/1538-3881/ab64fa

Rastello, S., Iorio, G., Mapelli, M., et al., Dynamical formation of Gaia BH1 in a young star cluster. 2023, *Monthly Notices of the RAS*, **526**, 740, DOI:10.1093/mnras/stad2757

Rebassa-Mansergas, A., Maldonado, J., Raddi, R., et al., Constraining the solar neighbourhood age-metallicity relation from white dwarf-main sequence binaries. 2021, *Monthly Notices of the RAS*, **505**, 3165, DOI:10.1093/mnras/stab1559

Roelofs, G. H. A., Rau, A., Marsh, T. R., et al., Spectroscopic Evidence for a 5.4 Minute Orbital Period in HM Cancri. 2010, *Astrophysical Journal, Letters*, **711**, L138, DOI:10.1088/2041-8205/711/2/L138

Simonetti, P., Vladilo, G., Silva, L., & Sozzetti, A., Statistical Properties of Habitable Zones in Stellar Binary Systems. 2020, *Astrophysical Journal*, **903**, 141, DOI:10.3847/1538-4357/abc074

Southworth, J., Rediscussion of eclipsing binaries. Paper XIX. The long-period solar-type system V454 Aurigae. 2024, *arXiv e-prints*, arXiv:2404.19443, DOI:10.48550/arXiv.2404.19443

Tanikawa, A., Cary, S., Shikauchi, M., Wang, L., & Fujii, M. S., Compact binary formation in open star clusters - I. High formation efficiency of Gaia BHs and their multiplicities. 2024, *Monthly Notices of the RAS*, **527**, 4031, DOI:10.1093/mnras/stad3294

Taylor, J. H. & Weisberg, J. M., A new test of general relativity - Gravitational radiation and the binary pulsar PSR 1913+16. 1982, *Astrophysical Journal*, **253**, 908, DOI:10.1086/159690

Tokovinin, A. & Moe, M., Formation of close binaries by disc fragmentation and migration, and its statistical modelling. 2020, *Monthly Notices of the RAS*, **491**, 5158, DOI:10.1093/mnras/stz3299

Wang, J., Fischer, D. A., Xie, J.-W., & Ciardi, D. R., Influence of Stellar Multiplicity on Planet Formation. II. Planets are Less Common in Multiple-star Systems with Separations Smaller than 1500 AU. 2014, *Astrophysical Journal*, **791**, 111, DOI:10.1088/0004-637X/791/2/111

Whitworth, A. P. & Lomax, O., Are the majority of Sun-like stars single? 2015, *Monthly Notices of the RAS*, **448**, 1761, DOI:10.1093/mnras/stv093

Zhang, H., Brandt, T. D., Kiman, R., et al., Dynamical masses and ages of Sirius-like systems. 2023a, *Monthly Notices of the RAS*, **524**, 695, DOI:10.1093/mnras/stad1849

Zhang, Z., Bowler, B. P., Dupuy, T. J., et al., The McDonald Accelerating Stars Survey: Architecture of the Ancient Five-planet Host System Kepler-444. 2023b, *Astronomical Journal*, **165**, 73, DOI:10.3847/1538-3881/aca88c

Contrib. Astron. Obs. Skalnaté Pleso **55/3**, 37 – 46, (2025)
https://doi.org/10.31577/caosp.2025.55.3.37

Accurate determination of binary star masses and distances using optical long-baseline interferometry

A. Gallenne

Instituto de Alta Investigación, Universidad de Tarapacá, Casilla 7D, Arica, Chile (E-mail: alexandre.gallenne@gmail.com)

Received: October 15, 2024; Accepted: January 22, 2025

Abstract. One of the most fundamental stellar parameters, mass, is often unavailable or measured with low accuracy, leading to weak constraints on stellar structure and evolution. Observing binary stars through a combination of interferometry and spectroscopy provides a unique opportunity to obtain highly precise dynamical mass measurements. Additionally, double-lined spectroscopic binaries offer independent distance measurements with extreme accuracy, enabling direct tests of Gaia parallaxes. I will demonstrate that by combining interferometric and spectroscopic observations, masses and distances with accuracy levels as high as 0.05% can be achieved for various types of binary systems, including binary Cepheids, eclipsing binaries, and standard binaries.

Key words: binaries: general – Stars: fundamental parameters – Stars: variables: Cepheids – Instrumentation: high angular resolution

1. Introduction

In the Araucaria project (Gieren et al., 2005), various techniques are employed to measure distances, with the goal of understanding the influence of population effects on key standard candles such as Cepheids, RR Lyrae stars, red clump stars, and the stars at the tip of the red-giant branch (Gieren et al., 2005). Binary systems play a crucial role in this effort, as highlighted by our work on eclipsing binaries, which has yielded the most accurate distance measurements for both the Large and Small Magellanic Clouds (Graczyk et al., 2020; Pietrzyński et al., 2019).

Binary stars are the only tool that enables direct and precise measurements of stellar mass and distance. In the case of double-lined spectroscopic binaries, their geometric distance can be determined, offering an independent benchmark for other methods, such as next Gaia data release (Gaia Collaboration et al., 2016). The mass is a fundamental parameter for understanding stellar structure and evolution, and accurate measurements are essential to assess consistency with theoretical models and tighten constraints. However, stellar parameters like the effective temperature ($T_{\rm eff}$) and radius (R), predicted by different stellar

evolution codes, can currently show discrepancies when compared to empirical values, leading to a broad range of possible ages for a given system. Comparing different evolutionary codes for a given age reveals discrepancies for both high- and low-mass stars, primarily due to the poorly constrained physics of stellar interiors (Huber, 2016). Stellar interior models vary in several aspects, initial chemical compositions, the treatment of convective core overshooting, rotational mixing, and the mixing length parameter (Marigo et al., 2017; Bressan et al., 2012; Dotter et al., 2008; Pietrinferni et al., 2004). High-precision measurements allow for tighter constraints on the evolutionary models, leading to a deeper understanding of stellar interior physics (e.g. Higl et al., 2018; Claret & Torres, 2018).

Over the years, the precision of stellar parameters ($T_{\rm eff}, R$, and M) has steadily improved through studies of eclipsing binary systems and large ground- and space-based photometric surveys (e.g., the Optical Gravitational Lensing Experiment, the Wide Angle Search for Planets, Kepler, the Large Synoptic Survey Telescope, and the Transiting Exoplanet Survey Satellite). By combining radial velocity (RV) data with photometric observations during eclipses, a precision level of approximately 1-3% is routinely achieved (e.g. Pribulla et al., 2018; Pilecki et al., 2018; Graczyk et al., 2015). However, recent studies indicate that a precision much better than 1% in stellar mass is required to reliably determine stellar interior model parameters (e.g., overshooting, initial helium abundance, etc. Higl et al., 2018; Valle et al., 2017).

Another model-independent method for measuring stellar masses and geometric distances with binary systems at sub-1% accuracy involves combining spectroscopic and astrometric observations (see e.g. Gallenne et al., 2016; Torres et al., 2009; Zwahlen et al., 2004). This technique requires no assumptions. Recently, it was applied to a Galactic binary Cepheid, yielding the most accurate distance and mass measurements for a Milky Way Cepheid (Gallenne et al., 2018a). However, astrometric measurements require the system to be spatially resolved, which can be challenging with single-dish telescopes. Optical long-baseline interferometry (LBI) offers a much better angular resolution, allowing for the detection of close binary systems (< 20 mas). LBI has proven its efficiency in providing both angular resolution and accuracy for such close binary stars (see, e.g. Pribulla et al., 2018; Gallenne et al., 2014, 2013; Le Bouquin et al., 2013).

I present my latest results using cutting-edge interferometric instruments combined with high-precision RV measurements. I will discuss three types of binary systems: eclipsing binaries (EBs), binary Cepheids, and standard binary stars. All of our systems are well-detached, which simplifies the analysis.

2. Eclipsing Binaries

In our quest for precise and accurate distance measurements for the Araucaria Project (Gieren et al., 2005), EBs serve as a very powerful tool. By combining contemporaneous radial velocities and photometric measurements, we can determine very precise linear radii. When these are paired with angular radii obtained from a well-calibrated surface brightness-colour relation (SBCR), the result is precise distance measurements. In 2019, we used EBs and a newly calibrated SBCR to determine the distance to the LMC with 1% accuracy (Pietrzyński et al., 2019; Gallenne et al., 2018b) and to the SMC with 2% (Graczyk et al., 2020).

Our newly calibrated SBCR (Pietrzyński et al., 2019) was specifically tailored to our LMC EBs with a colour range $2 < V - K < 2.8$. I am currently working on extending this range to include EBs of different spectral types. This extended SBCR will undergo rigorous validation through independent observing methods. The only alternative approach for precisely and accurately measuring EB distances involves combining RV data with astrometry. However, the small angular separations between EB components make astrometric measurements with single-dish telescopes impossible. Interferometry remains the only technique capable of spatially resolving their orbital motion.

I used LBI to observe nearby eclipsing systems and determine their astrometric orbits. By combining these observations with high-precision RV, as shown in Fig. 1, I achieved very accurate distance measurements. The first system I observed, TZ For, was studied with the VLTI/PIONIER instrument in 2015, yielding a distance measurement with 0.4% precision (Gallenne et al., 2016, 2018b). Five additional systems were subsequently observed (Gallenne et al., 2019) delivering the same level of precision. This level of accuracy is directly competitive with Gaia and will serve as a benchmark for parallax validation and for testing the accuracy of the extended SBCR.

During this work, I achieved stellar mass measurements with an as good as 0.04%. Such precise mass determinations are remarkable and can be used to test and calibrate stellar evolution models. As mentioned earlier, different evolutionary codes yield discrepant mass predictions for high- and low-mass stars, while they generally agree for solar-type stars, which is expected since the Sun is used to calibrate these models.

Achieving greater precision and accuracy in distance measurements was not possible due to the primary source of error being the systematic uncertainty from PIONIER's wavelength calibration (0.35%). To overcome this limitation, I transitioned the project to the VLTI/GRAVITY instrument and expanded the sample to include standard binary stars of various spectral types. Thanks to a dedicated internal reference laser source, this instrument is expected to achieve a wavelength calibration accuracy of approximately 0.02% in high-resolution spectral mode.

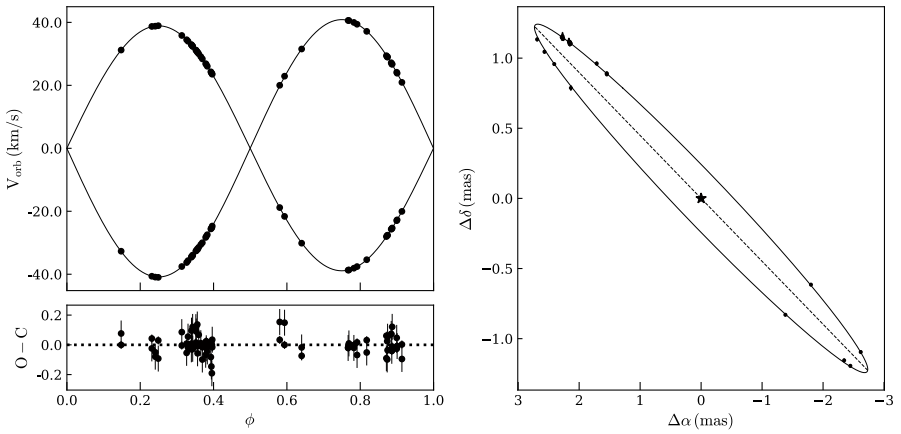


Figure 1. Left: radial velocities of the primary and the secondary star in the TZ For system. Right: astrometric orbit of the secondary component relative to the primary.

3. Standard Binary stars

Given the remarkable initial results on eclipsing binaries, it became evident to me that the sample of stars should be expanded to include non-eclipsing systems. Obtaining extremely precise masses for stars of various spectral types is essential for calibrating models at various evolutionary stages, as mentioned earlier. Moreover, there are no reference stars with the required distance precision and accuracy to validate Gaia parallaxes.

I observed 35 binary systems with GRAVITY and also acquired new high signal-to-noise ratio spectra with the VLTI/UVES spectrograph. In Gallenne et al. (2023), we published the results for 10 of these systems, achieving a precision of as good as 0.03% for both masses and distances, thanks to high-precision RVs($\sim$ 200 m s^{-1}) and astrometry ($\sim$ 20μas). Fig. 2 illustrates the high-precision orbit derived from my dataset.

This work yielded two key findings. First, we confronted our precise mass measurements, along with other observables (e.g., $T_{\rm eff}$, radii, ...), with four stellar evolution models. Theoretical predictions fail in matching observations of two components with a single isochrone, suggesting that further refinement of stellar models is necessary, especially when dealing with non-solar-type stars, as the models are often tailored to match solar characteristics. Second, we also compared our orbital parallaxes with Gaia and showed that for half of the stars, Gaia measurements deviate by more than 1σ, despite their RUWE value being below the commonly accepted cutoff of 1.4 for reliable Gaia astrometry. Further analysis suggests a correlation between this discrepancy and the brightness of

the systems, the brighter the star, the larger the deviation. Since these stars have $G < 10$, the discrepancy could be related to saturation effects.

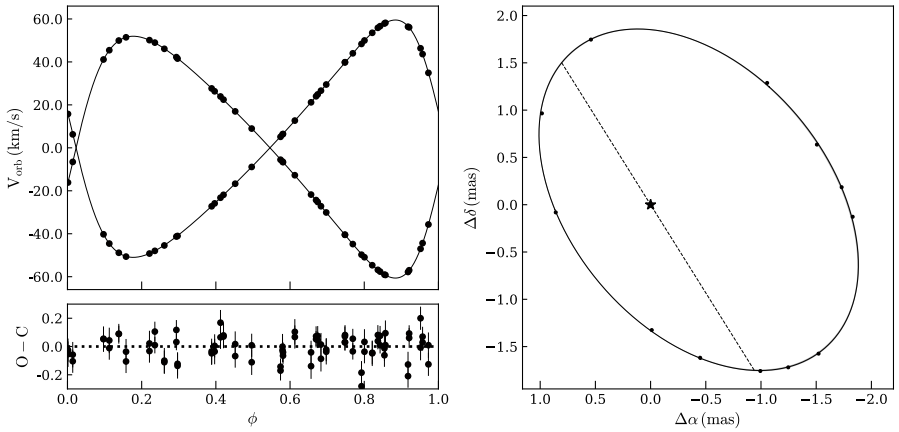


Figure 2. Left: radial velocities of the primary and the secondary components of the HD224974 system. Right: GRAVITY astrometric orbit of the secondary relative to the primary.

4. Binary Cepheids

LBI is also a powerful technique for studying binary Cepheids. In the context of the extragalactic distance scale, Cepheids are essential primary distance indicators due to their period-luminosity relation (PLR). However, calibrating this PLR can be challenging since it requires direct distance measurements. Prior to Gaia, the calibration was partially based on 19 Galactic Cepheids with trigonometric parallax measurements (Benedict et al., 2007; Kervella et al., 2014; Riess et al., 2018). However, their average accuracy was limited to 9%, making it difficult to achieve the 1% precision required for a reliable luminosity calibration. With Gaia, the geometric calibration of 75 Cepheid luminosities seems to be precise to 1% (Riess et al., 2021). However, the accuracy still needs to be assessed. Gaia is still affected by a variable parallax offset (Lindegren et al., 2021) that depends on ecliptic latitude, chromatic effects due to colour variations during pulsation, and the influence of binarity. As a result, precise and accurate independent distance measurements are essential to verify Gaia's accuracy. Observing binary Cepheids is the only method able to deliver precise and accurate independent distance measurements.

Most known companions are too close to the Cepheid (< 40 mas) to be observed with an 8-meter class telescope. While orbits for several Cepheids have

been determined through RV measurements, LBI is the only method capable of spatially resolving these systems. In 2012, I initiated an interferometric observing campaign targeting the brightest northern and southern binary Cepheids. The aim of this project is to monitor the astrometric orbits of their companions and to measure dynamical masses and distances.

All binary Cepheids are single-line spectroscopic binaries because the brightness of the Cepheid outshines the companion at optical wavelengths, leading to a degeneracy between distance and mass measurements. Since most companions are main-sequence B stars, ultraviolet (UV) wavelengths offer the best chance to detect the companion's spectral lines, which will help resolve the mass-distance degeneracy. We therefore secured HST/STIS UV observations of some binary Cepheid systems and measured RVs of their orbiting companions, despite the challenges of broad and blended spectral lines. In Gallenne et al. (2018a), we combined astrometric data from the CHARA/MIRC combiner with both space- and ground-based RV measurements to achieve the most precise distance (1%) for the Cepheid V1334 Cyg, in addition to the most precise mass (3%) for a Galactic Cepheid. Fig. 3 illustrates the highly precise orbit derived.

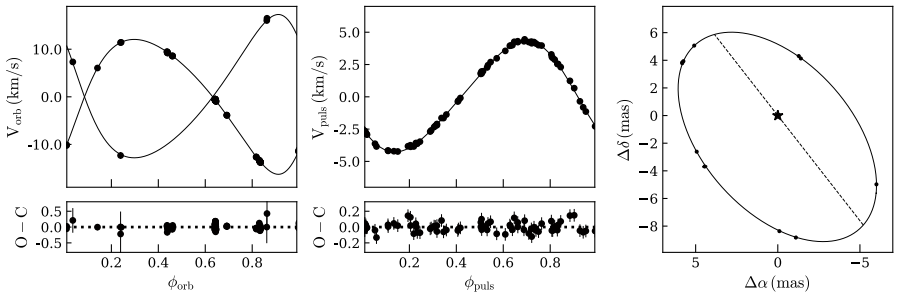


Figure 3. Left: Orbital velocity of the primary and the secondary components. Middle: Pulsation velocity of the primary (Cepheid). Right: MIRC astrometric orbit of the secondary relative to the primary.

Comparisons between our measured Cepheid mass and predictions from evolutionary models indicate that the models tend to overestimate the mass for the observed luminosity, even when factors like rotation and convective core overshooting are considered. This trend was also observed in another Cepheid system, Polaris, as reported by Evans et al. (2018).

We also compared our precise distance measurement with predictions from period-luminosity relations (PLRs). We found a discrepancy of 0.2-0.5 magnitudes when using PLRs calibrated with photometry, whereas those calibrated with direct distance measurements showed better agreement.

Recently, we conducted a similar analysis for another Cepheid, SU Cyg, for which RVs of the companion were also measured using HST/STIS spectra (Gallenne et al., 2025). We achieved even greater precision in our distance measurement, reaching a level of 0.5%, and obtained a 1% precision for the Cepheid's mass. A similar pattern to V1334 Cyg is observed, with discrepancies between our distance measurements and photometrically calibrated PLRs, as well as overestimated Cepheid mass predicted by evolutionary models.

5. Conclusions

Radial velocity measurements and interferometry offer a powerful approach to determine high-precision masses and distances of binary stars. This method is particularly efficient for close binary systems, where high angular resolution from interferometry is critical, enabling measurements of the mass with a precision as good as 0.03% and distance measurements accurate to sub-percent levels, offering crucial benchmarks for stellar models and calibration of other distance measurement techniques.

Obtaining such precise mass measurements offers a crucial test for stellar evolution models, which often fail to accurately reproduce key observables like temperature, radius, and luminosity simultaneously. Discrepancies emerge especially for non-solar-type stars, highlighting the need to refine assumptions about stellar interior, like convective core overshooting, rotation, or initial helium content. Consequently, high-precision mass data from binary systems is vital for enhancing the accuracy of these models.

There was previously no other method to verify the accuracy of Gaia parallaxes. Through this work, we achieved distance measurements with precision comparable to, or even exceeding, that of Gaia, offering a critical benchmark to identify potential biases in Gaia's data. We showed that for half of our sample, Gaia DR3 measurements deviate beyond 1σ, even though their RUWE values are below the widely accepted threshold of 1.4 for reliable Gaia astrometry. Additional analysis seems to indicate a correlation between this discrepancy and the brightness of the stars; specifically, brighter stars exhibit larger deviations. Given that these stars have $G < 10$, this discrepancy may be attributed to saturation effects, as well as the orbital motion that has not yet been considered.

Acknowledgements: I acknowledges the support of the Agencia Nacional de Investigación Científica y Desarrollo (ANID) through the FONDECYT Regular grant 1241073 and ANID-ALMA fund No. ASTRO20-0059.

References

Benedict, G. F., McArthur, B. E., Feast, M. W., et al., Hubble Space Telescope Fine Guidance Sensor Parallaxes of Galactic Cepheid Variable Stars: Period-

Luminosity Relations. 2007, *Astronomical Journal*, **133**, 1810, DOI:10.1086/511980

Bressan, A., Marigo, P., Girardi, L., et al., PARSEC: stellar tracks and isochrones with the PAdova and TRieste Stellar Evolution Code. 2012, *Monthly Notices of the RAS*, **427**, 127, DOI:10.1111/j.1365-2966.2012.21948.x

Claret, A. & Torres, G., The Dependence of Convective Core Overshooting on Stellar Mass: Additional Binary Systems and Improved Calibration. 2018, *Astrophysical Journal*, **859**, 100, DOI:10.3847/1538-4357/aabd35

Dotter, A., Chaboyer, B., Jevremović, D., et al., The Dartmouth Stellar Evolution Database. 2008, *Astrophysical Journal, Supplement*, **178**, 89, DOI:10.1086/589654

Evans, N. R., Karovska, M., Bond, H. E., et al., The Orbit of the Close Companion of Polaris: Hubble Space Telescope Imaging, 2007 to 2014. 2018, *Astrophysical Journal*, **863**, 187, DOI:10.3847/1538-4357/aad410

Gaia Collaboration, Prusti, T., de Bruijne, J. H. J., et al., The Gaia mission. 2016, *Astronomy and Astrophysics*, **595**, A1, DOI:10.1051/0004-6361/201629272

Gallenne, A., Evans, N. R., Kervella, P., et al., Multiplicity of Galactic Cepheids from long-baseline interferometry: V. High-accuracy orbital parallax and mass of SU Cygni. 2025, *Astronomy and Astrophysics*, **693**, A111, DOI:10.1051/0004-6361/202452346

Gallenne, A., Kervella, P., Evans, N. R., et al., A Geometrical 1% Distance to the Short-period Binary Cepheid V1334 Cygni. 2018a, *Astrophysical Journal*, **867**, 121, DOI:10.3847/1538-4357/aae373

Gallenne, A., Mérand, A., Kervella, P., et al., Multiplicity of Galactic Cepheids from long-baseline interferometry. II. The Companion of AX Circini revealed with VLTI/PIONIER. 2014, *Astronomy and Astrophysics*, **561**, L3, DOI:10.1051/0004-6361/201322883

Gallenne, A., Mérand, A., Kervella, P., et al., The Araucaria project: High-precision orbital parallaxes and masses of binary stars. I. VLTI/GRAVITY observations of ten double-lined spectroscopic binaries. 2023, *Astronomy and Astrophysics*, **672**, A119, DOI:10.1051/0004-6361/202245712

Gallenne, A., Monnier, J. D., Mérand, A., et al., Multiplicity of Galactic Cepheids from long-baseline interferometry. I. CHARA/MIRC detection of the companion of V1334 Cygni. 2013, *Astronomy and Astrophysics*, **552**, A21, DOI:10.1051/0004-6361/201321091

Gallenne, A., Pietrzyński, G., Graczyk, D., et al., The Araucaria Project: High-precision orbital parallax and masses of the eclipsing binary TZ For-

nacis. 2016, *Astronomy and Astrophysics*, **586**, A35, DOI:10.1051/0004-6361/201526764

Gallenne, A., Pietrzyński, G., Graczyk, D., et al., Fundamental properties of red-clump stars from long-baseline H-band interferometry. 2018b, *Astronomy and Astrophysics*, **616**, A68, DOI:10.1051/0004-6361/201833341

Gallenne, A., Pietrzyński, G., Graczyk, D., et al., The Araucaria project: High-precision orbital parallax and masses of eclipsing binaries from infrared interferometry. 2019, *Astronomy and Astrophysics*, **632**, A31, DOI:10.1051/0004-6361/201935837

Gieren, W., Pietrzynski, G., Bresolin, F., et al., Measuring Improved Distances to Nearby Galaxies: The Araucaria Project. 2005, *The Messenger*, **121**, 23

Graczyk, D., Maxted, P. F. L., Pietrzyński, G., et al., The Araucaria project. Precise physical parameters of the eclipsing binary IO Aquarii. 2015, *Astronomy and Astrophysics*, **581**, A106, DOI:10.1051/0004-6361/201526211

Graczyk, D., Pietrzyński, G., Thompson, I. B., et al., A Distance Determination to the Small Magellanic Cloud with an Accuracy of Better than Two Percent Based on Late-type Eclipsing Binary Stars. 2020, *Astrophysical Journal*, **904**, 13, DOI:10.3847/1538-4357/abbb2b

Higl, J., Siess, L., Weiss, A., & Ritter, H., An analysis of the TZ Fornacis binary system. 2018, *Astronomy and Astrophysics*, **617**, A36, DOI:10.1051/0004-6361/201833112

Huber, D., Precision Stellar Astrophysics in the Kepler Era. 2016, *ArXiv [eprint: 1604.07442]*

Kervella, P., Bond, H. E., Cracraft, M., et al., The long-period Galactic Cepheid RS Puppis. III. A geometric distance from HST polarimetric imaging of its light echoes. 2014, *Astronomy and Astrophysics*, **572**, A7, DOI:10.1051/0004-6361/201424395

Le Bouquin, J.-B., Beust, H., Duvert, G., et al., Masses and age of the chemically peculiar double-lined binary χ Lupi. 2013, *Astronomy and Astrophysics*, **551**, A121, DOI:10.1051/0004-6361/201220454

Lindegren, L., Bastian, U., Biermann, M., et al., Gaia Early Data Release 3. Parallax bias versus magnitude, colour, and position. 2021, *Astronomy and Astrophysics*, **649**, A4, DOI:10.1051/0004-6361/202039653

Marigo, P., Girardi, L., Bressan, A., et al., A New Generation of PARSEC-COLIBRI Stellar Isochrones Including the TP-AGB Phase. 2017, *Astrophysical Journal*, **835**, 77, DOI:10.3847/1538-4357/835/1/77

Pietrinferni, A., Cassisi, S., Salaris, M., & Castelli, F., A Large Stellar Evolution Database for Population Synthesis Studies. I. Scaled Solar Models and Isochrones. 2004, *Astrophysical Journal*, **612**, 168, DOI:10.1086/422498

Pietrzyński, G., Graczyk, D., Gallenne, A., et al., A distance to the Large Magellanic Cloud that is precise to one per cent. 2019, *Nature*, **567**, 200, DOI:10.1038/s41586-019-0999-4

Pilecki, B., Gieren, W., Pietrzyński, G., et al., The Araucaria Project: High-precision Cepheid Astrophysics from the Analysis of Variables in Double-lined Eclipsing Binaries. 2018, *Astrophysical Journal*, **862**, 43, DOI:10.3847/1538-4357/aacb32

Pribulla, T., Mérand, A., Kervella, P., et al., Physical parameters and ±0.2% parallax of the detached eclipsing binary V923 Scorpii. 2018, *Astronomy and Astrophysics*, **616**, A49, DOI:10.1051/0004-6361/201730673

Riess, A. G., Casertano, S., Yuan, W., et al., Cosmic Distances Calibrated to 1% Precision with Gaia EDR3 Parallaxes and Hubble Space Telescope Photometry of 75 Milky Way Cepheids Confirm Tension with ΛCDM. 2021, *Astrophysical Journal, Letters*, **908**, L6, DOI:10.3847/2041-8213/abdbaf

Riess, A. G., Casertano, S., Yuan, W., et al., New Parallaxes of Galactic Cepheids from Spatially Scanning the Hubble Space Telescope: Implications for the Hubble Constant. 2018, *Astrophysical Journal*, **855**, 136, DOI:10.3847/1538-4357/aaadb7

Torres, G., Claret, A., & Young, P. A., Binary Orbit, Physical Properties, and Evolutionary State of Capella (α Aurigae). 2009, *Astrophysical Journal*, **700**, 1349, DOI:10.1088/0004-637X/700/2/1349

Valle, G., Dell'Omodarme, M., Prada Moroni, P. G., & Degl'Innocenti, S., Statistical errors and systematic biases in the calibration of the convective core overshooting with eclipsing binaries. A case study: TZ Fornacis. 2017, *Astronomy and Astrophysics*, **600**, A41, DOI:10.1051/0004-6361/201628240

Zwahlen, N., North, P., Debernardi, Y., et al., A purely geometric distance to the binary star Atlas, a member of the Pleiades. 2004, *Astronomy and Astrophysics*, **425**, L45, DOI:10.1051/0004-6361:200400062

Contrib. Astron. Obs. Skalnaté Pleso **55/3**, 47 – 66, (2025)
https://doi.org/10.31577/caosp.2025.55.3.47

Symbiotic novae

U. Munari

INAF National Institute of Astrophysics, Astronomical Observatory of Padova, 36012 Asiago (VI), Italy (E-mail: ulisse.munari@inaf.it)

Received: November 21, 2024; Accepted: December 11, 2024

Abstract. (Invited Review) According to modern definition, a symbiotic nova is an otherwise normal nova (i.e. powered by *explosive* thermonuclear burning) that erupts within a symbiotic star, which is a binary where a WD accretes from a cool giant companion. Guided primarily by the very well observed eruptions of RS Oph in 2006 and 2021, and that of V407 Cyg in 2010, we describe the main multi-wavelength properties of symbiotic novae and their relation to classical novae, and propose a 3D model structure that identifies the emitting source location for hard and supersoft X-rays, radio syncrothron and thermal, permitted and forbidden emission lines. Very few symbiotic novae are known in the Galaxy, and we compile a revised catalog based on firm astrometric identification. The exciting prospect of an imminent new outburst of T CrB is also discussed.

Key words: binaries: symbiotic – novae, cataclysmic variables – circumstellar matter – jets and outflows – catalogs

1. A modern definition for symbiotic novae

Traditionally (eg. Gaposchkin, 1957; Allen, 1980; Kenyon, 1986; Warner, 1995), the term 'symbiotic nova' has indicated a symbiotic star undergoing a large amplitude ($\Delta V \geq$ 4 mag) and very long lasting outburst (several decades to a century), clearly distinct from the smaller amplitude ($\Delta V \sim$2 mag) and much faster eruptions (from several months to a few years) characterizing most of the symbiotic binaries and usually referred to as 'ZAND' events, from the prototype Z And that has gone through several of them in its recorded history (eg. Tomov et al., 2016; Skopal et al., 2020). Over the last 10-20 yrs the accepted meaning has however drastically changed to

> *a symbiotic nova is an otherwise normal nova [i.e. powered by explosive thermonuclear burning] that erupts within a symbiotic binary*

which we will adopt in this review. Classical novae and symbiotic novae share similar properties in the way their white dwarfs (WD) accrete mass and then ignite the explosive burning. A classical nova is a compact interacting binary, where a WD accretes (usually via Roche lobe overflow and formation of an accretion disk) from a low-mass red dwarf companion (RD), orbiting in a few

hours at a distance of about a Solar radius. In the case of a symbiotic binary the companion to the WD is a red giant (RG), and to accommodate its much larger dimensions the orbital separation widens to a few astronomical units and the orbital period increases to a few years.

For both the classical and symbiotic novae, the accreted material goes accumulating in electron-degenerate conditions on the surface of the WD; diffusion from the outer layers of the WD allows enrichment in CNO nuclei (ensuing stronger explosions). Once the pressure at the base of the accumulated shell reaches a critical value around 10^{20} dyn/cm^2, nuclear burning of the accreted material sets in. Given its electron-degenerate state ($P \propto \rho^{\beta}$), the shell does not initially react by expanding to the increase in temperature, with the consequent ramping in energy released by the nuclear reactions ($\epsilon_{\rm CNO} \propto {\rm T}^{17}$) which leads to further increase in temperature. Within a few minutes, the temperature reaches the Fermi value (of the order of 10^8 K), at which point the electron degeneracy is suddenly lifted ($P \propto \rho T$), and the hyper-hot material in the shell violently expands at velocities in excess of the escape velocity from the WD ($v_e = \sqrt{2GM/R} \sim 9100$ km sec^{-1} at M=1.25 M$_\odot$; Arseneau et al. (2024)), effectively terminating the TNR (eg. Starrfield, 1989; Starrfield et al., 2008). Not the entire shell is however expelled, and the nuclear burning can continue (now in thermal equilibrium) in what has been left of the shell on the surface of the WD, a phase lasting for weeks–months and characterized by supersoft X-rays emission, which become observable when the ejecta turn optically-thin (eg. Schwarz et al., 2011).

The paths followed by classical and symbiotic novae diverge at this point, at the time when the shell is violently expelled by the WD. Unbind from the system, the ejected material travels the WD–RD orbital separation of a classical nova in a matter of minutes, after which (and for the time being) it basically keeps expanding on free ballistic trajectories into the circumstellar void, as beautifully demonstrated by Nova Per 1901 (Liimets et al., 2012) and other novae with spatially resolved ejecta (O'Brien & Bode, 2008). In a symbiotic nova instead, the circumstellar space up to hundreds of AU is filled by the thick and slow wind of the RG, and the fast expanding ejecta have to plow their way through it (Sokoloski et al., 2008; Evans et al., 2008). This results in a violent and efficient deceleration of the ejecta, and the associated massive shock-fronts power emission from the highest energies probed by Cherenkov telescopes all the way down to the synchrotron emission dominating at radio wavelengths. The first nova ever detected in γ-rays (by the *Fermi*-LAT satellite) has been, not incidentally, the symbiotic nova V407 Cyg in 2010 (Abdo et al., 2010).

The literature about observations and modeling of nova explosions is very rich, and well beyond the possibility of a balanced citation in a short review like the present one. Excellent summaries may be found in the books and proceedings of conferences devoted specifically to novae, like those edited by Bode & Evans (1989), Cassatella & Viotti (1990), Hernanz & José (2002), Bode & Evans (2008), Saikia & Anupama (2012), and Woudt & Ribeiro (2014).

Old meaning for 'symbiotic novae'. Before moving on, some words are in order about the *traditional* meaning of the term 'symbiotic nova', which is still - although rarely - in use. In the life-cycle of a typical symbiotic star as proposed by Munari (2019), the longest intervals are spent accreting onto the WD (at highly variable rates). In the (great) majority of the symbiotic stars the accreted envelope is non-degenerate, primarily because of the low mass of the WD. Once the conditions for nuclear burning are reached, the burning ignites non-explosively and continues in thermal equilibrium as long as enough hydrogen fuel is present in the shell, a phase lasting decades to centuries (Iben, 1982; Fujimoto, 1982b,a). The rise to optical maximum takes a few years to complete (∼3 yrs for V1016 Cyg and V3268 Sgr): these are the symbiotic novae according to the old definition (for which we propose the name SETE standing for Symbiotic stars Erupting in Thermal-Equilibrium). The shell is *not* ejected and remains in hydrostatic equilibrium, progressively contracting in radius and slowly rising in surface temperature as the hydrogen fuel is consumed. Once the burning shell shrinks to the radius and temperature of the nuclei of planetary nebulae, accretion-induced ingestion by the shell of limited amounts of mass triggers short-lived ZAND outbursts (as observed in 2015 for AG Peg; Tomov et al., 2016). The exhaustion of the hydrogen fuel in the shell eventually stops the burning, the strong emission lines and ultraviolet continuum die away, and the symbiotic star (now broadly resembling a field single RG) resumes the long-lasting and quiet accretion phase in preparation for a new cycle.

2. A revised catalog of Symbiotic Novae

From the previous section, the main difference between classical and symbiotic novae resides in the nature of the companion to the WD: a red dwarf versus a red giant. Considering that the in the infrared K band (i) cool dwarfs and cool giants differ by ∼10 in absolute M(K) magnitude, and (ii) the interstellar reddening plays a marginal role (A(K)=0.43×E_{B-V} for M spectral types), and (iii) the sensitivity of the 2MASS JHK survey is high enough to detect a red giant anywhere in the Galaxy, it seems a good choice to investigate the distribution of novae in 2MASS K band to segregate symbiotic novae from classical ones.

We started by assembling various compilations of Galactic Novae (from IAU, SIMBAD, Bill Gray, Koji Mukai, and others) and proceeded with pruning them from mis-entries. For ex., FU Ori - the prototype of erupting pre-main sequence stars - is still listed as Nova Ori 1939. We therefore retained only the objects for which there is observational evidence of an *explosive* TNR event on a WD (which excludes SETE objects). Next, we tried to obtain accurate astrometric coordinates and a measure of their error by going to the original sources of the epoch (for ex., SIMBAD coordinates for Nova Sgr 1935 are those of an unrelated Mira variable, ∼1 arcmin away from the true nova position, as clear from a finding chart of the epoch). For novae up to 1985, the prime source for

astrometric coordinates and finding charts is the reference catalogue and atlas of Duerbeck (1987), where in most cases the original discovery photographic plates were directly inspected and astrometrically measured in a modern way. For later novae, we went through the original discovery announcements (on IAUC, CBET, ATel, etc.), follow-up papers, and the catalog and atlas of CVs by Downes & Shara (1993); Downes et al. (1997, 2001). The quoted coordinates were critically re-evaluated and their errors estimated in parallel with direct inspection of POSS scans and 2MASS maps. Only novae identified with a high degree of confidence and not in blend with field stars were retained. The surviving objects were then cross-matched with Gaia DR3 (Gaia Collaboration, 2016, 2023) looking for possible nearby, faint field stars that could interfere with a firm identification of the progenitor. After this further pruning, the Gaia DR3 coordinates were adopted and the final list of novae was cross-matched with the 2MASS catalog (Skrutskie et al., 2006) within 1arcsec radius (including correction for proper motion).

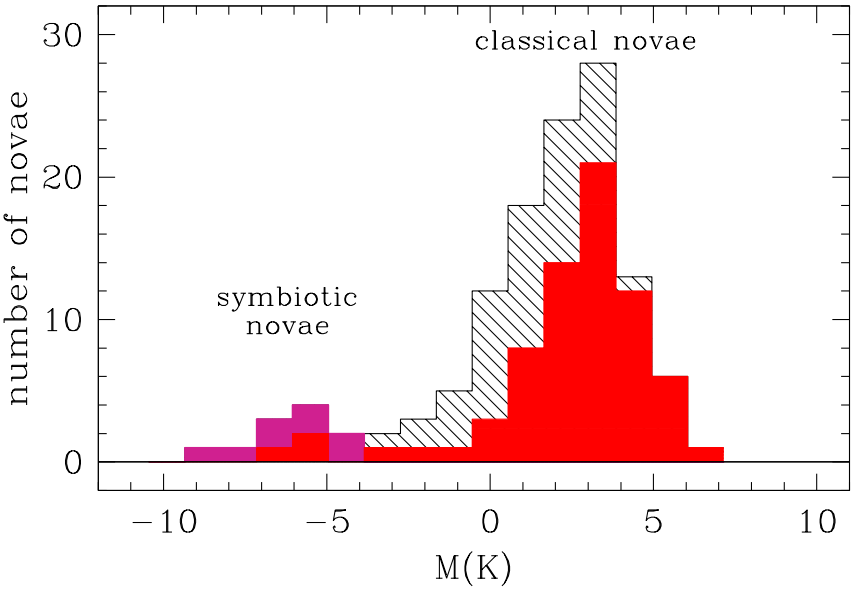


Figure 1. Distribution in absolute M(K) magnitude of all validated thermonuclear runaway novae with an accurate astrometric identification. Those containing a red giant (M(K)≤−4 mag) are listed in Tab. 1.

As a final step, the Gaia DR3 parallax was adopted to compute the absolute magnitude of novae in the K band (2.2 μm), which resulted in the distribution of Fig. 1. In this figure, the novae with an error on the parallax inferior to 25%,

Table 1. The symbiotic novae (novae with a red giant), corresponding to the objects with M(K)≤−4 in Fig. 1.

		Gaia DR3						Galactic		2MASS	
Name	Outbursts	RA	DEC	π [mas]	$\sigma(\pi)$ [mas]	BP	RP	long [deg]	lat [deg]	K_s	$(J-K_s)$
RS Oph	1898, 1933, 1958, 1967, 1985, 2006, 2021	17 50 13.159	−06 42 28.48	0.373	0.023	11.44	9.38	19.80	10.37	6.50	1.134
V745 Sco	1897, 1937, 1989, 2014	17 55 22.226	−33 14 58.55	0.100	0.076	16.54	13.25	357.36	−4.00	8.26	1.78
V3890 Sgr	1962, 1990, 2019	18 30 43.288	−24 01 08.9	0.048	0.045	15.82	12.75	9.20	−6.44	8.26	1.57
T CrB	1866, 1946	15 59 30.162	+25 55 12.61	1.092	0.028	9.91	7.62	42.37	48.16	4.81	1.19
V407 Cyg	1936?, 2010	21 02 09.819	+45 46 32.73	0.247	0.117	16.14	10.19	86.98	−0.48	3.3	2.4
EU Sct	1949	18 56 13.127	−04 12 32.41	0.072	0.037	17.60	14.53	29.73	−2.98	10.80	1.45
V1172 Sgr	1951	17 50 23.657	−20 40 29.82	0.104	0.047	18.13	14.97	7.64	3.34	11.03	1.54
V5581 Sgr	2009	17 44 08.460	−26 05 48.00	−0.04	0.145	20.34	13.96	2.25	1.76	7.92	2.09
V5590 Sgr	2012	18 11 03.700	−27 17 29.43	0.129	0.032	12.92	11.22	4.23	−4.04	7.35	1.95
V1534 Sco	2014	17 15 46.881	−31 28 30.31	0.113	0.070	17.91	14.10	354.33	3.99	9.58	1.68
V1708 Sco	2020	17 23 41.935	−31 03 07.60	0.073	0.071	18.66	14.72	355.65	2.84	9.75	1.88

are plotted in red, those with a larger error are dashed. Various novae with a red giant are listed in Gaia DR3 with a too large uncertain in the parallax, and consequently we derived their distances as an average of independent estimates found in literature; these systems are plotted in purple in Fig. 1. No correction for reddening is applied because it is reliably *measured* (not simply guessed) only for a tiny minority of all novae, and its impact - which is at the level of a few tenths of a magnitude at most - does not affect at all the distinction between classical and symbiotic novae in Fig. 1.

The distribution in Fig. 1 is clearly bi-modal. The more numerous group, which is that of classical novae (those with a red dwarf), presents a Gaussian-like distribution centered at M(K)=+3.2 mag. It is worth noticing that this value is about 1 mag brighter than the absolute K magnitude of main sequence K-type stars, suggesting that the same accretion disk that dominates the UV and optical energy distribution of old novae (Cassatella et al., 1990, 2004) extends its influence also into the infrared.

The smaller group in Fig. 1, is that of symbiotic novae, with a mean absolute magnitude of M(K)≈ −5.8 mag, which is close to the mean M(K)= −5.9 mag derived by Munari et al. (2021) for the accreting-only symbiotic stars. This similarity can be read as an indication that the population of red giants in field symbiotic stars and in symbiotic novae is the same, and presumably also their mass lose rates. The symbiotic novae in Fig. 1 (those with $M(K) \leq -4.0$ mag) are listed in Tab. 1, with quoted values taken from Gaia DR3 and 2MASS catalogues. Those with more than one recorded eruption (symbiotic *recurrent* novae) are listed at the top.

3. The distinctive presence of the red giant wind

We remarked above how the primary differences between classical and symbiotic novae originate from the wind of the red giant filling the circumstellar space of symbiotic novae, and how it interacts with the radiation output and the fast ejecta of the outbursting WD.

3.1. Flash ionization of the red giant wind

A feature unique to symbiotic novae actually manifests even before the fast ejecta begin slamming onto the pre-existing slow wind of the RG. It originates from the strong UV-flash originating from the burning shell during the TNR and its immediate aftermath. The flash is really short-lived: in the nova models by Starrfield et al. (2008), the shell surface temperature drops to $1{\times}10^5$ K in ∼300sec and ∼500sec for WDs of 1.35 and 1.25 $M_\odot$ mass, respectively.

In a classical nova, such a short-lived UV-flash precedes the discovery of the nova at optical wavelengths by ∼one day, and will go unnoticed while traveling through the empty circumstellar space. On the contrary, in a symbiotic nova, the RG wind that permeates the circumstellar space absorbs the photons of the UV-flash and get ionized. The ionized gas starts immediately to recombine, glowing very brightly in the process. The recombination time scale (in hours) goes as $t_{\rm rec} = 0.66\, T_e^{0.8}\, n_e^{-1}$ (Ferland, 2003), where T_e is the electron temperature in 10^4 K units, and n_e is the electron density in 10^9 cm^{-3} units. Both lines and continuum are emitted by the recombining wind.

Emission Lines. The emission lines component from the flashed wind are quite sharp (FWHM∼40 km sec^{-1}, as the outflow velocity of the RG wind is rather low), and are visible on-top the broad pedestal originating from the fast expanding ejecta (see top-left of Fig. 2). The evolution of the recombining Hα component over the first few days of the V407 Cyg (2010), RS Oph (2021), and V3890 Sgr (2019) outbursts is compared in Fig. 2. The e-folding recombination times are respectively 100, 60 and 13 hours, corresponding to electronic densities of $6.6{\times}10^6$, $1.1{\times}10^7$ and $5.0{\times}10^7$ cm^{-3}. From Fig. 2 its is clear that prompt access to a telescope with a standing-by high-resolution spectrograph (resolving power ≥20,000) is mandatory to successfully detect the presence of emission lines from the recombining wind and record the details of their very fast evolution.

The narrow emission lines from the flashed wind are invariably accompanied by a similarly sharp and slightly blue-shifted *absorption* component. It originates from the outer parts of the slowly outflowing RG wind, which remains neutral through the recombination process (which is equivalent to say that there is enough column density in the circumstellar material to absorb *all* the ionizing photons emitted during the initial UV-flash). While the narrow emission component traces gas which is roughly symmetric around the central binary, the blue-shifted narrow absorption provides a measure of the terminal wind velocity (at least in the direction probed by the line-of-sight to the observer).

From the spectra in Fig. 2, such terminal wind velocity is −38, −60, and −65 km sec^{-1} for V407 Cyg, RS Oph, and V3890 Sgr, respectively.

Nebular continuum. If the passage of a classical nova at peak optical brightness corresponds to the maximum angular extension of the optically-thick pseudo-photosphere of the expanding ejecta, in a symbiotic nova it generally marks the time when the continuum radiation from the recombining wind reaches its peak output, roughly corresponding to the maximum mass reached by the ionized fraction of the RG wind. For ex., in the case of the 2019 outburst of V3890 Sgr, the continuum emission from flashed wind declined in brightness by 4× before the ejecta could take over, as illustrated by the V-band lightcurve in the lower-right panel of Fig. 2; unsurprisingly, the e-folding time of the recombining RG wind estimated from the narrow Hα component is the same as derived from the emission in the continuum.

Radio thermal emission. The UV-flashed wind of the RG emits free-free radiation that should be detectable at radio wavelengths within 1-2 days of TNR onset, before the stronger synchrotron emission from the shocked ejecta takes over. The geometrical arrangement and flux level for this prompt free-free radio emission should be similar to that of the RG wind kept ionized by the long-term burning WDs in SETE objects, which has been modeled by Taylor & Seaquist (1984), among others. A fair fraction of symbiotic stars with burning WDs is radio-emitter at cm-wavelengths, with brightness temperature and α spectral index ($S_\nu \propto \nu^\alpha$) suggestive of thermal emission from an outflowing wind (eg. Seaquist et al., 1984; Seaquist & Taylor, 1990; Seaquist et al., 1993). The main difficulty to observe at radio wavelengths this prompt free-free emission resides in the (very) fast response time required to access suitable radio telescopes before the recombination wave (proceeding inside-out because of the density gradient in the RG wind) completes its job and the synchrotron emission from the shocked ejecta takes over.

The earliest radio observation for the 2014 outburst of V745 Sco started 2.6 days past optical maximum (Molina et al., 2024), 2.0 days for V3890 Sgr in 2019 (Nyamai et al., 2023), and 2 to 5 days for RS Oph in 2021 (Williams et al., 2021; Sokolovsky et al., 2021). They all were already affected by the rapidly growing contribution of the synchrotron emission from the shocked ejecta, at an epoch when the thermal emission from the flashed wind was declining if not already extinguished. Better luck could favor the coming and much anticipated outburst of T CrB (in 2025-2026 ?), for which proposals have been approved at basically all radio facilities to be triggered by the announcement of a new outburst. A few of them specifically aim to obtain a "picture at rest" of the circumstellar medium before the ejecta will slam onto it, by imaging the prompt free-free thermal emission from the UV-flashed wind within hours of the outburst discovery.

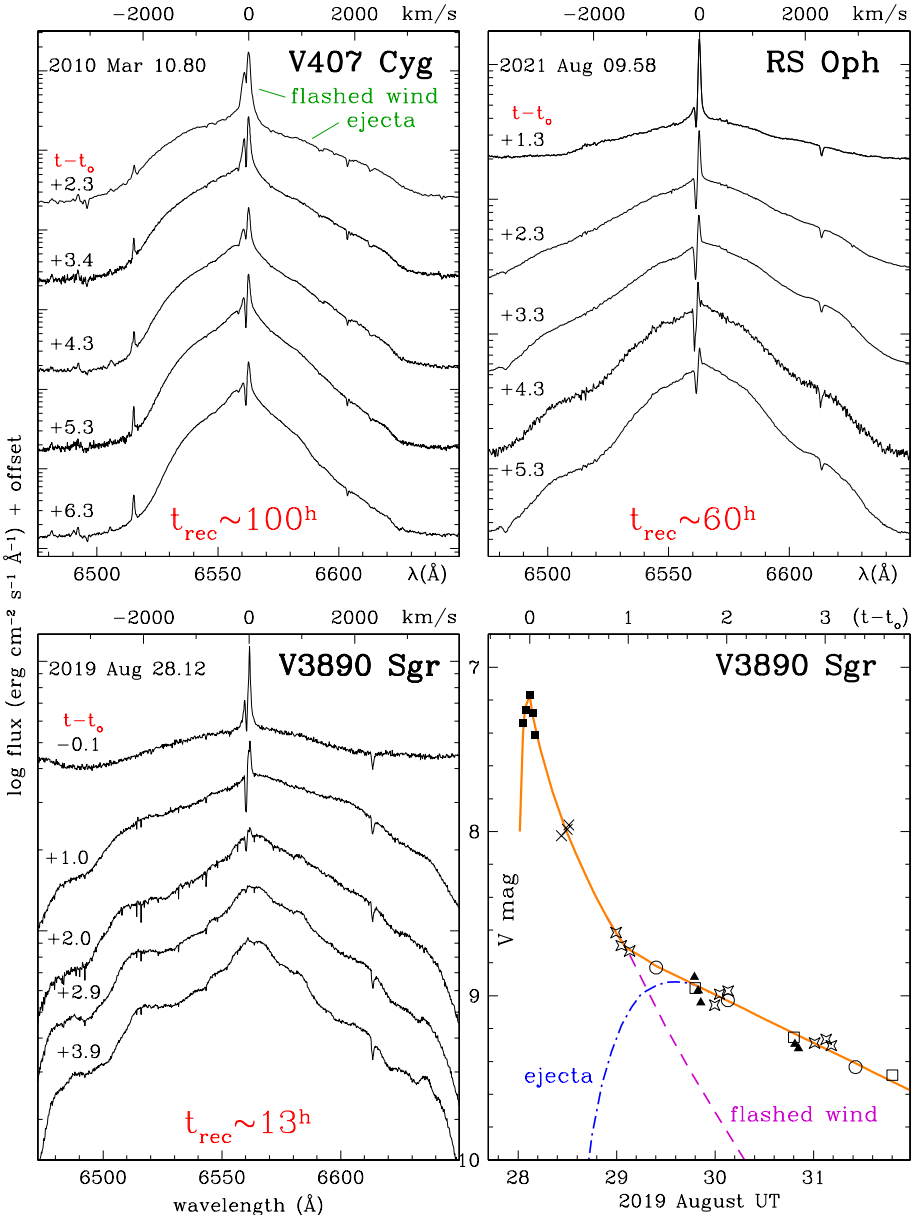


Figure 2. High-resolution Hα profiles covering the first days for the outburst of three symbiotic novae, to highlight the sharp component from the recombining flashed-wind of the RG and the broad one from the expanding ejecta. For comparison, the early photometric evolution of V3890 Sgr is deconvolved into the same two components (data from Munari et al., 2011; Munari & Valisa, 2021, F. Walter private comm.)

3.2. Deceleration of the ejecta by the red giant wind

The second feature unique to symbiotic novae is the violent deceleration of the nova ejecta as they plow through the pre-existing circumstellar material, fed by the slow wind of the RG. The ejecta are shocked and give origin to copious non-thermal emission over the entire wavelength range, from radio synchrotron to the TeV energies mapped by Cherenkov telescopes (Acciari et al., 2022; H. E. S. S. Collaboration et al., 2022). For RS Oph, the multi-wavelength results gathered from the 2006 and 2021 eruptions are very similar, which may be read as an indication that the cavity shaped by preceding eruptions is refilled by the wind of the red giant well in time for the following outburst, a results probably applicable also to the other symbiotic novae that were less intensively observed compared to RS Oph.

DEOP. The multi-wavelength appearance and fate of the shocked ejecta rest ultimately with the geometric arrangement of the circumstellar medium. Without the presence of the WD companion, the wind of the RG would fill the circumstellar space in a roughly spherically-symmetric manner. The gravitational pull of the WD deflects instead toward the orbital plane the mass-loss from the RG (eg. Mohamed & Podsiadlowski, 2012; Skopal & Cariková, 2015), creating a *Density Enhancement on the Orbital Plane* (DEOP). The more wind is deflected toward DEOP, the less is left to flow perpendicular to the orbital plane: ejecta launched into polar directions then suffer from only limited deceleration, while those on the orbital plane slam onto a much denser medium able to efficiently absorb (all) their kinetic momentum. For a given WD mass and RG mass-loss rate, a WD orbiting closer to the RG is more efficient in deflecting the RG wind away from polar directions and onto DEOP.

Bipolar radio-synchrotron lobes. Direct imaging of the expanding ejecta of RS Oph, years past the 2006 outburst, have been obtained with HST in [OIII] 5007 line (Ribeiro et al., 2009) and with Chandra in X-rays (Montez et al., 2022). Detecting such faint signals from years-old ejecta requires careful PSF-subtraction and image deconvolution. More direct and detailed images of the expanding ejecta can be obtained in the radio with VLBI techniques (very long baseline interferometry). Their milli-arcsec capabilities allow prompt resolution of the structure of the ejecta already within a few weeks of the eruption. An example of the results obtained with EVN (European VLBI Network) for the outbursts of V407 Cyg (2010) and RS Oph (2021) are shown in Fig. 3: the radio-emitting ejecta are shaped into wide bipolar lobes expanding perpendicularly to DEOP. The radio emission is of synchrotron origin, as supported by the absorption-corrected α spectral slope and by the huge brightness temperature ($10^7/10^8$ K), which is orders of magnitude hotter than associated to thermal processes (10^4 K).

The angular expansion of radio lobes can be transformed into corresponding space velocity by knowledge of the distance and the orbital inclination, fairly well known for both V407 Cyg and RS Oph (4.0 and 2.7 kpc, $\sim$80° and 57°,

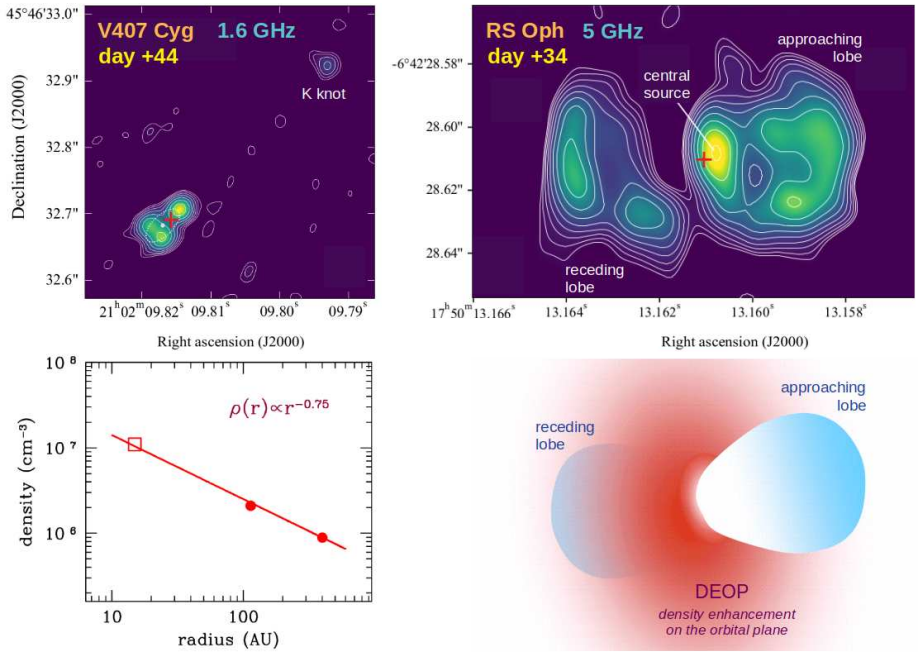


Figure 3. Top: VLBI high resolution radio maps of the 2010 and 2021 outbursts of the symbiotic novae V407 Cyg and RS Oph. The red cross marks the astrometric position from Gaia. Bottom right: cartoon highlighting the location of DEOP and the extinction it excerpts on the receding lobe of RS Oph (compare with panel directly above). Bottom left: the radial dependence of density within DEOP of RS Oph (data from Giroletti et al., 2020; Munari et al., 2022; Lico et al., 2024).

respectively). The time dependence of the space velocity of their radio lobes is compared in Fig. 4. The radio lobes of RS Oph have kept expanding at a high and constant v_{exp}=8150 km s^{-1} space velocity since the earliest radio epoch (day +14), which indicates that (*i*) the deceleration along the polar directions was completed already within the first two weeks, (*ii*) the WD orbiting close to the RG (1.5 AU orbital separation, Brandi et al., 2009) has been very effective in deflecting toward DEOP the wind of the RG, with a minimal amount of material present above 50 AU on the polar directions, and (*iii*) the terminal space velocity of the radio lobes is still a fairly large fraction of the initial launch velocity. The radio lobes of V407 Cyg have been instead decelerating all the way through the radio observing epochs, slowing from 6000 km s^{-1} on day +20 to 2800 km s^{-1} on day +91. This leads to conclude that the WD orbiting the RG at great distance (> 30 AU orbital separation, Hinkle et al., 2013) was not particularly effective in deflecting the wind of the RG away from polar directions, with enough gas

still present 250 AU above DEOP to keep the ejecta of V407 Cyg decelerating for months. Considering the velocities observed in RS Oph and V407 Cyg, and the respective deceleration profiles, it seems safe to infer that the initial launch velocity was similar for them both and probably close to 10,000/12,000 km s^{-1}.

The radio lobes of RS Oph, thanks to the 57° orbital inclination, have allowed to directly *"see"* DEOP for the first time in a symbiotic system. DEOP in RS Oph has been kept ionized by the WD burning nuclearly for the first three months of the outburst, so covering the whole set of radio observing epochs (day +14 to +64). An ionized DEOP is very effective in producing free-free absorption of the synchrotron radiation from the receding lobe which moves in the background to DEOP. Because the density within DEOP declines radially away from the central binary (cf. the lower-left panel of Fig. 3), also the free-free opacity declines in pace, with the net result that the receding lobe becomes visible only once its leading edge has moved behind DEOP outer regions of sufficiently low optical depth, which happens around day +20/+21, following the geometrical arrangement sketched in the lower-right panel of Fig. 3.

Before leaving this section about large-scale radio structures, it is worth mentioning an interesting and unexpected feature visible in the radio map of Fig. 3 for V407 Cyg: a knot of emission (labelled "K"), appears moving radially away - and along the same direction as the bipolar lobes - at a velocity (700 km sec^{-1}) that projects it back to the central binary ∼6.5 yrs before the 2010 eruption, when V407 Cyg was undergoing a spectacular surge in the accretion rate onto the WD (Kolotilov et al., 2003), similar to what happened to T CrB in the 8 yrs preceding its 1946 outburst (Payne-Gaposchkin & Wright, 1946). Clearly, during such super-active accretion phases (SAP) preceding the nova explosion, the WD of symbiotic novae can expel isolated and massive blobs of material along the orbital polar axes. It will be worth searching for similar blobs on radio maps collected at the time of the next eruption of T CrB, considering the new SAP phase it has recently undergone during 2015-2023 (Munari et al., 2016). It will also be worth to re-inspect the abundant spectroscopic material collected during the SAP phase of V407 Cyg (eg. Tatarnikova et al., 2003) and search for spectral counterparts to the ejection of the "K" radio blob.

Shrinking of emission lines. An easily observable manifestation of the violent deceleration of the ejecta in a symbiotic nova is the rapid narrowing of the *broad component* (cf. identification at top-left of Fig. 2) of the emission lines (eg. Shore et al., 2011; Munari et al., 2011; Banerjee et al., 2014). The left panels of Fig. 4 show the shrinking of Hα for the recent outbursts of V407 Cyg and RS Oph, characterized by slopes (FWHM $\propto$ t$^{\theta}$) of θ=−0.59 and −0.73, respectively [for simplicity, in the rest of this paper Hα will be used as proxy for permitted emission lines in general]. The narrowing of Hα proceeds very smoothly, supporting an origin in ejecta that expand through a medium that extends also very smoothly over the traveled distance, without discontinuities or sudden changes in the radial density gradient. By integrating over the behavior in Fig. 4, and taking v_{exp}=FWHM/2.355 as representative of the bulk velocity

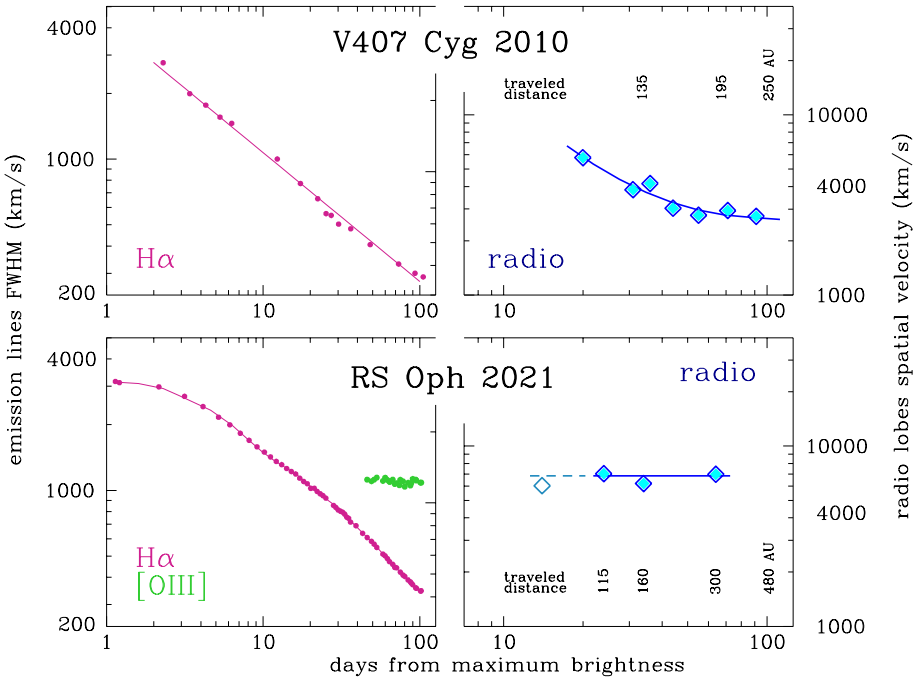


Figure 4. Comparing the evolution of the FWHM of Balmer and [OIII] emission lines (left) and the space velocity of the radio bipolar jets (right) for V407 Cyg and RS Oph (data from Munari et al., 2011; Munari & Valisa, 2022; Lico et al., 2024)

of the gas, the distance traveled by the Hα emitting ejecta in the first 100 days is 15 and 14 AU for V407 Cyg and RS Oph, respectively. Such a limited dimension fits very nicely with the central synchrotron radio source (cf upper-right of Figure 3) of RS Oph, that when visible for the first 40 days past the initial outburst remained unresolved at the EVN restoring ellipsoidal beam of 10×12 milli-arcsec, corresponding to an upper limit of 13 AU to its radius. The fact that over the initial 100 days the radio lobes travel for 250-500 AU in the polar directions, while the Hα emitting ejecta cover just 14-15 AU under constant deceleration, clearly indicate as the (main) source of Hα emission the ejecta moving close to the orbital plane and slamming onto DEOP.

3.3. X-rays

The evolution in X-rays of RS Oph has been monitored at ∼daily cadence with the *Swift* satellite for both the 2006 and 2021 outbursts. The energy distributions of X-rays have been deconvolved into hard and supersoft components by Page et al. (2022), from which we import the data plotted on the top row of Fig. 5.

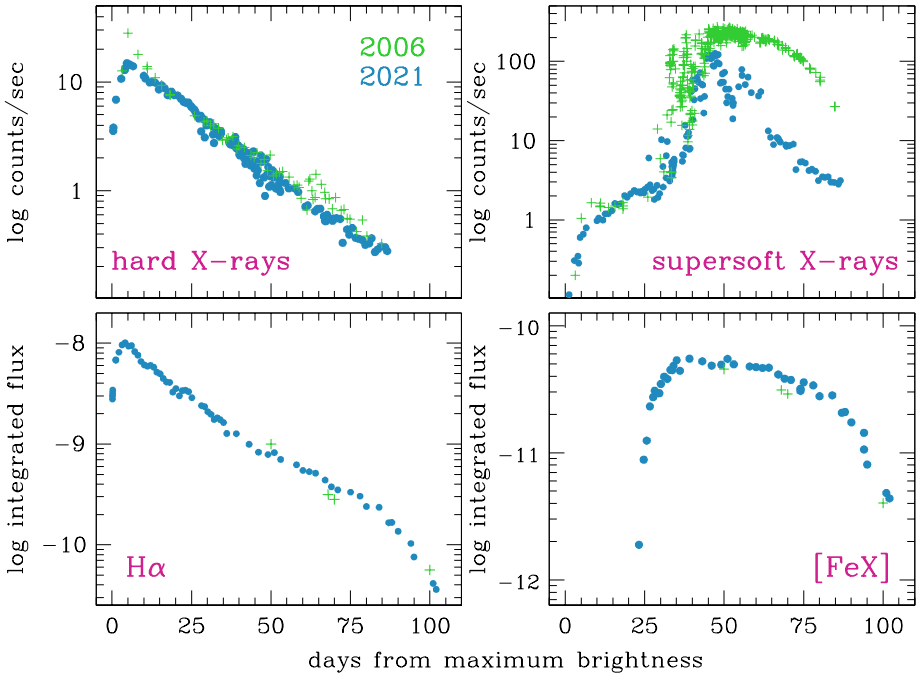


Figure 5. Comparing the evolution in flux for the 2006 and 2021 outbursts of RS Oph for hard X-rays, super-soft X-rays, permitted and coronal emission lines (data from Page et al., 2022; Munari & Valisa, 2022).

SUPERSOFT X-RAYS. They come directly from the central WD which is burning nuclearly at the surface, and become visible around day +25 when the medium around the WD clears enough to turn optically thin. Coronal emission lines appear at the same time (cf. the flux evolution of [FeX] 6375 Å plotted in the lower-right panel of Fig. 5), because they form in the circumstellar material now exposed to the hard radiation emanating from the burning WD. The coronal emission lines behaved very smoothly with time and very similar for the 2006 and 2021 eruptions, supporting identical burning phases on the WD for the two outbursts. The sharp decline in flux of the coronal lines suggests that the nuclear burning ends around day +85, which also coincides with the drop in supersoft X-rays observed during the 2006 event.

The excitation of coronal lines integrates the WD output over the 4π solid angle, and such lines are therefore well suited to trace the real output of the burning WD. On the contrary, supersoft X-rays - which are seen coming directly from the burning WD - are particularly sensitive to inhomogeneities in the absorbing material crossing the line-of-sight. This explains the rapid switch on/off episodes at the start of the SSS phase in 2006 (Osborne et al., 2011). On the

contrary, the SSS started smoothly in 2021 but significantly under-performed at later epochs compared to 2006; such difference has been modeled by Ness et al. (2023) in terms of different column density of absorbing material at the two outbursts. The opposite behavior of supersoft X-rays seen in 2006 and 2021, both during their rise to maximum and decline from, probably relates to the fact that the WD+RG binary was at opposite orbital phases at the time of the two eruptions. Therefore the line-of-sight to the WD may have probed at grazing incidence, in one eruption the inner wall of the cavity shaped into DEOP by the ejecta, and instead the outer atmosphere/inner wind of the RG at the other.

HARD X-RAYS. The hard X-rays originate from the ejecta colliding with the pre-existing material. The flux evolution of hard X-rays is identical for 2006 and 2021 (upper-left panel of Fig. 5), suggesting that RG wind had similarly refilled the circumstellar space after the previous eruption and that the ejecta impacted with the same mass and velocity (momentum). The decline in hard X-ray is continuous, very smooth, and without glitches, indicating a similarly smooth, continuous and extended distribution of the target slow material. This is the same conclusion we drawn above from the FWHM evolution of Hα, a fact suggesting that Hα and hard X-rays come from the same location within the binary system. This is also supported by the time-dependence of the *flux* radiated in Hα, which is plotted in the lower-left panel of Fig. 5, which is exactly the same as that of hard X-rays from the panel above.

3.4. Summary: a multi-wavelength 3D picture

Putting all together the information from the previous sections about the size, velocity and time evolution at radio, optical, and X-rays, a 3D picture of RS Oph (serving also as a guideline for symbiotic novae in general) can be assembled as illustrated in Fig. 6.

The WD ejecta are lunched symmetrically by the WD at 10,000 to 12,000 km sec^{-1} initial velocity. They interact with the pre-existing circumstellar material primarily at two distinct locations.

One location is very close to the central binary, at the inner radius of DEOP (the density enhancement on the orbital plane formed by the gravitational focusing of the RG wind by the orbiting WD). The high density and long radial extent of DEOP keeps the ejecta decelerating very smoothly for weeks/months, and the shock interface travels only a short distance, $\sim$15 AU in 100 days at which point the ejecta have been practically arrested (velocities $\leq$150 km sec^{-1}). The DEOP/ejecta interface is the location from where originates most of the hard X-rays, the central radio-synchrotron component, and the permitted optical emission lines. This interface is also probably the place where the high-energy γ-rays (visible in the first days of the outburst) are produced.

The other location is toward the poles of the orbital plane, where the density of pre-existing material is much lower compared to DEOP. Perpendicular to the orbital plane the deceleration is much less effective, and the ejecta launched in

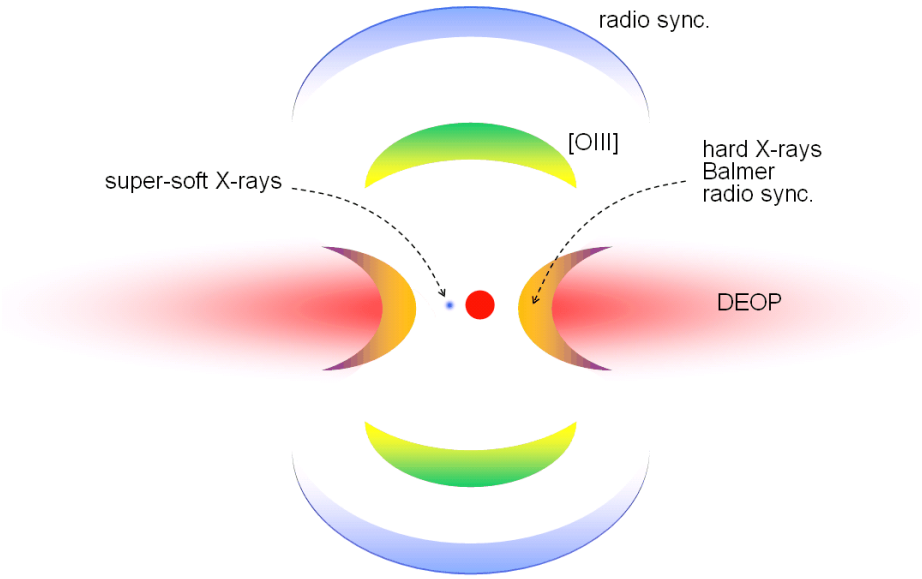


Figure 6. Artistic impression showing the location of key emission features in RS Oph around day +35 of the outburst (drawing not to scale). The WD + RG binary is at the center, DEOP (density enhancement on the orbital plane) is seen edge-on, and the polar directions run vertically.

that direction, after 100 days are still traveling at thousands of km sec^{-1}, having crossed hundreds of AU. The shocked outer edge of the resulting bipolar lobes is the location of the synchrotron emission dominating at radio cm-wavelengths.

The forbidden emission lines are observed in RS Oph to move at constant and high velocity, much larger that for permitted lines, as illustrated in the lower-left panel of Fig. 4. With all probability they form in the inner regions of the bipolar lobes, which move at a reduced velocity compared with their outer edges, turning visible once the local density dilutes below the critical value for collisional de-excitation of their upper metastable levels.

The cavity in the pre-existing circumstellar material shaped by ejecta plowing through them is efficiently and quickly refilled by the wind of the red giant: each outburst of RS Oph has behaved exactly the same, even those separated by just 9 years (like 1958 and 1967). The accretion disk around the WD is even quicker to reform, ∼250 days being enough to restore both pre-outburst disk brightness and flickering activity (Munari & Tabacco, 2022).

4. An imminent eruption of T CrB ?

The two known outbursts of T CrB in 1866 and 1946 are separated by 80 yrs, and other 80yrs will bring us to 2026. The 1946 eruption was preceded by a SAP phase lasting ∼8 yrs, and a new SAP characterized T CrB from 2015 to 2023 (Munari et al., 2016) leading to the natural conclusion that a new eruption may be imminent. Such a view has been shared by many (eg. Schaefer, 2023; Zamanov et al., 2023), with the beneficial results of an intensified pre-eruption monitoring of T CrB and the submission of proposals to most of the ground and space observing facilities; proposals waiting to be triggered at the very first announcement of the outburst ! Such an alertness from the community, the expected peak V∼3 mag brightness, and the proximity of T CrB to us (just 0.9 kpc distance and negligible interstellar reddening), with all probabilities will results is such a wealth of multi-wavelength information to keep people busy for long in understanding and modeling them, leading to a significant leap forward in our understanding of novae in general and their symbiotic subclass in particoular.

Acknowledgements. We acknowledge the INAF 2023 Minigrant funding program and the Conference Organizers for financial support. We thank K. Page, F. Walter, R. Lico, and P. Valisa for permission to use their data in drawing some of the figures.

References

Abdo, A. A., Ackermann, M., Ajello, M., et al., Gamma-Ray Emission Concurrent with the Nova in the Symbiotic Binary V407 Cygni. 2010, *Science*, **329**, 817, DOI:10.1126/science.1192537

Acciari, V. A., Ansoldi, S., Antonelli, L. A., et al., Proton acceleration in thermonuclear nova explosions revealed by gamma rays. 2022, *Nature Astronomy*, **6**, 689, DOI:10.1038/s41550-022-01640-z

Allen, D. A., On the late-type components of slow novae and symbiotic stars. 1980, *Monthly Notices of the RAS*, **192**, 521, DOI:10.1093/mnras/192.3.521

Arseneau, S., Chandra, V., Hwang, H.-C., et al., Measuring the Mass–Radius Relation of White Dwarfs Using Wide Binaries. 2024, *Astrophysical Journal*, **963**, 17, DOI:10.3847/1538-4357/ad2168

Banerjee, D. P. K., Joshi, V., Venkataraman, V., et al., Near-IR Studies of Recurrent Nova V745 Scorpii during its 2014 Outburst. 2014, *Astrophysical Journal, Letters*, **785**, L11, DOI:10.1088/2041-8205/785/1/L11

Bode, M. F. & Evans, A., eds. 1989, *Classical novae* (John Wiley & Sons)

Bode, M. F. & Evans, A., eds. 2008, *Classical Novae* (Cambridge Univ. Press), DOI:10.1017/CBO9780511536168

Brandi, E., Quiroga, C., Mikołajewska, J., Ferrer, O. E., & García, L. G., Spectroscopic orbits and variations of RS Ophiuchi. 2009, *Astronomy and Astrophysics*, **497**, 815, DOI:10.1051/0004-6361/200811417

Cassatella, A., González-Riestra, R., & Selvelli, P., eds. 2004, ESA Special Publication, Vol. **1283**, *INES Access Guide No. 3 - Classical Novae*

Cassatella, A., Selvelli, P. L., Gilmozzi, R., Bianchini, A., & Friedjung, M., IUE observations of faint old novae. 1990, in *Accretion-Powered Compact Binaries*, ed. C. W. Mauche (Cambridge Univ. Press), 373–376

Cassatella, A. & Viotti, R., eds. 1990, Lecture Notes in Physics, Vol. **369**, *Physics of Classical Novae* (Springer-Verlag)

Downes, R., Webbink, R. F., & Shara, M. M., A Catalog and Atlas of Cataclysmic Variables-Second Edition. 1997, *Publications of the ASP*, **109**, 345, DOI:10.1086/133900

Downes, R. A. & Shara, M. M., A Catalog of Cataclysmic Variables. 1993, *Publications of the ASP*, **105**, 127, DOI:10.1086/133139

Downes, R. A., Webbink, R. F., Shara, M. M., et al., A Catalog and Atlas of Cataclysmic Variables: The Living Edition. 2001, *Publications of the ASP*, **113**, 764, DOI:10.1086/320802

Duerbeck, H. W. 1987, *A reference catalogue and atlas of galactic novae* (D. Reidel Publ.)

Evans, A., Bode, M. F., O'Brien, T. J., & Darnley, M. J., eds. 2008, Astronomical Society of the Pacific Conference Series, Vol. **401**, *RS Ophiuchi (2006) and the Recurrent Nova Phenomenon*

Ferland, G. J., Quantitative Spectroscopy of Photoionized Clouds. 2003, *Annual Review of Astron and Astrophys*, **41**, 517, DOI:10.1146/annurev.astro.41.011802.094836

Fujimoto, M. Y., A Theory of Hydrogen Shell Flashes on Accreting White Dwarfs - Part Two - the Stable Shell Burning and the Recurrence Period of Shell Flashes. 1982a, *Astrophysical Journal*, **257**, 767, DOI:10.1086/160030

Fujimoto, M. Y., A theory of hydrogen shell flashes on accreting white dwarfs. I - Their progress and the expansion of the envelope. II - The stable shell burning and the recurrence period of shell flashes. 1982b, *Astrophysical Journal*, **257**, 752, DOI:10.1086/160029

Gaia Collaboration, The Gaia mission. 2016, *Astronomy and Astrophysics*, **595**, A1, DOI:10.1051/0004-6361/201629272

Gaia Collaboration, Gaia Data Release 3. Summary of the content and survey properties. 2023, *Astronomy and Astrophysics*, **674**, A1, DOI:10.1051/0004-6361/202243940

Gaposchkin, C. H. P. 1957, *The Galactic Novae* (Dover Pub.)

Giroletti, M., Munari, U., Körding, E., et al., Very long baseline interferometry imaging of the advancing ejecta in the first gamma-ray nova V407 Cygni. 2020, *Astronomy and Astrophysics*, **638**, A130, DOI:10.1051/0004-6361/202038142

H. E. S. S. Collaboration, Aharonian, F., Ait Benkhali, F., et al., Time-resolved hadronic particle acceleration in the recurrent nova RS Ophiuchi. 2022, *Science*, **376**, 77, DOI:10.1126/science.abn0567

Hernanz, M. & José, J., eds. 2002, American Institute of Physics Conference Series, Vol. **637**, *Classical Nova Explosions* (AIP)

Hinkle, K. H., Fekel, F. C., Joyce, R. R., & Wood, P., Infrared Spectroscopy of Symbiotic Stars. IX. D-type Symbiotic Novae. 2013, *Astrophysical Journal*, **770**, 28, DOI:10.1088/0004-637X/770/1/28

Iben, I., J., Hot accreting white dwarfs in the quasi-static approximation. 1982, *Astrophysical Journal*, **259**, 244, DOI:10.1086/160164

Kenyon, S. J. 1986, *The symbiotic stars* (Cambridge Univ. Press)

Kolotilov, E. A., Shenavrin, V. I., Shugarov, S. Y., & Yudin, B. F., UBVJHKLM photometry of the symbiotic Mira V407 Cyg in 1998 2002. 2003, *Astronomy Reports*, **47**, 777, DOI:10.1134/1.1611218

Lico, R., Giroletti, M., Munari, U., et al., High-resolution imaging of the evolving bipolar outflows in symbiotic novae: the case of RSOphiuchi 2021 nova outburst. 2024, *arXiv e-prints*, arXiv:2407.05794, DOI:10.48550/arXiv.2407.05794

Liimets, T., Corradi, R. L. M., Santander-García, M., et al., A Three-dimensional View of the Remnant of Nova Persei 1901 (GK Per). 2012, *Astrophysical Journal*, **761**, 34, DOI:10.1088/0004-637X/761/1/34

Mohamed, S. & Podsiadlowski, P., Mass Transfer in Mira-type Binaries. 2012, *Baltic Astronomy*, **21**, 88, DOI:10.1515/astro-2017-0362

Molina, I., Chomiuk, L., Linford, J. D., et al., The symbiotic recurrent nova V745 Sco at radio wavelengths. 2024, *Monthly Notices of the RAS*, **534**, 1227, DOI:10.1093/mnras/stae2093

Montez, R., Luna, G. J. M., Mukai, K., Sokoloski, J. L., & Kastner, J. H., Expanding Bipolar X-Ray Structure After the 2006 Eruption of RS Oph. 2022, *Astrophysical Journal*, **926**, 100, DOI:10.3847/1538-4357/ac4583

Munari, U., The Symbiotic Stars. 2019, in *The Impact of Binary Stars on Stellar Evolution*, ed. G. Beccari & H. Boffin, arXiv:1909.01389

Munari, U., Dallaporta, S., & Cherini, G., The 2015 super-active state of recurrent nova T CrB and the long term evolution after the 1946 outburst. 2016, *New Astronomy*, **47**, 7, DOI:10.1016/j.newast.2016.01.002

Munari, U., Giroletti, M., Marcote, B., et al., Radio interferometric imaging of RS Oph bipolar ejecta for the 2021 nova outburst. 2022, *Astronomy and Astrophysics*, **666**, L6, DOI:10.1051/0004-6361/202244821

Munari, U., Joshi, V. H., Ashok, N. M., et al., The 2010 nova outburst of the symbiotic Mira V407 Cyg. 2011, *Monthly Notices of the RAS*, **410**, L52, DOI:10.1111/j.1745-3933.2010.00979.x

Munari, U. & Tabacco, F., Flickering Returns as RS Oph Reestablishes Quiescent Conditions Following its 2021 Nova Outburst. 2022, *Research Notes of the American Astronomical Society*, **6**, 103, DOI:10.3847/2515-5172/ac72ae

Munari, U., Traven, G., Masetti, N., et al., The GALAH survey and symbiotic stars - I. Discovery and follow-up of 33 candidate accreting-only systems. 2021, *Monthly Notices of the RAS*, **505**, 6121, DOI:10.1093/mnras/stab1620

Munari, U. & Valisa, P., The 2021 outburst of RS Oph. A pictorial atlas of the spectroscopic evolution: the first 18 days. 2021, *arXiv e-prints*, arXiv:2109.01101, DOI:10.48550/arXiv.2109.01101

Munari, U. & Valisa, P., The 2021 outburst of RS Oph: a pictorial atlas of the spectroscopic evolution. II. From day 19 to 102 (solar conjunction). 2022, *arXiv e-prints*, arXiv:2203.01378, DOI:10.48550/arXiv.2203.01378

Ness, J. U., Beardmore, A. P., Bode, M. F., et al., High-resolution X-ray spectra of RS Ophiuchi (2006 and 2021): Revealing the cause of SSS variability. 2023, *Astronomy and Astrophysics*, **670**, A131, DOI:10.1051/0004-6361/202245269

Nyamai, M. M., Linford, J. D., Allison, J. R., et al., Synchrotron emission from double-peaked radio light curves of the symbiotic recurrent nova V3890 Sgr. 2023, *Monthly Notices of the RAS*, **523**, 1661, DOI:10.1093/mnras/stad1534

O'Brien, T. & Bode, M., Resolved nebular remnants. 2008, in *Classical Novae*, ed. M. F. Bode & A. Evans (Cabridge Univ. Press), 285–305

Osborne, J. P., Page, K. L., Beardmore, A. P., et al., The Supersoft X-ray Phase of Nova RS Ophiuchi 2006. 2011, *Astrophysical Journal*, **727**, 124, DOI:10.1088/0004-637X/727/2/124

Page, K. L., Beardmore, A. P., Osborne, J. P., et al., The 2021 outburst of the recurrent nova RS Ophiuchi observed in X-rays by the Neil Gehrels Swift Observatory: a comparative study. 2022, *Monthly Notices of the RAS*, **514**, 1557, DOI:10.1093/mnras/stac1295

Payne-Gaposchkin, C. & Wright, F. W., The Photographic Light-Curve of T Coronae Borealis. 1946, *Astrophysical Journal*, **104**, 75, DOI:10.1086/144834

Ribeiro, V. A. R. M., Bode, M. F., Darnley, M. J., et al., The Expanding Nebular Remnant of the Recurrent Nova RS Ophiuchi (2006). II. Modeling of Combined Hubble Space Telescope Imaging and Ground-based Spectroscopy. 2009, *Astrophysical Journal*, **703**, 1955, DOI:10.1088/0004-637X/703/2/1955

Saikia, D. F. & Anupama, G. C., eds. 2012, Bull. Astr. Soc. India, Vol. **40**, *Novae from radio to gamma rays* (Astron. Soc. India)

Schaefer, B. E., The B & V light curves for recurrent nova T CrB from 1842-2022, the unique pre- and post-eruption high-states, the complex period changes, and the upcoming eruption in 2025.5 ± 1.3. 2023, *Monthly Notices of the RAS*, **524**, 3146, DOI:10.1093/mnras/stad735

Schwarz, G. J., Ness, J.-U., Osborne, J. P., et al., Swift X-Ray Observations of Classical Novae. II. The Super Soft Source Sample. 2011, *Astrophysical Journal, Supplement*, **197**, 31, DOI:10.1088/0067-0049/197/2/31

Seaquist, E. R., Krogulec, M., & Taylor, A. R., A Highly Sensitive Radio Survey of Symbiotic Stars at 3.6 Centimeters. 1993, *Astrophysical Journal*, **410**, 260, DOI:10.1086/172742

Seaquist, E. R. & Taylor, A. R., The Collective Radio Properties of Symbiotic Stars. 1990, *Astrophysical Journal*, **349**, 313, DOI:10.1086/168315

Seaquist, E. R., Taylor, A. R., & Button, S., A Radio Survey of Symbiotic Stars. 1984, *Astrophysical Journal*, **284**, 202, DOI:10.1086/162399

Shore, S. N., Wahlgren, G. M., Augusteijn, T., et al., The spectroscopic evolution of the symbiotic-like recurrent nova V407 Cygni during its 2010 outburst. I. The shock and its evolution. 2011, *Astronomy and Astrophysics*, **527**, A98, DOI:10.1051/0004-6361/201015901

Skopal, A. & Cariková, Z., Wind mass transfer in S-type symbiotic binaries. I. Focusing by the wind compression model. 2015, *Astronomy and Astrophysics*, **573**, A8, DOI:10.1051/0004-6361/201424779

Skopal, A., Shugarov, S. Y., Munari, U., et al., The path to Z And-type outbursts: The case of V426 Sagittae (HBHA 1704-05). 2020, *Astronomy and Astrophysics*, **636**, A77, DOI:10.1051/0004-6361/201937199

Skrutskie, M. F., Cutri, R. M., Stiening, R., et al., The Two Micron All Sky Survey (2MASS). 2006, *Astronomical Journal*, **131**, 1163, DOI:10.1086/498708

Sokoloski, J. L., Rupen, M. P., & Mioduszewski, A. J., Uncovering the Nature of Nova Jets: A Radio Image of Highly Collimated Outflows from RS Ophiuchi. 2008, *Astrophysical Journal, Letters*, **685**, L137, DOI:10.1086/592602

Sokolovsky, K., Aydi, E., Chomiuk, L., et al., VLA observations of the 2021 eruption of RS Oph. 2021, *The Astronomer's Telegram*, **14886**, 1

Starrfield, S., Thermonuclear processes and the classical nova outburst. 1989, in *Classical Novae*, ed. M. F. Bode & A. Evans (John Wiley & Sons), 39–60

Starrfield, S., Iliadis, C., & Hix, W. R., Thermonuclear processes. 2008, in *Classical Novae*, ed. M. F. Bode & A. Evans (Cambridge Univ. Press), 77–101

Tatarnikova, A. A., Marrese, P. M., Munari, U., Tomov, T., & Yudin, B. F., Spectral observations of the symbiotic Mira variable V407 Cyg in 1993 2002. 2003, *Astronomy Reports*, **47**, 889, DOI:10.1134/1.1626192

Taylor, A. R. & Seaquist, E. R., Radio emission from symbiotic stars : a binary model. 1984, *Astrophysical Journal*, **286**, 263, DOI:10.1086/162594

Tomov, T. V., Stoyanov, K. A., & Zamanov, R. K., AG Pegasi - now a classical symbiotic star in outburst? 2016, *Monthly Notices of the RAS*, **462**, 4435, DOI:10.1093/mnras/stw2012

Warner, B. *Cataclysmic variable stars*, , Vol. **28** (Cambridge Univ. Press)

Williams, D., O'Brien, T., Woudt, P., et al., AMI-LA, e-MERLIN and MeerKAT radio detections of RS Oph in outburst. 2021, *The Astronomer's Telegram*, **14849**, 1

Woudt, P. A. & Ribeiro, V. A. R. M., eds. 2014, Astronomical Society of the Pacific Conference Series, Vol. **490**, *Stella Novae: Past and Future Decades*

Zamanov, R., Boeva, S., Latev, G. Y., et al., Accretion in the recurrent nova T CrB: Linking the superactive state to the predicted outburst. 2023, *Astronomy and Astrophysics*, **680**, L18, DOI:10.1051/0004-6361/202348372

Contrib. Astron. Obs. Skalnaté Pleso **55/3**, 67 – 74, (2025)
https://doi.org/10.31577/caosp.2025.55.3.67

High-angular-resolution studies of symbiotic novae

M. Otulakowska-Hypka

Astronomical Observatory Institute, Faculty of Physics and Astronomy, Adam Mickiewicz University, Słoneczna 36, 60-286 Poznan, Poland
(E-mail: magdaot@amu.edu.pl)

Received: November 19, 2024; Accepted: March 2, 2025

Abstract. Novae stars have fascinated observers around the world for centuries. They are eruptive close binary stellar systems consisting of a white dwarf and a secondary stellar component, which in rare cases is a red giant. Such systems are called symbiotic novae. Since the nova phenomenon is unexpected in most cases, there is a lack of observations and understanding, especially of the very early phases of their eruptions. To resolve and understand these early epochs, very fast and exceptionally high-angular-resolution methods of observations are needed. Symbiotic novae are the right systems for studies in the infrared, thus the optical interferometry is the ideal solution in this case. We discuss three of them, namely RS Oph, V3890 Sgr, and T CrB.

Key words: binaries – close binaries – cataclysmic stars – symbiotic stars – novae – optical interferometry – high-angular-resolution – RS Oph – V3890 Sgr – T CrB

1. Introduction to novae and motivation

Novae have been one of the most intriguing objects in the sky since the early days of astronomy. These unexpected, sudden, and relatively short increases in brightness attract the attention of astronomers and fascinate observers. The nature of a nova phenomenon has been a mystery for many centuries until very recently.

Walker (1954) first showed that a famous nova DQ Herculis is in fact a short-period binary system. This was a breakthrough discovery raising the question of whether all novae are binaries. Later, spectroscopic observations confirmed this hypothesis for these objects (Greenstein & Kraft, 1959). Next, the same conclusion was drawn for dwarf novae by Kraft (1962), who introduced a binary star model of such stars, where the cool star fills its Roche lobe and transfers matter to the hot companion star through a disk-like structure.

Then the whole standard model of a cataclysmic system developed during the next years. Krzeminski & Kraft (1964) introduced a stream in the binary model of WZ Sge, while Warner & Nather (1971) and Smak (1971), based on observations of another dwarf nova, U Gem, discussed the nature of the hot

spot. Walker & Chincarini (1968) interpreted the hot stellar component as the origin of the outbursts, in contrast to the previous conclusions of Krzeminski (1965), which allowed the proper theoretical work to begin (Paczyński, 1971). All these discoveries, dating back only $\sim$ 50 years, allowed us to slowly begin to understand the nature of cataclysmic variables (CV) in general and novae in particular (Robinson, 1976; Patterson, 1984).

Although our understanding of novae is not yet complete, the standard CV model that evolved over the years is supported by the observational data that are constantly flowing to us. We now know that novae are semi-detached binary stellar systems which erupt. Such an explosion of a nova occurs on the surface of the hot stellar component, i.e. a white dwarf (WD), while the secondary is a less evolved star, typically a main-sequence (MS) object or a red giant (RG). The secondary is a donor star as it fills the Roche lobe and loses material to its companion. This transported matter forms an accretion disc around the WD and gradually falls to its surface. Thus, WD slowly gains mass. At critical mass the matter becomes degenerate and a thermonuclear runaway (TNR) starts (Warner, 1995). Up to 10^{-4} $M_{\odot}$ of the material is removed from the system (Chomiuk et al., 2021) at speeds of hundreds or even thousands of kilometers per second.

Some time after the explosion the whole system returns to the state of active accretion and another accumulation of matter, until the next eruption. The entire cycle repeats with recurrence time depending on the mass accretion rate and the mass of the WD (Shara et al., 2018). So, the recurrence times differ significantly between diverse systems. In the case of classical novae (CN), these are times of the order of thousands of years (Shara et al., 2012).

If a system recur on timescales of the order of at most hundreds of years, it is called a *recurrent* nova (RN). Such binaries are rare, since we know only 10 RN in our Galaxy. RN systems containing a red giant as a donor star are known as *symbiotic recurrent novae* (SyRN). They are even rarer (4/10 of the known Galactic RN), namely: T CrB, V745 Sco, RS Oph, and V3890 Sgr. The surroundings of SyRN are complex, because in addition to both the stellar components, they may include additional gas and dust. What is more, a circumbinary, possibly spiral structures in the binary orbital plane as well as stellar wind effects must be also taken into account (Mohamed & Podsiadlowski, 2012).

Recently, a number of very interesting and important discoveries have been made, significantly expanding our knowledge about novae. Among others, e.g. the works on shocks of the ejecta (H. E. S. S. Collaboration et al., 2022) or gamma ray emission (Acciari et al., 2022), strong X-ray emission (Ness et al., 2023), coronal line emission in the UV, optical and IR, and others (Molaro et al., 2023). Although, there are still some open questions, that are nicely listed e.g. in an excellent recent review of Chomiuk et al. (2021). Some of these questions are about the nature of the physical processes that make the ejecta spherical or aspherical, the way the mass is ejected in nova eruptions, especially very early, the location of the dust produced in nova ejecta, or the kinematics of the dust.

The only way to address such questions is the use of near-infrared interferometry (Chesneau & Banerjee, 2012).

2. Recent interferometric observations of novae

Interferometric observations do not provide an image of an object; instead, the parameters of the interferometric fringes can be analyzed and modeled. They are a measure of the sizes and shapes of the observed celestial bodies. An additional spectroscopic signal, delivered with the interferogram, allows us to create synthetic three-dimensional data cubes with images of astronomical objects together with corresponding spectra. This is a great advantage of interferometry over other methods of observation, and thus it is sometimes possible to spatially locate regions of emission of specific spectral lines. Another benefit is the unprecedented and unique spatial resolution of milliarcseconds. For a review of the method, see, e.g. Monnier (2003) or Eisenhauer et al. (2023). The past decades have been a time of beautiful development of optical interferometry. There is already a number of published works showing results of this method applied to novae, among them the famous Nova Delphini 2013 (Schaefer et al., 2014). When it comes to the objects of our interest, the previous eruption of RS Oph has been observed with the use of interferometry, with first-generation instruments. Barry et al. (2008) showed already on day 3.8 that the size of the expanding matter was $4.0 - 6.2$ mas in the N-band continuum of the Keck Interferometer Nuller. On day 5.5 the size of $\sim 3 - 6$ mas, depending on the continuum or emission lines chosen in the K-band of VLTI/AMBER, was reported by Chesneau et al. (2007). In turn Lane et al. (2007) used PTI in the K-band and found the size of RS Oph's ejecta to be ~ 3 mas on days $4 - 11$, ~ 6 mas on days $14 - 29$, and $\sim 2 - 3$ mas on days $49 - 121$. Monnier et al. (2006) reported ~ 3 mas for up to 3 months since the eruption in the H-band and K-band of IOTA, Keck, and PTI. Thus, the size estimates of RS Oph after the 2006 eruption were inconclusive.

Recently, there have been new attempts to resolve novae with the use of state-of-the-art interferometers, among them the second-generation instruments of the Very Large Telescope Interferometer (VLTI)[1]. This was possible because V3890 Sgr and RS Oph erupted lately and thus, such observations were acquired and are now being analyzed. For both objects, we performed parametric model fitting with the use of the PMOIRED tool (Mérand, 2022). An example fit is shown in Fig. 1.

V3890 Sgr was observed with the Gravity instrument at VLTI (R=4000, K-band). The broad emission HeI (2.0587μm) line was detected, with a complex shape and several bumps over several thousands of km/s. This target was only marginally resolved, only in the line. The differential phases were characterized by an S-shaped signal and the closure phases were noisy. Nevertheless, it was

[1] https://www.eso.org/sci/facilities/paranal/telescopes/vlti.html

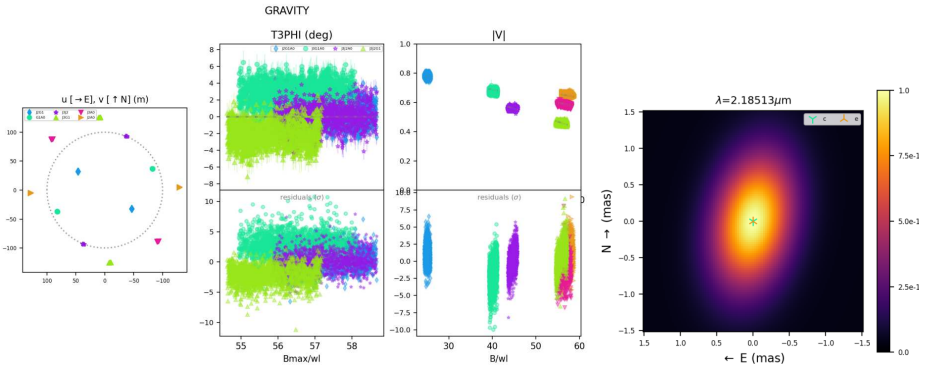


Figure 1. An example simple model of the continuum for RS Oph on day 5 after the last eruption, based on VLTI/Gravity data, performed with the use of the PMOIRED tool. Left: the *u*-*v* covarage representing the configuration of the telescopes used; Center: the closure phase (T3PHI) and visibility (V) signals with models (upper) and residuals (lower panel); Right: the resulting synthetic image of the continuum emission region, modeled as an elongated Gaussian profile. The model represents the size of the source properly (see visibility), whereas does not explain the small closure phase shifts. This means that the continuum-emitting region is clearly elongated but it is in fact more asymmetric than this simple model shows. The following complete modeling of the VLTI data show bipolar ejected matter perpendicular to this continuum signal (Otulakowska-Hypka et al., in preparation).

possible to create a model of the system in this resolved spectral range, showing a bipolar structure.

Next, for RS Oph all the available interferometric instruments were used to monitor the system at several epochs. The amount of data collected in this case was substantial: diverse spectral bands and spectral resolutions, different structures detected in specific lines, plus the overall evolution in time. A detailed description of this analysis is far beyond the scope of this paper and will be published separately (Otulakowska-Hypka et al., in preparation). However, the main findings of this part are that the entire structure of the ejected matter was exceptionally clumpy, also bipolar, and evolved very quickly.

In particular, we modeled the emission lines regions in the spectrum using a number of components of the Gaussian profile. The derived models allowed us to draw conclusions about the sizes and shapes of emitting regions. In addition, observations at different time epochs allowed us to measure the expansion rate of the nova shell and thus calculate the distance to the object (see also Kaczmarek et al. in these proceedings). In both the studied SyRN, apart from the central structure, we found two components located far from the center: blue- and

redshifted, representing the bipolar outflows from the systems, confirming the theory of the bipolar model of the ejected material in novae, already at very early epochs.

3. Near future of T CrB

T CrB is the second oldest known RN, with its first observed eruption in 1866 and the last one in 1946. The recurrence time of this star is $\sim$ 80 years, and thus we are now waiting for the next, very rare, once-in-a-lifetime opportunity to observe its eruption.

The visual brightening of T CrB rise from V=10 mag to V=2 mag as it is located at only $\sim$ 900 pc. This proximity gives an opportunity to study spatial structure in unprecedented detail. There is no better source with more optimal parameters for our scientific goal and from the point of view of the available interferometers.

There are observational indications that this next outburst is about to occur soon. Namely, a brightening in the optical bands that lasted from 2014 until recently and a pre-eruption dip. Similar photometric behavior was present before the 1946 outburst (Schaefer, 2023). Like most of the world-wide astronomical community, we look forward to the coming T CrB outburst and plan to monitor it closely with optical interferometers: before, during, and after the eruption. Among other things, we are, of course, interested in the morphology and kinematics of the event and its evolution. In addition, we will monitor the secondary eruption of T CrB, any signs of renewed accretion during the first weeks after eruption, to determine its influence on mass transfer to the WD. The best we can hope for is to resolve the stellar components. It is only possible for such a nearby nova, and only now – with the use of the second-generation instruments at VLTI and CHARA[2].

4. Conclusions

V3890 Sgr and RS Oph have recently erupted and T CrB is expected to erupt soon. This makes the current times a wonderful epoch to study these systems, given their rarity and recurrence times.

With the data of the two SyRN that are ready, and when T CrB erupts, we investigate the morphology and kinematics of the novae ejecta, as well as their asymmetry and very complex geometry, which are seen in emission lines and in the continuum. Such modeling of interferometric data is difficult and requires novel approaches, especially in the case of complex novae systems.

Optical interferometry gives us unprecedented angular resolution that is needed for comparison with existing detailed 3-D numerical simulations (e.g. Booth et al. (2016)), and to address the open questions in the theory of novae.

[2]the Center for High Angular Resolution Astronomy, https://www.chara.gsu.edu

Understanding eruptions of RN is important not only for cataclysmic variable stars. It also applies to the subjects of shock propagation (as compared to those in supernovae), as well as search of Type Ia supernovae progenitors. RN are one of the most promising objects in this context, since their white dwarfs are very massive, close to the Chandrasekhar limit, and the mass accretion rate is high.

Acknowledgements. We acknowledge support of the Polish National Science Center[3] grant 2019/32/C/ST9/00577 and the "Initiative of Excellence - Research University" (ID-UB) programme[4] at the Adam Mickiewicz University in Poznań, Poland.

References

Acciari, V. A., Ansoldi, S., Antonelli, L. A., et al., Proton acceleration in thermonuclear nova explosions revealed by gamma rays. 2022, *Nature Astronomy*, **6**, 689, DOI:10.1038/s41550-022-01640-z

Barry, R. K., Danchi, W. C., Traub, W. A., et al., Milliarcsecond N-Band Observations of the Nova RS Ophiuchi: First Science with the Keck Interferometer Nuller. 2008, *Astrophysical Journal*, **677**, 1253, DOI:10.1086/529422

Booth, R. A., Mohamed, S., & Podsiadlowski, P., Modelling the circumstellar medium in RS Ophiuchi and its link to Type Ia supernovae. 2016, *Monthly Notices of the RAS*, **457**, 822, DOI:10.1093/mnras/stw001

Chesneau, O. & Banerjee, D. P. K., Interferometric studies of novae in the infrared. 2012, *Bulletin of the Astronomical Society of India*, **40**, 267, DOI:10.48550/arXiv.1210.2507

Chesneau, O., Nardetto, N., Millour, F., et al., AMBER/VLTI interferometric observations of the recurrent Nova RS Ophiuchii 5.5 days after outburst. 2007, *Astronomy and Astrophysics*, **464**, 119, DOI:10.1051/0004-6361:20066609

Chomiuk, L., Metzger, B. D., & Shen, K. J., New Insights into Classical Novae. 2021, *Annual Review of Astron and Astrophys*, **59**, 391, DOI:10.1146/annurev-astro-112420-114502

Eisenhauer, F., Monnier, J. D., & Pfuhl, O., Advances in Optical/Infrared Interferometry. 2023, *Annual Review of Astron and Astrophys*, **61**, 237, DOI:10.1146/annurev-astro-121622-045019

Greenstein, J. L. & Kraft, R. P., The Binary System Nova DQ Herculis. I. The Spectrum and Radial Velocity during the Eclipse Cycle. 1959, *Astrophysical Journal*, **130**, 99, DOI:10.1086/146700

H. E. S. S. Collaboration, Aharonian, F., Ait Benkhali, F., et al., Time-resolved hadronic particle acceleration in the recurrent nova RS Ophiuchi. 2022, *Science*, **376**, 77, DOI:10.1126/science.abn0567

[3]https://ncn.gov.pl

[4]https://idub.amu.edu.pl/

Kraft, R. P., Binary Stars among Cataclysmic Variables. I. U Geminorum Stars (dwarf Novae). 1962, *Astrophysical Journal*, **135**, 408, DOI:10.1086/147280

Krzeminski, W., The Eclipsing Binary U Geminorum. 1965, *Astrophysical Journal*, **142**, 1051, DOI:10.1086/148375

Krzeminski, W. & Kraft, R. P., Binary Stars among Cataclysmic Variables. V. Photoelectric and Spectroscopic Observations of the Ultra-Short Binary Nova WZ Sagittae. 1964, *Astrophysical Journal*, **140**, 921, DOI:10.1086/147995

Lane, B. F., Sokoloski, J. L., Barry, R. K., et al., Interferometric Observations of RS Ophiuchi and the Origin of the Near-Infrared Emission. 2007, *Astrophysical Journal*, **658**, 520, DOI:10.1086/511414

Mérand, A., Flexible spectro-interferometric modelling of OIFITS data with PMOIRED. 2022, in Society of Photo-Optical Instrumentation Engineers (SPIE) Conference Series, Vol. **12183**, *Optical and Infrared Interferometry and Imaging VIII*, ed. A. Mérand, S. Sallum, & J. Sanchez-Bermudez, 121831N

Mohamed, S. & Podsiadlowski, P., Mass Transfer in Mira-type Binaries. 2012, *Baltic Astronomy*, **21**, 88, DOI:10.1515/astro-2017-0362

Molaro, P., Izzo, L., Selvelli, P., et al., ^{7}Be detection in the 2021 outburst of RS Oph. 2023, *Monthly Notices of the RAS*, **518**, 2614, DOI:10.1093/mnras/stac2708

Monnier, J. D., Optical interferometry in astronomy. 2003, *Reports on Progress in Physics*, **66**, 789, DOI:10.1088/0034-4885/66/5/203

Monnier, J. D., Barry, R. K., Traub, W. A., et al., No Expanding Fireball: Resolving the Recurrent Nova RS Ophiuchi with Infrared Interferometry. 2006, *Astrophysical Journal, Letters*, **647**, L127, DOI:10.1086/507584

Ness, J. U., Beardmore, A. P., Bode, M. F., et al., High-resolution X-ray spectra of RS Ophiuchi (2006 and 2021): Revealing the cause of SSS variability. 2023, *Astronomy and Astrophysics*, **670**, A131, DOI:10.1051/0004-6361/202245269

Paczyński, B., Evolutionary Processes in Close Binary Systems. 1971, *Annual Review of Astron and Astrophys*, **9**, 183, DOI:10.1146/annurev.aa.09.090171.001151

Patterson, J., The evolution of cataclysmic and low-mass X-ray binaries. 1984, *Astrophysical Journal, Supplement*, **54**, 443, DOI:10.1086/190940

Robinson, E. L., The structure of cataclysmic variables. 1976, *Annual Review of Astron and Astrophys*, **14**, 119, DOI:10.1146/annurev.aa.14.090176.001003

Schaefer, B. E., The B & V light curves for recurrent nova T CrB from 1842-2022, the unique pre- and post-eruption high-states, the complex period changes, and the upcoming eruption in 2025.5 ± 1.3. 2023, *Monthly Notices of the RAS*, **524**, 3146, DOI:10.1093/mnras/stad735

Schaefer, G. H., Brummelaar, T. T., Gies, D. R., et al., The expanding fireball of Nova Delphini 2013. 2014, *Nature*, **515**, 234, DOI:10.1038/nature13834

Shara, M. M., Mizusawa, T., Zurek, D., et al., The Inter-eruption Timescale of Classical Novae from Expansion of the Z Camelopardalis Shell. 2012, *Astrophysical Journal*, **756**, 107, DOI:10.1088/0004-637X/756/2/107

Shara, M. M., Prialnik, D., Hillman, Y., & Kovetz, A., The Masses and Accretion Rates of White Dwarfs in Classical and Recurrent Novae. 2018, *Astrophysical Journal*, **860**, 110, DOI:10.3847/1538-4357/aabfbd

Smak, J., Eruptive Binaries. II. U Geminorum. 1971, *Acta Astronomica*, **21**, 15

Walker, M. F., Nova DQ Herculis (1934): an Eclipsing Binary with Very Short Period. 1954, *Publications of the ASP*, **66**, 230, DOI:10.1086/126703

Walker, M. F. & Chincarini, G., Image-Tube Spectroscopic Studies of Rapid Variables. I. Spectroscopic and Photometric Observations of SS Cygni. 1968, *Astrophysical Journal*, **154**, 157, DOI:10.1086/149747

Warner, B. 1995, Cambridge Astrophysics, Vol. **28**, *Cataclysmic variable stars, 1st edn.* (Cambridge University Press), DOI:10.1017/CBO9780511586491, ISBN: 9780511586491

Warner, B. & Nather, R. E., Observations of rapid blue variables - II. U Geminorum. 1971, *Monthly Notices of the RAS*, **152**, 219, DOI:10.1093/mnras/152.2.219

Contrib. Astron. Obs. Skalnaté Pleso **55/3**, 75 – 80, (2025)
https://doi.org/10.31577/caosp.2025.55.3.75

X-raying the wind interactions of massive binaries

What we have learned from 25 years of observations

G. Rauw

STAR Institute, Université de Liège, Allée du 6 Août, 19c, Bât B5c, 4000 Liège, Belgium (E-mail: g.rauw@uliege.be)

Received: October 18, 2024; Accepted: December 9, 2024

Abstract. The collision of radiatively-driven stellar winds in massive binary systems should produce a strong X-ray emission. This emission is expected to display a phase-locked modulation due to a changing orbital separation (in eccentric systems) and/or a changing optical depth along our line of sight towards the wind interaction region. The current generation of X-ray satellites allowed the study of a number of massive binaries. They notably demonstrated that not all O + O binaries are X-ray bright and that some systems display rather complex orbital variations. In this contribution, we highlight the properties of a few systems that were recently studied with *XMM-Newton*.

Key words: stars: early-type – stars: winds – X-rays: stars

1. Introduction

Hot, massive stars of spectral-type O have energetic stellar winds that are driven by their huge radiation pressure (Vink, 2022). These winds associate considerable mass-loss rates of order $10^{-6}\,M_\odot\,yr^{-1}$ and large velocities of several $1000\,km\,s^{-1}$. Because the majority of these O-type stars reside in binary or higher multiplicity systems (Sana et al., 2012), the stellar winds of the stars in those systems are bound to interact with each other. When the winds collide, their huge kinetic energy is transformed into heat leading to post-shock plasma temperatures of millions of K (Stevens et al., 1992). The collision of stellar winds in O + O binary systems should thus produce a hot plasma emitting copious X-rays, and these systems should exhibit X-ray over-luminosities compared to single O-type stars. Owing to the orbital motion of the stars, the observable X-ray emission is further expected to be modulated by the variations of the orbital separation (in eccentric systems) and/or the changing optical depth along our line of sight towards the wind interaction region (Pittard & Parkin, 2010).

The actual emission and its variability depend on the efficiency of cooling processes via radiative recombination and inverse Compton scattering (Stevens et al., 1992; Pittard, 2009; Mackey et al., 2023). These cooling processes are

usually rather efficient in the wind interaction zones of close, short-period binaries and this should lead to strong hydrodynamic instabilities that reduce the X-ray emission of the wind interaction zone (Kee et al., 2014). On the contrary, wide, long-period binaries often feature an adiabatic wind interaction zone which should be more stable and is expected to display an X-ray emission that varies as $1/r$ where r is the instantaneous orbital separation between the binary components (Stevens et al., 1992). Whilst some prominent colliding wind binaries host Wolf-Rayet stars (e.g., WR 140, V 444 Cyg) the focus of the present contribution is on O + O binary systems.

2. The X-ray emission of massive binaries

The X-ray emission of massive stars was serendipitously discovered with the *EINSTEIN* satellite in the late 1970s (Harnden et al., 1979; Seward et al., 1979). Many of the brighter sources found among the O-type stars in these early observations were indeed binaries (Chlebowski, 1989). The *EINSTEIN* data already unveiled the existence of a simple scaling relation between the X-ray and bolometric luminosities of O-type stars ($L_{\rm X}/L_{\rm bol} \sim 10^{-7}$), and this relation was confirmed and refined by observations with subsequent satellites such as *ROSAT* and most recently *Chandra* and *XMM-Newton* (Berghoefer et al., 1997; Nazé, 2009). Over the last two and a half decades, the current generation of X-ray satellites shed new light on the X-ray properties of massive stars in general and massive binaries in particular (for reviews see e.g., Rauw & Nazé, 2016; Rauw, 2022, and references therein). The emerging global picture of colliding wind systems is more complicated than anticipated: whilst some emblematic systems are indeed bright and variable X-ray emitters, not all O+O binaries display a strong X-ray emission. Indeed, observations of large samples of O-type stars showed no strong difference in $L_{\rm X}/L_{\rm bol}$ between known binaries and presumably single O-type stars (e.g., Nazé, 2009; Rauw et al., 2015). As it turns out, X-ray over-luminosity of massive binaries is more the exception rather than the rule!

In long-period eccentric systems, this situation could partially result from a selection effect. To illustrate this, we consider the system HD 168112 (O4.5IV((f)) + O5.5V(n)((f)) which has an orbital period of 514 d and an eccentricity $e = 0.75$ Blomme et al. (2024). The X-ray emission of this systems displays a well-defined $1/r$ variation as expected for an adiabatic wind-wind collision (Rauw et al., 2024a). However, if we consider that a system would be classified as overluminous if its X-ray luminosity exceeds the canonical $L_{\rm X}/L_{\rm bol} \sim 10^{-7}$ by at least a factor of two, then HD 168112 meets this criterion only during about 10% of its orbital period, when the stars are close to periastron. Over the rest of the orbit, the emission is fully consistent with the level expected without any colliding wind contribution. Therefore, a single snapshot X-ray observation of such a long period eccentric system could easily miss the detection of the emission from the wind interaction zone if it would not be taken at times close to periastron.

Some eccentric colliding wind systems display hysteresis-like variations in their X-ray flux instead of the simple $1/r$ relation. This phenomenon is observed in systems with relatively short orbital periods such as HD 166734 (O7.5If + O9I(f), $P = 34.5$ d, $e = 0.62$, Nazé et al., 2017) and Cyg OB2 #8a (O6I + O5.5III, $P = 21.9$ d, $e = 0.18$, Mossoux et al., 2020). For a same value of r, these systems display a stronger emission at the phase before periastron than at the symmetric phase after periastron. In those binaries, the cooling regime probably changes from essentially adiabatic around apastron to radiative near periastron. The instabilities that occur in the radiative wind interaction zone around periastron could then lead to a collapse of the shock onto the star with the weaker wind (Nazé et al., 2017). This situation can even result in accretion of clumps of wind material onto the star with the weaker wind (Kashi, 2020). For instance, in the case of HD 166734, Kashi (2020) estimated that about $1.3 \times 10^{-8}\,M_\odot$ would be accreted at each orbital cycle. Once the stars move again away from each other the wind-wind interaction takes some time to rebuild, thus explaining the hysteresis behaviour.

However, not all short-period eccentric O+O systems follow the above description. For instance, HD 93205 (O3V + O8V, $P = 6.08$ d, $e = 0.37$, Morrell et al., 2001) displays a very different X-ray light curve (Fig. 1) when the data from twenty years of *XMM-Newton* observations are folded with the ephemerides of Morrell et al. (2001). Indeed, in this system, the strongest X-ray emission is observed after periastron. Whilst this could hint at a different origin for the X-ray variations, we stress that the ephemeris of this system need revision. Indeed, Morrell et al. (2001) diagnosed a rather significant apsidal motion at a rate of $1.95°\,\mathrm{yr}^{-1}$ and this secular precession of the orbit could impact our interpretation of the X-ray light curve of this system.

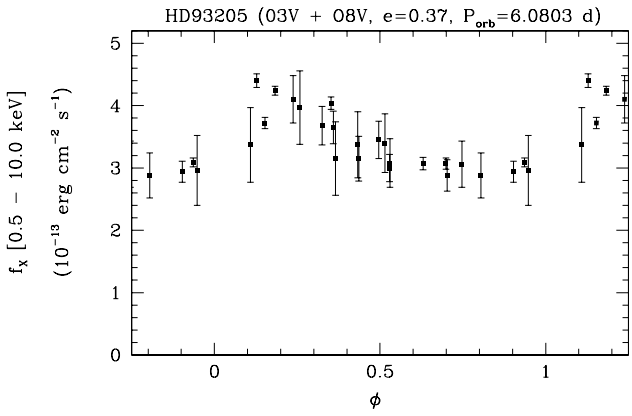


Figure 1. Variations of the observed X-ray flux of HD 93205 as a function of orbital phase according to the ephemerides of Morrell et al. (2001).

X-ray spectral variations in systems with circular orbits can be used to probe the properties of the stellar winds. For instance, in the case of HDE 228766 (Of^+/WN8ha + O7III-I, $P = 10.7$ d, Rauw et al., 2014), X-ray observations performed at both conjunction phases and one quadrature phase were used to investigate the variations of the X-ray flux as a function of energy. The observation with the Of^+/WN8ha star in front displayed a heavily attenuated X-ray spectrum, especially at low energies. The observed energy dependence of this attenuation was found to be in excellent agreement with the theoretically expected energy dependence of the opacity of the wind of this star. A significantly more complicated situation was found for HD 149404 (O7.5I(f) + ON9.7, $P = 9.8$ d, Rauw et al., 2024b). The variations of the X-ray emission between the conjunction phases with either the O7.5I(f) or the ON9.7 star in front have a lower amplitude and are grey as they do not display any significant energy dependence. The only way to explain this situation is to assume that these variations are dominated by occultation rather than absorption effects. Occultation can come from the stellar bodies, but given the low orbital inclination ($\leq 31°$) such a scenario seems rather unlikely. An alternative could be that the winds of the stars would consist of optically thick clumps. Indeed, in such a case, the ensuing attenuation of the X-ray emission would depend on the geometrical cross section of the clumps and not on their opacity.

3. Conclusions and future perspectives

The X-ray data on O+O binaries that were collected with *XMM-Newton* and *Chandra* considerably changed our understanding of wind-wind collisions. Among the most important findings, we can cite

- the fact that the majority of these binaries are not X-ray overluminous,
- the fact that wide eccentric systems with adiabatic wind interactions follow a $1/r$ X-ray flux dependence as predicted by theory,
- the fact that the wind interaction zones in shorter period eccentric systems switch between adiabatic and radiative regimes, possibly with accretion at periastron,
- the possibility that optically-thick clumps could be responsible for the grey flux attenuation seen in some systems, whilst others display instead a strongly energy dependent wind opacity as expected for photoelectric absorption by a stellar wind.

More detailed studies become possible, notably thanks to JAXA's *XRISM* mission and its high-resolution spectrograph *Resolve*. Whilst they will focus on a few bright sources, more targets will become accessible thanks to ESA's next X-ray observatory *Athena*. Indeed, some colliding wind binaries exhibit a strong

Fe XXV line at an energy of 6.7 keV. The formation of this line requires temperatures that are only reached in the plasma of the wind-wind collision and not in the winds of single massive stars. This line thus offers an excellent diagnostics of the physical conditions of the shocked plasma (Mossoux & Rauw, 2021). These binaries will be ideal targets for high-resolution X-ray spectroscopy with the *X-IFU* microcalorimeter spectrograph onboard *Athena* (Barret et al., 2023).

Acknowledgements. I'd like to express my gratitude to my collaborators Drs Yaël Nazé, Enmanuelle Mossoux, Ronny Blomme and Sophie Rosu, and to the referee Dr Jonathan Mackey. This work was supported by Belspo via the HERMeS PRODEX contract and via travel grant nr 40028245 awarded by the FRS-FRNS (Belgium).

References

Barret, D., Albouys, V., Herder, J.-W. d., et al., The Athena X-ray Integral Field Unit: a consolidated design for the system requirement review of the preliminary definition phase. 2023, *Experimental Astronomy*, **55**, 373, DOI:10.1007/s10686-022-09880-7

Berghoefer, T. W., Schmitt, J. H. M. M., Danner, R., & Cassinelli, J. P., X-ray properties of bright OB-type stars detected in the ROSAT all-sky survey. 1997, *Astronomy and Astrophysics*, **322**, 167

Blomme, R., Rauw, G., Volpi, D., Nazé, Y., & Abdul-Masih, M., The colliding-wind binary HD 168112. 2024, *Astronomy and Astrophysics*, **687**, A106, DOI:10.1051/0004-6361/202450227

Chlebowski, T., X-Ray Emission from O-Type Stars: Parameters Which Affect It. 1989, *Astrophysical Journal*, **342**, 1091, DOI:10.1086/167667

Harnden, F. R., J., Branduardi, G., Elvis, M., et al., Discovery of an X-ray star association in VI Cygni (Cyg OB2). 1979, *Astrophysical Journal, Letters*, **234**, L51, DOI:10.1086/183107

Kashi, A., Wind collision and accretion simulations of the massive binary system HD 166734. 2020, *Monthly Notices of the RAS*, **492**, 5261, DOI:10.1093/mnras/staa203

Kee, N. D., Owocki, S., & ud-Doula, A., Suppression of X-rays from radiative shocks by their thin-shell instability. 2014, *Monthly Notices of the RAS*, **438**, 3557, DOI:10.1093/mnras/stt2475

Mackey, J., Jones, T. A. K., Brose, R., et al., Inverse-Compton cooling of thermal plasma in colliding-wind binaries. 2023, *Monthly Notices of the RAS*, **526**, 3099, DOI:10.1093/mnras/stad2839

Morrell, N. I., Barbá, R. H., Niemela, V. S., et al., Optical spectroscopy of X-Mega targets - II. The massive double-lined O-type binary HD 93205. 2001, *Monthly Notices of the RAS*, **326**, 85, DOI:10.1046/j.1365-8711.2001.04500.x

Mossoux, E., Pittard, J. M., Rauw, G., & Nazé, Y., Search for non-thermal X-ray emission in the colliding wind binary Cygnus OB2 #8A. 2020, *Astronomy and Astrophysics*, **636**, A109, DOI:10.1051/0004-6361/201936735

Mossoux, E. & Rauw, G., LIFELINE: The program for the simulation of the X-ray line profiles in massive colliding wind binaries. 2021, *Astronomy and Astrophysics*, **646**, A89, DOI:10.1051/0004-6361/202039437

Nazé, Y., Hot stars observed by XMM-Newton. I. The catalog and the properties of OB stars. 2009, *Astronomy and Astrophysics*, **506**, 1055, DOI:10.1051/0004-6361/200912659

Nazé, Y., Gosset, E., Mahy, L., & Parkin, E. R., An X-ray view of HD 166734, a massive supergiant system. 2017, *Astronomy and Astrophysics*, **607**, A97, DOI:10.1051/0004-6361/201630303

Pittard, J. M., 3D models of radiatively driven colliding winds in massive O+O star binaries - I. Hydrodynamics. 2009, *Monthly Notices of the RAS*, **396**, 1743, DOI:10.1111/j.1365-2966.2009.14857.x

Pittard, J. M. & Parkin, E. R., 3D models of radiatively driven colliding winds in massive O + O star binaries - III. Thermal X-ray emission. 2010, *Monthly Notices of the RAS*, **403**, 1657, DOI:10.1111/j.1365-2966.2010.15776.x

Rauw, G., X-Ray Emission of Massive Stars and Their Winds. 2022, in *Handbook of X-ray and Gamma-ray Astrophysics*, ed. C. Bambi & A. Santangelo, 108

Rauw, G., Blomme, R., Nazé, Y., Volpi, D., & Fernandez-Vera, S., Ups and downs in the X-ray emission of the colliding wind binaries HD 168112 and HD 167971. 2024a, *Astronomy and Astrophysics*, **687**, A197, DOI:10.1051/0004-6361/202450158

Rauw, G., Lizin, S., Rosu, S., & Mossoux, E., Phase-resolved XMM-Newton observations of the massive post-RLOF system HD 149404. 2024b, *Astronomy and Astrophysics*, **686**, A152, DOI:10.1051/0004-6361/202348721

Rauw, G., Mahy, L., Nazé, Y., et al., Phase resolved X-ray spectroscopy of HDE 228766: Probing the wind of an extreme Of^+/WNLha star. 2014, *Astronomy and Astrophysics*, **566**, A107, DOI:10.1051/0004-6361/201423885

Rauw, G. & Nazé, Y., X-ray emission from interacting wind massive binaries: A review of 15 years of progress. 2016, *Advances in Space Research*, **58**, 761, DOI:10.1016/j.asr.2015.09.026

Rauw, G., Nazé, Y., Wright, N. J., et al., X-Ray Emission from Massive Stars in Cyg OB2. 2015, *Astrophysical Journal, Supplement*, **221**, 1, DOI:10.1088/0067-0049/221/1/1

Sana, H., de Mink, S. E., de Koter, A., et al., Binary Interaction Dominates the Evolution of Massive Stars. 2012, *Science*, **337**, 444, DOI:10.1126/science.1223344

Seward, F. D., Forman, W. R., Giacconi, R., et al., X-rays from Eta Carinae and the surrounding nebula. 1979, *Astrophysical Journal, Letters*, **234**, L55, DOI:10.1086/183108

Stevens, I. R., Blondin, J. M., & Pollock, A. M. T., Colliding Winds from Early-Type Stars in Binary Systems. 1992, *Astrophysical Journal*, **386**, 265, DOI:10.1086/171013

Vink, J. S., Theory and Diagnostics of Hot Star Mass Loss. 2022, *Annual Review of Astron and Astrophys*, **60**, 203, DOI:10.1146/annurev-astro-052920-094949

Contrib. Astron. Obs. Skalnaté Pleso **55/3**, 81 – 90, (2025)
https://doi.org/10.31577/caosp.2025.55.3.81

Apsidal motion in massive binaries: or how to sound stellar interiors

S. Rosu[1,2]

[1] *Département d'Astronomie, Université de Genève, Chemin Pegasi 51, 1290 Versoix, Switzerland, (E-mail: sophie.rosu@unige.ch)*

[2] *Department of Physics, KTH Royal Institute of Technology, The Oskar Klein Centre, AlbaNova, SE-106 91 Stockholm, Sweden*

Received: October 28, 2024; Accepted: December 12, 2024

Abstract. One of the most efficient and reliable observational technique allowing to probe the internal structure of a star is the determination of the apsidal motion in close eccentric binary systems. This secular precession of the binary orbit's major axis depends on the tidal interactions occurring between the two stars. The rate of this motion is directly related to the internal structure of the stars, in particular their inner density profile.

The most common way to derive the apsidal motion of a binary from observations, together with the fundamental parameters of the stars, is the analysis of the times of minima of the eclipses. While this technique has been used for decades, it returned to popularity lately thanks to the incredible precision of observations acquired with space-borne facilities such as TESS and Kepler, among others. Aside, a less common – but not less accurate though – method to determine a binary's apsidal motion rate is through the fit of the stars' radial velocity curves as a function of time. This technique relies on radial velocities collected over a (very) long timescale. While it points out the utility of gathering spectroscopic data of the same object over several decades, requiring dealing with the tricky task of combining and simultaneously analysing data from a variety of Earth-based instruments having their own characteristics each, it also gives old spectroscopic observations a second lease of life.

But what do you think if we decide to simultaneously and consistently analyse both spectroscopic and photometric data, that is to say, all available data of the same binary, rather than ignoring part of them? This challenging objective comes with a real deserved reward: consistent physical and orbital parameters for the binaries, including the apsidal motion rate, are obtained with unprecedented accuracy. The confrontation of the observationally determined parameters to theoretical models of stellar structure and evolution then allows us to finely constrain the internal structure of the stars.

This powerful technique has been known for years but has been seldom applied to massive stars. I will highlight its interest and reveal recent results concerning several massive binaries.

While standard 1D stellar evolution models predict stars having a smaller internal stellar structure constant, that is to say, stars having a smaller density contrast, than expected from observations, I demonstrate that the addition

of mixing inside the models helps to solve, at least partially, this discrepancy. Whether this additional mixing might be fully explained by rotational mixing is under investigation. Ongoing studies with the non-perturbative code `MoBiDICT` show that the perturbative model assumption is not justified in highly distorted stars, in which cases the apsidal motion is underestimated, exacerbating even more the need for enhanced mixing inside the models.

Key words: stars: early-type – stars: evolution – stars: massive – binaries: eclipsing – binaries: spectroscopic

1. The origin of the apsidal motion

In the Keplerian problem, the two stars of a binary, assumed to be point-like particles, orbit one another on elliptic orbits which maintain a constant orientation in space over time; Only the true anomaly (the positions of the stars on their orbit) changes with time (see Fig. 1). While this two-body problem is arguably valid for wide eccentric binaries, it is inappropriate for close eccentric binaries as the three-dimensional extension of the stars cannot be ignored. The stars exert on one another tidal forces which are responsible for the exchange of angular momentum in the system as well as the stellar deformations and the ensuing non-spherical gravitational fields of the stars. The major observable consequence of these tidal interactions on the orbital motion is the apsidal motion, that is to say, the precession of the line of apsides with time (see Fig. 1). I here insist upon the fact that this motion is a purely Newtonian (i.e. non-Keplerian) motion. It should not be mistaken with the relativistic apsidal motion which contributes to the total rate of apsidal motion in a binary system though, but is of minor importance for most binaries.

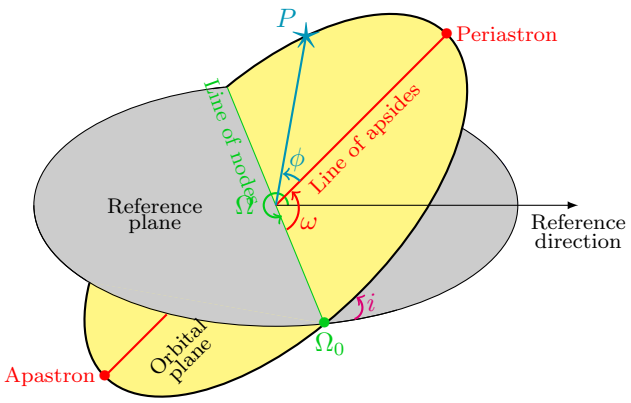


Figure 1. Definition of the orbital elements of a binary system.

Although relatively small, on the order of a few degrees per year, this apsidal motion has been measured in hundreds of binaries. I here refer to Rosu et al. (2024, figure 2), Hong et al. (2016, figure 6), and Zasche et al. (2020, figure 15) for the most up-to-date sample of binaries in our Galaxy, the Large and Small Magellanic Clouds, for which an apsidal motion determination exists in the literature.

I explain how we can measure the apsidal motion rate in a binary and illustrate it by one well-chosen specific case in Sect. 2. In Sect. 3, I introduce the apsidal motion equations and their link to the internal stellar structure constants. In Sect. 4, I show how to use these latter to sound the interior of stars through the confrontation of observationally-determined stellar and orbital parameters with dedicated 1D stellar structure and evolution models as well as 3D non-perturbative models. I review the study of the apsidal motion in (massive) binaries in Sect. 5.

2. From observations to the apsidal motion determination

The determination of the apsidal motion rate $\dot{\omega}$ is made following two different approaches (see Rosu, 2024, for a more careful explanation):

1. In an eclipsing binary, both the depths of the eclipses and their phase depend upon the orbital separation at conjunction phase that itself depends on the orientation of the ellipse with respect to our line of sight, that is to say, to ω. The adjustment of a set of lightcurves and/or times of minimum of the eclipses taken at different epochs therefore allows the determination of $\dot{\omega}$;

2. In a spectroscopic binary, the stars' radial velocities (RVs) depend upon $\cos\omega(t)$. The adjustment of the RV curves explicitly accounting for the linear rate of change of ω allows us to derive a value for $\dot{\omega}$.

While the former technique, thanks to the high-quality photometric data such as TESS, allows the determination of accurate apsidal motion rates using much shorter timespans than the decades of observations necessary for the RV adjustments, this latter technique turns out to be more powerful and accurate provided sufficient data are available (Rauw et al., 2016; Rosu, 2022; Rosu et al., 2020b, 2022a,b, 2023). Among all binaries, the short-period eccentric eclipsing double-line spectroscopic binaries for which photometric, spectroscopic, and RV data are available, are the most promising and intrinsically invaluable systems. Not only they are the only ones for which we can constrain the stars' fundamental properties (masses, radii) in a model independent way, but also their apsidal motion rate is used to probe the internal structure of the stars (see Sect. 3). Examples of such binaries are HD 152248 and HD 152219: Rosu et al. (2020b) and Rosu et al. (2022a) derived $\dot{\omega} = 1.84 \pm 0.08^\circ\,\mathrm{yr}^{-1}$ and $\dot{\omega} = 1.198 \pm 0.300^\circ\,\mathrm{yr}^{-1}$, respectively, based on the global adjustment of the RVs and lightcurves of the system (see Figs 2 and 3).

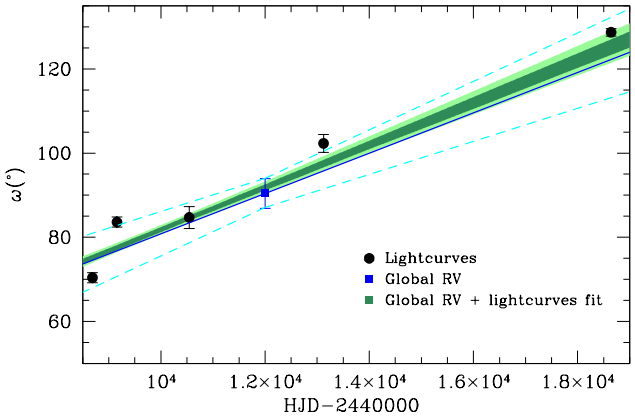


Figure 2. Values of ω as a function of time inferred from the RVs (blue and cyan), lightcurves (black), and both simultaneously (green) of HD 152248. Credit: Rosu et al. (2020b), reproduced with permission ©ESO.

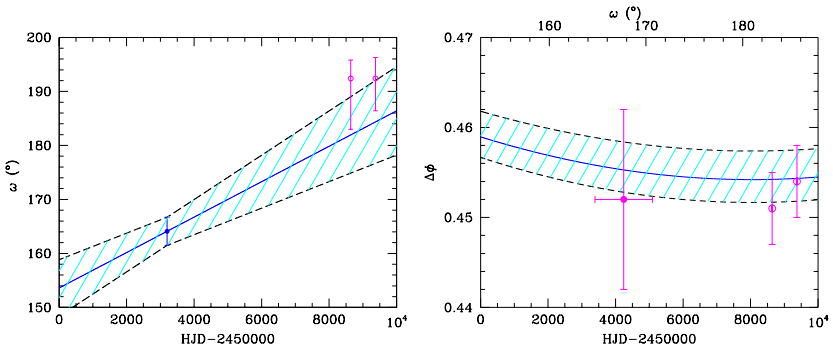


Figure 3. *Left panel:* Values of ω (left panel) and the phase difference $\Delta\phi$ between the primary and secondary eclipses (right panel) as a function of time inferred from the RVs (blue and cyan) and lightcurves (pink) of HD 152219. Figures from Rosu et al. (2022a).

3. Apsidal motion equations and internal stellar structure constants

In the perturbative case, the apsidal motion rate of a binary is the sum of the Newtonian contribution $\dot{\omega}_{\rm N}$ and a general relativistic correction $\dot{\omega}_{\rm GR}$. The Newtonian term has the following expression according to Sterne (1939) under the

assumption that only the contributions arising from the second-order harmonic distorsions of the gravitational potential are considered:

$$\dot{\omega}_{\rm N} = \frac{2\pi}{P_{\rm orb}} \left[15 f(e) \left\{ k_{2,1} q \left(\frac{R_1}{a} \right)^5 + \frac{k_{2,2}}{q} \left(\frac{R_2}{a} \right)^5 \right\} \right.$$
$$\left. + g(e) \left\{ k_{2,1} (1+q) \left(\frac{R_1}{a} \right)^5 \left(\frac{P_{\rm orb}}{P_{\rm rot,1}} \right)^2 + k_{2,2} \frac{1+q}{q} \left(\frac{R_2}{a} \right)^5 \left(\frac{P_{\rm orb}}{P_{\rm rot,2}} \right)^2 \right\} \right]. \quad (1)$$

In this expression, $q = m_2/m_1$ is the mass ratio, $P_{\rm orb}$ is the orbital period of the system, a is the semi-major axis of the orbit, R_* the radius, $k_{2,*}$ the internal structure constant, and $P_{{\rm rot},*}$ the rotational period of the considered star, and $f(e)$ and $g(e)$ are functions of the eccentricity of the orbit which expressions are given in e.g., Rosu (2021). The expression of $\dot{\omega}_{\rm GR}$ is attributed to Shakura (1985) and depends on $P_{\rm orb}, e, m_1$, and m_2.

The internal stellar structure constant k_2 is an algebraic expression of the η_2 function evaluated at the stellar surface, itself solution of the Clairaut-Radau differential equation (Hejlesen, 1987) that depends on the density profile inside the star (see Rosu, 2024, for more details). In a nutshell, k_2 is a measure of the density stratification between the core and the external layers of the star: The higher the k_2, the more homogeneous the star in terms of density ($k_2 = 0.75$ for an homogeneous sphere of constant density); On the contrary, the smaller the k_2, the higher the radial density gradient inside the star. As the star evolves, its k_2 decreases as the stellar core contracts while the stellar envelope expands. This renders k_2 a good indicator of stellar evolution just like the hydrogen mass fraction in the stellar core (see figures 12 and 15 in Rosu et al., 2020a).

In the apsidal motion equation, all terms appearing in the expressions of $\dot{\omega}_{\rm N}$ and $\dot{\omega}_{\rm GR}$ can be derived from observations, except for $k_{2,1}$ and $k_{2,2}$. In the case of a twin system, meaning both stars share the same properties in terms of mass, radius, and effective temperature, we can assume the stars also share the same density profile, so the same k_2. In this lucky case, we can solve the apsidal motion equation for k_2 and get an observational determination for this latter quantity. In the general case of a non-twin system, the situation is slightly more complex; I refer to Rosu et al. (2022a,b); Rosu (2024) for a thorough discussion and analysis of these cases. For the sake of this paper, I will focus on twin binaries only, with a particular attention to HD 152248 (Rosu et al., 2020a,b; Fellay et al., 2024).

4. Without enhanced mixing in the models, impossible to reproduce the observations... even in 3D

Dedicated stellar structure and evolution models were built for HD 152248 using the `Clés` code (Scuflaire et al., 2008) and its `min-Clés` routine to search

for best-fit models of the stars in terms of observational properties using the Levenberg-Marquardt minimisation technique (Rosu et al., 2020a). Overshooting was implemented in the models as a step-function through the overshooting parameter $\alpha_{\rm ov}$ while additional mixing was introduced through the turbulent diffusion implemented as a partial mixing process with velocities of the elements being the product of the turbulent diffusion coefficient D_T to the radial abundance gradient of the element. As such, the turbulent diffusion acts as reducing the abundance gradient of the elements. Both the overshooting and the turbulent diffusion increase the main-sequence lifetime of the stars as they bring additional hydrogen from the external layers to its core, hence fuel for nuclear reactions. Rosu et al. (2020a) showed that including overshooting in their models but no turbulent diffusion did not allow the simultaneous reproduction of the stellar mass, radius, and position in the Hertzsprung-Russell (HR) diagram of HD 152248 (see dotted purple track in Fig. 4). Indeed, to reproduce these observational parameters, the authors had to introduce a certain amount of turbulent diffusion and this, especially as the overshooting was small (see dashed green track in Fig. 4). However, the best-fit models obtained this way had systematically too high a k_2 value. Rosu et al. (2020a) further showed that to reproduce the apsidal motion rate and the k_2 of the stars in addition to the previously mentioned parameters, they had to introduce even more mixing in the models (see orange track in Fig. 4). That the standard models predict stars that are too homogeneous in terms of density stratification compared to what is expected from the observations is a key result that could not be achieved for this system without the study of the apsidal motion. At this juncture, it is of primordial importance to understand the physical origin of this required enhanced mixing required in the models. Rosu et al. (2020a) built stellar evolution models with the `GENEC` code (Eggenberger et al., 2008) including stellar rotation and suspected from their preliminary study that rotationally induced mixing is certainly the key, though further investigations are needed and ongoing.

We here note that these results were corroborated using the same method for the massive binaries HD 152219 (Rosu et al., 2022a), and CPD-41° 7741 and HD 152218 (Rosu et al., 2022b), and independently using 2D hydrodynamical simulations for these three binaries (Baraffe et al., 2023).

Whether this need of enhanced mixing in the models is due to the inherent 1D stellar modelling is a question worth asking, and answering. We used the `MoBiDICT` (Modelling Binaries Deformations Induced by Centrifugal and Tidal forces) code (Fellay & Dupret, 2023), a non-perturbative method that computes the entire precise 3D deformed structure of each component including the effets of stellar deformations on the mass redistribution, as opposed to the perturbative model assumption adopted in the 1D stellar modelling that considers the centrifugal and tidal forces as small perturbations of the spherical symmetry and only accounts for leading terms. `MoBiDICT` calculates the instantaneous non-perturbative tidal acceleration perturbation and its consequence on the apsidal motion (Fellay & Dupret, 2023; Fellay et al., 2024).

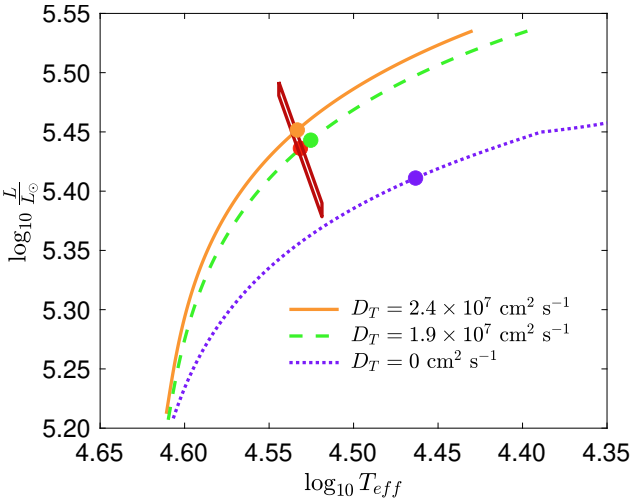


Figure 4. HR diagram for HD 152248: evolutionary tracks of `Clés` models. The observational values and their error bars are represented in red. The dots over-plotted on the tracks correspond to the models that fit the observational k_2. Credit: Rosu et al. (2020a), reproduced with permission ©ESO.

Fellay & Dupret (2023) demonstrated that the perturbative models significantly underestimate the deformations of binaries measured through η_2, a fortiori when stars have significant envelope mass compared to their total mass and when binaries have small orbital separation (i.e. a is comparable to the stellar radii) (see the adapted figure 11 in Rosu, 2024). The apsidal motion rate is affected the same way: The higher the envelope mass compared to the total stellar mass, the higher the relative difference between the non-perturbative and perturbative $\dot{\omega}$. This is illustrated in Fig. 5 for four kind of twin binaries and different values of the eccentricity. Low-mass main-sequence (MS) stars and reg giants (RGB) reach the most significant discrepancies with up to 70% and 40% errors on the $\dot{\omega}$ determination at small orbital separation and low eccentricity. For a given orbital separation but higher eccentricity, the discrepancy is even higher as the stars get closer during periastron passage, therefore exacerbating the stellar deformations and the ensuing impact on the apsidal motion rate.

Fellay et al. (2024) applied `MoBiDICT` to four well-known twin binaries (HD 152248, PV Cas, IM Per, and Y Cyg) to compare their obtained parameters to those from 1D stellar modelling. The authors included overshooting in the models as the only mixing process to avoid any degeneracies between different mixing mechanisms as explored by Rosu et al. (2020a, 2022a). Fellay et al. (2024) found that a systematic higher overshooting parameter was necessary in the `MobiDICT` code than in the 1D stellar models (see their table 2). This stands

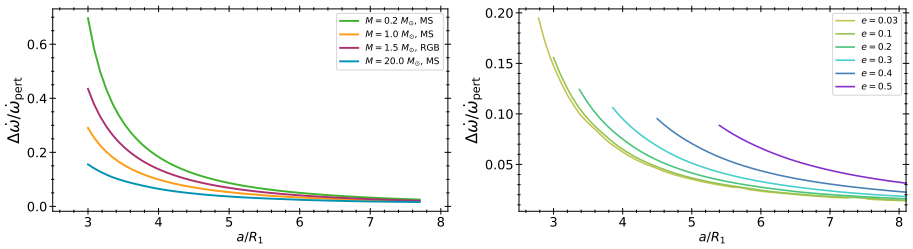


Figure 5. Apsidal motion relative difference as a function of the orbital separation normalised by the stellar radii for four twin binaries and $e = 0.1$ (*left panel*), and for 20 $M_\odot$ main-sequence stars but different values of e (*right panel*). Figure adapted from Fellay et al. (2024).

from the higher deformations in the non-perturbative approach that lead to smaller k_2 and hence, additional mixing is necessary to reproduce the internal density stratification. Far from solving the enhanced mixing issue encountered with 1D standard stellar models, the non-perturbative modelling enhances it. Furthermore, the non-perturbative approach, though being small compared to the perturbative approach, is on the same order of magnitude as the general relativistic correction and cannot be ignored anymore in the study of the apsidal motion in close eccentric binaries (see table 3 in Fellay et al., 2024).

5. Status quo of the apsidal motion

Close eccentric (massive) binaries might undergo apsidal motion, which means their longitude of periastron might precess in time, as a consequence of the tidal interactions that occur between the two stars. This motion has been measured in hundreds of systems during the last decades, historically using the times of minima of the eclipses, a method that returned to popularity lately thanks to the incredible precision of observations acquired with space-borne facilities such as TESS and Kepler, among others. The other less common but potentially more accurate method to derive the apsidal motion rate of the system is through the fit of the stars' radial velocity curves as a function of time provided a sufficient long timespan of the spectroscopic observations is available. In the lucky but challenging case of an eccentric eclipsing double-line spectroscopic binary, the simultaneous analysis of all spectroscopic and photometric data allows us to derive consistent physical and orbital parameters for the binaries, including the apsidal motion rate.

Far from being an observational curiosity, the measure of the apsidal motion rate in a binary is a powerful and robust means to sound the interior of the stars. In the perturbative case assumption, the apsidal motion rate is directly

proportional to the internal stellar structure constants k_2 of the stars, a measure of the stars' inner density profile. Thus, the measure of the apsidal motion rate of a binary system allows us to efficiently and reliably probe the interior of stars.

Through the confrontation of 1D stellar evolution models to the observational constraints of massive eccentric binaries, we reached the conclusion that the inner density profiles of the stars, measured through k_2 and $\dot{\omega}$, can only be reproduced provided enhanced mixing is included in the models. Indeed, standard model prescriptions predict stars having a smaller density contrast between the core and the external layers of the stars, than what is expected from the observations. The physical origin behind this enhanced mixing is most probably rotational mixing, though it is still under investigation. The results obtained with the 3D non-perturbative `MoBiDICT` code showed that the perturbative case assumption systematically underestimates the apsidal motion rate. As a matter of consequence, even more mixing needs to be included in `MoBiDICT` to reproduce the internal structure of the stars, exacerbating even more the results obtained with the 1D models. The more affected systems seem to be the massive stars which, despite their lower envelope mass compared to their total mass, are usually found in closer binaries and thus suffer more important deformations. It is therefore about time to adopt a perturbative approach to study those systems.

References

Baraffe, I., Clarke, J., Morison, A., et al., A study of convective core overshooting as a function of stellar mass based on two-dimensional hydrodynamical simulations. 2023, *Monthly Notices of the RAS*, **519**, 5333, DOI:10.1093/mnras/stad009

Eggenberger, P., Meynet, G., Maeder, A., et al., The Geneva stellar evolution code. 2008, *Ap&SS*, **316**, 43, DOI:10.1007/s10509-007-9511-y

Fellay, L. & Dupret, M. A., MoBiDICT: New 3D static models of close synchronised binaries in hydrostatic equilibrium. 2023, *A&A*, **676**, A22, DOI:10.1051/0004-6361/202346175

Fellay, L., Dupret, M. A., & Rosu, S., Underestimation of the tidal force and apsidal motion in close binary systems by the perturbative approach: Comparisons with non-perturbative models. 2024, *A&A*, **683**, A210, DOI:10.1051/0004-6361/202348134

Hejlesen, P. M., Studies in stellar evolution. III - The internal structure constants. 1987, *A&AS*, **69**, 251

Hong, K., Lee, J. W., Kim, S.-L., Koo, J.-R., & Lee, C.-U., Apsidal motions of 90 eccentric binary systems in the Small Magellanic Cloud. 2016, *MNRAS*, **460**, 650, DOI:10.1093/mnras/stw955

Rauw, G., Rosu, S., Noels, A., et al., Apsidal motion in the massive binary HD 152218. 2016, *A&A*, **594**, A33, DOI:10.1051/0004-6361/201628766

Rosu, S., What apsidal motion reveals about the interior of massive binary stars. 2021, *BSRSL*, **90**, 1, DOI:10.25518/0037-9565.10017

Rosu, S. 2022, Apsidal Motion in O-Star Binaries - Constraining the internal structure of the stars, PhD thesis, ULiège - Université de Liège [Sciences], Liège, Belgium

Rosu, S., Apsidal Motion in Massive Binaries: Or How to Sound Stellar Interiors Without Asteroseismology. 2024, *Bulletin de la Société Royale des Sciences de Liège*, **in press**

Rosu, S., Fellay, L., Rauw, G., & Dupret, M.-A., Apsidal motion in (massive) binaries. 2024, *special issue of the Central European Astrophysical Bulletin (CEAB)*, **in press**

Rosu, S., Noels, A., Dupret, M. A., et al., Apsidal motion in the massive binary HD 152248. Constraining the internal structure of the stars. 2020a, *A&A*, **642**, A221, DOI:10.1051/0004-6361/202038380

Rosu, S., Quintero, E. A., Rauw, G., & Eenens, P., New insight into the massive eccentric binary HD 165052: self-consistent orbital solution, apsidal motion, and fundamental parameters. 2023, *MNRAS*, **521**, 2988, DOI:10.1093/mnras/stad780

Rosu, S., Rauw, G., Conroy, K. E., et al., Apsidal motion in the massive binary HD 152248. 2020b, *A&A*, **635**, A145, DOI:10.1051/0004-6361/201937285

Rosu, S., Rauw, G., Farnir, M., Dupret, M. A., & Noels, A., Apsidal motion in massive eccentric binaries in NGC 6231. The case of HD 152219. 2022a, *A&A*, **660**, A120, DOI:10.1051/0004-6361/202141304

Rosu, S., Rauw, G., Nazé, Y., Gosset, E., & Sterken, C., Apsidal motion in massive eccentric binaries: The case of CPD-41° 7742, and HD 152218 revisited. 2022b, *A&A*, **664**, A98, DOI:10.1051/0004-6361/202243707

Scuflaire, R., Théado, S., Montalbán, J., et al., CLÉS, Code Liégeois d'Évolution Stellaire. 2008, *Ap&SS*, **316**, 83, DOI:10.1007/s10509-007-9650-1

Shakura, N. I., On the Apsidal Motion in Binary Stars. 1985, *Soviet Astronomy Letters*, **11**, 224

Sterne, T. E., Apsidal motion in binary stars. 1939, *MNRAS*, **99**, 451, DOI:10.1093/mnras/99.5.451

Zasche, P., Wolf, M., Kučáková, H., et al., First apsidal motion and light curve analysis of 162 eccentric eclipsing binaries from LMC. 2020, *A&A*, **640**, A33, DOI:10.1051/0004-6361/202037822

Contrib. Astron. Obs. Skalnaté Pleso **55/3**, 91 – 97, (2025)
https://doi.org/10.31577/caosp.2025.55.3.91

Distribution of cataclysmic variables in our Galaxy and their position in the HR diagram in the Gaia era

R. Canbay

Istanbul University, Institute of Graduate Studies in Science, Programme of Astronomy and Space Sciences, 34116, Istanbul, Türkiye
(E-mail: rmzycnby@gmail.com)

Received: November 6, 2024; Accepted: January 14, 2025

Abstract. In this study, the distances of stellar systems classified as cataclysmic variables in the literature were determined by using the distance compiled from the Bailer-Jones et al. (2021). The spatial distributions of cataclysmic variables in the heliocentric Galactic coordinate system are obtained and their positions in the Hertzsprung-Russell (HR) diagram constructed from Gaia colors are discussed.

Key words: Star: Cataclysmic binaries – Galaxy: Stellar dynamics and kinematics – Galaxy: Solar neighborhood

1. Introduction

Cataclysmic variables (CVs) are binary star systems consisting of a white dwarf (WD) as the primary component and a low-mass main-sequence star that fills its Roche lobe. Matter is transferred from the secondary to the primary through a gas stream and an accretion disk. In magnetic CVs, such as those in the polar (P) subgroup, the strong magnetic field of the WD completely prevents the formation of an accretion disk. Instead, material is channeled onto the WD through accretion columns and channels. In intermediate polars (IPs), the magnetic fields are weaker and insufficient to fully suppress the formation of an accretion disk, resulting in the formation of a disrupted, partial accretion disk influenced by the WD's magnetic field.

Townsley & Bildsten (2002) showed that the position of CVs on the Hertzsprung-Russell (HR) diagram (Hertzsprung, 1911; Russell, 1914) is determined by their evolutionary parameters, including the temperature of the WD , the mass of the donor star, and the luminosity of the accretion disk. However, due to the limited sample size of CVs and the inherent challenges in determining their distances, an analysis of their absolute magnitude distribution has not been possible until recently. With the advent of Gaia, this limitation has been overcome. Abril et al. (2020) found that the CVs obtained from Gaia DR2 are distinctly clustered according to their orbital periods, while also being dispersed

between the main sequence and WD regions of the HR diagram. The authors observed a relationship between orbital period, color, and absolute magnitude. This is, in fact, consistent with the expected behavior from the CV evolutionary model; as the orbital periods of evolved CVs shorten, the luminosity of the secondary star decreases, causing the WD and the accretion disk, which are already dominant, to become even more prominent. This applies to magnetic systems as well, though no disk structure is observed in those cases. Abrahams et al. (2022) used Gaia DR2 and EDR3 data to explore a new relationship between color ($G_{\rm BP} - -G_{\rm RP}$), absolute magnitude ($M_{\rm G}$), and orbital period ($P_{\rm orb}$), as well as to investigate the period gap and angular momentum loss mechanisms in cataclysmic variables.

2. Data and Analysis

Canbay et al. (2023) reported 4,149 systems with astrometric and photometric data in the Gaia DR3 data release and classified as CVs. The Gaia DR3 catalogue for CVs, including their equatorial coordinates $(\alpha, \delta)_{\rm J2000}$, their trigonometric parallaxes ($\overline{\omega}$) and Gaia magnitudes G, $G_{\rm BP}$, $G_{\rm RP}$, was obtained from Gaia Collaboration et al. (2023). Distances calculated using the Bailer-Jones et al. (2021) Bayesian method based on Gaia DR3 trigonometric parallaxes were also included in the catalog. Canbay et al. (2023) compared the distances ($d = 1000/\overline{\omega}$) of CVs calculated from Gaia's trigonometric parallaxes with the distances ($d_{\rm BJ}$) obtained by the Bailer-Jones et al. (2021) method with respect to the brightness G. The analysis showed that for systems with $G \leq 18.5$ mag, the scattering in the distance measurements is significantly smaller than for fainter systems. To minimize potential uncertainties in the distance estimates, the sample was restricted to $G \leq 18.5$ mag, resulting in the identification of 1,714 CV systems that satisfied this criterion. Starting with 1,714 CV systems, controls were performed based on the subtypes of the systems included in the analyses, and the system distances and brightness limits were updated. After excluding five systems as outliers, the analysis was carried out using a final sample of 1,709 systems.

Photometric data are affected by the interstellar medium. In this study, Schlafly & Finkbeiner (2011) dust map was utilized to correct the photometric data for absorptions and reddening. By inputting Galactic coordinates (l, b), the absorption value $A_\infty(V)$ in the V-band valid up to the Galactic boundary was obtained from the dust map. Given that the distances of the CVs are known, the absorption value between the Sun and the stellar system was calculated using the relation by Bahcall & Soneira (1980):

$$A_{\rm d}(V) = A_\infty(V)\left[1 - \exp\left(\frac{-\mid d \times \sin b \mid}{H}\right)\right], \tag{1}$$

In this equation, $d_{\rm BJ}$ represents the distances of the CVs as determined by Bailer-Jones et al. (2021), d denotes the Galactic latitude of the system, H is the dust scale height, and $A_{\rm d}(V)$ is the reduced absorption value. For this study, the dust scale height was adopted as H=125pc (Marshall et al., 2006). The reduced color excess of the systems was determined using the relation $E_{\rm d}(B-V) = A_{\rm d}(V)/3.1$. The total absorptions in G, $G_{\rm BP}$, and $G_{\rm RP}$ bands were obtained by using relations given as follows:

$$\begin{aligned} A(G) &= 0.83627 \times 3.1E_{\rm d}(B-V), \\ A(G_{\rm BP}) &= 1.08337 \times 3.1E_{\rm d}(B-V), \\ A(G_{\rm RP}) &= 0.63439 \times 3.1E_{\rm d}(B-V). \end{aligned} \tag{2}$$

The selective absorption coefficients in Equation (2) were taken from Cardelli et al. (1989). Using these coefficients, the total extinction values were determined, allowing for the calculation of de-reddened apparent magnitudes in the G, BP and RP-bands, denoted as G_0, $G_{\rm BP}$ and $G_{\rm RP}$, respectively. The absolute magnitudes $M_{\rm G}$ of CVs were calculated using the distance modulus formula $G_0 - M_{\rm G} = 5 \times \log(d_{\rm BJ}) - 5$, where $d_{\rm BJ}$ is the distance obtained from Bailer-Jones et al. (2021).

3. Results

The distribution of CVs, categorized into subgroups within the heliocentric rectangular Galactic coordinate system, is presented in Figure 1, with the corresponding results provided in Table 1.

The spatial distribution of the CVs used in this study reveals a concentration towards the galactic center. It displays trends similar to the Galactic coordinate distributions (X, Y, Z) reported by Canbay et al. (2023). For the 1,587 CVs in the study, the median values of d and (X, Y, Z) are 989 and (80, 93,-18) pc, respectively. These values are consistent with the median values found in the 1,709 sample analyzed in the study. The overall trends are consistent, with both studies showing a concentration of all CVs toward the Galactic center. Figure 2 shows their distribution based on absolute brightness $M_{\rm G}$ and $(G_{\rm BP} - G_{\rm RP})_0$ colors.

Considering the HR diagram obtained for CVs under the study, a focus on classifying them according to their components reveals a boundary separating WDs from main sequence stars, as identified by Gentile Fusillo et al. (2019). Furthermore, the study by Gaia Collaboration et al. (2019) analyzed the color-magnitude diagrams of variable stars, illustrating the distribution of subtypes, including Z Andromedae (Z And), U Geminorum (U Gem), and CVs. When applying this boundary to our dataset, it is observed that CVs are distributed across both the WD region, dominated by WDs, and the Z And region, dominated by giant components. Objects situated between these two regions are

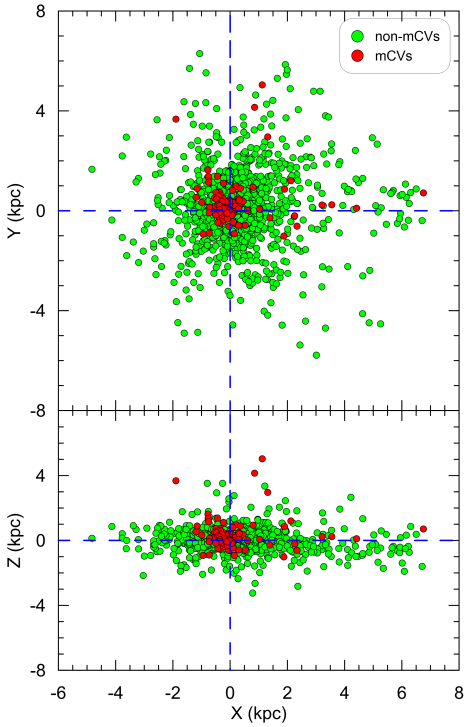


Figure 1. The spatial distribution of CVs with respect to the Sun. X, Y and Z are heliocentric rectangular galactic coordinates

Table 1. The median distances ($\tilde{d}$) and heliocentric rectangular Galactic coordinates ($\tilde{X}$, $\tilde{Y}$, $\tilde{Z}$) of CVs in the sample. Values are separately listed for All CVs, non-magnetic (non-mCVs) and magnetic (mCVs) systems. N denotes the number of objects.

Group	N	$\tilde{d}$ (pc)	$\tilde{X}$ (pc)	$\tilde{Y}$ (pc)	$\tilde{Z}$ (pc)
All CVs	1709	956	74	76	-11
non-mCVs	1577	1003	92	93	-13
mCVs	132	578	-54	-4	19

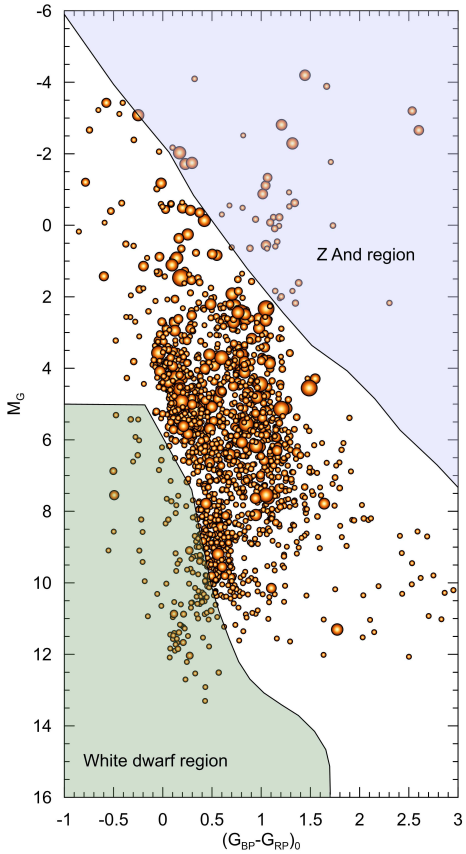


Figure 2. Distribution of known CVs in the HR diagram of Gaia DR3 data. The size of each point represents the relative parallax errors σ_ω/ω value of the all CVs.

inferred to exhibit a dominance of main sequence components (Figure 2). However, as shown in Figure 2, the majority of CVs are located in the main sequence (MS) region, suggesting that MS components are generally more prevalent. This finding aligns with the conventional definition of CVs, which consist of a WD and a low-mass MS star. Both components contribute significantly to the luminosity and color index of the system. Consequently, the observed colors and absolute magnitudes reflect the binary system as a whole, rather than the characteristics of each component individually. While the smaller, hotter WD dominates the luminosity at certain wavelengths, particularly in the ultraviolet, the MS star makes a substantial contribution to the system's luminosity at optical wavelengths. Therefore, the classification and interpretation of CVs within the HR diagram should account for the combined properties of the binary system, rather

than isolating the contributions of each component.

Abril et al. (2020) demonstrated that the distribution of CVs in the HR diagram forms distinct clusters corresponding to different stages of evolution. Their analysis revealed a trend where CVs with shorter orbital periods are fainter and exhibit bluer colors, a characteristic primarily influenced by the white dwarf's luminosity and the declining contribution from the donor star. These clusters align with standard evolutionary models of CVs. Abrahams et al. (2022) eidentified a relationship between the $(G_{\mathrm{BP}} - G_{\mathrm{RP}})$ color index, absolute magnitude , and orbital period . Their findings indicated that non-magnetic CVs adhere to a predictable pattern consistent with angular momentum loss mechanisms driving their evolution. Moreover, these studies underscore the significant influence of the accretion disk on the overall luminosity and color of CV systems. Our findings are consistent with these trends, as evidenced by the clustering of CVs in our HR diagram between the main sequence and white dwarf regions. When compared with the results of Abril et al. (2020) and Abrahams et al. (2022), our data corroborate the observed color and magnitude transitions driven by orbital period. The accretion disk significantly influences the luminosity and color index of CV systems. In non-magnetic CVs, the accretion disk's luminosity can overshadow the contributions of the white dwarf and secondary star, especially during high accretion states. Conversely, in magnetic CVs such as polars, the absence of a disk results in a lower overall luminosity, with the primary contributions coming from the white dwarf and accretion columns. A subset of CVs in our sample appears to exhibit luminosities characteristic of giant stars. This apparent discrepancy may arise from several factors; Misclassification: The observational blending of CVs with background or nearby giant stars could artificially inflate their luminosity measurements. Spectroscopic confirmation is essential to disentangle such cases. Physical Activity: In some CVs, the secondary star might exhibit enhanced activity, such as magnetic cycles or starspots, that temporarily boost the system's brightness. Additionally, high accretion rates or transient outbursts could contribute to the observed luminosity. Further spectroscopic and photometric investigations are essential to determine whether these systems are truly misclassified or if their elevated luminosities result from intrinsic activity. Refining these classifications will enhance our understanding of CV evolution and their distribution within the HR diagram.

Acknowledgements. This work has been supported in part by the Scientific and Technological Research Council of Türkiye (TÜBİTAK) 119F072. This work has been supported in part by Istanbul University: Project number NAP-33768.

References

Abrahams, E. S., Bloom, J. S., Szkody, P., Rix, H.-W., & Mowlavi, N., Informing the Cataclysmic Variable Sequence from Gaia Data: The Orbital-period-Color-

Absolute-magnitude Relationship. 2022, *Astrophysical Journal*, **938**, 46, DOI:10.3847/1538-4357/ac87ab

Abril, J., Schmidtobreick, L., Ederoclite, A., & López-Sanjuan, C., Disentangling cataclysmic variables in Gaia's HR diagram. 2020, *Monthly Notices of the RAS*, **492**, L40, DOI:10.1093/mnrasl/slz181

Bahcall, J. N. & Soneira, R. M., The universe at faint magnitudes. I. Models for the Galaxy and the predicted star counts. 1980, *Astrophysical Journal, Supplement*, **44**, 73, DOI:10.1086/190685

Bailer-Jones, C. A. L., Rybizki, J., Fouesneau, M., Demleitner, M., & Andrae, R., Estimating Distances from Parallaxes. V. Geometric and Photogeometric Distances to 1.47 Billion Stars in Gaia Early Data Release 3. 2021, *Astronomical Journal*, **161**, 147, DOI:10.3847/1538-3881/abd806

Canbay, R., Bilir, S., Özdönmez, A., & Ak, T., Galactic Model Parameters and Spatial Density of Cataclysmic Variables in the Gaia Era: New Constraints on Population Models. 2023, *Astronomical Journal*, **165**, 163, DOI:10.3847/1538-3881/acbead

Cardelli, J. A., Clayton, G. C., & Mathis, J. S., The relationship between IR, optical, and UV extinction. 1989, in IAU Symposium, Vol. **135**, *Interstellar Dust*, ed. L. J. Allamandola & A. G. G. M. Tielens, 5–10

Gaia Collaboration, Eyer, L., Rimoldini, L., et al., Gaia Data Release 2. Variable stars in the colour-absolute magnitude diagram. 2019, *Astronomy and Astrophysics*, **623**, A110, DOI:10.1051/0004-6361/201833304

Gaia Collaboration, Vallenari, A., Brown, A. G. A., et al., Gaia Data Release 3. Summary of the content and survey properties. 2023, *Astronomy and Astrophysics*, **674**, A1, DOI:10.1051/0004-6361/202243940

Gentile Fusillo, N. P., Tremblay, P.-E., Gänsicke, B. T., et al., A Gaia Data Release 2 catalogue of white dwarfs and a comparison with SDSS. 2019, *Monthly Notices of the RAS*, **482**, 4570, DOI:10.1093/mnras/sty3016

Hertzsprung, E., Ueber die Verwendung photographischer effektiver Wellenlaengen zur Bestimmung von Farbenaequivalenten. 1911, *Publikationen des Astrophysikalischen Observatoriums zu Potsdam*, **63**

Marshall, D. J., Robin, A. C., Reylé, C., Schultheis, M., & Picaud, S., Modelling the Galactic interstellar extinction distribution in three dimensions. 2006, *Astronomy and Astrophysics*, **453**, 635, DOI:10.1051/0004-6361:20053842

Russell, H. N., Relations Between the Spectra and Other Characteristics of the Stars. 1914, *Popular Astronomy*, **22**, 331

Schlafly, E. F. & Finkbeiner, D. P., Measuring Reddening with Sloan Digital Sky Survey Stellar Spectra and Recalibrating SFD. 2011, *Astrophysical Journal*, **737**, 103, DOI:10.1088/0004-637X/737/2/103

Townsley, D. M. & Bildsten, L., Faint Cataclysmic Variables in Quiescence: Globular Cluster and Field Surveys. 2002, *Astrophysical Journal, Letters*, **565**, L35, DOI:10.1086/339052

Contrib. Astron. Obs. Skalnaté Pleso **55/3**, 98 – 102, (2025)
https://doi.org/10.31577/caosp.2025.55.3.98

Insights from mid-infrared interferometric observations of the symbiotic nova RS Ophiuchi

F. Kaczmarek[1], M. Otulakowska-Hypka[1], F. Millour[2], N. Nardetto[2], C. Paladini[3], A. Mérand[4], C.A. Hummel[4], J. Mikołajewska[5], B. Lopez[2], F. Patat[4], M. Wittkowski[4], A. Meilland[2] and A. Domiciano de Souza[2]

[1] *Astronomical Observatory Institute, Faculty of Physics and Astronomy, Adam Mickiewicz University, Słoneczna 36, PL-60-286 Poznań, Poland*

[2] *Université Côte d'Azur, Observatoire de la Côte d'Azur, CNRS, Laboratoire Lagrange, 06304 Nice Cedex 4, France*

[3] *European Southern Observatory, Alonso de Córdova 3107, Vitacura, Santiago, Chile*

[4] *European Southern Observatory, Karl-Schwarzschild-Str. 2, 85748 Garching bei München, Germany*

[5] *Nicolaus Copernicus Astronomical Center, Polish Academy of Sciences, Bartycka 18, 00716 Warsaw, Poland*

Received: November 15, 2024; Accepted: February 7, 2025

Abstract. RS Oph is one of the best studied recurrent novae, with its last outburst in 2021 triggering an extensive observational campaign across the whole electromagnetic spectrum, which led to the accumulation of an impressive amount of data. Here, we present the preliminary results of our analysis of interferometric data, which allowed us to provide insights into the structure and kinematics of the expanding nova shell.

Key words: optical interferometry – symbiotic novae – cataclysmic variables

1. Introduction

The stellar components of the RS Oph symbiotic binary system are a M2III red giant (Zamanov et al., 2018) and a massive, carbon-oxygen white dwarf ($M_{WD} = 1.2{-}1.4\,M_{\odot}$), with the system having an orbital period of 453.6 days (Brandi et al., 2009). Due to the high mass of the white dwarf, close to the Chandrasekhar limit, RS Oph is considered one of the most likely candidates to eventually explode in a type Ia supernova event (Mikołajewska & Shara, 2017). Historically, RS Oph has experienced seven recorded outbursts, with the most recent occurring in 2021. Additionally, a review of archival data by Schaefer (2010) suggests the possibility of two previously undocumented outbursts.

In this poster, we present the results of our analysis of spectro-interferometric data gathered using the VLTI/MATISSE instrument (Lopez et al., 2022) at

two different epochs: 5.5 days and 24.5 days post-outburst. These observations were conducted across three mid-infrared (MIR) bands: L (2.8−4.2 μm), M (4.5−5.0 μm), and N (8.0−13.0 μm). However, after reducing and calibrating the data, only the L-band data proved to be of sufficient quality to be included in the subsequent analysis.

2. Methodology

1. Initially, we created single-component models for RS Oph, one for each emission component (L-band continuum, as well as Pfδ 3.30 μm, Pfγ 3.74 μm, and Brα 4.05 μm lines). To achieve this, we utilized the LITpro modelling software (Tallon-Bosc et al., 2008). We employed elongated uniform disks and elongated Gaussian ellipses to fit visibilities of the continuum and the individual lines. With the position of each component fixed at (0, 0) and the total flux normalized to 1, the only adjustable parameters were the position angle of the major axis, the elongation ratio, and, depending on the model used, the minor axis diameter or FWHM.

2. The single-component models were centro-symmetric, meaning that the closure phase of these models was equal to zero - a reasonable assumption for the continuum and the Pfδ and Pfγ lines, given that their closure phases did not significantly deviate from zero. However, these models cannot be used for the Brα line-component, as the shape of its closure phase curve indicated a departure from centro-symmetry. This observation led us to adopt a two-component model for the Brα line-component. This approach involved simultaneously fitting geometric models to the visibilities of the continuum- and Brα line-forming regions. The parameters previously determined for the continuum in the single-component modelling were kept fixed, as was the component's position at (0, 0). However, the parameters for the Brα line-forming region, including the major axis position angle, elongation ratio, minor axis diameter/FWHM, and the component's position relative to the continuum, were allowed to vary freely. The results of two-component modelling are presented on Fig. 1.

3. Modelling results

1. The closure phase values for the continuum-, Pfδ- and Pfγ-forming regions are close to zero, suggesting that these components are centro-symmetric. In contrast, the region associated with the emission of the Brα line shows a clear deviation from centro-symmetry.

2. In the models obtained for the 1st epoch, the continuum-forming region has a position angle of 160°±2°, similar to the Pfδ- and Pfγ-forming regions (158°±4° and 151°±6°, respectively). These observations track ma-

terial ejected in the event of the nova outburst, which is expanding in the orbital plane of the binary system.

3. The position angle of the Brα line-forming region, determined from the two-component modelling of data from the 1st epoch, is 132°±8° - a difference of $\sim 30°$ compared to the continuum-forming region. Such a difference suggests that this component tracks bipolar ejection within the system.

4. The position angle of all emission components from the 2nd epoch observations is 170°−180°. After 24.5 days since the nova outburst, only the emission of material expanding in the orbital plane of RS Oph remains detectable in these data.

5. Model fits for the 2nd epoch demonstrate a significant size increase in the case of all components (they are ∼2−3 times larger compared to models obtained for the 1st epoch), indicating the expansion of the envelope following the nova outburst.

Our findings demonstrate that the structure of an expanding material is more complex than a simple model of spherical ejection. Indeed, similar conclusions emerge from the analysis of observational data collected during the last two outbursts of RS Oph. Near-infrared observations conducted only 5.5 days after detection of 2006 outburst by VLTI/AMBER interferometer revealed ring-like structure expanding with velocity of $v_{\rm rad} \sim 1800\,{\rm km\,s^{-1}}$ and faster ($v_{\rm rad} \sim 2500 - 3000\,{\rm km\,s^{-1}}$) structure expanding in the East-West direction (Chesneau et al., 2007). The similar structure, now understood as an expanding bipolar outflow, can also be seen at radio (e.g., O'Brien et al. 2006; Sokoloski et al. 2008; Rupen et al. 2008; Munari et al. 2022) and X-ray wavelengths (Montez et al., 2022). The asymmetric geometry of ejected material can be traced as early as only 2 days after the outbursts, as evident from spectro-polarimetric observations of Nikolov et al. (2023).

We note that in our contribution we summarise the preliminary findings from the analysis of MATISSE data, and a thorough investigation of the velocity distribution of the expanding nova ejecta is beyond the scope of this paper. It will, however, constitute a part of a more comprehensive analysis of MIR interferometric data of RS Oph and the results of which will be presented soon (Kaczmarek et al., in prep.).

Acknowledgements. Based on observations collected at the European Southern Observatory under ESO programme 107.22UL.005. This research has made use of the Jean-Marie Mariotti Center `LITpro` service co-developed by CRAL, IPAG and LAGRANGE. This research was supported by the Polish National Science Centre grant 2019/32/C/ST9/00577 and the "Excellence Initiative - Research University" program (ID-UB) at A. Mickiewicz University in Poznań, Poland.

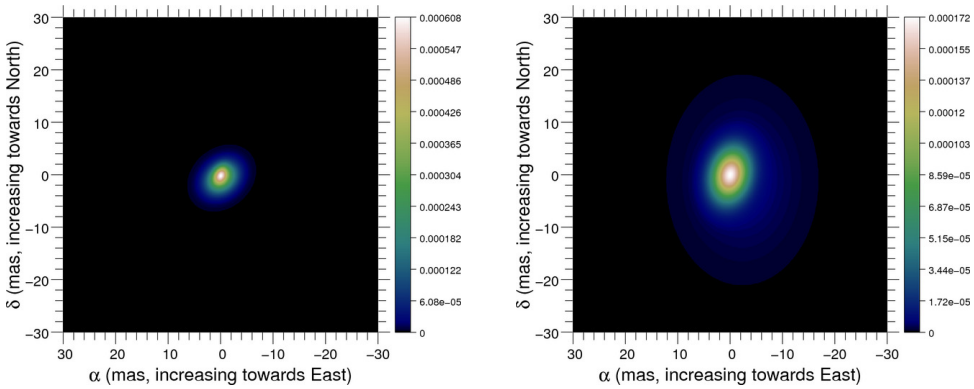


Figure 1. Geometry of the continuum- and Brα line-emitting regions derived from two-component modelling of 2021 outburst of RS Oph. The model used is an elongated Gaussian ellipse. The left panel shows results obtained for 1st epoch, while the right panel - for 2nd epoch.

References

Brandi, E., Quiroga, C., Mikołajewska, J., Ferrer, O. E., & García, L. G., Spectroscopic orbits and variations of RS Ophiuchi. 2009, *Astronomy and Astrophysics*, **497**, 815, DOI:10.1051/0004-6361/200811417

Chesneau, O., Nardetto, N., Millour, F., et al., AMBER/VLTI interferometric observations of the recurrent Nova RS Ophiuchii 5.5 days after outburst. 2007, *Astronomy and Astrophysics*, **464**, 119, DOI:10.1051/0004-6361:20066609

Lopez, B., Lagarde, S., Petrov, R. G., et al., MATISSE, the VLTI mid-infrared imaging spectro-interferometer. 2022, *Astronomy and Astrophysics*, **659**, A192, DOI:10.1051/0004-6361/202141785

Mikołajewska, J. & Shara, M. M., The Massive CO White Dwarf in the Symbiotic Recurrent Nova RS Ophiuchi. 2017, *Astrophysical Journal*, **847**, 99, DOI:10.3847/1538-4357/aa87b6

Montez, R., Luna, G. J. M., Mukai, K., Sokoloski, J. L., & Kastner, J. H., Expanding Bipolar X-Ray Structure After the 2006 Eruption of RS Oph. 2022, *Astrophysical Journal*, **926**, 100, DOI:10.3847/1538-4357/ac4583

Munari, U., Giroletti, M., Marcote, B., et al., Radio interferometric imaging of RS Oph bipolar ejecta for the 2021 nova outburst. 2022, *Astronomy and Astrophysics*, **666**, L6, DOI:10.1051/0004-6361/202244821

Nikolov, Y., Luna, G. J. M., Stoyanov, K. A., et al., Transient and asymmetric dust structures in the TeV-bright nova RS Oph revealed by spectropolarimetry. 2023, *Astronomy and Astrophysics*, **679**, A150, DOI:10.1051/0004-6361/202346997

O'Brien, T. J., Bode, M. F., Porcas, R. W., et al., An asymmetric shock wave in the 2006 outburst of the recurrent nova RS Ophiuchi. 2006, *Nature*, **442**, 279, DOI: 10.1038/nature04949

Rupen, M. P., Mioduszewski, A. J., & Sokoloski, J. L., An Expanding Shell and Synchrotron Jet in RS Ophiuchi. 2008, *Astrophysical Journal*, **688**, 559, DOI: 10.1086/525555

Schaefer, B. E., Comprehensive Photometric Histories of All Known Galactic Recurrent Novae. 2010, *Astrophys. J., Suppl. Ser.*, **187**, 275, DOI:10.1088/0067-0049/187/2/275

Sokoloski, J. L., Rupen, M. P., & Mioduszewski, A. J., Uncovering the Nature of Nova Jets: A Radio Image of Highly Collimated Outflows from RS Ophiuchi. 2008, *Astrophysical Journal, Letters*, **685**, L137, DOI:10.1086/592602

Tallon-Bosc, I., Tallon, M., Thiébaut, E., et al., LITpro: a model fitting software for optical interferometry. 2008, in Society of Photo-Optical Instrumentation Engineers (SPIE) Conference Series, Vol. **7013**, *Optical and Infrared Interferometry*, ed. M. Schöller, W. C. Danchi, & F. Delplancke, 70131J

Zamanov, R. K., Boeva, S., Latev, G. Y., et al., The recurrent nova RS Oph: simultaneous B- and V- band observationsof the flickering variability. 2018, *Monthly Notices of the RAS*, **480**, 1363, DOI:10.1093/mnras/sty1816

Contrib. Astron. Obs. Skalnaté Pleso **55/3**, 103 – 107, (2025)
https://doi.org/10.31577/caosp.2025.55.3.103

ER UMa: a dwarf nova that continues to amaze

E.P. Pavlenko[1], K.A. Antonyuk[1], S.Yu. Shugarov[2,3], O.I. Antonyuk[1] and N.V. Pit[1]

[1] *Crimean astrophysical observatory of RAS, Crimea (E-mail: eppavlenko@gmail.com)*

[2] *Astronomical Institute of the Slovak Academy of Sciences 059 60 Tatranská Lomnica, The Slovak Republic*

[3] *Sternberg Astronomical Institute, MSU, 119234 Moscow, Russia*

Received: December 2, 2024; Accepted: January 28, 2025

Abstract. ER UMa is a well known SU UMa-type dwarf nova with a number of outstanding properties. It is the prototype of a small group of dwarf novae with a high frequency of superoutbursts and a short orbital period. Our multicolor $BVRcIc$ investigation of ER UMa carried out at the Crimean astrophysical observatory in 2020 showed that in some occasions ER UMa may be a "bridge" between the subclasses of ER UMa-type stars and nova-like ones.

Key words: dwarf novae – superhumps – photometry

1. Introduction

ER UMa was identified as a cataclysmic variable in 1986 (Green et al., 1986). In 1992 this object was classified as a dwarf nova by Kato & Kunjaya (1995). For the first time, ER UMa was found to have superhumps with a period of 0.06549-0.06573 days (Kato et al., 2003), which is an attribute of SU UMa-type dwarf novae. Soon this object became a prototype of a special small group of ER UMa dwarf novae with a short interval between neighboring super-outbursts (super-cycle) of 19-50 days and a short (3-4 days) interval between neighboring normal outbursts (cycle) (Kato & Kunjaya, 1995). From a theoretical point of view, Osaki (1995) suggested that such a short cycle requires an unusually high mass transfer rate within the disk instability theory, which is not described by the theory of standard evolution of compact binaries. Thorstensen & Taylor (1997) found the orbital period of ER UMa equal to 0.06366 days and concluded that the orbital inclination is low. Gao et al. (1999) and Kjurkchieva & Marchev (2010) were first to observe negative superhumps during rise of an superoutburst and during a quiescence, respectively. Ohshima et al. (2012) were first to detect negative superhumps during the 2011 superoutburst, which had not been previously observed not only in ER UMa but also in SU UMa-type dwarf novae in general. Next, Ohshima et al. (2012), Zemko et al. (2013, 2014) found a correlation between the frequency of normal outbursts and the appearance and disappearance of negative superhumps, thereby confirming the theoretical

prediction (Osaki & Kato, 2013) that the appearance of negative superhumps, triggered by the tilt of the accretion disk, should entail a decrease in the frequency of normal outbursts, since in this case it will take more time for enough matter to accumulate in the disk to trigger thermal instability.

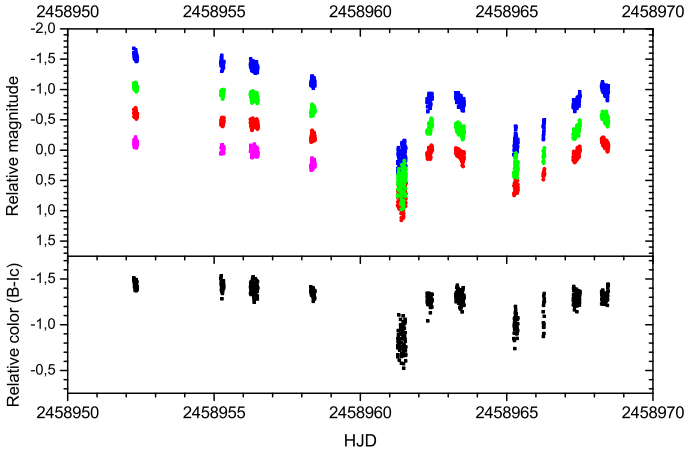


Figure 1. Top: Long-term light curve of ER UMa. The data is shown in blue (B), green (V), red (Rc) and magenta (Ic). Bottom: Color-indice $B - Ic$.

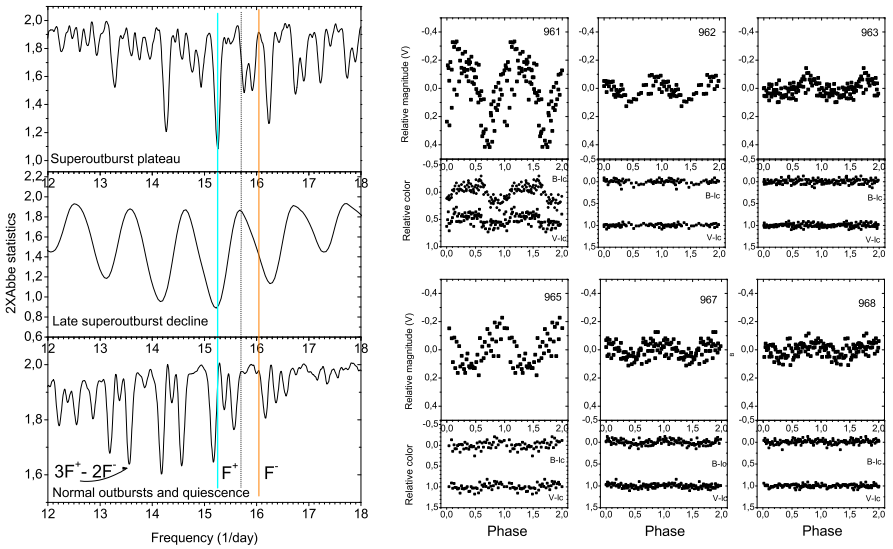
2. Observations and Result

We have undertaken a $BVRcIc$ study of ER UMa to determine the behavioral features of the object in one of the 2020 supercycles. Our observations have been carried out at the 1.25-m telescope of the Crimean astrophysical observatory with CCD ProLine PL23042 during 11 nights. Observations covered part of the superoutburst, two normal outbursts and quiescence in between (see Fig 1). The object became bluer in the outbursts and redder in the minimum. ER UMa displayed a short-term light variations both during the superoutburst, normal outbursts and quiescence in between. We calculated periodograms for three nights of the superoutburst plateau, two nights of the late superoutburst decline and quiescence + normal outbursts using method of Stellingwerf (1978), Pel'T (1980). The result is shown in the Fig 2a.

One could see that there are no clear evidences both of orbital and negative superhump period. However the positive superhumps with period of 0.0656 d (F=15.26), 0.0657 d (F=15.23) and P=0.0659 d (F=15.17) and their one-day aliases were registered along all stages of superoutburst and in quiescence including normal outbursts. A combination of frequencies that practically coincides with the frequency $3F(+) - 2F(-)$, where $F(+)$ and F(-) are frequences of positive and negative superhumps respectively and their daily aliases are also present at the stage "quiescence + normal outbursts".

The selected data of quiescence and normal outbursts folded on the period 0.0659 d is presented in the Fig 2b. A strange detail draws attention: a strong increase in the amplitude of brightness variations at the end of superoutburst (JD ...961) up to $0^m.4$. The possible explanation could be the appearance of another temporary source of variatons – "impulsive" or "faded" negative superhumps, which can affect the positive superhumps, increasing or decreasing the amplitude.

There are also no prominent variations of color-indices $B-Ic$ and $V-Ic$ for all curves with exception for JD . . . 961, . . . 965 and . . . 967. The object is bluest close to maximum light. Note that similar color indices of positive superhumps (blue at the phase of the superhump maximum on some nights and constant at all phases on others) were also recorded for RZ LMi by Shugarov et al. (2018).



a) b)

Figure 2. a) Periodograms for different states of ER UMa. The position of the frequencies of the positive ($F+$) and negative (F-) superhumps taken from (Kato et al., 2003) and (Ohshima et al., 2012) respectively is marked with a blue and orange line respectively, and those of the orbital period is shown by a black dotted line.
b) Examples of phased light curves folded with 0.0659d period and their color-indices for the data in normal outbursts and quiescence. For each curve the last three digits of the Julian date are given.

3. Discussion

The presence of positive superhumps in the quiescent state and normal outbursts was an unexpected effect. This means that the accretion disk in the ER UMa

continued to be in a state of thermal and tidal instability after the end of the superoutburst, similar to some nova-like stars. Kato et al. (2016) found that another ER UMa-type dwarf nova with an anomalously short supercycle, RZ LMi, can behave as a nova-like in some seasons, i.e., exhibit positive superhumps throughout the supercycle. Since this behavior was transient, Kato named the star "RZ Leonis Minoris Bridging between ER Ursae Majoris-Type Dwarf Nova and Novalike System". It is worth recalling that in the early stages of studying RZ LMi, the possible belonging of this system to the UX UMa-type nova-likes was suggested by Ringwald (1993), and to the VY Scl-type nova-likes by Pikalova & Shugarov (1995).

4. Conclusion

According to our observations, ER UMa in one of the 2020 supercycle showed positive superhumps during superoutburst and complex signal at "quiescence + normal outbursts" state. This signal consists of a dominant one - positive superhumps and possibly temporary one - negative superhumps. The evidence of positive superhumps of ER UMa found during all phases of one of the 2020 supercycle gives reason to suspect that this dwarf nova, like RZ LMi, in some occasions may be a bridge between the subclasses of ER UMa-type stars and nova-like ones.

Acknowledgements. SS is grateful for financial support from grants APVV-20-0148, VEGA 2/0030/21 and VEGA 2/0031/22.

References

Gao, W., Li, Z., Wu, X., Zhang, Z., & Li, Y., Superhumps in a Peculiar SU Ursae Majoris-Type Dwarf Nova, ER Ursae Majoris. 1999, *Astrophysical Journal, Letters*, **527**, L55, DOI:10.1086/312398

Green, R. F., Schmidt, M., & Liebert, J., The Palomar-Green Catalog of Ultraviolet-Excess Stellar Objects. 1986, *Astrophysical Journal, Supplement*, **61**, 305, DOI:10.1086/191115

Kato, T., Ishioka, R., Isogai, K., et al., RZ Leonis Minoris bridging between ER Ursae Majoris-type dwarf nova and nova-like system. 2016, *Publications of the ASJ*, **68**, 107, DOI:10.1093/pasj/psw101

Kato, T. & Kunjaya, C., Discovery of a Peculiar SU UMa-Type Dwarf Nova ER Ursae Majoris. 1995, *Publications of the ASJ*, **47**, 163

Kato, T., Nogami, D., & Masuda, S., Unusual Phase Reversal of Superhumps in ER Ursae Majoris. 2003, *Publications of the ASJ*, **55**, L7, DOI:10.1093/pasj/55.2.L7

Kjurkchieva, D. & Marchev, D., Large-Amplitude Modulations of the Cataclysmic Star ER UMa. 2010, *Publications de l'Observatoire Astronomique de Beograd*, **90**, 147

Ohshima, T., Kato, T., Pavlenko, E. P., et al., Discovery of Negative Superhumps during a Superoutburst of 2011 January in ER Ursae Majoris. 2012, *Publications of the ASJ*, **64**, L3, DOI:10.1093/pasj/64.4.L3

Osaki, Y., A Model for a Peculiar SU Ursae Majoris-Type Dwarf Nova ER Ursae Majoris. 1995, *Publications of the ASJ*, **47**, L11

Osaki, Y. & Kato, T., The Cause of the Superoutburst in SU UMa Stars is Finally Revealed by Kepler Light Curve of V1504 Cygni. 2013, *Publications of the ASJ*, **65**, 50, DOI:10.1093/pasj/65.3.50

Pel'T, Y. 1980, *Frequency analysis of astronomical time series.*

Pikalova, O. D. & Shugarov, S. Y., The Photometric Investigation of RZ LMi. 1995, in Astrophysics and Space Science Library, Vol. **205**, *Cataclysmic Variables*, ed. A. Bianchini, M. della Valle, & M. Orio, 173–173

Ringwald, F. A., The Cataclysmic Variables from the Palomar-Green Survey. 1993, *Publications of the ASP*, **105**, 805, DOI:10.1086/133235

Shugarov, S. Y., Katysheva, N. A., Chochol, D., Krushevska, V. N., & Vozyakova, O. V., Superhump and outburst activity of the cataclysmic variable RZ LMi in the U- and optical passbands. 2018, *Astrophysics and Space Science*, **363**, 100, DOI:10.1007/s10509-018-3299-9

Stellingwerf, R. F., Period determination using phase dispersion minimization. 1978, *Astrophysical Journal*, **224**, 953, DOI:10.1086/156444

Thorstensen, J. R. & Taylor, C. J., Orbital Periods for the Interesting Old Novae V446 HER and V533 HER. 1997, in American Astronomical Society Meeting Abstracts, Vol. **191**, *American Astronomical Society Meeting Abstracts*, 109.04

Zemko, P., Kato, T., & Shugarov, S. Y., Detection of Change in Supercycles in ER Ursae Majoris. 2013, *Publications of the ASJ*, **65**, 54, DOI:10.1093/pasj/65.3.54

Zemko, P., Shugarov, S., Kato, T., & Katysheva, N., Study of a long and short—term variability of ER Ursae Majoris. 2014, *Contributions of the Astronomical Observatory Skalnate Pleso*, **43**, 319

Contrib. Astron. Obs. Skalnaté Pleso **55/3**, 108 – 111, (2025)
https://doi.org/10.31577/caosp.2025.55.3.108

Long term *UBVRI* photometric and spectral monitoring of nova KT Eri during 2009-2023

S.Yu. Shugarov[1,2], **P.Yu. Golysheva**[2], **S. Dallaporta**[3] **and U. Munari**[4]

[1] *Astronomical Institute of the Slovak Academy of Sciences*
059 60 Tatranská Lomnica, The Slovak Republic(E-mail: shugarov@ta3.sk)
[2] *Sternberg Astronomical Institute, MSU, 119234 Moscow, Russia*
[3] *ANS Collaboration, c/o Asronomical Observatory, 36012 Asiago (VI), Italy*
[4] *INAF Padova, 36012 Asiago (VI), Italy*

Received: November 20, 2024; Accepted: January 9, 2025

Abstract. We present a status report of our intensive and long-term *UBVRI* photometric monitoring of nova KT Eri since its outburst in 2009. The old-nova in quiescence is characterized by very high excitation conditions (HeII 4686 being constantly the strongest emission line in optical spectra) and a complex-pattern photometric variability of one mag amplitude in which multi-periodicities (from hours to years) are mixed with chaotic activity of similar amplitude. Mean color and brightness levels are the same for pre- and post-outburst quiescence.

Key words: nova – spectrum – outburst – color variations

1. The discovery and observations of KT Eri

KT Eri was discovered by K. Itagaki on 2009 November 25.536 UT at 8.1 mag, already on a fast (t_2=6.6 days) decline from maximum brightness reached on November 14.67 UT at unfiltered 5.4 mag (Hounsell et al., 2010). Although several properties of KT Eri suggest it could be a recurrent nova, searches for previous outbursts proved (so far) unfruitful (Jurdana-Šepić et al., 2012; Schaefer et al., 2022).

In January 2010 we begun an intensive *UBVRI* photometric monitoring of KT Eri, with a broad assortment of 18–125cm telescopes located in Slovak Republic, Crimea, and Italy. All the photometry has been calibrated against the same photometric sequence presented in Tab. 1 and Fig.1, which has been carefully tighted to the Landolt's system of equatorial standards (Landolt, 2009). Our color- and light-curves of KT Eri over 2009-2023 are shown in Fig. 2.

We are also keeping KT Eri under spectroscopic monitoring with the Asiago 1.22m + B&C in low-resolution and absolute flux modes. The mean post-outburst spectrum of KT Eri relative to the 2012–2020 period is presented in Fig. 3, with little changes present among different observing epochs. The very high excitation conditions affecting KT Eri are really apparent by HeII 4686 Å being costantly the strongest emission line of the whole optical range.

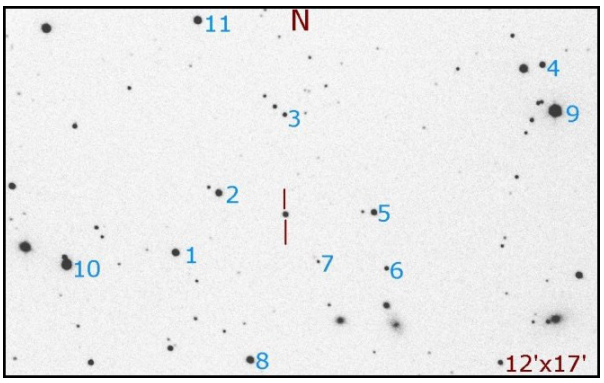


Figure 1. Identification of our photometric comparison sequence around KT Eri.

Table 1. Magnitudes and colors of the photometric comparison sequence in Fig.1.

star	V	U-B	B-V	V-R_C	R_C-I_C	star	V	U-B	B-V	V-R_C	R_C-I_C
1	12.820	0.81	0.998	0.575	0.503	7	16.345	0.01	0.565	0.370	0.334
2	13.267	1.10	1.256	0.816	0.644	8	12.694	0.88	0.981	0.571	0.488
3	15.197	-0.01	0.540	0.386	0.388	9	10.172	0.07	0.540	0.37	0.31
4	13.844	0.41	0.740	0.454	0.381	10	11.561	0.09	0.55	0.32	0.34
5	13.719	0.93	0.981	0.562	0.474	11	12.420	0.31	0.590	0.387	0.336
6	15.099	-0.07	0.540	0.361	0.339						

2. Results

Our color- and light-curves of KT Eri are presented in Fig. 2. The decline time from 2009 maximum is derived to be t_3=13 days, confirming the classification

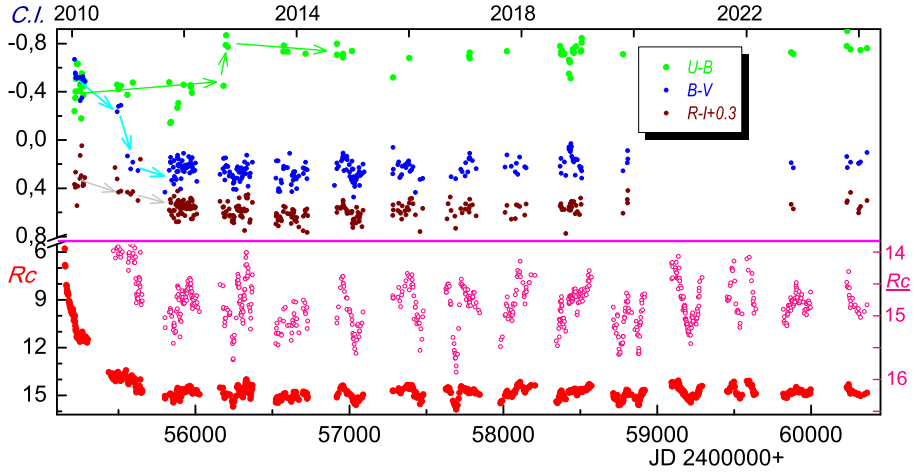


Figure 2. The overall light curve of KT Eri in R (lower panel) and color indices (upper panel) during the outburst and in quiescence. For a better visualization, the R-band lightcurve of the lower panel is plotted on both full and expanded scales (cf. ordinates on the left and right axes).

as a fast nova. KT Eri returned quickly to quiescence, leveling off at the same R=15.3 mag characterizing its pre-outburst brightness on Palomar plates. The

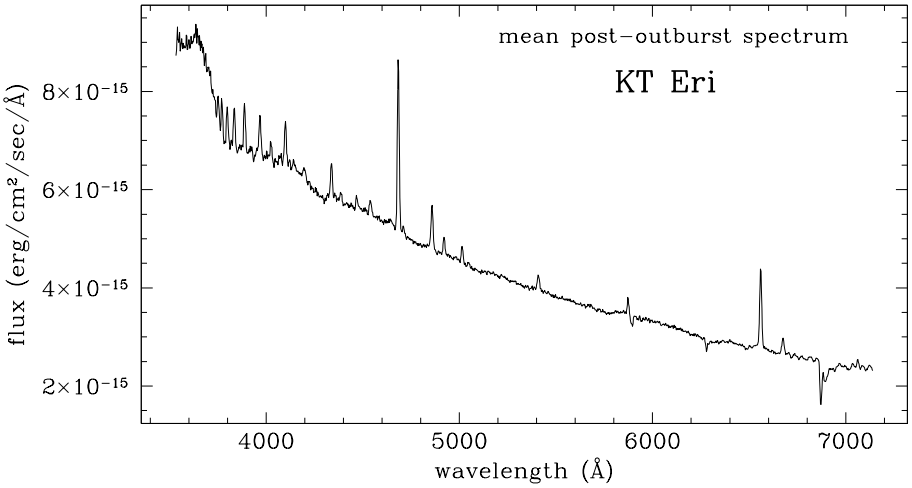


Figure 3. The mean optical spectrum of KT Eri during 2012–2020 yrs.

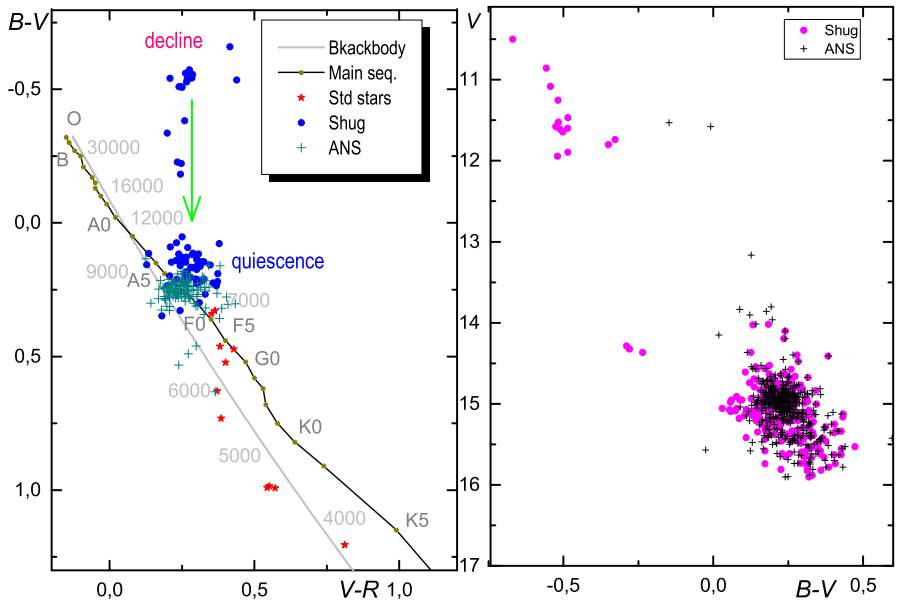


Figure 4. The two-color (left) and color-magnitude (right) diagrams. "Std stars" – positions of neighboring stars (from Tab. 1); "Shug" and "ANS"-positions of KT Eri, obtained by Shugarov and ANS Collaboration (Asiago) teams accordingly.

total outburst amplitude is about ∼10 mag. Note that the maximum outburst amplitude (∼ 19 mag) among classical Nova stars was detected at V1500 Cyg: (Harevich et al., 1975; Honda et al., 1975), The photometric post-outburst quiescence shows the same large variability (∼1 mag) inferred from inspection of pre-outburst photographic plates (Jurdana-Šepić et al., 2012). It is characterized by various time scales or multi-periodicities, intricately connected and not easy to isolate because not always all of them are present at the same time, which are mixed with a strong chaotic activity that may reach an amplitude of 0.7 mag over a few tens of minutes. The broad assortment of photometric times scales affecting KT Eri (from hours to years, eg. Munari & Dallaporta, 2014; Schaefer et al., 2022) has already been noted. We plan to carry out a comprehensive analysis in search for persistent periodicities by combining pre- and post-outburst available data.

The star track on the $B-V$, $V-R$ planes is plotted in Fig. 4. Apart from bluer $B-V$ colors during the decline from 2009 outburst maximum, the star has remained rather stable in color during quiescence, $B-V$=+0.22, $V-R$=+0.25.

Acknowledgements. SS is grateful for financial support from grants APVV-20-0148, VEGA 2/0030/21 and VEGA 2/0031/22. PG: the study was conducted under the state assignment of Lomonosov Moscow State University. UM acknowledges support from INAF 2023 Minigrant funding program.

References

Harevich, V., Bocharov, A. N., Shugarov, S. Y., et al., Nova Cygni 1975. 1975, *IAU Circulars*, **2839**, 1

Honda, M., Osawa, K., Osada, K., et al., Nova Cygni 1975. 1975, *IAU Circulars*, **2826**, 1

Hounsell, R., Bode, M. F., Hick, P., et al., The outburst light curve of Nova KT Eridani from Solar Mass Ejection Imager (SMEI) observations. 2010, *The Astronomer's Telegram*, **2558**, 1

Jurdana-Šepić, R., Ribeiro, V. A. R. M., Darnley, M. J., Munari, U., & Bode, M. F., Historical light curve and search for previous outbursts of Nova KT Eridani (2009). 2012, *Astronomy and Astrophysics*, **537**, A34, DOI:10.1051/0004-6361/20111780610.1086/141960

Landolt, A. U., UBVRI Photometric Standard Stars Around the Celestial Equator: Updates and Additions. 2009, *Astronomical Journal*, **137**, 4186, DOI:10.1088/0004-6256/137/5/4186

Munari, U. & Dallaporta, S., BVRI photometry of Nova KT Eri 2009 in quiescence and the 752 day period. 2014, *New Astronomy*, **27**, 25, DOI:10.1016/j.newast.2013.07.008

Schaefer, B. E., Walter, F. M., Hounsell, R., & Hillman, Y., The nova KT Eri Is a recurrent nova with a recurrence time-scale of 40-50 yr. 2022, *Monthly Notices of the RAS*, **517**, 3864, DOI:10.1093/mnras/stac2923

Contrib. Astron. Obs. Skalnaté Pleso **55/3**, 112 – 116, (2025)
https://doi.org/10.31577/caosp.2025.55.3.112

A look into the behaviour of BF Cygni after 2009

M. Tomova

Institute of Astronomy and NAO, Bulgarian Academy of Sciences, POBox 136, BG-4700 Smolyan, Bulgaria

Received: November 15, 2024; Accepted: December 27, 2024

Abstract. The last active phase of the eclipsing symbiotic binary BF Cygni began in 2006 and continues up to now. In 2009 Balmer satellite components indicating a bipolar collimated outflow with a variable velocity and intensity appeared in the spectrum. In this contribution we will examine the spectral behaviour of the system with emphasis on its burst during 2017. The satellite components of some lines indicating collimated ejection from the system disappeared for some time during the optical maximum and appeared again. The data are interpreted in the framework of the model of collimated stellar wind.
Key words: binaries: symbiotic – stars: mass-loss – stars: individual: BF Cyg

1. Introduction

BF Cyg is an eclipsing binary with an orbital period of 757.2 days (Fekel et al., 2001), whose eclipses (orbital minima) are observed well in both quiescence and outbursts (Skopal et al., 2015). The last active phase of BF Cyg began in 2006 and continues up to now. During this period its light is modulated by the orbital motion and shows photometric minima with a variable depth and shape. The residual of the depth of the first five minima is examined in a number of articles of Tomov et al. (2015, 2017, 2019); Tomov & Tomova (2018) and is interpreted in the framework of the model of the collimated stellar wind for Z And (Tomov et al., 2014).

In 2009 a collimated bipolar ejection of material from the system was observed for the first time (Skopal, Tomov & Tomova, 2013). The profile of the Balmer lines transformed – satellite emission components, located approximately symmetrically to the central emission, appeared. From that moment on, these satellite components are present in the spectrum, sometimes both emission components are present, and at other times only the red one (see Fig. 1, where our observations of the Hβ line up to and including 2016 are presented). In 2015 and 2017 during the development of a new activity were observed 1-mag bursts with gradual fading to the pre-outburst level lasting for about 1 year (Shchurova et al., 2019). Skopal et al. (2017) noted that around mid-February 2017 BF Cyg is around its peak brightness of the burst and the line spectrum was dominated

by hydrogen lines with a sharp absorption at about $-70\,\mathrm{km\,s^{-1}}$, and before the maximum the Balmer lines were accompanied by satellite emissions at about -400 and $+200\,\mathrm{km\,s^{-1}}$.

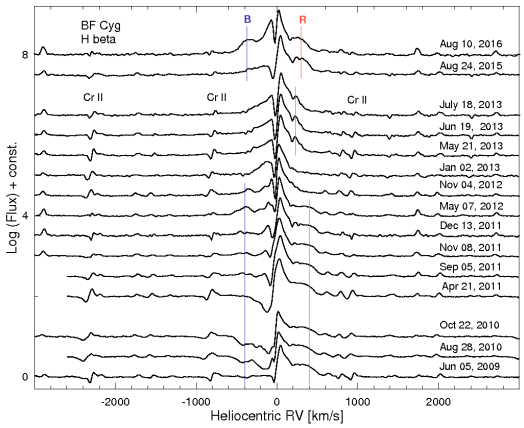


Figure 1. The spectral evolution of Hβ line, June 2009 – August 2016

We observed the system with a high resolution at the end of 2016, during the burst in 2017 and in September 2018 after the orbital minimum as well. Aim of our investigation is to analyse the profiles of some visual lines in the spectrum, to trace their evolution and to consider the changes of the mechanism of loss of mass of the outbursting compact object. Here we introduce preliminary results of our investigation.

2. Observations

The system BF Cyg was observed with the ESpeRo Echelle spectrograph (Bonev et al., 2017) of the 2m RCC telescope of the National Astronomical Observatory Rozhen, Bulgaria. The spectral resolution was ∼30 000. The spectra were reduced by means of IRAF (Tody, 1993). In our study we considered only the lines in the ranges of Hβ, HeI λ 4922 Å, HeI λ 5016 Å, FeII λ 5169 Å.

3. Spectral behaviour

3.1. The Hβ line

Our spectra from Dec. 11, 2016 and Sept. 02, 2018 showed a Hβ line consisting from two-peaks central emission component and a narrow absorption with $RV = -10, -15\,\mathrm{km\,s^{-1}}$ (see Fig. 2). Clearly visible emission components were present on both sides of the central component of the 2016 spectrum. These

emission components were not visible in the 2017 spectra, which showed a rather broad emission component, diminished by broad blue absorption, in some cases up to about $-500\,\mathrm{km\,s^{-1}}$. It reached up to about $-370\,\mathrm{km\,s^{-1}}$ in 2018. The presence of such components in the profile indicates a mass outflow from the outbursting compact object. We approximated the profile of the Hβ line with different number of Gauss functions. At first the central component was approximated and its contribution was subtracted from the emission in the area of the satellite components, in order to determine their parameters more precisely. Each satellite component of the Dec. 2016 profile was approximated with one Gaussian (see Fig. 2). Using the parameters from the approximation and the orbital inclination, $i = 75°$, and assuming that the bipolar outflow is perpendicular to the orbital plane, its opening angle was calculated $\theta = 10\overset{\circ}{.}2 \pm 0\overset{\circ}{.}3$. This value is comparable to that obtained by Skopal, Tomov & Tomova (2013), $\theta = 15\overset{\circ}{.}2 \pm 1\overset{\circ}{.}5$, for the period 2009–2012.

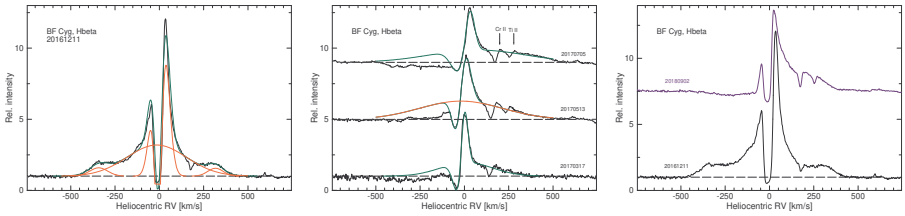


Figure 2. *Left and middle panel:* Approximation of Hβ line. Observed spectra are in black. Gaussians of components are in orange. Resulting curves approximating the observed spectra are in green. The satellite components are seen on the left panel. *Right panel:* Comparison of the profiles before and after the burst.

We applied the same approach to the 2017 spectra but we were unable to find confident presence of the red satellite emission component there. CrII and TiII lines are present over the red wing of the Hβ line, show strong P Cyg profile in this period and influence the red wing intensity. The red wing of the Hβ line in March and May 2017 is well approximated by a broad emission component (Fig. 2, middle). In July 2017 a weak red satellite emission is probably present, but we were unable to separate it from the rest of the emission of the Hβ wing. In addition, a multicomponent blue absorption up to about $-500\,\mathrm{km\,s^{-1}}$ is present in the Hβ profile on this date. Therefore we can not conclude that the satellite components are present in the Hβ line during our observations in 2017, but

rather a broad emission component of wind, whose blue part is diminished by P Cyg absorption.

The satellite components are probably present in the Hβ line in the spectrum of Sept. 2018. A red emission and a blue absorption components have been fitted on this spectrum, but these fits have large error and are not reliable.

3.2. The FeII 42 lines

The FeII 42 lines are presented in Fig. 3. The Hβ and FeII 42 lines show the same characteristics – a narrow P Cyg absorption, broad red emission and broad blue absorption, but different velocities – lower for the lines of FeII 42. This shows that the loss of mass which is observed in Hβ, is observed also in FeII 42 lines.

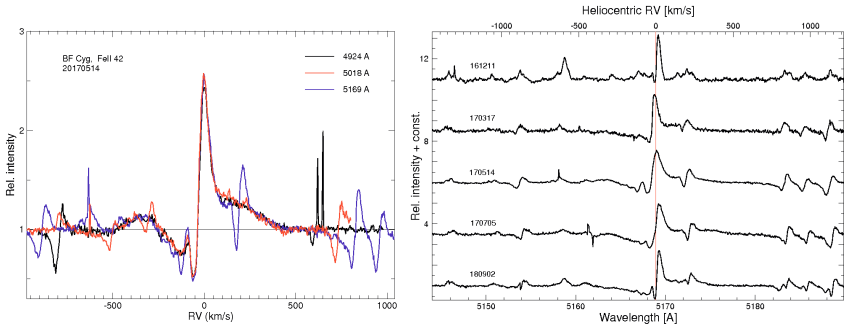


Figure 3. *Left panel:* Example of FeII 42 line profiles. A broad red emission and a broad blue absorption components are visible. The narrow P Cyg absorption is also present. An additional emission on the short wavelengths side of the blue absorption component is seen on this date, as well. *Right panel:* Evolution of the FeII 42 5169 Å line in our spectra during Dec. 2016 – Sept. 2018.

4. Conclusion

We present preliminary results from our study of the Hβ and FeII 42 line profiles before, during and after the burst in 2017. These lines contained clearly visible components indicating mass-outflow from the system. Based on approximation of the Hβ line profile we can not conclude that the satellite components are present in the 2017 observations, but rather a broad emission component of wind, whose blue part is diminished by P Cyg absorption. In Sept. 2018 the satellite components are probably restored.

Acknowledgements. The idea and a part of the implementation of this study belongs to DSc Nikolai Tomov, who passed away in 2022. We thank Dr. K. Stoyanov

for the acquiring part of the spectra. The research infrastructure this research was done with is funded by the Ministry of Education and Science of Bulgaria (support for the Bulgarian National Roadmap for Research Infrastructure, project D01-326/04.12.2023).

References

Bonev et al.: 2017, *BulgAJ*, **26**, 67

Fekel, F.C., Hinkle, K.H., Joyce, R.R., Skrutskie M.F., : 2001, *Astron.J*, **121**, 2219

Shchurova, A., Skopal, A., Shugarov, S., et al.: 2019, *Contrib. Astron. Obs. Skalnate Pleso*, **49**, 411

Skopal, A., Tomov, N.A., & Tomova, M.T.: 2013, *A&A*, **551**, L10

Skopal, A., Sekeráš, M., Tomov, N.A., Tomova, M.T., Tarasova, T.N., & Wolf, M.: 2015, *AcPol CTU Proc.*, **2**, 277

Skopal, A., Sekeráš, M., Shugarov, S., & Shagatova, N.: 2017, *ATel* 10086

Tody, D.: 1993, *Astronomical Data Analysis Software and Systems II*, **52**, 173

Tomov, N.A., & Tomova, M.T.: 2018, *Publ. Astron. Soc. Rudjer Boskovic*, **18**, 147

Tomov, N.A., Tomova, M.T., & Bisikalo, D.V.: 2014, *AN*, **335**, 178

Tomov, N.A., Tomova, M.T., & Bisikalo, D.V.: 2015, *AN*, **336**, 690

Tomov, N.A., Tomova, M.T., & Bisikalo, D.V.: 2017, *Ap&SS*, **362**, 220

Tomov, N.A., Tomova, M.T., & Bisikalo, D.V.: 2019, *BulgAJ*, **30**, 60

Contrib. Astron. Obs. Skalnaté Pleso **55/3**, 117 – 121, (2025)
https://doi.org/10.31577/caosp.2025.55.3.117

Doppler imaging of the contact binary DU Boo

E.B. Yorulmaz[1,2], **İ. Özavcı**[1,2], **E. Bahar**[1,2], **H.V. Şenavcı**[1,2], **G.A.J. Hussain**[3] **and O. Kochukhov**[4]

[1] *Ankara University, Faculty of Science, Astronomy & Space Sciences Department, Tandogan, TR-06100 Ankara, Türkiye (E-mail: ebyorulmaz@ankara.edu.tr)*

[2] *Ankara University, Astronomy and Space Sciences Research and Application Center (Kreiken Observatory), Incek Blvd., TR-06837 Ahlatlıbel, Ankara, Türkiye*

[3] *European Space Agency (ESA), European Space Research and Technology Centre (ESTEC), Keplerlaan 1, 2201 AZ Noordwijk, The Netherlands*

[4] *Department of Physics and Astronomy, Uppsala University, Box 516, S-75120 Uppsala, Sweden*

Received: October 30, 2024; Accepted: January 7, 2025

Abstract. The early-type contact binary DU Boo exhibits consistent O'Connell effect for many years. Studies in the literature of the system are insufficient to explain this consistency in the observed O'Connell effect. Based on this gap in the literature, the aim of this study is to investigate the surface brightness distribution of the system using the Doppler imaging technique as well as the mid-resolution time series spectra.

Key words: binary stars – O'Connell effect – Doppler imaging technique

1. Introduction

Asymmetries can be observed in the light curves of binary stars, due to various astrophysical reasons. The difference in the maximum levels of the light curve is called the O'Connell effect. The most widely accepted theory for the causes of this asymmetry is the presence of either hot or cool photospheric spots.

With a relatively long orbital period (P = 1.056 days), DU Boo binary system, which consists of two A7V-type (Pribulla et al., 2006) components, exhibits a significant O'Connell effect in addition to the total eclipse in its light curve (See Fig. 1). Unlike typical late-type contact binaries, DU Boo exhibits a highly stable spot configuration and hence light curve asymmetry. The asymmetry has been addressed using the cool spot approach placed near the neck region (Djurašević et al., 2013). In the case of cool spots, the formation of these asymmetries is associated with the thickness of the convective layer and the presence of differential rotation.

However, in A-type contact binary stars, the outer convective zone is very thin (Rucinski, 1974). Nevertheless, cool spot modeling has been still applied in the literature to explain the observed asymmetries in such early-type systems. In the case of hot spots, the asymmetry is generally explained by extra flux in light curves resulting from mass transfer (Shaw, 1994). Another study by Pribulla et al. (2011), who performed the spectral analysis of the system, suggested that the bump in the BF profiles, especially at the 0.25 phase, could be due to the presence of a hot spot.

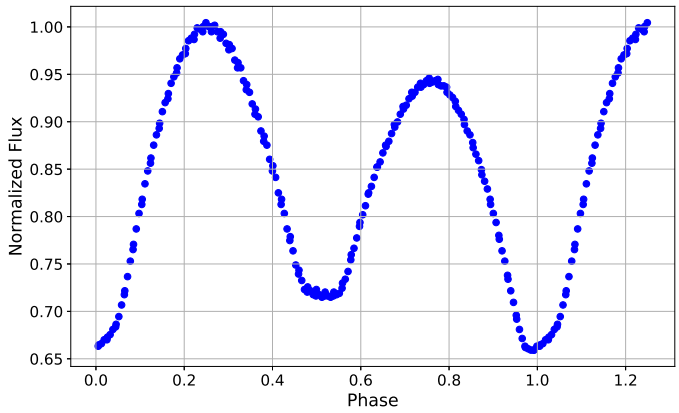


Figure 1. An example TESS light curve of DU Boo plotted using a part of sector 16 data.

2. Observations & methods

The mid-resolution (R $\sim$ 15000) spectra of DU Boo and standard stars were obtained using the Whoppshel spectrograph attached to the T80 Prof. Dr. Berahitdin Albayrak Telescope, covering the wavelength range between 4000-7800 Å. All spectra were reduced using standard IRAF packages. Normalization procedure was carried out using a python code improved by our research group (NSpec).

The iLSD code (Kochukhov et al., 2010) was used to create LSD profiles to enhance the SNR (Signal-to-Noise Ratio) values of spectra. This was done using a line list from the VALD3 database (Pakhomov et al., 2017) that is suited to the astrophysical properties of the components. The observation log of spectra and SNR values are given in Table. 1.

Table 1. Spectral observation log and SNR values.

Date	HJD (2450000+)	Phase	Exposure (s)	SNR (Spectra)	SNR (LSD)
16/07/2022	9777.3958	0.1469	3600	56	2300
14/07/2022	9775.3718	0.2301	3600	73	2800
14/07/2022	9775.4136	0.2697	3600	71	2800
12/07/2022	9773.3735	0.3375	3600	75	3900
12/07/2022	9773.4156	0.3774	3600	72	3500
24/04/2022	9694.4844	0.6241	3600	74	3900
20/04/2022	9690.2843	0.6463	3600	83	4600
20/04/2022	9690.3314	0.6909	3600	76	4600
21/07/2022	9782.3271	0.8172	3600	62	3700
21/07/2022	9782.3690	0.8569	3600	56	3600

In order to reconstruct surface brightness distribution of both components, we used the modified version of the dots code (Collier Cameron, 1997) which is based on a 3-temperature approximation that represents photosphere, hot and cool spots. Since the photospheric temperatures of the components are 7800 K and 7600 K, the maximum and minimum temperatures are defined as 8800 K and 6700 K for the primary component, and 8600 K and 5900 K for the secondary component, respectively.

The presence of a dip structure in the LSD velocity profile corresponding to the component is indicative of a hot spot, whereas the presence of a bump structure is associated with a cool spot (e.g. Rozelot & Neiner (2016)).

LSD profiles and the surface brightness distribution maps of the system are shown in Fig. 2 and Fig. 3, respectively.

3. Results & conclusion

In this study, the surface brightness distributions of the components of DU Boo have been reconstructed using Doppler imaging technique to investigate whether the asymmetry in the system is due to a hot or cool spot. In Fig. 2, blue arrows indicate a hot spot in the neck region around phase 0.25, pointing a stream of matter or a bright region, consistent with the suggestion made by Pribulla et al. (2011).

The surface brightness distribution map of the system and the TESS light curve both consistently suggest that the flux increase observed at phase 0.25 on the light curve is likely caused by a hot spot. In the case of DU Boo, hot spot on the neck region of the components can be explained using the mass transfer scenario proposed by Shaw (1994).

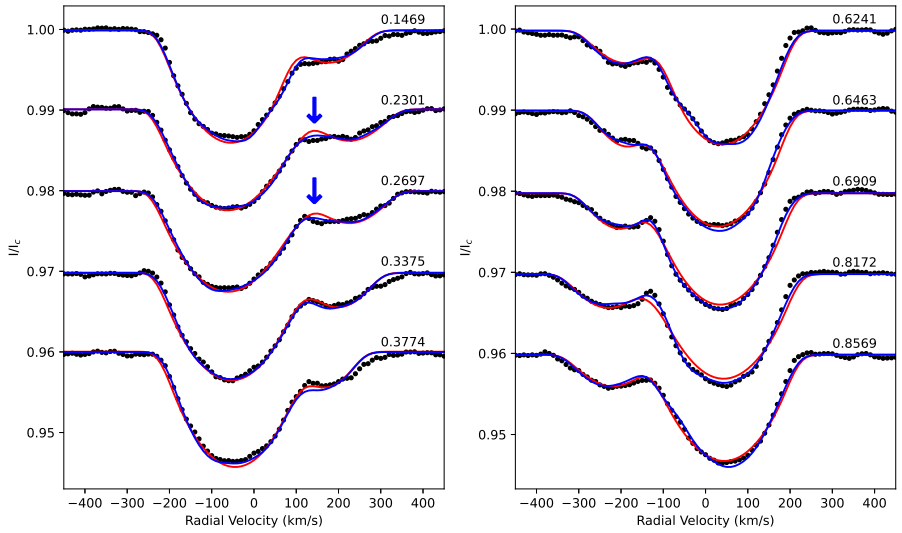


Figure 2. Observational LSD profiles (black dots), synthetic model fit (red solid line) and best fit models generated by the reconstructed process (blue solid line).

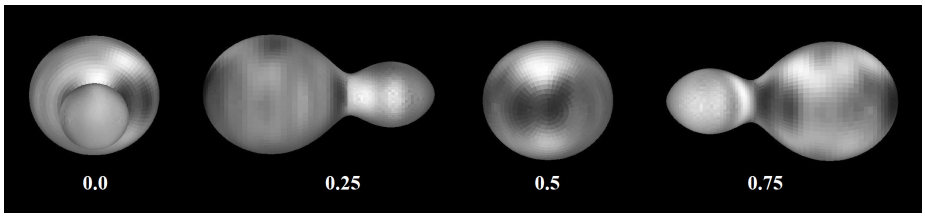


Figure 3. Surface brightness distrubution of the system at four main phases.

Although longer exposure times result in phase smearing, they do not significantly affect the determination of dominant spot characteristics at a specific stage. However, shorter exposure times can help produce higher-resolution maps of the spots.

References

Collier Cameron, A., Eclipse mapping of late-type close binary stars. 1997, *Monthly Notices of the RAS*, **287**, 556, DOI:10.1093/mnras/287.3.556

Djurašević, G., Baştürk, Ö., Latković, O., et al., Photometric Analysis of HS Aqr, EG Cep, VW LMi, and du Boo. 2013, *Astronomical Journal*, **145**, 80,

DOI:10.1088/0004-6256/145/3/80

Kochukhov, O., Makaganiuk, V., & Piskunov, N., Least-squares deconvolution of the stellar intensity and polarization spectra. 2010, *Astronomy & Astrophysics*, **524**, A5

Pakhomov, Y., Piskunov, N., & Ryabchikova, T., VALD3: Current Developments. 2017, in Astronomical Society of the Pacific Conference Series, Vol. **510**, *Stars: From Collapse to Collapse*, ed. Y. Y. Balega, D. O. Kudryavtsev, I. I. Romanyuk, & I. A. Yakunin, 518

Pribulla, T., Rucinski, S. M., Lu, W., et al., Radial Velocity Studies of Close Binary Stars. XI. 2006, *Astronomical Journal*, **132**, 769, DOI:10.1086/505536

Pribulla, T., Vaňko, M., Chochol, D., Hambálek, Ľ., & Parimucha, Š., O'Connell effect in early-type contact binaries: du Boo and AG Vir. 2011, *Astronomische Nachrichten*, **332**, 607, DOI:10.1002/asna.201111569

Rozelot, J.-P. & Neiner, C. *Cartography of the Sun and the Stars*, , Vol. **914** (Springer)

Rucinski, S. M., Binaries. II. A- and W-type Systems. The W UMa-type Systems as Contact. 1974, *Acta Astronomica*, **24**, 119

Shaw, J. S., Near-contact binaries. 1994, *Mem. Societa Astronomica Italiana*, **65**, 95

Contrib. Astron. Obs. Skalnaté Pleso **55/3**, 122 – 140, (2025)
https://doi.org/10.31577/caosp.2025.55.3.122

Pulsations in binary stars – a short review

S.J. Murphy

Centre for Astrophysics, University of Southern Queensland, Toowoomba, QLD 4350, Australia (E-mail: simon.murphy@unisq.edu.au)

Received: November 13, 2024; Accepted: December 12, 2024

Abstract. Asteroseismology has become an indispensable method for measuring stellar ages and radii, while binary systems remain the most prevalent tool for determining stellar masses. The synergy of the two, namely pulsating stars in binary systems, offer even more than the sum of their parts. The sometimes-overwhelming number of pulsation models to be examined for asteroseismic modelling can be tightly constrained when dynamical masses for both components are available. Binaries offer twice the opportunity to measure an asteroseismic age, which is then applicable to both components of a system, often providing ages for stars that are otherwise very difficult to determine. Some stellar physics, such as the strength of internal mixing or of core overshoot, is so difficult to infer that only in binary systems do sufficient constraints exist to advance our asteroseismic models. The pulsations themselves can also be used to infer dynamical masses through pulsation timing, while eclipsing binaries provide opportunities to test asteroseismic scaling relations. In these proceedings of an invited talk I selectively review the synergies afforded by pulsations in binaries, even when their companions are undetectable. I also describe how the field is changing as we become more data rich through each generation of large photometric survey.

Key words: asteroseismology – binaries: general – binaries: eclipsing – stars: oscillations – stars: variables: general

1. Introduction

Most stellar properties exhibit great variation across spectral types. Temperature and mass are obvious examples, but rotation rates and binary fraction are important yet often under-appreciated additions. Along the main sequence alone, rotation periods range from under 1 d for some B and A stars, to over 30 d for late-type dwarfs (Reinhold & Hekker, 2020). Meanwhile, the binary fraction drops by a factor of 10–15 from B primaries to M primaries (Moe & Di Stefano, 2017; Offner et al., 2023)[1]. The implications of these two effects are substantial when one considers that the majority of new binary stars were being found spectroscopically until recently (Halbwachs et al., 2023; Holl et al., 2023).

[1]Strongly dependent on orbital period.

The rotational broadening of spectral lines makes identification of binaries much harder for many reasons. When lines are very broad, it can become challenging to distinguish all but the strongest lines from the continuum. It is therefore almost impossible to tell when you are dealing with lines from two stars (a double-lined spectroscopic binary, or 'SB2'), rather than from one. Further, if those spectral lines can be detected for even one of the stars, measuring the line centres is also challenging (cf. Rucinski 1999), so it is not trivial to detect any variations in radial velocity (as a single-lined spectroscopic binary, or 'SB1'). To further complicate matters, stars of B and A spectral types often pulsate (Kurtz, 2022; Hey & Aerts, 2024; Murphy et al., 2024), with typical pulsation velocities exceeding $1\,\mathrm{km\,s^{-1}}$ (Kjeldsen & Bedding, 1995). Those pulsations can induce radial velocity shifts and also spectral line profile variations (e.g. Rieutord et al. 2023; Pollard et al. 2024), further obfuscating any spectroscopic signature of a binary companion. Clearly, a complete survey of binarity amongst these stars will require non-spectroscopic techniques.

The present era has seen a photometric revolution with the launch of space-based missions such as CoRoT, *Kepler* and TESS, as well as ground-based surveys such as ASAS and KELT. Although motivated by the search for transiting planets, these missions have detected eclipsing binaries (EBs) with ease and in large numbers. The observing strategy is also perfect for asteroseismology – the study of stellar pulsations (see Bowman & Bugnet 2024 for an introductory review). It is no surprise, then, that the all-sky observing strategy of TESS has picked up countless pulsating stars in EBs (Southworth & Bowman, 2022; Kahraman Aliçavuş et al., 2022, 2023; Eze & Handler, 2024). These will be discussed later in this review. The long and almost uninterrupted time-series from *Kepler* and to some extent from TESS have also facilitated the detection of many pulsation timing binaries (Murphy et al., 2018; Dholakia et al., 2024), which will also be covered in this review. The prospects for discovering more pulsators in binaries look good for both methods, with the continued operation of TESS and with the upcoming Roman Space Telescope (Huber et al., 2023), PLATO mission (Aerts & Tkachenko, 2024), and Earth 2.0 (ET) telescope (Ge et al., 2022).

A similar short review on pulsating stars in binary systems was written as a conference proceedings in 2018 (Murphy, 2018). The intention is for the present review to be synergistic with the earlier one and to provide updates in the field since then. For instance, the 2018 review covered compact pulsators in detail, and while TESS observations of compact pulsators have been published (e.g. Bognár et al. 2020; Baran et al. 2023), rather few reports have appeared of binaries amongst them (cf. Lee et al. 2022). Compact objects therefore do not feature in this review (they were not part of the talk upon which this review is based, either). Early-type pulsators in EBs, on the other hand, have had a TESS renaissance, and so receive substantial coverage here. A particularly significant development since 2018 has been the discovery of tidally trapped pulsations (Handler et al., 2020; Fuller et al., 2020), which are also extensively reviewed.

Nonetheless, there is naturally some overlap with the earlier review, particularly pertaining to pulsation timing but also to solar-like oscillators in binaries, which were cornerstones of the review talks then and now.

This review is laid out as follows. A few exemplary asteroseismic analyses of main-sequence solar-like oscillators in binaries are presented in Sec. 2, and their post-main-sequence counterparts are reviewed in Sec. 3. A comprehensive update on pulsation timing over the past six years is provided in Sec. 4 along with a look at future prospects of this technique. Sec. 5 explores the newly described class of tidally trapped pulsations, where the effect of tides on the pulsations can be so great that the tidal axis becomes the pulsation axis. Finally, Sec. 6 describes the surge of discoveries of early-type pulsators in eclipsing binaries, and lessons that can be learned from such studies.

2. Main-sequence solar-like oscillators in binaries

2.1. Photometry

The *Kepler* LEGACY sample contains 66 well-characterised main-sequence solar-like oscillators (Lund et al., 2017), and many more such oscillators with more complicated power spectra were also observed. The detection of stochastic oscillations in main-sequence stars requires high cadence observations and long time-series. With *Kepler*, this means short-cadence mode (60-s) observations, and the LEGACY sample only included stars with at least 1 yr of data. TESS, by comparison, had a less-short cadence of 120 s[2], and an overall redder bandpass, in which the oscillation amplitudes appear reduced. The all-sky sampling strategy also disfavours the collation of longer time-series except at the ecliptic poles. Nonetheless, a few dozen main-sequence solar-like oscillators were also found with TESS (Hatt et al., 2023), along with many more subgiants and giants. Naturally, some of these were known spectroscopic binaries, although none were reported to have two sets of oscillations in the same light curve (i.e. none were double-pulsator binaries, or PB2s[3]).

PB2s are promising from an asteroseismic perspective. The 2018 review provided multiple examples of solar-like oscillators in PB2s (Appourchaux et al., 2015; White et al., 2017; Li et al., 2018) and explained their significance. In short, such systems should have the same age and metallicity, meaning that the frequency content of their combined power spectrum is governed largely by their difference in mass. This makes them valuable tests of stellar evolution and pulsation models. However, stars with mass ratios close to unity, such that the luminosity of one doesn't pale in comparison to the other, are predicted to be rare (Moe & Di Stefano, 2017), and it appears that we also detect far fewer than are predicted to exist (Miglio et al. 2014, see discussion in Murphy 2018). New

[2]TESS now has many different cadences available, from the 20-s 'ultra-short' cadence to the original 1800-s full frame images (FFIs). The FFI cadence has now dropped to 200 s.

[3]named in analogy to the SB2s of spectroscopy

simulations that include *Gaia* data as priors are in preparation (Mazzi et al., 2024), and there is hope that the faster cadence (25 s) of the PLATO mission will yield many more PB2s.

2.2. Radial velocities

Asteroseismology of solar-like oscillators in velocity space (as opposed to photometry) was not covered in the 2018 review. There are pros and cons to using radial velocities (Bedding & Kjeldsen, 2007). The signal to noise ratio in velocity observations is usually better, because the granulation background is much smaller. In principle, this means that for cooler stars, where convection is more vigorous, velocities are more likely to yield a detection. The drawback is that single-target, ground-based velocity campaigns are more challenging to organise and have stringent technical requirements: it takes a short exposure to sample the oscillations, and so the spectrograph must be capable of a fast readout. Meanwhile, it takes a large aperture to gather enough photons in a short exposure. Hence, while rather few instruments meet the technical requirements, the capabilities can even exceed space-based photometers. Fig. 1 shows the known solar-like oscillators from both photometry and radial velocities.

The coolest main-sequence star in which oscillations have been detected is ϵ Indi A, which is an interesting case in the context of pulsations in binaries because the system is multiple (Fig. 2). The companions ϵ Ind Ba and Bb are among the best studied brown dwarfs, while ϵ Ind Ab is the nearest cold-Jupiter system to Earth. Asteroseismology of ϵ Indi A has revealed a frequency of maximum power, $\nu_{\rm max}$, of 5265 μHz – the highest so far of any solar-like oscillator – which in turn allows its mass to be inferred at $M = 0.782\,{\rm M}_\odot$ (Lundkvist et al., 2024). It also has an asteroseismic large spacing, $\Delta\nu$, of 201.25 μHz, which corresponds to an age younger than 4 Gyr (Campante et al., 2024). These asteroseismic measurements not only verify the distance to the system independent of parallax, but also provide important constraints on the brown dwarf properties, which are the only examples well constrained and nearby enough to have allowed a test of substellar cooling with time for a T dwarf. Thus the ϵ Indi system is a textbook example of the powerful synergy of asteroseismology and binary star analyses.

3. Solar-like oscillators beyond the main sequence

We have focussed so far on systems currently having companions, but as stars evolve up the red giant branch (RGB) and their radii expand, they can become common envelope binaries and eventually mergers (Paczynski, 1976). From the outside, it is impossible to distinguish a single 2.5-$M_\odot$ star that has evolved to become a red giant, from a 1.5 + 1.0-$M_\odot$ pair that merged on the RGB. However, their oscillation spectra can tell them apart. The Brunt-Väisälä frequency of the

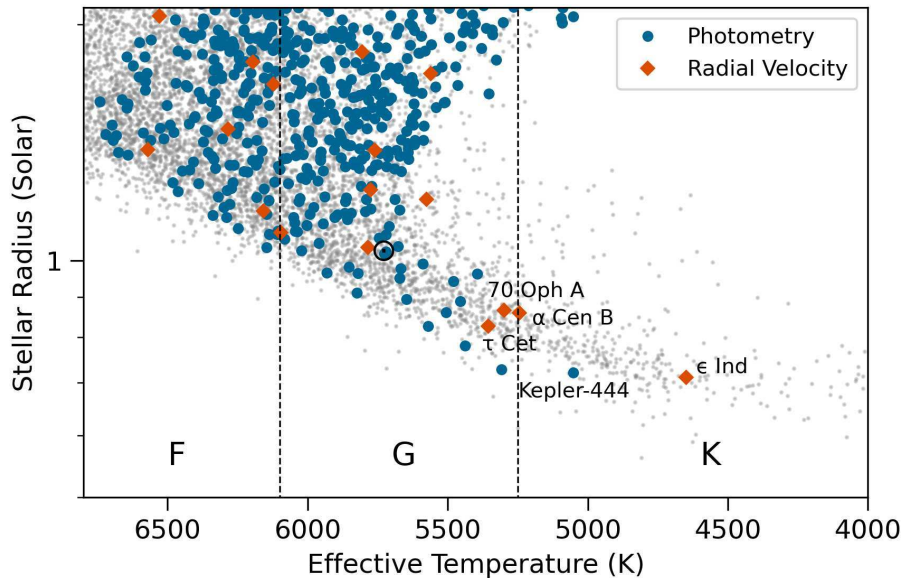


Figure 1. Stellar radius–effective temperature diagram highlighting seismic detections from *Kepler* and TESS photometry (blue circles; Mathur et al. 2017; Hatt et al. 2023), and radial-velocity campaigns (red diamonds; see e.g., Arentoft et al. 2008; Kjeldsen et al. 2008, and references therein). The stellar background sample (grey dots) is taken from the TESS Input Catalog (TIC; Stassun et al. 2019). The Sun is represented by its usual symbol. Approximate spectral type ranges (F, G, and K) are delimited by the vertical dashed lines. ϵ Indi (K5 V) is the coolest seismic dwarf observed to date (its interferometric radius and effective temperature were used to place it in the diagram; Rains et al. 2020). Figure and caption reproduced from Campante et al. (2024).

merger product looks similar to the original 1.5-$M_\odot$ primary, and significantly different from a 2.5-$M_\odot$ single star of the same luminosity (Rui & Fuller, 2021).

In the age of space photometry, red giants are often characterised by their period spacings, $\Delta\Pi$, and their frequency spacings, $\Delta\nu$. Specifically, it is common to plot many stars in the $\Delta\Pi$–$\Delta\nu$ plane, where RGB stars fall on a well-defined sequence. Deheuvels et al. (2022) showed that merger products can be identified in this diagram. Ordinarily, intermediate-mass red giants, which reach the core-helium burning phase with non-degenerate cores, lie above the RGB sequence in this diagram. But if those stars attained their mass by merger, especially after one of those stars developed a degenerate core, they instead lie under the RGB sequence. Hence, it is only the relatively uncommon case where two stars merge on the main sequence that leaves no asteroseismic fingerprints.

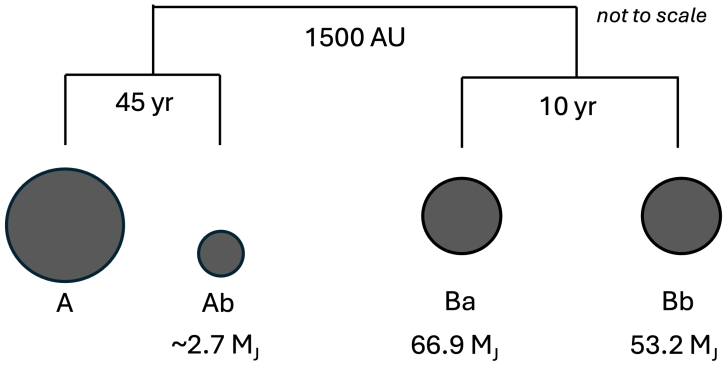


Figure 2. Mobile diagram for the ϵ Ind system. System properties are from Lundkvist et al. (2024), Campante et al. (2024), and references therein.

Binaries can also be detected indirectly before they merge, via evidence of substantial mass loss by Roche lobe overflow (RLOF) onto a companion. Ordinarily, stars might lose up to $0.2\,M_\odot$ through wind-driven mass loss as they ascend the red giant branch. Then, when they begin core helium burning, they settle onto a line called the zero-age helium burning (ZAHeB) line that is sharp in $\nu_{\rm max}$ both observationally and in models. (This is entirely analogous to the ZAMS forming a well-defined lower edge to the main sequence in luminosity space.) Li et al. (2022) found a handful of stars that fell to the wrong side of the ZAHeB line. They showed that these stars must have had non-degenerate cores (i.e. high main-sequence masses $\gtrsim 2.2\,M_\odot$) when they ascended the RGB, but their observed asteroseismic quantities ($\Delta\nu$ and $\nu_{\rm max}$) indicate their masses are now much lower ($\lesssim 1.6\,M_\odot$). These stars therefore lost substantial mass – much more than is explained via wind-driven mass loss – suggesting they donated it to an otherwise undetected companion.

Other tell-tale signs of significant mass loss are conspicuously low masses on the RGB. The 13.8-Gyr age of the Universe puts a lower limit on the mass of an RGB star of approximately 0.8–$1.0\,M_\odot$, yet Li et al. (2022) discovered dozens of red giants with masses significantly lower than this limit. Since "stellar winds driven by radiation and pulsation can only remove up to $0.2\,M_\odot$," they argue, those stars must have undergone more extreme mass loss, with RLOF onto a companion being the prime culprit. A specific example concerns the low-mass, core helium burning star KIC 4937011, which is a member of the cluster NGC 6819. This ~2.4-Gyr-old cluster has a main-sequence turn-off mass of $\sim 1.6\,M_\odot$, yet the asteroseismic mass of KIC 4937011 is $0.74\,M_\odot$ (Matteuzzi et al., 2024). Not only is this star too low mass to be a red giant given the age of the cluster, the same is true given the age of the Universe. Matteuzzi

et al. (2024) hypothesise that KIC 4937011 has lost around $1.0\,M_\odot$ of material through common envelope ejection in its recent history.

Of course, not all systems destined to experience common envelopes or RLOF have yet begun to lose mass. If a star does not overflow its Roche lobe at the tip of the RGB, it will have another chance as it ascends the asymptotic giant branch (AGB). This is the fate of any core-helium-burning red giants with companions in orbits of $200 < P_{\rm orb}({\rm d}) \lesssim 3000$ (Oomen et al., 2018), which includes several hundred known binaries with oscillating RG components (Themeßl et al., 2018; Beck et al., 2024). In some cases, the pulsations of the companion to the red giant are also detectable, and in some of *those* cases, those pulsations can be used to derive an orbital solution. That is the subject of the next section.

4. Pulsation timing orbits

The orbits of binary systems can be obtained by timing the pulsations of one (or more) components in the system. In its simplest form, the method is the classical O-C method (Barnes & Moffett, 1975; Sterken, 2005), which has been adapted to readily combine signals from many different pulsation modes (Murphy et al., 2014). There are also implementations analogous to frequency-modulated radios, where the stellar pulsations are the carrier frequencies modulated by the binary motion (Shibahashi & Kurtz, 2012; Shibahashi et al., 2015). These variations on a methodological theme have been confirmed with other techniques, such as RVs and eclipses (Barlow et al., 2011b,a; Kurtz et al., 2015). The 2018 review (Murphy, 2018) covered pulsation timing in detail, most of which will not be repeated here. Instead, the following paragraphs will cover the advancements from 2018, what can be expected in the near future, and will conclude with another demonstration of the synergy of pulsations and binary analyses.

As of 2018, a few hundred pulsation timing binaries were known, most of which contain one or more δ Sct pulsators (Murphy et al., 2018)[4]. Other classes of variables are not expected to yield many pulsation-timing binaries (Compton et al., 2016; Hermes, 2018), yet that number is not zero. For instance, Hey et al. (2019) applied the technique to six rapidly oscillating Ap stars, yielding two candidate (but unconfirmed) binaries. Otani et al. (2022) derived a convincing pulsation timing orbit from the subdwarf B star in AQ Col, but caution should generally be applied when dealing with subdwarfs because their modes undergo sporadic period changes (Mackebrandt et al., 2020). It is occasionally useful, of course, to be able to use pulsation timing to know when a star is *not* in a binary, too (Szewczuk & Daszyńska-Daszkiewicz, 2018; Murphy et al., 2020b). This has been applied to rule out stellar companions as false positives in transiting exoplanet searches (Hey et al., 2021).

[4]Some $21 \pm 6\%$ of these δ Sct stars are not the original primaries of their systems, and have *received* mass through RLOF in their binary evolution

The precision of orbital solutions can be greatly enhanced by combining pulsation timing with other methods. For instance, radial velocity is the time-derivative of the light arrival-time delay probed by pulsation timing, and the complementarity of the mathematical functions yields solutions more precise than doubling the precision of either method alone (e.g. Murphy et al. 2016; Derekas et al. 2019; Lampens et al. 2021). These two methods both operate along the radial projection of the orbit, hence ultimately confer the same information. The next frontier was to incorporate astrometry data into the analysis, as the astrometric plane is perpendicular to the radial vector.

The only analysis to have combined pulsation timing and astrometry is that of the α Pic system by Dholakia et al. (2024). It had long been suspected that α Pic was binary, but neither RVs nor astrometry could adequately sample its 1316-d orbit. Using three pulsation modes of α Pic A, Dholakia et al. (2024) used TESS data to measure variations in light arrival times, constraining the orbital period, and jointly fitted astrometric data from Hipparcos. The addition of astrometry allowed an orbital inclination to be inferred in addition to the usual orbital parameters from radial analyses, and further parameters such as a mass ratio then follow from comparison of the photocentre motion to the amplitude of the light arrival-time delays. Many more joint astrometric solutions can be expected following Gaia DR4, when intermediate astrometric data are released.

Most pulsation timing studies conducted thus far have been based on *Kepler* data, with a few TESS systems having been investigated ad-hoc (e.g. Yang et al. 2021; Vaulato et al. 2022). The use of multi-mission photometry is also on the rise (Lyu & Yang, 2023; Zieba et al., 2024). The first systematic pulsation timing study on TESS photometry has now been conducted (Dholakia et al., 2024), which used data from the first four years, corresponding to TESS Sectors 1–55. A disadvantage of TESS photometry compared to *Kepler* is the gaps in coverage due to TESS's step-and-stare observing strategy (Ricker et al., 2015). Dholakia et al. (2024) therefore also evaluated the minimum number of Sectors of observation required to reliably infer the orbital parameters. As TESS continues observing, the number of systems discovered and the quality of individual orbits are both expected to increase. In 2025, the launch of PLATO will provide yet another source of high duty cycle light curves for such analyses.

Improvements to pulsation timing are not limited to the inclusion of more data. In fact, some developments have focussed on better use of the data at hand. A drawback of the original method was the need to subdivide the time-series to look for pulsational phase shifts in each subdivision. This can be obviated by forward-modelling the light arrival-time delays onto the light curve itself. Hey et al. (2020b,a) built and provided the tools to apply this, which could be extended to include other parametric phenomena such as eclipse models in future (Prša et al., 2022). Dispensing with the need to subdivide the light curve is particularly advantageous when probing small orbits, which naturally includes most of the EB population. Murphy et al. (2016) had to introduce corrections

for undersampling of the orbits when subdividing, but there is no such need when forward modelling.

Yet more discoveries abound in the judicious application of pulsation timing to other *Kepler* data sets. Simply by extending the search space beyond the $T_{\rm eff}$ range of the Murphy et al. (2018) catalogue, new systems have been found in *Kepler* data (Manzoori, 2020; Yang, 2022; Murphy et al., 2020a). And use of the collateral 'smear' data on the *Kepler* CCD to produce light curves for otherwise saturated targets has yielded even more (Pope et al., 2019). A systematic application of pulsation timing to eclipsing systems is yet to be undertaken and is an obvious future direction.

One specific system exemplifies the combined power of asteroseismology and binary studies, and also happens to have been too cool (KIC $T_{\rm eff}$ = 5406 K) to have been captured in the primary pulsation-timing survey. KIC 9773821 is a RG–δ Sct binary in which both components have oscillations detected with *Kepler*, i.e. it is a PB2. The δ Sct pulsations confer a pulsation timing orbit, but the stochastic nature of the RG oscillations do not. The sharp spectral lines of the RG permit an RV orbit, while the broad δ Sct lines do not. Studied together, these allow a joint orbital model including a mass ratio (Murphy et al., 2021). Asteroseismology of the RG gives its mass, which then also gives the δ Sct mass via the orbital mass ratio. However, that RG mass is 2.1 $M_\odot$, so the RG core was never degenerate. This made it difficult to tell if the RG was core He burning, or on the RGB instead, hence its age was uncertain. This dilemma was solved using the δ Sct star – the RGB scenario would have required the δ Sct star to be somewhat younger and hotter; so hot, in fact, that it would lie outside the δ Sct instability strip. Although this is not unheard of (Bowman & Kurtz 2018; Murphy et al. 2019; Sharma et al. 2022; Hey & Aerts 2024; Mombarg et al. 2024, cf. Kahraman Aliçavuş et al. 2024),[5] this argument was one of many indicating that the primary had to be core helium burning, and illustrates the benefit of combining asteroseismic and binary analyses.

5. Tidally trapped pulsations

Some orbits are too small for pulsation timing to be effective, even with the latest methods. This includes an entirely new class of pulsating binaries – tidally trapped pulsators. These are a subset of the broader class of tidally perturbed pulsators, where the two components of the binary are sufficiently close that tidal forces affect the pulsations. First discovered in *Kepler* data (Hambleton et al., 2013; Balona, 2018), these systems sprang to the fore with TESS, starting with U Gru (Bowman et al., 2019), and several studies followed shortly thereafter (Lee, 2021; Southworth, 2021; Steindl et al., 2021; Van Reeth et al., 2022). The first systematic search for such systems produced five new discoveries in a well-referenced study by Van Reeth et al. (2023).

[5] Sharma et al. 2022, in particular, cited the many investigations into this.

The hallmark of tidally trapped pulsations are pulsation amplitudes that vary strongly with orbital phase and in addition to the effects of eclipses masking the pulsator. The amplitude variation results from tidally-induced asphericity, and Fuller et al. (2020) described the three resulting phenomena. The first is tidal alignment. Ordinarily the stellar rotation axis is the axis of symmetry for pulsations. Not so in close binaries, where tidal braking of the stellar rotation (Tassoul & Tassoul, 1992a,b) and tidal distortion lead to the tidal axis being the axis of alignment instead. Hence, the pulsation pole comes into and out of view twice each orbital cycle. The second phenomenon is tidal trapping, wherein the modes themselves are spatially confined to either the tidal poles or the tidal equator, further affecting their visibility over an orbital cycle. The third phenomenon is tidal amplification. This effect occurs when modes are able to propagate closer to the stellar surface. A pulsation wave's outer turning point is defined by the acoustic cutoff frequency, which depends on the surface gravity and is ordinarily independent of latitude. But in a close binary, the surface gravity is markedly lower at the L1 Lagrangian point, allowing the modes to propagate closer to the surface and become 'amplified'.

More work on tidally trapped pulsators can be expected in the near future as different geometries are observed for the first time (e.g. systems viewed from the tidal poles), and as modellers keep pace with the rate of observations to include the effects of tides on the pulsation models.

6. Pulsators in eclipsing binaries

The proliferation of space-based light curves, particularly resulting from TESS's all-sky coverage, has dramatically increased the number of known eclipsing binaries (Prša et al., 2022). This is particularly the case for B stars, which were not observed in large numbers by *Kepler* due the avoidance of bright stars and due to the *Kepler* field lying out of the galactic plane (Koch et al., 2010). TESS's smaller size lends itself to observing brighter stars than *Kepler* and has indirectly resulted in many of the newly-discovered EBs being A stars, which strike a balance between being bright and numerous (IJspeert et al. 2021; Southworth, these proceedings). It is no surprise, then, that the number of studies on pulsating stars in EBs suddenly shot up in the TESS era (Southworth et al., 2020; Budding et al., 2021; Lee & Hong, 2021; Southworth et al., 2021; Erdem et al., 2022). While most of these 'early' studies concerned single systems, it was not long before ensembles were also collated (Southworth & Bowman, 2022; Kahraman Aliçavuş et al., 2022, 2023; Ulaş & Ulusoy, 2023; Catanzaro et al., 2024; Eze & Handler, 2024).

The talk upon which this review is based had concluded with a couple of lessons learned by the author from recent studies of pulsators in EBs, and so this review concludes the same way. The first of those lessons was that spin-orbit alignment of binary systems cannot always be assumed. This lesson came

from the VV Ori system, consisting of a β Cep pulsator and an SPB star in a 1.49-d orbit, recently reported to show changes in the primary's inclination and changes in the totality of its eclipses (Southworth et al., 2021; Budding et al., 2024). Earlier analyses of many other systems as part of the BANANA project ('Binaries Are Not Always Neatly Aligned') held the same clues, wherein systems with good alignment and others with misalignment were found (Albrecht et al., 2009, 2011, 2012, 2014).

The second lesson came from the triple system V1031 Ori, which has a δ Sct component. That lesson was that Gaia distances for binaries and multiples are not yet trustworthy (as of Gaia DR3). The distance to this system from the EB analysis has yielded 210 ± 26 pc (Lee, 2021), which compares favourably to earlier comprehensive studies (215 ± 25 pc, Andersen et al. 1990) and Hipparcos (205 ± 30 pc, van Leeuwen 2007). However, it is somewhat discrepant with the distance from Gaia EDR3 [588^{+389}_{-198} pc (geometric) and 734^{+290}_{-258} pc (photogeometric); see Lee 2021 for details]. Even in the full DR3 release, the `gspphot` distance is inaccurate at $150.8^{+3.3}_{-3.6}$ pc, though it is now underestimated rather than overestimated. The problem is not universal – HD 23642 is another EB with a δ Sct component and has good agreement between the distance derived from eclipses (134.7 ± 2 pc, Southworth et al. 2023) and from Gaia (`gspphot` $= 137.6 \pm 1$ pc in DR3). Pending updated astrometry in Gaia DR4, V1031 Ori serves as a caution.

Acknowledgements. SJM was supported by the Australian Research Council (ARC) through Future Fellowship FT210100485.

References

Aerts, C. & Tkachenko, A., PLATO Complementary Science. 2024, in *8th TESS/15th Kepler Asteroseismic Science Consortium Workshop*, 22

Albrecht, S., Reffert, S., Snellen, I. A. G., & Winn, J. N., Misaligned spin and orbital axes cause the anomalous precession of DI Herculis. 2009, *Nature*, **461**, 373, DOI: 10.1038/nature08408

Albrecht, S., Winn, J. N., Carter, J. A., Snellen, I. A. G., & de Mooij, E. J. W., The Banana Project. III. Spin-Orbit Alignment in the Long-period Eclipsing Binary NY Cephei. 2011, *Astrophysical Journal*, **726**, 68, DOI:10.1088/0004-637X/726/2/68

Albrecht, S., Winn, J. N., Fabrycky, D. C., Torres, G., & Setiawan, J., The BANANA Survey: Spin-Orbit Alignment in Binary Stars. 2012, in IAU Symposium, Vol. **282**, *From Interacting Binaries to Exoplanets: Essential Modeling Tools*, ed. M. T. Richards & I. Hubeny, 397–398

Albrecht, S., Winn, J. N., Torres, G., et al., The BANANA Project. V. Misaligned and Precessing Stellar Rotation Axes in CV Velorum. 2014, *Astrophysical Journal*, **785**, 83, DOI:10.1088/0004-637X/785/2/83

Andersen, J., Clausen, J. V., & Nordstrom, B., Absolute dimensions of eclipsing binaries. XVI. V1031 Orionis. 1990, *Astronomy and Astrophysics*, **228**, 365

Appourchaux, T., Antia, H. M., Ball, W., et al., A seismic and gravitationally bound double star observed by Kepler. Implication for the presence of a convective core. 2015, *Astronomy and Astrophysics*, **582**, A25, DOI:10.1051/0004-6361/201526610

Arentoft, T., Kjeldsen, H., Bedding, T. R., et al., A Multisite Campaign to Measure Solar-like Oscillations in Procyon. I. Observations, Data Reduction, and Slow Variations. 2008, *Astrophysical Journal*, **687**, 1180, DOI:10.1086/592040

Balona, L. A., The effect of tides on self-driven stellar pulsations. 2018, *Monthly Notices of the RAS*, **476**, 4840, DOI:10.1093/mnras/sty544

Baran, A. S., Van Grootel, V., Østensen, R. H., et al., Short-period pulsating hot-subdwarf stars observed by TESS. I. Southern ecliptic hemisphere. 2023, *Astronomy and Astrophysics*, **669**, A48, DOI:10.1051/0004-6361/202244888

Barlow, B. N., Dunlap, B. H., & Clemens, J. C., Radial Velocity Confirmation of a Binary Detected from Pulse Timings. 2011a, *Astrophysical Journal, Letters*, **737**, L2, DOI:10.1088/2041-8205/737/1/L2

Barlow, B. N., Dunlap, B. H., Clemens, J. C., et al., Fortnightly fluctuations in the O-C diagram of CS 1246. 2011b, *Monthly Notices of the RAS*, **414**, 3434, DOI:10.1111/j.1365-2966.2011.18645.x

Barnes, III, T. G. & Moffett, T. J., Photometric properties and evidence of duplicity for SZ Lyncis. 1975, *Astronomical Journal*, **80**, 48, DOI:10.1086/111712

Beck, P. G., Grossmann, D. H., Steinwender, L., et al., Constraining stellar and orbital co-evolution through ensemble seismology of solar-like oscillators in binary systems. A census of oscillating red giants and dwarf stars in Gaia DR3 binaries. 2024, *Astronomy and Astrophysics*, **682**, A7, DOI:10.1051/0004-6361/202346810

Bedding, T. R. & Kjeldsen, H., Observations of solar-like oscillations. 2007, *Communications in Asteroseismology*, **150**, 106, DOI:10.1553/cia150s106

Bognár, Z., Kawaler, S. D., Bell, K. J., et al., TESS first look at evolved compact pulsators. Known ZZ Ceti stars of the southern ecliptic hemisphere as seen by TESS. 2020, *Astronomy and Astrophysics*, **638**, A82, DOI:10.1051/0004-6361/202037470

Bowman, D. M. & Bugnet, L., Asteroseismology. 2024, *arXiv e-prints*, arXiv:2410.01715, DOI:10.48550/arXiv.2410.01715

Bowman, D. M., Johnston, C., Tkachenko, A., et al., Discovery of Tidally Perturbed Pulsations in the Eclipsing Binary U Gru: A Crucial System for Tidal Asteroseismology. 2019, *Astrophysical Journal, Letters*, **883**, L26, DOI:10.3847/2041-8213/ab3fb2

Bowman, D. M. & Kurtz, D. W., Characterizing the observational properties of δ Sct stars in the era of space photometry from the Kepler mission. 2018, *Monthly Notices of the RAS*, **476**, 3169, DOI:10.1093/mnras/sty449

Budding, E., Love, T., Blackford, M. G., Banks, T., & Rhodes, M. J., Absolute parameters of young stars: V Puppis. 2021, *Monthly Notices of the RAS*, **502**, 6032, DOI:10.1093/mnras/stab381

Budding, E., Southworth, J., Pavlovski, K., et al., The enigmatic multiple star VV Ori. 2024, *Monthly Notices of the RAS*, **527**, 6389, DOI:10.1093/mnras/stad3586

Campante, T. L., Kjeldsen, H., Li, Y., et al., Expanding the frontiers of cool-dwarf asteroseismology with ESPRESSO. Detection of solar-like oscillations in the K5 dwarf epsilon Indi. 2024, *Astronomy and Astrophysics*, **683**, L16, DOI:10.1051/0004-6361/202449197

Catanzaro, G., Frasca, A., Alonso-Santiago, J., & Colombo, C., TESS photometry and CAOS spectroscopy of six eclipsing binaries with Am components. 2024, *Astronomy and Astrophysics*, **685**, A133, DOI:10.1051/0004-6361/202449332

Compton, D. L., Bedding, T. R., Murphy, S. J., & Stello, D., Binary star detectability in Kepler data from phase modulation of different types of oscillations. 2016, *Monthly Notices of the RAS*, **461**, 1943, DOI:10.1093/mnras/stw1092

Deheuvels, S., Ballot, J., Gehan, C., & Mosser, B., Seismic signature of electron degeneracy in the core of red giants: Hints for mass transfer between close red-giant companions. 2022, *Astronomy and Astrophysics*, **659**, A106, DOI:10.1051/0004-6361/202142094

Derekas, A., Murphy, S. J., Dálya, G., et al., Spectroscopic confirmation of the binary nature of the hybrid pulsator KIC 5709664 found with the frequency modulation method. 2019, *Monthly Notices of the RAS*, **486**, 2129, DOI:10.1093/mnras/stz875

Dholakia, S., Murphy, S. J., Huang, C. X., Venner, A., & Wright, D., A catalog of binary stars from phase modulation in the first four years of TESS Mission photometry. 2024, *arXiv e-prints*, arXiv:2410.19729, DOI:10.48550/arXiv.2410.19729

Erdem, A., Sürgit, D., Özkardeş, B., et al., V410 Puppis: A useful laboratory for early stellar evolution. 2022, *Monthly Notices of the RAS*, **515**, 6151, DOI:10.1093/mnras/stac2150

Eze, C. I. & Handler, G., β Cephei Pulsators in Eclipsing Binaries Observed with TESS. 2024, *Astrophysical Journal, Supplement*, **272**, 25, DOI:10.3847/1538-4365/ad39c5

Fuller, J., Kurtz, D. W., Handler, G., & Rappaport, S., Tidally trapped pulsations in binary stars. 2020, *Monthly Notices of the RAS*, **498**, 5730, DOI:10.1093/mnras/staa2376

Ge, J., Zhang, H., Zang, W., et al., ET White Paper: To Find the First Earth 2.0. 2022, *arXiv e-prints*, arXiv:2206.06693, DOI:10.48550/arXiv.2206.06693

Halbwachs, J.-L., Pourbaix, D., Arenou, F., et al., Gaia Data Release 3. Astrometric binary star processing. 2023, *Astronomy and Astrophysics*, **674**, A9, DOI:10.1051/0004-6361/202243969

Hambleton, K. M., Kurtz, D. W., Prša, A., et al., KIC 4544587: an eccentric, short-period binary system with δ Sct pulsations and tidally excited modes. 2013, *Monthly Notices of the RAS*, **434**, 925, DOI:10.1093/mnras/stt886

Handler, G., Kurtz, D. W., Rappaport, S. A., et al., Tidally trapped pulsations in a close binary star system discovered by TESS. 2020, *Nature Astronomy*, **4**, 684, DOI:10.1038/s41550-020-1035-1

Hatt, E., Nielsen, M. B., Chaplin, W. J., et al., Catalogue of solar-like oscillators observed by TESS in 120-s and 20-s cadence. 2023, *Astronomy and Astrophysics*, **669**, A67, DOI:10.1051/0004-6361/202244579

Hermes, J. J., Timing by Stellar Pulsations as an Exoplanet Discovery Method. 2018, in *Handbook of Exoplanets*, ed. H. J. Deeg & J. A. Belmonte (Springer International Publishing AG), 6

Hey, D. & Aerts, C., Confronting sparse Gaia DR3 photometry with TESS for a sample of around 60 000 OBAF-type pulsators. 2024, *Astronomy and Astrophysics*, **688**, A93, DOI:10.1051/0004-6361/202450489

Hey, D., Murphy, S., Foreman-Mackey, D., et al., Maelstrom: A Python package for identifying companions to pulsating stars from their light travel time variations. 2020a, *The Journal of Open Source Software*, **5**, 2125, DOI:10.21105/joss.02125

Hey, D. R., Holdsworth, D. L., Bedding, T. R., et al., Six new rapidly oscillating Ap stars in the Kepler long-cadence data using super-Nyquist asteroseismology. 2019, *Monthly Notices of the RAS*, **488**, 18, DOI:10.1093/mnras/stz1633

Hey, D. R., Montet, B. T., Pope, B. J. S., Murphy, S. J., & Bedding, T. R., A Search for Transits among the Delta Scuti Variables in Kepler. 2021, *Astronomical Journal*, **162**, 204, DOI:10.3847/1538-3881/ac1b9b

Hey, D. R., Murphy, S. J., Foreman-Mackey, D., et al., Forward Modeling the Orbits of Companions to Pulsating Stars from Their Light Travel Time Variations. 2020b, *Astronomical Journal*, **159**, 202, DOI:10.3847/1538-3881/ab7d38

Holl, B., Sozzetti, A., Sahlmann, J., et al., Gaia Data Release 3. Astrometric orbit determination with Markov chain Monte Carlo and genetic algorithms: Systems with stellar, sub-stellar, and planetary mass companions. 2023, *Astronomy and Astrophysics*, **674**, A10, DOI:10.1051/0004-6361/202244161

Huber, D., Pinsonneault, M., Beck, P., et al., Asteroseismology with the Roman Galactic Bulge Time-Domain Survey. 2023, *arXiv e-prints*, arXiv:2307.03237, DOI:10.48550/arXiv.2307.03237

IJspeert, L. W., Tkachenko, A., Johnston, C., et al., An all-sky sample of intermediate- to high-mass OBA-type eclipsing binaries observed by TESS. 2021, *Astronomy and Astrophysics*, **652**, A120, DOI:10.1051/0004-6361/202141489

Kahraman Aliçavuş, F., Çoban, Ç. G., Çelik, E., et al., Discovery of delta Scuti variables in eclipsing binary systems II. Southern TESS field search. 2023, *Monthly Notices of the RAS*, **524**, 619, DOI:10.1093/mnras/stad1898

Kahraman Aliçavuş, F., Gümüş, D., Kırmızıtaş, Ö., et al., Candidate Eclipsing Binary Systems with a δ Scuti Star in Northern TESS Field. 2022, *Research in Astronomy and Astrophysics*, **22**, 085003, DOI:10.1088/1674-4527/ac71a4

Kahraman Aliçavuş, F., Handler, G., Chowdhury, S., et al., On the Existence of "Maia variables". 2024, *arXiv e-prints*, arXiv:2404.16988, DOI:10.48550/arXiv.2404.16988

Kjeldsen, H. & Bedding, T. R., Amplitudes of stellar oscillations: the implications for asteroseismology. 1995, *Astronomy and Astrophysics*, **293**, 87

Kjeldsen, H., Bedding, T. R., Arentoft, T., et al., The Amplitude of Solar Oscillations Using Stellar Techniques. 2008, *Astrophysical Journal*, **682**, 1370, DOI:10.1086/589142

Koch, D. G., Borucki, W. J., Basri, G., et al., Kepler Mission Design, Realized Photometric Performance, and Early Science. 2010, *Astrophysical Journal, Letters*, **713**, L79, DOI:10.1088/2041-8205/713/2/L79

Kurtz, D. W., Asteroseismology Across the Hertzsprung-Russell Diagram. 2022, *Annual Review of Astron and Astrophys*, **60**, 31, DOI:10.1146/annurev-astro-052920-094232

Kurtz, D. W., Hambleton, K. M., Shibahashi, H., Murphy, S. J., & Prša, A., Validation of the frequency modulation technique applied to the pulsating δ Sct-γ Dor eclipsing binary star KIC 8569819. 2015, *Monthly Notices of the RAS*, **446**, 1223, DOI:10.1093/mnras/stu2075

Lampens, P., Vermeylen, L., Frémat, Y., et al., Orbital solutions derived from radial velocities and time delays for four Kepler systems with A/F-type (candidate) hybrid pulsators. 2021, *Astronomy and Astrophysics*, **647**, A139, DOI:10.1051/0004-6361/202039389

Lee, J. W., Tidally perturbed oblique pulsations in the hierarchical triple system V1031 Orionis. 2021, *Publications of the ASJ*, **73**, 809, DOI:10.1093/pasj/psab044

Lee, J. W. & Hong, K., β Cephei Pulsations in the High-mass Eclipsing System CW Cephei. 2021, *Astronomical Journal*, **161**, 32, DOI:10.3847/1538-3881/abbfff

Lee, J. W., Hong, K., Kim, H.-Y., & Park, J.-H., The pre-He white dwarfs in eclipsing binaries - IV. WASP 1814+48 with multiperiodic pulsations. 2022, *Monthly Notices of the RAS*, **515**, 4702, DOI:10.1093/mnras/stac2151

Li, Y., Bedding, T. R., Li, T., et al., Asteroseismology of KIC 7107778: a binary comprising almost identical subgiants. 2018, *Monthly Notices of the RAS*, **476**, 470, DOI:10.1093/mnras/sty222

Li, Y., Bedding, T. R., Murphy, S. J., et al., Discovery of post-mass-transfer helium-burning red giants using asteroseismology. 2022, *Nature Astronomy*, **6**, 673, DOI:10.1038/s41550-022-01648-5

Lund, M. N., Silva Aguirre, V., Davies, G. R., et al., Standing on the Shoulders of Dwarfs: the Kepler Asteroseismic LEGACY Sample. I. Oscillation Mode Parameters. 2017, *Astrophysical Journal*, **835**, 172, DOI:10.3847/1538-4357/835/2/172

Lundkvist, M. S., Kjeldsen, H., Bedding, T. R., et al., Low-amplitude Solar-like Oscillations in the K5 V Star Epsilon Indi A. 2024, *Astrophysical Journal*, **964**, 110, DOI:10.3847/1538-4357/ad25f2

Lyu, X. & Yang, M., Hidden Companions Detected by Asteroseismology. II. A Long-period Noneclipsing Binary System Revealed by Kepler and TESS. 2023, *Astrophysical Journal, Letters*, **943**, L7, DOI:10.3847/2041-8213/acb056

Mackebrandt, F., Schuh, S., Silvotti, R., et al., The EXOTIME project: signals in the O-C diagrams of the rapidly pulsating subdwarfs DW Lyn, V1636 Ori, QQ Vir, and V541 Hya. 2020, *Astronomy and Astrophysics*, **638**, A108, DOI:10.1051/0004-6361/201937172

Manzoori, D., Linear and non-linear tidal oscillations and mode identification in the eccentric binary system KIC 3858884. 2020, *Monthly Notices of the RAS*, **498**, 1871, DOI:10.1093/mnras/staa2207

Mathur, S., Huber, D., Batalha, N. M., et al., Revised Stellar Properties of Kepler Targets for the Q1-17 (DR25) Transit Detection Run. 2017, *Astrophysical Journal, Supplement*, **229**, 30, DOI:10.3847/1538-4365/229/2/30

Matteuzzi, M., Hendriks, D., Izzard, R. G., et al., Anomalously low-mass core-He-burning star in NGC 6819 as a post-common-envelope phase product. 2024, *arXiv e-prints*, arXiv:2408.11095, DOI:10.48550/arXiv.2408.11095

Mazzi, A., Miglio, A., Girardi, L., Corsaro, E., & Thomsen, J., Gaining insights into binary populations by combining photometric and spectroscopic data with asteroseismology. 2024, in *EAS2024*, 2065

Miglio, A., Chaplin, W. J., Farmer, R., et al., Prospects for Detecting Asteroseismic Binaries in Kepler Data. 2014, *Astrophysical Journal, Letters*, **784**, L3, DOI:10.1088/2041-8205/784/1/L3

Moe, M. & Di Stefano, R., Mind Your Ps and Qs: The Interrelation between Period (P) and Mass-ratio (Q) Distributions of Binary Stars. 2017, *Astrophysical Journal, Supplement*, **230**, 15, DOI:10.3847/1538-4365/aa6fb6

Mombarg, J. S. G., Aerts, C., & Molenberghs, G., Probability distributions of initial rotation velocities and core-boundary mixing efficiencies of γ Doradus stars. 2024, *Astronomy and Astrophysics*, **685**, A21, DOI:10.1051/0004-6361/202449213

Murphy, S. J., Pulsating stars in binary systems: a review. 2018, *arXiv e-prints*, arXiv:1811.12659, DOI:10.5281/zenodo.1739519

Murphy, S. J., Barbara, N. H., Hey, D., Bedding, T. R., & Fulcher, B. D., Finding binaries from phase modulation of pulsating stars with Kepler - VI. Orbits for 10 new binaries with mischaracterized primaries. 2020a, *Monthly Notices of the RAS*, **493**, 5382, DOI:10.1093/mnras/staa562

Murphy, S. J., Bedding, T. R., Gautam, A., Kerr, R. P., & Mani, P., The δ Scuti stars of the Cep-Her Complex - I. Pulsator fraction, rotation, asteroseismic large spacings, and the ν_{max} relation. 2024, *Monthly Notices of the RAS*, **534**, 3022, DOI:10.1093/mnras/stae2226

Murphy, S. J., Bedding, T. R., Shibahashi, H., Kurtz, D. W., & Kjeldsen, H., Finding binaries among Kepler pulsating stars from phase modulation of their pulsations. 2014, *Monthly Notices of the RAS*, **441**, 2515, DOI:10.1093/mnras/stu765

Murphy, S. J., Hey, D., Van Reeth, T., & Bedding, T. R., Gaia-derived luminosities of Kepler A/F stars and the pulsator fraction across the δ Scuti instability strip. 2019, *Monthly Notices of the RAS*, **485**, 2380, DOI:10.1093/mnras/stz590

Murphy, S. J., Li, T., Sekaran, S., et al., A binary with a δ Scuti star and an oscillating red giant: orbit and asteroseismology of KIC 9773821. 2021, *Monthly Notices of the RAS*, **505**, 2336, DOI:10.1093/mnras/stab1436

Murphy, S. J., Moe, M., Kurtz, D. W., et al., Finding binaries from phase modulation of pulsating stars with Kepler: V. Orbital parameters, with eccentricity and mass-

ratio distributions of 341 new binaries. 2018, *Monthly Notices of the RAS*, **474**, 4322, DOI:10.1093/mnras/stx3049

Murphy, S. J., Saio, H., Takada-Hidai, M., et al., On the first δ Sct-roAp hybrid pulsator and the stability of p and g modes in chemically peculiar A/F stars. 2020b, *Monthly Notices of the RAS*, **498**, 4272, DOI:10.1093/mnras/staa2667

Murphy, S. J., Shibahashi, H., & Bedding, T. R., Finding binaries from phase modulation of pulsating stars with Kepler - IV. Detection limits and radial velocity verification. 2016, *Monthly Notices of the RAS*, **461**, 4215, DOI:10.1093/mnras/stw1622

Offner, S. S. R., Moe, M., Kratter, K. M., et al., The Origin and Evolution of Multiple Star Systems. 2023, in Astronomical Society of the Pacific Conference Series, Vol. **534**, *Protostars and Planets VII*, ed. S. Inutsuka, Y. Aikawa, T. Muto, K. Tomida, & M. Tamura, 275

Oomen, G.-M., Van Winckel, H., Pols, O., et al., Orbital properties of binary post-AGB stars. 2018, *Astronomy and Astrophysics*, **620**, A85, DOI:10.1051/0004-6361/201833816

Otani, T., Lynas-Gray, A. E., Kilkenny, D., et al., Anomalous Orbital Characteristics of the AQ Col (EC 05217-3914) System. 2022, *Astrophysical Journal*, **926**, 17, DOI:10.3847/1538-4357/ac3a72

Paczynski, B., Common Envelope Binaries. 1976, in IAU Symposium, Vol. **73**, *Structure and Evolution of Close Binary Systems*, ed. P. Eggleton, S. Mitton, & J. Whelan, 75

Pollard, K., Rea, B., Gunn, F., Luisi, J., & Zhou, Y., High-degree modes in the southern pole star: The δ Scuti star σ Octantis. 2024, in *8th TESS/15th Kepler Asteroseismic Science Consortium Workshop*, 55

Pope, B. J. S., Davies, G. R., Hawkins, K., et al., The Kepler Smear Campaign: Light Curves for 102 Very Bright Stars. 2019, *Astrophysical Journal, Supplement*, **244**, 18, DOI:10.3847/1538-4365/ab2c04

Prša, A., Kochoska, A., Conroy, K. E., et al., TESS Eclipsing Binary Stars. I. Short-cadence Observations of 4584 Eclipsing Binaries in Sectors 1-26. 2022, *Astrophysical Journal, Supplement*, **258**, 16, DOI:10.3847/1538-4365/ac324a

Rains, A. D., Ireland, M. J., White, T. R., Casagrande, L., & Karovicova, I., Precision angular diameters for 16 southern stars with VLTI/PIONIER. 2020, *Monthly Notices of the RAS*, **493**, 2377, DOI:10.1093/mnras/staa282

Reinhold, T. & Hekker, S., Stellar rotation periods from K2 Campaigns 0-18. Evidence for rotation period bimodality and simultaneous variability decrease. 2020, *Astronomy and Astrophysics*, **635**, A43, DOI:10.1051/0004-6361/201936887

Ricker, G. R., Winn, J. N., Vanderspek, R., et al., Transiting Exoplanet Survey Satellite (TESS). 2015, *Journal of Astronomical Telescopes, Instruments, and Systems*, **1**, 014003, DOI:10.1117/1.JATIS.1.1.014003

Rieutord, M., Petit, P., Reese, D., et al., Spectroscopic detection of Altair's non-radial pulsations. 2023, *Astronomy and Astrophysics*, **669**, A99, DOI:10.1051/0004-6361/202245017

Rucinski, S., Determination of Broadening Functions Using the Singular-Value Decomposition (SVD) Technique. 1999, in Astronomical Society of the Pacific Conference Series, Vol. **185**, *IAU Colloq. 170: Precise Stellar Radial Velocities*, ed. J. B. Hearnshaw & C. D. Scarfe, 82

Rui, N. Z. & Fuller, J., Asteroseismic fingerprints of stellar mergers. 2021, *Monthly Notices of the RAS*, **508**, 1618, DOI:10.1093/mnras/stab2528

Sharma, A. N., Bedding, T. R., Saio, H., & White, T. R., Pulsating B stars in the Scorpius-Centaurus Association with TESS. 2022, *Monthly Notices of the RAS*, **515**, 828, DOI:10.1093/mnras/stac1816

Shibahashi, H. & Kurtz, D. W., FM stars: a Fourier view of pulsating binary stars, a new technique for measuring radial velocities photometrically. 2012, *Monthly Notices of the RAS*, **422**, 738, DOI:10.1111/j.1365-2966.2012.20654.x

Shibahashi, H., Kurtz, D. W., & Murphy, S. J., FM stars II: a Fourier view of pulsating binary stars - determining binary orbital parameters photometrically for highly eccentric cases. 2015, *Monthly Notices of the RAS*, **450**, 3999, DOI:10.1093/mnras/stv875

Southworth, J., Rediscussion of eclipsing binaries. Paper 7: Delta Scuti, Gamma Doradus, and tidally-perturbed pulsations in RR Lyncis. 2021, *The Observatory*, **141**, 282, DOI:10.48550/arXiv.2109.10196

Southworth, J. & Bowman, D. M., High-mass pulsators in eclipsing binaries observed using TESS. 2022, *Monthly Notices of the RAS*, **513**, 3191, DOI:10.1093/mnras/stac875

Southworth, J., Bowman, D. M., & Pavlovski, K., A β Cephei pulsator and a changing orbital inclination in the high-mass eclipsing binary system VV Orionis. 2021, *Monthly Notices of the RAS*, **501**, L65, DOI:10.1093/mnrasl/slaa197

Southworth, J., Bowman, D. M., Tkachenko, A., & Pavlovski, K., Discovery of β Cep pulsations in the eclipsing binary V453 Cygni. 2020, *Monthly Notices of the RAS*, **497**, L19, DOI:10.1093/mnrasl/slaa091

Southworth, J., Murphy, S. J., & Pavlovski, K., δ Scuti pulsations in the bright Pleiades eclipsing binary HD 23642. 2023, *Monthly Notices of the RAS*, **520**, L53, DOI:10.1093/mnrasl/slad004

Stassun, K. G., Oelkers, R. J., Paegert, M., et al., The Revised TESS Input Catalog and Candidate Target List. 2019, *Astronomical Journal*, **158**, 138, DOI:10.3847/1538-3881/ab3467

Steindl, T., Zwintz, K., & Bowman, D. M., Tidally perturbed pulsations in the pre-main sequence δ Scuti binary RS Cha. 2021, *Astronomy and Astrophysics*, **645**, A119, DOI:10.1051/0004-6361/202039093

Sterken, C., The O-C Diagram: Basic Procedures. 2005, in Astronomical Society of the Pacific Conference Series, Vol. **335**, *The Light-Time Effect in Astrophysics: Causes and cures of the O-C diagram*, ed. C. Sterken, 3

Szewczuk, W. & Daszyńska-Daszkiewicz, J., KIC 3240411 - the hottest known SPB star with the asymptotic g-mode period spacing. 2018, *Monthly Notices of the RAS*, **478**, 2243, DOI:10.1093/mnras/sty1126

Tassoul, J.-L. & Tassoul, M., A comparative study of synchronization and circularization in close binaries. 1992a, *Astrophysical Journal*, **395**, 259, DOI:10.1086/171647

Tassoul, M. & Tassoul, J.-L., On the efficiency of Ekman pumping for synchronization in close binaries. 1992b, *Astrophysical Journal*, **395**, 604, DOI:10.1086/171680

Themeßl, N., Hekker, S., Southworth, J., et al., Oscillating red giants in eclipsing binary systems: empirical reference value for asteroseismic scaling relation. 2018, *Monthly Notices of the RAS*, **478**, 4669, DOI:10.1093/mnras/sty1113

Ulaş, B. & Ulusoy, C., Discovery of δ Sct components in eclipsing binary systems IQ CMa, AW men and W Vol. 2023, *Monthly Notices of the RAS*, **518**, 4180, DOI:10.1093/mnras/stac3345

van Leeuwen, F., Validation of the new Hipparcos reduction. 2007, *Astronomy and Astrophysics*, **474**, 653, DOI:10.1051/0004-6361:20078357

Van Reeth, T., Johnston, C., Southworth, J., et al., Tidally perturbed gravity-mode pulsations in a sample of close eclipsing binaries. 2023, *Astronomy and Astrophysics*, **671**, A121, DOI:10.1051/0004-6361/202245460

Van Reeth, T., Southworth, J., Van Beeck, J., & Bowman, D. M., V456 Cyg: An eclipsing binary with tidally perturbed g-mode pulsations. 2022, *Astronomy and Astrophysics*, **659**, A177, DOI:10.1051/0004-6361/202142833

Vaulato, V., Nascimbeni, V., & Piotto, G., TESS search for substellar companions through pulsation timing of δ Scuti stars. I. Discovery of companions around Chang 134 and V393 Car. 2022, *Astronomy and Astrophysics*, **668**, A110, DOI:10.1051/0004-6361/202244592

White, T. R., Benomar, O., Silva Aguirre, V., et al., Kepler observations of the asteroseismic binary HD 176465. 2017, *Astronomy and Astrophysics*, **601**, A82, DOI:10.1051/0004-6361/201628706

Yang, M., Hidden Companions Detected by Asteroseismology. I. Two Kepler Field Non-Eclipsing Binaries. 2022, *Universe*, **8**, 614, DOI:10.3390/universe8120614

Yang, T.-Z., Zuo, Z.-Y., Li, G., et al., TIC 308396022: δ Scuti-γ Doradus hybrid with large-amplitude radial fundamental mode and regular g-mode period spacing. 2021, *Astronomy and Astrophysics*, **655**, A63, DOI:10.1051/0004-6361/202142198

Zieba, S., Zwintz, K., Kenworthy, M., et al., The β Pictoris b Hill sphere transit campaign. II. Searching for the signatures of the β Pictoris exoplanets through time delay analysis of the δ Scuti pulsations. 2024, *Astronomy and Astrophysics*, **687**, A309, DOI:10.1051/0004-6361/202347754

Contrib. Astron. Obs. Skalnaté Pleso **55/3**, 141 – 151, (2025)
https://doi.org/10.31577/caosp.2025.55.3.141

Cepheids in spectroscopic binary systems - current status and recent discoveries

B. Pilecki

Centrum Astronomiczne im. M. Kopernika PAN, Warsaw, Poland
(E-mail: pilecki@camk.edu.pl)

Received: December 12, 2024; Accepted: January 11, 2024

Abstract. We present a summary of the current knowledge about Cepheids in binary systems. We focus on the most recent findings and discoveries, such as the highly increasing number of confirmed and candidate spectroscopic binary Cepheids and the progress in determining their physical parameters. This includes new and newly analyzed binary Cepheids in the Milky Way and Magellanic Clouds. We will provide an update on the project to increase the number of the most valuable Cepheids in double-lined binary (SB2) systems from six to more than 100. To date, we have confirmed 60 SB2 systems, including detecting a significant orbital motion for 37. We identified systems with orbital periods up to five times shorter than the shortest period reported before and systems with mass ratios significantly different from unity (suggesting past binary interactions, including merger events). Both features are essential to understanding how multiplicity affects the formation and destruction of Cepheid progenitors and how this influences global Cepheid properties. We will also present nine new systems composed of two Cepheids. Only one such double Cepheid system was known before.

Key words: stars: variables: Cepheids - binaries: spectroscopic - stars: oscillations - stars: evolution

1. Introduction

Classical Cepheids (hereafter also Cepheids) are crucial for various fields of astronomy, including stellar oscillations and the evolution of intermediate and massive stars, and have an enormous influence on modern cosmology (see, e.g., the review of Bono et al., 2024). Since the discovery of the relationship between their pulsation period and luminosity (the Leavitt Law, Leavitt & Pickering 1912), the Cepheids have been extensively used to measure distances in the Universe (Anderson, 2024). The recent local Hubble constant determination accurate to 1.4% (Riess et al., 2022), which shows a significant discrepancy with the value inferred from *Planck* data, depends sensitively on this period–luminosity (P–L) relation.

Theoretical studies of Cepheids are quite advanced (e.g., Bono et al. 1999, 2005; Valle et al. 2009). We know they are radially pulsating evolved intermediate and high-mass giants and supergiants, mostly located in a well-defined

position on the helium-burning loop (called the *blue loop*). A small fraction of Cepheids is expected to pulsate during their first crossing through the instability strip on their way to the red giant branch. Empirical relations of different types are also often obtained and applied (Soszynski et al., 2008; Storm et al., 2011; Riess et al., 2019; Espinoza-Arancibia et al., 2024; Pilecki, 2024). However, our knowledge about the physical properties of Cepheids is still limited. Theory predicts masses of Cepheids in the range of 3–13 $M_\odot$, but their measured masses clump between 3.6 $M_\odot$ and 5 $M_\odot$, with only one higher but uncertain value of 6.7 $M_\odot$ (Pilecki et al., 2018; Evans et al., 2018, 2024a). This makes the Cepheid mass–luminosity relation poorly constrained (Anderson et al., 2016). Moreover, the blue loops predicted by current evolution theory are too short to explain the existence of low-mass, short-period Cepheids (see, e.g., Ripepi et al., 2022; Espinoza-Arancibia et al., 2024).

In the last decade, the expected fraction of classical Cepheids in multiple systems has grown to about 80% (Kervella et al., 2019), indicating that we cannot ignore their multiplicity in our studies. The light of a companion directly affects the observed brightness of Cepheids, but the tidal deformation, mass transfer, and merger origin may also impact their intrinsic brightness. The binary interactions, changing the stellar rotation, chemical composition, and mass, may affect the evolution of Cepheids and influence their pulsation characteristics.

There are almost 15000 known classical Cepheids (Pietrukowicz et al., 2021), mainly in the MW (Pojmanski et al., 2005; Soszyński et al., 2020, and references therein) and the Magellanic Clouds (Soszyński et al., 2017). Although 80% of these Cepheids are expected to be members of binary systems, only about 0.1% of them have been found in eclipsing systems, and 0.2% in double-lined spectroscopic binaries (SB2), while both these features provide indispensable information about the physical properties of Cepheids.

Here, we summarize the current state regarding single and double Cepheids in binary systems. We will focus mainly on those that were or can be used to determine the physical parameters of Cepheids, thus primarily focusing on eclipsing and SB2 Cepheids.

2. Binarity of Cepheids

Since the discovery of the binarity of Polaris in 1929 (Moore, 1929), many Cepheids in binary systems in the Milky Way were identified. In the updated catalog of Szabados (2003)[1], there are 171 Cepheids that are either binary or suspected for binarity. For 31 of them, orbital elements are also provided. In the recent study based on a large set of new spectroscopic data from the VELOCE project (Anderson et al., 2024), 32 new Cepheids in single-lined spectroscopic binary (SB1) systems were found, and orbital solutions for 18 of them were provided (Shetye et al., 2024). Unfortunately, all Cepheids from these two samples

[1]https://webarch.konkoly.hu/cep/intro.html; last update in 2019

have main sequence companions that are hardly seen in the spectra. None of these Cepheids were found in an eclipsing system.

In the Milky Way, there are only two known binary Cepheids without a main sequence companion, for which lines of both components can be easily seen and analyzed. Each comprises two Cepheids, i.e., stars practically in the same evolutionary phase. More information on them is given in Section 3. There is also one candidate for an eclipsing binary Cepheid (Soszyński et al., 2020), most probably of SB1 type.

In the analysis of Cepheid variables in the OGLE project (Soszyński et al., 2017), six candidates for eclipsing binary Cepheids were identified in the Large Magellanic Cloud (LMC) galaxy. Five have already been confirmed as SB2 and analyzed (see Section 2.2). In the Small Magellanic Cloud (SMC) galaxy, there are five candidates for eclipsing binary Cepheids, most probably of SB1 type, of which none has been spectroscopically confirmed yet. However, the light-travel time effect was detected in the photometric time series for one of them (Rathour et al., 2024). A nice summary of binary candidates in the Magellanic Clouds is provided in Szabados & Nehéz (2012). Recently, a new method of detecting SB2 Cepheids was developed that increased the number of such systems by an order of magnitude (see Section 4).

2.1. Masses of Milky Way Cepheids

Almost all binary Cepheids in the Milky Way are single-lined spectroscopic binaries (SB1), making mass estimates for their components very uncertain, with typical accuracies of 10-20%. Such estimates were done for seven SB1 Cepheids (see, Evans et al., 2018, 2024a, and references therein). This is because most binary Cepheids have an early-type main-sequence companion (exhibiting few and broad lines), typically 2–5 mag fainter in the V band, making it extremely hard to determine its velocity and, thus, the mass of the Cepheid.

However, with considerable effort, more accurate mass measurements could be performed for a few Milky Way Cepheids closest to us. This became possible with the recent improvement in interferometric observations complemented with additional spectroscopic observations from space in far-UV, where companion lines are detectable and radial velocities (RVs) can be measured. However, such spectra are much harder to obtain, which results in the companion's RVs being generally calculated from a low number of spectra. These RVs are also measured separately from the Cepheid RVs, which introduces an extra parameter in the model and increases the measurement uncertainty. These Cepheids are V1334 Cyg (Gallenne et al., 2018), Polaris (Evans et al., 2024b), and SU Cyg (Gallenne et al., 2024).

2.2. Eclipsing binary LMC Cepheids

Analyzing Cepheids in double-lined eclipsing binaries is the only way to obtain a full physical parametrization of these important stars. Our spectroscopic observations proved the binarity of five eclipsing Cepheid candidates in the LMC, and their further study brought a wealth of data regarding properties of classical Cepheids, with accuracies of 0.5-2% for the most interesting Cepheid masses and radii (e.g., Pietrzyński et al., 2010; Pilecki et al., 2013, 2015, 2018). This study also identified several interesting cases, including a rare system composed of two Cepheids, OGLE-LMC-CEP-1718 (Gieren et al., 2014). As all these eclipsing Cepheids were accompanied by other giants (in a similar stage of evolution), the measured mass ratios mainly were close to unity, but surprisingly, for one system, significantly different masses ($M_2/M_1 \sim 0.7$) were found. This led to a conclusion that the system (OGLE-LMC-CEP-1812; Pietrzyński et al. 2011) was a triple before, and the Cepheid is a product of a merger (Neilson et al., 2015). It is estimated that even 30% of Cepheids may be such a product (Sana et al., 2012). For the summary, please see Pilecki et al. (2018).

3. Binary Double (BIND) Cepheids

Binary systems composed of two Cepheids are crucial for understanding the structure and evolution of these pulsating stars. Having two Cepheids in one system puts strong constraints on models as their ages have to be equal and physical parameters similar and related to their pulsation periods. We can also assume that both Cepheids were born with the same chemical composition. Moreover, the study of OGLE-LMC-CEP-1718 showed that the more evolutionary advanced component is slightly less massive (Pilecki et al., 2018), which may provide vital information for the ongoing discussion on the origin of the Cepheid mass discrepancy problem (Cassisi & Salaris, 2011; Anderson et al., 2016).

Although the first visually unresolved pairs of Cepheids (dubbed double Cepheids[2]) were identified almost 30 years ago (Alcock et al., 1995), for a long time, only one was spectroscopically confirmed as a binary system and analyzed, which made any statistical analysis impossible. A more extensive set of such stars occupying a wider parameter space would provide the opportunity to gain valuable insight into the pulsation and evolution of Cepheids through a comparative analysis of the differences between the components. All models would have to simultaneously predict correct mass and pulsation period ratios of both Cepheids (together with other observables) for several systems composed of the same age stars with almost the same initial composition.

Recently, we showed the first results of our observing program of nine candidates for new genuine binary double (BIND) Cepheids, of which two are in the

[2]Two Cepheids identified at the same position in the sky (for the used resolution), but not necessarily gravitationally bound.

LMC, five in the SMC, and two in the Milky Way. Our spectroscopic observations proved the binarity of all of them (Pilecki et al., 2024). The observations were challenging as some systems show very low orbital amplitudes, meaning very low inclinations or long orbital periods. Long orbital periods imply we could not yet cover complete orbital cycles with spectroscopic observations. Fortunately, in some cases, orbital periods could be determined by analyzing the light-travel time effect (LTTE) in the available photometric data, which helped constrain the orbital solutions. The orbital radial velocity curves after subtracting pulsational variability are shown in Fig. 1. For half of the sample, the ratios of pulsation periods of the components are exceptionally low, which may suggest binary interactions, such as mass transfer or merger events, in their past. This is also proved by a few preliminary mass ratios far from unity. This sample, together with OGLE-LMC-CEP-1812 mentioned above and OGLE-LMC-CEP-1347 described in Section 4, indicate that a significant fraction of Cepheids may be of binary origin. More details about BIND Cepheids can be found in Pilecki et al. (2024).

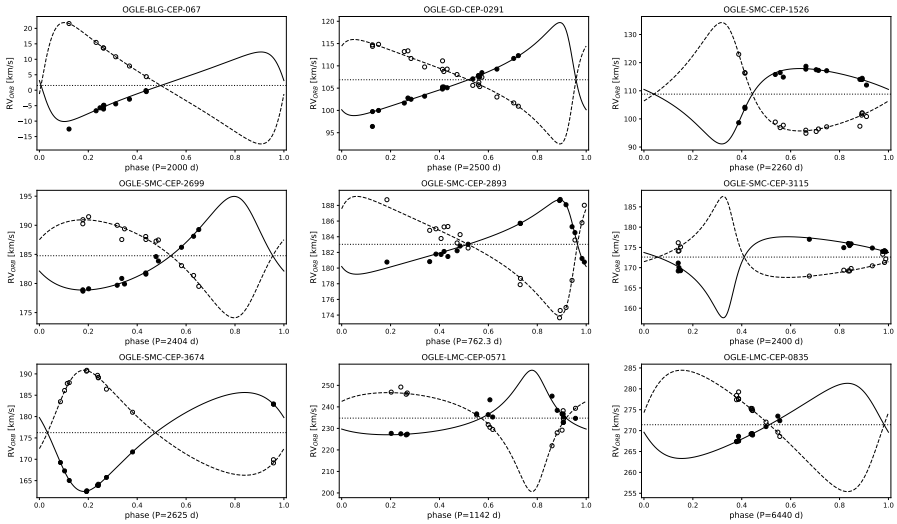


Figure 1. Orbital RV curves for nine new BIND Cepheids. Only for OGLE-SMC–CEP-2893 and OGLE-LMC-CEP-0571 do the orbital periods come from an orbital solution. For three SMC systems (1526, 2699, 3674) and one in the LMC (0835), the period is taken from the LTTE model, while for the rest, it is set to match the data and not to produce unphysical results.

4. New SB2 systems and candidates

Finding new binary Cepheids, especially in SB2 systems, is crucial for improving our knowledge about these stars. However, most of them have been evading detection for a long time. One good source for binary Cepheids was to look for eclipses, but this solution has three severe limitations. First, such systems are not numerous because a particular orbital orientation is needed for eclipses to occur. Second, according to current statistics, only about half of eclipsing systems involving Cepheids are double-lined, and third, the best places to look for them (the Galactic disk and Magellanic Clouds) have already been examined, and we do not expect many more such binaries to be found there. Therefore, we decided to look for another possible source that had not yet been considered and remained unexplored.

In Pilecki et al. (2021), we proposed a novel method of identification of Cepheids in SB2 systems according to which Cepheids that are excessively bright for their periods, have similar or redder colors, and have lower than average pulsation amplitudes are strongly suspected of forming binaries. There are about 100 such candidates in the Magellanic Clouds. Using the first collected data for a limited sample, we showed that this method is about 95% efficient, confirming SB2 status for 17 out of 18 analyzed Cepheids in the LMC galaxy (Pilecki et al., 2021; Pilecki, 2022). Our current sample of SB2 Cepheids in the LMC, SMC, and Milky Way consists of 60 objects, ten times more than what was known before the project. For 37 of them, an anticorrelated orbital motion of both Cepheid and the companion was detected. This is the ultimate proof that they are gravitationally bound and indicates the orbital periods are relatively short. Preliminary orbital solutions were obtained for 24, with periods of up to about seven years (for the longest periods with the help of the LTTE analysis). Three of them and one for which the orbit is not yet fully constrained are presented in Fig. 2.

One of the most interesting objects in the sample is the binary double-mode Cepheid OGLE-LMC-CEP-1347. It has an orbital period of only 58.6 days, about five times shorter than the shortest known before for a binary Cepheid (Pilecki et al., 2022). The Cepheid itself is the shortest-period one ever found in a binary system and the first double-mode Cepheid in a spectroscopically double-lined binary. OGLE-LMC-CEP-1347 is most probably on its first crossing through the instability strip, as inferred from both its short period and fast period increase, consistent with evolutionary models, and from the short orbital period (not expected for binary Cepheids whose components have passed through the red giant phase). Our evolutionary analysis yielded a first-crossing Cepheid with a mass between 3 and 3.5 $M_{\odot}$ (lower than any measured Cepheid mass). The companion is a stable star, at least two times fainter and less massive than the Cepheid (mass ratio q=0.56), while also redder and thus at the subgiant or more advanced evolutionary stage. To match these characteristics, the Cepheid has to be a product of binary interaction, most likely a merger of

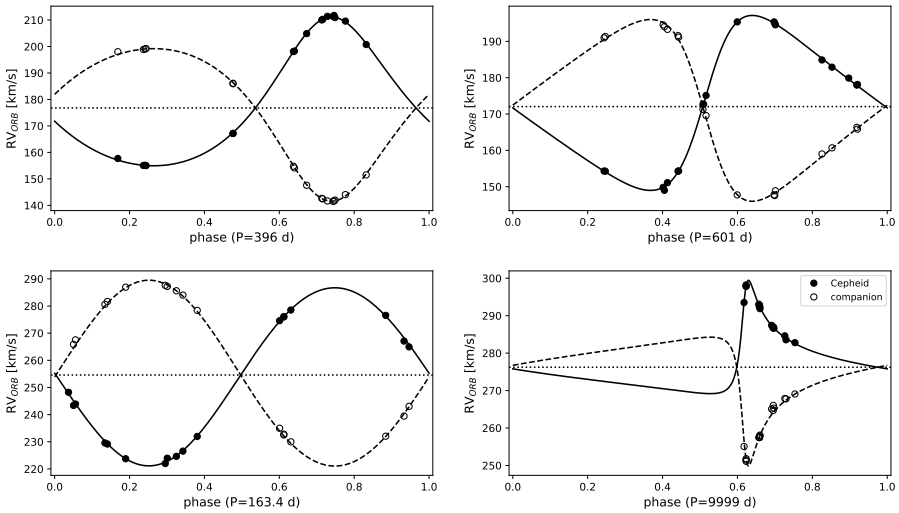


Figure 2. Preliminary orbits for four example double-lined binary Cepheids. The orbital period is not yet constrained for the last one.

two less massive stars, which makes it the second known classical Cepheid of binary origin. The orbital and pulsational radial velocity curves are shown in Fig. 3

Acknowledgements. The research that led to the presented results received funding from the Polish National Science Center grant SONATA BIS 2020/38/E/ST9/00486.

References

Alcock, C., Allsman, R. A., Axelrod, T. S., et al., The MACHO Project LMC Variable Star Inventory.I.Beat Cepheids-Conclusive Evidence for the Excitation of the Second Overtone in Classical Cepheids. 1995, *Astronomical Journal*, **109**, 1653, DOI:10.1086/117392

Anderson, R. I., On Cepheid distances in the H_0 measurement. 2024, *arXiv e-prints*, arXiv:2403.02801, DOI:10.48550/arXiv.2403.02801

Anderson, R. I., Saio, H., Ekström, S., Georgy, C., & Meynet, G., On the effect of rotation on populations of classical Cepheids. II. Pulsation analysis for metallicities 0.014, 0.006, and 0.002. 2016, *Astronomy and Astrophysics*, **591**, A8, DOI:10.1051/0004-6361/201528031

Anderson, R. I., Viviani, G., Shetye, S. S., et al., VELOcities of CEpheids (VELOCE). I. High-precision radial velocities of Cepheids. 2024, *Astronomy and Astrophysics*, **686**, A177, DOI:10.1051/0004-6361/202348400

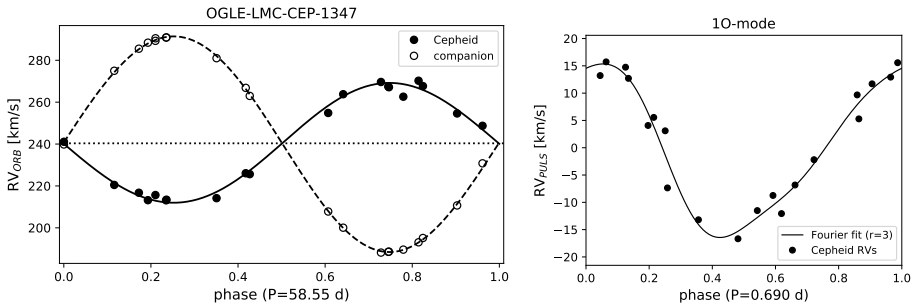


Figure 3. (left) Orbital radial velocity curve with the 1O-mode pulsation of the Cepheid subtracted. The orbit is circular, and the amplitude ratio indicates the companion is about 2 times less massive. (right) Pulsational RV curve for 1O mode with orbital motion subtracted. The scatter of the Cepheid RVs around the fits comes mostly from the unaccounted 2O pulsation.

Bono, G., Braga, V. F., & Pietrinferni, A., Cepheids as distance indicators and stellar tracers. 2024, *Astronomy and Astrophysics Reviews*, **32**, 4, DOI:10.1007/s00159-024-00153-0

Bono, G., Caputo, F., Castellani, V., & Marconi, M., Theoretical Models for Classical Cepheids. II. Period-Luminosity, Period-Color, and Period-Luminosity-Color Relations. 1999, *Astrophysical Journal*, **512**, 711, DOI:10.1086/306815

Bono, G., Marconi, M., Cassisi, S., et al., Classical Cepheid Pulsation Models. X. The Period-Age Relation. 2005, *Astrophysical Journal*, **621**, 966, DOI:10.1086/427744

Cassisi, S. & Salaris, M., A Classical Cepheid in a Large Magellanic Cloud Eclipsing Binary: Evidence Of Shortcomings in Current Stellar Evolutionary Models? 2011, *Astrophysical Journal, Letters*, **728**, L43, DOI:10.1088/2041-8205/728/2/L43

Espinoza-Arancibia, F., Pilecki, B., Pietrzyński, G., Smolec, R., & Kervella, P., Empirical instability strip for classical Cepheids. I. The Large Magellanic Cloud galaxy. 2024, *Astronomy and Astrophysics*, **682**, A185, DOI:10.1051/0004-6361/202347804

Evans, N. R., Gallenne, A., Kervella, P., et al., The Orbit and Mass of the Cepheid AW Per. 2024a, *Astrophysical Journal*, **972**, 145, DOI:10.3847/1538-4357/ad5e7d

Evans, N. R., Proffitt, C., Carpenter, K. G., et al., The Mass of the Cepheid V350 Sgr. 2018, *Astrophysical Journal*, **866**, 30, DOI:10.3847/1538-4357/aade03

Evans, N. R., Schaefer, G. H., Gallenne, A., et al., The Orbit and Dynamical Mass of Polaris: Observations with the CHARA Array. 2024b, *Astrophysical Journal*, **971**, 190, DOI:10.3847/1538-4357/ad5e7a

Gallenne, A., Evans, N. R., Kervella, P., et al., Multiplicity of Galactic Cepheids from long-baseline interferometry V. High-accuracy orbital parallax and mass of SU Cygni. 2024, *arXiv e-prints*, arXiv:2411.06647, DOI:10.48550/arXiv.2411.06647

Gallenne, A., Kervella, P., Evans, N. R., et al., A Geometrical 1% Distance to the Short-period Binary Cepheid V1334 Cygni. 2018, *Astrophysical Journal*, **867**, 121, DOI:10.3847/1538-4357/aae373

Gieren, W., Pilecki, B., Pietrzyński, G., et al., The Araucaria Project. OGLE-LMC-CEP-1718: An Exotic Eclipsing Binary System Composed of Two Classical Overtone Cepheids in a 413 Day Orbit. 2014, *Astrophysical Journal*, **786**, 80, DOI:10.1088/0004-637X/786/2/80

Kervella, P., Gallenne, A., Remage Evans, N., et al., Multiplicity of Galactic Cepheids and RR Lyrae stars from Gaia DR2. I. Binarity from proper motion anomaly. 2019, *Astronomy and Astrophysics*, **623**, A116, DOI:10.1051/0004-6361/201834210

Leavitt, H. S. & Pickering, E. C., Periods of 25 Variable Stars in the Small Magellanic Cloud. 1912, *Harvard College Observatory Circular*, **173**, 1

Moore, J. H., Note on the Long-Period System of Polaris. 1929, *Publications of the ASP*, **41**, 56, DOI:10.1086/123907

Neilson, H. R., Izzard, R. G., Langer, N., & Ignace, R., The strange evolution of the Large Magellanic Cloud Cepheid OGLE-LMC-CEP1812. 2015, *Astronomy and Astrophysics*, **581**, L1, DOI:10.1051/0004-6361/201526716

Pietrukowicz, P., Soszyński, I., & Udalski, A., Classical Cepheids in the Milky Way. 2021, *Acta Astronomica*, **71**, 205, DOI:10.32023/0001-5237/71.3.2

Pietrzyński, G., Thompson, I. B., Gieren, W., et al., The dynamical mass of a classical Cepheid variable star in an eclipsing binary system. 2010, *Nature*, **468**, 542, DOI:10.1038/nature09598

Pietrzyński, G., Thompson, I. B., Graczyk, D., et al., The Araucaria Project: Accurate Determination of the Dynamical Mass of the Classical Cepheid in the Eclipsing System OGLE-LMC-CEP-1812. 2011, *Astrophysical Journal, Letters*, **742**, L20, DOI:10.1088/2041-8205/742/2/L20

Pilecki, B., Revealing a numerous population of double-lined binary Cepheids. in , *XL Polish Astronomical Society Meeting*, ed. E. Szuszkiewicz, A. Majczyna, K. Małek, M. Ratajczak, E. Niemczura, U. Bąk-Stęślicka, R. Poleski, M. Bilicki, & Ł. Wyrzykowski, Vol. **12**, 174–177

Pilecki, B., Fundamentalization of Periods for First- and Second-overtone Classical Cepheids. 2024, *Astrophysical Journal, Letters*, **970**, L14, DOI:10.3847/2041-8213/ad5b54

Pilecki, B., Gieren, W., Pietrzyński, G., et al., The Araucaria Project: High-precision Cepheid Astrophysics from the Analysis of Variables in Double-lined Eclipsing Binaries. 2018, *Astrophysical Journal*, **862**, 43, DOI:10.3847/1538-4357/aacb32

Pilecki, B., Graczyk, D., Gieren, W., et al., The Araucaria Project: the First-overtone Classical Cepheid in the Eclipsing System OGLE-LMC-CEP-2532. 2015, *Astrophysical Journal*, **806**, 29, DOI:10.1088/0004-637X/806/1/29

Pilecki, B., Graczyk, D., Pietrzyński, G., et al., Physical parameters and the projection factor of the classical Cepheid in the binary system OGLE-LMC-CEP-0227. 2013, *Monthly Notices of the RAS*, **436**, 953, DOI:10.1093/mnras/stt1529

Pilecki, B., Pietrzyński, G., Anderson, R. I., et al., Cepheids with Giant Companions. I. Revealing a Numerous Population of Double-lined Binary Cepheids. 2021, *Astrophysical Journal*, **910**, 118, DOI:10.3847/1538-4357/abe7e9

Pilecki, B., Thompson, I. B., Espinoza-Arancibia, F., et al., Discovery of a Binary-origin Classical Cepheid in a Binary System with a 59 day Orbital Period. 2022, *Astrophysical Journal, Letters*, **940**, L48, DOI:10.3847/2041-8213/ac9fcc

Pilecki, B., Thompson, I. B., Espinoza-Arancibia, F., et al., Cepheids with giant companions. II. Spectroscopic confirmation of nine new double-lined binary systems composed of two Cepheids. 2024, *Astronomy and Astrophysics*, **686**, A263, DOI:10.1051/0004-6361/202349138

Pojmanski, G., Pilecki, B., & Szczygiel, D., The All Sky Automated Survey. Catalog of Variable Stars. V. Declinations 0 arcd - +28 arcd of the Northern Hemisphere. 2005, *Acta Astronomica*, **55**, 275, DOI:10.48550/arXiv.astro-ph/0508017

Rathour, R. S., Hajdu, G., Smolec, R., et al., Non-evolutionary effects on period change in Magellanic Cepheids. I. New binary systems revealed from light travel time effect. 2024, *Astronomy and Astrophysics*, **686**, A268, DOI:10.1051/0004-6361/202349117

Riess, A. G., Casertano, S., Yuan, W., Macri, L. M., & Scolnic, D., Large Magellanic Cloud Cepheid Standards Provide a 1% Foundation for the Determination of the Hubble Constant and Stronger Evidence for Physics beyond ΛCDM. 2019, *Astrophysical Journal*, **876**, 85, DOI:10.3847/1538-4357/ab1422

Riess, A. G., Yuan, W., Macri, L. M., et al., A Comprehensive Measurement of the Local Value of the Hubble Constant with 1 km s^{-1} Mpc^{-1} Uncertainty from the Hubble Space Telescope and the SH0ES Team. 2022, *Astrophysical Journal, Letters*, **934**, L7, DOI:10.3847/2041-8213/ac5c5b

Ripepi, V., Chemin, L., Molinaro, R., et al., The VMC survey - XLVIII. Classical cepheids unveil the 3D geometry of the LMC. 2022, *Monthly Notices of the RAS*, **512**, 563, DOI:10.1093/mnras/stac595

Sana, H., de Mink, S. E., de Koter, A., et al., Binary Interaction Dominates the Evolution of Massive Stars. 2012, *Science*, **337**, 444, DOI:10.1126/science.1223344

Shetye, S. S., Viviani, G., Anderson, R. I., et al., VELOcities of CEpheids (VELOCE): II. Systematic search for spectroscopic binary cepheids. 2024, *Astronomy and Astrophysics*, **690**, A284, DOI:10.1051/0004-6361/202450185

Soszynski, I., Poleski, R., Udalski, A., et al., The Optical Gravitational Lensing Experiment. The OGLE-III Catalog of Variable Stars. I. Classical Cepheids in the Large Magellanic Cloud. 2008, *Acta Astronomica*, **58**, 163

Soszyński, I., Udalski, A., Szymański, M. K., et al., Additional Galactic Cepheids from the OGLE Survey. 2020, *Acta Astronomica*, **70**, 101, DOI:10.32023/0001-5237/70.2.2

Soszyński, I., Udalski, A., Szymański, M. K., et al., Concluding Henrietta Leavitt's Work on Classical Cepheids in the Magellanic System and Other Updates of the OGLE Collection of Variable Stars. 2017, *Acta Astronomica*, **67**, 103, DOI:10.32023/0001-5237/67.2.1

Storm, J., Gieren, W., Fouqué, P., et al., Calibrating the Cepheid period-luminosity relation from the infrared surface brightness technique. I. The p-factor, the Milky Way relations, and a universal K-band relation. 2011, *Astronomy and Astrophysics*, **534**, A94, DOI:10.1051/0004-6361/201117155

Szabados, L., Database on Binaries among Galactic Classical Cepheids. 2003, *Information Bulletin on Variable Stars*, **5394**, 1

Szabados, L. & Nehéz, D., Binarity among Cepheids in the Magellanic Clouds. 2012, *Monthly Notices of the RAS*, **426**, 3148, DOI:10.1111/j.1365-2966.2012.21872.x

Valle, G., Marconi, M., Degl'Innocenti, S., & Prada Moroni, P. G., Uncertainties on the theoretical predictions for classical Cepheid pulsational quantities. 2009, *Astronomy and Astrophysics*, **507**, 1541, DOI:10.1051/0004-6361/200912004

Contrib. Astron. Obs. Skalnaté Pleso **55/3**, 152 – 164, (2025)
https://doi.org/10.31577/caosp.2025.55.3.152

Binary Cepheids: Insights from a simulation-based approach

P. Karczmarek

Nicolaus Copernicus Astronomical Center, Polish Academy of Sciences, Bartycka 18, 00-716 Warszawa, Poland (E-mail: pkarczmarek@camk.edu.pl)

Received: November 22, 2024; Accepted: January 7, 2025

Abstract. The growing evidence that the majority of stars are born in binary or multiple stars is causing a paradigm shift in our thinking about Cepheids from single to binary and possible multiple systems, and calls for action to include the presence and influence of companion(s) in the theories of stellar evolution and pulsations. Companions might alter every parameter of pulsating stars, from their apparent magnitude, to their pulsation cycles and internal structure, including mass gain/loss. These changes – to some degree – should affect every Cepheid, and anticipating them through simulations, as well as discovering them though observations, is paramount for refining models of stellar pulsations and gaining detailed knowledge about pulsation mechanisms. I present the current state of knowledge regarding binary Cepheids, discuss the strengths and limitations of various detection techniques, and explore how simulations can help observations by providing insights that are currently unattainable through observational means alone.

Key words: astronomical simulations – Delta Cepheid variable stars – binary stars – Cepheid distance

1. Introduction

Classical Cepheids (hereinafter Cepheids) are radially pulsating stars, widely used in astrophysics to determine distances and constrain theoretical models of stellar evolution and pulsations. They are such potent sources of information because of their special location on the Hertzsprung-Russell diagram inside the instability strip confined by the luminosity ($2 - 5\,L_{\odot}$) and effective temperature ($4000 - 7000\,K$), which drive their pulsations. As Cepheids' outer layers expand and contract, causing periodic changes in the physical parameters (radius, effective temperature, surface gravity, and luminosity), Cepheids' brightness also changes periodically, with periods ranging between about 2 and 100 days, correlating with their mean luminosity. This period-luminosity (P-L) relation (Leavitt Law, Leavitt & Pickering, 1912) renders Cepheids essential for accurate determinations of extragalactic distances and the Hubble constant (Riess et al., 2022).

Metallicity is another important factor that affects the Cepheid mean luminosity in the sense that metal-rich Cepheids are systematically brighter than their metal-poor counterparts (Breuval et al., 2022). The effect of metallicity is preserved in the shape of Cepheid light curves and because of that the information about the metalllicity can be retrieved from the photometric observations alone (Hocdé et al., 2023) when spectroscopic observations are inaccessible. In fact, metallicity, together with luminosity, effective temperature, and other parameters that describe the internal structure of Cepheids and govern their evolution (e.g. overshooting, rotation), are implemented in the newest generations of codes for the light curve modeling (e.g. De Somma et al., 2022). Such modeled light curves – when compared to the observed ones – give insight into physical features of Cepheids that could not be examined otherwise, and advance our knowledge about these pulsators, which turns them into even more precise tools for distance determination.

This advancement has been built upon the assumption that Cepheids are single stars. However, recent theoretical and empirical studies concur that at least 60 – 80% of Galactic Cepheids are in fact binary stars (Szabados, 2003; Mor et al., 2017; Kervella et al., 2019a), and a significant percentage of them (30 – 40%) are in multiple systems (Evans et al., 2005; Dinnbier et al., 2024).

Binary Cepheids, especially in eclipsing systems, are highly desired configurations, because they make unique stellar laboratories where stellar parameters (particularly masses and radii) of each companion can be determined independently and very accurately, and next used to further constrain stellar and pulsation models. An example of the remarkable utility of Cepheids in binary eclipsing systems is the determination of the dynamical mass of the Cepheid OGLE-LMC-CEP0227 with an unprecedented accuracy of 1% (Pietrzyński et al., 2010), which resolved the long-standing mass discrepancy problem (Keller, 2008), i.e. the discrepancy between Cepheid masses derived from stellar and pulsational models.[1] Pietrzyński et al. (2010) found that the dynamical mass of OGLE-LMC-CEP0227 agrees with the pulsational mass, thus challenging evolutionary models to identify the missing processes responsible for producing Cepheids that would reconcile this mass discrepancy.

Unfortunately, the overwhelming majority of known Cepheids remain categorized as single stars. In the Milky Way (MW) out of more than 3000 classical Cepheids (Pietrukowicz et al., 2021) about 200 have confirmed companions (Szabados, 2003; Kervella et al., 2019a; Kervella et al., 2019b; Shetye et al., 2024), which constitutes only about 6% of all known MW Cepheids. In the Small and Large Magellanic Clouds (SMC, LMC) out of about 10,000 Cepheids Soszyński et al. (2015) known are only about 70 Cepheids in binary systems (Szabados & Nehéz, 2012; Pilecki et al., 2021, 2024), which accounts for less than 1%. Such a gap between the percentage of observed binary Cepheids and the expected ones

[1] This discrepancy is about 20 – 30% in the sense that the pulsational masses are systematically smaller than the evolutionary ones.

(60 – 80%) indicates a strong selection bias due to the limitations of various detection techniques.

For example, binary Cepheids reported by Pilecki et al. (2021) all have companions that are giant stars. In fact, the large brightness of their companions that makes these Cepheids appear brighter than expected and thus above the P-L relation was the reason these stars were chosen for the spectroscopic analysis in the first place (see Fig. 1). A different criterion allowed Evans (1992) to recognize binary Cepheids with blue and hot main sequence companions due to larger than expected brightness in the ultraviolet domain; however, such observations could only be made from space and for the brightest of Cepheids ($V < 8$ mag). Binary Cepheid candidates can also be selected through the analysis of their photometric amplitudes in different passbands (Klagyivik & Szabados, 2009); especially a high A_V/A_B ratio can indicate a blue companion (either physical or on the line of sight) because the light from the blue companion reduces A_B more severely than A_V. Additionally, radial velocity amplitudes ($A_{\rm RV}$) of Cepheid + companion pairs are larger than single Cepheids due to the $A_{\rm RV}$ of orbital motion superimposed on the $A_{\rm RV}$ of pulsation, and can be another indicator of binarity through the parameter $A_{\rm RV}/A_B$, which should be larger for binaries than for single Cepheids (Klagyivik & Szabados, 2009). Another two methods allowed for detection of angularly resolved binary Cepheids due to the common proper motion of Cepheid + companion pairs (Kervella et al., 2019a) and due to the anomaly in Cepheids' proper motion (Kervella et al., 2019b).

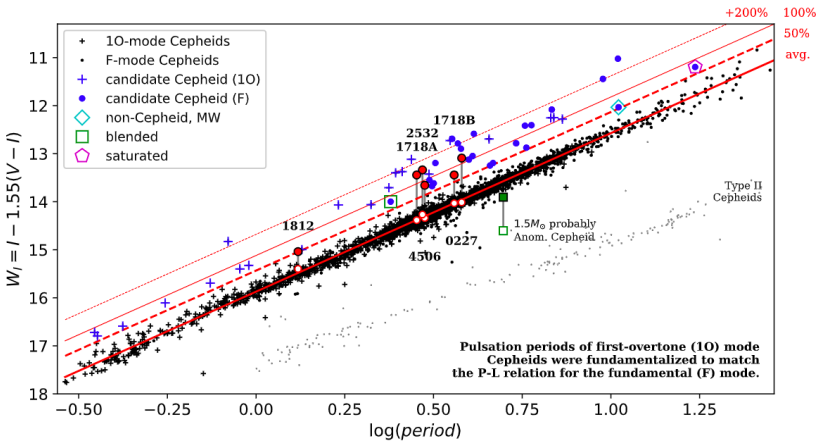


Figure 1. The P-L relation for the reddening-free Wesenheit index. Confirmed binary Cepheids are marked as red circles, while the candidates for binary Cepheids – as blue circles and plus signs. Figure excerpted from Pilecki et al. (2021); for a full description the reader is referred to the source publication.

The variety of methods and their applications demonstrate that no single technique can reliably detect binary Cepheids with all types of companions, while the gap between the expected and actual detections of binary Cepheids suggests that all the current methods combined are insufficient for identifying binary Cepheids with all possible companion types. This gap also highlights a 'blind spot' in our understanding of Cepheid evolution – which may predominantly occur in binary or multiple systems – and of Cepheids' characteristics, which might be affected – or even shaped – by interactions with their companion(s). In order to bridge this gap we resort to simulations of binary Cepheids.

2. Insights from binary population synthesis methods

Binary population synthesis (BPS) codes (e.g. Izzard et al., 2006; Belczynski et al., 2008) rely on approximate formulas to evolve stars from the main sequence until the compact object stage[2], enabling the simulation of vast populations (hundreds of thousands) of binary systems over billions of years. While BPS codes are computationally efficient, they simplify evolutionary processes and omit more complex interactions, making them tools suited for deriving statistical properties of large populations of binaries rather than studying individual systems in detail.

Synthetic populations of binary Cepheids are free from the selection bias inherent to limitations of the observing techniques. They allow us to explore the full range of physical and orbital characteristics that Cepheids and their companions can exhibit as they evolve together (orbital periods, eccentricities, mass ratios, companion types) – only a small fraction of which is accessible through observations. Moreover, synthetic populations are unaffected by reddening, a factor that significantly influences distance determinations. Additionally, while reddening changes Cepheids' apparent color to more red, hot main-sequence companions shift it to more blue, resulting in a complex, poorly understood combined effect. The synthetic population enables to separate the two factors by eliminating the reddening effect altogether.

The BPS codes can be executed with different values/distributions of input parameters: metallicity, star formation history, initial mass function, binary fraction, etc., resulting in many variants of synthetic populations. By comparing these variants one can explore the effects that each parameter has on the evolution and orbital/physical characteristics of binary Cepheids. This analysis can be performed by altering one parameter at a time, an approach achievable only through simulations, as the observed properties of binary Cepheids result from the complex interplay of all parameters.

[2]More specifically, the final stage of evolution can be a compact object (a white dwarf, a neutron star, or a black hole), or a supernova remnant, which is not a compact object but is the final stage of star's evolution.

Below I present a subjective compilation of findings regarding classical Cepheids in binary systems that were made possible thanks to the BPS approach, presented in Karczmarek et al. (2022) and Karczmarek et al. (2023). Simulations of binary Cepheids made by other authors (Neilson et al., 2015; Dinnbier et al., 2024) and simulations of other types of classical pulsators in binary systems, such as anomalous Cepheids (Gautschy & Saio, 2017), metal-rich RR Lyrae (Bobrick et al., 2024), and ultra-low-mass pulsators exhibiting RR-Lyrae pulsations (Karczmarek et al., 2017), although beyond the scope of this paper, are mentioned for the sake of completeness.

2.1. Effect on the extragalactic distance scale

Binary Cepheids with giant companions are easily detectable as outliers above the P-L relation (see Fig. 1). For the purpose of distance determinations using the Cepheid P-L relation these outliers are always removed so that their presence does not shift the P-L relation towards brighter magnitudes. However, the remaining binary Cepheids with companions that are not bright enough to be classified as outliers can still contribute to the shift of the P-L relation, just with a lesser effect. Given that 60 – 80% of Cepheids have companions, which add extra light to the Cepheid apparent brightness, the majority of Cepheids would reside slightly above the P-L relation, shifting it towards brighter magnitudes. Their compound contribution can result in a non-negligible shift that cannot be estimated from observations alone because such binary Cepheids cannot be distinguished from the single ones and properly addressed. This effect has long been assumed in the literature as negligible in the context of distance determinations, but a quantification of this phenomenon was done only recently by Karczmarek et al. (2023).

The authors used the BPS code StarTrack (Belczynski et al., 2008) to evolve 200,000 binary systems with masses between 2.5 and 12 $M_\odot$ and metallicities Z = 0.004, 0.008, 0.02, which correspond to the metallicites of Cepheids in the SMC, LMC, and MW, respectively. By varying other BPS parameters they created a total of 48 variants of synthetic populations, which allowed them to assess the most probable configuration of parameters, i.e. the one that reflects best the observed characteristics of Cepheids. The effect of binarity was controlled by the binarity percentage, $f_{\rm bin}$, which was arbitrarily set to one of 5 values: 0% (only single Cepheids), 25%, 50%, 75%, 100% (only binary Cepheids).

The authors calculated the changes in the slope and the zero point of the P-L relations in various passbands (from B to K, including Wesenheit indices) for populations of Cepheids with different binarity fractions, taking as a reference point the population with $f_{\rm bin} = 0\%$. They reported that the shifts in the P-L slopes due to binarity are negligible within errors, but the shifts in the zero points can be as severe as 0.05 mag (the shift in the B-band for $f_{\rm bin} = 100\%$). This result however needs to be put in the context of cosmic distance determinations. The distance derived using the P-L method is in fact a difference between two

zero points of the P-L relations, calculated for a reference and target galaxy (i.e. the distance modulus, μ). Therefore the final shift in the zero points needs to take into account the binarity percentage in the reference and target galaxies. The final shift will be the largest if the $f_{\rm bin}$ of the reference galaxy is drastically different from the $f_{\rm bin}$ of the target galaxy, and vice versa. If the $f_{\rm bin}$ of the two galaxies is the same, a very small shift is possible due to the population effects (e.g. different metallicities). The matrices in Fig. 2 show all the possible shifts in distance moduli, $\Delta\mu$, between the target and reference galaxies for the V and K bands. The conclusion of this study is that the effect of binarity depends on the passband of the P-L relation used for the distance determination, and is the smallest when the binarity percentages in the reference and target galaxies are similar.

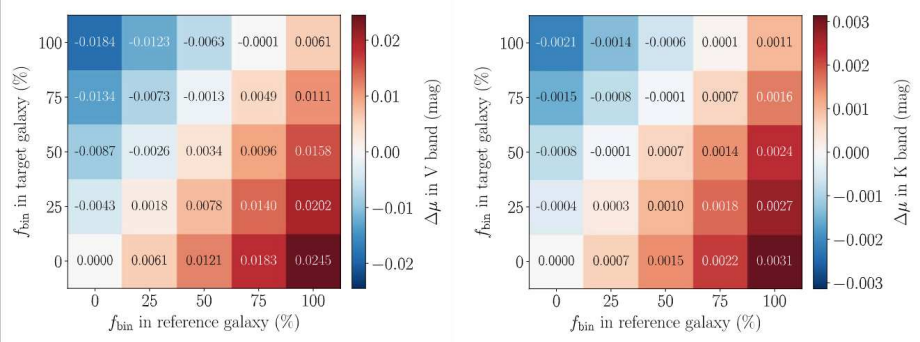


Figure 2. V- and K-band grids of possible values of distance modulus shifts, $\Delta\mu$, as a function of the binarity percentage in the reference (Z = 0.008) and target (Z = 0.02) galaxies. Figure excerpted from Karczmarek et al. (2023); for a full description the reader is referred to the source publication.

In the Wesenheit index W_H, $\Delta\mu$ ranges from -0.004 to 0.004 mag. If we introduce a random shift from this range to the distance moduli of all 37 galaxies hosting supernovae type Ia and Cepheid variables (Riess et al., 2022), we will not shift the value of the Hubble constant, but we will increase its spread by $0.07\,{\rm km\,s^{-1}\,Mpc^{-1}}$ or 0.1%. This result is indeed negligible for the current goal of achieving the 1% precision of the Hubble constant but might become relevant in the future in pursue of even higher precision.

2.2. Relation between the mass ratio and magnitude difference

The magnitude difference, also known as contrast, is the difference in brightness between the Cepheid[3] and its companion. The relation of the magnitude difference to the mass ratio (companion to Cepheid) was first explored by Anderson & Riess (2018), not through the BPS method but assuming a typical Cepheid of a 20-day pulsation period and accompanied by a main-sequence companion. They showed that the contrast decreases as the mass ratio increases and is the smallest for the mass ratio equal to 1. Secondly, the contrast is systematically larger in the H band than in the V band (i.e. Cepheids' companions are fainter in the H band) which is expected since the companions are main-sequence stars and therefore are systematically hotter and bluer than Cepheids. This relation between the mass ratio and contrast was further explored and expounded by Karczmarek et al. (2022) who used the BPS code StarTrack with parameters as described in section 2.1. They found a satisfactory agreement with Anderson & Riess (2018)'s results (see Fig. 3); additionally they presented for the first time the mass ratio-contrast relation for binary Cepheids traversing the instability strip while in the Hertzsprung gap (the co-called first crossing) and for binary Cepheids with giant companions. Comparison with the empirical data hints to the possibility that some of the observed binary Cepheids might be in fact first crossers as they seem to reside in Fig. 3 below the trend created by the 'blue loopers' (i.e. Cepheids on their second and third crossing).

Another interesting application of the mass ratio-contrast relation is that the mass ratio can be estimated from the knowledge of the contrast between the Cepheid and its companion, which in turn can be obtained from high-precision interferometric measurements (e.g. Gallenne et al., 2019).

2.3. Percentage of binary Cepheids in the Large Magellanic Cloud

The binarity percentage among MW Cepheids (60 – 80%) presented in section 1 might not be a universal value. Observational data alone are not sufficient to estimate the percentage of binaries among Cepheids in other galaxies (e.g. the LMC or SMC). However, they can help estimating this percentage in tandem with the BPS method. Karczmarek et al. (2022) put together two pieces of information: the number of Cepheids in eclipsing binaries in the LMC observed during 29 years of the Optical Gravitational Lensing Experiment project (OGLE, Soszyński et al., 2008; Pilecki et al., 2018) and the number of binary Cepheids with giant companions from their synthetic population,[4] which constitute 3 – 5% of the entire synthetic population of binary Cepheids. By comparing

[3]This difference vary as the Cepheid changes its brightness during the pulsation cycle. A simple approximation of the contrast value is made by assuming a fixed brightness of a Cepheid, equal to its mean brightness.

[4]In order to compare both numbers, the number of synthetic binary Cepheids with giant companions had to be trimmed to account for orbital periods below 29 yr and favorable inclination angles $i \geq 83$ deg that allow detection through eclipses.

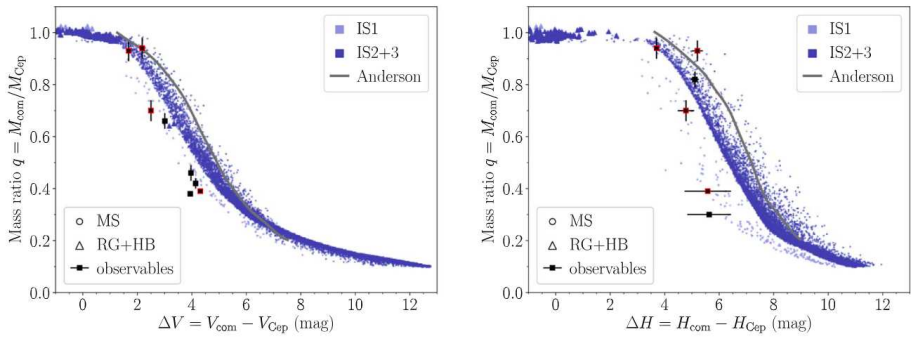


Figure 3. Magnitude difference (contrast) between MW Cepheids and their companions in the V (left) and H (right) bands vs. mass ratio. Empirical data are marked as black squares; systems present on both panels are additionally marked in red. Figure excerpted from Karczmarek et al. (2022); for a full description the reader is referred to the source publication.

the two numbers to each other and to the total number of Cepheids known in the LMC (Soszyński et al., 2015) Karczmarek et al. (2022) estimated the percentage of binary Cepheids in the LMC to be at least 55%, and most likely much higher, i.e. closer to 100%.

3. Beyond binaries – prospects in simulation-based approaches

The extra light contributing to the apparent brightness of Cepheids, discussed extensively in section 2.1, does not have to come from a gravitationally bound companion but from a blend, i.e. a star that coincidentally lies along the Cepheid's line of sight. Because of that all Cepheids with additional light are considered *candidates* for binary stars until their binarity is confirmed through spectroscopy or astrometry. However, these follow-up observations are highly time-consuming and may ultimately reveal that the Cepheid is merely a blend and not an exciting new discovery of a binary system. Therefore, an effective pre-selection of binary candidates is crucial to achieving a higher confirmation rate of binary Cepheids in subsequent follow-up studies.

A promising method to detect additional light in the apparent brightness of Cepheids coming from blue and hot stars was proposed by Madore (1977). As a Cepheid undergoes its pulsation cycle, its effective temperature and luminosity change periodically, leading to corresponding changes in the Cepheid's color. These variations can be represented on the color-color diagram of $U - B$ versus $B - V$, as a loop-shaped pattern that closely resembles a descending straight

line. When contaminated with additional light coming from a hot blue star, the loop deforms into more open and horizontal (see Fig. 4). The shape of the deformation holds information about the effective temperature and luminosity of the contaminating star, but is insufficient to determine whether the contaminator is gravitationally bound to a Cepheid. This piece of information can be obtained from a synthetic population of binary Cepheids. If the contaminator lies on the Hertzsprung-Russell diagram in the location frequently occupied by Cepheid companions, it is more probably a true Cepheid companion rather than a blend.

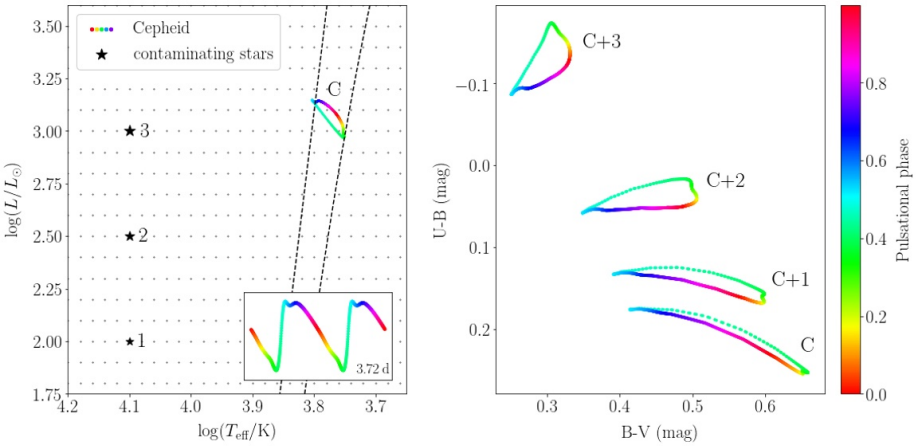


Figure 4. The location of a Cepheid (colorful loop) and three hotter constant stars (black stars) on the Hertzsprung-Russell diagram (left) is transformed on the color–color diagram (right), where the loops labeled as C+1, C+2, C+3 are deformed due to the contamination light coming from the stars 1, 2, 3, respectively.

Last but not least, a growing number of binary Cepheids identified today are often found to be either triple systems (Anderson et al., 2015) or binaries in which the Cepheids themselves resulted from mergers (Neilson et al., 2015; Pilecki et al., 2022) – indicating an origin in triple systems as well. The similar conclusion was reached by Dinnbier et al. (2024) who conducted the state-of-the-art n-body simulations of star clusters of various masses and densities, embedded in a galaxy, and consisting only of binary systems. They showed that mergers are very common among Cepheid progenitors, and prevent about 30% of them from evolving into Cepheids. On the other hand, one in five Cepheids forms as a result of a merger between stars with masses below the minimum threshold required for the Cepheid stage, meaning that had they not merged, they would have never become Cepheids. The binary percentage that Dinnbier et al. (2024)

derived from their n-body simulations is 42%, and underestimates the observed binary Cepheid percentage (60 – 80%) by approximately a factor of 2. This suggests that Cepheid progenitors should rather be formed in triple systems, not binaries.

Observations and simulations of binary Cepheids continue to surprise us with discoveries that call for the paradigm shift in our thinking about Cepheids from single to binary to triple and possibly multiple systems. Some simulations and models can continue with approximating Cepheids as single stars, especially when their objectives require using near-infrared passbands or/and cleaning the sample from outliers. Other ones will have to be adjusted to include the effect of companions in the calculations, as neglecting their presence might lead to inaccurate estimations of Cepheid features. The outcomes of BPS models might to some extent help to determine when single-star approximations remain valid and when multi-star simulations become necessary. The outcomes might also guide future observational campaigns, suggesting optimal observational strategies and facilitating the identification of new binary systems. The results of BPS studies and of other simulation-based approaches help us to broaden our knowledge about the formation and evolution of Cepheids and might prove essential in addressing long-standing Cepheid-related problems, such as the mass discrepancy, age discrepancy, or wind-induced mass loss.

Acknowledgements. Support from the European Research Council (ERC) under the European Union's Horizon 2020 research and innovation program (grant agreements No. 695099 and No. 951549), the Polish Ministry of Science and Higher Education through the grant DIR/WK/2018/09, the Polish National Science Centre through grants BEETHOVEN (2018/31/G/ST9/03050) and MAESTRO (UMO-2017/26/A/ST9/00446) is acknowledged. This paper is part of the Araucaria Project, an international collaboration, whose purpose is to provide an improved local calibration of the extragalactic distance scale out to distances of a few megaparsecs (araucaria.camk.edu.pl).

References

Anderson, R. I. & Riess, A. G., On Cepheid Distance Scale Bias Due to Stellar Companions and Cluster Populations. 2018, *Astrophysical Journal*, **861**, 36, DOI:10.3847/1538-4357/aac5e2

Anderson, R. I., Sahlmann, J., Holl, B., et al., Revealing δ Cephei's Secret Companion and Intriguing Past. 2015, *Astrophysical Journal*, **804**, 144, DOI:10.1088/0004-637X/804/2/144

Belczynski, K., Kalogera, V., Rasio, F. A., et al., Compact object modeling with the StarTrack population synthesis code. 2008, *The Astrophysical Journal Supplement Series*, **174**, 223

Bobrick, A., Iorio, G., Belokurov, V., et al., RR Lyrae from binary evolution: abundant, young, and metal-rich. 2024, *Monthly Notices of the Royal Astronomical Society*, **527**, 12196

Breuval, L., Riess, A. G., Kervella, P., Anderson, R. I., & Romaniello, M., An Improved Calibration of the Wavelength Dependence of Metallicity on the Cepheid Leavitt Law. 2022, *Astrophysical Journal*, **939**, 89, DOI:10.3847/1538-4357/ac97e2

De Somma, G., Marconi, M., Molinaro, R., et al., An updated metal-dependent theoretical scenario for Classical Cepheids. 2022, *The Astrophysical Journal Supplement Series*, **262**, 25

Dinnbier, F., Anderson, R. I., & Kroupa, P., Exploring the dynamical evolution of Cepheid multiplicity in star clusters and its implications for B-star multiplicity at birth. 2024, *Astronomy and Astrophysics*, **690**, A385, DOI:10.1051/0004-6361/202347641

Evans, N. R., A Magnitude-limited Survey of Cepheid Companions in the Ultraviolet. 1992, *Astrophysical Journal*, **384**, 220, DOI:10.1086/170865

Evans, N. R., Carpenter, K. G., Robinson, R., Kienzle, F., & Dekas, A. E., High-mass triple systems: the classical cepheid Y carinae. 2005, *The Astronomical Journal*, **130**, 789

Gallenne, A., Kervella, P., Borgniet, S., et al., Multiplicity of Galactic Cepheids from long-baseline interferometry-IV. New detected companions from MIRC and PIONIER observations. 2019, *Astronomy & Astrophysics*, **622**, A164

Gautschy, A. & Saio, H., On binary channels to anomalous Cepheids. 2017, *Monthly Notices of the RAS*, **468**, 4419, DOI:10.1093/mnras/stx811

Hocdé, V., Smolec, R., Moskalik, P., Ziółkowska, O., & Rathour, R. S., Metallicity estimations of MW, SMC, and LMC classical Cepheids from the shape of the V-and I-band light curves. 2023, *Astronomy & Astrophysics*, **671**, A157

Izzard, R. G., Dray, L. M., Karakas, A. I., Lugaro, M., & Tout, C. A., Population nucleosynthesis in single and binary stars-i. model. 2006, *Astronomy & Astrophysics*, **460**, 565

Karczmarek, P., Hajdu, G., Pietrzyński, G., et al., Synthetic Population of Binary Cepheids. II. The effect of companion light on the extragalactic distance scale. 2023, *The Astrophysical Journal*, **950**, 182

Karczmarek, P., Smolec, R., Hajdu, G., et al., Synthetic Population of Binary Cepheids. I. The Effect of Metallicity and Initial Parameter Distribution on Characteristics of Cepheids' Companions. 2022, *The Astrophysical Journal*, **930**, 65

Karczmarek, P., Wiktorowicz, G., Iłkiewicz, K., et al., The occurrence of binary evolution pulsators in classical instability strip of RR Lyrae and Cepheid variables. 2017, *Monthly Notices of the RAS*, **466**, 2842, DOI:10.1093/mnras/stw3286

Keller, S. C., Cepheid Mass Loss and the Pulsation-Evolutionary Mass Discrepancy. 2008, *Astrophysical Journal*, **677**, 483, DOI:10.1086/529366

Kervella, P., Gallenne, A., Evans, N. R., et al., Multiplicity of Galactic Cepheids and RR Lyrae stars from Gaia DR2. II. Resolved common proper motion pairs. 2019a, *Astronomy & Astrophysics*, **623**, A117

Kervella, P., Gallenne, A., Remage Evans, N., et al., Multiplicity of Galactic Cepheids and RR Lyrae stars from Gaia DR2. I. Binarity from proper motion anomaly. 2019b, *Astronomy and Astrophysics*, **623**, A116, DOI:10.1051/0004-6361/201834210

Klagyivik, P. & Szabados, L., Observational studies of Cepheid amplitudes-I. Period-amplitude relationships for Galactic Cepheids and interrelation of amplitudes. 2009, *Astronomy & Astrophysics*, **504**, 959

Leavitt, H. S. & Pickering, E. C., Periods of 25 Variable Stars in the Small Magellanic Cloud. 1912, *Harvard College Observatory Circular*, **173**, 1

Madore, B. F., The frequency of Cepheids with companions: a photoelectric approach. 1977, *Monthly Notices of the Royal Astronomical Society*, **178**, 505

Mor, R., Robin, A. C., Figueras, F., & Lemasle, B., Constraining the thin disc initial mass function using Galactic classical Cepheids. 2017, *Astronomy and Astrophysics*, **599**, A17, DOI:10.1051/0004-6361/201629464

Neilson, H. R., Izzard, R. G., Langer, N., & Ignace, R., The strange evolution of the Large Magellanic Cloud Cepheid OGLE-LMC-CEP1812. 2015, *Astronomy & Astrophysics*, **581**, L1

Pietrukowicz, P., Soszyński, I., & Udalski, A., Classical Cepheids in the Milky Way. 2021, *Acta Astronomica*, **71**, 205, DOI:10.32023/0001-5237/71.3.2

Pietrzyński, G., Thompson, I., Gieren, W., et al., The dynamical mass of a classical Cepheid variable star in an eclipsing binary system. 2010, *Nature*, **468**, 542

Pilecki, B., Gieren, W., Pietrzyński, G., et al., The Araucaria project: high-precision Cepheid astrophysics from the analysis of variables in double-lined eclipsing binaries. 2018, *The Astrophysical Journal*, **862**, 43

Pilecki, B., Pietrzyński, G., Anderson, R. I., et al., Cepheids with Giant Companions. I. Revealing a Numerous Population of Double-lined Binary Cepheids. 2021, *Astrophysical Journal*, **910**, 118, DOI:10.3847/1538-4357/abe7e9

Pilecki, B., Thompson, I. B., Espinoza-Arancibia, F., et al., Discovery of a Binary-origin Classical Cepheid in a Binary System with a 59 day Orbital Period. 2022, *Astrophysical Journal, Letters*, **940**, L48, DOI:10.3847/2041-8213/ac9fcc

Pilecki, B., Thompson, I. B., Espinoza-Arancibia, F., et al., Cepheids with giant companions. II. Spectroscopic confirmation of nine new double-lined binary systems composed of two Cepheids. 2024, *Astronomy and Astrophysics*, **686**, A263, DOI:10.1051/0004-6361/202349138

Riess, A. G., Yuan, W., Macri, L. M., et al., A comprehensive measurement of the local value of the Hubble constant with 1 km s- 1 Mpc- 1 uncertainty from the Hubble Space Telescope and the SH0ES team. 2022, *The Astrophysical journal letters*, **934**, L7

Shetye, S. S., Viviani, G., Anderson, R. I., et al., VELOcities of CEpheids (VELOCE): II. Systematic search for spectroscopic binary cepheids. 2024, *Astronomy and Astrophysics*, **690**, A284, DOI:10.1051/0004-6361/202450185

Soszyński, I., Poleski, R., Udalski, A., et al., The Optical Gravitational Lensing Experiment. The OGLE-III Catalog of Variable Stars. I. Classical Cepheids in the Large Magellanic Cloud. 2008, *Acta Astronomica*, **58**, 163, DOI:10.48550/arXiv.0808.2210

Soszyński, I., Udalski, A., Szymański, M. K., et al., The OGLE Collection of Variable Stars. Classical Cepheids in the Magellanic System. 2015, *Acta Astronomica*, **65**, 297, DOI:10.48550/arXiv.1601.01318

Szabados, L., Cepheids: observational properties, binarity and GAIA. 2003, in Astronomical Society of the Pacific Conference Series, Vol. **298**, *GAIA Spectroscopy: Science and Technology*, ed. U. Munari, 237

Szabados, L. & Nehéz, D., Binarity among Cepheids in the Magellanic Clouds. 2012, *Monthly Notices of the RAS*, **426**, 3148, DOI:10.1111/j.1365-2966.2012.21872.x

Contrib. Astron. Obs. Skalnaté Pleso **55/3**, 165 – 171, (2025)
https://doi.org/10.31577/caosp.2025.55.3.165

SWIPE: Stars WIth Pulsations and Eclipses

J. Southworth

Astrophysics Group, Keele University, Staffordshire, ST5 5BG, UK
(E-mail: taylorsouthworth@gmail.com)

Received: November 15, 2024; Accepted: November 19, 2024

Abstract. Eclipses and pulsations are the two primary ways in which the physical properties of stars can be deduced and used to improve our understanding of stellar theory. An obvious idea is to combine these two analyses into the study of pulsating stars in eclipsing binaries. This is the aim of the SWIPE project. This paper summarises the scientific arguments, current status and future plans of the project.

Key words: stars: fundamental parameters — stars: binaries: eclipsing — stars: oscillations

1. Introduction

Detached eclipsing binary stars (dEBs) are our primary source of direct measurements of the physical properties of stars. It is possible to determine their *bulk properties* – mass, radius, density, surface gravity – directly from empirical measurements (Andersen, 1991; Torres et al., 2010). These quantities can be determined to accuracies surpassing 0.2%, for example AI Phe (Maxted et al., 2020) and V505 Per (Southworth, 2021a). They are a crucial check and calibration source for the theoretical stellar models on which modern astrophysics is based. As examples, dEBs have been used to study the strength of internal mixing in high-mass stars (Tkachenko et al., 2020), calibrate the mass–radius relation in low-mass stars (Chen et al., 2014), help determine the properties of transiting planets (Southworth, 2009), and as a rung in the cosmological distance ladder (Pietrzyński et al., 2019; Freedman et al., 2020). Unfortunately, very high-precision masses and radii are needed for useful constraints on stellar theory (Valle et al., 2016; Constantino & Baraffe, 2018).

Asteroseismology is another prolific route towards understanding the stars, in particular their *interior properties* (Aerts et al., 2010). Pressure- (p-) mode pulsations are widespread in solar-like oscillators, and δ Scuti (Murphy et al., 2019) and β Cephei (Stankov & Handler, 2005) stars. Gravity- (g-) mode oscillations manifest in γ Doradus stars (Kaye et al., 1999) and the slowly-pulsating B (SPB) stars (Waelkens, 1991). Of these, the g-mode pulsations offer most promise as they penetrate deep inside stars and thus are affected by physical phenomena in the stellar interior. They have been used to constrain the rotational profile of stars (Aerts et al., 2019), angular momentum transport (e.g.

Mombarg et al., 2019) and internal mixing (Pedersen et al., 2021). A limitation of this method is that the masses and radii of individual stars are not known *a priori* so useful constraints can only be obtained through analysis of significant samples of stars.

An obvious avenue for an improved understanding of the behaviour of stars is to combine the power of binarity and asteroseismology by studying pulsating stars in dEBs. Once masses and radii are precisely known, the measured pulsation frequencies become a sensitive test of theoretical models. Pulsating stars in EBs have been known for decades (Tempesti, 1971; Knipe, 1971), but the data quality for detailed analysis was only recently achieved with space missions such as *CoRoT, Kepler* and TESS (Southworth, 2021c). Examples of recent work in this area include KIC 9850387 (Sekaran et al., 2021), KIC 4142768 (Guo et al., 2019) and HD 74423 (Handler et al., 2020).

We have therefore initiated a project: *Stars WIth Pulsations and Eclipses* (SWIPE) where we aim to perform detailed analysis of a sample of pulsating stars in dEBs to determine their masses, radii, luminosities and oscillation frequencies. These will be used to constrain stellar phenomena such as angular momentum transport, rotational profiles, and internal mixing.

2. Sample selection

Early work on pulsating stars in eclipsing binaries (EBs) was hindered by the difficulty of identifying such objects, particularly in cases where the oscillation amplitudes are low and/or the frequencies are comparable to the length of an observing night. The commencement of large-scale ground-based photometric surveys primarily targeted at the detection of transiting extrasolar planets (e.g. HATNet, HATSouth, KELT and SuperWASP) has been helpful, but the low data quality and severe aliasing due to diurnal effects compromise the usefulness of observations from these surveys.

The main advances in this work have instead been realised primarily through space-based data from *CoRoT, Kepler* and TESS. Whilst *Kepler* remains the source of the best light curves, the faintness and relatively low number of its targets hinders work on pulsating dEBs. TESS (Ricker et al., 2015) has observed the vast majority of the bright stars in the sky, but in most cases the observations are split into 27-d intervals obtained in different years so have a low frequency resolution. The archives of these space missions are nevertheless suffused with pulsating stars in EBs. Gaulme & Guzik (2019) analysed the full *Kepler* database to find 303 examples, and hundreds of δ Scuti stars in EBs have been catalogued (Kahraman Aliçavuş et al., 2017, 2022; Shi et al., 2022; Chen et al., 2022).

Southworth & Bowman (2022a) presented a catalogue of 26 high-mass pulsators in EBs, based on TESS data and including preliminary analyses of 18 of these objects. This sample of stars was identified visually via inspection of the

TESS light curves of known EBs. We found eight objects showing stochastic low-frequency (SLF) variability (Bowman et al., 2019), 16 definite or possible β Cephei stars, and 11 definite or possible SPBs. Eze & Handler (2024) have since presented a catalogue of 78 β Cephei stars in EBs using TESS data.

Whilst there are many δ Scuti stars known in EBs (see references above), eclipsing SPB and γ Dor stars appear to be much rarer. This reflects the prevalence of these objects in the single-star population. Southworth & Van Reeth (2022) presented the discovery of γ Dor pulsations in four known dEBs (CM Lac, MZ Lac, RX Dra and V2077 Cyg), again from visual inspection of TESS data. A fifth, V456 Cyg, was analysed in more detail as we found it to be only the second object known with tidally perturbed high-order g-mode pulsations (Van Reeth et al., 2022). A set of five more EBs showing tidally perturbed g-mode pulsations has been analysed by Van Reeth et al. (2023). We have since discovered more dEBs containing signatures of SLF, β Cephei, SPB, δ Scuti and γ Dor pulsations.

3. A SWIPE status report

Early results for several objects have been published, concentrating on the higher-mass objects in our sample. Two examples are the first and second β Cephei pulsators with a precise mass measurement: V453 Cyg and VV Ori (Southworth et al., 2020, 2021); in both cases the stars were well-studied dEBs whose TESS data led to the discovery of the pulsational signature. A subsequent study of VV Ori by Budding et al. (2024) used extensive spectroscopy to revise the mass measurements upwards by a statistically significant amount (masses of $M_1 = 11.56 \pm 0.14$ and $4.81 \pm 0.06\,\mathrm{M}_\odot$ compared to $M_1 = 10.9 \pm 0.1$ and $4.09 \pm 0.05\,\mathrm{M}_\odot$ from Terrell et al. 2007).

An emerging trend is the prevalence of pulsations affected by binarity, specifically showing evidence for tidal excitation, perturbation or tilting. Theoretical analyses of these phenomena have been described by Fuller et al. (2020) and Guo (2020). Spectroscopic follow-up has been obtained for nine of the objects in the catalogue of Southworth & Bowman (2022a) and all five γ Dor EBs named above, among other objects, and analysis of the data for AR Cas, AL Scl, V453 Cyg, V446 Cep and RX Dra has begun. Tab. 1 summarises our published work to the present. A basic webpage[1] has been established to document the project, but remains a work in progress. Spectroscopic observations have been obtained for approximately 20 systems in addition to those mentioned above, using the Isaac Newton, William Herschel, Mercator, Nordic Optical and Calar Alto 2.2 m telescopes .

In the near future the PLATO satellite (Rauer et al., 2024) will obtain light curves of *Kepler*-like quality over a much larger field of view, to detect

[1] `https://www.astro.keele.ac.uk/jkt/swipe/`

Table 1. EBs containing pulsating stars where a reasonably detailed analysis has been published as part of the SWIPE project, given in decreasing order of mass.

Target	Pulsation	Spectral type	Period (d)	Ref.
V1765 Cyg	SLF	B0.5 Ib + B1 V	13.374	(1)
V453 Cyg	β Cep, tidal	B0.4 IV + B0.7 IV	3.889	(2)
V346 Cen	Tidally excited	B1 III + B2 V	6.322	(3)
VV Ori	β Cep, tidal	B1 V + B4 V	1.485	(4)
V1388 Ori	β Cep or SPB	B2.5 IV + B3 V	1.485	(5)
IQ Per	SPB	B8 V + A6 V	1.744	(6)
KIC 4851217	γ Dor, δ Sct, tidal	A7 V + A7 IV	2.470	(7)
V1229 Tau	δ Sct	A0 Vp(Si) + Am	2.461	(8)
RR Lyn	γ Dor, δ Sct, tidal	A6 IVm + F0 Vm	9.945	(9)
KIC 9851944	γ Dor, δ Sct, tidal	F1 V + F2 IV	2.164	(10)
V456 Cyg	γ Dor, tidal	A2 Vm + F3 V	0.892	(11)
GK Dra	γ Dor, δ Sct	F1 V + F2 IV	9.974	(12)

References: (1) Southworth (2023); (2) Southworth et al. (2020); (3) Pavlovski et al. (2023); (4) Southworth et al. (2021); (5) Southworth & Bowman (2022b); (6) Southworth (2024b); (7) Jennings et al. (2024b); (8) Southworth et al. (2023); (9) Southworth (2021b); (10) Jennings et al. (2024a); (11) Van Reeth et al. (2022); (12) Southworth (2024a).

Earth-like planets via the transit method. The PLATO Multiple Star Working Group (MSWG) has been established to co-ordinate work on multiple stars using PLATO observations (Southworth & Maxted, these proceedings).

Acknowledgements. We acknowledge support from the Science and Technology Facilities Council (STFC) under grant number ST/Y002563/1.

References

Aerts, C., Christensen-Dalsgaard, J., & Kurtz, D. W. 2010, *Asteroseismology* (Astron. and Astroph. Library, Springer Netherlands, Amsterdam)

Aerts, C., Mathis, S., & Rogers, T. M., Angular momentum transport in stellar interiors. 2019, *ARA&A*, **57**, 35

Andersen, J., Accurate masses and radii of normal stars. 1991, *A&ARv*, **3**, 91

Bowman, D. M., Burssens, S., Pedersen, M. G., et al., Low-frequency gravity waves in blue supergiants revealed by high-precision space photometry. 2019, *Nature Astronomy*, **3**, 760

Budding, E., Southworth, J., Pavlovski, K., et al., The enigmatic multiple star VV Ori. 2024, *MNRAS*, **527**, 6389

Chen, X., Ding, X., Cheng, L., et al., Detection of δ Scuti pulsators in the eclipsing binaries observed by TESS. 2022, *ApJS*, **263**, 34

Chen, Y., Girardi, L., Bressan, A., et al., Improving PARSEC models for very low mass stars. 2014, *MNRAS*, **444**, 2525

Constantino, T. & Baraffe, I., Significant uncertainties from calibrating overshooting with eclipsing binary systems. 2018, *A&A*, **618**, A177

Eze, C. I. & Handler, G., β Cephei pulsators in eclipsing binaries observed with TESS. 2024, *ApJS*, **272**, 25

Freedman, W. L., Madore, B. F., Hoyt, T., et al., Calibration of the tip of the red giant branch. 2020, *ApJ*, **891**, 57

Fuller, J., Kurtz, D. W., Handler, G., & Rappaport, S., Tidally trapped pulsations in binary stars. 2020, *MNRAS*, **498**, 5730

Gaulme, P. & Guzik, J. A., Systematic search for stellar pulsators in the eclipsing binaries observed by Kepler. 2019, *A&A*, **630**, A106

Guo, Z., Tidal asteroseismology: possible evidence of nonlinear mode coupling in an equilibrium state in Kepler eclipsing binary KIC 3230227. 2020, *ApJ*, **896**, 161

Guo, Z., Fuller, J., Shporer, A., et al., KIC 4142768: an evolved γ Doradus/δ Scuti hybrid pulsating eclipsing binary with tidally excited oscillations. 2019, *ApJ*, **885**, 46

Handler, G., Kurtz, D. W., Rappaport, S. A., et al., Tidally trapped pulsations in a close binary star system discovered by TESS. 2020, *Nature Astronomy*, **4**, 684

Jennings, Z., Southworth, J., Pavlovski, K., & Van Reeth, T., Physical properties of the eclipsing binary KIC 9851944 and analysis of its tidally perturbed p- and g-mode pulsations. 2024a, *MNRAS*, **527**, 4052

Jennings, Z., Southworth, J., Rappaport, S. A., et al., Characterization of the δ Scuti eclipsing binary KIC 4851217 and its tertiary companion as well as detection of tidally tilted pulsations. 2024b, *MNRAS*, **533**, 2705

Kahraman Aliçavuş, F., Gümüş, D., Kırmızıtaş, Ö., et al., Candidate Eclipsing Binary Systems with a δ Scuti Star in Northern TESS Field. 2022, *RAA*, **22**, 085003

Kahraman Aliçavuş, F., Soydugan, E., Smalley, B., & Kubát, J., Eclipsing binary stars with a δ Scuti component. 2017, *MNRAS*, **470**, 915

Kaye, A. B., Handler, G., Krisciunas, K., Poretti, E., & Zerbi, F. M., Gamma Doradus stars: defining a new class of pulsating variables. 1999, *PASP*, **111**, 840

Knipe, G. F. G., The light curve and orbital elements of V539 Arae. 1971, *A&A*, **14**, 70

Maxted, P. F. L., Gaulme, P., Graczyk, D., et al., The TESS light curve of AI Phoenicis. 2020, *MNRAS*, **498**, 332

Mombarg, J. S. G., Van Reeth, T., Pedersen, M. G., et al., Asteroseismic masses, ages, and core properties of γ Doradus stars using gravito-inertial dipole modes and spectroscopy. 2019, *MNRAS*, **485**, 3248

Murphy, S. J., Hey, D., Van Reeth, T., & Bedding, T. R., Gaia-derived luminosities of Kepler A/F stars and the pulsator fraction across the δ Scuti instability strip. 2019, *MNRAS*, **485**, 2380

Pavlovski, K., Southworth, J., Tkachenko, A., Van Reeth, T., & Tamajo, E., High-mass eclipsing binaries: a testbed for models of interior structure and evolution – Accurate fundamental properties and surface chemical composition for V1034 Sco, GL Car, V573 Car and V346 Cen. 2023, *A&A*, **671**, A139

Pedersen, M. G., Aerts, C., Pápics, P. I., et al., Internal mixing of rotating stars inferred from dipole gravity modes. 2021, *Nature Astronomy*, **5**, 715

Pietrzyński, G., Graczyk, D., Gallenne, A., et al., A distance to the Large Magellanic Cloud that is precise to one per cent. 2019, *Nature*, **567**, 200

Rauer, H., Aerts, C., Cabrera, J., et al., The PLATO Mission. 2024, *arXiv.2406.05447*

Ricker, G. R., Winn, J. N., Vanderspek, R., et al., Transiting Exoplanet Survey Satellite (TESS). 2015, *Journal of Astronomical Telescopes, Instruments, and Systems*, **1**, 014003

Sekaran, S., Tkachenko, A., Johnston, C., & Aerts, C., A comparison of the dynamical and model-derived parameters of the pulsating eclipsing binary KIC 9850387. 2021, *A&A*, **648**, A91

Shi, X.-d., Qian, S.-b., & Li, L.-J., New pulsating stars detected in EA-type eclipsing-binary systems based on TESS data. 2022, *ApJS*, **259**, 50

Southworth, J., Homogeneous studies of transiting extrasolar planets. II. Physical properties. 2009, *MNRAS*, **394**, 272

Southworth, J., Rediscussion of eclipsing binaries. VI. The F-type system V505 Persei. 2021a, *The Observatory*, **141**, 234

Southworth, J., Rediscussion of eclipsing binaries. VII. Delta Scuti, gamma Doradus and tidally-perturbed pulsations in RR Lyncis. 2021b, *The Observatory*, **141**, 282

Southworth, J., Space-based photometry of binary stars: from Voyager to TESS. 2021c, *Universe*, **7**, 369

Southworth, J., Rediscussion of eclipsing binaries. XV. The B-type supergiant system V1765 Cygni. 2023, *The Observatory*, **143**, 254

Southworth, J., Rediscussion of eclipsing binaries. XVI. The δ Scuti / γ Dor hybrid pulsator GK Draconis. 2024a, *The Observatory*, **144**, 24

Southworth, J., Rediscussion of eclipsing binaries. XXI. The totally-eclipsing B-type system IQ Persei. 2024b, *The Observatory*, **144**, 278

Southworth, J., Bowman, D., Tkachenko, A., & Pavlovski, K., Discovery of β Cep pulsations in the eclipsing binary V453 Cygni. 2020, *MNRAS*, **497**, L19

Southworth, J. & Bowman, D. M., High-mass pulsators in eclipsing binaries observed using TESS. 2022a, *MNRAS*, **513**, 3191

Southworth, J. & Bowman, D. M., Rediscussion of eclipsing binaries. X. The pulsating B-type system V1388 Orionis. 2022b, *The Observatory*, **142**, 161

Southworth, J., Bowman, D. M., & Pavlovski, K., A β Cephei pulsator and a changing orbital inclination in the high-mass eclipsing binary system VV Orionis. 2021, *MNRAS*, **501**, L65

Southworth, J., Murphy, S. J., & Pavlovski, K., δ Scuti pulsations in the bright Pleiades eclipsing binary HD 23642. 2023, *MNRAS*, **520**, L53

Southworth, J. & Van Reeth, T., Four bright eclipsing binaries with γ Doradus pulsating components: CM Lac, MZ Lac, RX Dra and V2077 Cyg. 2022, *MNRAS*, **515**, 2755

Stankov, A. & Handler, G., Catalogue of galactic β Cephei stars. 2005, *ApJS*, **158**, 193

Tempesti, P., The eclipsing binary AB Cassiopeiae as a delta Scuti star. 1971, *IBVS*, **596**, 1

Terrell, D., Munari, U., & Siviero, A., Observational studies of early-type binary stars: VV Orionis. 2007, *MNRAS*, **374**, 530

Tkachenko, A., Pavlovski, K., Johnston, C., et al., The mass discrepancy in intermediate- and high-mass eclipsing binaries: The need for higher convective core masses. 2020, *A&A*, **637**, A60

Torres, G., Andersen, J., & Giménez, A., Accurate masses and radii of normal stars: modern results and applications. 2010, *A&ARv*, **18**, 67

Valle, G., Dell'Omodarme, M., Prada Moroni, P. G., & Degl'Innocenti, S., Calibrating convective-core overshooting with eclipsing binary systems. The case of low-mass main-sequence stars. 2016, *A&A*, **587**, A16

Van Reeth, T., Johnston, C., Southworth, J., et al., Tidally perturbed gravity-mode pulsations in a sample of close eclipsing binaries. 2023, *A&A*, **671**, A121

Van Reeth, T., Southworth, J., Van Beeck, J., & Bowman, D. M., V456 Cyg: an eclipsing binary with tidally perturbed g-mode pulsations. 2022, *A&A*, **659**, A177

Waelkens, C., Slowly pulsating B stars. 1991, *A&A*, **246**, 453

Contrib. Astron. Obs. Skalnaté Pleso **55/3**, 172 – 181, (2025)
https://doi.org/10.31577/caosp.2025.55.3.172

A catalogue of δ Sct pulsators in binary systems in 2024

A. Liakos

Institute for Astronomy, Astrophysics, Space Applications and Remote Sensing, National Observatory of Athens, Metaxa & Vas. Pavlou St., GR-15236, Athens, Greece (E-mail: alliakos@noa.gr)

Received: October 10, 2024; Accepted: January 14, 2025

Abstract. The updated catalogue of δ Sct stars in binary systems as well as their statistical properties are presented. Thanks to the Kepler, K2 and TESS space missions, this version of the catalogue contains more than 1000 δ Sct pulsators in binaries. The sample is divided according to the Roche Geometry of the binary systems in order to check for any systematic differences in the pulsators' evolution due to the proximity of the companion star. Statistics, demographics, and distributions of these pulsating stars within the H-R and mass-radius diagrams are provided. We notice that the absolute parameters have been accurately determined for only approximately 10% of the whole sample. Additionally, updated correlations between pulsation and orbital periods and evolutionary status are presented. This work aims to motivate the researchers for systematic analyses of such objects in order to increase the sample of systems with well known physical properties.

Key words: asteroseismology – catalogs – stars: binaries (including multiple): close – stars: oscillations (including pulsations) – stars: variables: delta Scuti – stars: binaries: general – stars: binaries: eclipsing

1. Introduction

δ Scuti stars (DS) are short-period pulsating variables that can oscillate in both radial and non-radial modes. The radial and low-order non-radial modes are driven by the kappa mechanism (Baker & Kippenhahn, 1962; Aerts et al., 2010; Balona et al., 2015), while the higher-order non-radial modes result from turbulent pressure in the hydrogen convective zone (Antoci et al., 2014; Grassitelli et al., 2015). These stars typically have masses between 1.4 and 2.5 $M_{\odot}$, temperatures ranging from approximately 6000 to 9500 K, and belong to luminosity classes III-V. Most of them are found within the classical instability strip (Murphy et al., 2019).

Although the first DS-members of binary systems were discovered in '70s (e.g. Hudson et al., 1971), since the early '00s there was not any systematic listing of them, mainly due to the limited discoveries. DS in binaries were difficult to be detected before 2000 mostly because the photometric accuracy of

photometers and first generations CCDs was lower than the amplitudes of their oscillations. The first list of these stars (eight in total) was published by Mkrtichian et al. (2002), who introduced the term 'Oscillating Eclipsing Algols' (oEA stars) for semidetached eclipsing systems with a mass accretor DS component. Later on, Mkrtichian et al. (2004, 2005) announced a few more similar systems, while Soydugan et al. (2006a,b) published 25 cases expanding also to the detached type systems. The latter works proposed also a correlation between the orbital ($P_{\rm orb}$) and pulsation ($P_{\rm pul}$) periods. Liakos et al. (2012, hereafter paper I) increased the sample of these systems to 74 and established the $P_{\rm orb}$-$P_{\rm pul}$ relation. The boundary between the end of the 'dark ages' and the beginning of the 'renaissance' era for this topic was the launch of the NASA/Kepler mission in 2009 (Koch et al., 2010). After the first data release (DR1) of Kepler in 2014, the systematic discoveries of this kind of systems increased. Liakos & Niarchos (2017, hereafter paper II) published an updated catalogue hosting 203 DS in 199 systems and found that there is a limit of 13 days in $P_{\rm orb}$ beyond that $P_{\rm orb}$ and $P_{\rm pul}$ are uncorrelated. After the end of Kepler and K2 missions, the NASA/TESS mission (Ricker et al., 2015) was launched in 2018. A few months later the TESS-DR1 was announced, leading to hundreds of new discoveries. Correlations between the fundamental parameters of the stars of this kind of systems according to their Roche geometry (e.g. $P_{\rm orb}$-$P_{\rm pul}$, $\log g$-$P_{\rm pul}$ correlations) were updated by Liakos (2017, for semidetached systems) and Liakos (2020, for detached systems).

Due to the aforementioned space missions, hundreds of new systems of this kind have been discovered and to date (i.e. August 2024) they have reached the number of 1048 DS in 1043 binary systems. However, there is still limited information on the absolute properties of their DS members. It should be noted that in ESA/Gaia DR3 (Gaia Collaboration et al., 2023) there are a lot of radial velocities available for eclipsing binaries with a DS member, which it is expected to increase the number of DS with accurately determined physical properties. Therefore, after the scheduled end of TESS and the fourth data release (DR4) of Gaia in 2025, as well as the launch of the ESA/PLATO mission (Rauer et al., 2016) in 2026, it is anticipated that this topic will enter through its 'golden ages' regarding the exponential increase of the sample and the information on the physical properties of the DS.

2. Demographics and statistical properties

The sources of the present catalogue are: a) the previous catalogues given in papers I and II, b) papers on satellite data mining and long lists of new cases (e.g. Murphy et al., 2018; Gaulme & Guzik, 2019; Kahraman Aliçavuş et al., 2022), and c) personal checks on the old rejected and ambiguous cases using satellite short-cadence data and new ground-based observations. Table 1 contains the demographics of all DS-members of binary systems according to their type

Table 1. Demographics of DS in binary systems according to the type of variability and Roche geometry of their host systems. Values in parentheses denote the number of DS with determined mass and radius.

Variability type	Detached	Semidetached	Unclassified	All
SB2+E	35(31)	34(34)	5(1)	74(66)
E and el	40(15)	53(32)	399(11)	492(58)
SB1+E or SB1(2)+el	19(17)	15(12)	8(3)	42(32)
SB1 and SB2	27(7)	0	11(5)	38(12)
O–C and PM and Vis.	348(6)	0	54(1)	402(7)
Sum	469(76)	102(78)	477(21)	1048(175)

SB1(2)=Single (Double) lined spectroscopic binary, E=Eclipsing binary, el=ellipsoidal variable, O−C=binarity detected through the periodic variation of the pulsational period, PM=binarity detected though the phase modulation of the pulsations, Vis.=Visual binary.

Table 2. Demographics of DS in binary systems according to our knowledge on their dominant pulsational ($P_{\rm pul}$) and orbital ($P_{\rm orb}$) periods.

	$P_{\rm pul}$ & $P_{\rm orb}$	Only $P_{\rm pul}$	Only $P_{\rm orb}$	All
Detached	200	5	264	469
Semidetached	99	0	2	101
Unclassified	350	59	69	478
Sum	649	64	335	1048

of variability and Roche geometry. In the same table, the respective numbers of DS, whose the physical properties have been determined, are also given. It should to be noted that to date only 66 DS out of 1048 belong to both eclipsing (E) and double-lined spectroscopic systems (SB2), which are considered as the utmost tools for determining the absolute properties. There are also another 32 DS with derived physical parameters that belong either to SB1+E or to SB1(2)+ellipsoidal systems and consist the second more reliable group for the physical parameters calculation. The absolute parameters of the rest 77 stars were determined using assumptions (e.g. the mass of the primary was assumed based on its spectral type).

Table 2 lists the DS in binary systems according to their geometry and our knowledge on their $P_{\rm orb}$ and $P_{\rm pul}$. Systems with only the $P_{\rm pul}$ known are those for which DS-type pulsations have been detected and their duplicity has been confirmed, but there is no exact value of their $P_{\rm orb}$ (e.g. wide orbit systems). On the other hand, those with only the $P_{\rm orb}$ known are those for which their $P_{\rm orb}$ has been determined, they present DS-type pulsations, but due to the limited time resolution of their data (e.g. long-cadence data of Kepler, K2, and TESS), their dominant pulsation frequency may be higher than the nyquist frequency

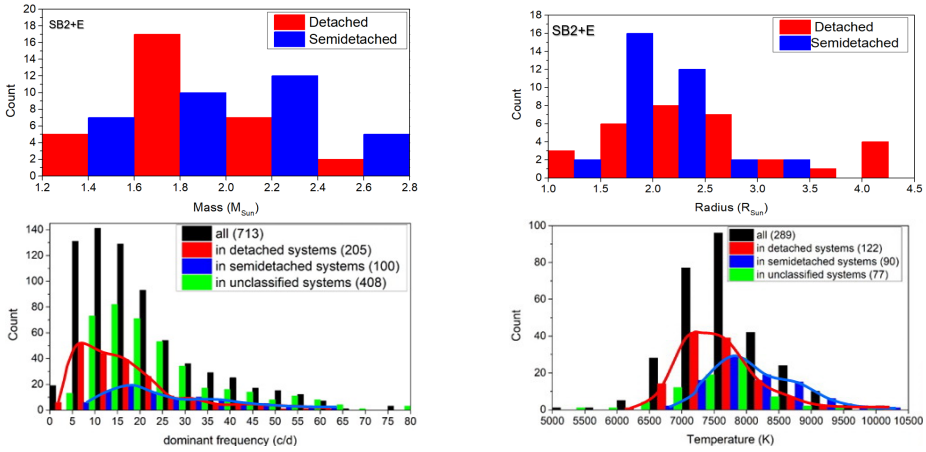


Figure 1. Distributions of the: a) masses (upper left), b) radii (upper right), c) dominant frequencies (lower left), and d) temperatures (lower right) of the DS in binaries according to their Roche geometry.

of these data sets (i.e. ~ 24 d^{-1}).

The statistical properties of DS in binaries are illustrated in Fig. 1. In this figure, for the masses and radii plots, we used only the DS that belong to SB2+E systems (Table 1). These plots show that DS in semidetached systems appear more compact. For the dominant frequencies and temperatures plots, we used 713 (Table 2) and 289 DS, respectively and we notice that the DS in detached systems exhibit slower pulsations and are slightly cooler in comparison with those in semidetached systems. It should be noted that the used aforementioned quantities were taken directly from the literature. The masses and radii of the SB2+E systems were derived from light and radial velocities curves modelling. The temperatures of the stars were derived either from spectral classification or they were given their catalogue values (i.e. Kepler or TESS or GAIA).

Using short- or medium- cadence data of the aforementioned space missions (i.e. time resolutions 1-2 min and 10 min, respectively) and personal observations using the 1.2 m Kryoneri telescope (Xilouris et al., 2018) for $\sim$ 25 cases lacking space data, we examined in total 272 previously rejected and ambiguous cases of older catalogues (Soydugan et al., 2006b, papers I and II). Particularly, we searched the data of these stars/systems in order to detect either pulsations or eclipses. We found that 66 cases still remain ambiguous either for the pulsations exhibition or the pulsations type. For these systems, only long- and/or medium- cadence space data exist so far, which are not sufficient to determine with high certainty their potential pulsational properties. For another 40 cases, except for the eclipses search, we did not apply any other method to check whether a DS star of the list belongs to a binary system, so they remained as

ambiguous regarding their duplicity. Finally, 166 cases were definitely rejected mostly due to the absence of pulsations.

3. Correlations

Using a much larger sample than that of the previous studies (i.e. papers I and II), we re-tested the correlation between $P_{\rm orb}$ and $P_{\rm pul}$ (Fig. 2). For this plot, systems that lack of modelling (i.e. previously categorized as unclassified) and have: a) $P_{\rm orb} > 20$ d and/or b) eccentric orbits are classified directly as detached systems. Therefore, the remaining 351 unclassified systems in Fig. 2 are short-period systems that lack of modelling.

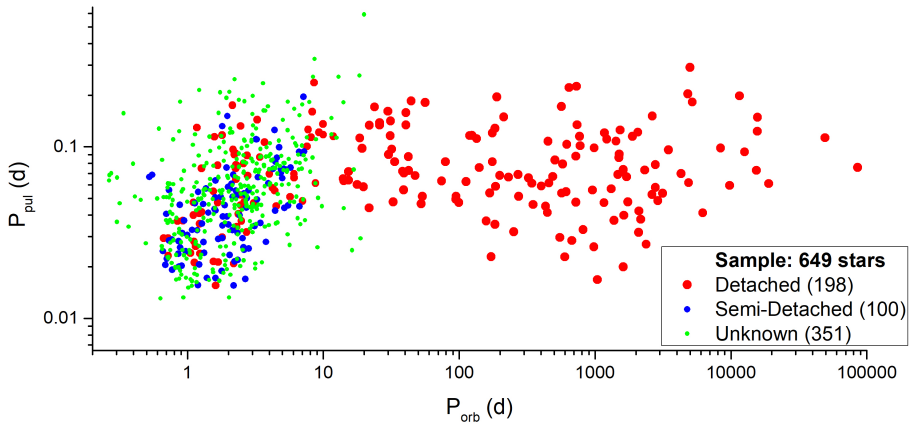


Figure 2. $P_{\rm orb}$-$P_{\rm pul}$ plot of the DS in binaries according to their Roche geometry.

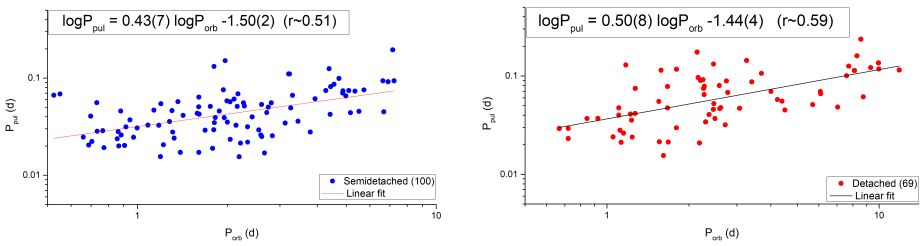


Figure 3. Linear fittings on the $P_{\rm orb}$-$P_{\rm pul}$ points of semidetached systems (left) and detached systems with $P_{\rm orb} < 12.5$ d (right).

Regarding the 198 detached systems, we applied the following methods to re-determine the threshold of $P_{\rm orb}$ beyond which $P_{\rm orb}$ and $P_{\rm pul}$ are uncorrelated. We fitted polynomial and exponential curves on the data points and by calculating their local extrema we found a limit of $P_{\rm orb}$=12.5 d and 13 d, respectively. Moreover, we performed linear fittings on datasets with various $P_{\rm orb}$ ranges (i.e. up to 6, 10, 14, 18, 20, 26, 34, 40, and 45 days) and calculated the respective correlation coefficients (r). The two best correlations were found for the datasets with $P_{\rm orb} < 10$ d and $P_{\rm orb} < 14$ d, which is in very good agreement with the previous two methods. For semidetached systems, we just applied linear fitting on all data (100 systems), since there is no system with $P_{\rm orb} > 7.5$ d within this subgroup. The fittings on the aforementioned datasets and the correlation formulae along with their respective r are shown in Fig. 3.

Another informative correlation is that between the evolutionary status ($\log g$) and the dominant $P_{\rm pul}$ of the binary DS. We performed linear fittings on the $\log g - P_{\rm pul}$ values (Fig. 4) of DS members of: a) semidetached systems, b) detached systems with $P_{\rm orb} < 12.5$ d, and c) detached systems with $P_{\rm orb} > 12.5$ d. In contrast with our previous work (paper II), the DS in semidetached and short-period detached systems have very similar relations (within the error limits) between $\log g - P_{\rm pul}$. On the other hand, very interestingly, for DS in detached systems with $P_{\rm orb} > 12.5$ d, these quantities seem uncorrelated. In any case, the comparison between the relations of the DS in binaries with that of single DS (see Fig. 4) shows clearly that they follow different trend, which undoubtedly is related to the existence of the companion star. However, the most important in this plot is the fact the binary DS preserve their pulsations longer in comparison with the single DS.

4. Evolutionary diagrams

Based on the new sample, we plot the DS of binary systems within the Mass-Radius and H–R diagrams in Fig. 5. For the Mass-Radius diagram, we include all the DS with somehow determined absolute parameters (Table 1). In this plot, the DS that belong to SB2+E are denoted with different symbols. Regarding the H–R diagram, the sample was larger, since both temperature and luminosity can be more easily determined in comparison with the mass and the radius. Both diagrams clearly show that the vast majority of binary DS are Main-Sequence stars in contrast with the single DS (Uytterhoeven et al., 2011). Only a few cases have been found below the Zero-Age (ZAMS) or beyond the Terminal-Age (TAMS) Main-Sequence. Their vast majority lie within the classical instability strip (IS), and only a few cases are located beyond its blue limit (IS-B). On the contrary, there are many DS very close to the red boundary of IS (IS-R) and some of them are found beyond that. It should to be noted that this region of the H–R diagram has an overlap with the γ Dor type pulsators, while there are numerous cases of pulsating stars with hybrid DS-γ Dor behaviour.

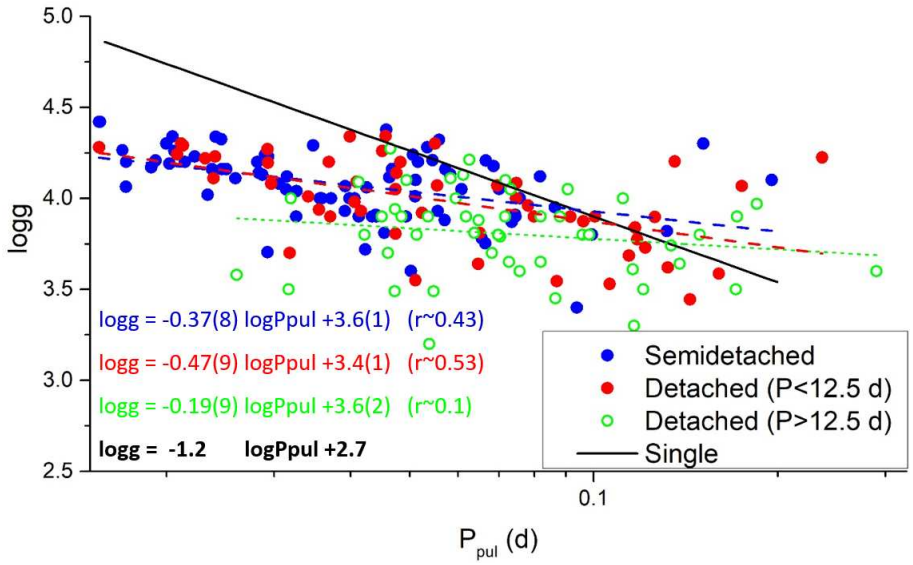


Figure 4. Correlations between $\log g$ and $P_{\rm pul}$ of binary DS according to their Roche geometry and $P_{\rm orb}$. The coloured lines are linear fittings on the different data sets (see text), while the black line, which represents the single DS, is given for comparison.

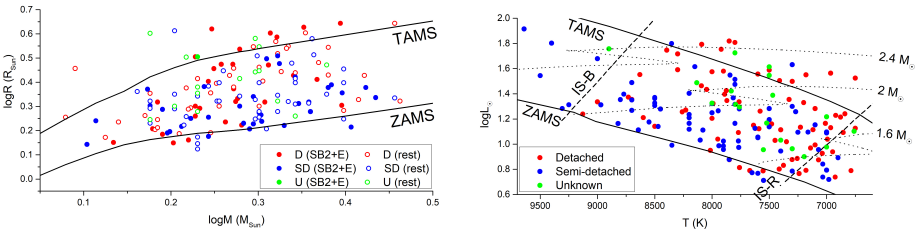


Figure 5. Mass-radius (left) and H–R (right) diagrams of DS in binaries.

5. Conclusions

This work contains the demographics and some statistical results on the largest catalogue of DS in binary systems to date, which contains 1048 DS in 1043 systems. The online form of the catalogue is given at https://alexiosliakos.weebly.com/catalogue.html. The sample was divided according to the Roche geometry of the host systems of the DS. The vast majority of the binary DS are Main-Sequence stars and they are located within the classical instability strip. The correlation between $P_{\rm orb}$-$P_{\rm pul}$ has been well established for both detached and semidetached systems, while the limit of 12.5-13 d in $P_{\rm orb}$ beyond that these

quantities are uncorrelated has been constrained with three different methods.

The DS in binary systems have masses between 1.25-2.9 $M_{\odot}$, radii between 1.3-4.4 $R_{\odot}$, and temperatures between 6700-9800 K. Their dominant pulsation frequencies range between 3.5-77 d^{-1}, but those in detached systems show a distribution peak within the range 5-10 d^{-1}, while those in semidetached binaries have a peak between 15-20 d^{-1}. There is correlation between evolutionary stage and the dominant frequency of the binary DS that is similar between the members of short-period detached and semidetached binaries but totally different from that of single DS. In general, the younger the star the highest the dominant pulsation frequency. Moreover, we still argue that the existence of the companion star plays significant role in the earlier initiation of the pulsations and their longer preservation in comparison with the single DS stars.

Although the sample is now relatively large, the sub-sample of the binary DS with accurately determined absolute properties is still rather small (66 cases). Therefore, we strongly encourage the community to obtain radial velocities measurements of the more than 400 eclipsing systems of the catalogue that lack information on their absolute parameters. This will lead to the sample increase, which in turn, will lead us to reach the ultimate goals that are the: i) setting of further constrains on the evolution of these stars and ii) checking of the influence of the proximity effects on their pulsational behaviour.

Acknowledgements. The author acknowledges financial support from the NOA's internal fellowship 'SPECIES' (No. 5094). This study is partially based on observations made with the 1.2 m Kryoneri telescope, Corinthia, Greece, which is operated by the Institute for Astronomy, Astrophysics, Space Applications and Remote Sensing of the National Observatory of Athens, Greece.

References

Aerts, C., Christensen-Dalsgaard, J., & Kurtz, D. W. 2010, *Asteroseismology*

Antoci, V., Cunha, M., Houdek, G., et al., The Role of Turbulent Pressure as a Coherent Pulsational Driving Mechanism: The Case of the δ Scuti Star HD 187547. 2014, *Astrophysical Journal*, **796**, 118, DOI:10.1088/0004-637X/796/2/118

Baker, N. & Kippenhahn, R., The pulsations of models of δ Cephei stars. 1962, *Zeitschrift für Astrophysik*, **54**, 114

Balona, L. A., Daszyńska-Daszkiewicz, J., & Pamyatnykh, A. A., Pulsation frequency distribution in δ Scuti stars. 2015, *Monthly Notices of the RAS*, **452**, 3073, DOI:10.1093/mnras/stv1513

Gaia Collaboration, Vallenari, A., Brown, A. G. A., et al., Gaia Data Release 3. Summary of the content and survey properties. 2023, *Astronomy and Astrophysics*, **674**, A1, DOI:10.1051/0004-6361/202243940

Gaulme, P. & Guzik, J. A., Systematic search for stellar pulsators in the eclipsing binaries observed by Kepler. 2019, *Astronomy and Astrophysics*, **630**, A106, DOI:10.1051/0004-6361/201935821

Grassitelli, L., Fossati, L., Langer, N., et al., Relating turbulent pressure and macroturbulence across the HR diagram with a possible link to γ Doradus stars. 2015, *Astronomy and Astrophysics*, **584**, L2, DOI:10.1051/0004-6361/201527289

Hudson, K. I., Chiu, H.-Y., Maran, S. P., Stuart, F. E., & Vokac, P. R., Automated and Conventional Photometry of the Short-Period Variable Star 14 Aurigae. 1971, *Astrophysical Journal*, **165**, 573, DOI:10.1086/150922

Kahraman Aliçavuş, F., Gümüş, D., Kırmızıtaş, Ö., et al., Candidate Eclipsing Binary Systems with a δ Scuti Star in Northern TESS Field. 2022, *Research in Astronomy and Astrophysics*, **22**, 085003, DOI:10.1088/1674-4527/ac71a4

Koch, D. G., Borucki, W. J., Basri, G., et al., Kepler Mission Design, Realized Photometric Performance, and Early Science. 2010, *Astrophysical Journal, Letters*, **713**, L79, DOI:10.1088/2041-8205/713/2/L79

Liakos, A., Asteroseismology of Kepler Algol-type oscillating eclipsing binaries. 2017, *Astronomy and Astrophysics*, **607**, A85, DOI:10.1051/0004-6361/201731247

Liakos, A., Asteroseismology of two Kepler detached eclipsing binaries. 2020, *Astronomy and Astrophysics*, **642**, A91, DOI:10.1051/0004-6361/202038065

Liakos, A. & Niarchos, P., Catalogue and properties of δ Scuti stars in binaries. 2017, *Monthly Notices of the RAS*, **465**, 1181, DOI:10.1093/mnras/stw2756

Liakos, A., Niarchos, P., Soydugan, E., & Zasche, P., Survey for δ Sct components in eclipsing binaries and new correlations between pulsation frequency and fundamental stellar characteristics. 2012, *Monthly Notices of the RAS*, **422**, 1250, DOI:10.1111/j.1365-2966.2012.20704.x

Mkrtichian, D. E., Kusakin, A. V., Gamarova, A. Y., & Nazarenko, V., Pulsating Components of Eclipsing Binaries: New Asteroseismic Methods of Studies and Prospects. 2002, in Astronomical Society of the Pacific Conference Series, Vol. **259**, *IAU Colloq. 185: Radial and Nonradial Pulsationsn as Probes of Stellar Physics*, ed. C. Aerts, T. R. Bedding, & J. Christensen-Dalsgaard, 96

Mkrtichian, D. E., Kusakin, A. V., Rodriguez, E., et al., Frequency spectrum of the rapidly-oscillating mass-accreting component of the Algol-type system AS Eri. 2004, *Astronomy and Astrophysics*, **419**, 1015, DOI:10.1051/0004-6361:20040095

Mkrtichian, D. E., Rodríguez, E., Olson, E. C., et al., Pulsations in eclipsing binaries. 2005, in Astronomical Society of the Pacific Conference Series, Vol. **333**, *Tidal Evolution and Oscillations in Binary Stars*, ed. A. Claret, A. Giménez, & J. P. Zahn, 197

Murphy, S. J., Hey, D., Van Reeth, T., & Bedding, T. R., Gaia-derived luminosities of Kepler A/F stars and the pulsator fraction across the δ Scuti instability strip. 2019, *Monthly Notices of the RAS*, **485**, 2380, DOI:10.1093/mnras/stz590

Murphy, S. J., Moe, M., Kurtz, D. W., et al., Finding binaries from phase modulation of pulsating stars with Kepler: V. Orbital parameters, with eccentricity and mass-ratio distributions of 341 new binaries. 2018, *Monthly Notices of the RAS*, **474**, 4322, DOI:10.1093/mnras/stx3049

Rauer, H., Aerts, C., Cabrera, J., & PLATO Team, The PLATO Mission. 2016, *Astronomische Nachrichten*, **337**, 961, DOI:10.1002/asna.201612408

Ricker, G. R., Winn, J. N., Vanderspek, R., et al., Transiting Exoplanet Survey Satellite (TESS). 2015, *Journal of Astronomical Telescopes, Instruments, and Systems*, **1**, 014003, DOI:10.1117/1.JATIS.1.1.014003

Soydugan, E., İbanoğlu, C., Soydugan, F., Akan, M. C., & Demircan, O., The connection between the pulsational and orbital periods for eclipsing binary systems. 2006a, *Monthly Notices of the RAS*, **366**, 1289, DOI:10.1111/j.1365-2966.2005.09889.x

Soydugan, E., Soydugan, F., Demircan, O., & İbanoğlu, C., A catalogue of close binaries located in the δ Scuti region of the Cepheid instability strip. 2006b, *Monthly Notices of the RAS*, **370**, 2013, DOI:10.1111/j.1365-2966.2006.10628.x

Uytterhoeven, K., Moya, A., Grigahcène, A., et al., The Kepler characterization of the variability among A- and F-type stars. I. General overview. 2011, *Astronomy and Astrophysics*, **534**, A125, DOI:10.1051/0004-6361/201117368

Xilouris, E. M., Bonanos, A. Z., Bellas-Velidis, I., et al., NELIOTA: The wide-field, high-cadence, lunar monitoring system at the prime focus of the Kryoneri telescope. 2018, *Astronomy and Astrophysics*, **619**, A141, DOI:10.1051/0004-6361/201833499

Contrib. Astron. Obs. Skalnaté Pleso **55/3**, 182 – 195, (2025)
https://doi.org/10.31577/caosp.2025.55.3.182

Magnetic activity in close binary systems

Zs. Kővári[1,2]

[1] *Konkoly Observatory, HUN-REN Research Centre for Astronomy and Earth Sciences, H-1121 Budapest, Konkoly Thege út 15-17., Hungary (E-mail: kovari@konkoly.hu)*

[2] *HUN-REN CSFK, MTA Centre of Excellence, H-1121 Budapest, Konkoly Thege út 15-17., Hungary*

Received: November 15, 2024; Accepted: December 1, 2024

Abstract. Tidal forces in close binary systems have diverse impacts on magnetic activity. The synchronicity characteristic of close systems counteracts magnetic braking, thereby sustaining rapid rotation—a key factor in increased levels of magnetic activity. Tidal effects can also work against the slowing down of rotation during stellar evolution, when the star inflates into a red giant. A notable manifestation of the effect of binarity on activity in such systems is the appearance of active longitudes, which are thought to arise from the excitation of non-axisymmetric dynamo modes. Through some recent examples, the dinamo operation in RS CVn and BY Dra type systems is briefly reviewed in terms of spot cycles, active longitudes, flare activity, and differential rotation.

Key words: binaries: close, binaries: eclipsing – stars: late-type, stars: activity, stars: starspots, stars: flare, stars: imaging

1. Introduction

Indicators of magnetic activity known on the Sun, such as dark photospheric spots, bright chromospheric plages, flares and coronal X-ray and radio emission, are common in late-type stars with convective envelopes. Detached close binary systems with such an active late-type component (e.g., RS CVn or BY Dra type systems) provide a unique environment where magnetic fields, tidal forces, and stellar dynamics interact in highly complex and extreme ways. The proximity of the stars can amplify the effects of magnetism, driving phenomena such as intense starspot activity, frequent flaring, and strong chromospheric and coronal emissions. These magnetic processes not only affect the observable characteristics of the stars but also play a critical role in shaping the long-term evolution of the binary system itself.

One of the key elements that makes the study of magnetic activity in close binaries so compelling is the multifaceted role of tidal interactions. Tidal synchronization can enhance magnetic activity by speeding up rotation, which in turn powers the dynamo processes that generate strong magnetic fields. The long-period group of RS CVn binaries typically consists of such systems with

evolved but still rapidly rotating active components. Moreover, tidal forces distort the stars' shapes, which introduces non-axisymmetry, yielding variations in the internal plasma flows and surface conditions, ultimately altering the magnetic dynamo (see, e.g., Moss & Tuominen, 1997; Sokoloff & Piskunov, 2002; Moss et al., 2002). This affects observable signs of magnetic activity, such as the distribution of starspots (e.g., Sethi & Martin, 2024), but may also contribute to the modulation of long-term magnetic behavior. However, tidal interactions also play a central role in orbital evolution, as the angular momentum exchange driven by tides and magnetic braking can lead to significant changes in the orbital period, eventually causing the stars to spiral closer together or even merge.

The combination of magnetic activity and tidal interactions creates a dynamic and evolving system, where changes in one aspect (such as rotation or orbital configuration) can ripple through and affect the magnetic, radiative, and mechanical properties of the stars. Therefore, by studying these systems, we can gain deeper insights into stellar magnetic dynamos, the role of magnetic activity in stellar evolution, and the complex interplay between stellar interiors, surfaces, and orbital dynamics. But understanding these processes in close binaries has broader implications, such as for the study of solar activity or even the evolution of exoplanetary systems around active stars.

In the recent past, high-resolution spectrographs, and space-based observatories, has significantly advanced the study of active close binaries. The surface of the spotted components can be studied in great detail with the Doppler imaging technique, which provides sufficiently robust and reliable results with adequate time (rotational phase) coverage, in contrast to photometric spot models, where the mapping of the surface of the star is only possible to a very limited extent (e.g. Kővári & Bartus, 1997; Luger et al., 2021).

In the following review, we go through the most prominent observable characteristics of magnetic dynamos operating in detached close binary systems with the help of selected examples from recent observational studies. However, due to space limitations, we cannot deal with the semi-detached or contact binaries (Algols, W UMa systems) in this review (but see a former review on the topic by Guinan & Giménez 1993, or a more recent statistical study by Kouzuma 2019), nor can we cover the theoretical foundations of the topic. Readers interested in the latter can be recommended, e.g., the series of papers by Schrijver & Zwaan (1991) and Holzwarth & Schüssler (2000, 2003a,b).

2. Observables of magnetic activity in close binaries

2.1. Starspots

Starspots are the most prominent manifestations of magnetic fields on the surface of stars. Their role is crucial for understanding stellar magnetic activity. By studying them we gain insights into the underlying stellar dynamos. But in binary systems, starspots provide clues also about the interactions between

the stars, for example in relation to rotational synchronization by tidal forces. Moreover, from the observation of the starspots, it is even possible to infer the interbinary magnetic interactions, at least to some extent, which can affect orbital dynamics as well. However, there is no doubt that monitoring starspot activity over time helps in understanding magnetic cycles and ultimately the mechanisms that generate and sustain magnetic fields.

Starspots can be observed using different methods of which we highlight the three most important here. *Photometric spot modeling* of light curves (see, e.g., the summary by Savanov, 2013) reveals spots as they rotate in and out of view, but the time series (i.e. 1-dimensional information) is not sufficient for spatial resolution. High-resolution spectroscopy, on the other hand, offers a more detailed approach through the *Doppler imaging* technique (e.g., Carroll et al., 2008, 2012, see also their references), where distortions in spectral lines caused by the star's rotation help create surface maps showing starspot locations. In more advanced observations, long-baseline optical/near-infrared *interferometry* allows for direct imaging of a star's surface, resolving starspots as dark regions, though this technique relies on highly specialized instrumentation and has strong constraints regarding the target itself. For a comparison of simultaneous visualizations of the spotted surface of the giant component in the RS CVn system σ Gem made with these three different imaging techniques, we cite the work of Roettenbacher et al. (2017).

2.2. Active longitudes

The formation spot concentrations along a certain longitude range (but sometimes even at high latitudes around the rotational poles), with lifetimes of the order of months to years, that is active or preferred longitudes, are commonly observed phenomena in active close binaries (Berdyugina & Tuominen, 1998). In synchronized systems these activity centres can form and also bind to certain orbital phases (e.g., Oláh, 2006). Active longitudes, however, require breaking the axial symmetry. This is consistent with the expectation of non-axisymmetric dynamo modes due to symmetry-breaking tidal forces (Moss & Tuominen, 1997). Another condition for the excitation of stable, non-axisymmetric fields is that the differential rotation is not too strong (Moss et al., 1995). We note that this has been verified for synchronously rotating components in close binaries in many cases (Kővári et al., 2017), which is not surprising because tidal coupling is expected to diminish differential rotation.

Certainly, the long-term monitoring of these structures provide insight into the large-scale structure and evolution of the stellar magnetic fields. The location of the active longitudes in the reference frame of the orbit was investigated by Oláh (2006) for 12 close binaries. According to the study, active longitudes on giants in RS CVn-type systems can typically be linked to substellar positions, however, in the case of active subgiant components, the picture is not so clear, rather mixed. At the same time, for main-sequence stars of BY Dra type

systems, the spots are mostly concentrated in quadrature positions. However, other studies led to somewhat contradictory results (cf. Berdyugina & Tuominen, 1998; Samujllo & Kiraga, 2007; Sethi & Martin, 2024).

2.3. Activity cycles

The solar activity cycle is recorded for hundreds of years, and this database can be extended to orders of magnitude longer timescales using various proxies recorded on Earth that reflect changes in solar activity. However, the long-term data collected for active close binaries cannot yet be compared to that of the Sun, either in terms of the time base or the regularity. Nevertheless, from the long-term brightness fluctuations observed in RS CVn and BY Dra type stars were explained long ago by the fact that the active components in such binaries rotate relatively rapidly as a result of tidal synchronization, which ultimately manifests itself in strong chromospheric activity. In other words, from the point of view of activity cycles, binarity has a role mostly in creating/maintaining rapid rotation. That is, the difference is not so much between an active single star and a star similar to it but in a binary system. In terms of dynamo operation, rotation, differential rotation and the evolutionary stage play a more important role (cf. Baliunas et al., 1996; Brun & Browning, 2017; Käpylä et al., 2023).

In a recent statistical study by Martínez et al. (2022), the authors examined 120 RS CVn-type (but including some BY Dra-type) stars from the Southern Hemisphere, and for 91 systems they were able to detect activity cycles. In fact, however, the activity cycles determined so far for active stars (again: not only strictly speaking for members in close binary systems) usually seem to be time-varying quasi-cycles, i.e. instead of precisely defined periods, only approximate averages can be determined. Moreover, in many cases multiple cycles were detected—just like on the Sun. As a reference here are some studies that contain also close binaries in a significant part: Buccino & Mauas (2009); Oláh et al. (2009, 2013); Özdarcan (2021).

2.4. Active coronae and flares

In the most accepted solar flare model (e.g., Kopp & Pneuman, 1976), the release of magnetic energy is caused by the reconnection of magnetic field lines. In addition, however, other possible mechanisms are known to induce reconnection in either the solar, or stellar magnetospheres, see e.g., in Hood & Priest (1979); Charbonneau et al. (2001); Forbes (2010); Priest (2014), etc. However, in close binaries, the binary nature itself plays the decisive role in the formation of flares in many cases. Radio and X-ray observations of close binaries suggest that in several such systems the extent of magnetic structures is comparable to the separation between the companion stars (e.g., Lestrade et al., 1985; Siarkowski et al., 1996; Peterson et al., 2010; Hummel & Beasley, 2020, etc.). This indicates that the magnetic activity is not only bound to one or the other component, but

is actually of interbinary origin. That is, we see the direct result of the magnetic interaction between the components. One such characteristic interaction is when the corotating giant magnetic loops present on both stars are large enough to reach each other and become entangled, and therefore the flux tubes can be temporarily bridged (Simon et al., 1980).

The role of interbinary magnetic fields in flare activity is still not fully understood. However, it is very likely that these interacting fields are not only responsible for the total quiescent X-ray light, but may also be the source of large, long-lasting energetic X-ray flares, as suggested by Singh & Pandey (2022). All of this seems to be supported by the recent finding by (Oláh et al., 2021), according to which it is reasonable to suspect that a large fraction of red giants showing enhanced flare activity found in the *Kepler* field do belong to close binary systems.

We note however, that it is not absolutely necessary to assume an interbinary magnetic entanglement since rapid rotation maintained by synchronization alone can increase the level of flare activity of such red giant components. Moreover, other types of interaction processes are also possible; e.g. van den Oord (1988) long ago drew attention to the fundamental role of the proximity of the companion star in the formation of filament support and flares in close binaries.

3. V471 Tau: a poster child for active close binaries

We illustrate the effect of close binarity on the magnetic activity through the example of V471 Tau, an eclipsing binary system of an active K2 red dwarf star and a white dwarf, i.e., a post-common envelope binary, also, a pre-cataclysmic system. V471 Tau is an actual astrophysical laboratory for studying many aspects of stellar evolution (what's more, the system is probably triple, see Kundra et al., 2022). To reveal the main characteristics of the K star's magnetic activity, in our recent study (Kővári et al., 2021) we used space photometry from *TESS*, high-resolution spectroscopy from the CFHT-ESPaDOnS data archive[1], and X-ray observations from various space instruments. Note, that in such post-common envelope binary systems X-ray emission can originate from either the white dwarf or the corona of the active K star.

The rotation of the K2 dwarf is locked tidally to the orbital period of the eclipsing system of $\approx$0.52 d. One of the direct consequences of tidal locking is that the hemisphere of the K-star facing the white dwarf is constantly exposed to the hot star's radiation, which heats it up. On the basis of spectral synthesis we found that the surface temperature of the K star indeed varies along the orbital phase: an average temperature rise of $\approx$100 K around ϕ=0.5 phase (so when the white dwarf is in front) indicates the irradiance effect in both the 2005 and 2014/15 observing seasons; see Fig. 1. Meanwhile, the hemisphere of the K2 star facing the hot component is more covered with cool spots; see our Fig. 2 for

[1]https://www.cadc.hia.nrc.gc.ca/AdvancedSearch/

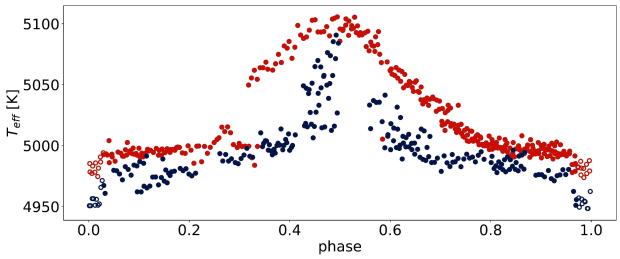


Figure 1. Variation of the surface temperature of the K2V component of V471 Tau along the orbital phase due to the irradiation effect. Temperature values were derived individually for each observed spectrum (red dots for the 2005 season, black dots for 2014/15). Open circles around zero phase correspond to those unaffected spectra that were observed when the white dwarf was eclipsed.

the results of Doppler imaging for both seasons. Moreover, despite the ten-year difference between the Doppler images shown in the figure, the surface spot distribution of the star K2 is remarkably stable. It is particularly noteworthy that the phase of the most dominant spot essentially coincides with the phase facing the white dwarf. This permanent cool spot, or say active longitude, may be coupled to the orbital phase (cf. Schrijver & Zwaan, 1991).

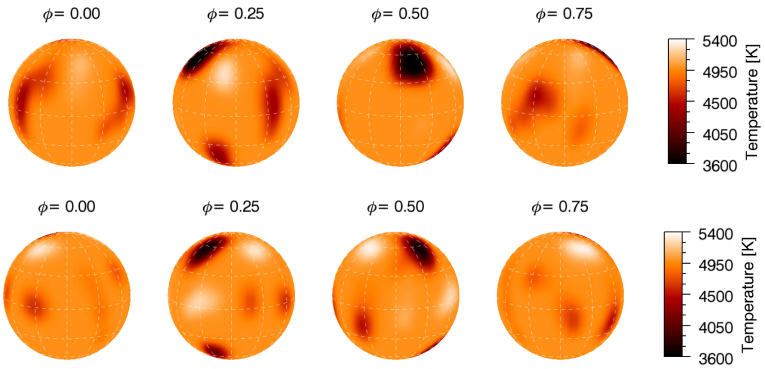


Figure 2. Doppler image of the K2V component of V471 Tau from 2005 data (top panel) and from 2014/15 data (bottom panel). Both surface temperature maps are plotted in quarter rotation phases; ϕ=0.0 corresponds to the phase when the white dwarf is eclipsed, ϕ=0.5 is the phase facing the white dwarf. Note the stable spot configuration despite a decade of time difference between the images.

Our thorough Doppler study in Kővári et al. (2021) also provided the opportunity to follow the changes in the spot distribution within a short period

of time (i.e., within a few days or a few weeks). The cross-correlation technique presented therein is one of the best known and most established ways to measure the differential rotation of the stellar surface (Donati & Collier Cameron, 1997). Briefly, surface differential rotation can be measured by cross-correlation of the consecutive Doppler images along the astrographic longitude. On the resulting cross-correlation function map, the strongest correlation pattern gives the most probable latitudinal velocity distribution. The pattern can be fitted with a quadratic rotation law in the usual form known from the solar case:

$$\Omega(\beta) = \Omega_{\rm eq}(1 - \alpha_{\rm DR} \sin^2 \beta), \tag{1}$$

where $\Omega(\beta)$ is the angular velocity at β latitude, $\Omega_{\rm eq}$ is the angular velocity of the equator, and $\alpha_{\rm DR}$ is the dimensionless surface shear parameter. An improved version of the technique (dubbed `ACCORD`, see e.g., Kővári et al., 2004, 2012, 2015), which uses the average of cross-correlations, is even more robust, i.e. less sensitive to rapid stochastic changes in the arrangement of spots.

For the K2 star of V471 Tau, the surface shear parameter was found to be $\alpha_{\rm DR} = 0.0026 \pm 0.0006$, which indicates an almost solid body rotation. This finding confirms the assumption that in the case of such a close binary, tidal locking inhibits the differential rotation. Further evidence of such tidal confinement can be seen in Fig. 3, which compares the shear parameters for various single and close binary stars with different rotation periods. The plot is an updated ver-

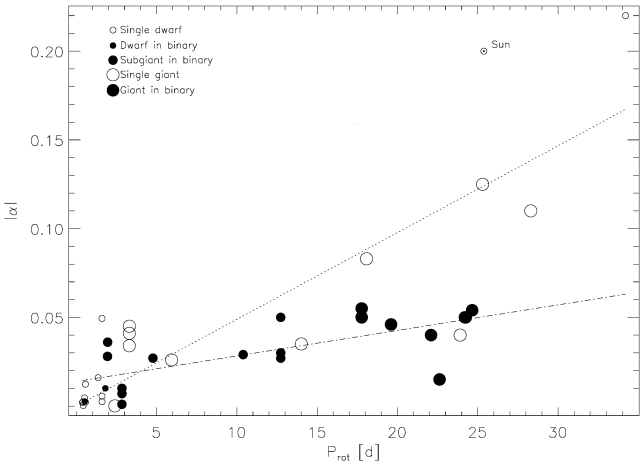


Figure 3. Surface shear parameter (α) vs. rotation period ($P_{\rm rot}$) graph for active spotted stars (updated from Kővári et al., 2017). Open circles fitted with a dashed straight line correspond to single active stars, filled black circles fitted with a dash–dotted straight line represent active stars in close binary systems. Symbol size increases from dwarfs to subgiants to giants.

sion of the surface shear parameter vs. rotation period graph ($|\alpha|$–$P_{\rm rot}$ graph) from Kővári et al. (2017). The dotted and dash-dotted lines denote the linear fits for single stars and stars in close binary systems, respectively, with slopes of $|\alpha| \propto 0.0049 P_{\rm rot}$[d] and $|\alpha| \propto 0.0014 P_{\rm rot}$[d]. The diagram clearly indicates bimodality, i.e., that close binarity does play a role in inhibiting the differential rotation of the convective envelope.

In connection with V471 Tau, we mention one more activity characteristic that raises the importance of close binarity: the inter-binary Hα emission in 2014/15. Based on long-term X-ray observations, the star was close to its maximum activity during this period (Kővári et al., 2021, see their Fig. 13). The Hα behaviour in Fig. 4 shows absorption centered around 0.0 phase and the emission between 0.35-0.65 phase, this latter around the phase of the most prominent cool spot (cf. Fig. 2). Being within the radial velocity range of the K2 dwarf, these features are localized on the surface of the red dwarf. However, there is a very different emitting phenomenon located between the centre of mass of the system and the white dwarf. This emission is stronger in the first half of the orbital phase, but still visible during the second half. This suggests the presence of a clump of emitting plasma corotating with the system in the vicinity of the inner Lagrangian (L1) point, as already reported by Young et al. (1991, see their Fig. 3), who also found external Hα emission component, originated from the inter-binary space beyond the centre of mass of the system, expanding towards the white dwarf, very similar to our result plotted in Fig. 4.

It is quite possible that the extra Hα emission from the inter-binary space might have something to do with the enhanced X-ray luminosity in 2015, i.e., around activity maximum. We suspect that during the magnetic cycle, around activity maximum more and/or more extended magnetic loops develop high above the surface of the K2 star, reaching one stellar radius (Guinan et al., 1986), and this way more cool material enters the upper atmosphere in trapped clumps, similar to solar prominences (cf. Collier Cameron & Robinson, 1989). Normally, such a clump of cool material appears in absorption in Hα, exactly what we actually see on the 'far side' of the K2 star around zero phase. However, it can get into emission when heated due to the UV radiation from the white dwarf. The physical process behind heating proposed first by Young et al. (1988) involves fluorescence-induced Hα emission (see also Bois et al., 1991). This scenario could explain the Hα line variability around activity maximum (Fig. 4) when extended loops with cool material trapped in them are present.

Finally, we mention here a special group of active binaries: those close binaries in which both components are magnetically active, so that their magnetospheres can interact directly with each other (Oláh & Kővári, 1997). In such cases, the rotation and orbital motion of the stars can lead to a slow overall winding of the coupled magnetic fields, allowing a gradual accumulation of magnetic energy that can eventually be released as an interbinary flare (Cherkis & Lyutikov, 2021). Note that something similar happened in UX Ari (G5V+K0IV), when the corotating, giant magnetic loops present on both stars

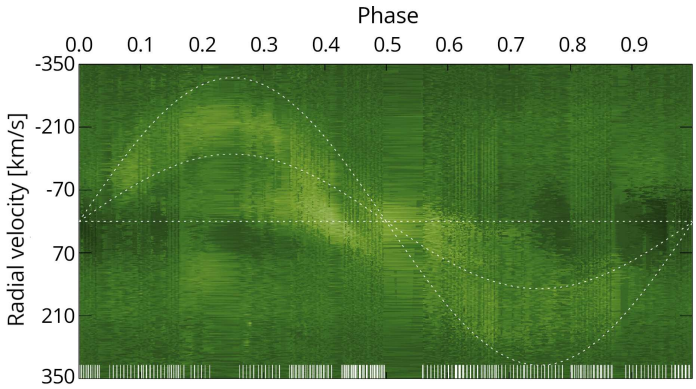


Figure 4. Dynamic Hα spectrum of V471 Tau from the 2014/15 data. The individual 1-D Hα spectra along the orbital phase are plotted in the rest frame of the K2 star. Dark green corresponds to deep absorption, while light yellow indicates strong emission. The large amplitude ($\approx$320 km s^{-1}) sine curve marks the radial velocity of the white dwarf, the smaller amplitude ($\approx$150 km s^{-1}) sinusoid is the radial velocity of the centre of mass of the binary system. Tick marks at the bottom indicate the phases of the observations.

interacted and flux tubes temporarily connected the components (Simon et al., 1980). Such connecting flux loops can also pave the way for mass transfer between the two stellar components (see, e.g. Ferreira & Mendoza-Briceño, 2005), which can even be observed in the form of orbital period changes (cf., Decampli & Baliunas, 1979). Another interesting target is DQ Tau, in which the orbit of the two $\sim$0.65$M_\odot$ mass pre-main sequence components is highly eccentric, therefore at periastron encounters the magnetospheres of the components collide and trigger each other, resulting in magnetic reconnection and so, as a result, recurring flares can be observed in these orbital phases (Salter et al., 2010).

4. Active red giants in long period RS CVn systems

In long period RS CVn systems with an active cool giant component, tidal synchronization helps maintain rapid rotation, even though blowing up to a giant star would just slow down the rotation. This process has a fundamental influence on dynamo operation, which is illustrated by some examples of great importance.

One notable target is σ Gem, a close binary with an active red giant primary that rotates synchronously with the orbital period ($P_{\rm rot} \approx P_{\rm orb} \approx$20 d). What makes the star really interesting is that its differential rotation was found to be antisolar, i.e. the equatorial band rotates the slowest (α=$-$0.04$\pm$0.01). We note that so far only a few stars have been confirmed to exhibit antisolar differential

rotation and there is good reason to assume that these are mostly subgiants or giants (cf. Kővári et al., 2017, see their Table 1). Kővári et al. (2015) also reported a significant poleward flow of $\sim$0.3km s^{-1} for σ Gem, which was measured using spot tracking. According to Kitchatinov & Rüdiger (2004) antisolar differential rotation may result from a fast meridional flow, if some driving mechanism is able to maintain it. Such driver candidates are large-scale thermal inhomogeneities (i.e., large starspots) and/or tidal effects in close binary systems. σ Gem meets both criteria, so the measurements and the theoretical basis verify each other.

A common feature of long period RS CVn giants is that large starspots develop on their surface from time to time, which can persist for several months and can cause modulation with an amplitude of up to $\sim$0.3-0.8 mag in the V band. However, it is not common for these activity centres to be bound to the orbit. The most recent long-baseline optical and infrared interferometric starspot observations of ζ And have revealed beyond any doubt that the spots can also appear at high latitudes, even covering the rotation poles. In addition, significant asymmetries can occur between the hemispheres regarding the appearance of spots (cf. Roettenbacher et al., 2016). This suggests highly asymmetric dynamo modes, i.e. a dynamo operation other than the Sun's, e.g., with mixed parity modes (Bushby, 2003). What is more, decades-long photometry of such overactive RS CVn giants showed that their long-term peak-to-peak brightness variation can be as much as one magnitude (Oláh et al., 2014), and these long-term changes are defintely not periodic, often a mixture of aperiodic and trend-like changes. Based on all this, it can be concluded that the dynamo of such RS CVn giants is non-solar in nature, in some cases chaotic (cf. Strassmeier et al., 2024).

Acknowledgements. This research was funded by the Hungarian National Research, Development, and Innovation Office grant KKP-143986. The financial support of the Austrian–Hungarian Action Foundation grant 117öu4 is also acknowledged.

References

Baliunas, S. L., Nesme-Ribes, E., Sokoloff, D., & Soon, W. H., A Dynamo Interpretation of Stellar Activity Cycles. 1996, *Astrophysical Journal*, **460**, 848, DOI: 10.1086/177014

Berdyugina, S. V. & Tuominen, I., Permanent active longitudes and activity cycles on RS CVn stars. 1998, *Astronomy and Astrophysics*, **336**, L25

Bois, B., Lanning, H. H., & Mochnacki, S. W., Spectroscopy of V471 Tau. II. Observations of the H(alpha) Line. 1991, *Astronomical Journal*, **102**, 2079, DOI: 10.1086/116032

Brun, A. S. & Browning, M. K., Magnetism, dynamo action and the solar-stellar connection. 2017, *Living Reviews in Solar Physics*, **14**, 4, DOI:10.1007/s41116-017-0007-8

Buccino, A. P. & Mauas, P. J. D., Long-term chromospheric activity of non-eclipsing RS CVn-type stars. 2009, *Astronomy and Astrophysics*, **495**, 287, DOI:10.1051/0004-6361:200810985

Bushby, P. J., Strong asymmetry in stellar dynamos. 2003, *Monthly Notices of the RAS*, **338**, 655, DOI:10.1046/j.1365-8711.2003.06080.x

Carroll, T. A., Kopf, M., & Strassmeier, K. G., A fast method for Stokes profile synthesis. Radiative transfer modeling for ZDI and Stokes profile inversion. 2008, *Astronomy and Astrophysics*, **488**, 781, DOI:10.1051/0004-6361:200809981

Carroll, T. A., Strassmeier, K. G., Rice, J. B., & Künstler, A., The magnetic field topology of the weak-lined T Tauri star V410 Tauri. New strategies for Zeeman-Doppler imaging. 2012, *Astronomy and Astrophysics*, **548**, A95, DOI:10.1051/0004-6361/201220215

Charbonneau, P., McIntosh, S. W., Liu, H.-L., & Bogdan, T. J., Avalanche models for solar flares (Invited Review). 2001, *Solar Physics*, **203**, 321, DOI:10.1023/A:1013301521745

Cherkis, S. A. & Lyutikov, M., Magnetic Topology in Coupled Binaries, Spin-orbital Resonances, and Flares. 2021, *Astrophysical Journal*, **923**, 13, DOI:10.3847/1538-4357/ac29b8

Collier Cameron, A. & Robinson, R. D., Fast Hα variations on a rapidly rotating, cool main-sequence star-II. Cloud formation and ejection. 1989, *Monthly Notices of the RAS*, **238**, 657, DOI:10.1093/mnras/238.2.657

Decampli, W. M. & Baliunas, S. L., What tides and flares do to RS Canum Venaticorum binaries. 1979, *Astrophysical Journal*, **230**, 815, DOI:10.1086/157140

Donati, J. F. & Collier Cameron, A., Differential rotation and magnetic polarity patterns on AB Doradus. 1997, *Monthly Notices of the RAS*, **291**, 1, DOI:10.1093/mnras/291.1.1

Ferreira, J. M. & Mendoza-Briceño, C. A., Coronal mass transfer in interbinary loops. 2005, *Astronomy and Astrophysics*, **433**, 1055, DOI:10.1051/0004-6361:20041926

Forbes, T., Models of coronal mass ejections and flares. 2010, in *Heliophysics: Space Storms and Radiation: Causes and Effects*, ed. C. J. Schrijver & G. L. Siscoe, 159

Guinan, E. F. & Giménez, A., Magnetic Activity in Close Binaries. 1993, in Astrophysics and Space Science Library, Vol. **177**, *Astrophysics and Space Science Library*, ed. J. Sahade, G. E. McCluskey, & Y. Kondo, 51

Guinan, E. F., Wacker, S. W., Baliunas, S. L., Loesser, J. G., & Raymond, J. C., Evidence of large-scale structures in the atmosphere of the active K-dwarf component of V471 Tauri. 1986, in ESA Special Publication, Vol. **263**, *New Insights in Astrophysics. Eight Years of UV Astronomy with IUE*, ed. E. J. Rolfe & R. Wilson, 197–200

Holzwarth, V. & Schüssler, M., Stability of magnetic flux tubes in close binary stars. 2000, *Astronomische Nachrichten*, **321**, 175, DOI:10.1002/1521-3994(200008)321:3<175::AID-ASNA175>3.0.CO;2-V

Holzwarth, V. & Schüssler, M., Dynamics of magnetic flux tubes in close binary stars. I. Equilibrium and stability properties. 2003a, *Astronomy and Astrophysics*, **405**, 291, DOI:10.1051/0004-6361:20030582

Holzwarth, V. & Schüssler, M., Dynamics of magnetic flux tubes in close binary stars. II. Nonlinear evolution and surface distributions. 2003b, *Astronomy and Astrophysics*, **405**, 303, DOI:10.1051/0004-6361:20030584

Hood, A. W. & Priest, E. R., Kink Instability of Solar Coronal Loops as the Cause of Solar Flares. 1979, *Solar Physics*, **64**, 303, DOI:10.1007/BF00151441

Hummel, C. A. & Beasley, A., Linking radio flares with spots on the active binary UX Arietis. 2020, in IAU Symposium, Vol. **354**, *Solar and Stellar Magnetic Fields: Origins and Manifestations*, ed. A. Kosovichev, S. Strassmeier, & M. Jardine, 418–420

Käpylä, P. J., Browning, M. K., Brun, A. S., Guerrero, G., & Warnecke, J., Simulations of Solar and Stellar Dynamos and Their Theoretical Interpretation. 2023, *Space Science Reviews*, **219**, 58, DOI:10.1007/s11214-023-01005-6

Kővári, Zs. & Bartus, J., Testing the stability and reliability of starspot modelling. 1997, *Astronomy and Astrophysics*, **323**, 801

Kővári, Zs., Korhonen, H., Kriskovics, L., et al., Measuring differential rotation of the K-giant ζ Andromedae. 2012, *Astronomy and Astrophysics*, **539**, A50, DOI:10.1051/0004-6361/201118177

Kővári, Zs., Kriskovics, L., Künstler, A., et al., Antisolar differential rotation of the K1-giant σ Geminorum revisited. 2015, *Astronomy and Astrophysics*, **573**, A98, DOI:10.1051/0004-6361/201424138

Kővári, Zs., Kriskovics, L., Oláh, K., et al., A confined dynamo: Magnetic activity of the K-dwarf component in the pre-cataclysmic binary system V471 Tauri. 2021, *Astronomy and Astrophysics*, **650**, A158, DOI:10.1051/0004-6361/202140707

Kővári, Zs., Oláh, K., Kriskovics, L., et al., Rotation-differential rotation relationships for late-type single and binary stars from Doppler imaging. 2017, *Astronomische Nachrichten*, **338**, 903, DOI:10.1002/asna.201713400

Kővári, Zs., Strassmeier, K. G., Granzer, T., et al., Doppler imaging of stellar surface structure. XXII. Time-series mapping of the young rapid rotator LQ Hydrae. 2004, *Astronomy and Astrophysics*, **417**, 1047, DOI:10.1051/0004-6361:20034187

Kitchatinov, L. L. & Rüdiger, G., Anti-solar differential rotation. 2004, *Astronomische Nachrichten*, **325**, 496, DOI:10.1002/asna.200410297

Kopp, R. A. & Pneuman, G. W., Magnetic reconnection in the corona and the loop prominence phenomenon. 1976, *Solar Physics*, **50**, 85, DOI:10.1007/BF00206193

Kouzuma, S., Starspots in contact and semi-detached binary systems. 2019, *Publications of the ASJ*, **71**, 21, DOI:10.1093/pasj/psy140

Kundra, E., Hambálek, Ľ., Vanaverbeke, S., et al., Variability of eclipse timing: the case of V471 Tauri. 2022, *Monthly Notices of the RAS*, **517**, 5358, DOI:10.1093/mnras/stac2812

Lestrade, J. F., Mutel, R. L., Preston, R. A., & Phillips, R. B., High-angular Resolution Observations of Stellar Binary Systems. 1985, in Astrophysics and Space Science Library, Vol. **116**, *Radio Stars*, ed. R. M. Hjellming & D. M. Gibson, 275–282

Luger, R., Foreman-Mackey, D., Hedges, C., & Hogg, D. W., Mapping Stellar Surfaces. I. Degeneracies in the Rotational Light-curve Problem. 2021, *Astronomical Journal*, **162**, 123, DOI:10.3847/1538-3881/abfdb8

Martínez, C. I., Mauas, P. J. D., & Buccino, A. P., Activity cycles in RS CVn-type stars. 2022, *Monthly Notices of the RAS*, **512**, 4835, DOI:10.1093/mnras/stac755

Moss, D., Barker, D. M., Brandenburg, A., & Tuominen, I., Nonaxisymmetric dynamo solutions and extended starspots on late-type stars. 1995, *Astronomy and Astrophysics*, **294**, 155

Moss, D., Piskunov, N., & Sokoloff, D., Nonaxisymmetric cool spot distributions and dynamo action in close binaries. 2002, *Astronomy and Astrophysics*, **396**, 885, DOI:10.1051/0004-6361:20021370

Moss, D. & Tuominen, I., Magnetic field generation in close binary systems. 1997, *Astronomy and Astrophysics*, **321**, 151

Oláh, K., Active Longitudes in Close Binaries. 2006, *Astrophysics and Space Science*, **304**, 145, DOI:10.1007/s10509-006-9096-x

Oláh, K., Kővári, Zs., Günther, M. N., et al., Toward the true number of flaring giant stars in the Kepler field. Are their flaring specialities associated with their being giant stars? 2021, *Astronomy and Astrophysics*, **647**, A62, DOI:10.1051/0004-6361/202039674

Oláh, K., Kolláth, Z., Granzer, T., et al., Multiple and changing cycles of active stars. II. Results. 2009, *Astronomy and Astrophysics*, **501**, 703, DOI:10.1051/0004-6361/200811304

Oláh, K. & Kövári, Zs., Doubly Active Binaries. 1997, in *The Earth and the Universe*, ed. G. Asteriadis, A. Bantelas, M. E. Contadakis, K. Katsambalos, A. Papdimitriou, & I. N. Tziavos, 151

Oláh, K., Moór, A., Kővári, Zs., et al., Magnitude-range brightness variations of overactive K giants. 2014, *Astronomy and Astrophysics*, **572**, A94, DOI:10.1051/0004-6361/201424695

Oláh, K., Moór, A., Strassmeier, K. G., Borkovits, T., & Granzer, T., Long-term photometry of three active red giants in close binary systems: V2253 Oph, IT Com and IS Vir. 2013, *Astronomische Nachrichten*, **334**, 625, DOI:10.1002/asna.201211846

Özdarcan, O., Spectroscopic and photometric analysis of 21 chromospherically active variables: Activity cycles and differential rotation. 2021, *Publications of the Astron. Soc. of Australia*, **38**, e027, DOI:10.1017/pasa.2021.21

Peterson, W. M., Mutel, R. L., Güdel, M., & Goss, W. M., A large coronal loop in the Algol system. 2010, *Nature*, **463**, 207, DOI:10.1038/nature08643

Priest, E. 2014, *Magnetohydrodynamics of the Sun*, DOI:10.1017/CBO9781139020732

Roettenbacher, R. M., Monnier, J. D., Korhonen, H., et al., No Sun-like dynamo on the active star ζ Andromedae from starspot asymmetry. 2016, *Nature*, **533**, 217, DOI:10.1038/nature17444

Roettenbacher, R. M., Monnier, J. D., Korhonen, H., et al., Contemporaneous Imaging Comparisons of the Spotted Giant σ Geminorum Using Interferometric, Spectroscopic, and Photometric Data. 2017, *Astrophysical Journal*, **849**, 120, DOI:10.3847/1538-4357/aa8ef7

Salter, D. M., Kóspál, Á., Getman, K. V., et al., Recurring millimeter flares as evidence for star-star magnetic reconnection events in the DQ Tauri PMS binary system. 2010, *Astronomy and Astrophysics*, **521**, A32, DOI:10.1051/0004-6361/201015197

Samujllo, M. & Kiraga, M., Evolution of Magnetic Flux Tubes in Convective Envelopes of Close Binary Stars. 2007, *Acta Astronomica*, **57**, 347

Savanov, I. S., Starspot detection and properties. 2013, in IAU Symposium, Vol. **294**, *Solar and Astrophysical Dynamos and Magnetic Activity*, ed. A. G. Kosovichev, E. de Gouveia Dal Pino, & Y. Yan, 257–268

Schrijver, C. J. & Zwaan, C., Activity in tidally interacting binaries. 1991, *Astronomy and Astrophysics*, **251**, 183

Sethi, R. & Martin, D. V., Tight stellar binaries favour active longitudes at sub- and antistellar points. 2024, *Monthly Notices of the RAS*, **529**, 4442, DOI:10.1093/mnras/stae717

Siarkowski, M., Pres, P., Drake, S. A., White, N. E., & Singh, K. P., Corona(e) of AR Lacertae. II. The Spatial Structure. 1996, *Astrophysical Journal*, **473**, 470, DOI:10.1086/178159

Simon, T., Linsky, J. L., & Schiffer, F. H., I., IUE spectra of a flare in the RS Canum Venaticorum-type system UX Arietis. 1980, *Astrophysical Journal*, **239**, 911, DOI:10.1086/158178

Singh, G. & Pandey, J. C., An X-Ray Study of Coronally Connected Active Eclipsing Binaries. 2022, *Astrophysical Journal*, **934**, 20, DOI:10.3847/1538-4357/ac7716

Sokoloff, D. & Piskunov, N., Swing excitation and magnetic activity in close binary systems. 2002, *Monthly Notices of the RAS*, **334**, 925, DOI:10.1046/j.1365-8711.2002.05583.x

Strassmeier, K. G., Kővári, Zs., Weber, M., & Granzer, T., Long-term Doppler imaging of the star XX Trianguli indicates chaotic non-periodic dynamo. 2024, *Nature Communications*, **15**, 9986, DOI:10.1038/s41467-024-54329-4

van den Oord, G. H. J., Filament support and flares in binaries. 1988, *Astronomy and Astrophysics*, **205**, 167

Young, A., Rottler, L., & Skumanich, A., Evidence for External Plasma around the K Dwarf Component of the Eclipsing Binary V471 Tauri. 1991, *Astrophysical Journal, Letters*, **378**, L25, DOI:10.1086/186133

Young, A., Skumanich, A., & Paylor, V., Fluorescence-induced Chromospheric H alpha Emission from the K Dwarf Component of V471 Tauri. I. The 1983 Epoch. 1988, *Astrophysical Journal*, **334**, 397, DOI:10.1086/166844

Contrib. Astron. Obs. Skalnaté Pleso **55/3**, 196 – 199, (2025)
https://doi.org/10.31577/caosp.2025.55.3.196

Pulsational characteristics of mass accreting stars in close binary systems

A. Miszuda

Nicolaus Copernicus Astronomical Centre, Polish Academy of Sciences, Bartycka 18, PL-00-716 Warsaw, Poland (E-mail: amiszuda@camk.edu.pl)

Received: November 15, 2024; Accepted: December 20, 2024

Abstract. Eclipsing binaries with pulsating components are a distinct subclass of binaries, merging orbital and pulsational analyses. In recent years that subclass led to the definition of a newly formed branch of tidal asteroseismology. While single-star pulsators are well understood, the effects of binarity and possible mass transfer on pulsational characteristics, particularly in mass-gaining stars, remain to be systematically explored. Here, I present preliminary results on the asteroseismic properties of a mass-accreting model for a $10\,M_\odot$ β Cephei-type star.

Key words: stars: binaries: close – stars: evolution – asteroseismology

1. Introduction

The recent years have brought an enormous progress in development and understanding of tidal asteroseismology. Handler et al. (2020) have reported the first ever observed case of a single p-mode tidally trapped δ Sct pulsation in a close binary star system, HD 74423. That discovery was followed by Kurtz et al. (2020), who discovered at least four separate tidally trapped oscillation modes in CO Cam system. As shown by Fuller et al. (2020), that exotic behaviour has its roots in mode coupling.

Further advancements have been made by recent studies, including Miszuda et al. (2021, 2022), who explored the role of mass transfer in affecting radial modes and mode instabilities in δ Sct stars. Expanding on this, Wagg et al. (2024) used Slowly Pulsating B (SPB) star models to show that mass-accreting binaries often exhibit amplitude variations in their period spacing patterns, with some patterns being out of phase. Additionally, Rui & Fuller (2021), Bellinger et al. (2024), and Henneco et al. (2024) demonstrated that asteroseismology can be used to distinguish merger products, by investigating how mass transfer affects the pulsation spectra of merger remnants. These studies collectively highlight the potential of asteroseismology in unveiling the complex effects of mass transfer and stellar mergers on the pulsational properties of stars.

The motivation for this research lies in the fact that stars within the mass range of β Cephei-type stars ($8 - 18\,M_\odot$) can be frequently found in binary or

multiple systems (Duchêne & Kraus, 2013), where mass transfer can significantly alter their evolution. This provides excellent conditions for studying the interplay between stellar pulsations and mass transfer.

2. Methodology

Using `MESA` (Modules for Experiments in Stellar Astrophysics, Paxton et al., 2011, version 23.05.1), I built a toy model of a binary system with $M_{\rm don,0} = 10\,{\rm M}_\odot$ and $M_{\rm acc,0} = 7\,{\rm M}_\odot$ initial masses in a $P_{\rm orb,0} = 3\,{\rm d}$ circular orbit. The binary was evolved through a phase of mass transfer until mass ratio reversal, i.e., $M_{\rm don} = 7\,{\rm M}_\odot$ and $M_{\rm acc} = 10\,{\rm M}_\odot$. At this point, all binary interactions were halted, and the mass-accreting star evolved as a single star until central hydrogen exhaustion.

Solar metallicity was assumed for each component, with exponential overshooting mixing applied to the hydrogen-burning core, with $f_{\rm ov} = 0.02$, following the Herwig (2000) prescription. Convective, semi-convective, and thermohaline mixing were incorporated with coefficients $\alpha_{\rm MLT} = 0.5$, $\alpha_{\rm SC} = 0.1$, and $\alpha_{\rm TH} = 1$, respectively.

For the sake of this paper I selected a model at $X_c = 0.1$ for the mass-accreting star and calculated theoretical pulsations for $\ell = 0, 1, 2$ modes using `GYRE` (Townsend et al., 2018). This model is approximately 39.31 Myr old and is well past the mass transfer phase, which started at $X_c = 0.52$ (23.64 Myr) and ended at $X_c = 0.59$ (23.65 Myr). All computations were repeated for a single $M = 10\,{\rm M}_\odot$ star as a basis for comparison.

3. Results

For each pulsational model, I calculated the period spacing, ΔP, using $\ell = 1$ g-modes frequencies. As shown in Fig. 1, the main differences between the single-star and mass-accreting models are in amplitude deviation and phase shifts in the period spacing patterns. The single-star model exhibits a lower amplitude compared to the binary case. Additionally, the mass-accreting model is out of phase for periods between 3-4 days. A similar behaviour was observed by Wagg et al. (2024) for SPB star models.

Next, the ν_s/ν_b frequency ratios were computed for $\ell = 0, 1, 2$ p-modes, where ν_s is the frequency from the single-star model and ν_b is the frequency from the binary model, ensuring that they correspond to the same radial orders $n_{\rm pg}$ in both cases. The most noticeable deviations appear at low radial orders, between $n_{\rm pg} = 0$ and $n_{\rm pg} = 10$, suggesting that low-order p-modes may be sensitive to differences in the internal structure of stars that have undergone mass transfer. This behaviour will be the subject of in-depth study in our future work.

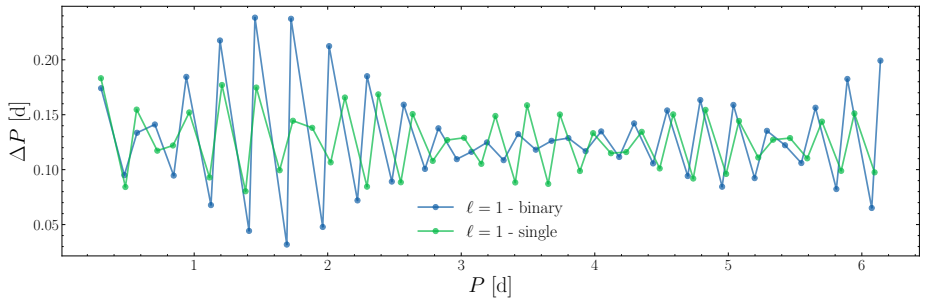


Figure 1. The period spacing patterns of the $\ell = 1$ g-modes for $M = 10\,\mathrm{M}_\odot$, $X_c = 0.1$ single (green line) and binary (blue line) models.

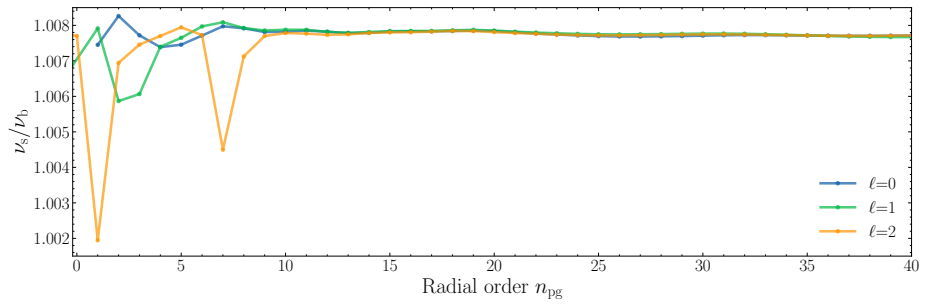


Figure 2. The frequency ratio patterns of the $\ell = 0, 1, 2$ p-modes for $M = 10\,\mathrm{M}_\odot$, $X_c = 0.1$ models.

4. Summary

The results presented in this proceedings suggest that mass accretion leads to measurable deviations in the pulsational properties of stars. This ongoing work will be expanded in a forthcoming paper by Miszuda & Guo (in preparation).

Acknowledgements. This work was supported by the Polish National Science Centre (NCN), grant number 2021/43/B/ST9/02972.

References

Bellinger, E. P., de Mink, S. E., van Rossem, W. E., & Justham, S., The Potential of Asteroseismology to Resolve the Blue Supergiant Problem. 2024, *Astrophysical Journal, Letters*, **967**, L39, DOI:10.3847/2041-8213/ad4990

Duchêne, G. & Kraus, A., Stellar Multiplicity. 2013, *Annual Review of Astron and Astrophys*, **51**, 269, DOI:10.1146/annurev-astro-081710-102602

Fuller, J., Kurtz, D. W., Handler, G., & Rappaport, S., Tidally trapped pulsations in binary stars. 2020, *Monthly Notices of the RAS*, **498**, 5730, DOI:10.1093/mnras/staa2376

Handler, G., Kurtz, D. W., Rappaport, S. A., et al., Tidally trapped pulsations in a close binary star system discovered by TESS. 2020, *Nature Astronomy*, **4**, 684, DOI:10.1038/s41550-020-1035-1

Henneco, J., Schneider, F. R. N., Hekker, S., & Aerts, C., Merger seismology: Distinguishing massive merger products from genuine single stars using asteroseismology. 2024, *Astronomy and Astrophysics*, **690**, A65, DOI:10.1051/0004-6361/202450508

Herwig, F., The evolution of AGB stars with convective overshoot. 2000, *Astronomy and Astrophysics*, **360**, 952

Kurtz, D. W., Handler, G., Rappaport, S. A., et al., The single-sided pulsator CO Camelopardalis. 2020, *Monthly Notices of the RAS*, **494**, 5118, DOI:10.1093/mnras/staa989

Miszuda, A., Kołaczek-Szymański, P. A., Szewczuk, W., & Daszyńska-Daszkiewicz, J., The eclipsing binary systems with δ Scuti component - II. AB Cas. 2022, *Monthly Notices of the RAS*, **514**, 622, DOI:10.1093/mnras/stac1197

Miszuda, A., Szewczuk, W., & Daszyńska-Daszkiewicz, J., The eclipsing binary systems with δ Scuti component - I. KIC 10661783. 2021, *Monthly Notices of the RAS*, **505**, 3206, DOI:10.1093/mnras/stab1597

Paxton, B., Bildsten, L., Dotter, A., et al., Modules for Experiments in Stellar Astrophysics (MESA). 2011, *Astrophysical Journal, Supplement*, **192**, 3, DOI:10.1088/0067-0049/192/1/3

Rui, N. Z. & Fuller, J., Asteroseismic fingerprints of stellar mergers. 2021, *Monthly Notices of the RAS*, **508**, 1618, DOI:10.1093/mnras/stab2528

Townsend, R. H. D., Goldstein, J., & Zweibel, E. G., Angular momentum transport by heat-driven g-modes in slowly pulsating B stars. 2018, *Monthly Notices of the RAS*, **475**, 879, DOI:10.1093/mnras/stx3142

Wagg, T., Johnston, C., Bellinger, E. P., et al., The asteroseismic imprints of mass transfer. A case study of a binary mass-gainer in the SPB instability strip. 2024, *Astronomy and Astrophysics*, **687**, A222, DOI:10.1051/0004-6361/202449912

Contrib. Astron. Obs. Skalnaté Pleso **55/3**, 200 – 210, (2025)
https://doi.org/10.31577/caosp.2025.55.3.200

Post-common-envelope planetary nebulae

D. Jones[1,2,3]

[1] *Instituto de Astrofísica de Canarias, 38205 La Laguna, Tenerife, Spain (E-mail: djones@iac.es)*

[2] *Departamento de Astrofísica, Universidad de La Laguna, E-38206 La Laguna, Tenerife, Spain*

[3] *Nordic Optical Telescope, Rambla José Ana Fernández Pérez 7, 38711, Breña Baja, Spain*

Received: November 27, 2024; Accepted: December 11, 2024

Abstract. Close-binary central stars of planetary nebulae offer a unique tool with which to study the critical and yet poorly understood common-envelope phase of binary stellar evolution. Furthermore, as the nebula itself is thought to comprise the ionised remnant of the ejected common envelope, such planetary nebulae can be used to directly probe the mass, morphology and dynamics of the ejecta. In this review, I summarise our current understanding of the importance of binarity in the formation of planetary nebulae as well as what they may be able to tell us about the common-envelope phase – including the possible relationships with other post-common-envelope phenomena like stellar mergers, novae and type Ia supernovae.

Key words: binaries: close – planetary nebulae: general – stars: jets

1. Introduction

It is now almost half a century since Paczynski (1976) first proposed the common-envelope (CE) scenario as the most viable pathway towards the formation of close binaries with an evolved component. Since then, the evidence for the importance of the CE has only grown, however key aspects of the processes at work remain enigmatic (Ivanova et al., 2013). At the time, Paczynski (1976) already recognised the importance of planetary nebulae (PNe) in understanding the CE phase, stating *"Observational discovery of a short period binary being a nucleus of a planetary nebula would provide very important support for the evolutionary scenario"*, and the first example was discovered that same year by Bond (1976). Subsequent studies of post-CE planetary nebulae (PNe) have already taught us much about the CE and they continue to represent a key tool with which to shed light on this critical phase of binary evolution (Jones, 2020).

From the perspective of the PN community, the principal interest in CE evolution is the ease with which it can explain the wide range of aspherical morphologies observed in PNe (Balick & Frank, 2002; García-Segura et al., 2018;

De Marco et al., 2022). However, until recently, there was a reluctance to accept that binarity was the primary shaping mechanism in PNe due to the lack of known binary central stars. In the early 2000s, only 16 post-CE PNe were known (a couple of which have since been shown to be wide binaries, false associations or non-PNe) leading to the estimate that roughly 10% of PNe hosted close binary stars (Bond, 2000). Exploitation of wide-field surveys, like OGLE, Kepler and TESS, has since led to an explosion of new discoveries (Miszalski et al., 2009; Jacoby et al., 2021; Aller et al., 2024), taking the total now to over 100 known post-CE central stars[1]. These studies have placed a hard lower limit on the binary fraction of 20%, while other probes (such as radial velocities, composite spectra and infrared excesses) have provided much higher estimates (perhaps as high as 80%; De Marco et al., 2004; Douchin et al., 2015).

The minimum 20% post-CE fraction already has one critical implication for our understanding of PNe – it is likely that some stars which our textbooks would say should produce an observable PN, in fact, do not. Simply put, based on the main sequence binary fraction and period distribution, one would not expect as many as 20% of all low- and intermediate-mass stars to experience a CE phase, let alone survive one without merging. The implication being that, if binaries appear over-abundant, then some single stars previously believed to be PN progenitors must not lead to observable PNe. Clearly, with such a large uncertainty on the true post-CE binary fraction in PNe (20–80%), it is similarly uncertain just what fraction of these single-star PN progenitors will not lead to PNe. However, there are indications that it may indeed be significant. Population synthesis studies have found that perhaps around one fifth of expected PN progenitors due not lead to observable PNe (potentially consistent with only binaries leading to PNe; Moe & De Marco, 2006), while as many as 50% of central stars exhibit properties that are inconsistent with single-star evolutionary tracks (Weidmann et al., 2020).

As a result of conservation of angular momentum during the ejection, the CE is always expected to be preferentially deposited in the orbital plane of the binary thus leading to nebular symmetry axes which lay perpendicular to this plane. While only nine PNe have been the subject of sufficiently detailed study to constrain both their nebular inclinations and central binary orbital inclinations, the correlation is striking and entirely consistent with the CE shaping each and every one (Hillwig et al., 2016). Indeed, the probability of finding such an alignment in these PNe by chance has been shown to be less than one in a million (Munday et al., 2020). Nonetheless, there is significant morphological diversity, even among this sample, meaning that, while the CE has clearly played a role in their shaping, the exact processes at work may vary appreciably (Hillwig et al., 2016).

Thus, it now seems beyond doubt that CE evolution is a critical aspect of PN formation and evolution, even though the precise details of this are still the

[1] A regularly updated list is maintained by the author at http://drdjones.net/bCSPN.

subject of active research (Jones & Boffin, 2017; Boffin & Jones, 2019). But, perhaps of greater interest for the wider astronomical community, we are now in a position to use post-CE PNe to try and understand the CE phase itself. The nebular material in these PNe is thought to comprise the ejected CE, offering a unique opportunity to study the ejecta directly (CE ejecta can also be observed in luminous red novae, but these represent "failed" CE events, where the stars merged before fully ejecting the donor's envelope). Furthermore, the short-lived nature of PNe (τ ~30 kyr) means that post-CE central stars of PNe have not yet had time to adjust their chemical and physical properties following the CE ejection. As such, post-CE PNe are an invaluable tool with which to study the CE phase leading to potentially interesting conclusions for a wide-range of other post-CE phenomena.

2. Pre-CE mass transfer

The first step towards using the population of post-CE central stars of PNe to try and understand the CE phase is to constrain the properties of individual post-CE central stars. Most have been discovered through their photometric variability meaning that only their orbital periods are known. In order to determine the properties of the stars themselves (masses, temperature, radii), one must obtain follow-up observations that allow for simultaneous modelling of light and radial velocity curves (e.g., Jones et al., 2022), and/or spectral analysis using model atmospheres (Hillwig et al., 2017).

While the number of central stars with well-constrained properties remains relatively small, principally due to the painstaking nature of the required follow-up observations and the complications of the modelling, one can already draw remarkable conclusions. Where the companion to the nebula progenitor is a main-sequence (MS) star, they are always[2] found to be inflated (often by a factor of $\times$2–3) with respect to isolated MS stars of the same mass (Jones et al., 2015). This inflation is almost certainly due to accretion, with further signposts of this accretion coming from the chemical contamination observed in the companion of the central star of The Necklace nebula (Miszalski et al., 2013).

Accretion during the CE phase is expected to be minimal (Sandquist et al., 1998), so it is probable that the accretion onto the companion happens before CE. Further evidence for accretion prior to the CE comes from the kinematical ages of the polar outflows observed in some post-CE PNe. These polar outflows, thought to be tracers of the mass transfer/accretion, are generally found to predate the ejection of the central nebula (and thus the ejection of the CE) by a few hundred to a few thousand years (Corradi et al., 2011; Miszalski et al.,

[2]Except the companion to the central star of PN M 3-1, which was found by Jones et al. (2019) to be of a normal size but extremely close to filling its Roche lobe (this system will be discussed more in section 5).

2011). It seems likely that this pre-CE mass transfer might be associated with a period of wind Roche-lobe overflow which could last for several thousands of years as indicated by the jets observed in Fleming 1 (Boffin et al., 2012).

It is important to note that there is little to no inflation observed in the MS companions of more evolved post-CE binaries (indeed these systems are excellent probes of the mass-radius relationship of late-type MS stars; Parsons et al., 2018). This might, at first, appear puzzling when one takes into account that the thermal timescales for these stars are too long for them to have relaxed back to a normal state. However, models predict that for intermediate values of accretion efficiency and rate, the response of fully convective stars is to become partially convective (Prialnik & Livio, 1985), and it is thus the convective layer formed in the outer envelope which expands rather than the star as a whole. The relaxation of this convective layer can then occur on a much shorter timescale (Jones et al., 2022).

3. Conditions to experience (and survive) a CE

The characterization of post-CE central stars has revealed a dearth of early type-companions (Brown et al., 2019). This is consistent with the idea that large mass ratios are required to initiate unstable Roche lobe overflow and thus a CE event (Pavlovskii & Ivanova, 2015). The same characterization efforts have also revealed a number of candidates to have experienced the CE while on the red giant branch (RGB). These stars are analogous to subdwarf B binaries (e.g., Schaffenroth et al., 2015) and serve as a clear demonstration that RGB CE events can both be survived (without merging) and produce an observable PN (Jones et al., 2022).

A handful of central stars have been shown to have white dwarf companions, being detected either by radial velocity variability (Boffin et al., 2012) or photometric variability due to tidal deformations (Santander-García et al., 2015) – as opposed to the sinusoidal photometric variability due to irradiation which is typical for MS companions. If one extrapolates from this to assume that all central stars showing photometric variability due to tidal deformations are double degenerates (DD; Hillwig et al., 2010), then a very significant fraction of all post-CE central stars are DD (particularly when one takes into account that these systems should be harder to detect due to the low amplitudes of variability for most configurations). These DD post-CE central stars may have formed through two consecutive CE phases (Nelemans & Tout, 2005), but their properties are more consistent with having avoided a CE when the first component evolved off the asymptotic giant branch (AGB), with the mass transfer at this stage being stable due to the initial mass ratio being close to unity (Woods et al., 2012). Understanding the frequency and properties (namely masses and orbital periods) of DD central stars of PNe will likely have important implications for

the constraining the pathways towards type Ia supernovae (Santander-García et al., 2015).

4. The missing mass problem

In the single-star scenario, the bright central shells of PNe contain only a small fraction of the mass that originally comprised the progenitor's envelope, with the vast majority residing in a very low surface brightness halo (Villaver et al., 2002). In the case of a CE event, the entirety of the donor's envelope is expected to be ejected on a very short timescale, subsequently forming the PN. Thus one would expect post-CE PNe to be significantly more massive than their single star counterparts, however Santander-García et al. (2022) showed that, in fact, there is very little difference between the masses of the two populations. Furthermore, studying the observed masses of four PNe for which data of the central stars permits the reconstruction of the CE phase and an estimation of the envelope mass, they found that the masses of the PNe represent only a fraction of the envelope masses of the donors (roughly 60% for the two DD systems analysed, but as low as 1% for Abell 63 which has a MS companion). This brings into question whether the nebulae surrounding post-CE central stars are indeed the ejected CE or rather the product of some much later phase of mass-loss when the CE has already dissipated (Corradi et al., 2015).

5. Nebular abundances and the link to novae

There are obvious links between post-CE PNe and novae, in particular the discovery of an ancient PN surrounding nova V458 Vul (Wesson et al., 2008a). However, there are also other less obvious connections. The central star of PN M 3-1 was found by Jones et al. (2019) to have a MS companion which is very close to Roche-lobe filling. This means that as the system evolves there is potential for mass transfer from the companion onto the central star in the relatively near future, possibly leading to a nova eruption inside the expanding PN similar to that of Nova V458 Vul.

Further connections between post-CE PNe and novae are found in their abundance patterns, with some of the shortest period central stars being associated with extreme abundance discrepancy PNe (Wesson et al., 2018). The abundances in these PNe are discrepant by a factor of five or more depending on whether they are derived using recombination lines or collisionally-excited emission lines. These discrepancies indicate the presence of a second (often centrally-concentrated) high-metallicty gas phase in these PNe (García-Rojas et al., 2016), where the abundances of this second gas phase are similar to those observed in neon novae (Wesson et al., 2008b).

6. Pre-PNe and the link to luminous red novae

Pre-PNe are thought to represent the intermediate phase between the central star having left the AGB but not yet being hot enough to fully ionise the surrounding nebula. As such, one might expect to find a similar post-CE fraction inside pre-PNe to that found in PNe. However, despite years of dedicated study, no post-CE central star has been found inside a pre-PN (see Hrivnak et al., 2011, 2017, 2022, 2024, and many, many more). This is perhaps indicative that the CE leads to a shortened pre-PN phase (reducing the likelihood of discovery) or even that pre-PNe and post-CE PNe represent distinct evolutionary pathways.

Intriguingly, the ejecta properties of luminous red novae – a class of transients associated with CE mergers – are strikingly similar to those of pre-PNe (Kamiński et al., 2018), offering a potential explanation for the dearth of surviving post-CE binaries in pre-PNe. However, it must be highlighted that much progress has been made linking the morphologies of pre-PNe with wide stellar companions (Decin et al., 2020), several of which are known in both pre-PNe (e.g., Sánchez Contreras et al., 2004) and PNe (e.g., Jones et al., 2017).

7. Conclusions

Binary evolution (both CE and wider) plays a key role in the formation of a significant fraction, perhaps the majority, of PNe (some might even argue all!). This makes PNe an important test bed with which to study binary stellar evolution – in particular the poorly understood CE phase, which has been demonstrated to be responsible for at least one fifth of all PNe. The fact that post-CE PNe should be among the youngest observable post-CE systems, potentially allowing for direct observations of both the ejected envelope and the surviving post-CE binary, furthermore makes them a unique probe of the CE.

The observed population of post-CE PNe confirms the theoretical expectations that the CE is preferentially ejected in the orbital plane of the binary and that a relatively large initial mass ratio is required in order for unstable mass transfer to occurr. There are also strong indications of pre-CE mass transfer which can chemically contaminate the companion (now the favoured hypothesis for the formation of carbon dwarfs; Whitehouse et al., 2021) as well as (temporarily) causing their radii to grow. However, not all properties of post-CE PNe are so easily understood – the so-called missing mass problem, and the origins of a second chemically-enriched gas phase in high abundance discrepancy nebulae are particularly puzzling. The resolution of these puzzles will undoubtedly further our understanding of the CE phase as well as of other CE progeny.

Acknowledgements. DJ would like to thank the organisers of Kopal 2024 for their kind invitation, which was particularly meaningful given that Zdeněk Kopal is his *academic* great-great grandfather (i.e. the PhD supervisor of his PhD supervisor's PhD supervisor's PhD supervisor).

DJ acknowledges support from the Agencia Estatal de Investigación del Ministerio de Ciencia, Innovación y Universidades (MCIU/AEI) and the European Regional Development Fund (ERDF) with reference PID-2022-136653NA-I00 (DOI: 10.13039/501100011033). DJ also acknowledges support from the Agencia Estatal de Investigación del Ministerio de Ciencia, Innovación y Universidades (MCIU/AEI) and the the European Union NextGenerationEU/PRTR with reference CNS2023-143910 (DOI: 10.13039/501100011033).

References

Aller, A., Lillo-Box, J., & Jones, D., Planetary nebulae seen with TESS: New and revisited short-period binary central star candidates from Cycles 1 to 4. 2024, *Astronomy and Astrophysics*, **690**, A190, DOI:10.1051/0004-6361/202450942

Balick, B. & Frank, A., Shapes and Shaping of Planetary Nebulae. 2002, *Annual Review of Astron and Astrophys*, **40**, 439, DOI:10.1146/annurev.astro.40.060401.093849

Boffin, H. M. J. & Jones, D. 2019, *The Importance of Binaries in the Formation and Evolution of Planetary Nebulae* (Springer Cham), DOI:10.1007/978-3-030-25059-1

Boffin, H. M. J., Miszalski, B., Rauch, T., et al., An Interacting Binary System Powers Precessing Outflows of an Evolved Star. 2012, *Science*, **338**, 773, DOI:10.1126/science.1225386

Bond, H. E., Objects common to the Catalogue of Galactic Planetary Nebulae and the General Catalogue of Variable Stars. 1976, *Publications of the ASP*, **88**, 192, DOI:10.1086/129923

Bond, H. E., Binarity of Central Stars of Planetary Nebulae. 2000, in Astronomical Society of the Pacific Conference Series, Vol. **199**, *Asymmetrical Planetary Nebulae II: From Origins to Microstructures*, ed. J. H. Kastner, N. Soker, & S. Rappaport, 115

Brown, A. J., Jones, D., Boffin, H. M. J., & Van Winckel, H., On the post-common-envelope central star of the planetary nebula NGC 2346. 2019, *Monthly Notices of the RAS*, **482**, 4951, DOI:10.1093/mnras/sty2986

Corradi, R. L. M., García-Rojas, J., Jones, D., & Rodríguez-Gil, P., Binarity and the Abundance Discrepancy Problem in Planetary Nebulae. 2015, *Astrophysical Journal*, **803**, 99, DOI:10.1088/0004-637X/803/2/99

Corradi, R. L. M., Sabin, L., Miszalski, B., et al., The Necklace: equatorial and polar outflows from the binary central star of the new planetary nebula IPHASX J194359.5+170901. 2011, *Monthly Notices of the RAS*, **410**, 1349, DOI:10.1111/j.1365-2966.2010.17523.x

De Marco, O., Akashi, M., Akras, S., et al., The messy death of a multiple star system and the resulting planetary nebula as observed by JWST. 2022, *Nature Astronomy*, **6**, 1421, DOI:10.1038/s41550-022-01845-2

De Marco, O., Bond, H. E., Harmer, D., & Fleming, A. J., Indications of a Large Fraction of Spectroscopic Binaries among Nuclei of Planetary Nebulae. 2004, *Astrophysical Journal, Letters*, **602**, L93, DOI:10.1086/382156

Decin, L., Montargès, M., Richards, A. M. S., et al., (Sub)stellar companions shape the winds of evolved stars. 2020, *Science*, **369**, 1497, DOI:10.1126/science.abb1229

Douchin, D., De Marco, O., Frew, D. J., et al., The binary fraction of planetary nebula central stars - II. A larger sample and improved technique for the infrared excess search. 2015, *Monthly Notices of the RAS*, **448**, 3132, DOI:10.1093/mnras/stu2700

García-Rojas, J., Corradi, R. L. M., Monteiro, H., et al., Imaging the Elusive H-poor Gas in the High adf Planetary Nebula NGC 6778. 2016, *Astrophysical Journal, Letters*, **824**, L27, DOI:10.3847/2041-8205/824/2/L27

García-Segura, G., Ricker, P. M., & Taam, R. E., Common Envelope Shaping of Planetary Nebulae. 2018, *Astrophysical Journal*, **860**, 19, DOI:10.3847/1538-4357/aac08c

Hillwig, T. C., Bond, H. E., Afşar, M., & De Marco, O., Binary Central Stars of Planetary Nebulae Discovered Through Photometric Variability. II. Modeling the Central Stars of NGC 6026 and NGC 6337. 2010, *Astronomical Journal*, **140**, 319, DOI:10.1088/0004-6256/140/2/319

Hillwig, T. C., Frew, D. J., Reindl, N., et al., Binary Central Stars of Planetary Nebulae Discovered Through Photometric Variability. V. The Central Stars of HaTr 7 and ESO 330-9. 2017, *Astronomical Journal*, **153**, 24, DOI:10.3847/1538-3881/153/1/24

Hillwig, T. C., Jones, D., De Marco, O., et al., Observational Confirmation of a Link Between Common Envelope Binary Interaction and Planetary Nebula Shaping. 2016, *Astrophysical Journal*, **832**, 125, DOI:10.3847/0004-637X/832/2/125

Hrivnak, B. J., Lu, W., Bakke, W. C., & Grimm, P. J., Variability in Protoplanetary Nebulae. IX. Evidence for Evolution in a Decade. 2022, *Astrophysical Journal*, **939**, 32, DOI:10.3847/1538-4357/ac938a

Hrivnak, B. J., Lu, W., Bohlender, D., et al., Are Proto-planetary Nebulae Shaped by a Binary? Results of a Long-term Radial Velocity Study. 2011, *Astrophysical Journal*, **734**, 25, DOI:10.1088/0004-637X/734/1/25

Hrivnak, B. J., Lu, W., Henson, G., & Hillwig, T. C., Variability in Protoplanetary Nebulae. X. Multiyear Periods as an Indicator of Potential Binaries. 2024, *Astronomical Journal*, **167**, 30, DOI:10.3847/1538-3881/ad0cc4

Hrivnak, B. J., Van de Steene, G., Van Winckel, H., et al., Where are the Binaries? Results of a Long-term Search for Radial Velocity Binaries in Proto-planetary Nebulae. 2017, *Astrophysical Journal*, **846**, 96, DOI:10.3847/1538-4357/aa84ae

Ivanova, N., Justham, S., Chen, X., et al., Common envelope evolution: where we stand and how we can move forward. 2013, *Astronomy and Astrophysics Reviews*, **21**, 59, DOI:10.1007/s00159-013-0059-2

Jacoby, G. H., Hillwig, T. C., Jones, D., et al., Binary central stars of planetary nebulae identified with Kepler/K2. 2021, *Monthly Notices of the RAS*, **506**, 5223, DOI:10.1093/mnras/stab2045

Jones, D., Observational Constraints on the Common Envelope Phase. 2020, in *Reviews in Frontiers of Modern Astrophysics; From Space Debris to Cosmology*, ed. P. Kabáth, D. Jones, & M. Skarka (Springer), 123–153

Jones, D. & Boffin, H. M. J., Binary stars as the key to understanding planetary nebulae. 2017, *Nature Astronomy*, **1**, 0117, DOI:10.1038/s41550-017-0117

Jones, D., Boffin, H. M. J., Rodríguez-Gil, P., et al., The post-common envelope central stars of the planetary nebulae Henize 2-155 and Henize 2-161. 2015, *Astronomy and Astrophysics*, **580**, A19, DOI:10.1051/0004-6361/201425454

Jones, D., Boffin, H. M. J., Sowicka, P., et al., The short orbital period binary star at the heart of the planetary nebula M 3-1. 2019, *Monthly Notices of the RAS*, **482**, L75, DOI:10.1093/mnrasl/sly142

Jones, D., Munday, J., Corradi, R. L. M., et al., The post-common-envelope binary central star of the planetary nebula Ou 5: a doubly eclipsing post-red-giant-branch system. 2022, *Monthly Notices of the RAS*, **510**, 3102, DOI:10.1093/mnras/stab3736

Jones, D., Van Winckel, H., Aller, A., Exter, K., & De Marco, O., The long-period binary central stars of the planetary nebulae NGC 1514 and LoTr 5. 2017, *Astronomy and Astrophysics*, **600**, L9, DOI:10.1051/0004-6361/201730700

Kamiński, T., Steffen, W., Tylenda, R., et al., Submillimeter-wave emission of three Galactic red novae: cool molecular outflows produced by stellar mergers. 2018, *Astronomy and Astrophysics*, **617**, A129, DOI:10.1051/0004-6361/201833165

Miszalski, B., Acker, A., Moffat, A. F. J., Parker, Q. A., & Udalski, A., Binary planetary nebulae nuclei towards the Galactic bulge. I. Sample discovery, period distribution, and binary fraction. 2009, *Astronomy and Astrophysics*, **496**, 813, DOI:10.1051/0004-6361/200811380

Miszalski, B., Boffin, H. M. J., & Corradi, R. L. M., A carbon dwarf wearing a Necklace: first proof of accretion in a post-common-envelope binary central star of a planetary nebula with jets. 2013, *Monthly Notices of the RAS*, **428**, L39, DOI:10.1093/mnrasl/sls011

Miszalski, B., Corradi, R. L. M., Boffin, H. M. J., et al., ETHOS 1: a high-latitude planetary nebula with jets forged by a post-common-envelope binary central star. 2011, *Monthly Notices of the RAS*, **413**, 1264, DOI:10.1111/j.1365-2966.2011.18212.x

Moe, M. & De Marco, O., Do Most Planetary Nebulae Derive from Binaries? I. Population Synthesis Model of the Galactic Planetary Nebula Population Produced by Single Stars and Binaries. 2006, *Astrophysical Journal*, **650**, 916, DOI:10.1086/506900

Munday, J., Jones, D., García-Rojas, J., et al., The post-common-envelope binary central star of the planetary nebula ETHOS 1. 2020, *Monthly Notices of the RAS*, **498**, 6005, DOI:10.1093/mnras/staa2753

Nelemans, G. & Tout, C. A., Reconstructing the evolution of white dwarf binaries: further evidence for an alternative algorithm for the outcome of the common-envelope phase in close binaries. 2005, *Monthly Notices of the RAS*, **356**, 753, DOI:10.1111/j.1365-2966.2004.08496.x

Paczynski, B., Common Envelope Binaries. 1976, in IAU Symposium, Vol. **73**, *Structure and Evolution of Close Binary Systems*, ed. P. Eggleton, S. Mitton, & J. Whelan, 75

Parsons, S. G., Gänsicke, B. T., Marsh, T. R., et al., The scatter of the M dwarf mass-radius relationship. 2018, *Monthly Notices of the RAS*, **481**, 1083, DOI:10.1093/mnras/sty2345

Pavlovskii, K. & Ivanova, N., Mass transfer from giant donors. 2015, *Monthly Notices of the RAS*, **449**, 4415, DOI:10.1093/mnras/stv619

Prialnik, D. & Livio, M., The outcome of accretion on to a fully convective star Expansion or contraction? 1985, *Monthly Notices of the RAS*, **216**, 37, DOI:10.1093/mnras/216.1.37

Sánchez Contreras, C., Gil de Paz, A., & Sahai, R., The Companion to the Central Mira Star of the Protoplanetary Nebula OH 231.8+4.2. 2004, *Astrophysical Journal*, **616**, 519, DOI:10.1086/424827

Sandquist, E. L., Taam, R. E., Chen, X., Bodenheimer, P., & Burkert, A., Double Core Evolution. X. Through the Envelope Ejection Phase. 1998, *Astrophysical Journal*, **500**, 909, DOI:10.1086/305778

Santander-García, M., Jones, D., Alcolea, J., Bujarrabal, V., & Wesson, R., The ionised and molecular mass of post-common-envelope planetary nebulae. The missing mass problem. 2022, *Astronomy and Astrophysics*, **658**, A17, DOI:10.1051/0004-6361/202142233

Santander-García, M., Rodríguez-Gil, P., Corradi, R. L. M., et al., The double-degenerate, super-Chandrasekhar nucleus of the planetary nebula Henize 2-428. 2015, *Nature*, **519**, 63, DOI:10.1038/nature14124

Schaffenroth, V., Barlow, B. N., Drechsel, H., & Dunlap, B. H., An eclipsing post common-envelope system consisting of a pulsating hot subdwarf B star and a brown dwarf companion. 2015, *Astronomy and Astrophysics*, **576**, A123, DOI:10.1051/0004-6361/201525701

Villaver, E., Manchado, A., & García-Segura, G., The Dynamical Evolution of the Circumstellar Gas around Low- and Intermediate-Mass Stars. II. The Planetary Nebula Formation. 2002, *Astrophysical Journal*, **581**, 1204, DOI:10.1086/344250

Weidmann, W. A., Mari, M. B., Schmidt, E. O., et al., Catalogue of the central stars of planetary nebulae. Expanded edition. 2020, *Astronomy and Astrophysics*, **640**, A10, DOI:10.1051/0004-6361/202037998

Wesson, R., Barlow, M. J., Corradi, R. L. M., et al., A Planetary Nebula around Nova V458 Vulpeculae Undergoing Flash Ionization. 2008a, *Astrophysical Journal, Letters*, **688**, L21, DOI:10.1086/594366

Wesson, R., Barlow, M. J., Liu, X. W., et al., The hydrogen-deficient knot of the 'born-again' planetary nebula Abell 58 (V605 Aql). 2008b, *Monthly Notices of the RAS*, **383**, 1639, DOI:10.1111/j.1365-2966.2007.12683.x

Wesson, R., Jones, D., García-Rojas, J., Boffin, H. M. J., & Corradi, R. L. M., Confirmation of the link between central star binarity and extreme abundance discrepancy factors in planetary nebulae. 2018, *Monthly Notices of the RAS*, **480**, 4589, DOI:10.1093/mnras/sty1871

Whitehouse, L. J., Farihi, J., Howarth, I. D., et al., Carbon-enhanced stars with short orbital and spin periods. 2021, *Monthly Notices of the RAS*, **506**, 4877, DOI:10.1093/mnras/stab1913

Woods, T. E., Ivanova, N., van der Sluys, M. V., & Chaichenets, S., On the Formation of Double White Dwarfs through Stable Mass Transfer and a Common Envelope. 2012, *Astrophysical Journal*, **744**, 12, DOI:10.1088/0004-637X/744/1/12

Contrib. Astron. Obs. Skalnaté Pleso **55/3**, 211 – 216, (2025)
https://doi.org/10.31577/caosp.2025.55.3.211

A new route to massive helium-rich hot subdwarfs

Z. Li[1,2,3], **Y. Zhang**[4], **H. Chen**[1,2,3], **H. Ge**[1,2,3], **D. Jiang**[1,2,3], **J. Li**[1,2,3], **X. Chen**[1,2,3] **and Z. Han**[1,2,3]

[1] *Yunnan Observatories, Chinese Academy of Sciences, Kunming, 650216, People's Republic of China (E-mail: lizw@ynao.ac.cn, cxf@ynao.ac.cn)*

[2] *Key Laboratory for the Structure and Evolution of Celestial Objects, Chinese Academy of Science, People's Republic of China*

[3] *International Centre of Supernovae, Yunnan Key Laboratory, Kunming, 650216, People's Republic of China*

[4] *Zhoukou Normal University, East Wenchang Street, Chuanhui District, Zhoukou, 466001, People's Republic of China*

Received: December 5, 2024; Accepted: February 12, 2025

Abstract. Hot subdwarf (SD) stars provide a valuable opportunity to study stellar evolution, binary evolution, and element diffusion. In the conventional binary evolution scenario, SDs are believed to be the stripped cores of red giants. Here, we propose a new formation process for massive hot subdwarfs called the asymptotic giant branch (AGB) common envelope (CE) channel, which involves a CE ejection with an AGB star. This alternative pathway can explain helium-rich SDs with $\log(n_{\rm He}/n_{\rm H}) > -1$ due to the partial hydrogen burning in the envelope.

Key words: hot subdwarfs – asymptotic giant branch

1. Introduction

Hot subdwarfs (SDs), located in the region of extremely horizontal branch on the HR diagram, represent an intermediate phase between the red giant branch (RGB) and white dwarf (WD) cooling sequence (Heber, 2016). The structure of SDs is relatively simple, consisting of a helium (He)-burning core and a thin hydrogen (H)-rich envelope. To achieve this structure, it is crucial to remove the H envelope when the star ascends to the RGB. However, it is insufficient to unbind this envelope for a RGB star by the internal mechanisms only. Binary interactions have been identified as an efficient way for stripping off the H-rich envelope from SD progenitors (e.g. Han et al., 2002).

There are three main channels through which SDs can form: (1) stable Roche lobe overflow channel: As the primary star (SD progenitor) fills its Roche lobe, the envelope is stripped in a stable manner; SD binaries produced from this channel typically have orbital periods ranging from hundreds to thousands of days;

(2) common envelope (CE) ejection channel: binary would enter into CE phase when binary mass transfer proceeds in a dynamically unstable way; successful ejection results in the formation of an SD; these binaries tend to have close orbits and various types of companion stars such as planets, brown dwarfs, main sequence stars, or WDs; (3) Merger channel: SDs are formed through the merger of two He WDs. These three pathways collectively offer reasonable explanations for the general characteristics observed in most SDs. However, theoretical models encounter difficulties when it comes to explaining certain peculiar properties exhibited by some SDs, such as their surface element abundance distribution.

The chemical peculiarity found on the surface of SDs is particularly intriguing, especially with regards to He abundance. Consequently, studying the distribution of surface abundances in SDs can provide valuable insights into their formation and evolution processes. Previous researches have shown that the distribution of He abundances spans a wide range ($-4 < \log(n_{\rm He}/n_{\rm H}) < 3$). Currently, there is no single unified theory that can account for this diversity in He abundance among SDs. In other words, the diversity of He abundance may suggest different formation pathways for SDs.

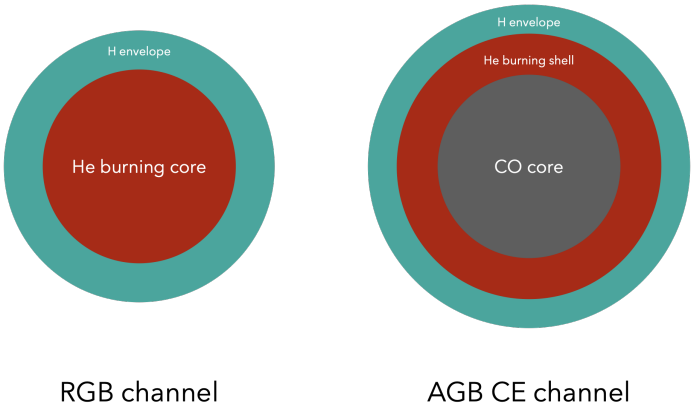


Figure 1. Initial SD structures for SDs from different channels. The cartoons are drawing not to scale.

Here we propose a novel mechanism involving an asymptotic giant branch (AGB) star undergoing CE ejection as one possible route leading to a specific type of SD. Unlike RGB stars where only H burning occurs in their cores, AGB stars have already burned their He cores into carbon-oxygen (CO) cores. As a result, an SD produced through the AGB CE channel would possess a large CO core along with surrounding H/He-burning shells and an outer H envelope, as shown in Figure 1. We found that such structure naturally explain some special SDs in the observations.

2. Methods

The simulations are conducted using the stellar evolution code Modules for Experiments in Stellar Astrophysics (MESA, version 12115; Paxton et al., 2015). We examine two scenarios of metallicity: $Z = 0.02$ and $Z = 0.001$. Additional important inputs are described by Li et al. (2024). The process of CE currently cannot be simulated by MESA. In this study, we approximate the CE process by assuming a high rate of mass loss ($> 10^{-3} M_{\odot}/\mathrm{yr}^{-1}$). Initially, we evolve a single star until it reaches the early-AGB, where the CE occurs. Then, we artificially remove the envelope with a high rate of mass loss until the H envelope mass drops below a predetermined value. We do not consider the case of stripping stars from thermal-pulse AGB because the complex physical processes of the thermal-pulse phase may lead to numerical difficulties when high mass-loss rates are assumed. In our simulations, the remaining H envelope mass is less than $0.01 M_{\odot}$, therefore, the stripping star would avoid the AGB phase since the H-envelope is too thin to ignite H shell burning.

Figure 2 shows an example illustrating how SDs can be formed through AGB CE channel. We start with an initial stellar mass of $3.0 M_{\odot}$ and metallicity $Z = 0.02$. The star evolves into early AGB phase before undergoing CE at the position indicated by the black open circle. Subsequently, we remove most of its envelope through a high mass-loss rate until only $0.01 M_{\odot}$ remains. This results in an SD with a total mass of $0.55 M_{\odot}$, initially containing a CO core of $0.33 M_{\odot}$. The thick line represents $\log L_{\mathrm{He}} > 0$, where $\log L_{\mathrm{He}}$ represents He-burning luminosity. After the end of He and H burning in the envelope, the SD ultimately transforms into a CO WD.

An interesting point is that the AGB CE scenario is quite similar to the so-called "born-again AGB stars" (Iben, 1984; Miller Bertolami, 2024). The born again scenario occurs at the late thermal pulse after the AGB stage, where most of the H envelope has already been lost through strong AGB winds. The He burning in the shell drives the thermal pulse and pushes the star back into giant branch. The biggest difference between these two models is the helium shell mass remained. In the AGB CE channel, the stripping processes occur at the early-AGB stage, resulting in SDs that still retain a significant part of He in the envelope. However, in the born again scenario, the majority of helium in the core has been fused into C/O, leaving typically less than $10^{-2} M_{\odot}$ of residual He (Miller Bertolami, 2024). Then the evolutionary timescales of the stars from AGB CE channel (from several 10^4 to several 10^6 yr) are longer than those of born again scenario ($\sim 10^4$ yr).

3. Results

We first compare our results with the observational data on $\log T_{\mathrm{eff}} - \log g$ plane. The three solid lines shown in the right panel of Figure 3 represent typical evolu-

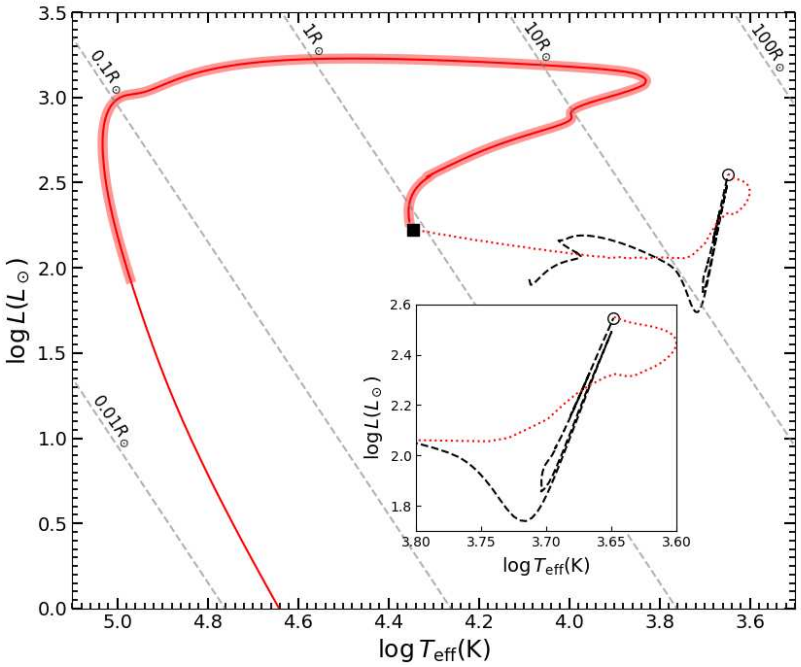


Figure 2. A typical example in constructing the SD from AGB CE channel. The black dashed line is for the evolutionary track of a $3.0M_{\odot}$ star with $Z = 0.02$ evolving from the MS to the AGB. The onset and termination of CE phase are shown in black open circle and black solid square, respectively. The produced SD mass is $0.55M_{\odot}$, and the thick red line represents the case of $\log L_{\rm He} > 0$. From Li et al. (2024).

tionary tracks for SDs with masses equal to 0.49, 0.55, and $0.68M_{\odot}$, respectively. These three tracks correspond to envelopes having identical masses ($0.01M_{\odot}$). The minimum He core mass obtained through AGB CE channel is $0.48M_{\odot}$, i.e., the track shown in the thick black line. The time intervals between adjacent asterisks are 2×10^5 years. For the three thick lines, the timescales for SDs are in the range of several million years, which is approximately 100 times shorter than that of SDs from RGB channel (typically around 100 million years for a 0.46 $M_{\odot}$ SD). This could potentially explain why there is a relatively low number of massive SDs compared to canonical SDs. The tracks for SDs from the AGB CE channel closely resemble the post-AGB evolutionary tracks. Consequently, the AGB CE channel can also explain certain peculiar objects previously classified as post-AGB stars, such as hot UV-bright stars in globular cluster and inflated hot SDs (Moehler et al., 2019; Ratzloff et al., 2020; Kumar et al., 2024).

In the right panel of Figure 3, we present the observational sample on the

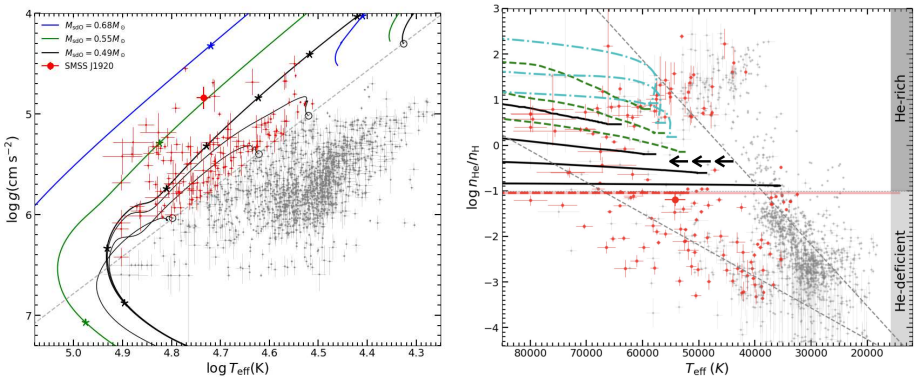


Figure 3. Right panel: The comparison between the SD evolutionary tracks and the observations in the $\log T_{\rm eff} - \log g$ plane. The observational SD samples are taken from Luo et al. (2021). Right panel: Helium abundance vs. effective temperature for the observations and SD tracks. From Li et al. (2024).

$T_{\rm eff} - \log(n_{\rm He}/n_{\rm H})$ plane. We construct various SD models with different He core masses and envelope masses, taking into account wind mass-loss from SDs as described by Krtička et al. (2016). During the AGB stage, H burning occurs in the shell and the produced SD stars generally have $\log(n_{\rm He}/n_{\rm H}) > 1$. Our models naturally reproduce the distribution of He-rich hot subdwarfs with high $\log T_{\rm eff}$. Unlike double He WD mergers and internal mixing in the hot flasher scenario, our models specifically aim to explain hot subdwarf binaries. Therefore, it would be easy to distinguish the formation channel of He-rich hot subdwarfs if there is a companion star.

4. Summary

In this study, we propose a novel pathway to SDs known as the AGB CE channel. SDs formed through this particular channel exhibit distinct structures compared to those produced by the conventional RGB channel. Consequently, there are significant variations in the physical properties of SDs between these two channels. We identify four characteristic traits of SDs originating from the AGB CE channel: high $\log T_{\rm eff}$ values, low $\log g$ values, He-rich atmospheres, and presence of companion stars. If an observational sample simultaneously exhibits all four features mentioned above, it suggests that the SD may be born via the AGB CE channel.

Acknowledgements. This work is supported by the Natural Science Foundation of China (grant Nos. 12125303, 12288102, 12090040/3, 11733008, 12473034, 11703081, 11422324, 12073070), the National Key R&D Program of China (grant Nos. 2021

YFA1600403, 2021 YFA1600400) and the International Centre of Supernovae, Yunnan Key Laboratory (No. 202302AN360001).

References

Han, Z., Podsiadlowski, P., Maxted, P. F. L., Marsh, T. R., & Ivanova, N., The origin of subdwarf B stars - I. The formation channels. 2002, *Monthly Notices of the RAS*, **336**, 449, DOI:10.1046/j.1365-8711.2002.05752.x

Heber, U., Hot Subluminous Stars. 2016, *Publications of the ASP*, **128**, 082001, DOI:10.1088/1538-3873/128/966/082001

Iben, Jr., I., On the frequency of planetary nebula nuclei powered by helium burningand on the frequency of white dwarfs with hydrogen-deficient atmospheres. 1984, *Astrophysical Journal*, **277**, 333, DOI:10.1086/161700

Krtička, J., Kubát, J., & Krtičková, I., Stellar wind models of subluminous hot stars. 2016, *Astronomy and Astrophysics*, **593**, A101, DOI:10.1051/0004-6361/201628433

Kumar, R., Moharana, A., Piridi, S., et al., Discovery of a hot post-AGB star in Galactic globular cluster E3. 2024, *Astronomy and Astrophysics*, **685**, L6, DOI:10.1051/0004-6361/202449777

Li, Z., Zhang, Y., Chen, H., et al., A New Route to Massive Hot Subdwarfs: Common Envelope Ejection from Asymptotic Giant Branch Stars. 2024, *Astrophysical Journal*, **964**, 22, DOI:10.3847/1538-4357/ad2206

Luo, Y., Németh, P., Wang, K., Wang, X., & Han, Z., Hot Subdwarf Atmospheric Parameters, Kinematics, and Origins Based on 1587 Hot Subdwarf Stars Observed in Gaia DR2 and LAMOST DR7. 2021, *Astrophysical Journal, Supplement*, **256**, 28, DOI:10.3847/1538-4365/ac11f6

Miller Bertolami, M. M., Primer on Formation and Evolution of Hydrogen-Deficient Central Stars of Planetary Nebulæ and Related Objects. 2024, *Galaxies*, **12**, 83, DOI:10.3390/galaxies12060083

Moehler, S., Landsman, W. B., Lanz, T., & Miller Bertolami, M. M., Hot UV-bright stars of galactic globular clusters. 2019, *Astronomy and Astrophysics*, **627**, A34, DOI:10.1051/0004-6361/201935694

Paxton, B., Marchant, P., Schwab, J., et al., Modules for Experiments in Stellar Astrophysics (MESA): Binaries, Pulsations, and Explosions. 2015, *Astrophysical Journal, Supplement*, **220**, 15, DOI:10.1088/0067-0049/220/1/15

Ratzloff, J. K., Kupfer, T., Barlow, B. N., et al., EVR-CB-004: An Inflated Hot Subdwarf O Star + Unseen WD Companion in a Compact Binary Discovered with the Evryscope. 2020, *Astrophysical Journal*, **902**, 92, DOI:10.3847/1538-4357/abb5b2

Contrib. Astron. Obs. Skalnaté Pleso **55/3**, 217 – 233, (2025)
https://doi.org/10.31577/caosp.2025.55.3.217

Are binary-star populations regionally different?

– in memory of Sverre Aarseth –

P. Kroupa[1,2]

[1] *Helmholtz-Institut fuer Strahlen und Kernphysik, University of Bonn, Nussallee 14-16, 53115 Bonn, Germany (E-mail: pkroupa@uni-bonn.de)*
[2] *Charles University in Prague, Faculty of Mathematics and Physics, Astronomical Institute, V Holešovičkách 2, CZ-18000 Praha, Czech Republic (E-mail: pavel.kroupa@mff.cuni.cz)*

Received: November 17, 2024; Accepted: January 27, 2025

Abstract. For synthesising star clusters and whole galaxies, stellar populations need to be modelled by a set of four functions that define their initial distribution of stellar masses and of the orbital properties of their binary-star populations. The initial binaries are dynamically processed in different embedded clusters explaining differences in the observed populations. The approach summarised here, for which the Aarseth Nbody codes have been instrumental, allows inference of the initial conditions of the globular cluster ω Cen and the quantification of the stellar merger rate as a function of stellar spectral type, of the role of multiples and mergers for the Cepheid population, and predictions of extragalactic observables. The observability of the four initial distribution functions and their physical and philosophical meaning are also briefly raised. Evidence for the variation of these functions on the physical conditions of star formation and future steps towards extensions to include higher-order multiple systems are touched upon.

Key words: stellar populations – initial binary star population – ω Cen – Cepheids – stellar mergers

1. Introduction

The primary distribution function defining the appearance as well as the dynamical and elemental-abundance evolution of a stellar population is the stellar initial mass function (IMF, $\xi(m)$). But what about specifying how the stars are distributed in binary or higher-order multiple systems? These provide star-relevant internal degrees of freedom that affect the stellar-dynamical and astrophysical evolution of stellar populations.

Concerning the stellar IMF, the number of stars with masses in the interval m to $m + \mathrm{d}m$ born in one embedded cluster is $\mathrm{d}N = \xi(m)\,\mathrm{d}m$. Its dependence on the metal abundance and density of the embedded cluster is reasonably well known (Kroupa *et al.*, 2024). The embedded clusters form in molecular cloud

clumps with a star-formation efficiency (SFE) near 30 per cent with half-mass radii $r_{\rm h} < 1\,{\rm pc}$ (Marks & Kroupa 2012; Zhou, Kroupa & Dib, 2024) and masses in stars, $M_{\rm ecl}$, ranging from about a dozen stars to many millions of stars, depending on the properties of the hosting molecular clouds as set by the host-galaxy's state (e.g. in self-regulated equilibrium or interacting). Observations of nearby molecular cloud clumps with ongoing star formation suggest the SFE to lie between a few and 30 per cent (e.g. Lada & Lada, 2003, fig. 25 in Megeath *et al.*, 2016, fig. 8 in Zhou, Dib & Kroupa, 2024) while Nbody calculations of the very well observed $1-2\,{\rm Myr}$ old Orion Nebula Cluster (mass $\approx 10^3\,M_\odot$), the NGC3603 very young cluster (mass $\approx 10^4\,M_\odot$), and the star-burst cluster R136 (mass $\approx 10^5\,M_\odot$) suggest SFE≈ 33 per cent in all cases (Kroupa, Aarseth & Hurley, 2001; Banerjee & Kroupa, 2018). A SFE near 33 per cent may be the characteristic effective SFE involved in an embedded cluster emerging from a molecular cloud clump. The region-wide or galaxy-wide IMF (gwIMF) follows by adding all stellar IMFs of all formed embedded clusters in the region, leading to the gwIMF evolving with the metal abundance and gas density (Jerabkova *et al.*, 2018).

Can a similar description of the binary-star properties of different stellar populations or galaxies be arrived at? A problem facing this goal is that no successful star-formation theory can be resorted to in order to perform this synthesis, since at present the simulations of star formation have neither achieved sufficient realism to match the small embedded clusters in the nearest star-forming cloud in Taurus-Auriga nor Orion Nebula type clusters (for a discussion see Kroupa *et al.* 2024).

2. Are stars born in binary or in higher-order multiple stellar systems?

Owing to the conservation of angular momentum pre-stellar molecular cloud cores within a clump form not one star but multiple stellar systems. These have stellar-dynamical decay time-scales of $10^4 - 10^5\,{\rm yr}$ leaving, within this time-scale, a population consisting of 50 or 33 per cent binaries and 50 or 66 per cent single stars if all cores were to spawn non-hierarchical triple or quadruple systems, respectively. Because $\approx 1\,{\rm Myr}$ old populations in low-density star-forming regions have a binary fraction near 1 this must imply that the vast majority of all stars form as binaries or hierarchical, dynamically stable higher-order systems (Goodwin & Kroupa, 2005). The fraction of higher-order multiple systems is sufficiently small (Goodwin *et al.*, 2007; Duchêne & Kraus, 2013; Offner *et al.*, 2023; Merle, 2024) to be neglected in deriving the relevant distribution functions. The above is true for late-type stars less massive than a few $M_\odot$ but more massive stars appear to be born with a triple and quadruple fraction near to unity (Offner *et al.*, 2023). Thus, it may be assumed to sufficient approximation

that the total fraction of multiple systems is $f_{\rm mult,birth} = 1$ at birth. Here

$$f_{\rm mult} = N_{\rm mult} / \left(N_{\rm sing} + N_{\rm mult} \right) \, , \tag{1}$$

where $N_{\rm mult}$ is the number of multiple systems and $N_{\rm sing}$ is the number of single stars in a star-count survey. For example, if we survey 100 main-sequence systems on the sky and 50 are binaries, 15 triples and 5 quadruples then $f_{\rm mult,ms} = 0.7$, while the observer misses 95 stars if none of the multiple systems are resolved. Triples and quadruples can thus be counted as binaries, setting $f_{\rm bin} \approx f_{\rm mult} = 0.7$ in this example.

3. The distribution functions

Given that late-type stars (massive stars obey different pairing rules, see e.g. Dinnbier *et al.*, 2024; the birth orbital-parameter distribution function defining massive stars still needing to be formulated) appear to form as binaries, secondarily to the stellar IMF, three additional birth distribution functions are needed to specify the dynamical internal degrees of freedom of a just born stellar population: the period distribution function, $f_{\rm P,birth}(P)$, the mass-ratio distribution function, $f_{\rm q,birth}(q)$ ($q = m_2/m_1 \leq 1$ with m_1, m_2 being the mass of the primary and secondary, respectively), and the eccentricity distribution function, $f_{\rm e,birth}(e)$. $\mathrm{d}N = f_{\rm x,birth}(x)\,\mathrm{d}x$ is the number – or fraction amongst all systems in a survey – of binary systems with orbital element x in the range x to $x + \mathrm{d}x$, with $x = P, q, e$. Note that P is customarily in days. If $a_{\rm AU}$ is the orbital semi-major axis in astronomical units then by Kepler's third law, $m_{\rm sys} = m_1 + m_2 = a^3_{\rm AU}/P^2_{\rm yr}$, where $P_{\rm yr} = 365.25\,P$ is the orbital period in years.

The following questions need to be answered: what are the mathematical forms of $f_{\rm P,birth}, f_{\rm q,birth}, f_{\rm e,birth}$, and if these exist, are these as dependent on the physical conditions of the gas clouds as is $\xi(m)$ (see "The Universality Hypothesis" in Kroupa 2011)? Answering these questions is not trivial because none of the distribution functions are observable: at any time a population of stars is surveyed, it is already at an evolved astrophysical stage (massive stars have evolved) and in an evolved stellar-dynamical state because stars begin to gravitationally interact in the dense embedded clusters as soon as they become ballistic particles. The properties of the binary population thus changes on the crossing time scale of the embedded cluster which is $\lesssim 0.3\,$Myr. The initial distribution functions thus never exist physically, but they are required for mathematically modelling stellar populations. They are "hilfskonstrukts" (Kroupa & Jerabkova, 2018).

For example consider a very low-mass embedded cluster in which a handfull of (say 4) binaries are observed to have formed within a clump with a half-mass radius $r_{\rm h} \approx 0.1\,$pc. With an average stellar mass of $0.3\,M_\odot$ and a star-formation efficiency of 1/3 the clump mass becomes $M_{\rm cl} \approx 8\,M_\odot$ such that it's crossing

time is $t_{\rm cross} = 2\,r_{\rm h}/\sigma \approx 0.33\,{\rm Myr}$, with

$$\sigma \approx (G\,M_{\rm cl}/r_{\rm h})^{1/2}\ , \tag{2}$$

being the nominal velocity dispersion and G the gravitational constant. Any wide binary that forms in such a low-density molecular cloud clump, i.e. a very low-mass embedded cluster, will thus have experienced a number of mild encounters with other binaries at an observation time of $0.5-1$Myr, with (in this case very mild) stellar-dynamical ejections likely having removed a few stars already by this time (Kroupa & Bouvier, 2003). More massive embedded clusters are more stellar-dynamically active therewith dynamically processing the initial population on a shorter time scale (Kroupa, 1995a).

Important note: In order to not affect the stellar IMF it is of paramount importance, when constructing an initial stellar population, to first create an array of stellar masses from a given $\xi(m)$ and to then pair stars chosen from this array into binaries or higher-order multiples such that some $f_{\rm q}$ is obeyed (Oh & Kroupa, 2016; Dinnbier *et al.* 2024; Dvorakova *et al.*, 2024).

Fig. 1 demonstrates the problem: About 1 Myr old populations in star-forming regions of low density have a significantly higher binary fraction than the main sequence (ms) stars in the Galactic field which have an average age of about 5 Gyr. This difference in the binary fractions, $f_{\rm bin,birth} \approx 1$ vs $f_{\rm bin,ms} \approx 0.5$, is readily explained through the disruption of binaries in the embedded clusters in which they formed through stellar-dynamical encounters.

Before describing the procedure how the birth distribution functions were arrived at a historical note is useful to appreciate the developments: By the late 1980s it was already well known that (i) binary systems form through three-body encounters in star clusters and these slow down the Nbody computations significantly, especially if multiple binary systems interact in the core of the clusters. And (ii) surveys of field stars were showing many of them to be binary systems (e.g. Abt 1983) such that some initial binary population appeared to be necessary when initialising the Nbody models. Therefore Sverre Aarseth spent much effort developing integration, transformation and regularisation methods to allow his Nbody codes to computationally handle such multiple systems while the stars evolve astrophysically. But the link between star clusters being the origin of the field population was not significantly entertained (e.g. Wielen 1971). In late-1992, a very excited Sverre Aarseth approached me at coffee time at the Institute of Astronomy in Cambridge and truly dragged me to his office to explain the newly-found implementation of chain regularisation into the Nbody code (later published in Mikkola & Aarseth, 1993). I was not able to follow the technical details of his explanations (being initially preoccupied with a cookie that had disagreeably melted into my coffee cup and with merely counting stars to obtain $\xi(m)$), but it dawned on me that this discovery improved his Nbody codes dramatically, making the Nbody integration of star clusters with a large initial binary population even more accessible (his codes were the most advanced

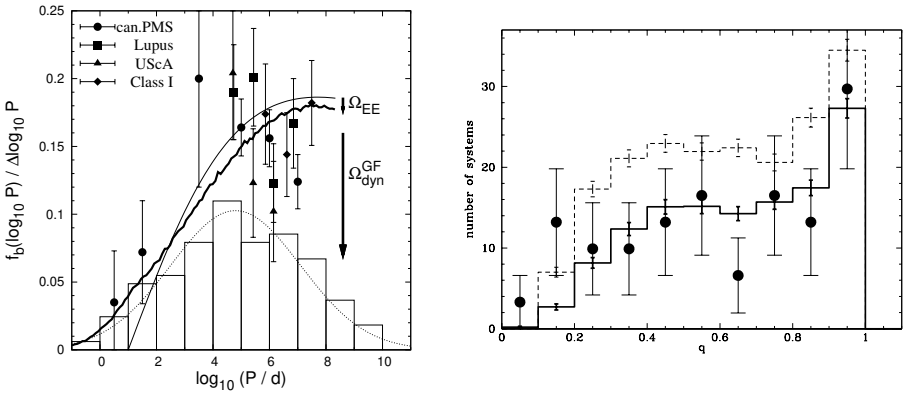


Figure 1. *Left panel*: The distribution functions of periods, $f_{\rm b} = f_{\rm bin}$, of about 1 Myr old late-type binary systems in star-forming regions as shown by solid symbols. The histogram shows the period distribution of main sequence G-dwarfs in the Galactic field (Duquennoy & Mayor 1991; Raghavan *et al.* 2010) which also matches that of K- and M-dwarfs that have a slightly lower binary fraction (see Fig. 2). For example, 8 per cent of all field-G dwarfs have a stellar companion with $10^3 < P/{\rm d} \leq 10^4$. The thin solid line is the birth distribution of periods, $f_{\rm P,birth}$ (Eq. 4). It evolves through pre-main sequence eigenevolution ($\Omega_{\rm EE}$) in about 10^5 yr per binary to the thick solid curve which is the initial period distribution function, $f_{\rm P,init}$. The stellar-dynamical encounters in the embedded clusters in which the stellar population is born in evolve (by the stellar dynamical operator, $\Omega^{\rm GF}_{\rm dyn}$) $f_{\rm P,init}$ to the observed period distribution function, $f_{\rm P,ms}$, in the Galactic field shown as the thin-dotted curve. $\Omega^{\rm GF}_{\rm dyn}$ is a function of the distribution of masses of the embedded clusters, $M_{\rm ecl}$, and their half-mass radii, $r_{\rm h}$. Adapted from fig. 1 in Marks, Kroupa & Oh (2011), for further details see there. *Right panel*: The mass-ratio distribution for primaries with masses $0.1 \leq m_1/M_\odot \leq 1.1$. The solid circles show the mass ratio distribution of the volume-limited Solar-neighbourhood sample of observed stars (Reid & Giziz, 1997). The dashed histogram is the initial ($f_{\rm q,init}$, Eq. 4) and the solid one is the model main-sequence Galactic-field population, $f_{\rm q,ms}$, computed according to Eq. 3. Note that the stellar dynamical processing in the birth embedded clusters reduces the number of binaries at all values of q and how the pre-main sequence eigenevolution leads to a near-perfect match between the observed peak and the model near $q \approx 1$ (the "pre-main sequence eigenevolution" peak in q). Adapted from fig. 17 in Kroupa (2008), for details see there.

already with fully code-integrated stellar evolution and the most advanced mathematical transformations of the equations of motions for efficient and accurate time integration). This development allowed the code to efficiently compute the dynamical interaction of compact sub-systems of evolving stars, and it just so happened to occur when the first high-resolution imaging and speckle interferometry observations of nearby star-forming regions done in the early 1990s (see

Kroupa 1995a for details) turned up the unexpected result that nearly all pre-main sequence stars there are binaries. I had witnessed these results when they were reported for the first time at a conference on binary systems in Atlanta in 1992, and it became apparent to me that the binaries probably break up in embedded clusters. But this needed to be shown with Nbody calculations. This is where the new chain regularisation came into play. The above demonstrates how different research developments can conspire to interfere constructively at just the right time to allow useful progress. The Aarseth suit of programmes (Aarseth 1999, 2003, 2008) contains a stand-alone fortran chain-regularisation code (chain.f) for integrating small-N systems, and given the importance of chain regularisation, a newer C-code, CATENA, was later developed by Jan Pflamm-Altenburg and applied to a Nbody study of the Trapezium star cluster (Pflamm-Altenburg & Kroupa 2006).

The procedure to derive the birth (and initial) distribution functions is as follows: the Galactic field population needs to be reproduced given the pre-main sequence constraints (e.g. Fig. 1). The constraint that $f_{\rm bin,birth} \approx 1$ for the pre-main sequence population stemming from the nearby (and thus common low-density) molecular cloud clumps suggests the birth period distribution function to be rising with P, since, by the Heggie-Hills law (Sec. 5) the close binaries are not significantly affected by stellar-dynamical encounters while the long-period ones are likely to be disrupted. Indeed, the data in the left panel of Fig. 1 tell us that the binary fraction for $P < 1000\,{\rm d}$ ($f_{\rm bin}(P < 10^3\,{\rm d}) \approx 13$ per cent) is similar in the pre-main sequence population as it is for the metal-rich Galactic-field population in the Solar neighbourhood. In order to arrive at a mathematical formulation of the plausible birth distribution functions, Kroupa (1995a) applied an iterative procedure. By performing Nbody simulations with an Aarseth (1999, 2003, 2008) code of star clusters until their dissolution (such that their stars become field stars) with different birth densities and starting with a first guess for $f_{\rm P,birth}$, $f_{\rm q,birth}$, $f_{\rm e,birth}$, the destruction of binary orbits through stellar-dynamical encounters was quantified. Sverre had to change the memory array structure in his Nbody software so I could do the computations of star clusters initially consisting of 100 per cent binary systems, a problem considered to be sacrilegious and heretical until then (Aarseth, 1993, private communication). For example, the seminal work on "The evolution of open clusters" by the PhD student of Sverre Aarseth, Elena Terlevich (1987), still relied on single-star simulations with an earlier Aarseth Nbody code. Returning to the present issue, a second round of simulations used improved $f_{\rm P,birth}$, $f_{\rm q,birth}$, $f_{\rm e,birth}$, with this being repeated until these distribution functions were consistent with the observational constraints evident in the left panel of Fig. 1 for the pre-main sequence stars and the field stars. "Consistent" here means according to inspection by eye. It would be wrong to attempt a formal fit, because the pre-main sequence observational data are for $\approx 1\,{\rm Myr}$ old systems that have already been dynamically processed to some degree despite stemming from low-density molecular clumps. And the Galactic field population stems from the superposition of many

dissolved embedded clusters, the distribution of which is unknown. The choice of action was therefore to seek $f_{\rm x,birth}$ such that an overall good reproduction of the $\approx 1\,$Myr and $\approx 5\,$Gyr old populations could be achieved through Nbody modelling. An important cross check was to ensure that the computed mass ratio and orbital eccentricity distributions were also, at the same time, consistent with the data available for the pre-main sequence and the field binaries. *This uniquely demonstrated that the field population can be arrived at by the stellar-dynamical processing of the birth population of binaries that is consistent with the observed binary systems in a pre-main sequence stellar population. For this to work, stars must form as binary systems in embedded clusters, implying that embedded clusters are the fundamental building blocks of galaxies (Kroupa 2005).*

The next step was to account for the observed correlations between P, q and e for systems with $P \lesssim 10^3\,$d. These correlations are obtained from the birth distributions via *pre-main sequence eigenevolution* which models the dissipative evolution of these three internal degrees of freedom during the first $\approx 10^5\,$yr of a binary's existence. To achieve a useful mathematical description of this, theoretical work on the tidal dissipation and tidal circularisation was accommodated (Kroupa, 1995b). Pre-main sequence eigenevolution leads to the shrinkage of an orbit, to its circularisation and to a change in the mass ratio, q, as the secondary component in the binary accretes gas from the accretion disk of the primary. The changes in P, q and e occur in dependence of the birth P. The formulation of pre-main sequence eigenevolution was improved slightly by Belloni *et al.* (2017) who took into account the properties of stellar populations in globular star clusters. Pre-main sequence eigenevolution thus changes the masses of some of the stars and leads to mergers such that the *initial* population (after the $\approx 10^5\,$yr evolution) has a larger mass in stars by a few percent and contains a few per cent mergers of all initial stars which are now single stars.

The so-arrived at comprehensive and computationally highly efficient approach was tested against the field population of nearby (and thus fully resolved truly single) and more distant (and thus unresolved binaries) stars in terms of star counts, i.e. their respective stellar luminosity functions, by computing star clusters until their dissolution (Kroupa 1995c). An additional test of the above birth distribution functions plus pre-main sequence eigenevolution theory was performed against the observations of the density profile, the velocity dispersion profile, the IMF and observed binary-star properties in the Orion Nebula Cluster and the Pleiades cluster (Kroupa, Aarseth & Hurley 2001). These calculations also demonstrated how an embedded cluster emerges through gas expulsion from its molecular cloud clump to become part of an OB association and a long-lived open star cluster.

In order to allow the rapid synthesis of entire stellar-field populations in galaxies assuming all stars form as binaries and in embedded clusters, the above was formalised in terms of operators that act on $f_{\rm P,birth}, f_{\rm q,birth}, f_{\rm e,birth}$ (Kroupa 2002). The mathematical formulation of the operators was achieved by Marks,

Kroupa & Oh (2011) in terms of the *pre-main sequence eigenevolution operator*, $\Omega_{\rm EE}$ and the *stellar-dynamical operator*, $\Omega_{\rm dyn}$. After applying $\Omega_{\rm EE}$ to evolve the birth to the initial distribution of binaries in one computational step, the population is stellar-dynamically processed by a second computational step by applying $\Omega_{\rm dyn} = \Omega_{\rm dyn}(M_{\rm ecl}, r_{\rm h})$ to obtain the dynamically processed initial population after a specified time. Because further dynamical processing of this remaining binary population largely halts after gas expulsion expands the cluster, freezing the stellar population and its binaries (apart from individual hardening events), the frozen population in a post-gas-expulsion young open cluster becomes its contribution to the Galactic field population.

In summary, we can write that at a given x, the operator $\Omega_{\rm dyn}$ reduces or increases $f_{\rm x}$ as a consequence of the stellar-dynamical processing in the cluster characterised by $M_{\rm ecl}, r_{\rm h}$, i.e. its density. We thus have the evolution of the birth population to the frozen main sequence (ms) one being computed via the following steps:

$$f_{\rm x,init}(x) = \Omega_{\rm EE}\, f_{\rm x,birth}(x) \implies f_{\rm x,ms}(x) = \Omega_{\rm dyn}(M_{\rm ecl}, r_{\rm h})\, f_{\rm x,init}(x)\ . \qquad (3)$$

Thereafter the same step as in the first part of Eq. 3 can be performed using the main-sequence version of $\Omega_{\rm EE}$ in order to correct the orbital elements of the short-period ms binaries for tidal circularisation (Kroupa, 1995b). The integration over (i.e. summation of) all such $\Omega_{\rm dyn}$-processed binary populations yields the field stellar population as it emanates from the population of embedded clusters that form at a given time. This is represented in Fig. 1 by $\Omega^{\rm GF}_{\rm dyn}$.

Therewith a formulation of the binary-star birth binary distribution functions that are valid for star formation in the Solar vicinity of the Galaxy is obtained,

$$\begin{aligned} \xi(m) \quad & \text{eq. } 5-8 \text{ in Kroupa } \textit{et al.}\ (2024), \\ f_{\rm P,birth}(q), f_{\rm q,birth}(P), f_{\rm e,birth}(e) \quad & \text{eq. } 3{\rm b}-8 \text{ in Kroupa (1995b),} \\ & \text{updated in Belloni } \textit{et al.}\ (2017). \end{aligned} \qquad (4)$$

4. Using the initial distribution functions

The usage of the stellar IMF, $\xi(m)$, for various problems in galactic, extragalactic and high-redshift problems is well documented (Hopkins 2018; Kroupa *et al.*, 2024).

Similarly, with the birth distribution functions, $f_{\rm P,birth}(q)$, $f_{\rm q,birth}(P)$, $f_{\rm e,birth}(e)$, in hand and assuming these to be invariant to the physical conditions, (Carney *et al.* 2005; Kroupa 2011) any population of any age can be synthesised. For example, *forbidden binaries* must exist (Kroupa, 1995b) – these are binaries that have been hardened through an encounter and appear above the eccentricity–period cutoff that arises from tidal circularisation. Such forbidden binaries circularise on the orbital time scale and allow insights into stellar interiors.

We can calculate the evolution of the birth binary population in the Orion Nebula Cluster and the Pleiades (Kroupa, Aarseth & Hurley, 2001). The initial conditions under which the globular cluster ω Cen, with its very small present-day binary fraction (Wragg *et al.*, 2024) and its associated retrograde field population (Carney *et al.*, 2005) most likely formed in can be inferred (Marks, Kroupa & Dabringhausen, 2022). This system is interesting, because Carney *et al.* (2005) note that the prograde metal-poor population of stars has an observed binary fraction that is not distinguishable from that of the metal-rich population, while the retrograde field population co-orbiting with ω Cen and of the same low metallicity has a much smaller binary fraction. These differences can be understood if the retrograde population was born in one or more dense star-burst clusters, the remnants of which today are evident as the ancient ω Cen. The implied high birth density of ω Cen of $\approx 10^8\,M_\odot/\mathrm{pc}^3$ (see fig. 10 in Marks *et al.* 2011) is of relevance also for the massive globular cluster 47 Tuc which is reported to likewise have an extremely low present-day binary fraction (Müller-Horn *et al.*, 2024).

Further, the relevance of star-cluster-induced binary-star mergers for the population of B[e] stars can be assessed: about 26–30 per cent of all O-type stars, 13-24 per cent of all B-type stars and 5-8 per cent of all A-type stars would be mergers (Dvořáková *et al.*, 2024). A substantial fraction of massive stars are thus probably mergers that were induced to happen through stellar-dynamical encounters in their young star clusters where they were born. The birth binary fraction of unity leads to profuse stellar-dynamical ejections of O and B type stars from their birth embedded clusters as shown by Nbody calculations (Oh & Kroupa, 2016) and as is now observed to be the case based on Gaia data (e.g. Stoop *et al.*, 2024; Carretero-Castrillo *et al.*, 2024).

We can also synthesise galactic field populations by adding the many contributions from all embedded clusters that have since dissolved leading to the prediction that star-forming late-type dwarf galaxies will have an overall binary fraction amongst its late-type stars of $f_{\rm bin,ms} \approx 0.8$, Milky-Way-type galaxies have $f_{\rm bin,ms} \approx 0.5$ (as is observed) and massive elliptical galaxies have $f_{\rm bin,ms} \approx 0.35$ (Marks & Kroupa, 2011). The dynamical evolution of the Cepheid population in a galaxy can be computed, giving insights, for example, into out-of-age Cepheids which are like blue stragglers and form after a binary system merges into the Cepheid instability strip (Dinnbier, Anderson & Kroupa, 2024).

Most of the above results relied heavily on the Aarseth Nbody codes to do the time-forward integrations of the equations of motions of the systems being studied. But these are CPU-time consuming and the development of the Ω-operators based on the Nbody results lead to the BIPOS1 programme. The programme BInary POpulation Synthesis 1 (BIPOS1) has been made publicly available to allow the rapid computation of dynamically processed stellar populations (Dabringhausen, Marks & Kroupa, 2022). The modelled population of galactic field stars turns out to be in excellent agreement with the observed population of M-, K- and G dwarfs (see Marks & Kroupa, 2011; Cifuentes *et*

al. 2024), accounts for the peak at $q \approx 1$ (Fig. 1) *after* the above theory was formulated, and also reproduces the correlation between the binary fraction and the mass of the primary star observed for Galactic field stars (Fig. 2).

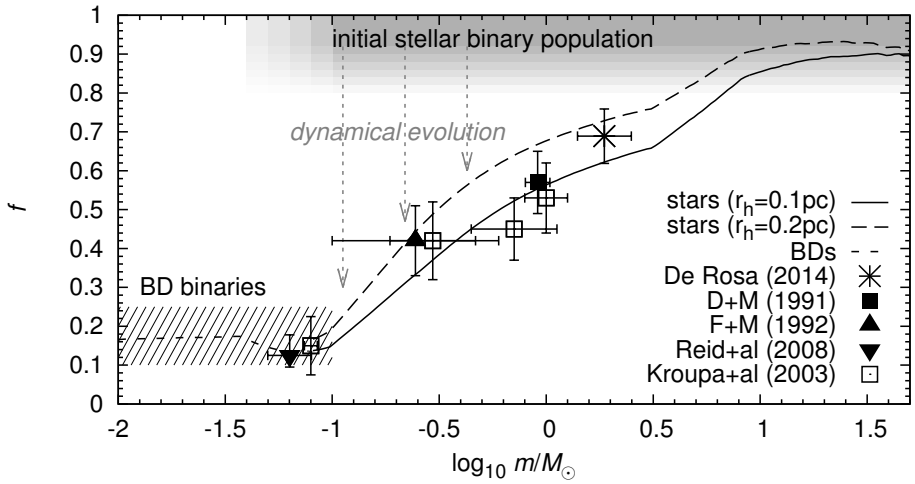


Figure 2. The binary fraction as a function of the primary mass. Stars are born in embedded clusters with half mass radii $r_{\rm h}$ as binaries. This birth stellar binary population has $f = f_{\rm bin,birth}(m_1) \approx 1$ *for all primary masses*, m_1. The stellar-dynamical encounters within the embedded clusters decrease $f_{\rm bin,birth}(m_1)$ more for smaller m_1 because less-massive binary systems are, on average, less bound. The calculations (via $\Omega_{\rm dyn}$) show the decrease to match the observed data of old Galactic field populations (depicted by the different symbols) very well. Brown dwarfs (BD) follow fundamentally different distribution functions to those of stars, and massive stars ($m_1 > 5\,M_\odot$) likewise have different pairing rules but appear to be born typically in triple and quadruple systems. This figure demonstrates that it is incorrect to take the observed decrease of the binary fraction with decreasing primary-star mass as a direct constraint on star-formation theory. Adapted from fig. 6 in Thies *et al.* (2015), for details see there.

5. The physical variation of the birth/initial distribution functions

The variation of $\xi(m)$ with metallicity, Z, and density of the embedded cluster is reasonably well understood (Kroupa *et al.*, 2024). From the empirical evidence it transpires that the gravitationally unstable gas clump which forms an embedded cluster does what theory broadly expected all along: in broad and simple terms, at high (e.g. Solar) metallicity, the collapse cannot be as deep because slightly

overdense gas cools rapidly and so fragments into typically less massive proto-stellar cores, while at low metallicity, the collapse is deeper reaching larger densities before individual proto-stars emerge thus leading to a more top-heavy stellar IMF in the embedded cluster that forms in the molecular cloud clump.

The three birth binary star distribution functions, $f_{\rm P,birth}, f_{\rm q,birth}, f_{\rm e,birth}$, most likely vary in an according and a coordinated fashion. In extracting their variation from the available data, one needs to take into account that a metal-poor gas cloud will collapse to a denser state than a metal-rich one such that the ensuing low-metallicity embedded cluster will lead to a lower overall binary fraction *if* the birth distribution functions were to be invariant, because more of the binary systems are disrupted in a denser embedded cluster. Since *hard* (i.e. close, see below) binaries have too small a cross section for significant stellar-dynamical processing, the number of these does not change significantly and this is independent of metallicity. *Soft* (i.e. wide, see below) low-Z binaries would however be depleted compared to their counterparts at $Z_\odot$. According to Eq. 1, the binary fraction for close binaries would thus be slightly smaller at low than at high metallicity but would be quite insensitive to Z, while the binary fraction of wide binaries would be smaller at low Z than at $Z_\odot$. The data by Lodieu *et al.* (2025) may be consistent with this interpretation – see below.

However, more likely $f_{\rm x,birth}(\log Z)$ will differ from $f_{\rm x,birth}(\log Z)$ by the same broad physics: the proto-stellar core collapses to a higher density before two proto-stars emerge probably leading to a higher fraction of close binaries at low metallicity, as discussed by Mazzola *et al.* (2020). Longer-period binaries may appear just as in the high-Z case through random associations in the molecular cloud filaments of protostars for late-type stars (see Kroupa *et al.* 2024 for a discussion). Since the molecular cloud core evolves to a denser state at low Z, it is probable that also the wider binaries will end up having shorter P values than their equivalent high-Z counterparts.

The hard/soft boundary is of importance here: *hard binaries* have orbital velocities that are larger than the bulk velocity dispersion in the embedded cluster in which they are born, while *soft binaries* have slower orbital velocities. *There is no universal hard/soft boundary apart from that for an embedded cluster at a given time.* The hard/soft boundary is proportional to $r_{\rm h}^{-1/2}$ (Eq. 2) such that this boundary is at a higher velocity for a low-Z embedded cluster than for a high-Z cluster of equal mass. The binary-star semimajor axes, a, are also probably systematically smaller at low-Z than at high-Z, scaling proportionally to $r_{\rm h}$. But because the orbital velocity of a binary system is proportional to $a^{-1/2}$ (eq. 142 in Kroupa 2008), the fraction of hard to soft binaries may remain the same in an embedded cluster of low metallicity compared to an equal-mass cluster at high metallicity. However, it may be, by the Heggie-Hills law ("*hard binaries harden, soft binaries soften*", Heggie, 1975; Hills, 1975), that the denser environment in the metal-poor embedded cluster hardens the tight binaries such that the fraction of *close* binaries ends up being larger in the metal-poor popu-

lation than in the metal-rich one.

The above discussion may be relevant for the discovery through large surveys by Moe, Kratter & Badenes (2019) and Mazzola *et al.* (2020) that iron-poor populations have a higher fraction of *close* binaries than metal-rich populations. These authors also find the fraction of close binaries to vary with the alpha-element abundances. The variation of the observed populations with the metal abundance thus appears to be complicated. However, what matters is that the cooling function of the gas depends primarily on the available atomic transitions such that Z is the relevant quantity. Thus, a population that is alpha-element enriched but iron poor might have the same binary star properties to a population that is iron rich and alpha-element poor. For example, according to Forbes *et al.* (2011, see also Wirth *et al.*, 2022), $[Z/H] = [Fe/H] + [\alpha/H]$. Returning to the samples by Moe *et al.* (2019, their fig. 3) and Mazzola *et al.* (2020, their fig. 5), their data appear to indicate that at near Solar metallicity ($[\mathrm{Fe/H}] \approx 0$) the fraction of close ($P < 10^4$ d) binaries in a survey amounts to about 20 per cent which is consistent with Fig. 1 (left panel). Fig. 3 in Moe *et al.* (2019) suggests that at $[\mathrm{Fe/H}] \approx -3$ this fraction increases to 60 per cent. In Fig. 6 in Mazzola *et al.* (2020) the published fraction reaches > 100 per cent at moderate low metallicity ($[\mathrm{Z/H}] \approx -0.8$), leaving no room for a contribution to the stellar population by wider binaries (with $P > 10^4$ d). In contrast to the above studies, Lodieu *et al.* (2025) find Solar-type stars at low "metallicity" ($[Fe/H] < -1.5$) to have a comparable/much smaller binary fraction to those at Solar metallicity for close binaries (< 8 AU)/wide binaries ($8 - 10^4$ AU), respectively. In view of the above results that appear to differ substantially in terms of the reported binary fraction of close binaries at low Z, it is therefore unclear how these quoted fractions are to be compared and care needs to be taken in precisely defining what is counted how.

The above information provides a suggestion how the current formulation of $f_{\mathrm{x,\,birth/init}}(Z \approx Z_\odot)$ given by Eq. 4 can be generalised to other values of Z. An iterative process of matching the observational constraints (e.g. by Carney *et al.*, 2005; Moe *et al.*, 2019; Mazzola *et al.*, 2020; Lodieu *et al.*, 2025) to Nbody-generated data, similarly to that performed by Kroupa (1995a,b), will be necessary to infer a viable model. Hereby smaller r_{h} values at low Z will need to be probed. The so-arrived at model for $f_{\mathrm{x,\,birth/init}}(Z)$ will then be of importance to test and check the theory of star formation (rather than the other way around).

In performing such tests of star-formation theory, it needs to be remembered that computer simulations of collapsing molecular cloud cores do not produce a measurable $f_{\mathrm{x,\,birth/init}}(Z)$ for the same reasons why these functions cannot be measured on the sky (the forming binaries break up due to encounters in these simulations while others are still forming). The theoretically produced $f_{\mathrm{x,\,birth/init}}(Z)$ can however be extracted by tracing the individual stellar particles back to where and in which stellar system they were born in, in order to quantify as well as is possible the values of P, q, e for this system. The theoreti-

cal $f_{\mathrm{x,\,birth/init}}(Z)$ can be constructed from the distributions of the so obtained quantities.

Metallicity and density dependent operators $\Omega_{\mathrm{EE}}(Z), \Omega_{\mathrm{dyn}}(r_{\mathrm{h}}, M_{\mathrm{ecl}} : Z)$ will then need to be quantified along the lines as performed by Marks, Kroupa & Oh (2011) to allow rapid dynamical synthesising of stellar populations being born in galaxies of different properties and at different redshifts as probed by Marks & Kroupa (2011) for the $Z \approx Z_{\odot}$ case.

6. Conclusions

The difference between the binary populations in star forming regions and the Galactic field can be understood if stars form mostly as binary systems and in embedded star clusters in molecular cloud clumps. Dynamical processing in these embedded clusters dissolves a large fraction of the soft binaries. The binary properties of Galactic field stellar populations are therewith reasonably well understood at Solar metallicity.

The Sun too may have had a binary companion orbiting it with a birth period $P \gtrsim 10^6$ d ($a \gtrsim 300$ AU) in order to be consistent with the current orbit of Neptune. Such orbits in fact dominate the birth period distribution function (Fig. 1). The existence of planetary systems around most stars is thus not in contradiction to all stars forming as binary systems. The finding that many exoplanetary systems appear to be "jumbled-up", i.e. not as regular and orderly as our Solar System (e.g. Zhu & Dong, 2021), may be due to the perturbations during the formation stage or thereafter by the not so distant companion star and stellar-dynamical encounters in their birth embedded clusters (Thies *et al.* 2011).

There is evidence that low-metallicity populations follow the trend already well documented by the variation of the stellar IMF. The sense may be that with decreasing metallicity the average stars appear to be more massive and consist of closer binaries at birth, and probably also with more similar companion masses. There is thus emerging evidence how the three birth distribution functions, $f_{\mathrm{P,birth}}(P : Z, m_1)$, $f_{\mathrm{q,birth}}(q : Z, m_1)$, $f_{\mathrm{e,birth}}(e : Z, m_1)$, differ form their metal-rich ($Z \approx Z_{\odot}$) counterparts such that, upon the dynamical processing in the low-metallicity embedded clusters, the survey results are obtained. However, as discussed above, some of the evidence appears to be contradictory.

In terms of challenges for the future to improve the mathematical description of birth distribution functions of stars: (A) the variation of these with metallicity and density of the embedded clusters in which stars are born will need to be studied. This will require Nbody simulations to quantify the stellar-dynamical processing of the distribution functions for plausible mass functions of embedded clusters that are likely to have spawned the stellar populations under study. For example, a field population might stem from one single massive star burst cluster or from a large population of less-massive embedded clusters. An example

of this is the work on ω Cen and its associated field population mentioned in the text. (B) The extension of the birth distribution functions to include triple and quadruple systems is needed. This is an interesting task to be mastered by seeking a mathematical description that preserves the above (Eq. 4) but accommodates additional companions without violating the stellar IMF.

As a final comment, the above and associated work shows that there is no single correction for unresolved binary systems for a given star-count survey because the dynamical histories of observed populations can differ such that their binary properties differ. For example, a low-mass molecular cloud in which low-mass embedded clusters emerge spawns a T Tauri association with a high binary fraction ($f_{\rm bin} \approx 0.8$). A neighbouring massive molecular cloud in which ONC- (or even NGC3603-) type star-burst embedded clusters condense spawns an OB association with an overall binary fraction $f_{\rm bin} \approx 0.4 - 0.5$. And, even if they are merely "hilfskonstrukts", the inference of the true birth/initial distribution functions are needed for efficiently modelling stellar populations. Finally, given some observational survey data, understanding the underlying stellar populations and their binary properties non-negotiably requires full understanding of their stellar-dynamical and astrophysical evolution. Without the monumentally fundamental Nbody-development work by Sverre Aarseth in Cambridge since the 1960s this would not have been possible to be achieved.

Acknowledgements. This work would have been entirely impossible without Sverre Aarseth (1934–2024), whose pioneering contributions to Nbody coding and simulations profoundly shaped the field. His mentorship and guidance were pivotal to my development as both a researcher and a person as well as for the work reported here. Sverre's legacy as a brilliant scientist and a generous mentor will continue to inspire the Nbody community. I sincerely thank Sverre Aarseth for his immensely kind reactions to my computational needs, incorporating the treatment of all stars as initial binaries, gas expulsion and the inclusion of the computation of a cluster's tidal tails. All these innovations to the codes allowed a significant amount of research I was involved with, and I will be forever indebted to Sverre for making this possible. I also acknowledge the DAAD Eastern-European Bonn-Prague exchange programme for support.

References

Aarseth, S.J.: 1999, *Publications of the ASP* **111**, 1333, DOI:10.1086/316455

Aarseth, S.J.: 2003, *Gravitational N-Body Simulations*, Cambridge University Press, Cambridge

Aarseth, S.J.: 2008, *Lecture Notes in Physics* **760**, 1, DOI:10.1007/978-1-4020-8431-7_1

Abt, H.A.: 1983, *Ann. Rev. Astron. Astrophys.* **21**, 343, DOI:10.1146/annurev.aa.21.090183.002015

Banerjee, S. and Kroupa, P.: 2018, *Astrophysics and Space Science* **424**, 143, DOI:10.1007/978-3-319-22801-3_6

Belloni, D., Askar, A., Giersz, M., Kroupa, P. and Rocha-Pinto, H.J.: 2017, *Monthly Notices of the RAS* **471**, 2812, DOI:10.1093/mnras/stx1763

Cifuentes, C., Caballero, J.A., Gonzalez-Payo, J., Amado, P.J., Bejar, V.J.S., et al.: 2024, *arXiv:2412.12264v1* ,

Carney B. W., Aguilar L. A., Latham D. W. and Laird J. B.: 2005, *Astronomical Journal* **129**, 1886, DOI:10.1086/427542

Carretero-Castrillo, M., Ribo, M., Paredes, J.M. and Benaglia, P: 2024, *Bulletin de la Société Royale des Sciences de Liège* **93**, 103, DOI:10.25518/0037-9565.12289

Dabringhausen, J., Marks, M. and Kroupa, P.: 2022, *Monthly Notices of the RAS* **510**, 413, DOI:10.1093/mnras/stab3288

Dinnbier F., Anderson R.I. and Kroupa P.: 2024, *Astronomy and Astrophysics* **690**, A385, DOI:10.1051/0004-6361/202347641

Duchêne, G. and Kraus, A.: 2013, *Ann. Rev. Astron. Astrophys.* **51**, 269, DOI:10.1146/annurev-astro-081710-102602

Duquennoy, A. and Mayor, M.: 1991, *Astronomy and Astrophysics* **248**, 485

Dvořáková N., Korčáková D., Dinnbier F. and Kroupa P.: 2024, *Astronomy and Astrophysics* **689**, A234, DOI:10.1051/0004-6361/202449586

Forbes, D., Spitler, L.R., Strader, J., Romanowsky, A.J., Brodie, J.P. and Foster, C.: 2011, *Monthly Notices of the RAS* **413**, 2943, DOI:10.1111/j.1365-2966.2011.18373.x

Goodwin, S. P. and Kroupa, P.: 2005, *Astronomy and Astrophysics* **439**, 565, DOI:10.1051/0004-6361:20052654

Goodwin, S.P., Kroupa, P., Goodman, A. and Burkert, A.: 2007, in *Protostars and Planets V*, ed.: B. Reipurth, D. Jewitt and K. Keil, University of Arizona Press, Tucson, 133

Heggie, D.C.: 1975, *Monthly Notices of the RAS* **173**, 729, DOI:10.1093/mnras/173.3.729

Hills, J.G.: 1975, *Astronomical Journal* **80**, 809, DOI:10.1086/111815

Hopkins, A.: 2018, *Publications of the Astron. Soc. of Australia* **35**, 39, DOI:10.1017/pasa.2018.29

Jerabkova, T., Hasani-Zonozi, A., Kroupa, P., Beccari, G., Yan, Z., Vazdekis, A. and Zhang, Z.-Y.: 2018, *Astronomy and Astrophysics* **620**, 39, DOI:10.1051/0004-6361/201833055

Kroupa, P.: 1995a, *Monthly Notices of the RAS* **277**, 1491, DOI:10.1093/mnras/277.4.1491

Kroupa, P.: 1995b, *Monthly Notices of the RAS* **277**, 1507, DOI:10.1093/mnras/277.4.1507

Kroupa, P.: 1995c, *Astrophysical Journal* **453**, 358, DOI:10.1086/176395

Kroupa, P.: 2002, *Binary Systems, Star Clusters and the Galactic-Field Population*, Habilitation Thesis, University of Kiel, Kiel

Kroupa, P.: 2005, *ESASP* **576**, 629, DOI:10.48550/arXiv.astro-ph/0412069

Kroupa, P.: 2008, in *The Cambridge N-Body Lectures, Lecture Notes in Physics 760*, ed.: S. Aarseth, C. Tout and R. Mardling, Springer-Verlag Berlin, Heidelberg, 181

Kroupa P.: 2011, *IAU Symp.* **270**, 141, DOI:10.1017/S1743921311000305

Kroupa, P., Aarseth, S. and Hurley, J.: 2001, *Monthly Notices of the RAS* **321**, 699, DOI:10.1046/j.1365-8711.2001.04050.x

Kroupa, P. and Bouvier, J.: 2003, *Monthly Notices of the RAS* **346**, 343, DOI:10.1046/j.1365-2966.2003.06645.x

Kroupa, P. and Jerabkova T.: 2018, in *The Impact of Binaries on Stellar Evolution*, eds.: G. Beccari and H.M.J. Boffin, Cambridge University Press, arXiv:1806.10605,

Kroupa, P., Gjergo, E., Jerabkova, T. and Yan, Z.: 2024, in *Encyclopedia of Astrophysics*, eds.: I. Mandel and F.R.N. Schneider, Elsevier Reference Module, arXiv:2410.07311,

Lada, C.J. and Lada, E.A.: 2003, *Ann. Rev. Astron. Astrophys.* **41**, 57, DOI:10.1146/annurev.astro.41.011802.094844

Lodieu, N., Pérez Garrido, A., Zhang, J.-Y., Martín, E.L., Rebolo, López, R., Pérez-Toledo, F., Clavero, R. and Nespral, D.: 2025, *Astronomy and Astrophysics, accepted* , DOI:10.48550/arXiv.2501.14462

Marks, M. and Kroupa, P.: 2011, *Monthly Notices of the RAS* **417**, 1702, DOI:10.1111/j.1365-2966.2011.19519.x

Marks, M., Kroupa, P. and Oh, S.: 2011, *Monthly Notices of the RAS* **417**, 1684, DOI:10.1111/j.1365-2966.2011.19257.x

Marks, M. and Kroupa, P.: 2012, *Astronomy and Astrophysics* **543**, A8, 10.1051/0004-6361/201118231

Marks, M., Kroupa, P. and Dabringhausen, J.: 2022, *Astronomy and Astrophysics* **659**, A96, DOI:10.1051/0004-6361/202141846

Mazzola, C.N., Badenes, C., Moe, M., Koposov, S.E., Kounkel, M., Kratter, K., etal.: 2020, *Monthly Notices of the RAS* **499**, 1607, DOI:10.1093/mnras/staa2859

Megeath, S.T., Gutermuth, R., Muzerolle, J., Kryukova, E., Hora, J. L., Allen, L.E., Flaherty, K., Hartmann, L., Myers, P.C., Pipher, J.L., Stauffer, J., Young, E.T. and Fazio, G. G.: 2016, *Astrophysical Journal* **151**, 5, DOI:10.3847/0004-6256/151/1/5

Merle T.: 2024, *Bulletin de la Société Royale des Sciences de Liège* **93**, 170, DOI: 10.25518/0037-9565.11641

Mikkola, S. and Aarseth, S.J.: 1993, *Celestial Mechanics & Dynamical Astronomy* **57**, 439, DOI:10.1007/BF00695714

Moe, M., Kratter, K.M. and Badenes, C.: 2019, *Astrophysical Journal* **875**, 61, DOI:10.3847/1538-4357/ab0d88

Müller-Horn, J., Göttgens, F., Dreizler, S., Kamann, S., Martens, S., Saracino, S. and Ye, C.S.: 2024, *arXiv:2412.13189v1* ,

Offner S. S. R., Moe M., Kratter K. M., Sadavoy S. I., Jensen E. L. N. and Tobin J. J.: 2023, in *Protostars and Planets VII*, ed.: S. Inutsuka, Y. Aikawa, T. Muto, K. Tomida and M.Tamura, Astronomical Society of the Pacific, San Francisco, 275

Oh, S. and Kroupa, P.: 2016, *Astronomy and Astrophysics* **590**, 107, DOI:10.1051/0004-6361/201628233

Pflamm-Altenburg, J. and Kroupa, P.: 2006, *Monthly Notices of the RAS* **373**, 295, DOI:10.1111/j.1365-2966.2006.11028.x

Raghavan, D., McAlister, H.A., Henry, T.J., Latham, D.W., Marcy, G.W., Mason, B.D., Gies, D.R., White, R.J. and Brummelaar, T.A.: 2010, *Astrophysical Journal, Supplement* **190**, 1, DOI:10.1088/0067-0049/190/1/1

Reid, I.N. and Gizis, J.E.: 1997, *Astronomical Journal* **113**, 2246, DOI:10.1086/118436

Stoop, M., de Koter, A., Kaper, L., Brands, S., Portegies Zwart, S., Sana, H., et al.: 2024, *Nature* **634**, 809, DOI:10.1038/s41586-024-08013-8

Terlevich, E.: 1987, *Monthly Notices of the RAS* **224**, 193, DOI:10.1093/mnras/224.1.193

Thies, I., Kroupa, P., Goodwin, S.P., Stamatellos, D. and Whitworth, A.P.: 2011, *Monthly Notices of the RAS* **417**, 1817, DOI:10.1111/j.1365-2966.2011.19390.x

Thies, I., Pflamm-Altenburg, J., Kroupa, P. and Marks, M.: 2015, *Astronomical Journal* **800**, 72, DOI:10.1088/0004-637X/800/1/72

Wielen, R.: 1971, *Astronomy and Astrophysics* **13**, 309

Wirth, H., Kroupa, P., Haas, J., Jerabkova, T., Yan, Z., Subr, L.: 2022, *Monthly Notices of the RAS* **516**, 3342, DOI:10.1093/mnras/stac2424

Wragg, F., Kamann, S., Saracino, S., Latour, M., Dreizler, S., Martens, S., Seth, A., Vaz, D. and van de Ven, G.: 2024, *Monthly Notices of the RAS* **535**, 781, DOI:10.1093/mnras/stae2333

Zhou, J.W., Kroupa, P. and Dib, S.: 2024, *Publications of the ASP* **136**, id.094301, DOI:10.1088/1538-3873/ad6f44

Zhou, J.W., Dib, S. and Kroupa, P.: 2024, *Publications of the ASP* **136**, id.094302, DOI:10.1088/1538-3873/ad77f4

Zhu, W. and Dong, S.: 2021, *Ann. Rev. Astron. Astrophys.* **59**, 291, DOI:10.1146/annurev-astro-112420-020055

Contrib. Astron. Obs. Skalnaté Pleso **55/3**, 234 – 237, (2025)
https://doi.org/10.31577/caosp.2025.55.3.234

Interrelated main-sequence MLR, MRR, MTR relations from planet hosting stars

V. Bakış[1], **Z. Eker**[1], **F. Soydugan**[2] **and S. Bilir**[3]

[1] *Akdeniz University, Faculty of Sciences, Dept. of Space Sci. and Technologies, Antalya, Türkiye (E-mail: volkanbakis@akdeniz.edu.tr)*

[2] *Çanakkale Onsekiz Mart University, Faculty of Sciences, Department of Physics, Çanakkale, Türkiye*

[3] *İstanbul University, Faculty of Sciences, Dept. of Astronomy and Space Sciences, İstanbul, Türkiye*

Received: October 27, 2024; Accepted: March 3, 2025

Abstract. In this study, we investigated the interrelated mass-luminosity, mass-radius, and mass-temperature relations of planet-hosting stars. The sample, which is chosen to be main-sequence systems, is divided into two metallicity regimes: one regime is below the average of all samples (z=0.017) and the other above it. Suitable figures represent the comparisons of each distinct metallicity regime.

Key words: stars:fundamental parameters – stars:host stars

1. Introduction

Understanding the relationships between stellar mass, luminosity, radius, and temperature is fundamental to the study of stellar astrophysics. These interrelated properties are particularly important for main-sequence stars, which constitute the majority of stars in our galaxy and are key targets in the search for exoplanets. Our previous work (Eker et al., 2018) on this topic has garnered significant attention, as evidenced by the diverse range of papers citing our research.

In this study, we focus on a carefully selected sample of main-sequence stars known to host planets. This sample provides a robust basis for examining the Mass-Luminosity, Mass-Radius, and Mass-Temperature relations for two metallicity regimes. Our dataset includes 856 host stars, whose physical parameters are obtained from the NASA Exoplanet Archive, representing a larger sample than that used in Eker et al. (2018), which was based on the components of double-lined detached eclipsing binaries.

2. MLR

We derive the MLR for planet-hosting stars with different metallicities. Using our sample, we generate mass-luminosity diagrams and fit functions for two distinct metallicity values. The results illustrate how metallicity influences the MLR, with higher metallicity stars generally showing different luminosity levels at the same mass compared to their lower metallicity counterparts. In Fig. 1, mass-luminosity data in our sample is shown with two metallicity values, which are shown in grey and black for z<0.017 and z>0.017, respectively. The metallicity value of z=0.017 is the average metallicity of the sample used in this study. The mass regimes are shown with vertical lines in the figure.

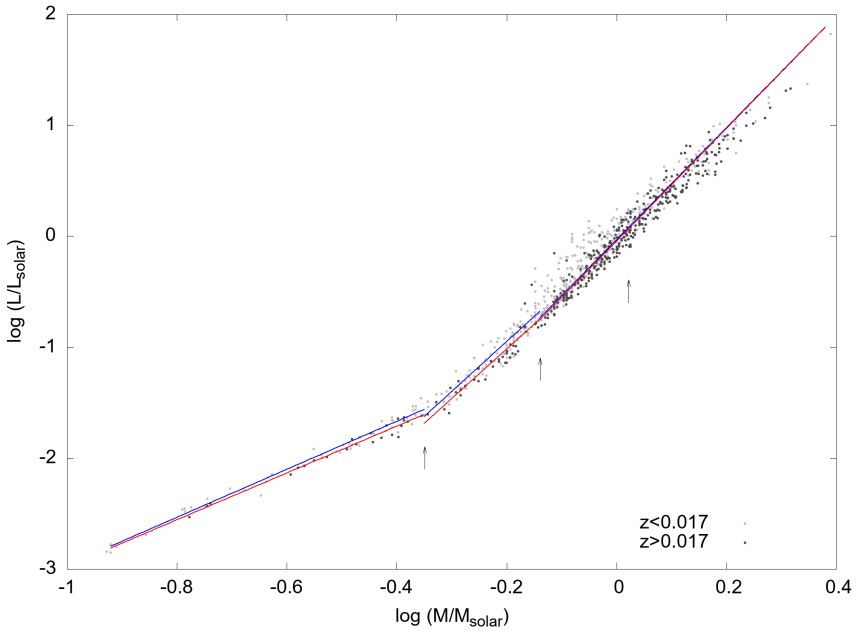
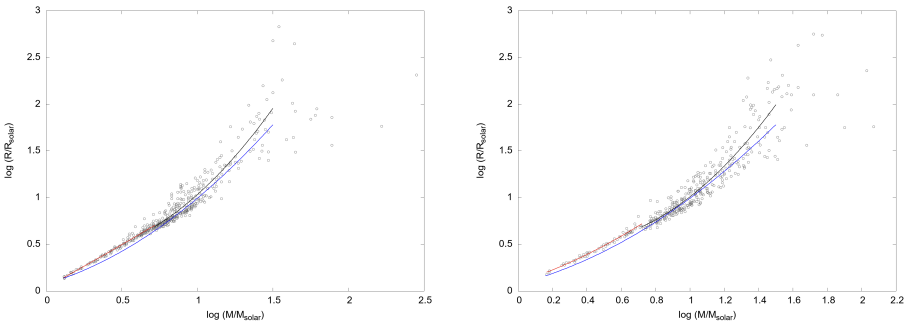


Figure 1. MLR from planet-hosting stars with different metallicities.

3. MRR

By understanding how a star's mass correlates with its radius, we can infer key properties of stars and their planetary systems. The MRR aids in determining the physical characteristics of exoplanets when the host star's parameters are known, allowing for more accurate modelling of planetary sizes and composi-



(a) Lower metallicity (z<0.017) (b) Higher metallicity (z>0.017)

Figure 2. Mass-radius relation (MRR) for planet-hosting stars with different metallicity regimes.

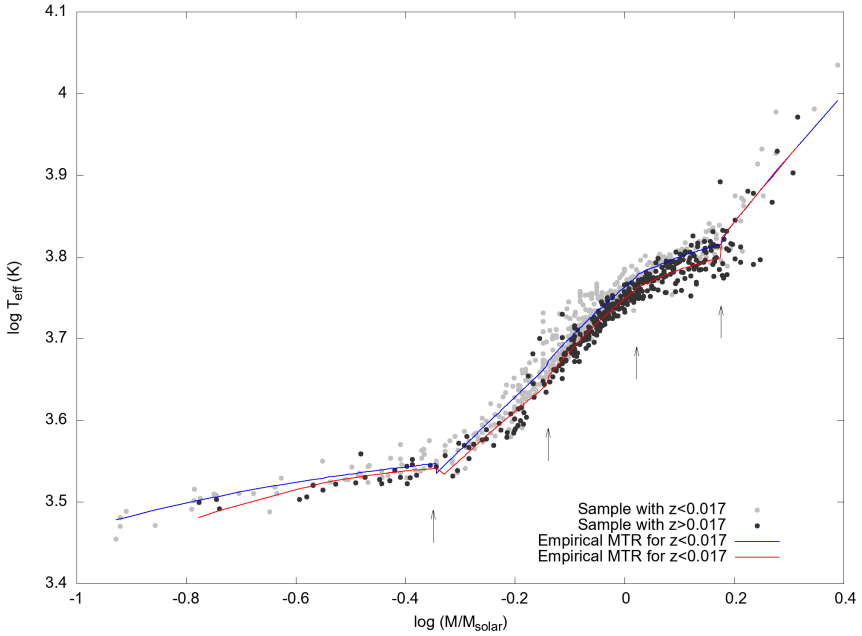


Figure 3. MTR from planet-hosting stars with lower (z<0.017) metallicity (grey data, blue model) and higher (z>0.017) metallicity (black data, red model).

tions. In our analysis, we derive the MRR for our sample of planet-hosting stars. The mass-radius diagrams presented in Fig. 2 show the fitted functions for stars with two different metallicity values. These functions illustrate how metallicity impacts the radius for a given stellar mass, providing insights into the structural differences and evolution of stars with varying compositions. The detailed mass-radius diagrams emphasize the need to account for metallicity when applying the MRR in exoplanet research and cluster studies.

4. MTR

By examining how stellar mass correlates with effective temperature, we can infer key characteristics of stars and their potential to host planets. In this study, we derive the MTR for our sample of planet-hosting stars. The mass-temperature diagrams presented in Fig. 3 illustrate the relationships between stellar mass and effective temperature, with fitted functions accounting for two distinct metallicity values. These functions reveal how metallicity influences the effective temperature for a given stellar mass, shedding light on the variations in stellar atmospheres and evolutionary pathways. The detailed mass-temperature diagrams emphasize the need to consider metallicity when applying the MTR, as it affects the star's temperature and, consequently, the interpretation of observational data.

Acknowledgements. We would like to express our gratitude for the financial support provided by the TÜBİTAK 1001 Project (Project No: 122R053), which significantly contributed to the realization of this study. This research has made use of the NASA Exoplanet Archive, which is operated by the California Institute of Technology, under contract with the National Aeronautics and Space Administration under the Exoplanet Exploration Program.

References

Eker Z., Bakış V., Bilir S., Soydugan F., Steer I., Soydugan E., Bakış H., et al., 2018, Monthly Notices of the RAS, 479, 5491. doi:10.1093/mnras/sty1834

Contrib. Astron. Obs. Skalnaté Pleso **55/3**, 238 – 242, (2025)
https://doi.org/10.31577/caosp.2025.55.3.238

The impact of a variable angular momentum loss on long-period sdB binaries

J.P. Sánchez Arias, M. Cabezas and J. Vos

Astronomical Institute of the Czech Academy of Sciences
251 65 Ondřejov, The Czech Republic(E-mail: sanchez@asu.cas.cz)

Received: November 15, 2024; Accepted: February 5, 2025

Abstract. We investigated the effect of different angular momentum loss during the mass transfer of long-period sdB binaries by implementing a variable angular momentum loss efficiency parameter in MESA code. Our preliminary results show the impact on the mass ratio, orbital period, and metallicity. In particular, the number of long-period sdBs produced is reduced for higher angular momentum loss efficiency.
Key words: evolution – mass-loss – subdwarfs

1. Introduction

Hot subdwarf B (sdB) binaries with main-sequence companions are thought to be outcomes of stable mass transfer from evolved red giants. The current and typical treatment of angular momentum loss during Roche-lobe overflow is performed by using fixed mass-loss fractions. However, using a static treatment from slow mass loss until the start of a common envelope does not predict many of the observed correlations and the actual angular momentum loss is not objectively known. The change of the angular momentum loss impacts the distribution of the final orbital period, mass ratio, and ultimately the total number of produced sdBs. To investigate the effect of different angular momentum loss during mass transfer in different stellar populations, we have implemented new subroutines in MESA with a variable angular momentum loss efficiency parameter.

1.1. Variable angular momentum loss efficiency in MESA

We replaced the current expression for the angular momentum loss in MESA, with the following expression which considers a variation in the rate of angular momentum loss between two extreme scenarios: $\dot{J}_{min}$ and $\dot{J}_{max}$:

$$\dot{J} = (1 - \xi)\dot{J}_{min} + \xi \dot{J}_{max} \tag{1}$$

where $0 \leq \xi \leq 1$ is the degree of mixture. The minimum rate of angular momentum loss, $\dot{J}_{min}$, accordingly to Vos et al. (2020), is given by:

$$\dot{J}_{\min} = J_z \frac{q^2}{(1+q)} \frac{\dot{M}_{RG}}{M_{RG}} \tag{2}$$

where $q = M_{\rm RG}/M_{comp}$ is the mass ratio between the evolved red giant (RG), which initiates mass transfer at a rate $\dot{M}_{RG}$ through Roche-lobe overflow and the companion at the main sequence. J_z is the angular momentum given by:

$$J_z = \frac{M_{RG}}{(1+q)} \frac{2\pi}{P} a^2 \left(1-e^2\right)^{\frac{1}{2}} \tag{3}$$

where P is the orbital period, a the binary separation, and e the eccentricity of the orbit. Following Bobrick et al. (2017), we considered:

$$\dot{J}_{max} = \dot{M}_{RG} \left[\left(\frac{q}{1+q} \right)^2 + (0.5 - 0.227 \log_{10} q)^2 \right] \frac{2\pi}{p} a^2 \left(1-e^2\right)^{\frac{1}{2}} \tag{4}$$

where $(0.5 - 0.227 \log_{10} q)$ provides an approximation for the distance between the center of the RG star to the L1 point where the mass transfer occurs, divided a (Frank et al., 2002). Next, we computed binary evolution for different values of ξ for the grid of models presented in Vos et al. (2020).

2. Simulations

We based our simulations on the grid computed by Vos et al. (2020) which was developed to study the impact of the chemical history of the Galaxy in observed binary populations. This grid encompasses a set of 2060 Galactic binaries which may potentially produce long-period composite sdB binaries forming at the present epoch. They were selected over a large population of systems representing all the binaries in the Galaxy considering detailed initial mass function, metalicities, age, and mass fraction for different population bins in modeling the Galaxy. The selection criteria for this set of binaries were the following:

- primary masses above 0.7 $M_\odot$ and below 2 $M_\odot$, to dismiss stars which remain at the main sequence and ignite the He core non-degenerately ;
- 1 <$M_{primary}$/ M_{comp} < 3;
- periods between 0.1 and 1.4 times the period corresponding to the Roche-lobe overflow at the tip of the red giant branch;
- and binaries which become sdB at the present day, i.e. in which the primary reaches the tip of the red giant branch no earlier than 300Myr before the present day and no later than 700Myr after the present day.

This set of runs produced 147 sdB binaries for $\xi = 0$, considering sdBs as those stars that reach effective temperatures above 20 000K during its core He-burning phase. In this work, we computed the same set of runs with $\xi = 0.1$ and compare the results with those for $\xi = 0$.

3. Results

In Fig. 1 we show the metallicity [Fe/H] vs. final orbital period, P (left panel) and the mass ratio, q vs. P (right panel), for the all sdB produced when considering $\xi = 0$ (blue circles) and 0.1 (orange circles). As mentioned in Vos et al. (2020), the maximum RG radius depends on the metallicity, therefore the final orbital periods of sdB binaries must also correlate with their initial metallicity. This strong correlation is shown in the left panel. It can also be observed that resulting orbital periods decrease when considering higher angular momentum loss. In overall, there are no major differences in these distributions for different values of ξ. However, the amount of resulting sdBs for both cases is different, even considering such a small change in the angular momentum loss. We obtained 132 sdBs for $\xi = 0.1$ compared with 147 for $\xi = 0$.

Fig. 2 shows the impact of different angular momentum loss efficiency for systems with the same initial parameters P, q, [Fe/H], and the sdB progenitor mass. Specifically, we considered three systems with the following initial parameters: one system with $P_1 = 430$ [d], $q_1 = 1.49$, $[\mathrm{Fe/H}]_1 = 0.367$, and 1.0 $M_\odot$; a second one with $P_2 = 349$ [d], $q_2 = 1.4$, $[\mathrm{Fe/H}]_2 = 0.1395$, and 1.2 $M_\odot$ and a third one with $P_3 = 163$ [d], $q_3 = 1.45$, $[\mathrm{Fe/H}]_3 = 0.0296$, and 1.8 $M_\odot$. For each of these systems, which are originally sdBs at $\xi = 0$, we compute a set of binary evolution models for $0 \leq \xi \leq 0.1$ with a step of $\Delta\xi = 0.01$. Colour-coding shows the values for ξ. Systems that result in sdB stars are marked with circles, sdA stars are marked with diamonds, while systems resulting in He-WDs or horizontal branch (HB) stars are marked with triangles and squares respectively. The diverse evolutionary pathways of binaries systems can be noticed in this P-q diagram by the existence of the main and secondary branches. These branches, formed by observed P-q relations, are indicated in the figure with red dashes ellipses. In this figure we can observe that for increasing values of ξ, the resulting orbital periods are lower. We also observed that even at low values of ξ, the progenitors lose a considerable amount of mass which prevents the ignition and results as He-WDs instead of sdBs.

4. Conclusions and future work

Our main conclusions for long period sdB binaries are summarized as follows:

– the resulting orbital period, P, decrease for higher values of ξ;

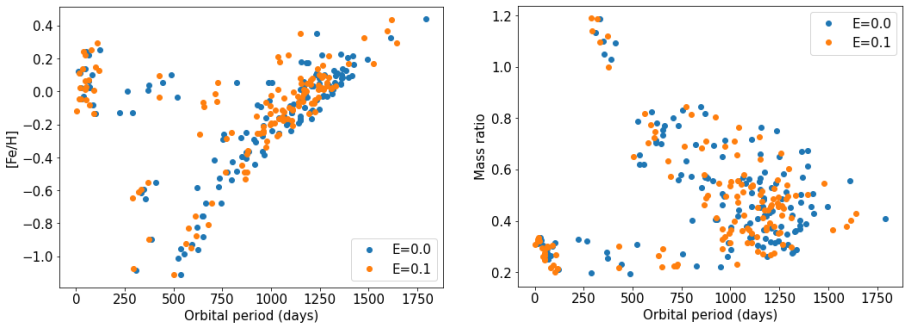


Figure 1. [Fe/H] vs. P and q vs. P distributions at the left and right panels, respectively, for the resulting sdBs when considering $\xi = 0$ (in blue) and 0.1 (in orange).

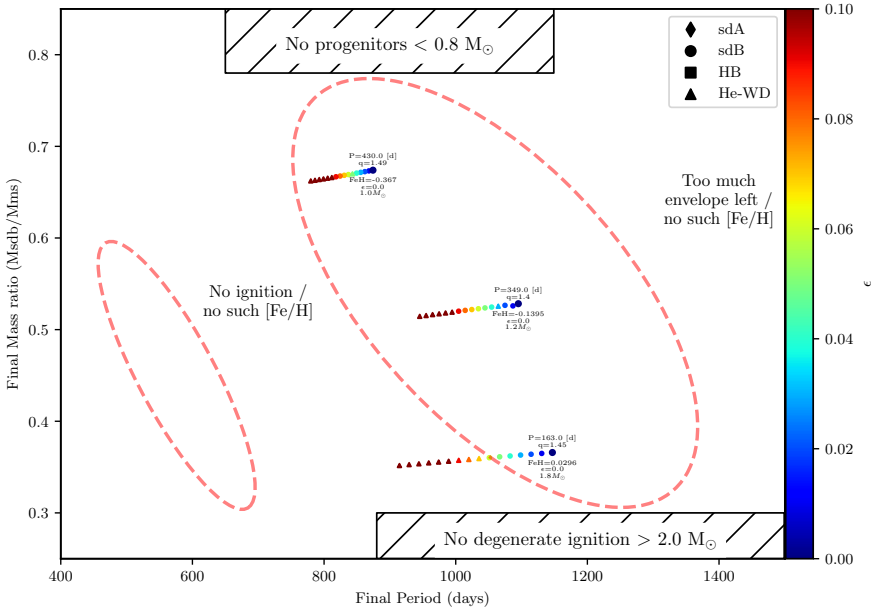


Figure 2. Effect of initial parameters: P, q, [Fe/H] and sdB progenitor mass on the final orbital periods and mass ratios, for small changes in ξ. We considered three systems with sdB progenitor masses of 1, 1.2 and 1.8 $M_{\odot}$, indicated in the figure along with the values for P, q, $[Fe/H]$. Systems that result in sdB stars are marked with circles, sdA stars are marked with diamonds, and systems resulting in He-WDs or HB stars are marked with triangles and squares, respectively. The locations of the main and second branches of the observed P-q relation are indicated in red dashed ellipses. Colour-coding shows the values for ξ considered.

– for long-period sdB binaries, the mass fraction slightly decreases when increasing the efficiency of the angular momentum loss efficiency;

– the small changes implemented in the angular momentum loss efficiency have a little impact in the observable distribution of the sdBs in the [Fe/H] vs. P and q vs. P planes;

– these same changes, however, impact the number of resulting sdB: the higher ξ, the lower the number of sdB produced;

– even for values of $\xi \leq 0.1$, the progenitors lose a considerable amount of mass which prevents the ignition and results as He-WDs, instead of sdBs.

The angular momentum loss significantly impacts the evolution of binary systems forming long period sdB stars. Variations in the angular momentum loss alter mass transfer dynamics and the final configuration of these systems. The present study will be extended for $\xi \leq 1$ and compared with observed systems to retrieve reliable constraints for the angular momentum loss.

Acknowledgements. This research was supported by the Grant Agency of the Czech Republic (GAČR 22-34467S).

References

Bobrick, A., Davies, M. B., & Church, R. P., Mass transfer in white dwarf-neutron star binaries. 2017, *Monthly Notices of the RAS*, **467**, 3556, DOI:10.1093/mnras/stx312

Frank, J., King, A., & Raine, D. J. 2002, *Accretion Power in Astrophysics: Third Edition*

Vos, J., Bobrick, A., & Vučković, M., Observed binary populations reflect the Galactic history. Explaining the orbital period-mass ratio relation in wide hot subdwarf binaries. 2020, *Astronomy and Astrophysics*, **641**, A163, DOI:10.1051/0004-6361/201937195

Contrib. Astron. Obs. Skalnaté Pleso **55/3**, 243 – 254, (2025)
https://doi.org/10.31577/caosp.2025.55.3.243

Populations of hierarchical stellar systems

A. Tokovinin

Cerro Tololo Interamerican Observatory – NSFs NOIRlab, Casilla 603, La Serena, Chile (E-mail: andrei.tokovinin@noirlab.edu)

Received: October 11, 2024; Accepted: December 10, 2024

Abstract. Triple and higher-order stellar systems are common products of star formation, and their frequency depends strongly on the mass. About 10 0000 hierarchies are expected within 100 pc, but only a quarter of those are presently catalogued. The diversity of their architectures is related to several processes responsible for formation and early evolution: pure N-body dynamics, dynamics with tides, fragmentation of disks and cores, and dissipative capture. Each mechanism leaves its characteristic imprints, illustrated by real systems matching the predicted features. Tentative classification of hierarchies into families assiciated with particular formation scenarios is a new emerging field. Large surveys play an increasing role in improving the multiplicity statistics and in finding rare systems. As an example, relative alignment of eclipsing binaries in triples with known inclinations of outer orbits is discussed, suggesting that only a quarter of such systems are aligned.

Key words: binaries: general – binaries: visual – binaries: close

1. Introduction

Statistics of binary stars in the field is known relatively well, starting from the best-studied group of solar-type stars and extending to smaller and larger masses (Offner et al., 2023). It became clear recently that the field binaries are a mixture of different populations. For example, the frequency of close pairs depends strongly on metallicity, while the frequency of wide pairs differs considerably between dense and sparse clusters (Deacon & Kraus, 2020) and also possibly depends on metallicity (Hwang et al., 2020). These differences are related to the formation mechanisms of binaries, but, unfortunately, their signatures are blurred in the statistics of the mixed field population.

Hierarchical stellar systems can be viewed as combinations of two or more elementary binaries. They are described by a larger number of parameters (periods P, mass ratios q, eccentricities e of each pair, mutual orbit orientation, period ratios). In this multi-parameter space, the signatures of formation processes might be more pronounced, compared to binaries. Hence the idea of classifying hierarchies into distinct families emerges (Tokovinin, 2021). Although such classification is still tentative or ambiguous, it might be a useful endeavor.

Remember that the empirical classification of biological species appeared well before its underpinning genetic roots were discovered.

Our current knowledge of hierarchies is still very incomplete. Using the estimated frequency of hierarchical systems plotted in Fig. 1 of Offner et al. (2023) and the number of Gaia stars in the 100-pc volume, I estimated a total of ∼10 000 hierarchies, while only 2225 are listed in the latest[1] update of the multiple star catalog, MSC (Tokovinin, 2018b). Hierarchies, like binaries, are discovered via combination of various observing techniques spanning the full range of periods. The Gaia DR3 catalog (Gaia Collaboration et al., 2021) has substantially improved the completeness by revealing all pairs wider than $\sim 1''$ and detecting their inner subsystems via astrometric accelerations, radial velocity (RV) variation, and other markers. Some of those nearby hierarchies were confirmed by directly resolving the inner pairs (Tokovinin, 2023b). As a result, the completeness of nearby hierarchies within 100 pc is substantially improved at wide separations (outer periods $P_{\rm out} > 10^5$ d), and it is very good when the inner pairs are also resolved by Gaia. Nevertheless, the plot of inner mass ratios and periods, $q_{\rm in}$ vs. $P_{\rm in}$, shows clear imprints of the observing techniques (see Fig. 7 in Tokovinin, 2023b). The discovery of the most interesting compact hierarchies is still largely dependent on the ground-based work and, so far, is barely helped by Gaia.

2. Formation mechanisms and families of hierarchies

The basic mechanisms producing binaries and hierarchies (Offner et al., 2023) are: (i) dynamical interactions, (ii) dynamics with tides, (iii) disk fragmentation, (iv) core or filament fragmentation, and (v) dissipative capture. These processes and their predictions regarding architecture of hierarchies are detailed below and illustrated by examples. However, association between formation mechanisms and real systems remains speculative; a given system can be possibly produced by alternative mechanisms. The sequence of events in formation and early evolution is called formation *scenario* — a term borrowed from binary evolution and cinema.

2.1. N-body dynamics

Originally, triple stars were studied as systems of gravitating point masses (Anosova, 1986). This approach established the criteria of dynamical stability (Mardling & Aarseth, 2001). The N-body dynamics makes clear predictions about architecture of triples: the orbits are randomly aligned, the period ratios are moderate (just above the stability limit), and the inner eccentricities are distributed thermally as $f(e_{\rm in}) \propto e_{\rm in}$ (e.g. Antognini & Thompson, 2016; Stone & Leigh, 2019).

[1]December 2023, https://www.ctio.noirlab.edu/~atokovin/stars/ and Vizier J/ApJS/235/6

One expects the N-body dynamics to dominate at large scales, on the order of distances between stars in the primordial clusters. Indeed, the properties of the relatively complete sample of wide low-mass Gaia hierarchies within 100 pc match the N-body predictions (Tokovinin, 2022a). The most intriguing member of this sample is the sextuple system V1311 Ori (Tokovinin, 2022b) composed of M-type dwarfs. It contains four Gaia sources in a non-hierarchical configuration with projected separations of $\sim 10^4$ au, and two of those sources are close resolved pairs. This system is still young (∼24 Myr) and might disintegrate into triple, binary, and single stars in the future.

Dynamical interactions at much smaller scales occur in hierarchical systems that become unstable owing to shrinking outer orbits or internal dynamics. Violent interactions during close approaches result in ejections (usually of the lowest-mass member) and tightening of the inner binary that absorbs the binding energy of the ejected star. This mechanism is largely responsible for producing massive runaway stars (Fujii & Portegies Zwart, 2011). Their peculiar velocities above 30 $\mathrm{km\,s^{-1}}$ indicate the spatial scale of disintegrating multiple systems on the order of 1 au or less. The remaining close binaries are even more massive than the runaways, so this process is most relevant for large masses.

2.2. Dynamics and tides

When separation between stars in the inner binary is comparable to their radii, the point-mass approximation is no longer valid because tides in the inner binaries came into play. Close binaries can be formed within triples with misaligned or eccentric outer orbits via Lidov-Kozai (L-K) cycles and related mechanisms (Eggleton & Kisseleva-Eggleton, 2006; Naoz, 2016). The empirical fact that close binaries are often found within triples seems to support this scenario; however, Moe & Kratter (2018) show that this mechanism can produce only a fraction of close binaries, and it is most efficient at the pre-main sequence (PMS) stage when the stars are large.

While close binaries indeed like to be accompanied (Hwang, 2023), their tertiary companions are often too distant to exert any dynamical influence. However, these apparent triples might contain intermediate-level subsystems, i.e. be quadruples of 3+1 architecture. This offers an interesting possibility of cascade L-K cycles (Hamers et al., 2015). First, they slowly modify the orientation of the intermediate orbit to the point when the inner triple starts these cycles and eventually forms a close inner pair with the help of tides. This happens well after the stars have contracted from their large PMS size. Recently, Powell et al. (2023) searched for intermediate subsystems in wide pairs containing eclipsing binaries (EBs) and found 20 new 3+1 quadruples.

2.3. Disk fragmentation and migration

The gravitational instability starts on large spatial scales and proceeds to smaller scales, as the gas gets denser while remaining cold (Vázquez-Semadeni et al., 2019). During this isothermal collapse stage, the Jeans mass decreases, prompting fragmentation. The cooling becomes inefficient for optically thick gas at densities corresponding to a spatial scale of ∼10 au; this prevents formation of closer pairs (so-called opacity limit to fragmentation). Conservation of the angular momentum slows down the accretion on to protostars: the incoming gas is temporarily retained in disk-like structures (Tu et al., 2024) which can become unstable and form companions at separations >10 au. Continuing accretion on to a binary results in the preferential growth of the companion (increases the mass ratio), and, generally, in its inward migration (Lai & Muñoz, 2023; Siwek et al., 2023). Using several simplifying assumptions, Tokovinin & Moe (2020) developed a statistical model of companion formation and migration that matches reasonably well the statistics of short-period binaries.

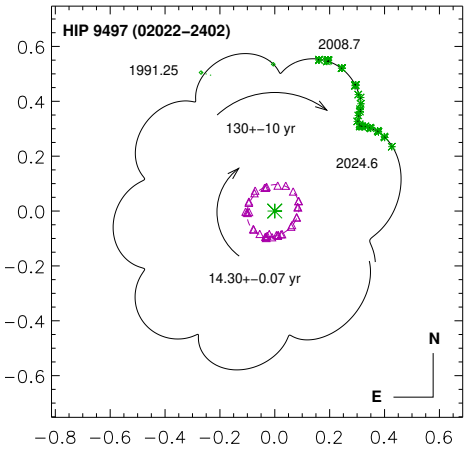


Figure 1. The double twin triple system HIP 9497 with recently updated orbits (Tokovinin, 2018a). The inner 14.3-yr orbit is well constrained, and the still uncertain outer period suggest a period ratio of 1:9, possibly in a mean motion resonance. Both orbits are quasi–circular. The masses of two stars in the inner pair are 0.6 $M_\odot$, the primary is of 1.2 $M_\odot$.

A tertiary companion can form by disk fragmentation. If the accretion continues, the companion can become as massive as the inner binary, and the system becomes a double twin where the inner and outer mass ratios are close to one. This mechanism implies dissipative interaction of stars with the disk, leading to quasi-circular and mutually aligned orbits. Many examples of such triples are known (Fig. 1). Quadruple systems of 3+1 architecture with roughly aligned orbits could also be formed inside-out by successive disk fragmentation and migration, especially the compact ones like HIP 41431 with periods of 2.9, 59 days, and 3.9 yr (Borkovits et al., 2019). Compact triple systems identified by eclipse time variations or by double eclipses (Borkovits et al., 2016; Rappaport et al., 2023) were plausibly formed by disk fragmentation and migration; their orbits

are typically very well aligned. The shortest known outer periods in compact triples are about 33 days (examples in Tokovinin, 2021).

2.4. Core fragmentation

A filament or a density peak within it (core) can fragment into several protostars. These stellar embryos continue to accrete the surrounding gas and to interact dynamically with each other, as demonstrated in computer simulations (Bate, 2019; Lee et al., 2019). Bound hierarchical systems are frequently formed during core collapse, although some of them later become disrupted. Dynamical interactions with neighbors imply misaligned and eccentric orbits in such triples. Two young quintuple systems, ξ Sco and κ Tuc, could be formed in this way (Tokovinin, 2020). Their particularity is the absence of close inner binaries, suggesting that, for some reason, the migration was not strong, if any; the outer separations are around 8 kau, and both hierarchies are members of young moving groups, suggesting formation in a low-density environment.

Dynamical interactions between nascent protostars occur on the free-fall (crossing) time scale; however, the gas accretion can continue longer, fed by the large-scale hierarchical collapse (Vázquez-Semadeni et al., 2019). Some stars can be ejected from the cloud, becoming low-mass orphans (Reipurth, 2000), while the remaining stars continue to gain mass from the common gas reservoir. This circumstance can explain why stellar masses in multiple systems do not correspond to a random draw from the IMF, being much more similar. In the extreme case, hierarchies containing 3 or 4 stars of nearly equal masses (triplets and quadruplets) can be formed. One such example is ϵ Cha, the core of the young (5 Myr) association, hosting three similar 2.5 $M_\odot$ stars (Tokovinin, 2023a). Here, the inner 6.4-yr orbit has an eccentricity of 0.73, and it is not aligned with the outer orbit, suggesting a violent dynamical history (unlike the double twins discussed above). This system could be formed by core collapse followed by the dynamical interplay between the seeds and accretion. Alternatively, it could result from dynamical decay of a 2+2 quadruple, but in such a case the remaining triple would acquire a recoil velocity and would leave the association, which is not observed.

Collapse and fragmentation can be triggered by gas compression during collision between two clouds. Early simulations by Whitworth (2001) demonstrate formation of a 2+2 quadruple with comparable masses in such triggered event. Unfortunately, this idea was not developed further theoretically, while many wide 2+2 quadruples composed of comparable-mass stars are known in the field and among PMS stars (Reipurth et al., 2024).

Generally speaking, however, formation of hierarchical systems during core collapse is not an event, but rather a process where continuing gas accretion and the associated migration play a crucial role. Apart from equalizing stellar masses, it shrinks the orbits and, presumably, aligns them. Extreme products of such process are compact 2+2 quadruples where four stars of similar masses

are packed in a small volume. Until recently, the shortest outer period of ∼1 yr was found in VW LMi (Pribulla et al., 2020). In 2023, this record was beaten by TIC 219006971 with an outer period of 168 days (Kostov et al., 2023) and by BU CMi with an outer period of 121 days (Pribulla et al., 2023). In all these 2+2 quadruples, the four stars have similar masses above 1 $M_\odot$, and all orbits are confined to one plane. If this reasoning is correct, there should be no compact 2+2 quadruples among low-mass M dwarfs because they have not accreted enough gas. Interestingly, among the 8 newly identified doubly eclipsing 2+2 quadruples containing contact pairs (Zasche et al., 2024), the least massive one is a K3 dwarf with an outer period of 22 yr (not compact).

2.5. Dissipative capture and close binaries

Close approaches of stars in a nascent mini-cluster can produce wide bound systems if the excessive kinetic energy is dissipated in their gas envelopes. At the same time, this causes a surge of accretion on to each star that can form close companions via disk fragmentation or shrink the orbit if the colliding star is already a binary. During such encounters, the accreted gas is not aligned with the original binary orbits or disks, which makes for a rapid orbit migration. Simulations of star formation show that dissipative collisions occur frequently (Bate, 2019; Kuruwita & Haugbølle, 2023) or may even be the dominant binary formation channel (Rozner et al., 2023). This mechanism can potentially explain the empirical relation between close (e.g. eclipsing) and wide binaries (Hwang, 2023) without evoking the L-K cycles.

3. The role of large surveys

Large surveys from ground and space dominate the current and future landscape of astronomical research and have profound impact in the area of stellar multiplicity. Yet, none of the existing surveys was designed for the study of binaries and multiples, and these detections are just by-products. Although a million of resolved Gaia binaries in El-Badry et al. (2021) greatly surpass the content of the WDS, many more binaries are missed by Gaia. Figure 2 represents various indicators of binarity available in DR3. One of those, for example, is the lack of astrometric solutions for pairs with separations from 0.1″ to 1″ and moderate magnitude differences, the so-called *Gaia hole* (Fig. 6 in Tokovinin, 2023b). Another non-trivial indicator is the variability of G-band fluxes in semi-resolved pairs (Holl et al., 2023). An excessive astrometric noise (large RUWE) can be caused not only by the motion of the photocenter, but also by blending with a faint semi-resolved companion. Surveys like Gaia become more productive when they are complemented by dedicated follow-up observations designed to overcome their limitations.

Statistical inferences from surveys must inevitably account for the selection biases. This can be achieved by two alternative strategies. The raw statistics

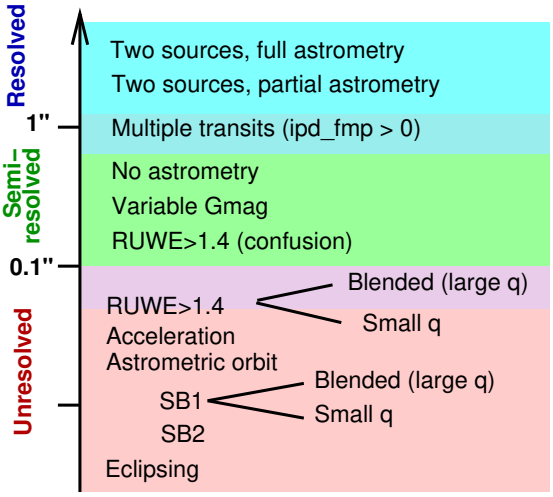


Figure 2. Schematic inventory of binarity indicators in Gaia. They are split into three broad groups: resolved (wide), semi-resolved, and unresolved (close) binaries. Each indicator has a complex and poorly known selection bias.

can be de-convolved from the selection and other effects. Alternatively, the true underlying statistics can be represented by a parametric model. The model is filtered by the selection function, and the result is compared to the observations to find the best-matching values of the parameters and their confidence intervals. Both approaches are found in the modern literature.

Apart from the statistics, large surveys find rare objects, like the two triply eclipsing sextuple systems discovered by TESS (Powell et al., 2021; Zasche et al., 2023). Existence of such objects challenges the theory and, thus, advances our understanding of the multiple-star formation.

Here is an example of my ongoing work based on surveys. Using the catalogs of EBs and the Gaia orbits, Czavalinga et al. (2023) identified 376 new compact hierarchies where astrometric or spectroscopic pairs contain inner short-period EBs (many of those are confirmed by the eclipse timing). Mutual alignment in such systems can be probed by the distribution of $x = |\cos i|$, where i is the inclination of the Gaia orbit. In aligned triples, one expects to find an excess of edge-on orbits with $x \approx 0$, while an isotropic orbit orientation corresponds to the uniform distribution of x. For all 1685 MSC triples with known outer inclinations (i.e. astrometric or visual orbits), x is indeed distributed uniformly. However, for the subset of 369 hierarchies containing EBs, a clear excess at $x < 0.3$ is seen, indicating mutual alignment within $\sim 20°$ (Fig. 3). The excess, however, contains only 1/4 of such triples (the rest have uniform x), and this fraction does not depend on the outer period. So, the majority (3/4) of compact triples with short-period inner subsystems appear to be not mutually aligned. This result does not contradict the known misalignment of close inner pairs in some emblematic hierarchies like Algol or Castor (Torres et al., 2022). However, it is in tension with the strong alignment of compact hierarchies found by Borkovits et al. (2016). Resolved triples also show a strong alignment at outer separations

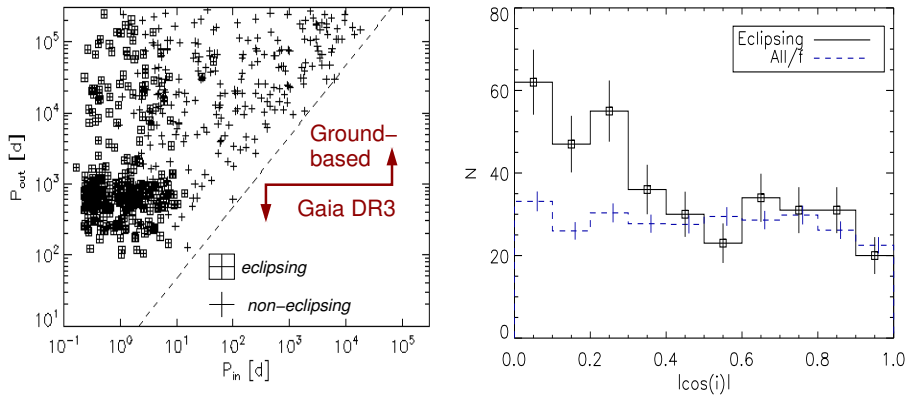


Figure 3. Mutual alignment in triple systems containing EBs. The left panel is a plot of outer and inner periods of all hierarchies with known outer inclinations. Outer periods below 1000 days are dominated by the Gaia sample of Czavalinga et al. (2023), longer periods result from ground-based observations. The dashed line is the dynamical stability limit; eclipsing subsystems are marked by squares. The right panel plots the histogram of $x = |\cos i|$ in the 369 hierarchies containing EBs and the scaled-down histogram for all hierarchies with known inclinations.

below ∼100 au (Tokovinin, 2017), but their inner subsystems are much wider than the EBs. The prevailing misalignment in the sample of Czavalinga et al. can be tested by dynamical analysis of compact hierarchies, e.g. a search for eclipse depth variations caused by precession (which, however, is slow).

A possible explanation of these findings might be related to the differences in the angular momentum of the accreted gas. When it is roughly constant, an aligned triple can form where the accretion of co-rotating gas does not shrink the orbits too much, like in the system shown in Fig. 1. If, on the other hand, a triple is formed by a dissipative capture, the accreted gas is strongly misaligned and efficiently shrinks the inner orbit, producing a close inner pair. More observational and theoretical work is needed to explore this scenario, and here the role of large surveys will be essential.

References

Anosova, J. P., Dynamical Evolution of Triple Systems. 1986, *Astrophysics and Space Science*, **124**, 217, DOI:10.1007/BF00656037

Antognini, J. M. O. & Thompson, T. A., Dynamical formation and scattering of hierarchical triples: cross-sections, Kozai-Lidov oscillations, and collisions. 2016, *Monthly Notices of the RAS*, **456**, 4219, DOI:10.1093/mnras/stv2938

Bate, M. R., The statistical properties of stars and their dependence on metallicity. 2019, *Monthly Notices of the RAS*, **484**, 2341, DOI:10.1093/mnras/stz103

Borkovits, T., Hajdu, T., Sztakovics, J., et al., A comprehensive study of the Kepler triples via eclipse timing. 2016, *Monthly Notices of the RAS*, **455**, 4136, DOI:10.1093/mnras/stv2530

Borkovits, T., Sperauskas, J., Tokovinin, A., et al., The compact multiple system HIP 41431. 2019, *Monthly Notices of the RAS*, **487**, 4631, DOI:10.1093/mnras/stz1510

Czavalinga, D. R., Mitnyan, T., Rappaport, S. A., et al., New compact hierarchical triple system candidates identified using Gaia DR3. 2023, *Astronomy and Astrophysics*, **670**, A75, DOI:10.1051/0004-6361/202245300

Deacon, N. R. & Kraus, A. L., Wide binaries are rare in open clusters. 2020, *Monthly Notices of the RAS*, **496**, 5176, DOI:10.1093/mnras/staa1877

Eggleton, P. P. & Kisseleva-Eggleton, L., A Mechanism for Producing Short-Period Binaries. 2006, *Astrophysics and Space Science*, **304**, 75, DOI:10.1007/s10509-006-9078-z

El-Badry, K., Rix, H.-W., & Heintz, T. M., A million binaries from Gaia eDR3: sample selection and validation of Gaia parallax uncertainties. 2021, *Monthly Notices of the RAS*, **506**, 2269, DOI:10.1093/mnras/stab323

Fujii, M. S. & Portegies Zwart, S., The Origin of OB Runaway Stars. 2011, *Science*, **334**, 1380, DOI:10.1126/science.1211927

Gaia Collaboration, Brown, A. G. A., Vallenari, A., et al., Gaia Early Data Release 3. Summary of the contents and survey properties. 2021, *Astronomy and Astrophysics*, **649**, A1, DOI:10.1051/0004-6361/202039657

Hamers, A. S., Perets, H. B., Antonini, F., & Portegies Zwart, S. F., Secular dynamics of hierarchical quadruple systems: the case of a triple system orbited by a fourth body. 2015, *Monthly Notices of the RAS*, **449**, 4221, DOI:10.1093/mnras/stv452

Holl, B., Fabricius, C., Portell, J., et al., Gaia Data Release 3. Gaia scan-angle-dependent signals and spurious periods. 2023, *Astronomy and Astrophysics*, **674**, A25, DOI:10.1051/0004-6361/202245353

Hwang, H.-C., The mystery in Gaia DR3 triples: occurrence rates, orientations, and eccentricities of wide tertiaries around close binaries. 2023, *Monthly Notices of the RAS*, **518**, 1750, DOI:10.1093/mnras/stac3116

Hwang, H.-C., Hamer, J. H., Zakamska, N. L., & Schlaufman, K. C., Very wide companion fraction from Gaia DR2: A weak or no enhancement for hot Jupiter hosts, and a strong enhancement for contact binaries. 2020, *Monthly Notices of the RAS*, **497**, 2250, DOI:10.1093/mnras/staa2124

Kostov, V. B., Borkovits, T., Rappaport, S. A., et al., TIC 219006972: a compact, coplanar quadruple star system consisting of two eclipsing binaries with an outer period of 168 d. 2023, *Monthly Notices of the RAS*, **522**, 90, DOI:10.1093/mnras/stad941

Kuruwita, R. L. & Haugbølle, T., The contribution of binary star formation via core fragmentation on protostellar multiplicity. 2023, *Astronomy and Astrophysics*, **674**, A196, DOI:10.1051/0004-6361/202244882

Lai, D. & Muñoz, D. J., Circumbinary Accretion: From Binary Stars to Massive Binary Black Holes. 2023, *Annual Review of Astron and Astrophys*, **61**, 517, DOI:10.1146/annurev-astro-052622-022933

Lee, A. T., Offner, S. S. R., Kratter, K. M., Smullen, R. A., & Li, P. S., The Formation and Evolution of Wide-orbit Stellar Multiples In Magnetized Clouds. 2019, *Astrophysical Journal*, **887**, 232, DOI:10.3847/1538-4357/ab584b

Mardling, R. A. & Aarseth, S. J., Tidal interactions in star cluster simulations. 2001, *Monthly Notices of the RAS*, **321**, 398, DOI:10.1046/j.1365-8711.2001.03974.x

Moe, M. & Kratter, K. M., Dynamical Formation of Close Binaries during the Pre-main-sequence Phase. 2018, *Astrophysical Journal*, **854**, 44, DOI:10.3847/1538-4357/aaa6d2

Naoz, S., The Eccentric Kozai-Lidov Effect and Its Applications. 2016, *Annual Review of Astron and Astrophys*, **54**, 441, DOI:10.1146/annurev-astro-081915-023315

Offner, S. S. R., Moe, M., Kratter, K. M., et al., The Origin and Evolution of Multiple Star Systems. 2023, in Astronomical Society of the Pacific Conference Series, Vol. **534**, *Protostars and Planets VII*, ed. S. Inutsuka, Y. Aikawa, T. Muto, K. Tomida, & M. Tamura, 275

Powell, B. P., Kostov, V. B., Rappaport, S. A., et al., TIC 168789840: A Sextuply Eclipsing Sextuple Star System. 2021, *Astronomical Journal*, **161**, 162, DOI:10.3847/1538-3881/abddb5

Powell, B. P., Kostov, V. B., & Tokovinin, A., A Hunting Expedition For High-Order Hierarchies. 2023, *Monthly Notices of the RAS*, **524**, 4296, DOI:10.1093/mnras/stad2065

Pribulla, T., Borkovits, T., Jayaraman, R., et al., BU Canis Minoris - the most compact known flat doubly eclipsing quadruple system. 2023, *Monthly Notices of the RAS*, **524**, 4220, DOI:10.1093/mnras/stad2015

Pribulla, T., Puha, E., Borkovits, T., et al., Secular changes in the orbits of the quadruple system VW LMi. 2020, *Monthly Notices of the RAS*, **494**, 178, DOI:10.1093/mnras/staa699

Rappaport, S. A., Borkovits, T., Gagliano, R., et al., A study of nine compact triply eclipsing triples. 2023, *Monthly Notices of the RAS*, **521**, 558, DOI:10.1093/mnras/stad367

Reipurth, B., Disintegrating Multiple Systems in Early Stellar Evolution. 2000, *Astronomical Journal*, **120**, 3177, DOI:10.1086/316865

Reipurth, B., Briceño, C., Geballe, T. R., et al., Haro 5-2: A New Pre-main-sequence Quadruple Stellar System. 2024, *Astronomical Journal*, **168**, 143, DOI:10.3847/1538-3881/ad5956

Rozner, M., Generozov, A., & Perets, H. B., Binary formation through gas-assisted capture and the implications for stellar, planetary, and compact object evolution. 2023, *Monthly Notices of the RAS*, **521**, 866, DOI:10.1093/mnras/stad603

Siwek, M., Weinberger, R., & Hernquist, L., Orbital evolution of binaries in circumbinary discs. 2023, *Monthly Notices of the RAS*, **522**, 2707, DOI:10.1093/mnras/stad1131

Stone, N. C. & Leigh, N. W. C., A statistical solution to the chaotic, non-hierarchical three-body problem. 2019, *Nature*, **576**, 406, DOI:10.1038/s41586-019-1833-8

Tokovinin, A., Orbit Alignment in Triple Stars. 2017, *Astrophysical Journal*, **844**, 103, DOI:10.3847/1538-4357/aa7746

Tokovinin, A., Dancing Twins: Stellar Hierarchies That Formed Sequentially? 2018a, *Astronomical Journal*, **155**, 160, DOI:10.3847/1538-3881/aab102

Tokovinin, A., The Updated Multiple Star Catalog. 2018b, *Astrophysical Journal, Supplement*, **235**, 6, DOI:10.3847/1538-4365/aaa1a5

Tokovinin, A., Nearby Quintuple Systems κ Tucanae and ξ Scorpii. 2020, *Astronomical Journal*, **159**, 265, DOI:10.3847/1538-3881/ab8af1

Tokovinin, A., Architecture of Hierarchical Stellar Systems and Their Formation. 2021, *Universe*, **7**, 352, DOI:10.3390/universe7090352

Tokovinin, A., Resolved Gaia Triples. 2022a, *Astrophysical Journal*, **926**, 1, DOI:10.3847/1538-4357/ac4584

Tokovinin, A., The Family of V1311 Ori: a Young Sextuple System or a Minicluster? 2022b, *Astronomical Journal*, **163**, 127, DOI:10.3847/1538-3881/ac4bc5

Tokovinin, A., Dynamics of Four Triple Systems. 2023a, *Astronomical Journal*, **165**, 165, DOI:10.3847/1538-3881/acbf32

Tokovinin, A., Exploring Thousands of Nearby Hierarchical Systems with Gaia and Speckle Interferometry. 2023b, *Astronomical Journal*, **165**, 180, DOI:10.3847/1538-3881/acc464

Tokovinin, A. & Moe, M., Formation of close binaries by disc fragmentation and migration, and its statistical modelling. 2020, *Monthly Notices of the RAS*, **491**, 5158, DOI:10.1093/mnras/stz3299

Torres, G., Schaefer, G. H., Monnier, J. D., et al., The Orbits and Dynamical Masses of the Castor System. 2022, *Astrophysical Journal*, **941**, 8, DOI:10.3847/1538-4357/ac9d8d

Tu, Y., Li, Z.-Y., Zhu, Z., & Hsu, C.-Y., Fragmentation of dense rotation-dominated structures fed by collapsing gravo-magneto-sheetlets and origin of misaligned 100 au-scale binaries and multiple systems. 2024, *Monthly Notices of the RAS*, **532**, 3135, DOI:10.1093/mnras/stae1639

Vázquez-Semadeni, E., Palau, A., Ballesteros-Paredes, J., Gómez, G. C., & Zamora-Avilés, M., Global hierarchical collapse in molecular clouds. Towards a comprehensive scenario. 2019, *Monthly Notices of the RAS*, **490**, 3061, DOI:10.1093/mnras/stz2736

Whitworth, A. P., Impulsively Triggered Binary Star Formation. in , *The Formation of Binary Stars*, ed. H. Zinnecker & R. Mathieu, Vol. **200**, 33

Zasche, P., Borkovits, T., Jayaraman, R., et al., V994 Herculis: a unique triply eclipsing sextuple star system. 2023, *Monthly Notices of the RAS*, **520**, 3127, DOI:10.1093/mnras/stad328

Zasche, P., Henzl, Z., Merc, J., Kára, J., & Kučáková, H., Eight new 2+2 doubly eclipsing quadruple systems detected. 2024, *Astronomy and Astrophysics*, **687**, A6, DOI:10.1051/0004-6361/202450400

Contrib. Astron. Obs. Skalnaté Pleso **55/3**, 255 – 262, (2025)
https://doi.org/10.31577/caosp.2025.55.3.255

Doubly eclipsing systems: Divide et impera

P. Zasche

Charles University, Faculty of Mathematics and Physics, Astronomical Institute, V Holešovičkách 2, CZ-180 00, Praha 8, Czech Republic
(E-mail: zasche@sirrah.troja.mff.cuni.cz)

Received: October 7, 2024; Accepted: January 7, 2025

Abstract. Multiply eclipsing systems are still quite new type of objects, but their number is still increasing: now reaching almost 1 thousand. They represent rather challenging task for modelling. Even in the case when having enough data for a complex analysis. There are many effects acting together, which have to be taken into account. However, for most of them still the dynamical interactions are small enough. Hence, at first, the systems can be considered as two independent triple systems. And for the analysis to use a well-known old method : Divide et impera.

Key words: binary stars – multiple systems – photometry

1. Introduction

The classical role of eclipsing binaries as a standstone of modern astrophysics was discussed elsewhere (e.g. Southworth 2012). However, nowadays the amount of detected eclipsing binaries reached a number of more than 2 millions. Hence, it is absolutely beyond the capacity of human beings to be able to analyse each particular binary in detail. Only some statistical properties of them are being studied sometimes.

Another way of thinking about the topic would be to focus on some very specific type of eclipsing systems, which still deal with much lower numbers. Objects observable, but rare enough, which are of high astrophysical importance. The multiply-eclipsing systems are definitely such type of objects. With these I mean those stars, where one can see different periods of various eclipses, where one periodicity obviously cannot easily explain all of the observed eclipses. Therefore, such systems can be either triply eclipsing triples, where the third body moves on an outer orbit (also typically co-planar) to the inner eclipsing pair causing the tertiary eclipses (of typically quite complicated shape). Or another scenario where we have a bound 2+2 system of two eclipsing inner binaries, which do not have to necessarily eclipse each other on their mutual orbit. Hence, the two eclipsing periods typically detected via photometry make them a so-called "doubly eclipsing system", i.e. two eclipsing periods apparently coming from one point source on the sky. We should more correctly classify them only as

candidates, because their mutual orbit is not known in general. However, the non-detection of any mutual movement of the two pairs around each other does not prevent us to classify these objects as doubly eclipsing.

The vast majority of such systems were discovered quite recently only due to continuous monitoring of the sky with different photometric surveys like OGLE (for example 32 detected doubly eclipsing binaries from the OGLE fields towards the Galactic Bulge, see Soszyński et al. 2016), or satellite telescopes like Corot, Kepler or recently TESS (about three hundred new systems detected by Kostov et al. 2022, Zasche et al. 2022b, and Kostov et al. 2024). Quite surprisingly, 20 years ago nobody in the astrophysical community knew anything about such kind of objects, the first one was V994 Her discovered by Lee et al. (2008). Nowadays, the number of candidates with two distinctive photometric periods reaches one thousand (980 published yet, state for the date of October 2024). Among these systems I count only these ones, which have both eclipsing periods published and are obviously not blends coming from two distinct close-by sources on the sky.

2. Methods for analysis

In principle, there are two possible methods for analysing these complicated systems.

1. Complete combined dynamical modelling of the whole 2+2 system. Joining all individual data into one dataset and running the full dynamical computation and modelling of LC, RV, ETV, or SED together. Process time-consuming and non-trivial, and demanding good starting values of parameters and well-observed data. This approach was being used by a group of people around T.Borkovits, and their analysis led to many interesting results on several dynamically interacting systems, e.g. Borkovits et al. (2021), or Pribulla et al. (2023).

2. Another possible approach would be used only for weakly bound quadruples, where their outer orbital periods are longer compared to the inner periods. It means where the mutual dynamical interaction is smaller and one can use some simplified approach via linearization of the whole modelling. I call this approach as "divide et impera". It means cutting the whole problem into smaller pieces. And then to solve the individual datasets independently with some simplified assumptions. In the following sections, I will present why such an approach is mostly sufficient.

Linearization in the problem would be to use linear ephemerides instead of complicated approach of ETV variation described with LITE or dynamical effects. Such an ETV is not known in the beginning and one has to use some preliminary assumption of the correct period for example. But with a linear ephemerides one can fit the individual light curves and radial velocity curves

and then season by season to join them together to some joint approach. For systems where the long mutual period A-B is long enough, such an approach is justifiable, as can be seen in our illustrative figure 1.

One can use such a method only when the outer period is long enough, and the dynamical interactions are generally small (the ratio of P_{AB}/P_A or P_{AB}/P_B large enough). Another necessary condition is that the number of datapoints in individual datasets is large enough when cutting the whole dataset into shorter intervals.

Here comes quite important point of our whole approach. Judging whether our method is adequate, or the ratio of periods is small enough should be done star-by-star by the one doing the analysis. For sure, the outer period should be an order of magnitude longer than both inner periods. And also the number of data points in every single cutted interval should be enough (at least dozens of photometric data points for each light curve).

Another step in the method also using this "divide et impera" approach would be for the disentangling of the combined light curve into the two individual light curves of both A and B pairs. Using a similar assumption, we shall use some preliminary fit of LC of pair A, subtract it from the combined photometry, and do the same with LC of pair B. Doing this procedure several times iteratively, one gets the final disentangled light curves of both A and B pairs. However, also here the simplification of the process is obvious - one has to have a linear ephemerides, and both light curves should be constant in shape over the time interval. When such an assumption is not fulfilled, then again one has to cut the whole interval into smaller pieces, for which the assumption is acceptable.

3. Usage of the method

One can ask whether the presented method is adequate for most of the doubly eclipsing 2+2 quadruples. Or it is too simplifying and can be used only for several systems. I will show that it is usable for most of the systems known nowadays.

What is the crucial parameter for judging whether the linearization is acceptable or not is the period of the outer orbit, or the ratio of inner to outer period. Because most of the studied systems detected as doubly eclipsing have inner orbital periods of days typically, the outer period of years or decades is certainly long enough. It means that the dynamical interactions would be small enough, and for example only the geometrical LITE can also be used for fitting of the ETV curve. On the other hand, when we deal with an outer period of hundreds of days like for BU CMi, where the outer period is only of 121 days (Pribulla et al., 2023), this simplification definitely cannot be used.

Therefore, for the decision on what is the fraction of all doubly eclipsing stars which can be studied in our way, I collected the published systems. This means that only these 2+2 quadruples definitely proved to orbit, where their mutual

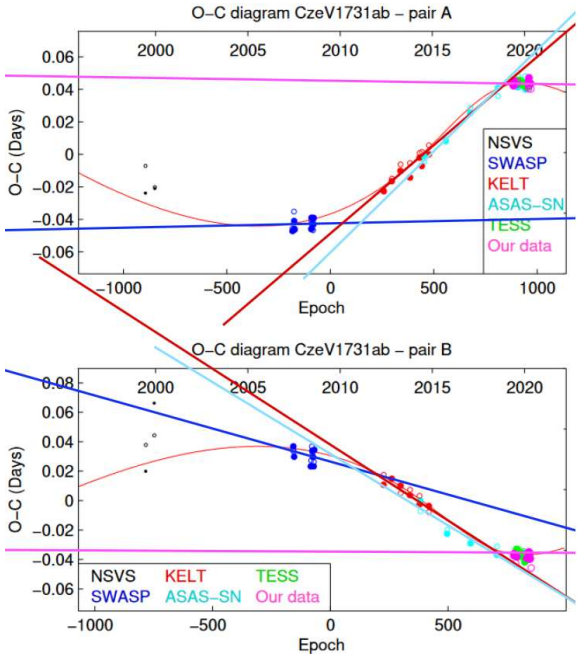


Figure 1. The ETV diagram of both A and B pairs of system CzeV1731. All individual datasets were analysed in some simplified approach with linear ephemerides, which were different for different time epochs.

orbit was derived. Surprisingly, among the known 980 doubly eclipsing systems still only 58 of them were published as bound 2+2 with derived orbits. These mutual-orbit solutions were published in these papers: Zasche & Henzl (2022), Rappaport et al. (2017), Zasche et al. (2022a), Zasche et al. (2024a), Powell et al. (2021), Kostov et al. (2021), Zasche et al. (2019), Pejcha et al. (2022), Rowden et al. (2020), Pribulla et al. (2023), Zasche et al. (2023b), Kostov et al. (2024), Rappaport et al. (2016), Kostov et al. (2023), Zervas et al. (2024), Ádám et al. (2023), Hajdu et al. (2019), Kővári et al. (2024), Zasche et al. (2023a), Borkovits et al. (2018), Zasche et al. (2020), Borkovits et al. (2021), and Zasche et al. (2024b).

As is clearly seen in our figure 2, most of the studied systems by our group are these ones having the outer periods of years or decades. It means those, where their dynamical interaction is in general very small. On the other hand, the group around T.Borkovits using their sophisticated dynamical modelling code sometimes deal with very dynamically interacting systems with much shorter outer periods. From the total 58 systems with derived orbits, only 4 have $P_{AB}/P_A < 100$, and only 6 have $P_{AB}/P_B < 100$.

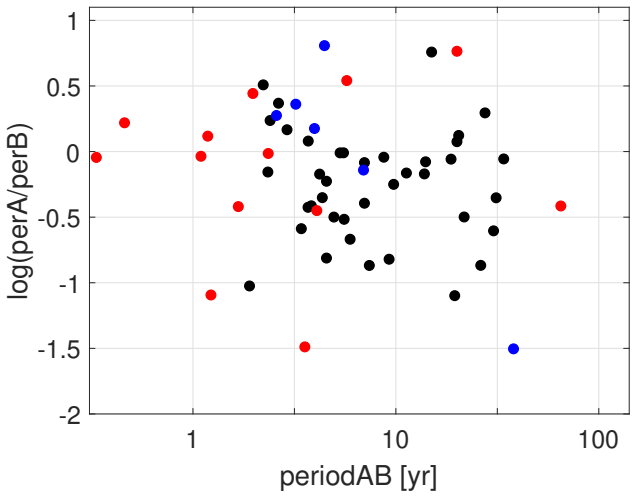


Figure 2. Plot of the doubly eclipsing systems with published outer mutual orbit of both pairs (pair A and pair B around a common barycenter). Distinction according to the author of the study for a particular system: black dots our systems, red dots by T.Borkovits et al., and blue dots by the other authors.

Worth of mentioning is a fact that apart from the number of data points and ratio of periods, there are also some other limitations for using our simplified approach. Cutting the whole interval into smaller pieces is one way, but the constancy of the shape of the light curve in every subset is an important task. The shape of the light curve cannot vary in time (like typical spot modulation for some contact binaries or late-type stars), or we should use multiple light curve templates over the whole time interval. The same applies also for the case where the inclination of either of the binaries is not constant in time. A similar problem should arise when rapid apsidal motion appears, and this effect changes the shape of the light curves when comparing the season-to-season data. Quite challenging would also be these systems, where some rapid ETV changes appear due to very eccentric orbits and the quadruple-star interactions, which can occur also on orbits with longer mutual periods, see e.g. Borkovits et al. (2015).

4. Conclusion

To summarize, I have shown that the simplified method of cutting the whole dataset into smaller pieces and using some assumptions of linear ephemerides is appropriately usable for the majority of known bound doubly eclipsing systems yet. On the other hand, probably the most interesting dynamically interacting quadruples on shorter orbits should be studied with a complete photo-dynamical

approach. And especially these systems (sometimes called as celestial mechanics laboratory) can give us some clue about the true origin of these complicated 2+2 quadruple systems.

Acknowledgements. This research has made use of the SIMBAD and VIZIER databases, operated at CDS, Strasbourg, France, and of NASA Astrophysics Data System Bibliographic Services. The research was partly supported by the project Cooperatio - Physics of Charles University in Prague.

References

Ádám, R. Z., Hajdu, T., Bódi, A., et al., Variable stars in the residual light curves of OGLE-IV eclipsing binaries towards the Galactic Bulge. 2023, *Astronomy and Astrophysics*, **674**, A170, DOI:10.1051/0004-6361/202346006

Borkovits, T., Albrecht, S., Rappaport, S., et al., EPIC 219217635: a doubly eclipsing quadruple system containing an evolved binary. 2018, *Monthly Notices of the RAS*, **478**, 5135, DOI:10.1093/mnras/sty1386

Borkovits, T., Rappaport, S., Hajdu, T., & Sztakovics, J., Eclipse timing variation analyses of eccentric binaries with close tertiaries in the Kepler field. 2015, *Monthly Notices of the RAS*, **448**, 946, DOI:10.1093/mnras/stv015

Borkovits, T., Rappaport, S. A., Maxted, P. F. L., et al., BG Ind: the nearest doubly eclipsing, compact hierarchical quadruple system. 2021, *Monthly Notices of the RAS*, **503**, 3759, DOI:10.1093/mnras/stab621

Hajdu, T., Borkovits, T., Forgács-Dajka, E., et al., Eclipse timing variation analysis of OGLE-IV eclipsing binaries towards the Galactic Bulge - I. Hierarchical triple system candidates. 2019, *Monthly Notices of the RAS*, **485**, 2562, DOI:10.1093/mnras/stz592

Kővári, Z., Strassmeier, K. G., Kriskovics, L., et al., A star under multiple influences. Magnetic activity in V815 Her, a compact 2+2 hierarchical system. 2024, *Astronomy and Astrophysics*, **684**, A94, DOI:10.1051/0004-6361/202348324

Kostov, V. B., Borkovits, T., Rappaport, S. A., et al., TIC 219006972: a compact, coplanar quadruple star system consisting of two eclipsing binaries with an outer period of 168 d. 2023, *Monthly Notices of the RAS*, **522**, 90, DOI:10.1093/mnras/stad941

Kostov, V. B., Powell, B. P., Rappaport, S. A., et al., Ninety-seven Eclipsing Quadruple Star Candidates Discovered in TESS Full-frame Images. 2022, *Astrophysical Journal, Supplement*, **259**, 66, DOI:10.3847/1538-4365/ac5458

Kostov, V. B., Powell, B. P., Rappaport, S. A., et al., 101 eclipsing quadruple star candidates discovered in TESS full frame images. 2024, *Monthly Notices of the RAS*, **527**, 3995, DOI:10.1093/mnras/stad2947

Kostov, V. B., Powell, B. P., Torres, G., et al., TIC 454140642: A Compact, Coplanar, Quadruple-lined Quadruple Star System Consisting of Two Eclipsing Binaries. 2021, *Astrophysical Journal*, **917**, 93, DOI:10.3847/1538-4357/ac04ad

Lee, C. U., Kim, S. L., Lee, J. W., et al., V994 Herculis: the multiple system with a quadruple-lined spectrum and a double eclipsing feature. 2008, *Monthly Notices of the RAS*, **389**, 1630, DOI:10.1111/j.1365-2966.2008.13708.x

Pejcha, O., Cagaš, P., Landri, C., et al., The complex dynamical past and future of double eclipsing binary CzeV343: Misaligned orbits and period resonance. 2022, *Astronomy and Astrophysics*, **667**, A53, DOI:10.1051/0004-6361/202244335

Powell, B. P., Kostov, V. B., Rappaport, S. A., et al., TIC 168789840: A Sextuply Eclipsing Sextuple Star System. 2021, *Astronomical Journal*, **161**, 162, DOI:10.3847/1538-3881/abddb5

Pribulla, T., Borkovits, T., Jayaraman, R., et al., BU Canis Minoris - the most compact known flat doubly eclipsing quadruple system. 2023, *Monthly Notices of the RAS*, **524**, 4220, DOI:10.1093/mnras/stad2015

Rappaport, S., Lehmann, H., Kalomeni, B., et al., A quintuple star system containing two eclipsing binaries. 2016, *Monthly Notices of the RAS*, **462**, 1812, DOI:10.1093/mnras/stw1745

Rappaport, S., Vanderburg, A., Borkovits, T., et al., EPIC 220204960: A Quadruple Star System Containing Two Strongly Interacting Eclipsing Binaries. 2017, *Monthly Notices of the RAS*, **467**, 2160, DOI:10.1093/mnras/stx143

Rowden, P., Borkovits, T., Jenkins, J. M., et al., TIC 278956474: Two Close Binaries in One Young Quadruple System Identified by TESS. 2020, *Astronomical Journal*, **160**, 76, DOI:10.3847/1538-3881/ab9d20

Soszyński, I., Pawlak, M., Pietrukowicz, P., et al., The OGLE Collection of Variable Stars. Over 450 000 Eclipsing and Ellipsoidal Binary Systems Toward the Galactic Bulge. 2016, *Acta Astronomica*, **66**, 405, DOI:10.48550/arXiv.1701.03105

Southworth, J., Eclipsing Binary Stars: the Royal Road to Stellar Astrophysics. 2012, in *Orbital Couples: Pas de Deux in the Solar System and the Milky Way*, ed. F. Arenou & D. Hestroffer, 51–58

Zasche, P., Borkovits, T., Jayaraman, R., et al., V994 Herculis: a unique triply eclipsing sextuple star system. 2023a, *Monthly Notices of the RAS*, **520**, 3127, DOI:10.1093/mnras/stad328

Zasche, P. & Henzl, Z., TIC 452991707 and TIC 452991693 as a Candidate Sextuple System with Three Eclipsing Binaries. 2022, *Acta Astronomica*, **72**, 103, DOI:10.32023/0001-5237/72.2.2

Zasche, P., Henzl, Z., & Kára, J., The first study of four doubly eclipsing systems. 2022a, *Astronomy and Astrophysics*, **659**, A8, DOI:10.1051/0004-6361/202142771

Zasche, P., Henzl, Z., Lehmann, H., et al., CzeV1731: The unique doubly eclipsing quadruple system. 2020, *Astronomy and Astrophysics*, **642**, A63, DOI:10.1051/0004-6361/202038656

Zasche, P., Henzl, Z., & Mašek, M., Multiply eclipsing candidates from the TESS satellite. 2022b, *Astronomy and Astrophysics*, **664**, A96, DOI:10.1051/0004-6361/202243723

Zasche, P., Henzl, Z., Mašek, M., et al., Detection of seven 2+2 doubly eclipsing quadruple systems. 2023b, *Astronomy and Astrophysics*, **675**, A113, DOI:10.1051/0004-6361/202346848

Zasche, P., Henzl, Z., Merc, J., Kára, J., & Kučáková, H., Eight new 2+2 doubly eclipsing quadruple systems detected. 2024a, *Astronomy and Astrophysics*, **687**, A6, DOI:10.1051/0004-6361/202450400

Zasche, P., Henzl, Z., & Wolf, M., Six new eccentric eclipsing systems with a third body. 2024b, *Astronomy and Astrophysics*, **683**, A158, DOI:10.1051/0004-6361/202348501

Zasche, P., Vokrouhlický, D., Wolf, M., et al., Doubly eclipsing systems. 2019, *Astronomy and Astrophysics*, **630**, A128, DOI:10.1051/0004-6361/201936328

Zervas, K., Christopoulou, P.-E., & Papageorgiou, A., Investigating Period Variability Mechanisms in Eclipsing Binary Stars through Eclipsing Time Variation Analysis: A Case Study of TZ Bootis. 2024, *Astrophysical Journal*, **961**, 97, DOI:10.3847/1538-4357/ad096a

Contrib. Astron. Obs. Skalnaté Pleso **55/3**, 263 – 269, (2025)
https://doi.org/10.31577/caosp.2025.55.3.263

Demographics of M dwarf binary exoplanet hosts discovered by TESS

R.A. Matson[1], **R. Gore**[2], **S.B. Howell**[3] **and D.R. Ciardi**[4]

[1] *U.S. Naval Observatory, 3450 Massachusetts Avenue NW, Washington, D.C. 20392, USA (E-mail: rachel.a.matson2.civ@us.navy.mil)*

[2] *Bay Area Environmental Research Institute, Moffett Field, CA 94035, USA*

[3] *NASA Ames Research Center, Moffett Field, CA 94035, USA*

[4] *NASA Exoplanet Science Institute, Caltech/IPAC, 1200 E. California Blvd., Pasadena, CA 91125, USA*

Received: November 27, 2024; Accepted: January 13, 2025

Abstract. M dwarfs have become increasingly important in the detection of exoplanets and the study of Earth-sized planets and their habitability. However, 20-30% of M dwarfs have companions that can impact the formation and evolution of planetary systems. We use high-resolution imaging and Gaia astrometry to detect stellar companions around M dwarf exoplanet hosts discovered by TESS and determine the separation, magnitude difference, and projected separation for each system. We find 47 companions around 216 M dwarfs and a multiplicity rate of 19.4+/-2.7% that is consistent with field M dwarfs. However, the projected separation for close binaries is shifted to larger separations, confirming the lack of close exoplanet host binaries seen in previous studies.

Key words: binary stars – planet hosting stars

1. Introduction

Nearly six thousand exoplanets have been confirmed to date[1], however, only ∼250 are known to be in binary star systems[2]. As most stars form in binaries or multiples (Duchêne & Kraus, 2013) and the presence of a stellar companion is expected to alter planet formation and evolution (e.g., Thebault & Haghighipour, 2015), the discovery and characterization of such systems provides important insight into planet formation and evolutionary processes. In particular, the architectures of planet hosting binary systems can elucidate which mechanisms are most impacted by a companion star.

Observational evidence from both radial velocity (RV) and transit planet surveys indicates planets occur less frequently in binaries with separations $\lesssim$100au, confirming the detrimental effect of a nearby stellar companion (e.g., Hirsch

[1] https://exoplanetarchive.ipac.caltech.edu/

[2] http://exoplanet.eu/planets_binary/

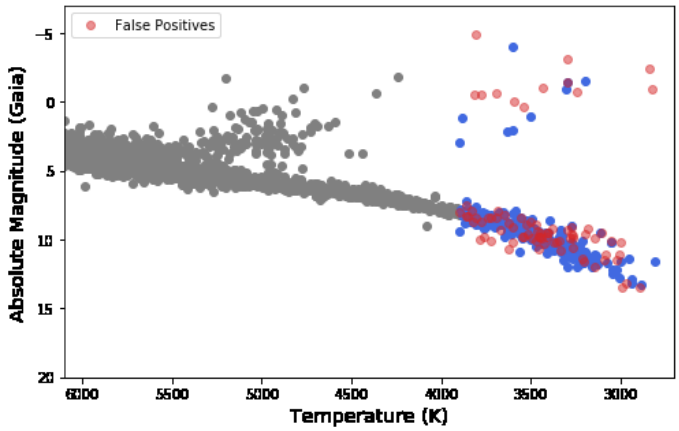


Figure 1. H-R diagram of TESS planet candidate host stars with our sample of M star TOIs shown in blue. We remove false positive and ambiguous TOIs (red dots) and the nine remaining TOIs that appear above the main sequence.

et al., 2021; Kraus et al., 2016). Such studies find fewer close companions around solar-type stars hosting giant planets (e.g., Ngo et al., 2016) and smaller short-period planets (e.g., Lester et al., 2021).

The prevalence of M dwarfs, as well as their low masses, small sizes, and cool temperatures, have made them prime targets for detecting Earth-sized planets and characterizing exoplanet atmospheres. The Transiting Exoplanet Survey Satellite (TESS) mission (Ricker et al., 2015) is focused on detecting exoplanets around nearby bright stars and includes tens of thousands of M dwarfs in its target list. Planets discovered by TESS provide the opportunity to assess the multiplicity of M dwarf exoplanet hosts, as their proximity enables follow-up observations sensitive to companions within a few astronomical units of the host star. Modest samples of TESS M dwarf host stars have shown evidence of fewer close binaries in planet hosting systems (Ziegler et al., 2020; Clark et al., 2022), similar to what has been found for solar-type stars. Here we provide an overview of our investigation of 216 M dwarf TESS Objects of Interest (TOIs) (Matson et al., 2024) to detect stellar companions and investigate the multiplicity of M dwarfs hosting short period transiting planets.

2. Sample & observations

High-resolution images of TOIs are used to detect stars that are not resolved in the TESS Input Catalog (TIC) or with seeing-limited photometry that may mimic or distort the signal of a transiting planet. These observations also allow us to assess the multiplicity of stars hosting transiting planets.

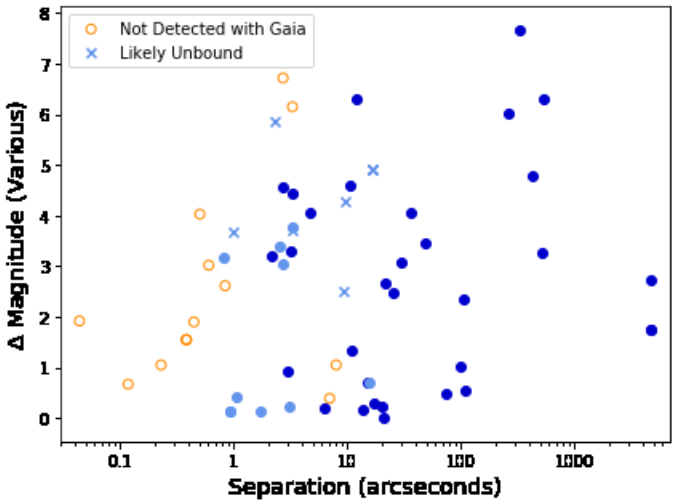


Figure 2. Magnitude difference and separation of companions to M dwarf TOIs. Companions detected with high-resolution imaging and unresolved by Gaia are shown as open circles. CPM companions detected using Gaia DR3 are plotted in blue, with companions also detected with high-resolution imaging shown in light blue. Blue ×'s indicate stars identified with high-resolution imaging that have parallax/proper motion data indicating they are unbound companions.

We selected TOIs with effective temperatures less than 3900 K from the TESS Exoplanet Follow-up Observing Program website (ExoFOP; NExScI, 2022). Targets listed as false positive or ambiguous planet candidates (as of 8 February 2024) were removed from the sample, as were stars with parameters consistent with giants (see Figure 1), resulting in a sample of 221 M dwarfs with confirmed or candidate transiting exoplanets. We then collected high-resolution imaging observations conducted as part of the TESS Follow-up Observing Program by our team and other groups available on ExoFOP.

2.1. High-resolution imaging

Speckle interferometry observations of 148 M dwarf TOIs were taken from 2019−2024 in narrow band filters centered at 562 and 832 nm. Observations were obtained with the 'Alopeke and Zorro speckle cameras on the Gemini 8.1 m North and South telescopes, respectively, and the NESSI speckle camera at the 3.5 m WIYN telescope. Details of the instruments, observing program, and data reduction procedures can be found in Howell et al. (2021, and references therein).

We also observed 85 M dwarf TOIs with near-infrared adaptive optics (AO) imaging using NIRC2 on the Keck-II 10 m telescope and PHARO on the 200 inch

Hale telescope at Palomar Observatory from 2018 – 2022. Both narrow (e.g., Br-γ, J_{cont}) and broad-band filters (e.g., K, H_{cont}) with central wavelengths near 2.2 μm were used depending on the magnitude of the target and the observing conditions. See Schlieder et al. (2021, and references within) for more information regarding the observing program, instruments, and data reduction.

2.2. ExoFOP Observations

High-resolution imaging data for an additional 41 M dwarfs in our sample were available on ExoFOP, including companion detections from the HRCam speckle imager on the SOAR 4.1m telescope (see Ziegler et al., 2020) and the Speckle Polarimeter on the 2.5 m SAI telescope (Safonov et al., 2017). These data increase the number of detected companions and expand the parameter space searched for each TOI due to the different sensitivities of each instrument.

3. Stellar companions

3.1. High-resolution imaging

Eight stellar companions to M dwarf TOIs were detected using speckle observations and twelve companions were detected with AO observations, two of which were also detected by speckle. The high-resolution imaging data extracted from ExoFOP contained an additional ten companions, resulting in a total of 28 companions around 24 TOIs in our sample. The companions have angular resolutions ranging from $0.04-16''$. The TOIs and detected companions were cross-matched with Gaia DR3 (Gaia Collaboration et al., 2023), revealing six pairs with dissimilar proper motions and parallaxes indicating they are not physically bound, which we treat as single stars. Six other companions were not resolved by Gaia or had no parallax and/or proper motion measurements and were assumed to be bound. The magnitude difference as a function of angular separation for the companions detected via high-resolution imaging are shown in Figure 2. Companions also found in Gaia are shown in light blue, with unbound companions marked as $\times$'s, while those unresolved by Gaia are shown as open orange circles.

3.2. Gaia astrometry

We also searched for wide companions to the M dwarf TOIs using Gaia DR3 and code adapted from El-Badry et al. (2021) to identify common proper motion (CPM) pairs. Thirty-eight companions were identified around 35 TOIs, with angular separations of $0.8 - 540''$. Four companions were brighter than the host star, implying the TOI is the secondary component, and removed from our analysis. The magnitude difference and separation of each CPM companion is shown as a blue dot in Figure 2, with companions also detected with high-resolution imaging shown in light blue.

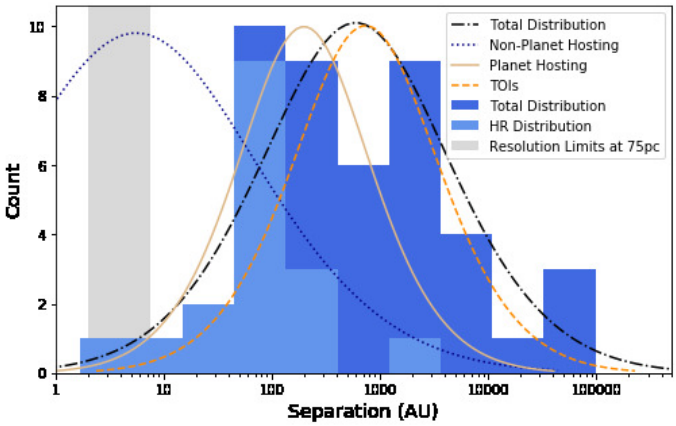


Figure 3. The projected separation distribution of companions detected around M dwarf TOI's, with the high-resolution imaging (HR) subset highlighted in light blue. A Gaussian fit to the data (dot dash line) peaks at $\mu = 596$ au ($\sigma = 11$ au). The separation distributions of non-planet hosting, planet hosting, and TOI M dwarfs from Clark et al. (2024, 2022) are shown for comparison. The gray shaded region depicts the inner angular resolution limits of the various high-resolution imaging techniques used in this study.

4. Results & discussion

Using high-resolution imaging and common proper motions we detect 47 companions around 42 M dwarf TOIs for a stellar multiplicity rate of $19.4 \pm 2.7\%$. These findings are slightly lower than the $\sim 24 \pm 2\%$ multiplicity rates observed for M dwarfs within 25pc (Winters et al., 2019) and 15pc (Clark et al., 2024), but consistent within the uncertainties. Studies of stellar companions to TOIs (e.g., Mugrauer et al., 2023) and confirmed exoplanet hosts (e.g., Michel & Mugrauer, 2024) using Gaia astrometry and close companions from the literature have found similar multiplicity rates of ∼19%. These results indicate short-period planet formation is a routine occurrence in binary stars, as our multiplicity rate generally agrees with field M dwarfs and other planet hosting stars.

To evaluate the separations of stellar companions to transiting exoplanet hosts, we calculate the projected physical separation of each companion from the primary star in astronomical units using the observed angular separation and Gaia distance. The separation distribution, shown in Figure 3, peaks at ∼600 au. This is considerably larger than the peaks in separation seen in other studies of M dwarf binaries, such as Clark et al. (2024), which shows a peak at ∼6 au and includes companions with separations of $0.07 - 300''$ for M dwarfs within 15pc. Although the M dwarfs in our sample are further away, with an average distance of 75 pc, high-resolution imaging allows us to probe down to ∼2 au for two-thirds of our sample. The inner angular resolution limits of all

high-resolution imaging techniques used in this survey are highlighted in gray in Figure 3, which, at a distance of 75pc, span separations of $2 - 7.5$ au. Thus, the shifted peak in our separation distribution can be attributed to fewer close companions in our sample and not our lack of sensitivity to such companions.

Clark et al. (2024) divided their M dwarf sample by stars with and without known planets, determining statistically significant differences in the separation peaks at 198 au and 5.6 au, respectively. The distributions for the non-planet and planet hosting M dwarfs are plotted in Figure 3, as well as the separation distribution for M dwarf TOIs from Clark et al. (2022), which peaks at 735 au. Although our peak separation is larger than the planet hosting sample in Clark et al. (2024), likely due to our broader survey limits, it is generally consistent with the two planet hosting distributions and differs considerably from the non-planet hosting systems. The deficit of close companions observed in exoplanet host systems is therefore clearly seen in our sample of M dwarf TOIs.

References

Clark, C. A., van Belle, G. T., Ciardi, D. R., et al., A Dearth of Close-in Stellar Companions to M-dwarf TESS Objects of Interest. 2022, *Astronomical Journal*, **163**, 232, DOI:10.3847/1538-3881/ac6101

Clark, C. A., van Belle, G. T., Horch, E. P., et al., The POKEMON Speckle Survey of Nearby M Dwarfs. III. The Stellar Multiplicity Rate of M Dwarfs within 15 pc. 2024, *Astronomical Journal*, **167**, 174, DOI:10.3847/1538-3881/ad267d

Duchêne, G. & Kraus, A., Stellar Multiplicity. 2013, *Annual Review of Astron and Astrophys*, **51**, 269, DOI:10.1146/annurev-astro-081710-102602

El-Badry, K., Rix, H.-W., & Heintz, T. M., A million binaries from Gaia eDR3: sample selection and validation of Gaia parallax uncertainties. 2021, *Monthly Notices of the RAS*, **506**, 2269, DOI:10.1093/mnras/stab323

Gaia Collaboration, Vallenari, A., Brown, A. G. A., et al., Gaia Data Release 3. Summary of the content and survey properties. 2023, *Astronomy and Astrophysics*, **674**, A1, DOI:10.1051/0004-6361/202243940

Hirsch, L. A., Rosenthal, L., Fulton, B. J., et al., Understanding the Impacts of Stellar Companions on Planet Formation and Evolution: A Survey of Stellar and Planetary Companions within 25 pc. 2021, *Astronomical Journal*, **161**, 134, DOI:10.3847/1538-3881/abd639

Howell, S. B., Scott, N. J., Matson, R. A., et al., The NASA High-Resolution Speckle Interferometric Imaging Program. 2021, *Frontiers in Astronomy and Space Sciences*, **8**, 10, DOI:10.3389/fspas.2021.635864

Kraus, A. L., Ireland, M. J., Huber, D., Mann, A. W., & Dupuy, T. J., The Impact of Stellar Multiplicity on Planetary Systems. I. The Ruinous Influence

of Close Binary Companions. 2016, *Astronomical Journal*, **152**, 8, DOI:10.3847/0004-6256/152/1/8

Lester, K. V., Matson, R. A., Howell, S. B., et al., Speckle Observations of TESS Exoplanet Host Stars. II. Stellar Companions at 1-1000 au and Implications for Small Planet Detection. 2021, *Astronomical Journal*, **162**, 75, DOI:10.3847/1538-3881/ac0d06

Matson, R. A., Gore, R., Howell, S. B., et al., Demographics of M Dwarf Binary Exoplanet Hosts Discovered by TESS. 2024, *arXiv e-prints*, arXiv:2412.08465, DOI:10.48550/arXiv.2412.08465

Michel, K.-U. & Mugrauer, M., Gaia search for (sub)stellar companions of exoplanet hosts. 2024, *Monthly Notices of the RAS*, **527**, 3183, DOI:10.1093/mnras/stad3196

Mugrauer, M., Rück, J., & Michel, K. U., Gaia search for stellar companions of TESS Objects of Interest IV. 2023, *Astronomische Nachrichten*, **344**, e20230055, DOI:10.1002/asna.20230055

NExScI. 2022, Exoplanet Follow-up Observing Program Web Service, DOI:10.26134/EXOFOP5

Ngo, H., Knutson, H. A., Hinkley, S., et al., Friends of Hot Jupiters. IV. Stellar Companions Beyond 50 au Might Facilitate Giant Planet Formation, but Most are Unlikely to Cause Kozai-Lidov Migration. 2016, *Astrophysical Journal*, **827**, 8, DOI:10.3847/0004-637X/827/1/8

Ricker, G. R., Winn, J. N., Vanderspek, R., et al., Transiting Exoplanet Survey Satellite (TESS). 2015, *Journal of Astronomical Telescopes, Instruments, and Systems*, **1**, 014003, DOI:10.1117/1.JATIS.1.1.014003

Safonov, B. S., Lysenko, P. A., & Dodin, A. V., The speckle polarimeter of the 2.5-m telescope: Design and calibration. 2017, *Astronomy Letters*, **43**, 344, DOI:10.1134/S1063773717050036

Schlieder, J. E., Gonzales, E. J., Ciardi, D. R., et al., Follow-up and Validation of K2 and TESS Planetary Systems with Keck NIRC2 Adaptive Optics Imaging. 2021, *Frontiers in Astronomy and Space Sciences*, **8**, 63, DOI:10.3389/fspas.2021.628396

Thebault, P. & Haghighipour, N., Planet Formation in Binaries. 2015, in *Planetary Exploration and Science: Recent Results and Advances*, ed. S. Jin, N. Haghighipour, & W.-H. Ip, 309–340

Winters, J. G., Henry, T. J., Jao, W.-C., et al., The Solar Neighborhood. XLV. The Stellar Multiplicity Rate of M Dwarfs Within 25 pc. 2019, *Astronomical Journal*, **157**, 216, DOI:10.3847/1538-3881/ab05dc

Ziegler, C., Tokovinin, A., Briceño, C., et al., SOAR TESS Survey. I. Sculpting of TESS Planetary Systems by Stellar Companions. 2020, *Astronomical Journal*, **159**, 19, DOI:10.3847/1538-3881/ab55e9

Contrib. Astron. Obs. Skalnaté Pleso **55/3**, 270 – 279, (2025)
https://doi.org/10.31577/caosp.2025.55.3.270

Spectroscopic and photometric study of a possible multiple system: V684 Mon

E. Kıran[1], **V. Bakış**[2] **and Ö.L. Değirmenci**[3]

[1] *Department of Astronomy and Space Sciences, Faculty of Science, Atatürk University, 25240, Erzurum, Türkiye (E-mail: evrim.kiran@atauni.edu.tr)*

[2] *Department of Space Sciences and Technologies, Faculty of Science, Akdeniz University, 07058, Antalya, Türkiye*

[3] *Department of Astronomy and Space Sciences, Faculty of Science, Ege University, 35100, Bornova - İzmir, Türkiye*

Received: November 15, 2024; Accepted: March 20, 2025

Abstract. Binary and multiple systems (MSs) are important objects since the fundamental physical parameters of those systems allow us to test stellar evolution models. Thanks to increasing satellite observations and advanced technology light measuring instruments in recent years, precise position and light measurements of double star systems can be made. With these highly sensitive data, new multiple systems are found and their natures are examined. In this study, we present spectroscopic and photometric solutions of V684 Mon.

Key words: stars – multiple systems – eclipsing binary systems

1. Introduction

Using precise satellite data, many candidates of binary or multiple systems are being discovered and their properties determined (e.g. Kervella et al. (2022); Gaia Collaboration et al. (2023); Kostov et al. (2024)). Formation and evolution of these systems are also interesting. Jiménez-Esteban et al. (2019) likened the wide multiple systems to mini star clusters with components born at the same time and with the same chemical composition. They indicated that wide multiple systems are excellent candidates for testing stellar models and for age indicators, as the component stars in these systems are separated wide enough to evolve independently. Star cluster and associations are suitable environments for testing the formation and evolution models of binary and MSs. Open star clusters are the most studied objects among stellar groups due to the young and middle-aged stars they contain and the fact that these stars can be in different stages of evolution. Kounkel et al. (2019) emphasized the importance of close binary fraction and properties of young stars, that provides an invaluable insight into the mechanisms behind the formation and evolution of multiples.

V684 Mon (HD 47755, TIC 220314428, GaiaDR3 3326715714242517248) was discovered by Koch et al. (1986) as a binary system with a period of $P =$

$1^d.8514195$ (Kim et al., 2018). The UBV colors of the system are given by Ducati (2002), V684 Mon system is a member of open cluster NGC 2264 (Tarricq et al., 2021). The system was also cataloged as WDS J06406+0947-A in Washington Visual Double Star Catalogue (Mason et al., 2001). WDS J06406+0947B and WDS J06406+0947C were listed as the visual components of V684 Mon, with an angular separation of 21".0 and 26".0 respectively. Apsidal motion of the system was studied by Zasche (2012). Spectroscopic and photometric solutions of V684 Mon were presented by Bradstreet et al. (2007).

2. Photometric and spectroscopic data

V684 Mon was observed by The Transiting Exoplanet Survey Satellite (TESS) (Ricker et al., 2015) in Sector 6 and Sector 33. The QuickLook Pipeline (QLP) light curves (LCs) produced by the MIT QuickLook Pipeline (QLP) (Huang et al., 2020) were used to improve the linear ephemerides and for the LCs solutions. Spectroscopic observations of V684 Mon stars were carried out on Turkish-Russian 150cm telescope (RTT150). TFOSC (TUG Faint Object Spectrograph and Camera) spectrograph with $R = 5099$ was used in the observations. The wavelength range of the obtained spectra is between 3350-9400 Å. Spectroscopic observations were made between January and March 2013. IRAF (Tody, 1986) was used to reduce the obtained spectra and measure of radial velocities (RVs).

3. Analysis

3.1. Improved ephemerides

Times of minimum data of V684 Mon obtained in this study from the TESS observations given in Figure 1 were used to improve the linear ephemerides of the system. The minimum times obtained by using Kwee van Worden method (Kwee & van Woerden, 1956) are shown in Figure 1 and used in the O-C analysis. We applied an unweighted least-squares fit to the primary and secondary eclipse times separately to obtain the following linear light elements in Eq (1) for primary minima:

$$MinI(HJD) = 2444617.789(3) + 1.851419(1) \times E, \quad (1)$$

3.2. Determination of orbital parameters

The RVs of the components were measured from the absorption line of HI (6562.8 Å) element. The wavelength shifts were measured by applying Gaussian fit to the reduced spectra and RVs were calculated. The RVs of V684 Mon system were plotted by using the improved ephemerids given in Eq. 1 and the radial velocity curve (RVC) of the system and O-C of RVs are given in Figure 2. The orbital parameters of the system are listed in Table 1.

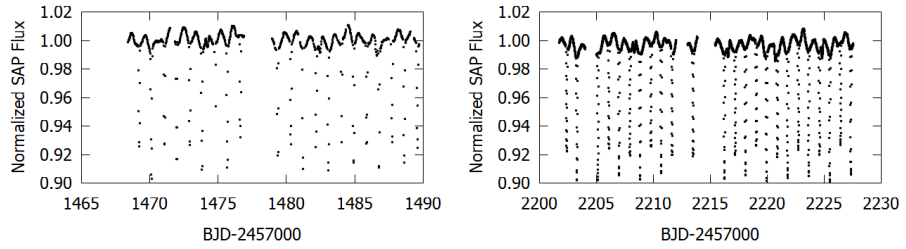


Figure 1. TESS light variation of V684 Mon system from Sector 6 (left) and 33 (right).

Table 1. The orbital parameters obtained from the radial velocity curve solution of V684 Mon.

Parameter	Value
e	0.027 ± 0.040
V_γ (kms^{-1})	6.0 ± 4.0
ω ($^\circ$)	336.9 ± 0.0
K_1 (kms^{-1})	193.2 ± 13.0
K_2 (kms^{-1})	164.3 ± 11.0
$a\sin i$ (R$_\odot$)	12.8 ± 0.4
q	1.19 ± 0.1

3.3. Photometric solutions

The PHOEBE 1 program developed by Prša & Zwitter (2005), which is the implementation of the Wilson-Devinney code (Wilson & Devinney, 1971), was used to analyze photometric data. Ducati (2002) gives the B-V color and V magnitude of the system as $-0^m.13$ and $8^m.44$ respectively. The temperature for V684 Mon was estimated from the given color value by using the relation given by Eker et al. (2020) as $T_{\rm eff}$= 15300K. The orbital parameters of the system given in Table 1 were used as initial parameters for the light curve (LC) solution. The gravitational darkening coefficients $g_{1,2}$ and albedo $A_{1,2}$ for both components with radiative atmosphere are taken as 1.0. van Hamme (1993) tables were used to calculate the edge darkening coefficients of the components. The observed data and the model of the initial solution and the residuals are shown Figure 3.

In Figure 3 (left panel), apart from two dominant eclipses (primary and secondary) eclipse-like light loss stand out. Those light losses are also seen as the dips at 248470, 248474, 248482 together with the pulsation variations in the

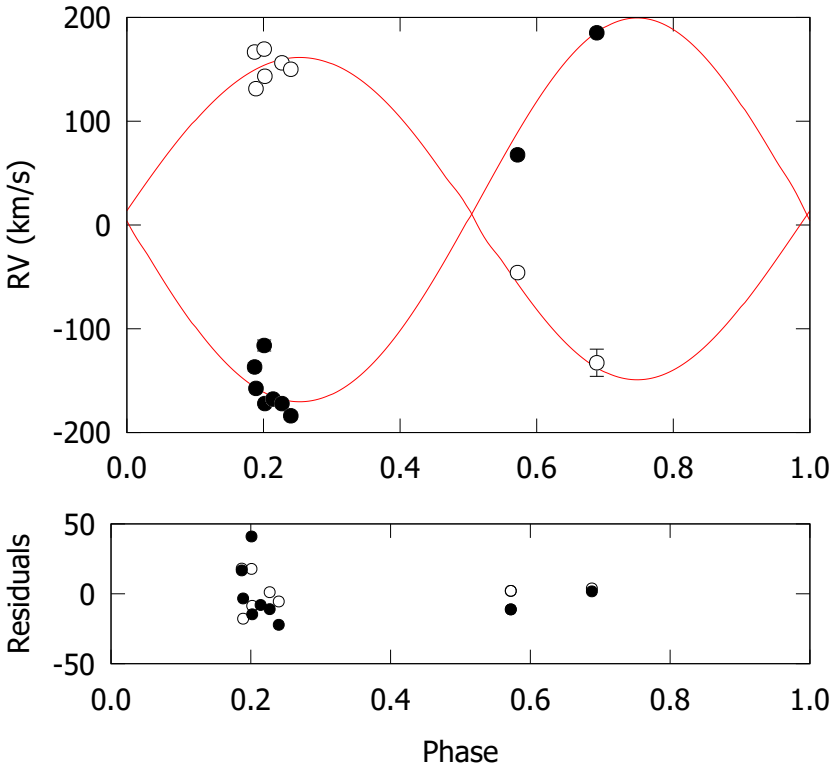


Figure 2. The radial velocities (upper panel) and corresponding residuals (right panel) of V684 Mon. The black filled and empty circles represent the primary and the secondary components, respectively. The red line represents the best-fit theoretical model.

residuals of the LC solution shown in the right panel clearly. LC analysis without removing these light changes from the LC would clearly cause systematic errors. Therefore, it was decided to characterize and remove the out-of-eclipse variations.

We checked for contamination within the TESS aperture from nearby sources. Figure 4 shows a 7x7 pixels TESS cutout centered on the target star. Two field stars are within 2 pixels of the target, WDS J06406+0947-B and C, both contaminating the extracted light curve. WDS J06406+0947-C is cataloged as an eclipsing binary system (V780 Mon) by Avvakumova et al. (2013) and the period of the system was given as 4.12 days by Kearns et al. (1997). However, we checked if there is any contamination within the TESS aperture.

Hence, we also take into account the visual components' WDS J06406+0947-B: is denoted as WDS-B and V780 Mon light contributions to the total light.

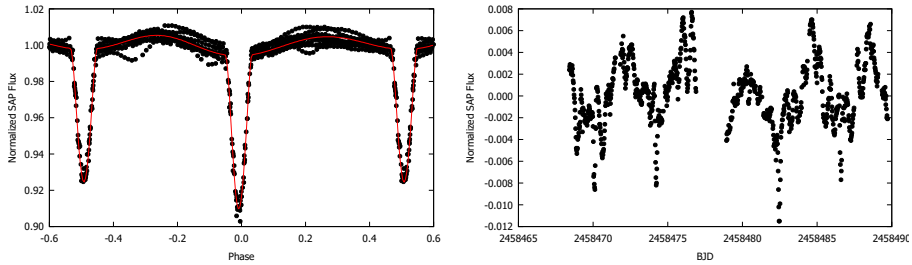


Figure 3. Left panel: TESS lightcurve (black symbols) and corresponding best-fit model (red) for V684 Mon. Right panel: shows the residuals of the solution.

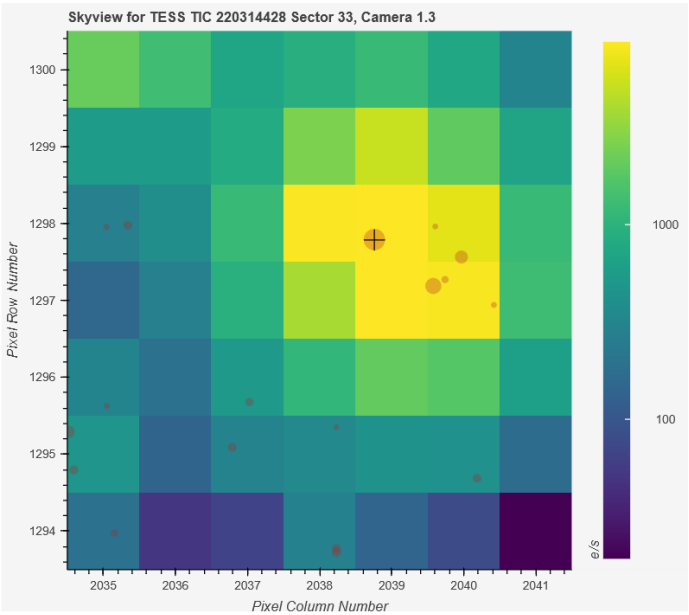


Figure 4. The pixel position of V684 Mon in TESS area.

Moreover, before the LC solutions of the EBs, we need to be sure if the light losses seen as the dips in Fig 3 are caused by one of visual components or not. The light contribution of the visual components, WDS-B and V780 Mon to the total light is approximately 0.15 and 0.04, respectively, according to the magnitudes given by Ducati (2002). The light contribution of the secondary EB system that seen in the TESS LC is about 0.01 (see Figure 3). If we take into account of this contribution and the magnitudes of V684 Mon (Ducati, 2002) and its visual components (Sung et al., 1997), we can assume that V780 Mon can provide such

light loss. The third light contribution was estimated as $l_{\mathrm{V684Mon+WDS-B}}$=0.806 and $l_{\mathrm{WDS-C+V780Mon}}$=0.113 for TESS LC solutions of V780 Mon and V684 Mon systems, individually.

V780 Mon system is listed as a member of relatively young open cluster NGC 2264. The system is considered as a detached with two main sequence star. We estimated the temperature of the system given by (Ducati, 2002) and attributed to the primary component. Assuming a circular orbit, the period was calculated as 4.14725 days by frequency analysis using the Period04 (Lenz & Breger, 2005) program. The LC of the system was analyzed under these assumptions and the results are presented in Table 2 and Figure 5.

Table 2. The PHOEBE solution of V780 Mon.

Parameter	Unit	Value
T_0	(days)	2458473.1839 ± 0.002
P	(days)	4.14725 (fixed)
i	(∘)	71.8 ± 0.2
q		0.2 (fixed)
$\Delta\ T\ (T_1/T_2)$	(K)	2.98 ± 0.07
$\Omega_{1,2}$		$6.39 \pm 0.1,\ 2.47 \pm 0.01$
l_{V780Mona}		0.185
l_{V780Monb}		0.007
$l_{\mathrm{(V684Mon+WDS-B)}}$		0.807 ± 0.001
$r_{1,2}$		$0.162 \pm 0.003,\ 0.193 \pm 0.002$

Table 3. The PHOEBE solution of V684 Mon.

Parameter	Unit	Value
T_0	(days)	$2444617.80476 \pm 0.00005$
P	(days)	1.85142 (fixed)
i	(∘)	76.51 ± 0.01
ω	(∘)	5.883 ± 0.006
$T_{\mathrm{eff}_{1,2}}$	(K)	15300(fixed), 13080 ± 11
$\Omega_{1,2}$		$6.731 \pm 0.003,\ 8.697 \pm 0.005$
$l_{\mathrm{v684\ Mona}}$		0.562
$l_{\mathrm{v684\ Monb}}$		0.311
$l_{\mathrm{(WDS-B+V780\ Mon)}}$		0.127 ± 0.001
$r_{1,2}$		$0.1826 \pm 0.0001,\ 0.1540 \pm 0.0001$

The residuals of the V780 Mon LC solution were analyzed by using the Period04 program. The sinusoidal wave function with different frequency and amplitude values were applied to the residual data. Then, by subtracting the si-

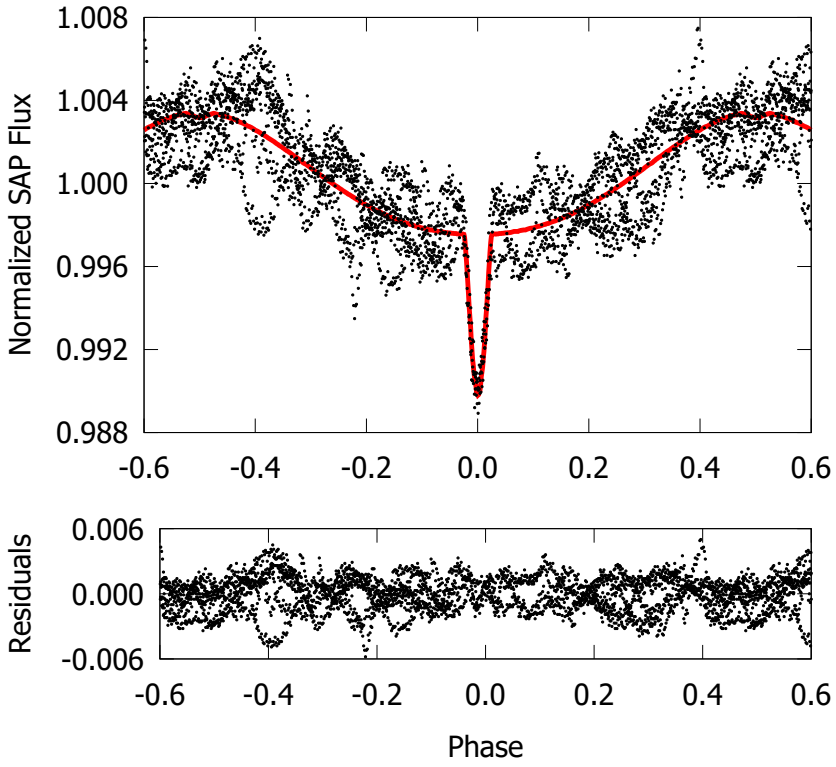


Figure 5. The TESS LC and residuals of the solutions of V780 Mon.

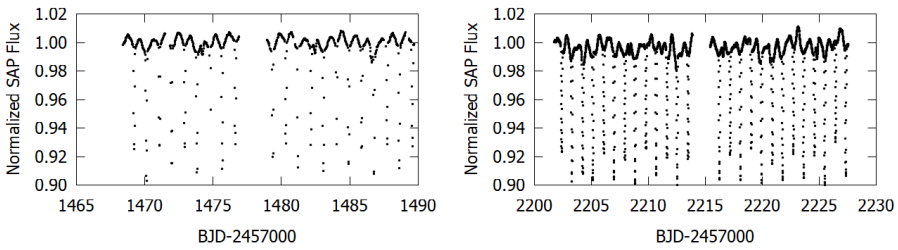


Figure 6. The pulsating-free LC of V684 Mon.

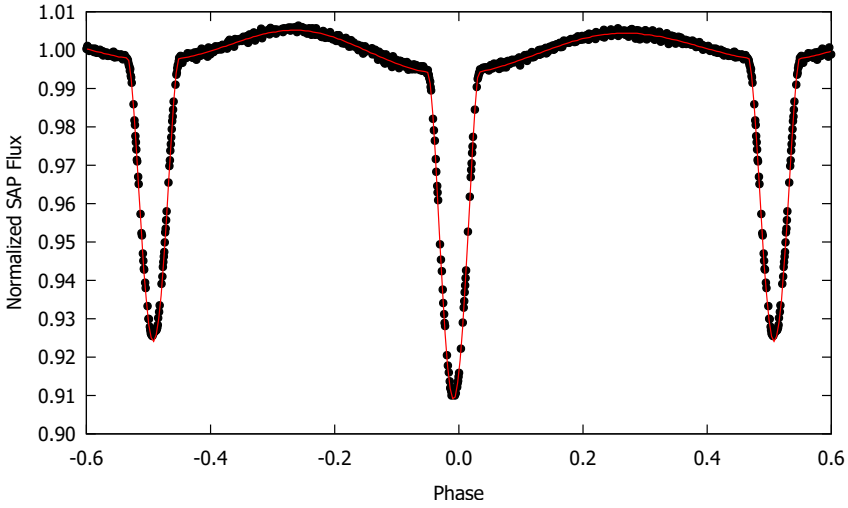


Figure 7. The LC solutions of V684 Mon.

nusoidal wave function from all the observational data (including the minima), a pulsating-free LC was obtained (see Figure 6). Finally, the LC of V684 Mon were analyzed. The results of the photometric solution are presented in Table 3.The fitting of the model of the observed data can be seen in Figure 7.

4. Conclusion

In this study, the spectroscopic and photometric solutions of the known eclipsing binary system V684 Mon system were presented. The photometric and spectroscopic solutions obtained in this study are consistent with those of the literature. We also investigated the photometric variation of V780 Mon which is near the V680 Mon. Although the TESS data are sufficient to roughly estimate the photometric parameters, ground-based spectroscopy is necessary to obtain full astrophysical data of this system. With the new spectroscopic observations that will be made in the future, more precise orbital parameters can be obtained to reach the astrophysical parameters of those systems and the evolution status can be discussed.

Acknowledgements. We thank the referee for her/his valuable comments fro this study. We gratefully acknowledge the support of the Turkish Scientific and Technological Research Council of Türkiye (TÜBİTAK) with the project 118C464. EK was supported with the BİDEP-2218 Post-Doctoral Research Fellowship Program of TÜBİTAK. We thank TÜRKİYE National Observatories, IKI, and KFU for partial support in using RTT150 (Russian Turkish 1.5-m telescope in Antalya) with project

number 13ARTT150-407. This paper includes data collected by the TESS mission which are publicly available from the Mikulski Archive for Space Telescopes (MAST). We acknowledge the use of TESS High-Level Science Products (HLSP) produced by the Quick-Look Pipeline (QLP) at the TESS Science Office at MIT, which are publicly available from the Mikulski Archive for Space Telescopes (MAST). Funding for the TESS mission is provided by NASA's Science Mission directorate. This work has made use of data from the European Space Agency (ESA) mission *Gaia* (https://www.cosmos.esa.int/gaia), processed by the *Gaia* Data Processing and Analysis Consortium (DPAC, https://www.cosmos.esa.int/web/gaia/dpac/consortium). Funding for the DPAC has been provided by national institutions, in particular, the institutions participating in the *Gaia* Multilateral Agreement. In this research, we benefited from the use of the SIMBAD database and the VizieR service operated at CDS, Strasbourg, France; and NASA's Astrophysics Data System Bibliographic Service. So, we tried to organize the conclusion of our study in contemplation of this possibility and without coming to a definitive pronounce on.

References

Avvakumova, E. A., Malkov, O. Y., & Kniazev, A. Y., Eclipsing variables: Catalogue and classification. 2013, *Astronomische Nachrichten*, **334**, 860, DOI:10.1002/asna.201311942

Bradstreet, D. H., Hargis, J. R., Sanders, S. J., & Etzel, P. B., Absolute Parameters for the Very Young, Hot Eclipsing Binary V684 Mon in NGC 2264. 2007, in American Astronomical Society Meeting Abstracts, Vol. **210**, *American Astronomical Society Meeting Abstracts #210*, 03.02

Ducati, J. R. 2002, VizieR Online Data Catalog: Catalogue of Stellar Photometry in Johnson's 11-color system., CDS/ADC Collection of Electronic Catalogues, 2237, 0 (2002)

Gaia Collaboration, Arenou, F., Babusiaux, C., et al., Gaia Data Release 3. Stellar multiplicity, a teaser for the hidden treasure. 2023, *Astronomy and Astrophysics*, **674**, A34, DOI:10.1051/0004-6361/202243782

Huang, C. X., Vanderburg, A., Pál, A., et al., Photometry of 10 Million Stars from the First Two Years of TESS Full Frame Images: Part I. 2020, *Research Notes of the American Astronomical Society*, **4**, 204, DOI:10.3847/2515-5172/abca2e

Jiménez-Esteban, F. M., Solano, E., & Rodrigo, C., A Catalog of Wide Binary and Multiple Systems of Bright Stars from Gaia-DR2 and the Virtual Observatory. 2019, *Astronomical Journal*, **157**, 78, DOI:10.3847/1538-3881/aafacc

Kearns, K. E., Eaton, N. L., Herbst, W., & Mazzurco, C. J., Rotation periods for stars in NGC 2264. 1997, *Astronomical Journal*, **114**, 1098, DOI:10.1086/118540

Kervella, P., Arenou, F., & Thévenin, F., Stellar and substellar companions from Gaia EDR3. Proper-motion anomaly and resolved common proper-motion pairs. 2022, *Astronomy and Astrophysics*, **657**, A7, DOI:10.1051/0004-6361/202142146

Kim, C. H., Kreiner, J. M., Zakrzewski, B., et al., A Comprehensive Catalog of Galactic Eclipsing Binary Stars with Eccentric Orbits Based on Eclipse Timing Diagrams. 2018, *Astrophysical Journal, Supplement*, **235**, 41, DOI:10.3847/1538-4365/aab7ef

Koch, R. H., Bradstreet, D. H., Hrivnak, B. J., Pfeiffer, R. J., & Perry, P. M., HD 47755, a new eclipsing binary. 1986, *Astronomical Journal*, **91**, 590, DOI:10.1086/114041

Kostov, V. B., Powell, B. P., Rappaport, S. A., et al., 101 eclipsing quadruple star candidates discovered in TESS full frame images. 2024, *Monthly Notices of the RAS*, **527**, 3995, DOI:10.1093/mnras/stad2947

Kounkel, M., Covey, K., Moe, M., et al., Close Companions around Young Stars. 2019, *Astronomical Journal*, **157**, 196, DOI:10.3847/1538-3881/ab13b1

Kwee, K. K. & van Woerden, H., A method for computing accurately the epoch of minimum of an eclipsing variable. 1956, *Bulletin Astronomical Institute of the Netherlands*, **12**, 327

Lenz, P. & Breger, M., Period04 User Guide. 2005, *Communications in Asteroseismology*, **146**, 53, DOI:10.1553/cia146s53

Mason, B. D., Wycoff, G. L., Hartkopf, W. I., Douglass, G. G., & Worley, C. E., The 2001 US Naval Observatory Double Star CD-ROM. I. The Washington Double Star Catalog. 2001, *Astronomical Journal*, **122**, 3466, DOI:10.1086/323920

Prša, A. & Zwitter, T., A Computational Guide to Physics of Eclipsing Binaries. I. Demonstrations and Perspectives. 2005, *Astrophysical Journal*, **628**, 426

Ricker, G. R., Winn, J. N., Vanderspek, R., et al., Transiting Exoplanet Survey Satellite (TESS). 2015, *Journal of Astronomical Telescopes, Instruments, and Systems*, **1**, 014003, DOI:10.1117/1.JATIS.1.1.014003

Sung, H., Bessell, M. S., & Lee, S.-W., UBVRI H(alpha) Photometry of the Young Open Cluster NGC 2264. 1997, *Astronomical Journal*, **114**, 2644, DOI:10.1086/118674

Tarricq, Y., Soubiran, C., Casamiquela, L., et al., 3D kinematics and age distribution of the open cluster population. 2021, *Astronomy and Astrophysics*, **647**, A19, DOI:10.1051/0004-6361/202039388

Tody, D., The IRAF Data Reduction and Analysis System. 1986, in Society of Photo-Optical Instrumentation Engineers (SPIE) Conference Series, Vol. **627**, *Instrumentation in astronomy VI*, ed. D. L. Crawford, 733

van Hamme, W., New Limb-Darkening Coefficients for Modeling Binary Star Light Curves. 1993, *Astronomical Journal*, **106**, 2096, DOI:10.1086/116788

Wilson, R. E. & Devinney, E. J., Realization of Accurate Close-Binary Light Curves: Application to MR Cygni. 1971, *Astrophysical Journal*, **166**, 605

Zasche, P., On the Apsidal Motion of Thirteen Eclipsing Binaries. 2012, *Acta Astronomica*, **62**, 97, DOI:10.48550/arXiv.1204.5578

Contrib. Astron. Obs. Skalnaté Pleso **55/3**, 280 – 285, (2025)
https://doi.org/10.31577/caosp.2025.55.3.280

Formation of compact hierarchical triples

A. Moharana[1,2], **K.G. Hełminiak**[1], **T. Pawar**[1] **and G. Pawar**[1]

[1] *Nicolaus Copernicus Astronomical Center, Polish Academy of Sciences, ul. Rabiańska 8, 87-100 Toruń, Poland*

[2] *Astrophysics Group, Keele University, Staffordshire, ST5 5BG, U.K.*

Received: November 15, 2024; Accepted: January 13, 2025

Abstract. Compact hierarchical triples (CHTs) are triple stars where the tertiary is in an orbit of period less than 1000 d. They were thought to be rare but we are discovering more of these systems recently, thanks to space-based missions like TESS, Kepler, and GAIA. In this work, we use orbital parameters obtained from these missions to constrain the formation process of CHTs. We also use spectroscopic and systemic parameters from our work, and the literature to understand the effects of metallicity and dynamics on the formation processes.

Key words: binaries: close – stars: formation

1. Introduction

Around 8% of all Solar-type stars exist in triple systems (Raghavan et al., 2010). This percentage increases are we go towards high-mass stars. This has increased interest in the detection, evolution, and formation of triple stars. New observations from space observatories have led to an exponential increase in the detection of these systems. This also led to the discovery of a new class of these triples, called compact hierarchical triples (CHTs; see Borkovits 2022 for a review). CHTs are triple stars where the tertiary star is in an orbit of period less than 1000 d. This roughly corresponds to an orbit size of less than 5 AU. This compactness can cause dynamical changes which can be monitored over a few years. Therefore, the effect of dynamics in the evolution of these systems can be constrained (Borkovits et al., 2022).

The sizes of CHTs are on the scales of planetary systems. Therefore, they are interesting sites for studying star formation. The current idea of triple star formation is that they form through the process of sequential disk-instability (DI+DI), where the tertiary is formed from disk instabilities in the circumbinary disk around the inner binary (Tokovinin, 2017). This was based on the observations of orbit alignment in triple stars. However, the analysis was done on triples whose semi-major axes were over 10 AU. In this work, we use estimates of orbital parameters of the present sample of CHTs to study the signatures of processes that are involved in the formation and evolution of CHTs.

2. Measurement of CHT parameters

Detecting stellar companions using eclipsing binaries (EBs) also allows us to measure the basic properties of the companion. While in some cases, we can only extract the idea about its orbit and lower mass limits, in some cases we can get all the stellar parameters of the tertiary. While accurate parameters of CHTs can be extracted using triply eclipsing systems, tripled-lined EBs and eclipse depth varying systems, it is extensive in process and therefore limited to a small sample (Moharana et al., 2024). The first large sample of CHTs was reported by Borkovits et al. (2016), where the authors used eclipse timing variations (ETVs) from Kepler EBs[1] to characterise the orbits of 222 triple systems. Out of 222 of these triples, 110 are CHTs. However, only 45 CHTs have robust solutions with observations which cover more than two times the outer orbital period. Following the same methodology, Hajdu et al. (2019) gave us 258 CHTs in the Galactic Bulge, using EBs from OGLE (Soszyński et al., 2016) from which we selected 177 CHTs with robust solutions. The parameters that these studies estimated are the EB orbital period (P_1), tertiary orbital period (P_2), projection of the outer semi-major axis ($a_2 \sin i_2$), tertiary orbital eccentricity (e_2), argument of periastron of the tertiary orbit (ω_2), and the tertiary mass function ($f(m_3)$). Czavalinga et al. (2023) used a different methodology to estimate around 376 CHTs. The Gaia collaboration released a catalogue of DR3 non-single-star orbital solutions (GAIA-NSS; Gaia Collaboration et al. 2023). Czavalinga et al. (2023) crossmatched the targets with EB catalogues from different sky surveys. They found that some systems have periods substantially longer than the EB orbital periods. The GAIA-NSS in most of these cases are likely to belong to outer orbits of tertiary stars in those systems. The parameters resulting from this survey were P_1, P_2, $a_2 \sin i_2$, e_2, and ω_2. The P_1 and P_2 distribution of the sample is presented in Fig.1.

3. Calculation of mass ratios

To get an estimate of the mass ratio, we need to connect the orbital parameters with masses using the tertiary mass function derived from Kepler's law,

$$f(m_3) = \frac{m_3^3 \sin^3 i}{(m_{\rm bin} + m_3)^2} = \frac{P_2 K^3}{2\pi G}(1 - e_2^2)^{3/2} \tag{1}$$

where $m_{\rm bin}$ is the total binary mass, and K is the semi-amplitude of RV signal or ETV signal. Eq.1 can be transformed into a cubic equation of $q_2 = m_C/m_{\rm bin}$ as the variable with the coefficients being functions of f and $m_{\rm bin}$. For the ETV surveys, we have estimates of f. Therefore in such a case, it is easy to numerically solve the following cubic equation, assuming a $m_{\rm bin}$ and $\sin i = 1$

[1] https://keplerebs.villanova.edu/

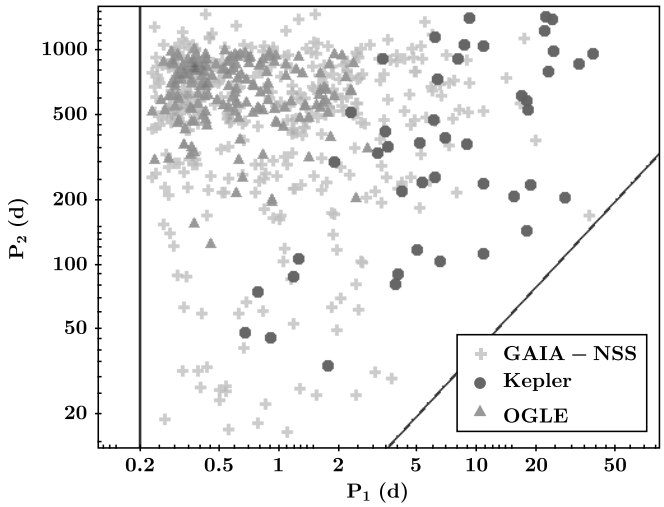


Figure 1. Distribution of orbital periods for the sample of CHTs used in this work. The grey lines mark the stability limits. The horizontal line on the left part of the plot represents the period limit for contact binaries while the slanted line on the right represents the limit for dynamical stability.

for simplicity[2],

$$m_{\rm bin} q_2^3 - f q_2^2 - 2 f q_2 - f = 0 \tag{2}$$

Solving this equation for parameters estimated from Czavalinga et al. (2023) is not straightforward as f is not available. The only unknown in the expression for f is K. For our approximation, we set

$$K = 2\pi a_2 / P_2 \tag{3}$$

where a_2 is available from GAIA-NSS solutions. From Eq.1 and taking $e_2 = 0$ for a simpler calculation, we get,

$$f_{\rm GAIA}(m_3) = \frac{4\pi^2 a_2^3}{G P_2^2} \tag{4}$$

We then estimate"ad-hoc" q_2 distribution from all the surveys, assuming $m_{\rm bin} = 2 M_\odot$. This assumption is based on the approximate idea that most of the known $m_{\rm bin}$ for the sample is spread around 2 $M_\odot$. The distribution was created by dividing the q_2 distribution into bins of size of 0.05. We also created an eccentricity distribution with a bin size of 0.03.

[2]From the current statistics of CHT inclinations (most systems are near co-planar), this approximation gives us a good estimate of the actual mass.

4. Discussion and conclusions

We obtain distributions of eccentricity and tertiary mass ratios of all the CHTs from the large sample surveys, GAIA-NSS, OGLE, and Kepler. we also estimate the individual distributions of each of the surveys. The similarities and dissimilarities of the distributions are discussed in the successive sections.

4.1. Eccentricity distribution of the tertiary orbit

The eccentricity distribution has a specific shape which shows cumulative probabilities of e_2 larger than that expected from a flat distribution (Fig.2). This is consistent with what was reported in Czavalinga et al. (2023) and was also observed in the eccentricity distribution of close binaries (Raghavan et al., 2010). But if we look at the e_2 distribution closely, we see a small variation of trends between the different surveys. Kepler and OGLE distributions tend to go subflat at eccentricities 0.1-0.25. Such a trend was observed for metal-poor CHTs in Moharana et al. (2024). Therefore this points at the Kepler sample being metal-poor. But OGLE also has a distribution similar to GAIA at eccentricities around 0.45-0.55. This could be a sign that OGLE has CHTs with distinct metallicities and not a homogenous metallicity distribution like GAIA.

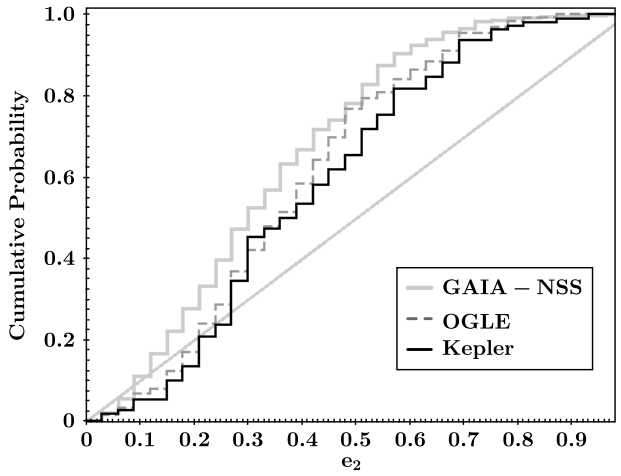


Figure 2. Cumulative probability distribution of e_2 for the sample of CHTs. The sub-samples of GAIA-NSS, OGLE, and Kepler are represented by grey-solid, grey-dashed, and black-solid lines respectively. The slanted grey line represents the expected trend for a flat distribution.

4.2. Bi-modality in mass ratio distribution

One of the expected outcomes of the DI+DI scenario of star formation is that it produces "twins", meaning that the mass ratio of the outer hierarchy to the inner hierarchy is 1. While deviations from 1 are expected, in our distribution we see bimodality, with two peaks at q_2 values smaller than 1 (Fig.3). This bi-modality could be due to bias in observation methodology as GAIA favours large q_2 and OGLE favours small q_2. But this bi-modality was seen in Moharana et al. (2024) where we found that young CHTs have q_2 closer to 1 while old CHTs have low q_2. This hints that the two peaks in our distribution could be due to two populations of different ages. The lower peak between 0.2 and 0.35 is mostly due to the OGLE sample. Therefore, the OGLE sample, which consists of CHTs in the Galactic Bulge, are old CHTs with their age in the order of giga-years.

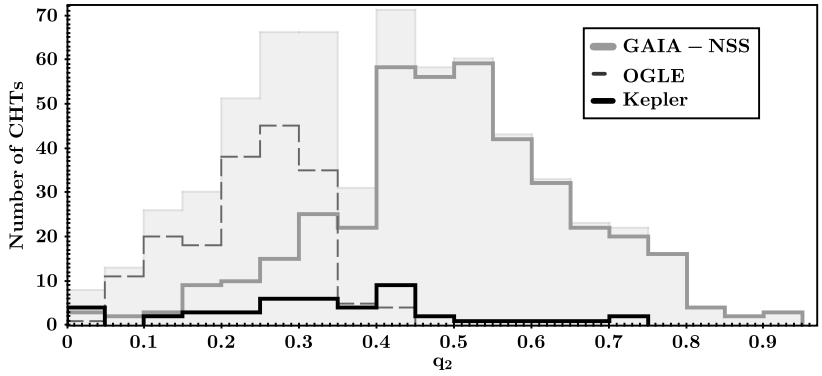


Figure 3. Distribution of q_2 for the large sample of CHTs (shaded histogram). The sub-samples of GAIA-NSS, OGLE, and Kepler are represented by grey-solid, grey–dashed, and black-solid lines respectively.

4.3. Dynamical processes and time evolution of distributions

The distributions of e_2 and q_2 are consistent with the DI+DI formation scenario but there is also a need to account for the additional dynamical processes that exist in CHTs. The shift in q_2 needs strong mechanisms for mass loss which cannot be explained by stellar evolution only. Moharana et al. (2024) proposed mass-loss by tidal dissipation which would also explain the abundance of planar CHTs. But there is also a possibility that the different q_2 are a result of dynamical interactions with the circumbinary accretion disk (CBAD) or complicated fragmentation and accretion in the CBAD (Borkovits et al., 2022). However, we lack a large sample of robust mutual inclination and age estimates to test these scenarios.

This deficiency will surely be improved with the upcoming large-scale missions that will study multiple stars. Further, our calculations are approximate and do not precisely estimate the q_2. This calls for detailed analyses of more CHTs and a better study of parameter distribution.

Acknowledgements. This work is funded by the Polish National Science Centre (NCN) through grant 2021/41/N/ST9/02746. A.M. acknowledges support from the UK Science and Technology Facilities Council (STFC) under grant number ST/Y002563/1. K.G.H. and G.P. acknowledge support from NCN grant 2023/49/B/ST9/01671.

References

Borkovits, T., Eclipsing Binaries in Dynamically Interacting Close, Multiple Systems. 2022, *Galaxies*, **10**, 9, DOI:10.3390/galaxies10010009

Borkovits, T., Hajdu, T., Sztakovics, J., et al., A comprehensive study of the Kepler triples via eclipse timing. 2016, *Monthly Notices of the RAS*, **455**, 4136, DOI:10.1093/mnras/stv2530

Borkovits, T., Rappaport, S. A., Toonen, S., et al., Von Zeipel - Lidov - Kozai cycles in action: Kepler triples with eclipse depth variations: KICs 6964043, 5653126, 5731312, and 8023317. 2022, *Monthly Notices of the RAS*, **515**, 3773, DOI:10.1093/mnras/stac1983

Czavalinga, D. R., Mitnyan, T., Rappaport, S. A., et al., New compact hierarchical triple system candidates identified using Gaia DR3. 2023, *Astronomy and Astrophysics*, **670**, A75, DOI:10.1051/0004-6361/202245300

Gaia Collaboration, Arenou, F., Babusiaux, C., et al., Gaia Data Release 3. Stellar multiplicity, a teaser for the hidden treasure. 2023, *Astronomy and Astrophysics*, **674**, A34, DOI:10.1051/0004-6361/202243782

Hajdu, T., Borkovits, T., Forgács-Dajka, E., et al., Eclipse timing variation analysis of OGLE-IV eclipsing binaries towards the Galactic Bulge - I. Hierarchical triple system candidates. 2019, *Monthly Notices of the RAS*, **485**, 2562, DOI:10.1093/mnras/stz592

Moharana, A., Hełminiak, K. G., Marcadon, F., et al., Spectroscopy of eclipsing compact hierarchical triples: I. Low-mass double-lined and triple-lined systems. 2024, *Astronomy and Astrophysics*, **690**, A153, DOI:10.1051/0004-6361/202450797

Raghavan, D., McAlister, H. A., Henry, T. J., et al., A Survey of Stellar Families: Multiplicity of Solar-type Stars. 2010, *Astrophysical Journal, Supplement*, **190**, 1, DOI:10.1088/0067-0049/190/1/1

Soszyński, I., Pawlak, M., Pietrukowicz, P., et al., The OGLE Collection of Variable Stars. Over 450 000 Eclipsing and Ellipsoidal Binary Systems Toward the Galactic Bulge. 2016, *Acta Astronomica*, **66**, 405, DOI:10.48550/arXiv.1701.03105

Tokovinin, A., Orbit Alignment in Triple Stars. 2017, *Astrophysical Journal*, **844**, 103, DOI:10.3847/1538-4357/aa7746

Contrib. Astron. Obs. Skalnaté Pleso **55/3**, 286 – 294, (2025)
https://doi.org/10.31577/caosp.2025.55.3.286

Orbital analysis of additional bodies around eclipsing binaries HT Vir and MR Del

F. Akar[1], Ö. Baştürk[2,3], E.M. Esmer[2,3,4], E. Sertkan[1], B.Güler[1] and M.B. Bayram[5]

[1] *Ankara University Graduate School of Natural and Applied Sciences, Department of Astronomy and Space Sciences, Ankara, Türkiye (E-mail: frknakar@ankara.edu.tr)*

[2] *Ankara University, Faculty of Science, Department of Astronomy and Space Sciences Ankara, Türkiye*

[3] *Ankara University Astronomy and Spaces Sciences Research & Application Center, Kreiken Observatory, Incek Blvd., Ankara, Türkiye*

[4] *Department of Physics and McDonnell Center for the Space Sciences, Washington University, St. Louis, MO 63130, USA*

[5] *Istanbul University Graduate School of Natural and Applied Sciences, Department of Astronomy and Space Sciences, Vezneciler, Istanbul, Türkiye*

Received: November 15, 2024; Accepted: January 20, 2025

Abstract. We analyze the orbital characteristics of additional bodies suggested to exist around the eclipsing binaries HT Vir and MR Del by utilizing both astrometric and eclipse timing data, with recent timing data primarily from TESS and astrometric data from Gaia. Our analysis shows that the available timing data for HT Vir closely follows the ETV trend induced by the companion suggested by the astrometric solution. For MR Del, we derived an orbital solution indicating a companion with an approximate semi-major axis of 150 AU. We also updated the ETV analysis for MR Del, finding a longer-period variation compared to previous studies.

Key words: binaries: eclipsing – stars: individual (HT Vir, MR Del) – techniques: astrometry – eclipse timing

1. Introduction

The existence and properties of additional bodies around eclipsing binaries have long been a topic of debate, with various techniques proposing the presence of such companions. The combination and analysis of data from different observational techniques allow for a comprehensive parameter set to be derived, providing valuable insights into the orbital dynamics, mass distribution, and evolutionary processes within these systems. By analyzing both eclipse timing variations (ETVs) and astrometric data of two selected eclipsing binaries, we

derive the properties of their companions suggested by these two observational techniques and compare the results.

HT Vir is a contact eclipsing binary system with a visual magnitude of 7.67 and an orbital period of 0.4077 days. It has a visual companion separated by 1.011 arcseconds, which is only 0.4 magnitudes fainter Gaia Collaboration et al. (2023). Zasche & Wolf (2007) combined the astrometric and timing data for HT Vir, deriving the orbital properties of a distant third body in the system, suggesting an astrometric orbit for this companion. Following this, Liao & Qian (2010) analyzed the eclipse timing variations of HT Vir and discovered a cyclic variation with a period of approximately 30 years. However, they noted that this cyclic change could stem from various causes, emphasizing the need for additional minimum timing observations to better understand the underlying mechanisms. Furthermore, Lu et al. (2001) identified the distant companion as a spectroscopic binary, establishing HT Vir as a quadruple system.

MR Del, on the other hand, is a detached eclipsing binary system with an orbital period of 0.5217 days and a visual magnitude of 9.20. The system also features a visual companion separated by only 1.654 arcseconds, as reported in Gaia DR3. Zasche et al. (2009) initially analyzed MR Del's astrometric data to investigate a resolved additional body and derived an orbital period of approximately 1996 years. However, ETV analyses of MR Del have suggested much shorter periodicities than those indicated by the astrometric data. In recent studies, both Özavcı et al. (2020) and Meng et al. (2021) identified a cyclic period variation in MR Del, with an approximate period of 18 years, likely driven by a Light-Time Effect (LiTE) caused by an additional companion.

Within this study, we aim to update the astrometric analyses for both HT Vir and MR Del, while conducting an ETV analysis exclusively for MR Del. Utilizing the latest timing data from TESS and astrometric data from Gaia, this approach provides a refined characterization of the additional bodies around these binary systems, enhancing our understanding of their orbital properties.

2. Data

2.1. Astrometry

We obtained the astrometric data, including epoch, angular separation and position angle and their associated uncertainties, from the Washington Double Star Catalogue, which includes Gaia data (Mason et al., 2001)[1]. We retrieved the parallax values used in the analysis from Gaia DR3.

2.2. Eclipse Timing

We collected the minimum timing data from various sources. For both systems, we retrieved TESS light curves from Mikulski Archive for Space Telescopes

[1] http://www.astro.gsu.edu/wds

(MAST) Portal[2]. We removed outliers and detrended the TESS light curves by dividing the data with second-degree polynomial fits to each half of each sector followed by a normalization to the median-level. We then calculated minima timings using the Xtrema software (Bahar et al., 2015) with the Kwee-van Woerden technique (Kwee & van Woerden, 1956). Additionally, we obtained eclipse timing data from the VarAstro[3], the BAV archive[4], and relevant literature. For MR Del, we conducted additional observations using the T35 telescope with a QSI 660 CCD camera at Ankara University's Kreiken Observatory and the IST40 telescope with a KAF 8300 camera at Istanbul University Observatory, from which we derived minimum timings as well.

Table 1. New timings of minima obtained for MR Del in this study

Eclipse Timing (BJD-TDB)	Error [days]	Type	Filter	Telescope
2460139.405707	0.000041	Primary	R	T35
2460525.456763	0.000057	Primary	V	IST40
2460529.369638	0.000069	Secondary	R	T35

3. Analysis

3.1. Astrometry

For the astrometric analysis, we used the ORBITIZE! code (Blunt et al., 2019) to determine the orbits and properties of the additional companions for both HT Vir and MR Del.

The parallel-tempered Affine-invariant Markov Chain Monte Carlo (MCMC) algorithm (Vousden et al., 2016) was employed in this analysis, producing a posterior distribution of orbital parameters. Some entries in the dataset lacked uncertainty values; to incorporate these entries into the analysis, we assigned the largest error present in the dataset to ensure consistent treatment. To ensure robust analysis, we utilized 100,000 posterior samples, representing plausible orbital configurations consistent with the data. The orbits and derived parameters of these companions are presented below in Figures 1 and 2, with the corresponding orbital parameters, represented as median values along with their uncertainties, listed in Table 2.

[2]https://archive.stsci.edu
[3]https://var.astro.cz
[4]https://www.bav-astro.eu

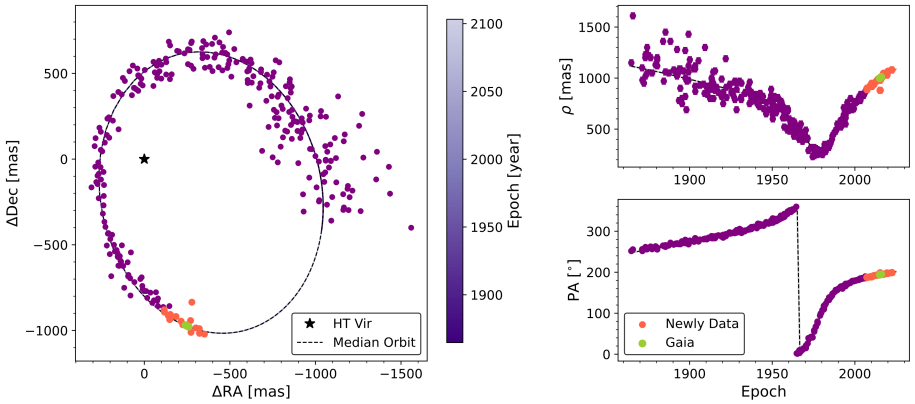


Figure 1. The left panel shows the relative orbit of the companion of HT Vir based on astrometric data, plotted using 1000 randomly selected orbits from the posterior distribution. The dashed black line represents the orbit generated using the median values of the parameters listed in Table 2. The top-right plot shows the angular separation, while the bottom-right plot presents the changes in position angle over time, in conjunction with the orbit. The yellow and orange data points represent new astrometric data added after the most recent astrometric study for this star.

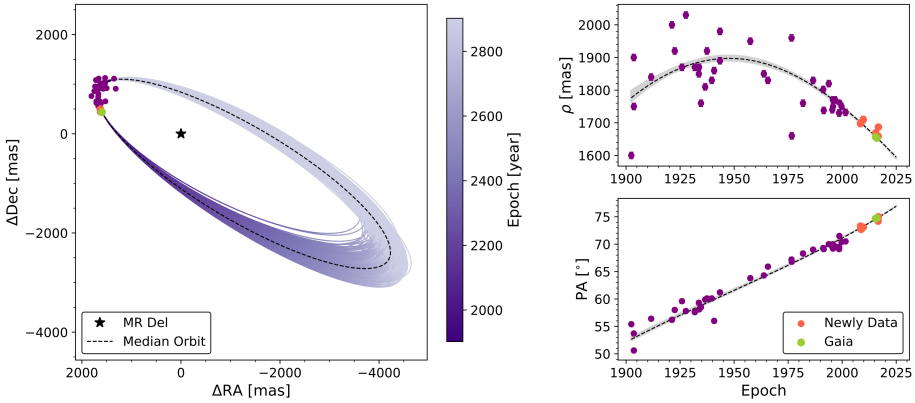


Figure 2. Relative orbit of the companion of MR Del. For a detailed description, see Figure 1.

3.2. Eclipse timing

For MR Del, we modeled the eclipse timing variation using our Python code, employing the affine-invariant MCMC algorithm developed by Foreman-Mackey

Table 2. Orbital Parameters for the visual tertiary components of HT Vir and MR Del.

Parameter	Unit	HT Vir	MR Del
Period	[yr]	238.5028 ± 0.0192	1772.7580 ± 65.1634
Semi-major axis	[AU]	64.4571 ± 0.2441	153.5693 ± 4.4432
Eccentricity	-	0.6200 ± 0.0001	0.4453 ± 0.0172
Inclination	[deg]	48.7555 ± 0.0029	72.1005 ± 0.3778
Argument of Periastron	[deg]	254.1245 ± 0.0046	352.0605 ± 3.9922
Longitude of Nodes	[deg]	176.7337 ± 0.0034	59.9052 ± 0.6592
Parallax	[mas]	15.7849 ± 0.0602	22.1742 ± 0.0230
Total Mass	[$M_\odot$]	4.7079 ± 0.0531	1.1511 ± 0.0403
Epoch of Periastron	[yr]	1976.5155 ± 0.0006	1926.8032 ± 10.1655
RMSE	[mas]	75.47	53.39
χ^2_ν ($\chi^2_{\nu,\mathrm{RA}} + \chi^2_{\nu,\mathrm{Dec}}$)	-	15.59	108.82

et al. (2013). In cases where minima timings lacked uncertainty values, we categorized the observations based on the methods used across the dataset. For each observational method such as pe:photoelectric, ccd: CCD photometry, we calculated an average uncertainty and assigned this value to entries missing error data, using the method-based average to maintain accuracy.

As a result of our analysis, we updated the ephemeris to best represent the O-C diagram, effectively mitigating the linear trend caused by accumulated uncertainties. The updated ephemeris is given by:

$$\text{Min I}(\text{BJD}_{\text{TDB}}) = 2459770.052326(256) + 0.52168927(3) \times E$$

Table 3. Orbital parameters and model fit statistics for MR Del.

Parameter	Unit	Value
P_3	[yr]	32.607 ± 1.115
e_3	–	0.389 ± 0.003
ω_3	[deg]	7.997 ± 0.011
T_0	[BJD_{TDB}]	2465503.752909 ± 557
A	[day]	0.00353 ± 0.00001
$a_{12} \sin i$	[AU]	0.663 ± 0.004
a_3	[AU]	10.750 ± 1.341
$f(M_3)$	[$M_\odot$]	0.00027 ± 0.00003
M_3	[$M_\odot$]	0.083 ± 0.008
Model Fit Statistics		
χ^2_ν	–	13.1757
AIC	–	2161.6425
BIC	–	2183.5931

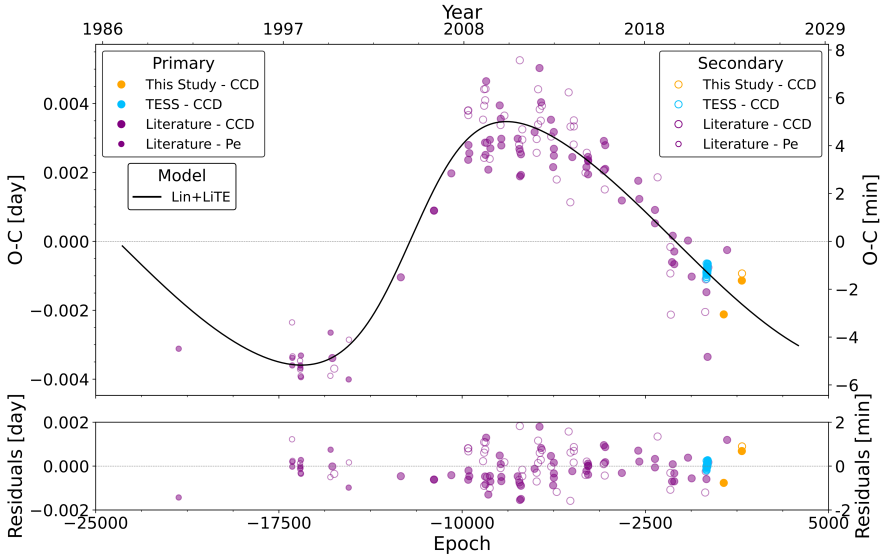


Figure 3. ETV diagram for MR Del.

4. Discussion and conclusion

In this study, we examined the orbital properties of the resolved tertiary bodies gravitationally bound to the eclipsing binary systems HT Vir and MR Del by utilizing both ETV and astrometric data. We focused on understanding how the properties derived from each dataset influence the other, particularly the effects of additional components on the observed eclipse timing variations. These findings contribute to a more refined understanding of the systems' orbital structures and dynamics.

(i) For the HT Vir system, the total mass was estimated to be approximately 4.7 $M_{\odot}$. Given that the combined mass of the binary system is estimated to be $M_{1,2} = 2.3M_{\odot}$, as determined by D'Angelo et al. (2006), the mass of the additional component can be calculated to be around 2.4 $M_{\odot}$. This significantly large mass is expected to cause a significant variation in the ETV diagram. By applying the REBOUND N-body simulation code (Rein & Liu, 2012) and using the orbital parameters derived for the additional component, we calculated the corresponding ETV variation. To align the observed minima timings of HT Vir with the expected ETV trend induced by this component, a slight linear correction was applied. This manual adjustment, not based on a fit, yielded $T_0 = 2448760.66470$ and $P = 0.407673$. The corrected minima timings closely followed the ETV trend caused by the additional component, highlighting its influence on the system's timing behavior.

Furthermore, the relatively large amplitude periodic variation observed in HT Vir can be partially explained by the presence of this additional componaion. However, recent observations suggest that the remaining variation does not follow the cyclic trend and might instead be linked to magnetic activity, as suggested by the O'Connell effect observed in the light curves of the systems and its F8 spectral type.

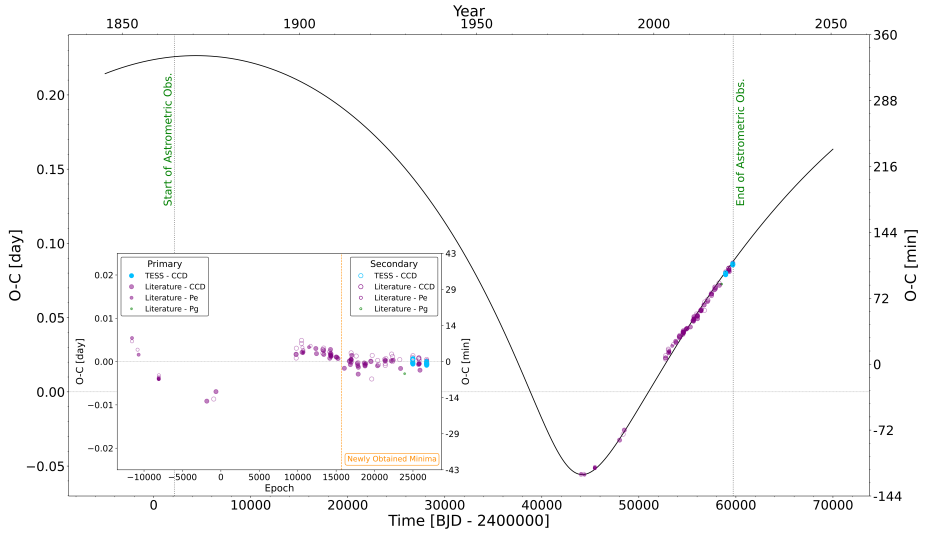


Figure 4. ETV analysis of HT Vir based on its astrometric solution. The figure shows the astrometric orbit of the companion and its corresponding ETV. The inset graph represents the O-C diagram for HT Vir itself. This diagram was generated using the ephemeris: Min I$(\mathrm{BJD_{TDB}}) = 2448760.673345(264) + 0.40767253(1) \times E$.

(ii) For the MR Del system, the astrometric analysis revealed an orbital period of approximately 1800 years for the additional companion. Such a long period suggests that this component's effect on the ETV diagram should manifest itself as a nearly linear trend, rather than the pronounced variation observed in HT Vir. Observations from both ground-based and space-borne telescopes, combined with recent data, have extended the period of the detected ETV variation, resulting in a longer-period signal compared to previous studies. Moreover, the high eccentricity of the orbit makes alternative explanations, such as magnetic activity-induced changes less likely, further supporting the presence of a long-period companion whose influence on MR Del's timing data can now be seen more clearly. The derived mass of the third body is close to the boundary between a star and a brown dwarf, indicating a significant influence on the ETV pattern and reinforcing its role in the system's dynamical evolution.

In addition, the ETV solution suggests the presence of an additional component that is likely closer to the binary system than the visually detected companion. This raises the possibility that the MR Del system could be a hierarchical quadruple system. However, to confirm this hierarchical configuration with certainty, ETV data covering at least two full cycles would be required. Based on the currently available data, it is challenging to draw definitive conclusions about the system's architecture.

These analyses highlight how ETV and astrometric studies can together reveal the presence and characteristics of additional bodies in binary systems, even when these bodies have orbital periods extending beyond typical observational baselines. Future observations, especially long-term timing data, are essential to refine these orbital solutions and deepen our understanding of the complex dynamical interactions within such systems.

Acknowledgements. We thank TÜBİTAK for their support with the 1001 grant for our project 122F358. We also thank the Council of Higher Education in Türkiye (YÖK) for their support with the ADEP projects carried out in Ankara University (FBA-2023-2698) and in Istanbul University (FBA-2022-39121). We also thank Ankara University Astronomy and Space Sciences Research and Application Center (Kreiken Observatory) and Istanbul University Observatory Application and Research Center for the observation time for the specified target. This research has made use of the Washington Double Star Catalog maintained at the U.S. Naval Observatory. This work has made use of data from the European Space Agency (ESA) mission *Gaia* (https://www.cosmos.esa.int/gaia), processed by the *Gaia* Data Processing and Analysis Consortium (DPAC, https://www.cosmos.esa.int/web/gaia/dpac/consortium). Funding for the DPAC has been provided by national institutions, in particular the institutions participating in the *Gaia* Multilateral Agreement. This paper includes data collected by the TESS mission. Funding for the TESS mission is provided by NASA's Science Mission Directorate.

References

Bahar, E., Šenavcı, H. V., & Başţürk, Ö., A Python-based GUI Software to Calculate Times of Maximum and Minimum: Xtrema. 2015, in Astronomical Society of the Pacific Conference Series, Vol. **496**, *Living Together: Planets, Host Stars and Binaries*, ed. S. M. Rucinski, G. Torres, & M. Zejda, 288

Blunt, S. C., Wang, J. J., Angelo, I., et al., orbitize!: A comprehensive code for orbit fitting of direct imaging and radial velocity data. 2019, *The Astronomical Journal*, **158**, 181, DOI:10.3847/1538-3881/ab3b47

D'Angelo, C., van Kerkwijk, M. H., & Rucinski, S. M., Contact Binaries with Additional Components. II. A Spectroscopic Search for Faint Tertiaries. 2006, *Astronomical Journal*, **132**, 650, DOI:10.1086/505265

Foreman-Mackey, D., Hogg, D. W., Lang, D., & Goodman, J., emcee: The MCMC Hammer. 2013, *Publications of the ASP*, **125**, 306, DOI:10.1086/670067

Gaia Collaboration, Vallenari, A., Brown, A. G. A., et al., Gaia Data Release 3. Summary of the content and survey properties. 2023, *Astronomy and Astrophysics*, **674**, A1, DOI:10.1051/0004-6361/202243940

Kwee, K. K. & van Woerden, H., A method for computing accurately the epoch of minimum of an eclipsing variable. 1956, *Bulletin Astronomical Institute of the Netherlands*, **12**, 327

Liao, W.-P. & Qian, S.-B., Detection of a Cyclic Period Change in the W UMa-Type System HT Virginis. 2010, *PASJ*, **62**, 521, DOI:10.1093/pasj/62.3.521

Lu, W., Rucinski, S. M., & Ogłoza, W., Radial Velocity Studies of Close Binary Stars. IV. 2001, *Astronomical Journal*, **122**, 402, DOI:10.1086/321131

Mason, B. D., Wycoff, G. L., Hartkopf, W. I., Douglass, G. G., & Worley, C. E., The 2001 US Naval Observatory Double Star CD-ROM. I. The Washington Double Star Catalog. 2001, *Astronomical Journal*, **122**, 3466, DOI:10.1086/323920

Meng, G., Zhang, L.-y., Han, X. L., et al., Photometric studies of five eclipsing binaries: RS Ser, V0449 Per, MR Del, V593 Cen, and V1095 Her. 2021, *MNRAS*, **503**, 324, DOI:10.1093/mnras/stab410

Özavcı, İ., Özuyar, D., Şenavcı, H. V., et al., Orbital Period Analysis of Four Eclipsing Binaries XY Boo, RW Com, MR Del and AK Her. 2020, *Acta Astronomica*, **70**, 33, DOI:10.32023/0001-5237/70.1.3

Rein, H. & Liu, S. F., REBOUND: an open-source multi-purpose N-body code for collisional dynamics. 2012, *Astronomy and Astrophysics*, **537**, A128, DOI:10.1051/0004-6361/201118085

Vousden, W. D., Farr, W. M., & Mandel, I., Dynamic temperature selection for parallel tempering in Markov chain Monte Carlo simulations. 2016, *Monthly Notices of the RAS*, **455**, 1919, DOI:10.1093/mnras/stv2422

Zasche, P. & Wolf, M., Combining astrometry with the light-time effect: The case of VW Cep, ζ Phe and HT Vir. 2007, *Astronomische Nachrichten*, **328**, 928, DOI:10.1002/asna.200710828

Zasche, P., Wolf, M., Hartkopf, W. I., et al., A Catalog of Visual Double and Multiple Stars With Eclipsing Components. 2009, *AJ*, **138**, 664, DOI:10.1088/0004-6256/138/2/664

Contrib. Astron. Obs. Skalnaté Pleso **55/3**, 295 – 300, (2025)
https://doi.org/10.31577/caosp.2025.55.3.295

Discovery of a third body around semi-detached binary V527 Dra through eclipse timing and radial velocity variations

H.V. Şenavcı[1,2], D. Bohlender[3], E. Bahar[1,2], S. Gu[4], İ. Özavcı[1,2], M. Yılmaz[1,2], E.B. Yorulmaz[1,2], O. Latković[5] and A. Čeki[5]

[1] *Ankara University, Faculty of Science, Astronomy & Space Sciences Department, Tandoğan, TR-06100, Ankara, Türkiye (E-mail: hvsenavci@ankara.edu.tr)*

[2] *Ankara University, Astronomy and Space Sciences Research and Application Center (Kreiken Observatory), İncek Blvd., TR-06837, Ahlatlıbel, Ankara, Türkiye*

[3] *Canadian Astronomy Data Centre & Dominion Astrophysical Observatory, Herzberg Astronomy and Astrophysics Research Centre, National Research Council of Canada 5071 West Saanich Road, Victoria, BC V9E 2E7, Canada*

[4] *Yunnan Observatories, Chinese Academy of Sciences, Kunming 650216, People's Republic of China*

[5] *Astronomical Observatory, Volgina 7, 11000 Belgrade, Serbia*

Received: October 2, 2024; Accepted: January 2, 2025

Abstract. The mid-eclipse times obtained using TESS data for the semi-detached binary V527 Dra show cyclic variations attributed to the presence of an additional body. Additionally, the broadening profiles (BFs) of V527 Dra, obtained from spectroscopic data gathered between 2020 and 2024, reveal a third peak with varying radial velocities over time, further indicating the presence of a third body. Therefore, in this study, using the radial velocity variations of the third component and the eclipse timing variations from the TESS data, we were able to constrain the orbital parameters of the third component.

Key words: Stars: individual: V527 Dra – (Stars:) binaries (including multiple): close – Techniques: radial velocities

1. Introduction & motivation

For eclipsing binaries, the continuous and high-precision observations gathered using space telescopes provide valuable insights into long-term phenomena like magnetic activity and hierarchical multiple star systems, often identified through eclipse timing variations (ETV) (see Kirk et al., 2016; Prša et al., 2022).

In a recent study by Čeki et al. (2024), we conducted a comprehensive analysis of the semi-detached eclipsing binary V527 Dra, utilizing both ground and space-based photometric data, as well as radial velocity measurements (see Čeki et al., 2024, for details). During the determination of radial velocities using the broadening function (BF) technique (Rucinski, 1999, 2002, 2004), we realized the presence of third peaks in the BFs, in addition to the broadening profiles of both components of V527 Dra. Furthermore, those peaks have different velocities in the 2020 and 2021 data as seen from Figure 1.

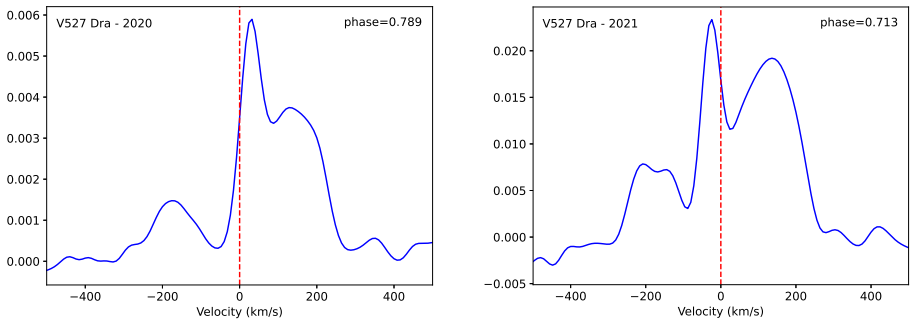


Figure 1. Example BFs of V527 Dra from 2020 and 2021 dataset. The red dashed lines show the velocity of 0 km s^{-1}. Figures are taken from Čeki et al. (2024).

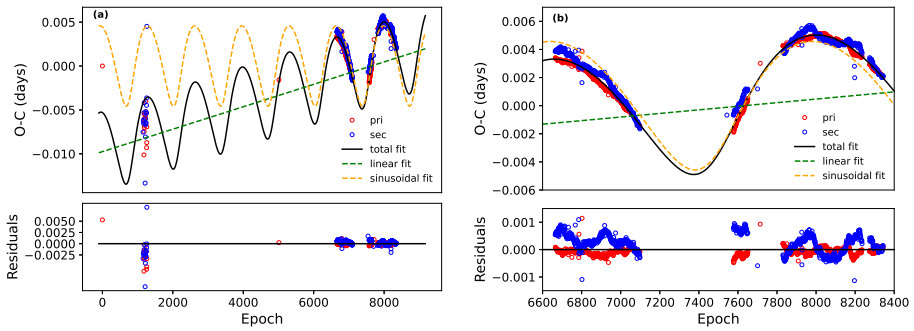


Figure 2. (a) The complete ETV diagram of V527 Dra, constructed using all available eclipse times, along with model fits incorporating the light-time effect (LiTE) and a linear trend. (b) A zoomed-in view focusing solely on the TESS data. Residuals are displayed below each plot. Figures are taken from Čeki et al. (2024).

In the same study by Čeki et al. (2024), we also investigated the eclipse timing variations (ETV) of V527 Dra, where the most of the mid eclipse times

were calculated from the TESS data. The overall ETV of the system exhibits a cyclic variation superimposed on a linear trend (see Figure 2). Under the Light-Time-Effect (LiTE) approximation and using the equations from Irwin (1952), the best-fitting LiTE model yielded a third body with a mass of $M_3 = 0.999 \pm 0.031\ M_\odot$ and with a period of $P_3 = 2.733 \pm 0.005$ yr, assuming that the third body's orbit is co-planar with the binary orbit. We explored whether an additional body with a mass of $0.999\ M_\odot$, as obtained from the ETV analysis, could be responsible for the observed third peak in the BFs of V527 Dra, which is the motivation of this study. A similar investigation already was conducted by our working group (see Čeki et al., 2024, for details) using two spectral dataset from 2020 and 2021, revealing that the RVs of the third peak are in fair agreement with the RV variation generated using the parameters obtained from the ETV analysis. In this study, we reinforce this agreement with the additional spectral data of the system.

2. New spectroscopic observations and RV determination

To investigate further whether this additional contribution originates from a physically bound component to the V527 Dra binary, we collected more spectroscopic data of the system at the Lijiang Observatory and the Dominion Astrophysical Observatory (DAO). The spectroscpic observations at the Lijiang Observatory were conducted using the YFOSC instrument mounted on the 2.4m Lijiang Telescope, with the resolution of R∼10000 and an exposure time of 450 seconds on April 21^{st}. The remaining spectroscpic data were obtained using the Cassegrain spectrograph attached to the 1.83 m Plaskett Telescope, offering a resolution of R∼15000 and an exposure time of 1800 seconds during the May - September observing season. HD 184499 (G0V) was also observed as the RV standard throughout the entire observing run. The data reduction was performed using the standard IRAF packages. Radial velocity measurements were obtained by fitting a sum of Gaussian profiles to the observed peaks in the BFs, specifically using a sum of three Gaussians. The optimal values for each Gaussian profile's parameters, including amplitude, width, and peak center, were determined through an optimization process. Two examples of fitted Gaussian profiles are shown in Figure 3.

3. Results and Discussion

Using Eqn. 1, we first determined the radial velocity variation of the additional body using the parameters obtained from the ETV analysis (see Čeki et al., 2024, for details), within the timespan covering the entire dataset. Figure 4 shows the radial velocities calculated from all observations, along with the radial velocity variation for the additional body (red dashed line). The results clearly

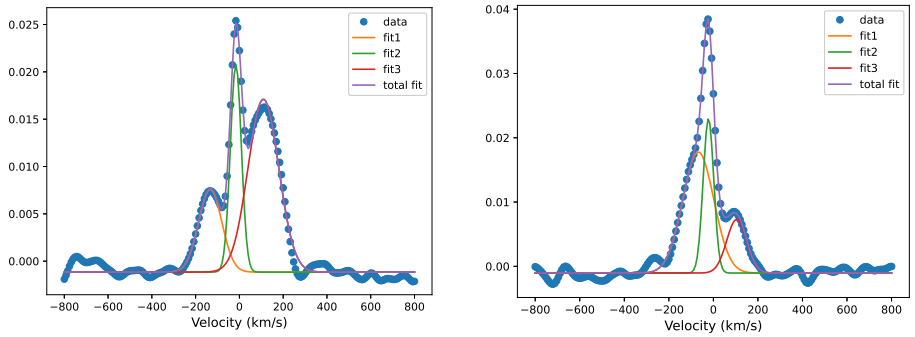


Figure 3. Two examples of Three-Gaussian profile fitting via an optimization process to the observed peaks in the BFs to determine the RVs of the components of V527 Dra.

indicate that the observed RV of the third component aligns well with the theoretical RV variation derived from the ETV analysis.

$$Vrad = \frac{2\pi a_3 \sin i_3}{P(1-e^2)^{1/2}}[\cos(\nu+\omega_3) + e\cos\omega_3] + V_{\gamma_3} \tag{1}$$

The radial velocity variation of the additional component (Eqn. 1) allows us to constrain $a_3 \sin i_3$ and V_{γ_3} parameters. In addition, since we determined $a_{12}sini_3$ and mass function $f(M_3)$ from the ETV analysis, and $M_{1,2}$ from the light and radial velocity curve analyses (Čeki et al., 2024), we were able to constrain M_3 and the orbital inclination of the third body i_3 using the equations below through an optimization process:

$$\frac{a_{12}\sin i_3}{a_3 \sin i_3} = \frac{M_3}{M_1+M_2}, f(M_3) = \frac{(M_3 \sin i_3)^3}{(M_1+M_2+M_3)^2} \tag{2}$$

Consequently the best-fitting RV variation, which is plottes as blue solid line in Figure 4, yielded the parameters $a_3 sini_3 = 1.875 \pm 0.222 AU$, $M_3 = 1.18 \pm 0.11 M_\odot$, $i_3 = 60.1 \pm 2.0°$ and $V_{\gamma_3} = -0.867 \pm 0.017$km/s.

From the simultaneous TESS, SDSS g',r' and i' light and velocity curve analysis of the system, Čeki et al. (2024) estimated the average third light contribution as $\ell_3$avg = 0.337. To calculate the amount of third light of the additional body with the mass of $M_3 = 1.18 M_\odot$ that we obtained from the RV variation, we used the mass-luminosity ($1.15\mathrm{M}^{3.36}$) and mass-radius ($\log R = 0.026 + 0.945 \log M$) relations given by Demircan & Kahraman (1991) and calculated the luminosity and the radius of the tertiary component to be $L_3 = 2.01 L_\odot$ and $R_3 = 1.24 R_\odot$, respectively. The third light is defined in terms of total flux in the given passband at maximum light as $\ell_3 = F_3 \ / \ (F_1+F_2+F_3)$ and the luminosity $L = 4\pi R^2 F$, where R is the radius of star and F is the bolometric

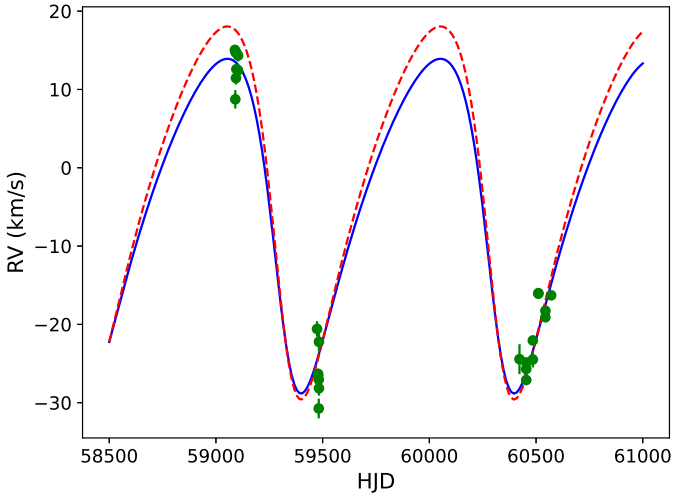


Figure 4. RV variation of the third body, of which the parameters were calculated from the ETV analysis, assuming a coplanar orbit with the binary system (red dashed lines). Green dots represent radial velocities of the third body derived from BFs. The blue solid line shows the RV variation of the third body after adjusting asini3 of the third body and systemic velocity of the triple system.

flux. Neglecting the difference between bolometric and passband-specific flux as well as the limb darkening and the gravity darkening, we could roughly obtain the third light (ℓ_3) via Eqn. 3 given below:

$$l_3 = \frac{L_3/R_3^2}{L_1/R_1^2 + L_2/R_2^2 + L_3/R_3^2} \tag{3}$$

The resulting light contribution of the tertiary component is $\ell_3 = 0.299$, which is quite consistent with the value obtained through the light curve analysis by Čeki et al. (2024).

Observing the radial velocity of the additional component combined with the parameters obtained from the ETV analysis offers a unique opportunity to determine the orbital parameters and the mass of the additional component more accurately. With further spectroscopic observations of V527 Dra, the orbital parameters of the additional body can be determined with greater precision, and the systemic velocity of the binary can be measured to confirm the physical connection.

Acknowledgements. Based on observations obtained at the Dominion Astrophysical Observatory, Herzberg Astronomy and Astrophysics Research Centre, National Research Council of Canada.

References

Demircan, O. & Kahraman, G., Stellar Mass / Luminosity and Mass / Radius Relations. 1991, *Astrophysics and Space Science*, **181**, 313, DOI:10.1007/BF00639097

Irwin, J. B., The Determination of a Light-Time Orbit. 1952, *ApJ*, **116**, 211, DOI:10.1086/145604

Kirk, B., Conroy, K., Prša, A., et al., Kepler Eclipsing Binary Stars. VII. The Catalog of Eclipsing Binaries Found in the Entire Kepler Data Set. 2016, *Astronomical Journal*, **151**, 68, DOI:10.3847/0004-6256/151/3/68

Prša, A., Kochoska, A., Conroy, K. E., et al., TESS Eclipsing Binary Stars. I. Short-cadence Observations of 4584 Eclipsing Binaries in Sectors 1-26. 2022, *Astrophysical Journal, Supplement*, **258**, 16, DOI:10.3847/1538-4365/ac324a

Rucinski, S., Determination of Broadening Functions Using the Singular-Value Decomposition (SVD) Technique. 1999, in Astronomical Society of the Pacific Conference Series, Vol. **185**, *IAU Colloq. 170: Precise Stellar Radial Velocities*, ed. J. B. Hearnshaw & C. D. Scarfe, 82

Rucinski, S. M., Radial Velocity Studies of Close Binary Stars. VII. Methods and Uncertainties. 2002, *Astronomical Journal*, **124**, 1746, DOI:10.1086/342342

Rucinski, S. M., Advantages of the Broadening Function (BF) over the Cross-Correlation Function (CCF). 2004, in American Astronomical Society Meeting Abstracts, Vol. **215**, *Stellar Rotation*, ed. A. Maeder & P. Eenens, 17

Čeki, A., Şenavcı, H. V., Latković, O., et al., Comprehensive analysis of the eclipsing binaries V527 Dra and V2846 Cyg. 2024, *Monthly Notices of the RAS*, **532**, 3582, DOI:10.1093/mnras/stae1709

Contrib. Astron. Obs. Skalnaté Pleso **55/3**, 301 – 306, (2025)
https://doi.org/10.31577/caosp.2025.55.3.301

A catalog of exoplanets around post-common envelope eclipsing binaries: CuPS-ETV

E. Sertkan[1], Ö. Baştürk[2,3], E.M. Esmer[2,3,4], F. Akar[1] and B. Güler[1]

[1] *Ankara University Graduate School of Natural and Applied Sciences, Department of Astronomy and Space Sciences, Ankara, Türkiye (E-mail: ezgi.sertkan@ankara.edu.tr)*

[2] *Department of Astronomy and Space Sciences, Faculty of Science, Ankara University, 06100 Ankara, Türkiye*

[3] *Ankara University Astronomy and Space Sciences Research & Application Center, Kreiken Observatory, Incek Blvd., Ankara, Türkiye*

[4] *Department of Physics and McDonnell Center for the Space Sciences, Washington University, St. Louis, MO 63130, USA*

Received: November 15, 2024; Accepted: January 24, 2025

Abstract. A significant part of circumbinary planet discoveries to date have been identified in post-common envelope binaries (PCEBs) using the Eclipse Timing Variations technique (ETV). The detectability of these additional bodies is largely thanks to the total masses, relative radii, and close proximity of the companions of these binary systems, which make ETV-based discoveries possible. Additionally, processes from earlier stages of binary star evolution may impact third-body formation around these systems. The CuPS-ETV catalog compiles the physical and observational properties of these systems and their companions from multiple sources in the literature. Organized for structured queries and visualizations, this catalog is a comprehensive and accessible resource designed to support population analyzes of PCEBs, exploring their complex dynamics and evolutionary patterns.

Key words: circumbinary planets, post-common envelope binaries, catalog, exoplanets

1. Introduction

We are developing the first catalog specific to PCEB systems with additional bodies discovered with the ETV technique, aiming to provide insights into the population and distribution of their physical parameters.

Post Common Envelope Binary systems (PCEB's) are binary star systems where at least one component has completed its main-sequence evolution. Additional objects have been proposed around such systems in the substellar mass regime, and most of these binary systems with evolved components consist of a hot sub-dwarf of spectral type O or B (sdOB), or a white dwarf (WD) primary

and a cool M-dwarf companion. These systems have short orbital periods, often on the order of hours, and their total masses are relatively small.

The progenitors of binary systems with evolved components are binary systems consisting of two main-sequence stars. During their evolution, the more massive primary component fills its Roche lobe and transfers mass to the companion. The companion, receiving this transferred material, may not be able to fully accrete the mass from the primary. As a result, the material that cannot be accreted by the companion surrounds the system, leading to a phase known as the "common envelope" (Paczynski, 1976). During the common envelope phase, the components of the binary lose angular momentum to the envelope and spiral-in to form a close binary. The material in the envelope spreads via angular momentum transfer (common envelope ejection). This process results in a binary system that has undergone a common envelope evolution, forming what is known as a Post-Common Envelope Binary (PCEB) system (Heber, 2016).

Binary systems that have undergone common envelope evolution are ideal to look for additional objects in the substellar mass regime with the eclipse timing method due to their small total masses and short orbital periods. Precise measurements of minimum eclipse times are possible thanks to the V-shaped minima profiles, and the Light Time Effect (LiTE) due to low-mass additional bodies is easily revealed with the help of small total mass of the binary (Baştürk et al., 2023). Magnetic activity in the low-mass companion star may cause ETVs, and determining whether variations are due to magnetic activity or LiTE involves calculating the required energy using the companion's physical parameters (Völschow et al., 2016).

Apsidal motion in eccentric binaries causes large ETV cycles, but strong tidal forces during the evolution of these compact systems typically lead to nearly circular orbits. Radial velocity studies support this, indicating circular orbits (Vučković et al., 2007), making apsidal motion an unlikely cause of ETVs in PCEBs. Other mechanisms, such as tidal interactions or gravitational wave effects, can result in loss or gain of angular momentum, which affects orbital periods in a secular fashion.

Substellar objects around such systems suggested based on the observed ETVs attract attention. Therefore, their long-term follow-up is required to reveal their nature, which can be best acheived through a custom catalog. For the development of such a catalog, we have conducted an extensive review of existing studies focused on PCEBs and additional bodies suggested around them based on the ETVs they display. We have systematically collected and organized data from various sources, ensuring that the information is comprehensive and readily usable for researchers.

We collect parameters related to binaries and their companions, organizing them into a user-friendly structure for future research. The catalog will be open-access and query-friendly, aiming to provide researchers with an organized

resource for analyzing the population and distribution of parameters related to PCEBs and their potential companions.

2. Catalog structure

The catalog is structured into four main layers:

1. **System layer:** Includes the orbital parameters of binary systems, such as orbital period, semi-major axis, and mass ratio.

2. **Star layer:** Contains the physical properties of the primary and secondary stars, including effective temperatures, masses, and radii.

3. **Planet layer:** Describes the proposed planets, providing details such as periods, masses, orbital distances, and eccentricities.

4. **Reference layer:** Links all layers using reference numbers and corresponding literature sources.

Users can merge these layers through reference numbers to track the origin of each dataset. Bar charts, such as the one in Fig. 1, provide visual representations of data sources.

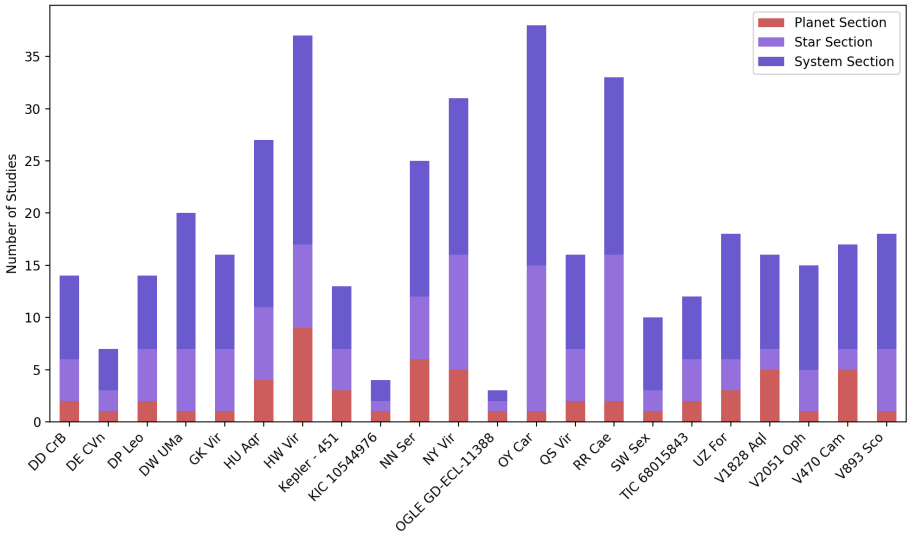


Figure 1. Number of studies referenced per dataset.

Table 1 provides a detailed overview of the four main layers in the catalog structure. The "method" in subscript is to denote which method is used to obtain the aforementioned parameter, e.g. q-search for the mass ratio (q).

Most of the primary stars in our catalog are either white dwarfs (WD) or *O* or *B*-type hot sub-dwarfs (sdOB). Both groups have cooler, low-mass secondaries. These findings may provide clues about their evolutionary paths and formation mechanisms of planetary mass objects around PCEBs (Zorotovic & Schreiber, 2013).

Table 1. The physical parameters included in the layers of the catalog with updated units.

System layer	**Star layer**	**Planet layer**	**Reference layer**
System Name	Star Name	Planet Name	System Name
Alternate Name	$T_{\rm eff}$ (K)	$P_{\rm orb}$ (days)	First Author/Year
T_0 (BJD-TDB)	$T_{\rm eff,method}$	$M_{\rm min}$ ($M_{\rm Jup}$)	Ref. Number
$P_{\rm orb}$ (days)	$\log g$	a (AU)	NASA/ADS Link
a ($R_\odot$)	$\log g_{\rm method}$	ω (deg)	
$a_{\rm method}$	M ($M_\odot$)	$T_{\rm per}$ (JD)	
q	$M_{\rm method}$	M (deg)	
$q_{\rm method}$	R ($R_\odot$)	Ref. Number	
i (deg)	$R_{\rm method}$		
$i_{\rm method}$	Ref. Number		
d (pc)			
Ref. Number			

An example of graphical representations of the information in the catalog can be a mass versus orbital period plot, which demonstrates the distribution of planetary discoveries across various techniques (Fig. 2). Another key plot, the Hertzsprung-Russell diagram, illustrates the temperature and radius distributions of the primary and secondary stars, based on the luminosities derived from standard relations (Fig. 3).

3. Results

Our catalog identifies 37 planets proposed around PCEBs. Notably, twenty-two substellar objects within planetary or brown dwarf mass limits ($M<80\ M_{\rm jup}$) have been suggested around systems where the primary star is a hot sub-dwarf

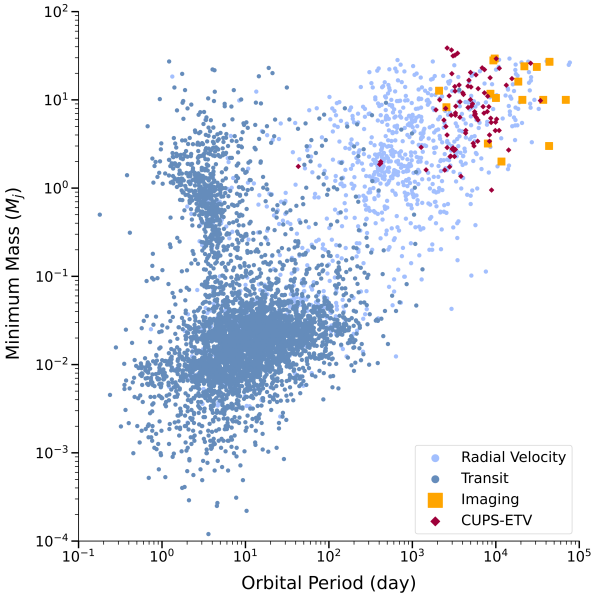


Figure 2. Distribution of planetary discoveries across techniques.

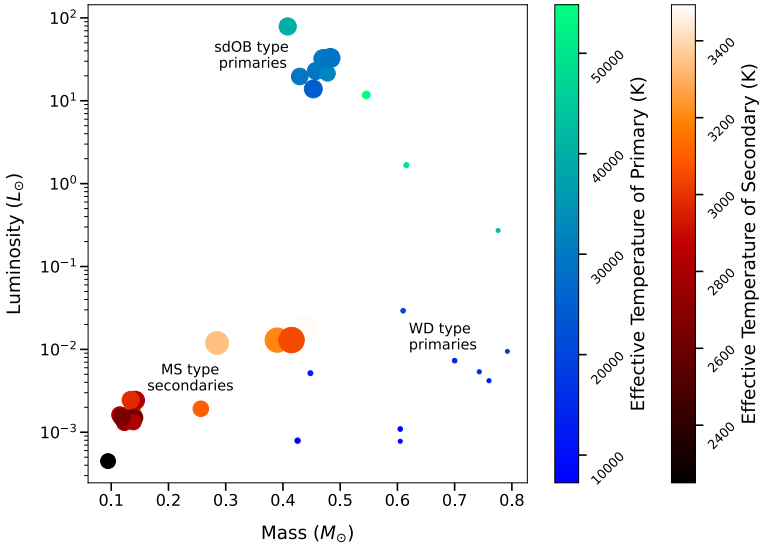


Figure 3. Mass-temperature-luminosity distribution of primary and secondary stars.

on the extreme horizontal branch of the Hertzsprung-Russell diagram or a white dwarf, while the companion star is a low-mass main-sequence star.

Our catalog provides a tool for the analysis of the population characteristics of these unique systems. The results highlight distinct groupings among the host stars and suggest diverse evolutionary scenarios for third-body formation in these environments.

4. Acknowledgements

We gratefully acknowledge the support of the Scientific and Technological Research Council of Türkiye (TÜBİTAK) with the project 122F358.

References

Baştürk, O., Esmer, E. M., Demir, E., & Selam, S. O., Eclipse Timing Variations Observed in PCEB Systems. 2023, in *10th Meeting on Hot Subdwarfs and Related Objects* (Liège: Bulletin de la Société Royale des Sciences de Liège)

Heber, U., Hot Subluminous Stars. 2016, *IOPScience*, **128**

Paczynski, B., Common Envelope Binaries. 1976, in IAU Symposium, Vol. **73**, *Structure and Evolution of Close Binary Systems*, ed. P. Eggleton, S. Mitton, & J. Whelan, 75

Vučković, M., Aerts, C., Østensen, R., et al., The binary properties of the pulsating subdwarf B eclipsing binary PG 1336-018 (NY Virginis). 2007, *Astronomy and Astrophysics*, **471**, 605, DOI:10.1051/0004-6361:20077179

Völschow, M., Schleicher, D. R. G., Perdelwitz, V., & Banerjee, R., Eclipsing time variations in close binary systems: Planetary hypothesis vs. Applegate mechanism. 2016, *Astronomy and Astrophysics*, **587**, A34, DOI:10.1051/0004-6361/201527333

Zorotovic, M. & Schreiber, M. R., Origin of apparent period variations in eclipsing post-common-envelope binaries. 2013, *Astronomy & Astrophysics, Series A*, **579**, A95, DOI:10.1051/0004-6361/201220321

Contrib. Astron. Obs. Skalnaté Pleso **55/3**, 307 – 312, (2025)
https://doi.org/10.31577/caosp.2025.55.3.307

Period changes in low-mass eclipsing binaries:

V1828 Aql, NSVS 2676703, and NSVS 6507557

M. Wolf[1], **L. Šmecler**[2,3], **H. Kučáková**[1,3,4,5], **T. Hynek**[6], **P. Zasche**[1], **K. Hornoch**[5] **and R.F. Auer**[3,7]

[1] *Astronomical Institute, Faculty of Mathematics and Physics, Charles University, Praha 8, Czech Republic (E-mail: Marek.Wolf@mff.cuni.cz)*
[2] *Observatory Valašské Meziříčí, Czech Republic*
[3] *Variable Star and Exoplanet Section of the Czech Astronomical Society*
[4] *Research Centre for Theoretical Physics and Astrophysics, Institute of Physics, Silesian University in Opava, Czech Republic*
[5] *Astronomical Institute, Academy of Sciences, Ondřejov, Czech Republic*
[6] *DARK SKY Beskydy, Park tmavé oblohy, Czech Republic*
[7] *South Moravian Observatory, Veverská Bítýška, Czech Republic*

Received: November 5, 2024; Accepted: January 11, 2025

Abstract. Low-mass stars belong to the most numerous component of our Galaxy. We present the new results of our long-term observational project to detect small variations in the orbital periods of low-mass and short-period eclipsing binaries. Three known systems, namely V1828 Aql, NSVS 2676703, NSVS 6507557, and their period changes visible in the current $O-C$ diagrams, are briefly discussed.

Key words: binaries: eclipsing – binaries: close – stars: low-mass – stars: individual (V1828 Aql, NSVS 2676703, NSVS 6507557)

1. Introduction and observations

Low-mass binaries (LMB) and their multiple systems play an important role in stellar astrophysics. Their origin and evolution are still not fully understood questions in star formation theory. Moreover, observations of low-mass stars show a severe discrepancy between estimated and modeled parameters, where the models give some 10-15% smaller radii than the observations, while their effective temperatures are some 5% higher (Ribas et al., 2008; Morales et al., 2013). Here, we focus on three detached low-mass eclipsing binaries of different spectral types. In V1828 Aql the hot subdwarf star is present as a primary, and the other two contain K and M dwarf components. Our previous studies on LMB were presented in Wolf et al. (2018, 2020, 2021).

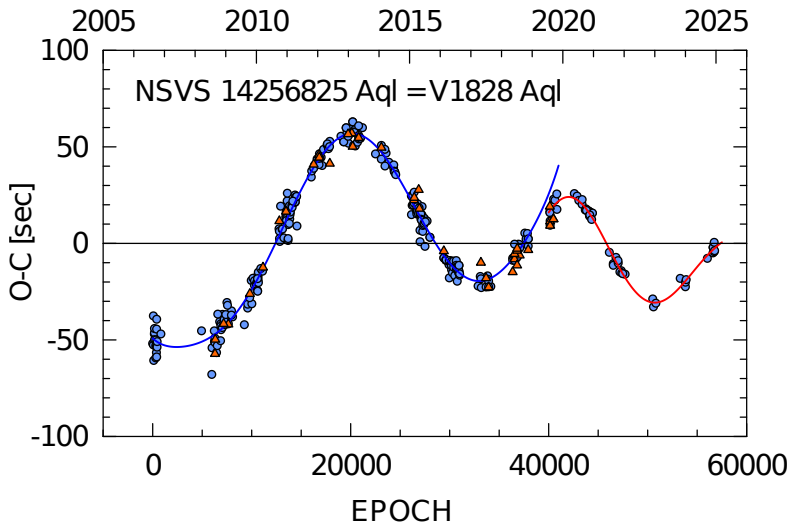


Figure 1. Period changes in the current $O-C$ diagram of NSVS 14256825 = V1828 Aql. Primary and secondary eclipses are plotted as blue circles and orange triangles, resp. The previous solution of LITE with the third body period $P_3 \simeq 9$ yr (blue curve) is no longer valid. Overall variations of $O-C$ values cannot be interpreted as a single LITE, sinusoidal oscillations of $O-C$ values are showing a decaying amplitude in recent years. Combination of several LITEs of additional bodies or a still unknown mechanism in binary systems can play a role.

LMBs are relatively faint objects with a short orbital period, rapid and deep eclipses, also interesting for amateur observers and their small telescopes with CCD techniques. Since 2006 systematic long-term light curve and eclipse monitoring of many eclipsing LMB has been made at several observatories:

- 65-cm Mayer telescope (D65) in Ondřejov observatory and CCD camera MII G2-3200 (Moravian Instruments, https://www.gxccd.com) with Johnson-Cousins BVRI filters in remote access,
- 40-cm Ritchey-Chrétien telescope at Dark Sky Beskydy observatory and CCD camera MII C3-Pro mono with Baader LRGB Halfa filters and remote access to the telescope, https://www.darkskybeskydy.cz
- 35-cm and 28-cm SCT Celestron telescopes at Valašské Meziříčí observatory with CCD camera G2-1600 and G2-4000, https://www.astrovm.cz/cz/
- 20-cm Newtonian telescope at South Moravian Observatory with CCD camera MII G2-1600, https://south-moravian-observatory.jimdofree.com/

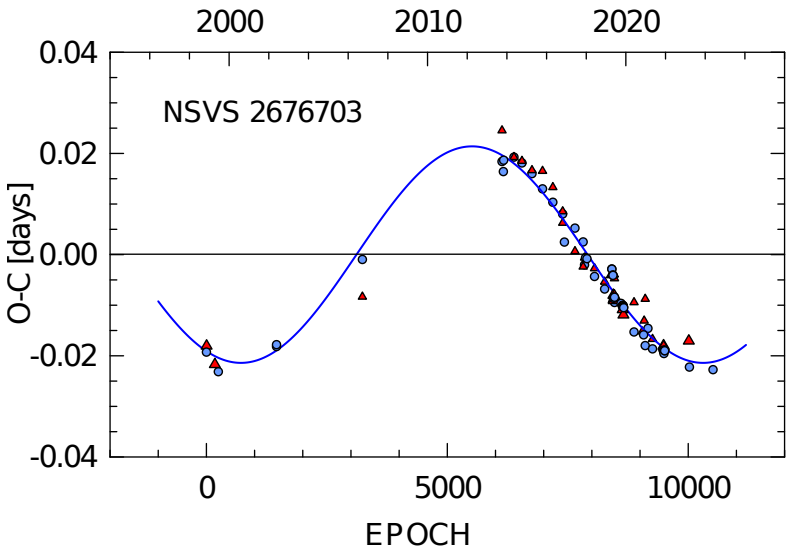


Figure 2. $O-C$ diagram for NSVS 2676703 for orbital period $P = 0.86743297$ days, where data from the TESS satellite (larger symbols) were also used. The blue sinusoidal curve represents our solution of LITE with the period of 22.8 yr and a relatively large semi-amplitude about 30 minutes. Assuming coplanar orbit and the masses of both components $M_1 = 1.2$ M$_\odot$ and $M_2 = 0.72$ M$_\odot$, the minimal mass of the third body follows $M_{3,\mathrm{min}} \simeq 0.9$ M$_\odot$. Unfortunately, such a bright third body is not visible in the TESS light curve solution.

2. Period variation and light time effect

The period analysis of three selected binaries was performed using all available mid-eclipse times found in the literature, as well as our newly measured times and those derived from TESS data. One of the best methods to detect the third body orbiting the eclipsing binary, in addition to astrometry and spectroscopy, is the light travel delay, or the so-called light time effect (LITE), associated with the orbital motion of the third body (Irwin, 1952; Mayer, 1990). Usually, this method is more sensitive to companions on a long-period orbit, and its semi-amplitude A is proportional to the mass and period of the third body as

$$A \sim M_3 \; P_3^{2/3}.$$

Moreover, low-mass binary components favor the detection of low-mass companions on short-period orbits (Pribulla et al., 2012). On the other hand, in the case of a shorter orbital period of the third body (usually less than one year), small dynamical perturbations of the inner orbit can occur that also create additional changes in the observed times; see Borkovits et al. (2011, 2016). In the

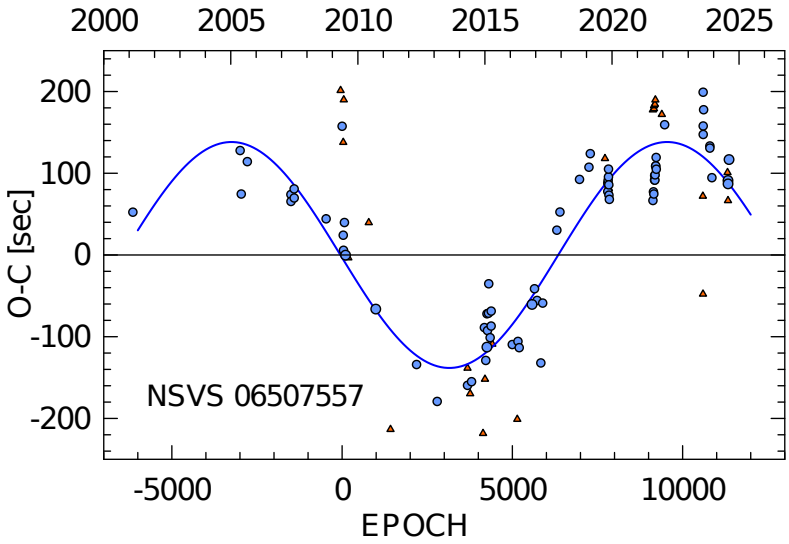


Figure 3. Current $O - C$ diagram for NSVS 6507557 with orbital period $P = 0.515089155$ days. See legend to Fig. 1. The blue sinusoidal curve represents possible LITE with a period of 15.3 yr and a semi amplitude of about 140 sec. Short time deviations from the overall sinusoidal course are clearly visible, esp. around the epochs 8000 – 9000 (larger symbols for TESS data). This points to another dynamical effect likely to occur in this system.

following, we present three examples of $O - C$ diagrams for systems in which the original solution of LITE turns out to be unsatisfactory or incomplete. They are discussed below and plotted in Figs. 1 – 3.

3. Discussion and conclusions

Just as among massive stars, we are also finding an increasing number of multiple systems among low-mass stars. This study provides accurate information on period changes and the possible multiplicity of three detached low-mass eclipsing binaries. Based on the presented analyses, we can conclude the following.

1. V1828 Aql = NSVS 14256825, one of the well-known PCEB HW Vir-type systems containing a very hot subdwarf B primary and M dwarf secondary. Several comprehensive period studies have been presented in the past. In the last one Zervas & Christopoulou (2024) suggest that the $O - C$ data can be well explained by the presence of two circumbinary planets. The inner planet with mass of 11 M_{Jup} revolves in a nearly circular orbit with the period of 7 yr. The outer orbiting body is unconstrained with a period range 20 – 50 yr and substellar mass 11 – 70 M_{Jup}. The authors also confirm the stability of

their solution for 100 Myr. We can conclude that this system belongs to several similar systems like HW Vir, HS0705+6700 and NN Ser, showing currently a decaying LITE amplitude in their $O - C$ diagrams.

2. In case of NSVS 2676703, only a part of the third-body orbital period is covered by precise and continuous timings. Further two decades of observations can bring more clarity to this interesting stellar object and to its period changes.

3. Concerning NSVS 6507557, there is a close faint object listed in the Gaia Archive (https://gea.esac.esa.int/archive/), about 2.5 mag fainter with a similar proper motion and distance. Its angular separation is 0.001145 deg = 4.122 arcsec and the parallax $\pi \simeq 8$ mas (distance 125 pc). This gives us a linear separation of a possible companion of 515 au. Simply, it is too far from being identified as an orbiting third body derived in this study with an orbital period of about 15 yr.

Unfortunately, to our knowledge, in the case of NSVS 2676703 and NSVS 6507557 no radial velocities have been published so far. Some presented results can therefore be considered preliminary. Further measurements of eclipses and radial velocities are desirable. The sample of well-known LMB needs to be increased, and observations of additional systems would be very useful. Multicolor photometry of individual systems and lists of mid-eclipse times are available upon request.

Acknowledgements. The research of MW and PZ was supported by the project Cooperatio-Physics of Charles University. HK and KH were supported by the RVO 67985815 project. The authors also thank Lenka Kotková, Ondřejov observatory, Jan Vraštil, Charles University Prague, and Marek Chrastina, Masaryk University Brno, for their important contribution to photometric observations. TH thanks Jan Zahajský (Supra Praha) and Martin Myslivec, who played a significant role in putting the whole set in the Beskydy observatory into operation. The following Internet-based resources were used: the SIMBAD database operated at CDS, Strasbourg, France, and the NASA Astrophysics Data System Bibliographic Services. This paper includes data collected by the Tess mission. The funding for the Tess mission is provided by the NASA Science Mission Directorate. This research is part of ongoing collaboration between professional astronomers and the Czech Astronomical Society, Variable Star and Exoplanet Section (https://var.astro.cz/en).

References

Borkovits, T., Csizmadia, S., Forgács-Dajka, E., & Hegedüs, T., Transit timing variations in eccentric hierarchical triple exoplanetary systems. I. Perturbations on the time scale of the orbital period of the perturber. 2011, *Astronomy and Astrophysics*, **528**, A53, DOI:10.1051/0004-6361/201015867

Borkovits, T., Hajdu, T., Sztakovics, J., et al., A comprehensive study of the Kepler triples via eclipse timing. 2016, *Monthly Notices of the RAS*, **455**, 4136, DOI:10.1093/mnras/stv2530

Irwin, J. B., The Determination of a Light-Time Orbit. 1952, *Astrophysical Journal*, **116**, 211, DOI:10.1086/145604

Mayer, P., Eclipsing Binaries with Light-time Effect. 1990, *Bulletin of the Astronomical Institutes of Czechoslovakia*, **41**, 231

Morales, J. C., Ribas, I., & Jordi, C., Fundamental properties of low-mass stars in eclipsing binary systems. 2013, in EAS Publications Series, Vol. **64**, *EAS Publications Series*, ed. K. Pavlovski, A. Tkachenko, & G. Torres, 103–110

Pribulla , T., Vaňko, M., Ammler-von Eiff, M., et al., The Dwarf project: Eclipsing binaries - precise clocks to discover exoplanets. 2012, *Astronomische Nachrichten*, **333**, 754, DOI:10.1002/asna.201211722

Ribas, I., Morales, J. C., Jordi, C., et al., Fundamental properties of low-mass stars. 2008, *Mem. Societa Astronomica Italiana*, **79**, 562, DOI:10.48550/arXiv.0711.4451

Wolf, M., Kučáková, H., Zasche, P., et al., Possible substellar companions in dwarf eclipsing binaries. SDSS J143547.87+373338.5, NSVS 7826147, and NSVS 14256825. 2021, *Astronomy and Astrophysics*, **647**, A65, DOI:10.1051/0004-6361/202039851

Wolf, M., Kučáková, H., Zasche, P., et al., Possible substellar companions in low-mass eclipsing binaries: GU Bootis and YY Geminorum. 2018, *Astronomy and Astrophysics*, **620**, A72, DOI:10.1051/0004-6361/201833708

Wolf, M., Kučáková, H., Zasche, P., et al., Possible companions in low-mass eclipsing binaries: V380 Dra, BX Tri, and V642 Vir. 2020, *Contributions of the Astronomical Observatory Skalnate Pleso*, **50**, 637, DOI:10.31577/caosp.2020.50.2.637

Zervas, K. & Christopoulou, P. E., NSVS 14256825: Period variation and orbital stability analysis of two possible substellar companions. 2024, *Astronomy and Astrophysics*, **691**, A115, DOI:10.1051/0004-6361/202450195

Contrib. Astron. Obs. Skalnaté Pleso **55/3**, 313 – 324, (2025)
https://doi.org/10.31577/caosp.2025.55.3.313

The present and the future of modeling eclipsing binary systems

A. Prša

Villanova University, Department of Astrophysics and Planetary Science, 800 Lancaster Ave, Villanova PA 19085, U.S.A. (E-mail: aprsa@villanova.edu)

Received: December 16, 2024; Accepted: January 21, 2025

Abstract. In September 2024, eclipsing binary star practitioners gathered in Litomyšl, Czech Republic, the birth town of Zdeňek Kopal, one of the most celebrated pioneers of our field, to discuss the latest developments and state-of-the-art. I was invited to present my own biased view of the present and the future of modeling eclipsing binary stars. In this contribution I attempt to make a clear distinction between approaches that are suited to individual objects and approaches that aim to deliver bulk results for large datasets. I stress that our motivation should be different: individual system analysis is warranted whenever there is potential to propose or improve our understanding of the underlying physics, while bulk analysis should be used to probe stellar formation and evolution channels. I briefly discuss two examples of tools to achieve the goals: PHOEBE for individual system analysis, and PHOEBAI for bulk analysis.

Key words: binary stars – eclipsing binaries – fundamental parameters – artificial intelligence

1. Introduction

Eclipsing binary stars (EBs) have long been recognized as *the* calibrators of stellar astrophysics. Most of what we know about the fundamental stellar properties stems from EB studies (Torres et al., 2010). Their favorable orbital alignment with the line of sight, and consequent eclipses, make them ideal astrophysical laboratories: a simple geometry coupled with well-understood dynamical laws allow us to obtain fundamental parameters without a-priori assumptions. Fig. 1 showcases the power of EBs: the masses, radii and luminosities of stars inferred from EB observations constitute the most accurate set of constraints for the theories of stellar formation and evolution. The uncertainties are generally below 2-3%, making the error-bars in Fig. 1 smaller than the symbols.

Binary systems do not discriminate on the spectral type or luminosity class; be it main sequence stars, red giants, or compact objects, be it flaring M-dwarfs or pulsating variables, be it tight mass-transferring systems or exoplanets, all these components are found in binary stars. Once we find them in an eclipsing

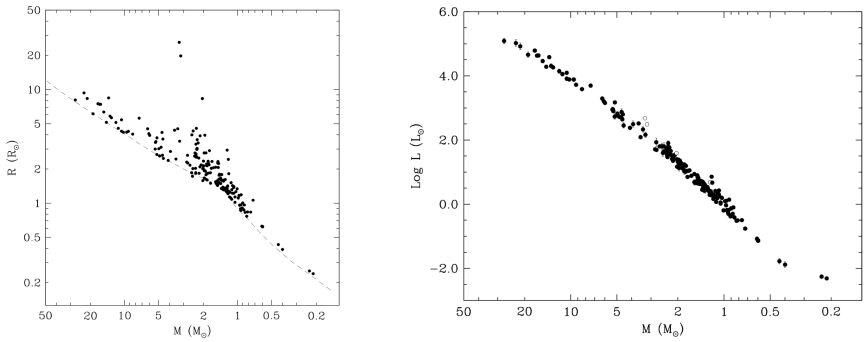


Figure 1. Radius-mass and luminosity-mass relationships for a sample of 94 EBs (Torres et al., 2010). The dashed line is the theoretical zero-age main sequence. Uncertainties in R, L and M are smaller than symbol sizes. Depicted with open symbols are stars classified as giants.

system, the path to fundamental parameters is straight-forward. For obvious reasons, colleagues who study these objects rely on masses and radii provided from EB analyses, which earns EB practitioners an occasional bottle of wine for their efforts. Further augmenting the importance of binaries is the observation that around 20% of binaries have tertiary components (Orosz, 2015), including circumbinary planets (Welsh et al., 2015); when all three components undergo eclipses, the uncertainties in fundamental parameters can reach ∼0.1% (Carter et al., 2011). It is thus of no surprise that Henry Norris Russell, in 1948, pointed out EBs as "the Royal Road" to stellar astrophysics.

2. The present

The 21st has been marked by an unprecedented advancement in data quality. NASA's *Kepler* mission, for example, routinely achieved photometric precision of the order of few tens of ppm (Borucki et al., 2010). *Kepler* observed ∼150,000 stars in the 105 square degree patch of the sky for 4 years with a 30-min cadence (and ∼1,000 stars with 2-min cadence) with 92% temporal completeness. In effect, for the first time we obtained a near-uninterrupted, ultra-precise set of observations for a few thousand EBs as well (Kirk et al., 2016). *Kepler*'s successor, *TESS* (Ricker et al., 2015), continued the census with thousands of targeted EBs (Prša et al., 2022) and ∼150,000 EBs in full frame images across the sky. While the majority of *TESS* EBs are observed continuously for about a month at a time, the dataset still represents a glimpse into EB complexities that remained hidden from ground-based observatories before. The latest space survey, Gaia (Gaia Collaboration et al., 2021), provides a stereoscopic vision of the Galaxy with simultaneous photometric, radial velocity, and astrometric ob-

Table 1. A table of EB parameters that can be inferred from a specific combination of observables. "Cal. LC" stands for flux-calibrated light curve, "SB1" stands for a single-lined spectroscopic binary, and "SB2" for the double-lined spectroscopic binary. The (✓) symbol corresponds to quantities that can be inferred from some but not all light curves. Adapted from Wrona & Prša (2024).

Parameter	Cal. LC	Cal. LC+ distance	2+ Cal. LCs	2+ Cal. LCs+dist.	2+ Cal. LCs+SB1	2+ Cal. LCs+SB2
t_0	✓	✓	✓	✓	✓	✓
P_0	✓	✓	✓	✓	✓	✓
i	✓	✓	✓	✓	✓	✓
$e\cos\omega$	✓	✓	✓	✓	✓	✓
$e\sin\omega$	✓	✓	✓	✓	✓	✓
$r_1 + r_2$	✓	✓	✓	✓	✓	✓
T_2/T_1	✓	✓	✓	✓	✓	✓
r_2/r_1	(✓)	(✓)	(✓)	(✓)	(✓)	✓
$q = M_2/M_1$	(✓)	(✓)	(✓)	(✓)	(✓)	✓
l_3	(✓)	(✓)	(✓)	(✓)	(✓)	(✓)
$\dot{P}$, $\dot{\omega}$, ...	(✓)	(✓)	(✓)	(✓)	(✓)	(✓)
$L_1 + L_2$		✓		✓		✓
L_1, L_2		✓		✓		✓
T_1, T_2			✓	✓	✓	✓
v_γ					✓	✓
M_1, M_2						✓
R_1, R_2				✓		✓
a				✓		✓

servations, with impressive first EB results for 400,000 systems (Mowlavi et al., 2023).

This explosion in photometric precision and temporal coverage put EB models to the test. At this level of precision, the models could no longer reliably reproduce observations, in part because of the missing physics, and in part because of the lack of the required numerical precision. PHOEBE (Prša & Zwitter, 2005) is one of the many codes that exhibited these inadequacies; this prompted a code rewrite in 2016 to remediate the situation.

Irrespective of the choice for the utilized model, the new decade brought on new requirements for modeling. EB practitioners have long realized that – depending on the types of observables available – the parameter space is non-linear and severely degenerate. Table 1 provides rule-of-thumb information content for available types of observables: it informs us what parameters we can infer from what types of observations. Thus, in general, to infer fundamental parameters (masses, radii, temperatures and luminosities), we need multi-band photometric and double-lined spectroscopic data.

Further, gone are the days where "solving" an EB means running an optimizer that minimizes the sum of squares of the residuals between the data

and the model, providing (unrealistically small) formal errors and publishing the results based on poorly sampled data with large scatter. Instead, the typical solution process involves several steps (Conroy et al., 2020):

Solution estimation: in order to ascertain convergence for the optimizers, the starting point in the parameter space needs to be reasonably close to a solution[1]. This is a task for estimators: methods that quickly analyze the data and provide a cursory solution. An example is an estimate of $e\cos\omega$ from eclipse separation in phase, or $r_1/a+r_2/a$ from eclipse widths, or $e\sin\omega$ from the eclipse duration ratios.

Solution optimization: once close, the solution needs to converge to a minimum as robustly as possible. This is usually achieved by finding the parameters that minimize the sum of squares of the residuals. Optimization is an iterative process that will typically follow the locally steepest slope towards the minimum. Once there, it will estimate formal errors from the covariance matrix. optimizers differential corrections (Wilson & Devinney, 1971), Nelder and Mead's simplex method (Kallrath & Linnell, 1987), and Powell's direction set method (Prša & Zwitter, 2007).

Solution sampling: the minimum reached must not be construed as the final solution: the topology of the parameter space near that minimum needs to be properly explored. That is a task for samplers: methods that traverse the vicinity of the parameter space and evaluate the probabilities in order to infer realistic parameter values. This is a computationally expensive and arduous process as parameter space needs to be traversed heuristically. Typical samplers include Markov Chain Monte Carlo methods (Foreman-Mackey et al., 2019), differential evolution (Storn & Price, 1997), etc. Inference is usually done within the Bayesian formalism, and the results are typically presented in a corner plot, with individual parameter posterior probability density functions and two-dimensional parameter cross-correlations (Conroy et al., 2020).

These components need to be utilized in unison in order to derive a compelling, credible solution for EB parameters given the data. The time cost of a typical modeling process is weeks to months, depending on the complexity of the parameter space, types of observations, and data quality and quantity.

3. The future

The 21st has also been marked by an unprecedented advancement in data quantity. Table 2 provides a rough census of observed or expected numbers of EBs in recent, currently ongoing, and imminent surveys.

[1]We deliberately stress *a* solution rather than *the* solution because, in most circumstances, there will not be a single, unequivocal model that uniquely explains the data.

Table 2. A census of recent, ongoing, and imminent surveys, along with their EB yield.

Survey	Data type	Years of operation	EB yield
K2	photometry	2014-18	∼1,000
Kepler	photometry	2009-13	∼3,000
NGTS	photometry	2015–	∼5,000
OGLE-II	photometry	1997-2000	∼6,000
Plato	photometry	2026?	∼8,000
ASAS	photometry	1997-2010	∼10,000
Galah	spectroscopy	2013–	∼15,000
OGLE-III	photometry	2001-09	∼40,000
ASAS-SN	photometry	2014–	∼40,000
TESS	photometry	2018–	∼150,000
OGLE-IV	photometry	2010–	∼500,000
ZTF	multi-band photometry	2018–	∼500,000
Gaia	photometry, astrometry, RVs	2013–	∼1.8 million
CSST	photometry, spectroscopy	2026?	∼2 million
LSST	multi-band photometry	2025–	∼10 million

It seems clear that, over the next ten years or so, we will have well over ten million EBs in our hands. In the previous section we have established that, typically, we need ∼weeks of computer time to robustly analyze EB observables. Thus, unless we are willing to accept that EB modeling remains a boutique[2] operation, we need faster approaches.

One such approach utilizes artificial intelligence (AI). We have been inundated with AI in our everyday lives, and for good reason. It powers technologies like virtual assistants, personalized recommendations, and smart home devices, making daily tasks more efficient and tailored to individual needs. In healthcare, AI enables early diagnosis through advanced imaging and predictive analytics (Secinaro et al., 2021), while in education, it supports personalized learning experiences (Chen et al., 2020). AI also enhances industries like transportation with autonomous vehicles and navigation systems, and it revolutionizes customer service through chatbots and automated support (Mohamad Suhaili et al., 2021).

AI has been proposed for EBs as well, for automated classification (see, for example, Čokina et al. 2021) and for bulk analysis (e.g., Prša et al. 2008). The appeal is undeniable: if AI could "look at" observables, recognize them as EBs, and deduce principal parameters in a fraction of a second, it would allow us to rapidly analyze large datasets. The question, then, is how accurately can this be done? Prša et al. (2008) trained a backpropagating neural network on syn-

[2]The task of solving 10 million EBs in the next 100 years would require ∼4000 astronomers and ∼8 million computer cores, along with a moratorium on further observations.

thetic light curves generated by PHOEBE (Prša & Zwitter, 2005; Prša et al., 2016) where the network was shown ∼32,000 light curves with 5 corresponding parameters: temperature ratio (T_2/T_1), sum of fractional radii ($R_1/a+R_2/a$), radial eccentricity ($e\sin\omega$), tangential eccentricity ($e\cos\omega$), and inclination ($\sin i$). They demonstrated that the trained network could attain the accuracy better than 10% for 90% of the sample. This allowed the authors to deploy the network on 2500+ EBs from OGLE and CALEB databases.

The principal problem with this type of approach is that, in the absence of post-festum tests, we do not know *which* 10% are not correctly characterized. Given that the neural network maps input (light curves) to output (parameters) opaquely, not only do we lack the ability to evaluate per-light curve accuracy, we also cannot attribute meaningful uncertainties to any obtained parameters. The remedy is to run post-festum tests, but these can be both computationally and temporally expensive, which defeats the initial purpose at least to some extent.

There exists an alternative, though: we can exchange the neural network's inputs and outputs. Instead of providing light curves as input, we provide parameters; instead of collecting parameters as output, we collect light curves. The network becomes an *emulator* of the physical engine. Assuming that the network can be trained adequately to encompass the non-linear properties of our complex, multivariate parameter space, each computation that takes minutes to complete using the physical model can take milliseconds using a trained network. Thus, the AI-powered engine becomes a drop-in replacement for the physical model. In our particular case, PHOEBAI replaces PHOEBE (cf. Fig. 2).

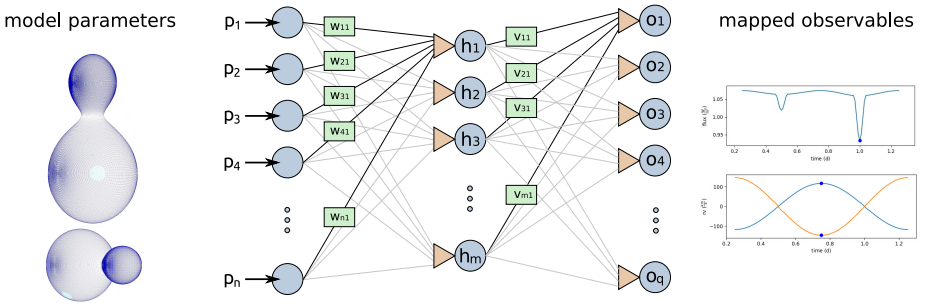


Figure 2. A schematic representation of the feed-forward neural network that acts as an emulator to the physical engine. Parameters p_i are mapped through connection weights w_{ij} across hidden layers h_j to the output units o_k, representing synthetic observables.

Let us first estimate the potential speed-up and establish a good motive for this effort. In Section 2 we estimate that, for the completion of the estimation, optimization, and sampling stages, we require $\sim 10^6$ forward model computa-

tions. If each model takes ∼2 minutes to compute , we are talking about 3.8 *years* of compute time on a single processor core. To handle this volume of computations in a reasonable time (say, 2 weeks), we need 100 cores – i.e., a computer cluster. For the neural network, on the other hand, the model can be "computed" within a millisecond. In that case, the net compute time becomes ∼1.5 hours *on a single processor*. Thus, AI holds promise of a $\sim 10^6$-fold speed-up.

There are certainly limitations to such an emulator, even if the underlying network is perfectly trained.

- The inputs and the outputs are fixed, determined by the network topology. If the network it trained with, say, 10 input parameters and it outputs, say, 500 fluxes in equidistant phases, we are restricted to using the same 10 parameters and the emulator will yield fluxes in those exact 500 phase points. The observations will thus need to be interpolated to the corresponding phase array for comparison with the model, and any other parameters present in the physical model will not play a role in the emulator.

- The network emulates phased light curves, so there can be no temporal variation in the data. Any variability that is not captured by the parameters used for training the network will inevitably skew the results to the extent of the degeneracy between included and omitted parameters. Any trends in the data, or more complex noise models, need to be accounted for either before (i.e., by detrending) or concurrently with sampling (i.e., by modifying the maximized probability function).

- Neural networks cannot be used on input that deviates from the training set: while they are well suited for interpolation, they are notoriously bad at extrapolation (Freeman & Skapura, 1991). Thus, if the training set does not cover the parameter space adequately, sampling will not be done correctly. It also means that, if the *density* of the covered parameter space is not representative of actual distributions, the results may be biased or suffer from undersampling systematics.

- The parameter space is inherently non-linear and highly degenerate. The choice of input parameters is thus crucial for emulator performance and result fidelity. Should any of the principal parameters be omitted, or if the chosen parameters are not orthogonal, the emulator will be misspecified and the results will be biased.

These limitations can be controlled with a careful optimization of the neural network topology and the construction of the training set. Once optimized and trained, the emulator is ready to be used as a drop-in replacement of the physical model. That includes the optimization stage and the sampling stage: given the data, the emulator is able to minimize the cost function and to sample the

probability density. It is able to do so in a ∼millionth of the physical model's time cost.

As proof of concept, we trained an emulator on 6 photometric parameters: the effective temperature ratio T_2/T_1, eccentricity e, argument of periastron ω, orbital inclination i, the sum of fractional radii $r_1 + r_2$, and their ratio r_2/r_1. For efficiency, we replaced e and ω with $e \sin \omega$ and $e \cos \omega$, and i with $\cos i$. The parameters were sampled from distributions that cover a wide enough range to encompass the case study light curves. The network was trained on ∼600k light curves synthesized using PHOEBE. As outputs, the network used phase-folded light curves sampled in 500 points. We denote this emulator PHOEBAI: PHOEBE via AI (Wrona & Prša, 2024).

The topology of the network was determined by the `RandomizedSearchCV` method (Bergstra & Bengio, 2012) from the `sklearn` library (Pedregosa et al., 2011). The method evaluated thousands of structures with varying numbers of hidden layers, nodes, and activation functions. The chosen shape was the simplest among the best performing in terms of minimizing the sum of residual squares between predicted and actual sets of light curves. It comprises four hidden layers with 512, 512, 512, and 1024 nodes, with the sigmoid activation function.

Application of this network was tested on a subset of EBs from the *TESS* EB catalog (Prša et al., 2022) that matched our training set distributions. The optimizer utilized differential evolution (Storn & Price, 1997) from the `scipy.optimize` library (Virtanen et al., 2020). The final results from this optimization were subsequently used as starting values for MCMC sampling using the emcee Python library (Foreman-Mackey et al., 2019).

During the sampling process, we employed 80 walkers and 4000 iterations to obtain posterior distributions. Fig. 3 compares PHOEBAI and PHOEBE performance on a detached EB, TIC 279097693. This is a typical (rather than cherry-picked) result from the test sample: it shows that PHOEBAI is able to accurately capture both the posteriors and parameter correlations.

4. Conclusions

As we continue to be inundated with high-quality data, we need to distinguish between "boutique" operation and bulk processing. When our understanding of the physical processes can be advanced by pointed investigations of individual objects, the well-established methods and codes remain indispensable. On the other hand, to understand large sample properties and parameter distributions that probe the outcomes of stellar formation and evolution principles, we need to rely on novel methods. One such method, presented in this paper, employs feed-forward neural networks. It is important to realize that it is not the only way or even the preferred way to model large swaths of data, but – as demonstrated here – PHOEBAI certainly shows promise in delivering robust results on par with

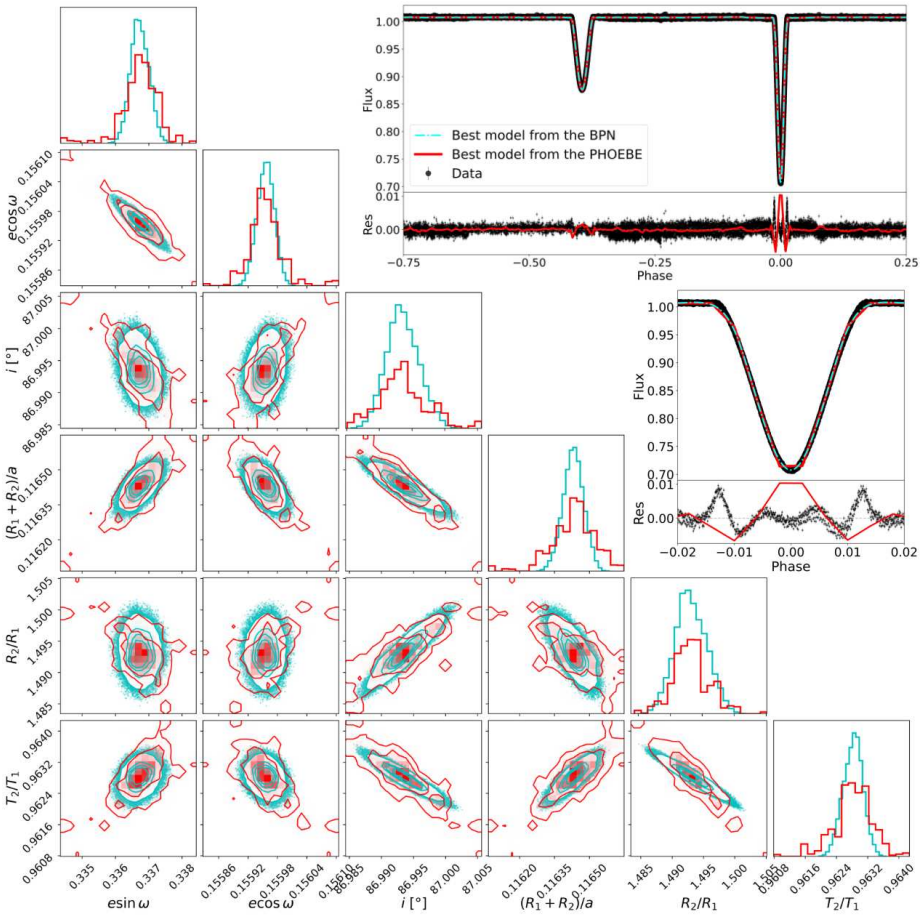


Figure 3. Sampling results for TIC 279097963, a detached EB observed by *TESS* in Sector 4. The top right panel depicts a phase-folded light curve with the best–fit PHOEBE model (red) and the best-fit PHOEBAI model (cyan), along with the residuals, plotted over data. The panel below zooms in on the primary eclipse, demonstrating that the residuals are due to the coarse phase sampling. The corner plot compares parameter posteriors (diagonal) and 2-D correlations (off-diagonal) for the 6 sampled parameters with PHOEBE (red) and PHOEBAI (cyan). PHOEBAI posteriors are better sampled but slightly narrower. Overall, there is a remarkable agreement between the two approaches, where PHOEBAI performed $\sim$250, 000 times faster than the PHOEBE sampler.

the physical engines. Above all, it remains vital to understand the limitations and ranges of application for both the physics-based models and the AI-based emulators and to use them appropriately.

Acknowledgements.
The author would like to acknowledge NASA award 23-ADAP23-0068 that funded in part the work presented in this paper.

References

Bergstra, J. & Bengio, Y., Random Search for Hyper-Parameter Optimization. 2012, *J. Mach. Learn. Res.*, **13**, 281–305

Borucki, W. J., Koch, D., Basri, G., et al., Kepler Planet-Detection Mission: Introduction and First Results. 2010, *Science*, **327**, 977, DOI:10.1126/science.1185402

Carter, J. A., Fabrycky, D. C., Ragozzine, D., et al., KOI-126: A Triply Eclipsing Hierarchical Triple with Two Low-Mass Stars. 2011, *Science*, **331**, 562, DOI:10.1126/science.1201274

Chen, L., Chen, P., & Lin, Z., Artificial Intelligence in Education: A Review. 2020, *IEEE Access*, **8**, 75264, DOI:10.1109/ACCESS.2020.2988510

Conroy, K. E., Kochoska, A., Hey, D., et al., Physics of Eclipsing Binaries. V. General Framework for Solving the Inverse Problem. 2020, *Astrophysical Journal, Supplement*, **250**, 34, DOI:10.3847/1538-4365/abb4e2

Foreman-Mackey, D., Farr, W. M., Sinha, M., et al. 2019, emcee v3: A Python ensemble sampling toolkit for affine-invariant MCMC, Zenodo

Freeman, J. A. & Skapura, D. M. 1991, *Neural networks: algorithms, applications, and programming techniques* (Redwood City, CA, USA: Addison Wesley Longman Publishing Co., Inc.), ISBN: 0-201-51376-5

Gaia Collaboration, Brown, A. G. A., Vallenari, A., et al., Gaia Early Data Release 3. Summary of the contents and survey properties. 2021, *Astronomy and Astrophysics*, **649**, A1, DOI:10.1051/0004-6361/202039657

Kallrath, J. & Linnell, A. P., A New Method to Optimize Parameters in Solutions of Eclipsing Binary Light Curves. 1987, *Astrophysical Journal*, **313**, 346, DOI:10.1086/164971

Kirk, B., Conroy, K., Prša, A., et al., Kepler Eclipsing Binary Stars. VII. The Catalog of Eclipsing Binaries Found in the Entire Kepler Data Set. 2016, *Astronomical Journal*, **151**, 68, DOI:10.3847/0004-6256/151/3/68

Mohamad Suhaili, S., Salim, N., & Jambli, M. N., Service chatbots: A systematic review. 2021, *Expert Systems with Applications*, **184**, 115461, DOI:10.1016/j.eswa.2021.115461

Mowlavi, N., Holl, B., Lecoeur-Taïbi, I., et al., Gaia Data Release 3. The first Gaia catalogue of eclipsing-binary candidates. 2023, *Astronomy and Astrophysics*, **674**, A16, DOI:10.1051/0004-6361/202245330

Orosz, J. A., Triple Stars Observed by Kepler. 2015, in Astronomical Society of the Pacific Conference Series, Vol. **496**, *Living Together: Planets, Host Stars and Binaries*, ed. S. M. Rucinski, G. Torres, & M. Zejda, 55

Pedregosa, F., Varoquaux, G., Gramfort, A., et al., Scikit-learn: Machine Learning in Python. 2011, *Journal of Machine Learning Research*, **12**, 2825

Prša, A., Conroy, K. E., Horvat, M., et al., Physics Of Eclipsing Binaries. II. Toward the Increased Model Fidelity. 2016, *Astrophysical Journal, Supplement*, **227**, 29, DOI:10.3847/1538-4365/227/2/29

Prša, A., Guinan, E. F., Devinney, E. J., et al., Artificial Intelligence Approach to the Determination of Physical Properties of Eclipsing Binaries. I. The EBAI Project. 2008, *Astrophysical Journal*, **687**, 542, DOI:10.1086/591783

Prša, A. & Zwitter, T., A Computational Guide to Physics of Eclipsing Binaries. I. Demonstrations and Perspectives. 2005, *Astrophysical Journal*, **628**, 426, DOI:10.1086/430591

Prša, A., Kochoska, A., Conroy, K. E., et al., TESS Eclipsing Binary Stars. I. Short-cadence Observations of 4584 Eclipsing Binaries in Sectors 1-26. 2022, *Astrophysical Journal, Supplement*, **258**, 16, DOI:10.3847/1538-4365/ac324a

Prša, A. & Zwitter, T., Introducing Powell's Direction Set Method to a Fully Automated Analysis of Eclipsing Binary Stars. 2007, in Astronomical Society of the Pacific Conference Series, Vol. **370**, *Solar and Stellar Physics Through Eclipses*, ed. O. Demircan, S. O. Selam, & B. Albayrak, 175

Ricker, G. R., Winn, J. N., Vanderspek, R., et al., Transiting Exoplanet Survey Satellite (TESS). 2015, *Journal of Astronomical Telescopes, Instruments, and Systems*, **1**, 014003, DOI:10.1117/1.JATIS.1.1.014003

Russell, H. N., The Royal Road of Eclipses. 1948, **7**, 181

Secinaro, S., Calandra, D., & Secinaro, A. e. a., The role of artificial intelligence in healthcare: a structured literature review. 2021, *BMC Med Inform Decis Mak*, **21**, 125, DOI:10.1186/s12911-021-01488-9

Storn, R. & Price, K., Differential Evolution – A Simple and Efficient Heuristic for Global Optimization over Continuous Spaces. 1997, *J. of Global Optimization*, **11**, 341–359, DOI:10.1023/A:1008202821328

Torres, G., Andersen, J., & Giménez, A., Accurate masses and radii of normal stars: modern results and applications. 2010, *Astronomy and Astrophysics Reviews*, **18**, 67, DOI:10.1007/s00159-009-0025-1

Čokina, M., Maslej-Krešňáková, V., Butka, P., & Parimucha, Š., Automatic classification of eclipsing binary stars using deep learning methods. 2021, *Astronomy and Computing*, **36**, 100488, DOI:10.1016/j.ascom.2021.100488

Virtanen, P., Gommers, R., Oliphant, T. E., et al., SciPy 1.0: Fundamental Algorithms for Scientific Computing in Python. 2020, *Nature Methods*, **17**, 261, DOI:10.1038/s41592-019-0686-2

Welsh, W. F., Orosz, J. A., Short, D. R., et al., Kepler 453 b - The 10th Kepler Transiting Circumbinary Planet. 2015, *Astrophysical Journal*, **809**, 26, DOI:10.1088/0004-637X/809/1/26

Wilson, R. E. & Devinney, E. J., Realization of Accurate Close-Binary Light Curves: Application to MR Cygni. 1971, *Astrophysical Journal*, **166**, 605, DOI:10.1086/150986

Wrona, M. & Prša, A., The Eclipsing Binaries via Artificial Intelligence. II. Need for Speed in PHOEBE Forward Models. 2024, *arXiv e-prints*, arXiv:2412.11837

Contrib. Astron. Obs. Skalnaté Pleso **55/3**, 325 – 339, (2025)
https://doi.org/10.31577/caosp.2025.55.3.325

Fourier disentangling of spectra in observational surveys

P. Hadrava

Astronomical Institute of the Czech Academy of Sciences, Boční II 1401, CZ-141 31 Praha 4, The Czech Republic (E-mail: had@asu.cas.cz)

Received: October 16, 2024; Accepted: January 16, 2025

Abstract. The usage of the Fourier disentangling of component spectra and orbital parameters of multiple stars is advantageous in follow-up campaigns to big photometric surveys. The perspectives of its applications in spectroscopic surveys are outlined.

Key words: stars: fundamental parameters – binaries: spectroscopic – stars: atmospheres

1. Introduction

The observations of binary and multiple stars reveal the fundamental parameters of stars, which are crucial not only for testing the theory of structure and evolution of stars, but also of stellar systems, galaxies, and of chemical evolution of the universe. Specifically, the spectroscopic observations of binaries provide an information about their absolute sizes and physical parameters of their atmospheres ($T_{\rm eff}$, $\log g$, abundances etc.). Due to the multiplicity of the stellar systems, the spectra of component stars are blended. In order to determine the atmospheric parameters of the components we need to separate their individual spectra from the observations. This can be done numerically (e.g. using the method of tomographic separation by Bagnuolo & Gies, 1991) if the Doppler shifts of the component spectra at different exposures are known. However, to recognize the dynamics of the system and the consequent Doppler shifts, it is desirable to have the component spectra separated (in order to measure their Doppler shifts similarly to the method of cross-correlation by Simkin, 1974). Thus, the mutually conditioned information about the dynamics and the spectra of the component stars is entangled in the sets of observed spectra and therefore must be sought in parallel. Methods of such a simultaneous search for the component spectra and the orbital parameters are called the disentangling of spectra. They were introduced by Simon & Sturm (1994), who solved the separation of spectra by means of the singular-value decomposition in the wavelength domain, and by Hadrava (1995) using a solution in the Fourier domain. (It should be noted that the term 'disentangling' is sometimes used also for procedures which do not solve the problem in its complexity.)

To get a complete information about the dynamics of a multiple stellar system, it is desirable to combine the spectroscopy with a photometry or interferometry which are sensitive to the inclination of the orbit. Moreover, as the photometry is less observationally demanding than the spectroscopy, it is usually available for a longer period of time. The light curves are thus more suitable for determining the orbital periods. Typically the photometric variability indicates targets worth of a spectroscopic follow-up. With the increasing number and extent of the space- and ground-based photometric surveys, the chances to find in their archives light curves needed to complement the spectra obtained in a campaign dedicated to objects of interest are growing. Disentangling is then an efficient method to interpret the observations.

There are also available spectroscopic surveys of stars. Because the method of disentangling is much less laborious than the classical procedure of measuring the radial velocities (RVs) and subsequent solution of RV-curves, it is more suitable for an automated search for orbital parameters from the observed spectra of multiple stars.

2. Disentangling in context of interpreting observations

Progress in science can generally only be achieved through a combination of theory and observation (experiment). A theory which is not based on empirically found facts and is not experimentally verified can be an interesting thought exercise, but in the end it may mislead from an understanding of nature. On the other hand, an observation that is not motivated by an actual theoretical question and whose results and consequences are not interpreted theoretically is useless. It may seem that the most reliable confirmation of a theory and the best interpretation of the observations would be a detailed theoretical prediction of the experimental results that agrees within the errors with the observations. However, any theoretical model is biased by our assumptions about importance of the various effects which may play a role in physics of the investigated object. Even a good agreement of a sophisticated theoretical model with a set of observations thus cannot guarantee that an alternative model would not fit a wider set better.

For example, it is used to model spectra of close binaries as a superposition of synthetic spectra radiated by small elements of the surfaces of the component stars. Each spectrum is computed from a non-LTE plane-parallel model atmosphere with local values of $T_{\rm eff}$ and $\log g$ which, according to the von Zeipel's theorem, correspond to the Roche model of the equipotential of a tidally distorted stellar surface. But, the Roche model is based on an assumption of hydrostatic equilibrium, which is inconsistent with the diffusion approximation of radiative transfer presumed by the von Zeipel's theorem. Such a sophisticated computation thus need not give a better result than a more pragmatic approximation using a single synthetic spectrum corresponding to a mean temperature

and gravity acceleration. This simple model is also often used as a template for RV measurements using the cross-correlation method. However, the components of binaries are often peculiar (for instance if they are fast rotators with a decretion disc), so that it is safer to avoid a use of any template or any assumption on structure of their atmospheres. This is what the disentangling enables.

3. Basic features of the disentangling

In its standard version, the method of disentangling assumes, that the only change in the spectra of binary components is their Doppler shift due to the orbital motion, but the method does not impose any restrictive presumption on their shape. Instead of templates needed in alternative methods to determine the Doppler shifts in individual exposures, the exposures in other orbital phases are used in disentangling to find the relative changes of RVs between the exposures and to solve for the orbital parameters. Naturally, the systemic velocity of the multiple system cannot be determined, unless some line in spectrum of a component is identified and the total value of its Doppler shift is measured. The spectra of components separated in the disentangling are their mean shapes over the period of observation. The separation of the component spectra has to be overdetermined, i.e. more exposures in different orbital phases are needed than is the number of components to be separated, in order to have a residual least squares, which are then minimized by the search for the parameters. The residual noise of the separated spectra decreases with the square root of the number of exposures, what makes their subsequent comparison with synthetic spectra easier and more reliable than an independent fit of individual exposures.

Because the Doppler shift of the continua is in practice unmeasurable, the disentangling is usually performed in limited regions of spectra normalized with respect to the continua. The contributions of the individual component stars to the continuum cannot therefore be separated and the line depths in the separated spectra are related to the level of continuum of the whole system. Consequently, a comparison of the disentangled spectra with theoretical models must take into account unknown multiplicative line-strength factors, together with the parameters of the rotational broadening and the Doppler shift due to the systemic velocity. Successful fit of one component by a synthetic spectrum decreases uncertainties in separating of other components. Hence, if there is an indication that the spectrum of some of the components is of a type for which we have reliable synthetic model (e.g. when the component is a main-sequence star), it is advantageous to perform the template-constrained disentangling, in which the spectrum of the one component is chosen from a set of the synthetic spectra and only the other(s) is computed as an unknown (see Hadrava, 2016, for explanation).

Possible changes of component spectra during the orbit or on a longer time scale can be investigated from differences between individual exposures and

their synthetic model computed as a superposition of the separated spectra Doppler shifted according to the corresponding RVs. The disentangling can be generalised to treat also changes of line profiles of individual components. The line-profile variations can often be expressed or at least approximated using a convolution of the intrinsic line profile with a time-variable broadening function dependent on a few parameters. The values of these parameters can be then found in the same way as the orbital parameters on which the broadening function of the Doppler shift (i.e. a shifted delta function) depends. The simplest case is the variation of line strength parametrized by a multiplicative factor. Another example are pulsations of a component star (see Hadrava et al., 2009). Fourier transform turns the convolution into multiplication and it thus splits the high-dimension linear problem of the separation of spectra into independent low-dimension solutions of each Fourier mode. This makes the Fourier disentangling fast and capable of further generalisations.

Any such generalisation should, however, be possible in both versions of disentangling – in the wavelength and in the Fourier domain. There appear sometimes claims (often misleading) in the literature about advantages and disadvantages of both methods. One alleged disadvantage should be a need to rebin the input spectra into an equidistant logarithmic scale. Regarding the wavelength dependence of the Doppler effect, it is a constant shift just in the logarithmic wavelength-scale, which is thus needed in both methods of disentangling as well as in any correct method of separation. Naturally, the difference from a linear wavelength-scale can be negligible in a narrow region of wavelengths, but it would be already an inaccuracy. If the Doppler shift should be represented by a unit off-diagonal matrix in the wavelength domain, then the input and output must be equidistant. It is possible to multiply this matrix from both sides by matrices performing the interpolation from the sampling of the input data and to the desired sampling of the output, but the outcome is the same as in subsequent interpolation, solution, and an additional resampling. The constant shift is given by a diagonal matrix (of unit complex numbers) in the Fourier representation, but the game takes place in the direct and inverse Fourier transform. It could also be adapted to any sampling of the input and output, but it is facilitated by a two-step procedure of interpolation into an equidistant sampling and then a use of Fast Fourier Transform (FFT). In any case, the overal procedure of spectra separation is in fact a linear interpolation from the input to output spectra. To minimize a smoothing by subsequent interpolations, it is recommendable to resample the input data into a finer scale than is the original resolution of the input spectra.

Another reservation about the Fourier disentangling repeated in a literature is that it does not allow to assign different weights to individual bins of input spectra. Usually it is not mentioned that the wavelength-domain disentangling does not enable to assign different weights to different Fourier modes, which is a more useful option. Possible dead pixels or cosmics in the input spectra can and should be eliminated in both methods during preprocessing of the data

before the resampling into the equidistant scale. On the other hand, a suitable weighting of different Fourier modes, i.e. of features on a long and short scale, enables to minimize an influence of unevenesses of continua and to strengthen the impact of narrow lines on solution of orbital parameters, or to combine the disentangling of spectra with different resolution. It is especially important in use of echelle spectra, where merging of the orders complicates finding of the continuum (see Hensberge, 2007). In some cases, like the Hα emission, the lines can be wider than the width of the order. It would be thus ideal to have to each high-resolution echelle spectrum also a simultaneous single-order low-resolution spectrum in wide region of wavelengths for flux normalisation.

A real advantage of the wavelength-domain disentangling is that it enables to separate the component spectra in a range enlarged on both sides of the input region for a short interval which enters the region only in some exposures due to non-zero Doppler shifts of the components. The solution in these intervals suffers more from the noise, but it is important that its absence does not violate the solution inside the sampled region. The choice of the region is equivalent to a multiplication of the whole spectrum by characteristic function of its interval, which means a convolution with its transform in the Fourier domain. In particular, the usage of FFT assumes a periodical repeating of the region, so that a line which disappears behind one edge of the region should appear at the other one. Its neglecting may disturb the solution at the region edges in a width comparable to the amplitude of the Doppler-shift. It is thus preferable to cut the regions of sampling in wavelengths where are no prominent lines (which is usually easy for early-type stars), or to choose a wider region and to skip a vicinity of its edges.

4. Disentangling in spectroscopic surveys

Disentangling of spectra obtained in follow-up campaigns focused on targets indicated in photometric surveys as possible binaries is a common practice. The recent development of space- and ground-based spectroscopic surveys opens a new option for study of multiple stars. As pointed out by Seeburger et al. (2024), the disentangling is a powerful technique to interpret the observed spectra, however, it may encounter slightly different problems when applied to spectroscopic surveys. In particular, spectra from such surveys can be of low resolution and available only from too few epochs. Low S/N and unsuitable distribution of the observations over the phases of orbital motion of individual objects can also be a problem. This is not necessarily always the case (see, e.g., Guo et al., 2022, who used more than six observations at resolving power $R \simeq 7500$ of each star). All these problems depend on the instrumentation used, strategy of the observations, as well as on duration of the survey, and they may diminish in a more distant future. If the survey has to yield a statistics of multiplicity of the stars, then its insufficient quality and completeness requires a careful treatment of

Table 1. Orbital parameters of 68 u Her (P in days, T in HJD-2400000, $K_{1,2}$ in km s^{-1}).

Solution	Kolbas+	43 spectra	4 spectra	$R \simeq 2000$
P	2.05102685(68)	2.050966(4)	2.050933(11)	2.050936(22)
T	47611.5007(15)	52302.226(2)	52302.227(3)	52302.221(7)
K_1	94.6±2.3	99.10(6)	97.98(16)	97.66±1.42
K_2	267.4±3.3	273.16	268.99	261.45
$q = K_1/K_2$	0.354	0.363(8)	0.364(2)	0.374(5)

selection effects. Nevertheless, Seeburger et al. (2024) present their implementation of disentangling, which should avoid the problem of few-epochs spectra replacing the search for orbital parameters by computation of the RVs only.

Considering simple double-lined spectroscopic binaries (SB2), it is true that three exposures are sufficient to separate the two spectra of components if their RVs are to be also disentangled, while at least five exposures are needed to disentangle all spectroscopic orbital parameters (i.e. the period P, periastron passage T, eccentricity e, longitude of periastron ω, and RV amplitudes $K_{1,2}$). In a review of existing codes for disentangling in their Tab. 1, Seeburger et al. (2024) claim that the KOREL code can solve only for orbital parameters and not RVs, what is not true. Any of these options can be chosen for any component, but the computation of RVs is rarely used because the choice of orbital parameters is more valuable. Although the authors justify the superiority of the template-independent methods, they are using templates to combine their disentangling with cross-correlation.

In order to test correctness and reliability of the operation of disentangling in a case of few-epochs data expected in spectroscopic surveys, it is advantageous to treat a subset selected from a large set of spectra. This makes it possible to check the reliability of results obtained from a limited data set against the results from a richer data set. As an example, let us take the eclipsing binary 68 u Her studied in detail by Kolbas et al. (2014). By analysing *Hipparcos* photometry and 43 high-resolution spectra (with $R \simeq 40000$) obtained at Calar Alto Observatory in 2008, the authors arrived at orbital parameters given here in the first column of Tab. 1.

In the present work we shall use another 43 spectra of Hα region secured in the years 2002-2007 using the CD700 camera ($R \simeq 13000$) at 2m Perek Telescope of Ondřejov Observatory. The KOREL disentangling shown in Fig. 1 separates the line profiles of the primary and secondary component and the water telluric lines, which are significant in this region (see the bottom three green lines). The disentangled orbital parameters are given in the second column of Tab. 1. The distribution of Bayesian probability of the parameters is shown in Fig. 2 by the error ellipse and isocontours corresponding to 1, 2, and 3-σ probability (see Hadrava, 2016, for explanation). The couples of parameters $P - T$ and $K_1 - q$

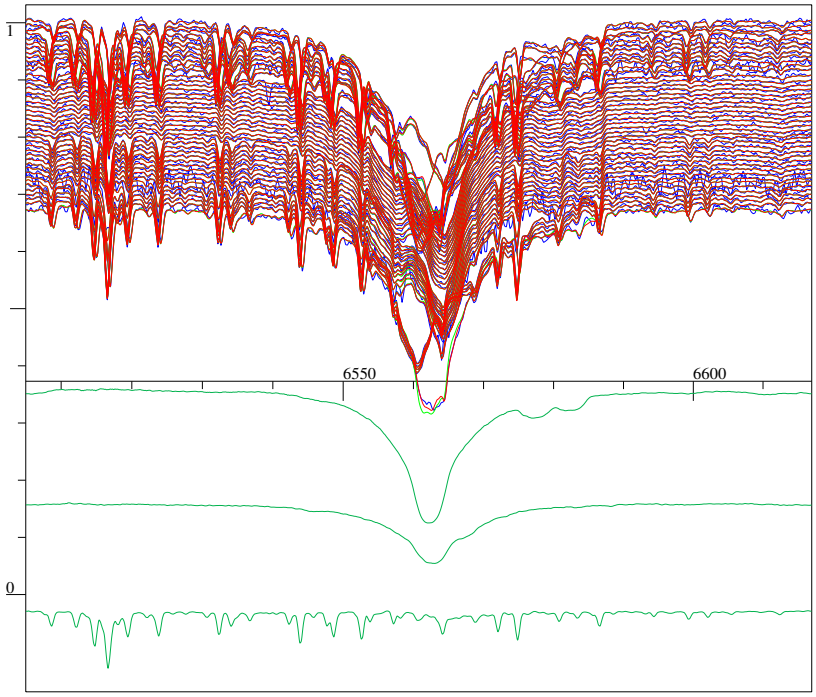


Figure 1. KOREL-disentangling of 43 Ondřejov spectra in Hα region of 68 u Her.

are anticorrelated with correlation coefficients -0.863 and -0.571, respectively.

If the initial conditions for the convergence of parameters contain a non-zero eccentricity, it quickly converges to zero in the case of 68 u Her. The longitude of periastron is thus chosen 90° to set the periastron passage identical with conjunction of the components (and a centre of eclipse). A negligible excentricity is a common case in short-period binaries due to their tidal circularization. An assumption of a circular orbit may thus simplify the search for orbital parameters and to decrease the number of needed exposures in short-lasting surveys. Unprecise initial estimates of velocity amplitudes also usually converge quite smoothly to the correct values. The orbital period which we obtained by adjusting an initial estimate to our spectroscopic data agrees with a relative error 2.97×10^{-5} with the ephemeris derived from the *Hipparcos* photometry. This is a satisfactory result regarding the fact that appart of the last exposure taken about 926 periods after the first one, all others are obtained within 604 periods. The search for period is, however, very sensitive to the initial conditions and often leads to a false local minimum.

To simulate data from a few-epochs survey, we can choose 4 exposures, which

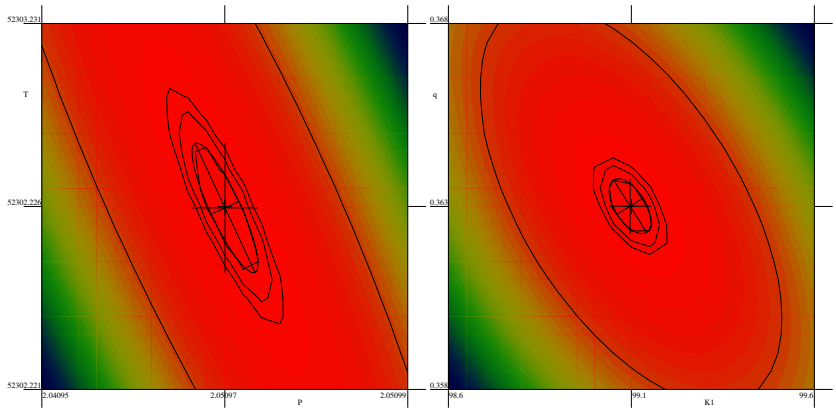


Figure 2. Distribution of probability of disentangled parameters in the plane $P - T$ (left panel) and $K_1 - q$ (right panel).

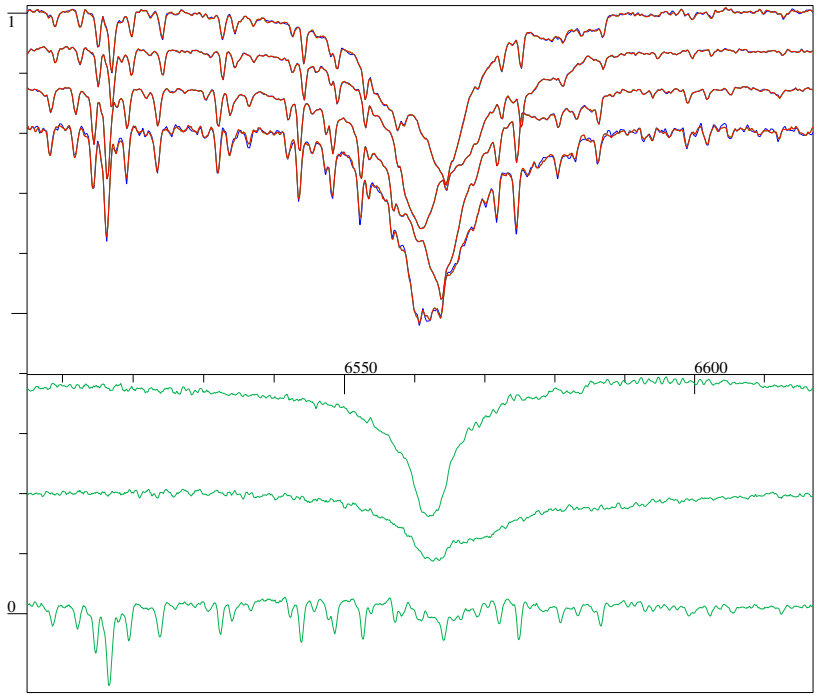


Figure 3. KOREL-disentangling of four Ondřejov spectra in Hα region of 68 u Her.

are a minimum needed to disentangle the three component spectra and RVs or the orbital parameters without e and ω. Because the second exposure in our set of spectra began immediately after the end of the first one, we shall choose the exposures 2-5. The disentangling of these four spectra shown in Fig. 3 reveals basically the same features as the results obtained from the whole set of 43 spectra (e.g. the CII doublet 6578 and 6582Å in the more massive primary), but naturally in a more noisy form. Because of a lower overdeterminacy, the input spectra are fitted more precisely than in the disentangling of the whole set (compare the input spectra displayed in blue lines with their fit in red), but their noise is more imprinted onto the separated spectra. The disentangled orbital parameters shown in the third column of Tab. 1 also agree with the previous solutions but with a higher error. For example, the relative error of the period with respect to the photometric ephemeris is 3.71×10^{-5} while the data span 292 periods. However, the period cannot be determined reliably from such scarce data. In our case, the first two exposures were taken at the beginning of the year 2002 and the next two in the summer 2003, so that periods shorter or longer for about $P/292 \simeq 0.007$d can give nearly the same orbital phases with one more or one less cycle. It can be seen from the distribution of residuals after the disentangling which is displayed in Fig. 4. Zooming in the vicinity of the central peak of the probability distribution, we can find that it has a fine structure. It is due to an interference of the sampling epochs. The central peak gets more compact and pronounced with increasing number of exposures, while the side lobes of the probability distribution diminish. For a disentangling of orbital parameters from a few-epochs spectroscopy, it is thus desirable to have an estimate of the orbital period (and possibly also the epoch of conjunction) from a photometric survey.

Instead of disentangling the orbital parameters, we can also disentangle independently RVs of all components in all exposures as suggested by Seeburger et al. (2024). In a template independent disentangling we have to fix RV of one exposure of each component to prevent the ambiguity in an additive constant to RVs of the component and the corresponding Doppler shift of its separated spectrum. In our present case of Hα region we can retain orbital parameters for the telluric lines, which are calculated from the coordinates of the star and to solve only for the strengths of these lines. If we start the convergence of RVs from values close to the solution found using disentangling of orbital parameters, we arrive at solution which is very similar in both the separated spectra and the RVs (see Tab. 2). Residual noise σ of the spectra in units of the continuum level is even slightly smaller compared to the disentangling of the orbital parameters (see the last line of Tab. 2) owing to a higher number of free parameters (6 RVs instead of P, T, and $K_{1,2}$). However, if the initial conditions of some RVs deviate significantly from this correct solution, the disentangling converges to a false minimum, separated spectra are distorted, and RVs of other components are also wrong. While in the disentangling of orbital parameters the RVs of each component in each exposure are bound to be consistent with other exposures, in

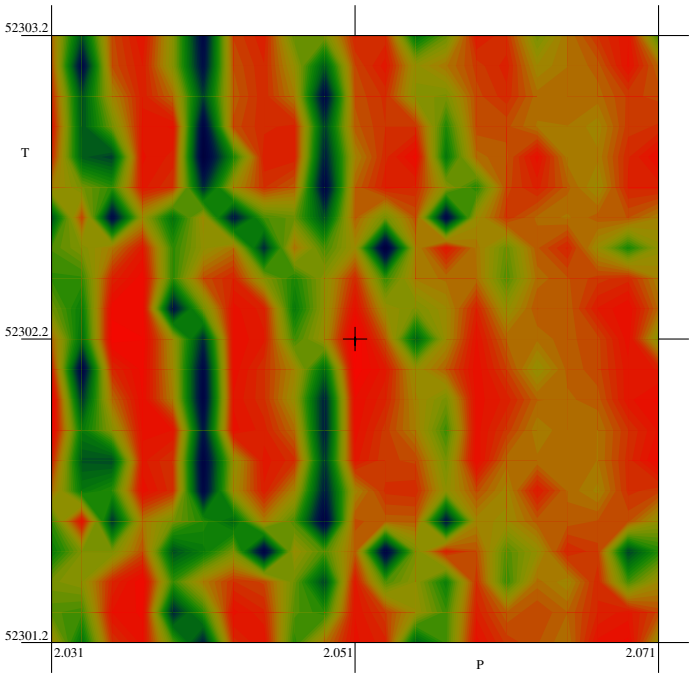


Figure 4. Distribution of residuals in the $P-T$ plane at disentangling of four spectra.

Table 2. Radial velocities disentangled in various solutions.

Spectra/parameters	43/orbit	4/orbit	4/RVs	43/orbit	4/orbit	4/RVs
HJD-2400000	RV_1	RV_1	RV_1	RV_2	RV_2	RV_2
52303.6811	96.8	94.9	97.6	−267.6	−259.9	−263.2
52308.6665	−77.0	−75.4	−81.0	204.6	206.9	199.5
52841.3914	70.5	63.6	62.4	−183.5	−176.2	−182.8
52903.3475	−53.4	−55.4	−56.0	148.8	152.7	149.2
$\sigma \times 10^3$	1.99	1.07	1.05			

their direct disentangling they are prone to fall into a false local minimum or to confuse to which component they belong. If there are available more exposures than the very minimum of three, then the disentangling of RVs has more free parameters than the disentangling of orbital parameters (especially if the period is known), which causes a higher instability of the solution. Regarding also the fact that the whole solution of orbital parameters offers more information about the observed systems, the decision to limit the disentangling to RVs is not much suitable.

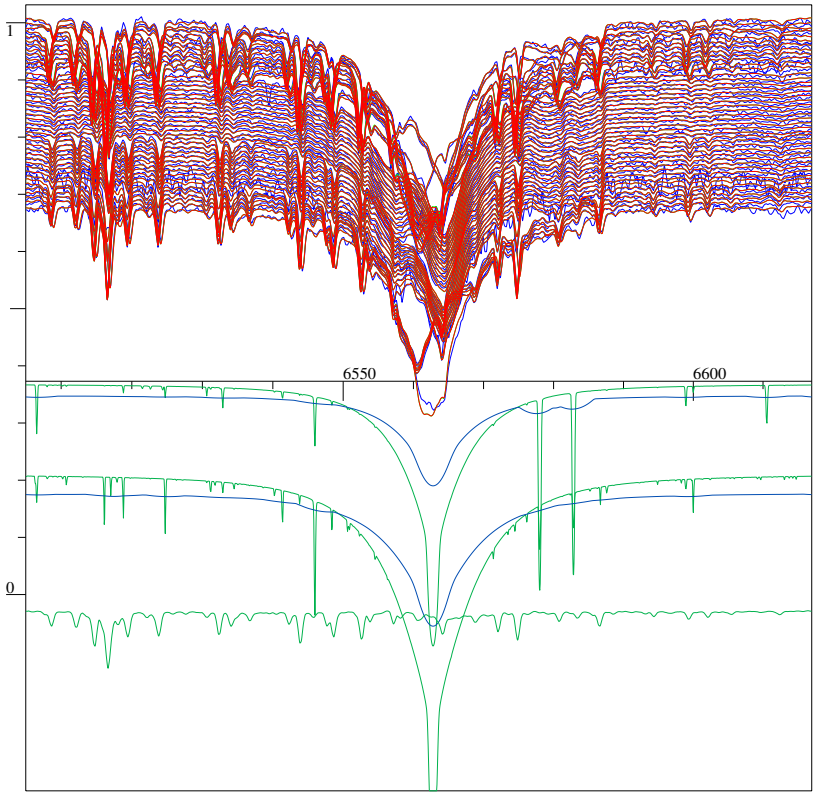


Figure 5. KOREL-disentangling of 68 u Her constrained by synthetic templates for 21000 K and 11750 K.

When we find that the disentangled spectra agree sufficiently with spectra of main-sequence stars or another type of objects for which model spectra are available, we can use for their further analysis a template-constrained disentangling. In the present case of 68 u Her we can use synthetic spectra computed using the code SPECTRUM, version 2.75, by Gray (1999), applied to the grid of LTE model atmospheres by Castelli & Kurucz (2003). If the spectra of one component and of the telluric lines are fixed to the result from the free disentangling, while the template of the other component is chosen from the set of synthetic spectra, and we converge its line strengths, rotational broadening, and systemic velocity, we find the best fit for the primary component at the temperature 21000 K and for the secondary at 11750 K. Disentangling constrained by both these templates is displayed in Fig. 5; here the green lines show the input synthetic spectra and the cyan their rotational broadening rescaled in depth. This

solution has a residual noise $\sigma = 3.09 \times 10^{-3}$, that is only for a half higher than that of the free disentangling. However, it does not show, e.g., the drop in red wing of Hα of the secondary which can be seen even in the disentangling of the subset of four spectra in Fig. 3. Using a quadratic fit also to three neighbouring synthetic templates for each component, we arrive at estimate of the temperatures of the component stars 21350 K and 11900 K, for which Kolbas et al. (2014) found 21600 ± 220 K and 12600 ± 550 K. The mean line-strength factors indicate the continuum of the primary to be at 0.750 and of the secondary at 0.232 of the total continuum, which is close to the *Hipparcos* photometric light ratio 0.739 ± 0.026 according to Kolbas et al. (2014). The systemic velocity of the primary is $\gamma_1 = -22.0\,\mathrm{km\,s^{-1}}$ and of the secondary $\gamma_2 = -6.2\,\mathrm{km\,s^{-1}}$.

The template-constrained disentangling of RVs can be performed even for a single exposure. This procedure can also select the templates which fit the observed spectrum best and it could be applied if a survey does not contain more than one exposure of a star. However, due to a higher noise, it is less sensitive than the disentangling of multiple exposures. This method is practically equivalent to a two-dimensional cross-correlation, with a difference that the rotational broadening is also obtained in this way.

To test the performance of the Fourier disentangling in a case of low signal-to-noise ratio and low-resolution spectra, we can add to our data an artificial noise and to blur them by convolving them with a Gaussian function or another kernel imitating the instrumental profile of the spectrograph in use. Our spectra of 68 u Her can be degraded to a resolution $R \sim 2000$ using a convolution with Gaussian of half-with 1.5 Å. Applying it to the above selected four spectra, we arrive by disentangling to the orbital parameters given in the fourth column of Tab. 1 and to the separated spectra shown in Fig. 6. As we can see, these results are still qualitatively consistent with those obtained from the spectra with a higher resolution. Naturally, the tinny telluric lines cannot be clearly distinguished, what may cause problems also in a case of binaries with late-type stars.

5. Discussion and conclusion

In addition to the few epochs of exposures and their random distribution in orbital phase, the low S/N ratio can also be an obstacle to a successful disentangling in spectroscopic surveys. As already mentioned, the residual noise of the separated spectra decreases with a number of the input exposures, but in a few-epochs data it cannot be reliably diminished. The limiting factor is not the absolute value of S/N, which is given by the ratio of (mostly photon) noise to the level of continuum, but its relation to the depth and width of the spectral lines, which are the carrier of information about the multiplicity of the stellar system. The same S/N can thus be sufficient to separate the components in

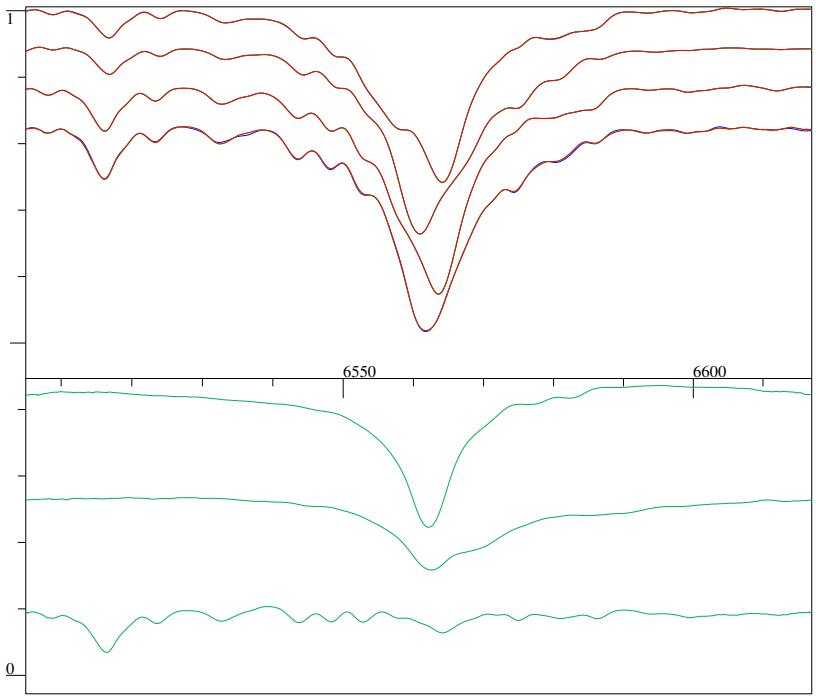


Figure 6. KOREL-disentangling of 68 u Her spectra with $R \sim 2000$.

some SB2 system, it may fail to detect a companion in some other system, or it may be completely unable to find RV-changes in yet another system.

Similarly, the applicability of a particular method of disentangling is not given by resolving power of the used spectrograph alone, but it also depends on the amplitude of RVs in the observed system and on the spectra of its components. Fourier disentangling enables to reach a sub-pixel precision in the determination of the Doppler shift (see Hadrava, 2009), but it does not mean a possibility to resolve and to separate dense narrow lines of late-type stars if they are below the resolution of the detector. The residual noise may mimic intrinsic spectral features in low resolution and low S/N spectra and no method can then yield a reliable disentangling of a low number of exposures.

Finally, the success of disentangling and reliability of its results for a particular system also depends on its possible intrinsic variability, e.g. due to pulsations, mass loss, spots etc. An automated application of disentangling to large spectroscopic surveys should thus be combined with a more sophisticated clasification and pre-selection of the targets like in the work by Škoda et al. (2020). Statistical conclusions from such studies should take into account the selection effects

of the detectability of the companion stars.

In spite of these complications, the disentangling of spectra is a method appropriate for treatment of multiple stars observed in spectroscopic surveys. The template-independent version is capable to interpret also spectra of systems with some peculiarities and the template-constrained disentangling can find parameters of stellar atmospheres of common stars. The disentagling of orbital parameters is preferable to the disentangling of radial velocities. It is desirable to combine the disentangling of spectra with a light-curve solution of data from photometric surveys.

Acknowledgements. This work has been supported by project RVO 67985815. It uses spectra collected with the 2m Perek Telescope at Ondřejov Observatory of the Astronomical Institute of the Czech Academy of Sciences.

References

Bagnuolo, William G., J. & Gies, D. R., Tomographic Separation of Composite Spectra: The Components of the O-Star Spectroscopic Binary AO Cassiopeiae. 1991, *Astrophysical Journal*, **376**, 266, DOI:10.1086/170276

Castelli, F. & Kurucz, R. L., New Grids of ATLAS9 Model Atmospheres. 2003, in IAU Symposium, Vol. **210**, *Modelling of Stellar Atmospheres*, ed. N. Piskunov, W. W. Weiss, & D. F. Gray, A20

Gray, R. O. 1999, SPECTRUM: A stellar spectral synthesis program, Astrophysics Source Code Library, record ascl:9910.002

Guo, Y., Liu, C., Wang, L., et al., The statistical properties of early-type stars from LAMOST DR8. 2022, *Astronomy and Astrophysics*, **667**, A44, DOI:10.1051/0004-6361/202244300

Hadrava, P., Orbital elements of multiple spectroscopic stars. 1995, *Astronomy and Astrophysics, Supplement*, **114**, 393

Hadrava, P., Notes on the disentangling of spectra. I. Enhancement in precision. 2009, *Astronomy and Astrophysics*, **494**, 399, DOI:10.1051/0004-6361:200810810

Hadrava, P., Disentangling of Stellar Spectra. 2016, in Astrophysics and Space Science Library, Vol. **439**, *Astronomy at High Angular Resolution*, ed. H. M. J. Boffin, G. Hussain, J.-P. Berger, & L. Schmidtobreick, 113

Hadrava, P., Šlechta, M., & Škoda, P., Notes on disentangling of spectra. II. Intrinsic line-profile variability due to Cepheid pulsations. 2009, *Astronomy and Astrophysics*, **507**, 397, DOI:10.1051/0004-6361/200912554

Hensberge, H., Removal of Instrumental Signatures in Echelle Spectra. 2007, in Astronomical Society of the Pacific Conference Series, Vol. **364**, *The Future of Photometric, Spectrophotometric and Polarimetric Standardization*, ed. C. Sterken, 275

Kolbas, V., Dervişoğlu, A., Pavlovski, K., & Southworth, J., Tracing CNO exposed layers in the Algol-type binary system u Her. 2014, *Monthly Notices of the RAS*, **444**, 3118, DOI:10.1093/mnras/stu1652

Seeburger, R., Rix, H.-W., El-Badry, K., Xiang, M., & Fouesneau, M., Autonomous disentangling for spectroscopic surveys. 2024, *Monthly Notices of the RAS*, **530**, 1935, DOI:10.1093/mnras/stae982

Simkin, S. M., Measurements of Velocity Dispersions and Doppler Shifts from Digitized Optical Spectra. 1974, *Astronomy and Astrophysics*, **31**, 129

Simon, K. P. & Sturm, E., Disentangling of composite spectra. 1994, *Astronomy and Astrophysics*, **281**, 286

Škoda, P., Podsztavek, O., & Tvrdík, P., Active deep learning method for the discovery of objects of interest in large spectroscopic surveys. 2020, *Astronomy and Astrophysics*, **643**, A122, DOI:10.1051/0004-6361/201936090

Contrib. Astron. Obs. Skalnaté Pleso **55/3**, 340 – 345, (2025)
https://doi.org/10.31577/caosp.2025.55.3.340

Enhanced spectral disentangling techniques for long-period hot subdwarf binaries

P. Németh[1], **J. Vos**[2] **and M. Cabezas**[2]

[1] *Astroserver.org, Fő tér 1, 8533 Malomsok, Hungary*
(E-mail: peter.nemeth@astroserver.org)

[2] *Astronomical Institute of the Czech Academy of Sciences*
251 65 Ondřejov, The Czech Republic

Received: November 14, 2024; Accepted: January 19, 2025

Abstract. Wavelength space binary spectral disentangling is discussed with a data-driven, steepest-descent chi-square minimizing, global fitting procedure that applies stacked synthetic spectra to render composites. With additional constraints such as Gaia distance, mass ratio, orbital period, and separation of the binary members the stellar parameter precision can be improved even for non-eclipsing systems. We follow the orbits of 36 systems of which we discuss JL 277 here.

Key words: composite spectrum binaries

1. Introduction

Composite spectrum binaries are systems where the observed spectrum is a blend of light from two stellar components. These are common among binaries with evolved stars like hot subdwarfs or (low-mass) white dwarfs with cool companions.

The main challenge is disentangling the contributions of each star, which requires robust methods to accurately derive the atmospheric parameters (e.g., temperature, gravity) and flux contributions from the composite spectrum. These entangled parameters in composite spectra lead to serious degeneracies and systematic errors. Overcoming these requires high signal-to-noise, multi-wavelength observations, and various assumptions or constraints on the systems.

Historically, high-precision stellar parameters were obtainable primarily from eclipsing binaries, where light curves provided direct constraints on component sizes and flux ratios. For non-eclipsing systems, the analysis relied heavily on assumptions and models, leading to larger uncertainties.

With the upcoming Gaia DR4 release, the landscape is changing. Spectral decomposition techniques, combined with precise mass ratios and astrometric data like orbital separations, offer a powerful approach to studying non-eclipsing binaries at a level of precision that previously was limited to single stars or eclipsing systems.

Both wavelength-domain (Simon & Sturm, 1994) and Fourier-domain disentangling (Hadrava 1995, Hadrava 1997, also in these proceedings) are designed to simultaneously solve for orbital parameters and to separate component spectra from a set of spectra sufficiently covering the orbital period. Our method of fitting the observed spectra by synthetic templates enables us to determine atmospheric parameters even from a single observation.

2. Spectral disentangling with XTGRID

We fit the observed composite spectrum with a synthetic model, constructed as a linear combination of two single-star synthetic spectra. The method is implemented in the chi-square minimizing, data-driven, global fitting procedure XTGRID (Németh et al., 2012). The fitting process adjusts the atmospheric parameters (e.g., effective temperature, surface gravity, metallicity) and the relative flux contributions iteratively until convergence is achieved. The primary goal is to derive accurate atmospheric parameters for both stars, disentangling their individual contributions from the observed composite spectrum at the given observed or assumed constraints. XTGRID can combine models from various stellar atmosphere codes and synthetic libraries to render composite models. We applied here TLUSTY models (Hubeny & Lanz, 2017) for the hot subdwarf and ATLAS models extracted from the BOSZ library (Bohlin et al., 2017) for the cool companions.

The observed spectrum is modeled iteratively using synthetic spectra generated for a range of stellar parameters. The synthetic composite spectrum $F_{\rm model}(\lambda)$ is expressed as:

$$F_{\rm model}(\lambda) = w_1 F_1(\lambda(1 - v_1/c)) + w_2 F_2(\lambda(1 - v_2/c)),$$

where $F_1(\lambda(1 - v_1/c))$ and $F_2(\lambda(1 - v_2/c))$ are the radial velocity corrected synthetic spectra of the two components, and w_1, w_2 are the respective weighting factors representing their flux contributions.

We incorporate observed mass ratios as additional constraints during the fitting process. The mass ratio provides a direct link between the stellar masses M_1 and M_2, which we use to limit the surface gravity ratios and the parameter space of the solutions. This helps to significantly reduce the degeneracy in the fit and improves the accuracy of derived stellar properties.

In non-eclipsing systems, the mass ratio obtained from radial velocity measurements gives us valuable information that previously was not fully utilized in spectral decomposition. By integrating this constraint, we effectively reduce the number of free parameters, thereby refining the solution.

The formation of hot subdwarfs is a direct result of the common envelope and/or Roche-lobe overflow evolution channels (Pelisoli et al., 2020), and the precise surface parameters of the components are keys to fine-tuning evolution models.

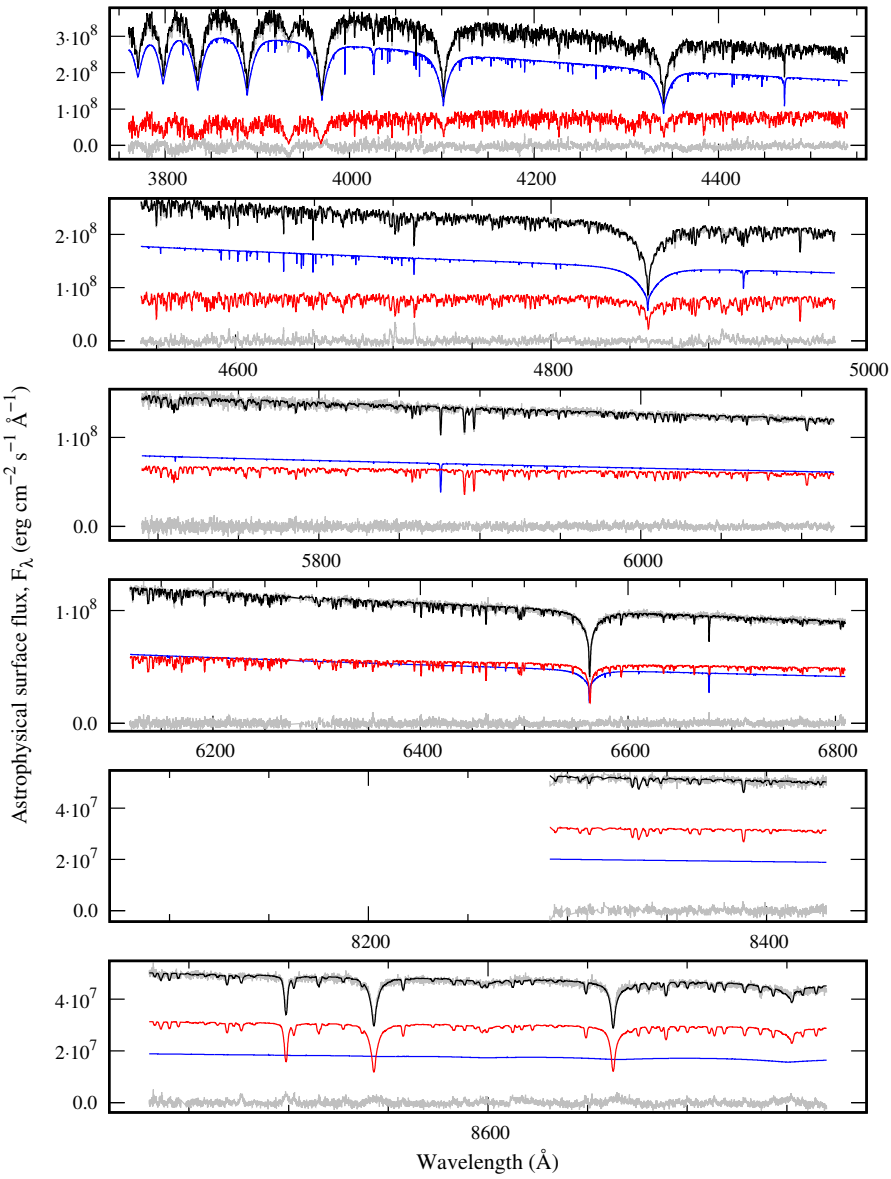


Figure 1. Best-fit XTGRID / TLUSTY+ATLAS composite model for JL 277 shown in *black*. The VLT / UVES observation is in *grey*, the TLUSTY model is in *blue*, and the ATLAS model is shown in *red*. At zero flux we show the fit residuals. The model parameters are available on request.

Figure 1 shows the best-fit spectral model for JL 277, an sdB+F5V type binary. The measured spectral energy distribution from ultraviolet, optical, and infrared measurements is available for many systems (e.g. Simbad VizieR service) and allows the flux contributions from the spectral model to be compared in much broader ranges as demonstrated for JL 277 in Figure 2.

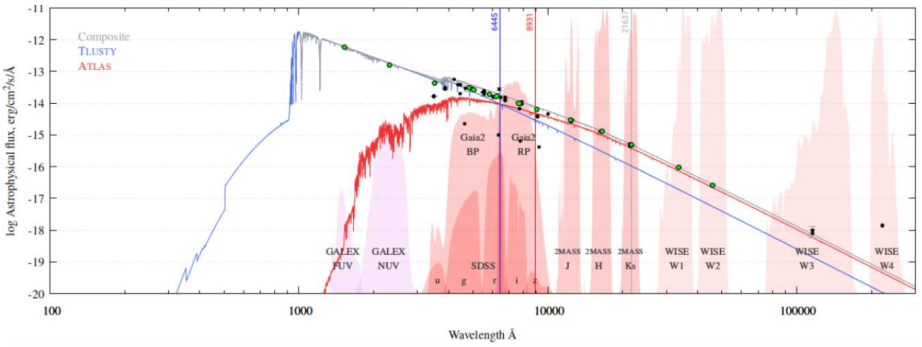


Figure 2. Spectral energy distribution of JL 277. All data points were taken from the VizieR Photometry Viewer service. The photometric data were de-reddened using $E(B-V) = 0.022$ mag (stilism.obspm.fr). The green points were used to match the slope of the passband convolved combined TLUSTY and ATLAS fluxes to the observations and the model was normalized to the observed SED in the 2MASS/K band.

3. Radial velocities

Radial velocity measurements of JL 277 were obtained by cross-correlating the observations with RV standard spectra. Figure 3 shows the radial velocity curve. These velocities allowed orbital parameters, semi-amplitudes, and the mass ratio to be determined assuming a Keplerian orbit within the AOTS database system (https://a15.astro.physik.uni-potsdam.de).

4. Future prospects with Gaia DR4

Gaia DR4 is expected to provide precise measurements of orbital separations for a large number of binary systems, including non-eclipsing binaries. This will enable a self-consistent analysis of these systems by combining spectroscopic data (from radial velocity and spectral fitting) with astrometric information. With the orbital size a, period P, and mass ratio q (already included in our fitting process), we can derive absolute masses M_1 and M_2. Consequently, the observed properties of each binary member can be matched to single-star models with commensurable precision.

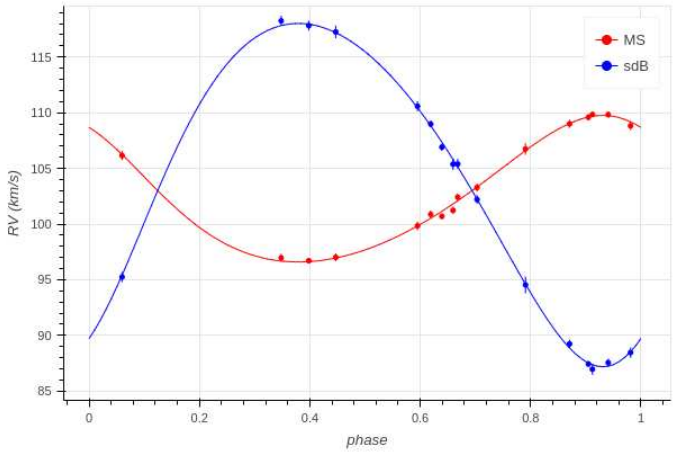


Figure 3. Radial velocity curve of JL 277 from the AOTS system.

Table 1. Orbital parameters of JL 277 extracted from the AOTS system.

Parameter	Value ± Error
P (days)	1090.3 ± 1.5
$T0$ (-2400000)	55827.0 ± 1.5
ω (deg)	3.52 ± 0.10
e	0.086 ± 0.010
K_1 (km/s)	14.470 ± 0.160
K_2 (km/s)	6.528 ± 0.067
q ($M_{\rm sdB}/M_{\rm MS}$)	0.451 ± 0.008

This approach offers a major advantage for the study of non-eclipsing binaries, allowing us to reach precision levels previously achievable only in eclipsing systems. By utilizing observed orbital characteristics, we can fully characterize the binary components, including their evolutionary states and masses, without relying on light curve data.

5. Summary

The inclusion of photometric data and mass ratios as constraints in spectral decomposition significantly enhances the accuracy of derived stellar parameters for non-eclipsing composite spectrum binaries. This methodology opens up new avenues for analyzing these systems with precision previously limited to eclipsing binaries. With the upcoming Gaia DR4 release, we anticipate further improvements in the accuracy of our method, allowing to investigate a wider range of

Table 2. Parameters of the members in JL 277.

Parameter	Primary±1σ	Secondary±1σ
$T_{\rm eff}$ (K)	24200±400	6050±150
$\log g$ (cgs)	5.29±0.09	4.10±0.10
M ($M_\odot$)	0.466±0.020	1.034±0.047
R ($R_\odot$)	0.252±0.003	1.499±0.030
L ($L_\odot$)	19.39±0.77	2.718±0.111
d (pc)	1014.5±20.5	

binaries and better understand their evolutionary stages. This work not only broadens the scope of precise binary star analysis but also has the potential to refine our understanding of binary star evolution, especially in cases involving hot subdwarfs, low-mass white dwarfs, and other evolved stellar components.

Another case study for the quasi Wolf-Rayet (He-rich sdO) and B7V binary HD 45166 is also available in these proceedings.

Acknowledgements. We thank the anonymous referee for their comments and suggestions, which have improved the clarity and quality of this manuscript. This research was supported by the Grant Agency of the Czech Republic (GAČR 22-34467S).

References

Bohlin, R. C., Mészáros, S., Fleming, S. W., et al., A New Stellar Atmosphere Grid and Comparisons with HST/STIS CALSPEC Flux Distributions. 2017, *Astronomical Journal*, **153**, 234, DOI:10.3847/1538-3881/aa6ba9

Hadrava, P., Orbital elements of multiple spectroscopic stars. 1995, *Astronomy and Astrophysics, Supplement*, **114**, 393

Hadrava, P., Relative line photometry of eclipsing binaries. 1997, *Astronomy and Astrophysics, Supplement*, **122**, 581, DOI:10.1051/aas:1997102

Hubeny, I. & Lanz, T., A brief introductory guide to TLUSTY and SYNSPEC. 2017, *arXiv e-prints*, arXiv:1706.01859, DOI:10.48550/arXiv.1706.01859

Németh, P., Kawka, A., & Vennes, S., A selection of hot subluminous stars in the GALEX survey - II. Subdwarf atmospheric parameters. 2012, *Monthly Notices of the RAS*, **427**, 2180, DOI:10.1111/j.1365-2966.2012.22009.x

Pelisoli, I., Vos, J., Geier, S., Schaffenroth, V., & Baran, A. S., Alone but not lonely: Observational evidence that binary interaction is always required to form hot subdwarf stars. 2020, *Astronomy and Astrophysics*, **642**, A180, DOI:10.1051/0004-6361/202038473

Simon, K. P. & Sturm, E., Disentangling of composite spectra. 1994, *Astronomy and Astrophysics*, **281**, 286

Contrib. Astron. Obs. Skalnaté Pleso **55/3**, 346 – 351, (2025)
https://doi.org/10.31577/caosp.2025.55.3.346

Weighing single-lined spectroscopic binaries using tidal RVs: the case of V723 Mon

K. Masuda[1], **T. Hirano**[2,3] **and M. Tomoyoshi**[1]

[1] *Department of Earth and Space Science, Osaka University, Osaka 560-0043, Japan (E-mail: kmasuda@ess.sci.osaka-u.ac.jp)*

[2] *Astrobiology Center, NINS, 2-21-1 Osawa, Mitaka, Tokyo 181-8588, Japan*

[3] *National Astronomical Observatory of Japan, NINS, 2-21-1 Osawa, Mitaka, Tokyo 181-8588, Japan*

Received: November 2, 2024; Accepted: December 10, 2024

Abstract. The tidal deformation of a star in a close binary not only produces the photometric flux variations (ellipsoidal variations, ELVs) but also causes the apparent radial velocity (RV) variations due to asymmetric distortion of the absorption lines. This "tidal RV" signal contains information equivalent to that from photometric ELVs, enabling its use in mass estimation for single-lined spectroscopic binaries (SB1s) and offering a potentially more robust approach against contaminating light relative to ELVs. In this work, we develop a quantitative model for the tidal RV signal and apply it to the binary system V723 Monocerotis, where both ELV and tidal RV signals are detected, and successfully determine the component masses using only the primary star's absorption lines. The masses derived from the tidal RV modeling show a reasonable agreement with those from an analysis based on ELVs that carefully accounts for the flux contamination from the secondary star. This result demonstrates that tidal RVs provide a useful alternative means for mass estimation in SB1s.

Key words: Radial velocity – Red giant stars – Tidal distortion

1. Introduction

Many important binary systems are observed as single-lined spectroscopic binaries (SB1s). In a tight SB1 that exhibits flux variations due to tidal deformation of the primary star (ellipsoidal variations, ELVs),[1] the binary mass can be determined by combining ELVs with the primary's radial velocity (RV) variations due to orbital motion and information of the primary's radius. This method has been used for the mass estimation in close binaries including X-ray systems, but it has been pointed out that contaminating light from sources other than the primary star, if not properly taken into account, can introduce systematic errors in the mass and inclination estimates (Kreidberg et al., 2012).

[1]In this work, the "primary" refers to the brighter component of an SB1 for which radial velocities are measured, and it is not necessarily more massive than the secondary.

In this work, we focus on spectroscopic effects of tidal deformation as an alternative means for binary mass estimation. The deformation of the primary star does not only change the apparent size of the star, it also changes the relative area of the approaching and receding parts of the visible stellar surface in phase with the orbit. This results in asymmetric distortion of the Doppler-broadened absorption lines, and induces apparent RV variations (e.g., Sterne, 1941; Kopal, 1959); see Figure 1. Because this "tidal RV" signal shares a common origin as ELVs, it should in principle enable mass estimation of an SB1 system using only the primary star's absorption lines from high-resolution spectroscopic data, providing a potentially more robust approach against flux contamination that reduces the photometric ELV amplitude. To test this concept, we develope a quantitative model of the tidal RV signal and apply it to the binary system V723 Monocerotis. The system consists of a red giant primary and a more compact, hotter subgiant secondary (El-Badry et al., 2022), where significant tidal deformation of the primary has enabled detection of both EVs and tidal RV signals (Jayasinghe et al., 2021; Masuda & Hirano, 2021).

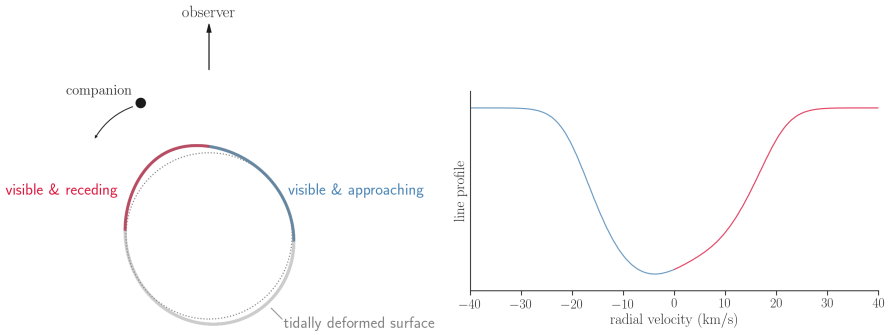


Figure 1. Schematic illustration of the tidal effect on the absorption line profile; figure from Masuda & Hirano (2021). *(Left)*— The thick gray line shows the equator of the red giant deformed by the companion. *(Right)*— The absorption line profile corresponding to the configuration shown in the left panel.

2. The tidal RV model

We model the RV signal due to the orbital motion and tidal deformation effects in the following steps. See Masuda & Hirano (2021) for more details.

1. The distributions of the flux and line-of-sight velocity over the surface of the primary star is computed adopting the Roche model, given the time of inferior conjunction (secondary star is in front) t_0, orbital period P, inclination i, primary's mass M_1, secondary's mass M_2, primary's radius R_1, gravity-darkening coefficient y, and two limb-darkening coefficients u_1

and u_2 for the quadratic law. The flux and velocity values are evaluated at 768 `HEALPix/healpy` pixels (Górski et al., 2005). The gravity- and limb-darkening coefficients are constrained to be around the values determined as a function of a single effective wavelength $\lambda_{\rm eff}$ using the relation in Claret & Bloemen (2011).

2. The flux and velocity distributions are used to compute the absorption line profile of the primary star, given the macroturbulence velocity ζ. For the macrotubulence velocity field, we adopt a radial–tangential model and assume the common velocity dispersions for both directions.

3. The line profile model was used to simulate the cross-correlation function (CCF) as results from cross-correlating the observed spectrum with a theoretical template spectrum, whose line profile is assumed to be a Gaussian with the standard deviation (in the velocity space) of β. The tidal RV, $v_{\rm tidal}$, is computed as the velocity corresponding to the CCF peak.

4. The center-of-mass velocities v_0 of the primary star due to orbital motion are computed as $v_0(t) = -K \sin\left[\frac{2\pi(t-t_0)}{P}\right] + \gamma$, where K is computed from the above M_1, M_2, i, and P, and γ is the RV zero point. Then the full physical model for the observed RVs is $v_{\rm model}(t) = v_0(t) + v_{\rm tidal}(t)$.

The above physical RV model is specified by the set of parameters $\theta = \{M_1, M_2, R_1, t_0, P, i, \zeta, \lambda_{\rm eff}, \beta, \gamma\}$, which are inferred from the RV data simlutaneously.

3. Application to V723 Mon

We use the model in the previous section to fit the RV data of V723 Mon from Strassmeier et al. (2012). The velocities were derived from high-resolution ($R = 55,000$), optical (338–882 nm) spectra from the STELLA échelle spectrograph (SES) on the 1.2 m STELLA-I telescope at the Teide Observatory (Strassmeier et al., 2004; Weber et al., 2008; Strassmeier et al., 2010), via a cross correlation analysis using a synthetic spectrum. We also adopt $v \sin i = 15.7 \pm 1.0$ km/s and $\zeta = 2.0 \pm 1.1$ km/s determined by forward-modeling the Subaru/IRD spectrum of this target as additional constraints; see Tomoyoshi et al. (2024) for details.

Figure 2 shows the inferred RV model along with the observed data. We successfully modeled the tidal RV signal (upper-middle panel), and obtained $M_1 = 0.46^{+0.12}_{-0.09}\,M_\odot$ and $M_2 = 2.5 \pm 0.2\,M_\odot$ using spectroscopic information (i.e., RVs and line widths) alone. Although we did not explicitly take into account the significant contamination of the secondary's flux in this system (El-Badry et al., 2022)., our results show a reasonable agreement with $M_1 = 0.44 \pm 0.06\,M_\odot$ and $M_2 = 2.8 \pm 0.3\,M_\odot$ obtained from the absolute flux and ELVs, after carefully modeling the secondary's flux contamination (El-Badry et al., 2022).

This serves as a proof of concept that modeling of tidal RVs is useful as an alternative means to measure the mass of tidally deformed SB1s. As shown in

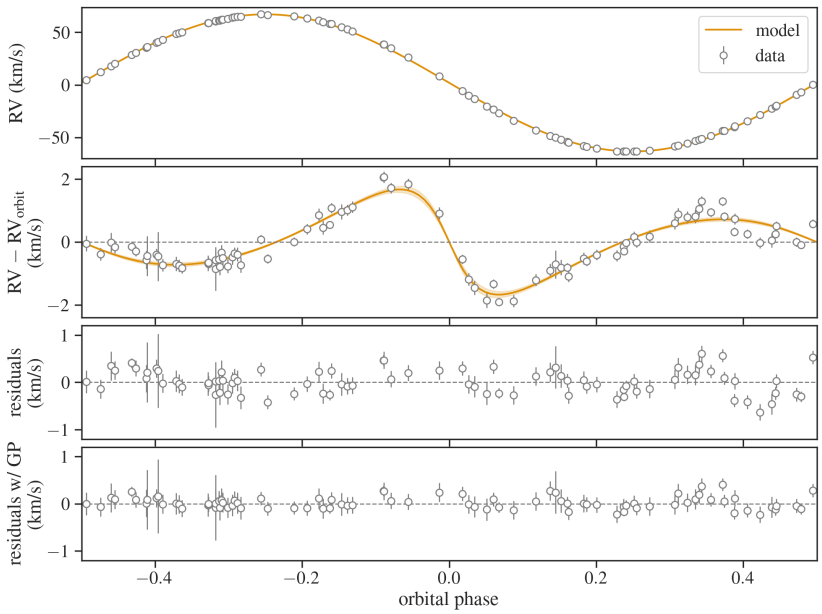


Figure 2. The observed and modeled RVs as a function of orbital phase. The white filled circles are the RV data from Strassmeier et al. (2012). The orange solid line and the shaded region respectively show the mean and standard deviation of the posterior models. *(Top)* — Raw RVs. *(Upper-middle)* — RVs relative to the orbital component plus γ ($v_{\rm tidal}$ in Section 2). *(Lower-middle)* — Residuals relative to the full physical model. *(Bottom)* — RVs relative to the full physical model + mean prediction of the Gaussian process noise model.

the corner plot for M_1, M_2, R_1, and i (Figure 3), however, our modeling (black contours) prefers $\sim 2\sigma$ larger i and smaller R_1 than those derived by El-Badry et al. (2022) (red crosses) so that the resulting $v \sin i$ remains similar. This could indicate a systematic error in the inclination estimate in our tidal RV modeling. If this bias is indeed present, one possible explanation is that our analytic CCF evaluation model may be overly simplified, as it assumes a uniform shape for all absorption lines. Reducing this type of systematic error may be possible by directly modeling the line shapes rather than using RV values derived from distorted lines. This approach will be explored in future work.

4. Summary and conclusion

We developed a quantitative model for the apparent RV variations due to orbital-phase-dependent tidal deformation of a star, and used it to determine the physical parameters of the binary system V723 Mon only using RVs and

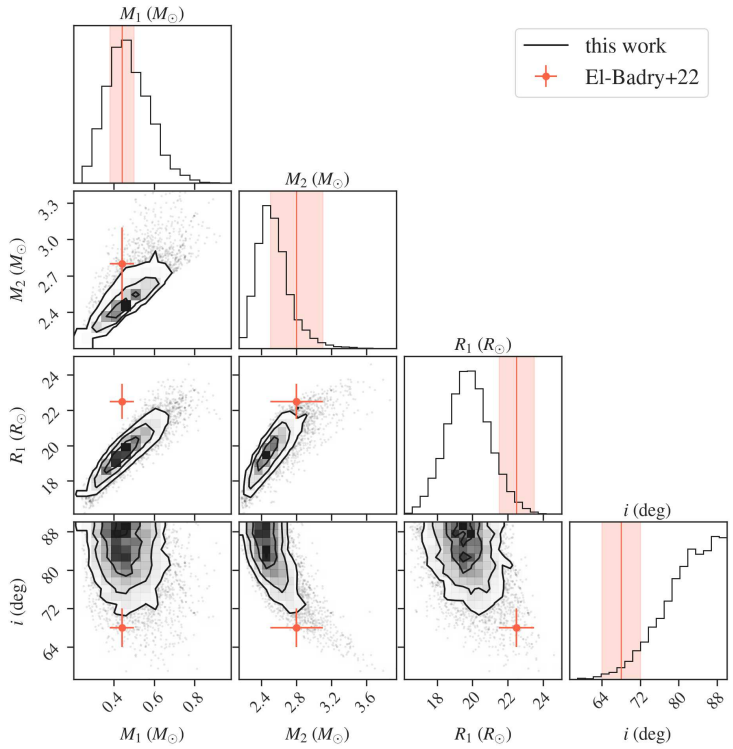


Figure 3. Corner plot for the posterior samples obtained from our tidal RV modeling (black contours and histograms). The red crosses are the values derived by El-Badry et al. (2022) using ELVs.

$v \sin i$ of the primary star. To our knowledge, this is the first quantitative mass measurement of an SB1 system using only spectroscopic data, independent of stellar models or absolute flux information. Although we did not explicitly model the secondary's significant flux, the masses derived ($M_1 = 0.46^{+0.12}_{-0.09}\,M_\odot$ and $M_2 = 2.5 \pm 0.2\,M_\odot$) align well with those from ellipsoidal variations ($M_1 = 0.44 \pm 0.06\,M_\odot$ and $M_2 = 2.8 \pm 0.3\,M_\odot$) and SED analysis that fully takes into account the significant secondary's flux (El-Badry et al., 2022). This demonstrates that tidal RV modeling offers a potentially useful alternative for mass measurements of tidally deformed SB1s of particular interest, such as X-ray faint, dormant compact object binaries that are being uncovered from ongoing large surveys. Comparing ELV- and tidal-RV-based results also reveals a possible inclination biases in tidal RV modeling, which may be mitigated by directly modeling phase-dependent line distortions. This is a task for future work.

Acknowledgements. The authors are grateful to the organizers of the conference "Binary and Multiple Stars in the Era of Big Sky Surveys." K.M. acknowledges support

by JSPS KAKENHI grant No. 21H04998.

References

Claret, A. & Bloemen, S., Gravity and limb-darkening coefficients for the Kepler, CoRoT, Spitzer, uvby, UBVRIJHK, and Sloan photometric systems. 2011, *Astronomy and Astrophysics*, **529**, A75, DOI:10.1051/0004-6361/201116451

El-Badry, K., Seeburger, R., Jayasinghe, T., et al., Unicorns and giraffes in the binary zoo: stripped giants with subgiant companions. 2022, *Monthly Notices of the RAS*, **512**, 5620, DOI:10.1093/mnras/stac815

Górski, K. M., Hivon, E., Banday, A. J., et al., HEALPix: A Framework for High-Resolution Discretization and Fast Analysis of Data Distributed on the Sphere. 2005, *Astrophysical Journal*, **622**, 759, DOI:10.1086/427976

Jayasinghe, T., Stanek, K. Z., Thompson, T. A., et al., A unicorn in monoceros: the 3 $M_\odot$ dark companion to the bright, nearby red giant V723 Mon is a non-interacting, mass-gap black hole candidate. 2021, *Monthly Notices of the RAS*, **504**, 2577, DOI:10.1093/mnras/stab907

Kopal, Z. 1959, *Close binary systems*

Kreidberg, L., Bailyn, C. D., Farr, W. M., & Kalogera, V., Mass Measurements of Black Holes in X-Ray Transients: Is There a Mass Gap? 2012, *Astrophysical Journal*, **757**, 36, DOI:10.1088/0004-637X/757/1/36

Masuda, K. & Hirano, T., Tidal Effects on the Radial Velocities of V723 Mon: Additional Evidence for a Dark 3 $M_\odot$ Companion. 2021, *Astrophysical Journal, Letters*, **910**, L17, DOI:10.3847/2041-8213/abecdc

Sterne, T. E., Notes on Binary Stars. IV. A Source of Spurious Eccentricity in Spectroscopic Binaries. 1941, *Proceedings of the National Academy of Science*, **27**, 168, DOI:10.1073/pnas.27.3.168

Strassmeier, K. G., Granzer, T., Weber, M., et al., The STELLA robotic observatory. 2004, *Astronomische Nachrichten*, **325**, 527, DOI:10.1002/asna.200410273

Strassmeier, K. G., Granzer, T., Weber, M., et al., The STELLA Robotic Observatory on Tenerife. 2010, *Advances in Astronomy*, **2010**, 970306, DOI:10.1155/2010/970306

Strassmeier, K. G., Weber, M., Granzer, T., & Järvinen, S., Rotation, activity, and lithium abundance in cool binary stars. 2012, *Astronomische Nachrichten*, **333**, 663, DOI:10.1002/asna.201211719

Tomoyoshi, M., Masuda, K., Hirano, T., et al., Weighing Single-lined Spectroscopic Binaries Using Tidal Effects on Radial Velocities: The Case of V723 Monocerotis. 2024, *arXiv e-prints*, arXiv:2410.22083, DOI:10.48550/arXiv.2410.22083

Weber, M., Granzer, T., Strassmeier, K. G., & Woche, M., The STELLA robotic observatory: first two years of high-resolution spectroscopy. 2008, in Society of Photo-Optical Instrumentation Engineers (SPIE) Conference Series, Vol. **7019**, *Advanced Software and Control for Astronomy II*, ed. A. Bridger & N. M. Radziwill, 70190L

Contrib. Astron. Obs. Skalnaté Pleso **55/3**, 352 – 356, (2025)
https://doi.org/10.31577/caosp.2025.55.3.352

Surface mapping of the young solar-like star V1358 Ori with the updated SpotDIPy code

E. Bahar[1,2], **İ. Özavcı**[1,2], **E.B. Yorulmaz**[1,2], **G.A.J. Hussain**[3] and **H.V. Şenavcı**[1,2]

[1] *Department of Astronomy and Space Sciences, Faculty of Science, Ankara University, Beşevler TR-06560 Yenimahalle, Ankara, Türkiye (E-mail: enbahar@ankara.edu.tr)*

[2] *Ankara University, Astronomy and Space Sciences Research and Application Center (Kreiken Observatory), İncek Blvd., TR-06837 Ahlatlı bel, Ankara, Türkiye*

[3] *European Space Agency (ESA), European Space Research and Technology Centre (ESTEC), Keplerlaan 1, 2201 AZ Noordwijk, The Netherlands*

Received: October 12, 2024; Accepted: January 19, 2025

Abstract. New features integrated into the open-source Doppler imaging code SpotDIPy were introduced, with an application performed on the young solar-like star V1358 Ori. A three-temperature approximation was adapted to the SpotDIPy code to reconstruct regions on the stellar surface that are both cooler and hotter than the photosphere. Additionally, the code was updated to enable simultaneous solutions of both spectroscopic and photometric data. The code has been improved both in terms of performance and user interface. The high-resolution spectra and the TESS light curve of V1358 Ori were simultaneously modeled for the first time using the new version of SpotDIPy, resulting in the surface brightness distribution of the star.

Key words: magnetic activity – starspots – solar-like stars

1. Introduction

The study of stellar surface brightness distributions, particularly in young solar-like stars, is crucial for understanding magnetic activity and its evolution. Although interferometry is applied for direct imaging of a limited number of stars, most stars require indirect techniques such as Doppler imaging, which is known as the only method capable of producing high-resolution surface brightness distributions. In this context, SpotDIPy (Bahar et al., 2024), an open-source code, was developed to generate surface brightness distributions using Doppler imaging and light curve inversion techniques. Initially, the code was based on a two-temperature model that accounted for cool spots and the photosphere. It was later extended to a three-temperature model by incorporating hot spots as

well, enabling a more comprehensive representation of surface brightness distribution. Additionally, SpotDIPy now supports simultaneous Doppler imaging and light curve inversion, which was applied to V1358 Ori to derive its surface brightness distribution.

2. SpotDIPy code

SpotDIPy is a Python-based Doppler imaging and light curve inversion code based on a three-temperature approximation. It has been designed to be as simple and user-friendly as possible, while offering a powerful interface for visualizing the results. Some of the key features of SpotDIPy are listed below.

- Constructs a surface grid consisting of surface elements with approximately equal areas, taking into account the oblateness of the star due to its rotation. Additionally, it incorporates the effect of gravity-darkening as described by Espinosa Lara & Rieutord (2011).
- Calculates limb-darkening effects for the relevant wavelength range or passband, based on each surface element's temperature, surface gravity (logg), and metallicity values using $ExoTiC{-}LD$ (Grant & Wakeford, 2024) Python package.
- Generates synthetic spectral line profiles considering the effects of macroturbulence and the instrumental profile.
- Accounts for differential rotation in the inversion process.
- Determine specific stellar parameters (such as *vsini*) using the grid search technique.

3. Observations

V1358 Ori was observed using the NARVAL high-resolution ($R \approx$65000) echelle spectropolarimeter, mounted on the 2-meter Bernard Lyot Telescope at the Observatoire Midi-Pyrénées, Pic du Midi, France, between January 3 and 16, 2019. A total of 10 spectra were obtained from PolarBase (Donati et al., 1997; Petit et al., 2014), covering approximately 1.5 stellar rotations. The light curve data were obtained from the TESS space telescope (Ricker et al., 2015), specifically using observations that coincided with the temporal coverage of the spectroscopic data.

4. Analyses and results

The surface brightness distribution of the star V1358 Ori was obtained using the SpotDIPy code by simultaneously modeling spectral line profiles and light curve data. Since the accuracy of the surface brightness distribution derived

from Doppler imaging is highly dependent on the signal-to-noise ratio (SNR) of the data, high SNR average line profiles were generated using the Least Squares Deconvolution technique (Donati et al., 1997). The input parameters required for Doppler imaging were adopted from the study by Kriskovics et al. (2019). While Kriskovics et al. (2019) used a range of temperatures in their Doppler imaging analysis, our approach employs a three-temperature model. Specifically, we adopted the quiet photosphere temperature of 6040 K from Kriskovics et al. (2019), and used the minimum and maximum spot temperatures reported in that study, 4500 K and 6400 K, as the representative temperatures for the cool and hot spot regions, respectively. Differential rotation was not considered in our Doppler imaging analysis. Given that the time span of our spectral and photometric data is approximately 1.5 stellar rotations (about 2 days), the effect of differential rotation are expected to be negligible within this time frame. The best-fit results obtained from the simultaneous analysis are shown in Figure 1, 2, and 3.

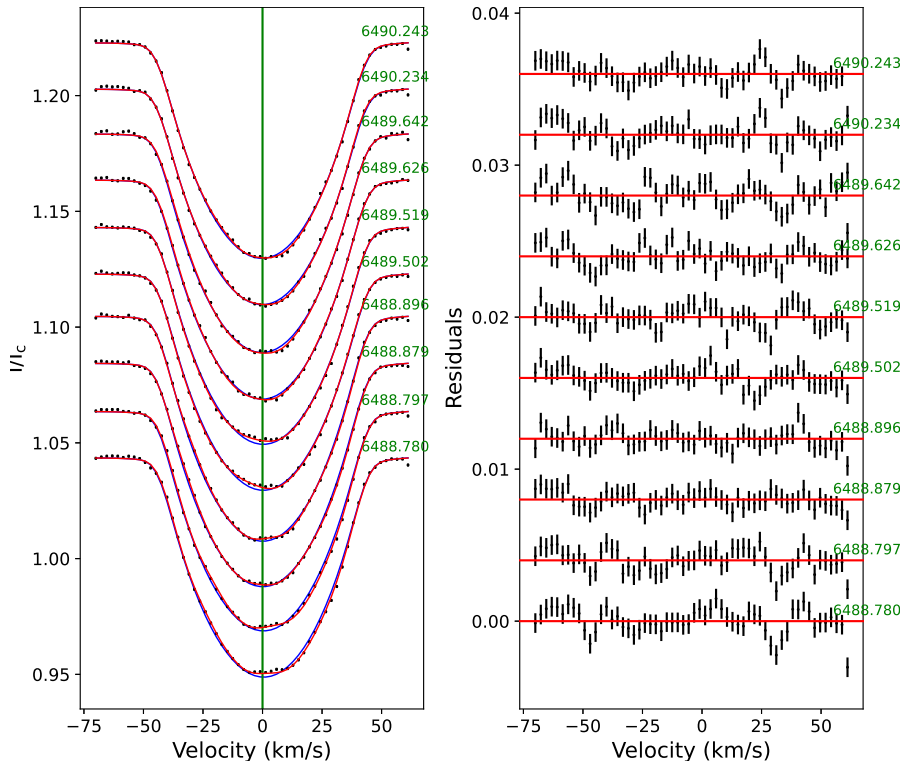


Figure 1. Left: the observed spectral line profiles (black dots), spotted model (red lines), and spotless model (blue lines). Right: residuals.

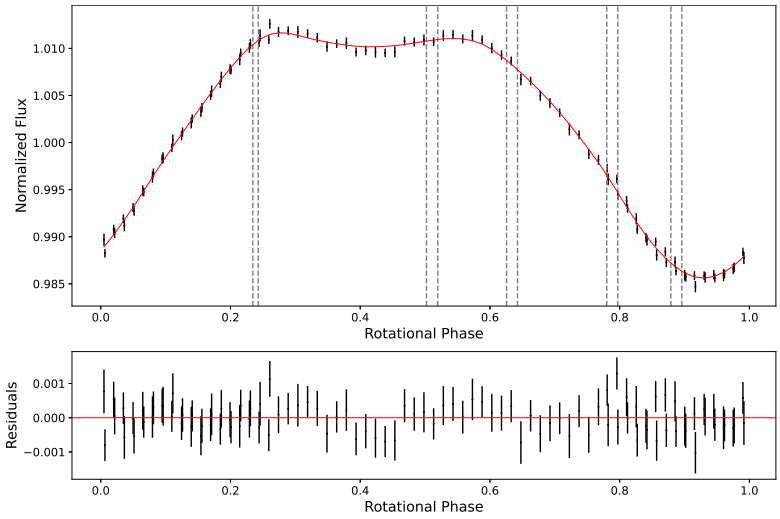


Figure 2. Top: the observed light curve (black dots) and the spotted model (red line). Vertical dashed lines corresponding to the mid-phase of the observed spectral data used in the Doppler imaging analysis. Bottom: residuals.

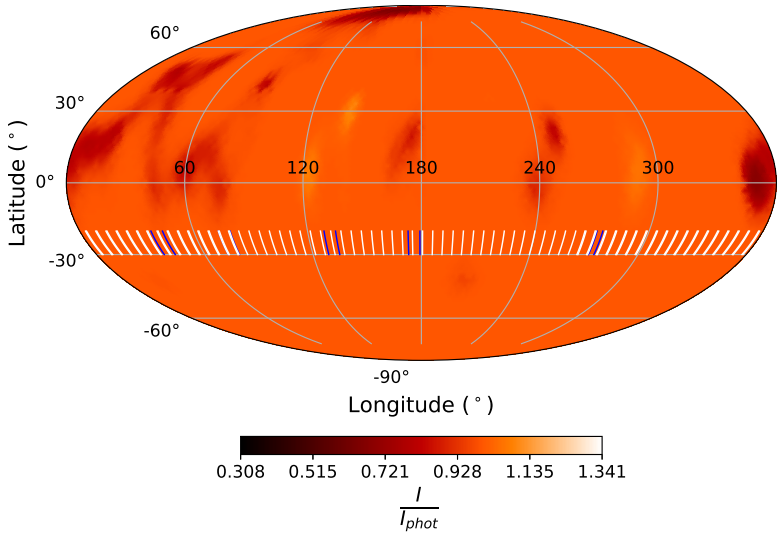


Figure 3. The surface brightness distribution map of V1358 Ori in Mollweide projection. The white and blue stripes show the distribution of photometric and spectral data used in this study along stellar longitude, respectively.

5. Conclusion and future work

In this study, using the SpotDIPy code, we obtained the surface brightness distribution of the young solar-like star V1358 Ori, revealing cool spots primarily at mid and high latitudes, especially near the equator. The results, derived from high signal-to-noise ratio (SNR) data, offer valuable insights into the star's magnetic activity. It is important to note that the uneven phase distribution of the spectral data, with a maximum phase gap of 0.347, may result in the appearance of artificial spots on the resulting map. The latest version of SpotDIPy has been upgraded to simultaneously model both spectral line profiles and light curves for single stars based on a three-temperature approximation. In the future, we plan to expand SpotDIPy's capabilities to generate surface brightness distributions for binary stars. SpotDIPy is available on GitHub (https://github.com/EnginBahar/SpotDIPy).

References

Bahar, E., Şenavcı, H. V., Işık, E., et al., First Chromospheric Activity and Doppler Imaging Study of PW And Using a New Doppler Imaging Code: SpotDIPy. 2024, *Astrophysical Journal*, **960**, 60, DOI:10.3847/1538-4357/ad055d

Donati, J. F., Semel, M., Carter, B. D., Rees, D. E., & Collier Cameron, A., Spectropolarimetric observations of active stars. 1997, *Monthly Notices of the RAS*, **291**, 658, DOI:10.1093/mnras/291.4.658

Espinosa Lara, F. & Rieutord, M., Gravity darkening in rotating stars. 2011, *Astronomy and Astrophysics*, **533**, A43, DOI:10.1051/0004-6361/201117252

Grant, D. & Wakeford, H. R., ExoTiC-LD: thirty seconds to stellar limb-darkening coefficients. 2024, *Journal of Open Source Software*, **9**, 6816, DOI:10.21105/joss.06816

Kriskovics, L., Kővári, Z., Vida, K., et al., Magnetic activity of the young solar analog V1358 Orinis. 2019, *Astronomy and Astrophysics*, **627**, A52, DOI:10.1051/0004-6361/201834927

Petit, P., Louge, T., Théado, S., et al., PolarBase: A Database of High-Resolution Spectropolarimetric Stellar Observations. 2014, *Publications of the ASP*, **126**, 469, DOI:10.1086/676976

Ricker, G. R., Winn, J. N., Vanderspek, R., et al., Transiting Exoplanet Survey Satellite (TESS). 2015, *Journal of Astronomical Telescopes, Instruments, and Systems*, **1**, 014003, DOI:10.1117/1.JATIS.1.1.014003

Contrib. Astron. Obs. Skalnaté Pleso **55/3**, 357 – 361, (2025)
https://doi.org/10.31577/caosp.2025.55.3.357

Eclipsing binary classification with machine learning techniques

B. Keskin[1] **and Ö. Baştürk**[2,3]

[1] *Ankara University, Graduate School of Natural & Applied Sciences, Astronomy & Space Sciences Department, Ankara, Türkiye*

[2] *Ankara University, Faculty of Science, Astronomy & Space Sciences Department, Ankara, Türkiye*

[3] *Ankara University, Astronomy & Space Sciences Research & Application Center, Kreiken Observatory, Ankara, Türkiye*

Received: November 14, 2024; Accepted: December 20, 2024

Abstract. We focus on the automated classification of eclipsing binary stars using deep learning methods to handle the vast data generated by large-scale photometric sky surveys. These surveys produce extensive datasets that are impractical for manual analysis. By using machine learning to classify eclipsing binary stars based on light curve morphology, this study aims to contribute to the efforts to efficiently process and accurately interpret massive data from projects Kepler, TESS and Gaia missions.

Key words: stars:binary stars, stars:eclipsing binaries, techniques:light curve classification, techniques:machine learning

1. Introduction

Eclipsing binaries, whose light curves show brightness variations from mutual eclipses, have large sets of photometric survey data. Automated data processing, leveraging supervised and unsupervised machine learning (ML) are essential to efficiently analyze these massive datasets and identifying patterns in time-series data.

Daza-Perilla et al. (2023) utilized ML to classify eclipsing binary stars (EBs) in the VISTA Variables of the Vía Láctea Survey (VVV), revealing time-series features in light curves and introducing a Compound Decision Tree (CDT) model for their classification. Čokina et al. (2021) classified eclipsing binary light curves into detached and over-contact classes. A hybrid of Bidirectional Long Short Term Memory (BiLSTM) and one dimensional Convolutional Neural Network (1D CNN), achieved 98% accuracy, and reached 100% when semi-detached binaries were excluded. Bódi & Hajdu (2021) used the Locally Linear Embedding (LLE) algorithm for classifying the Optical Gravitational Lensing Experiment (OGLE) eclipsing binary light curves based on their morphology. Süveges, M. et al. (2017) applied ML methods, including Functional Principal Component

Analysis (FPCA), Linear Discriminant Analysis (LDA), Random Forest (RF), and Self-Organizing Map (SOM), to classify eclipsing binaries based on light curve morphology using datasets from Catalog and Atlas of Eclipsing Binaries (CALEB), High Precision Parallax Collecting Satellite (HIPPARCOS), and Kepler. Kochoska, A. et al. (2017) proposed a combination of the t-distributed Stochastic Neighbor Embedding (t-SNE) and Density-Based Spatial Clustering of Applications with Noise (DBSCAN) algorithms for the purposes of eclipsing binary light curve classification. The polynomial chain (polyfit) and two-Gaussian models are used to characterize the geometry of the folded light curves. Classification is done according to the morphology parameter for a given system.

This study aims to contribute to the efforts in reliable and rapid classification of eclipsing binaries, enabling statistically reproducible results across vast astronomical databases. We classify a limited sample of eclipsing binary star candidates in the Gaia DR3 archive. We utilize Transiting Exoplanet Survey Satellite (TESS)[1] and Kepler[2] light curve data in the Villanova eclipsing binary catalogs, where the systems are ready to be labeled according to the morphology parameter (Matijevič et al., 2012), to train our CNN model. We then apply the trained model to classify our sample of eclipsing binaries from the Gaia Data Release 3 (DR3) archive.

2. Data and methods

Villanova Kepler and TESS eclipsing binary archives are used for training ML model. 2907 Kepler and 4349 TESS EB light curves are taken and labeled according to morphology parameter by the following criteria (Matijevič et al., 2012);

morph < 0.5 detached (D)
$0.5 <$ morph < 0.7 semidetached (SD)
$0.7 <$ morph < 0.8 overcontact (OC)
$0.8 <$ morp ellipsoidal (E)

The light curves are phase-folded by using light elements taken from Villanova archives and binned uniformly to standardize their resolution, ensuring consistency across datasets (Fig.1).

For classification, a small sample including 2106 EB's were selected from Gaia DR3 archive. We provide a few of these binned and phase-folded light curves in Fig.2 (left) as examples. Light curves had to be processed based on two Gaussian and a cosine function due to their sampling and intensity scaling as presented in Mowlavi, N. et al. (2023) (Fig.2 right).

[1] https://tessebs.villanova.edu
[2] https://keplerebs.villanova.edu

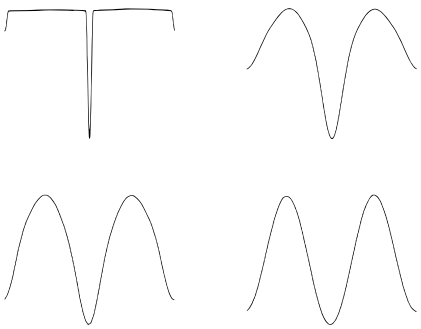


Figure 1. Sample detached (top left), semidetached (top right), overcontact (bottom left), ellipsoidal (bottom right) Kepler and TESS light curves.

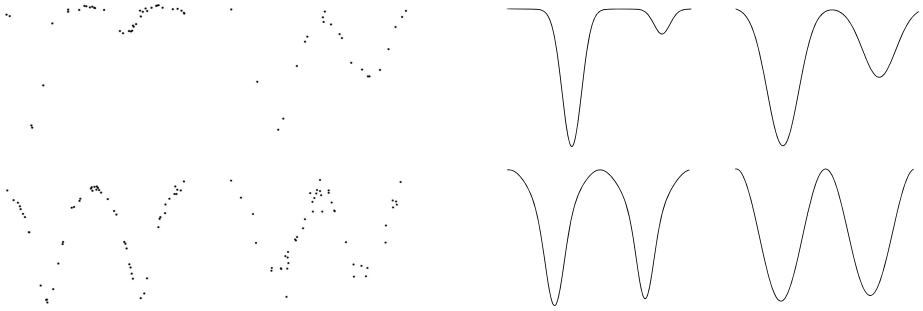


Figure 2. Sample Gaia DR3 light curves (left) and their modeled light curves (right).

The selected binaries are also in the Kepler or TESS archive. Out of 2106 EB's 789 are from Kepler archive and 1317 are from TESS archive. So we can crossmatch the labeled and the predicted classes.

We converted light curve data of Kepler and TESS EBs to Portable Network Graphic (PNG) image files by a Python code we developed for the task. Then these light curve images were splitted into 3 groups: 67% for training, 25% for validation and 8% for test. We used VGG-19 as the ML model. VGG-19 is a pretrained CNN from Visual Geometry Group (VGG) Department of Engineering Science, Oxford University. The number 19 stands for the number of layers with trainable weights. We chose VGG-19 for its ability to effectively extract nuanced features from light curve data, such as subtle variations in amplitude, shape and periodicity. VGG-19's fine-tuning, combined with the use of regularization techniques, provided results without overfitting. We used "reduce LR on plateau" and "early stopping" methods to avoid overfitting. We also conducted experiments with varying hyperparameters and confirmed that overtraining did not occur.

3. Results and discussion

We achieved 91% accuracy on Kepler and TESS test data and 64% accuracy on Gaia DR3 data as given with the confusion matrix in Fig.3. Our ML model is highly successful on semidetached class, while it tends to predict overcontact binaries as semidetached.

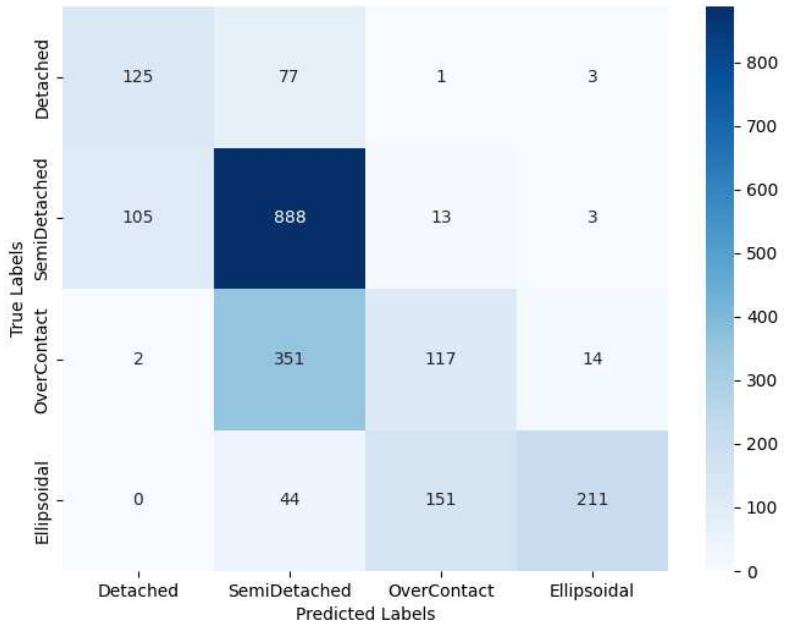


Figure 3. Confusion matrix.

Training of the ML model is one of the important steps. The Kepler and TESS light curves that we used for training should be modeled in the same way as the Gaia light curves. This is the reason why the model was successful in classifying the test data, but partially failed in classifying the Gaia data. We plan to explore additional modeling techniques, including smoothing and fitting analytic models, for improved consistency and interpretability in future studies.

Although model accuracy could probably be improved with a larger and more homogeneous dataset, our primary focus was to establish a proof of concept and identify potential challenges to this classification task. As part of our ongoing work, additional observation archives are being explored to expand the training dataset and improve the robustness and performance of the model.

We used "phase folding method" for the acquisition of the relevant light curve information. Harmonic analysis can be used to determine characteristics of the light curves. Integration of spot-induced effects as well as modulations

caused by reflection and ellipsoidal deformation in close binary systems could enhance the precision of future models, particularly for more detailed analysis of system parameters. Spot-induced variations are generally low-amplitude compared to the primary eclipse features in eclipsing binaries. Despite such variations, classification accuracy is found to be similar across diverse types of light curves with varying levels of spot activity.

References

Bódi, A. & Hajdu, T., Classification of OGLE Eclipsing Binary Stars Based on Their Morphology Type with Locally Linear Embedding. 2021, *The Astrophysical Journal Supplement Series*, **255**, 1, DOI:10.3847/1538-4365/ac082c

Čokina, M.and Maslej-Krešňáková, V., Butka, P., & Parimucha, Š.., Automatic classification of eclipsing binary stars using deep learning methods. 2021, *Astronomy and Computing*, **36**, 100488, DOI:10.1016/j.ascom.2021.100488

Daza-Perilla, I. V., Gramajo, L. V., Lares, M., et al., Automated classification of eclipsing binary systems in the VVV Survey. 2023, *Monthly Notices of the Royal Astronomical Society*, **520**, 828, DOI:10.1093/mnras/stad141

Kochoska, A., Mowlavi, N., Prša, A., et al., Gaia eclipsing binary and multiple systems. A study of detectability and classification of eclipsing binaries with Gaia. 2017, *A&A*, **602**, A110, DOI:10.1051/0004-6361/201629957

Matijevič, G., Prša, A., Orosz, J. A., et al., Kepler Eclipsing Binary Stars. III. Classification of Kepler Eclipsing Binary Light Curves with Locally Linear Embedding. 2012, *The Astronomical Journal*, **143**, 123, DOI:10.1088/0004-6256/143/5/123

Mowlavi, N., Holl, B., Lecoeur-Taïbi, I., et al., Gaia Data Release 3 - The first Gaia catalogue of eclipsing-binary candidates. 2023, *A&A*, **674**, A16, DOI:10.1051/0004-6361/202245330

Süveges, M., Barblan, F., Lecoeur-Taïbi, I., et al., Gaia eclipsing binary and multiple systems. Supervised classification and self-organizing maps. 2017, *A&A*, **603**, A117, DOI:10.1051/0004-6361/201629710

Contrib. Astron. Obs. Skalnaté Pleso **55/3**, 362 – 365, (2025)
https://doi.org/10.31577/caosp.2025.55.3.362

octans: Observed calculated diagram and light curves

M. Niaei[1,2] **and Ö. Baştürk**[3,4]

[1] *Ankara University Graduate School of Natural and Applied Sciences, Department of Astronomy and Space Sciences, Ankara, Türkiye (E-mail: astrosek@science.ankara.edu.tr)*

[2] *Informatics and Information Security Research Center, Türkiye*

[3] *Ankara University, Faculty of Science, Department of Astronomy and Space Sciences Ankara, Türkiye*

[4] *Ankara University Astronomy and Spaces Sciences Research & Application Center, Kreiken Observatory, Incek Blvd., Ankara, Türkiye*

Received: November 15, 2024; Accepted: March 3, 2025

Abstract. `octans` is a `Python` library designed for easy and robust calculation of light curve extrema timings and the construction of O-C diagrams. It also provides access to various databases to retrieve light curves and extrema times. While `octans` includes a user-friendly GUI (which is under construction), its primary focus is on sophisticated algorithms for deriving extrema timings from binary and variable star light curves.

Key words: light curve – minima – propagation of uncertainty

1. Introduction

A light curve measures periodic changes in flux from a celestial body over time, driven by external (extrinsic) or internal (intrinsic) properties. The unique features of a light curve reveal valuable information about the source. Changes in the orbital periods of binary stars can provide valuable insights into their orbital characteristics and the interactions between their components. These variations are visualized by plotting differences between observed timings of extrema ("O") and those computed from a linear ephemeris ("C"), forming O-C diagrams.

To create an O-C diagram, one must measure extrema times on a light curve. Various methods, such as the bisector of chords, Kwee-van Woerden (Kwee & van Woerden, 1956), direct measurement or determining local minima from the derivative of a fit function (Pilarčík et al., 2012), and Fielder (Pilarčík et al., 2012) techniques, have been employed to achieve the task. These methods involve finding the extremum point of a minimum profile in a discrete dataset. Most available software lack robust error propagation for these measurements. `octans` emphasizes accurate uncertainty estimation, though some techniques,

such as frequency analysis and Kwee-van Woerden method, either lack or underestimate error assessments due to their limitations.

2. octans code

`octans` is written in Python based on frequently used libraries in astronomy such as `astropy`, `astroquery`, `numpy`, pandas, `lightkurve` and more.

2.1. Light curve handling and retrieval

To handle light curve data, an `XLightCurve` object can be created using time, flux, and optionally flux error values. Observers can input their light curve data with built-in Python functions or libraries like `pandas` and `astropy`. For external data sources, `octans` provides methods to retrieve data from various astronomical archives and databases, including `Kepler` Borucki et al. (2010), `TESS` Ricker et al. (2015), `ASAS` Shappee et al. (2014), `var_astro`* Czech Astronomical Society (2024), and `ETD`* Czech Astronomical Society (2024).This is accomplished via the `Portal` class. Note that options marked with * may be modified or removed due to change in terms of use of VarAstro.

2.2. Measurements of minima timings

Light minima measurements are vital for observing eclipsing binaries, marking eclipse times on a light curve and aiding in studying orbital period changes. If the period varies, minima timings will deviate from those predicted by a fixed linear ephemeris.

2.3. Methods of measurement

`octans` has multiple classes where it encapsulate the data and functionalities. For instance to store time and error in time `octans` employs a class called `Minima`. It stores the timing as `astropy.time.Time` and its uncertainty as `astropy.time.TimeDelta`.

In order to analyze the time-series itself `octans` uses a class called `XLightCureve` which is inherited from `lightkurve.lightcurve`. So it already comes with all the functionalities of the object. `octans` adds some other functions on top of that.

2.4. Construction of an O-C diagram

`octans` employees a dataclass called `Minima`. It encapsulates each measured time and its associated uncertainty (must be called observed). Having an observed minimum time is enough to create an O-C diagram. Equipped with a previously observed minimum time and the period of variability one can calculate the

expected minima timings and store them in `Minima` dataclass. The next step would be the comparison of these values.

2.5. An example run

A sample code to retrieve O-C diagram from data available in VarAstro is shown in Listing 1 and the result is shown in Figure 1.

Listing 1 Retrieving O-C data from VarAstro using `octans`

```
from octans import Portal, Period
from matplotlib import pyplot as plt

name = "XY LEO"

# Create a Portal and Period Object
portal = Portal.from_name(name)
period = Period.from_name(name)

# Retrieve Periods from all available sources
# and get the value obtained from VarAstro
period_values = period.all()
var_astro_period_value = period_values[period_values["source"] == "
    VAS"].iloc[0].P

# Retrieve minima times from VarAstro
var_astro_minimas = portal.var_astro()

# Create O-C
var_astro_oc = var_astro_minimas.oc(period=var_astro_period_value)
var_astro_oc.smooth(s=0.02).plot(
    marker=".", color="red", linestyle="None"
)
plt.title(f"O-C Diagram of {name}")
plt.xlabel("Time (JD)")
plt.ylabel("O-C (JD)")
plt.tight_layout()
plt.show()
```

3. Conclusion

`octans` is a user-friendly software tool for astronomical light curve analysis, hosted on `GitHub` (https://github.com/mshemuni/octans) and available on `PyPi` (`pip install octans`). It operates with the reliability of widely-used `Python` packages, ensuring robust and efficient performance.

Acknowledgements. We thank TÜBİTAK for their support with the 1001 grant for our project 122F358.

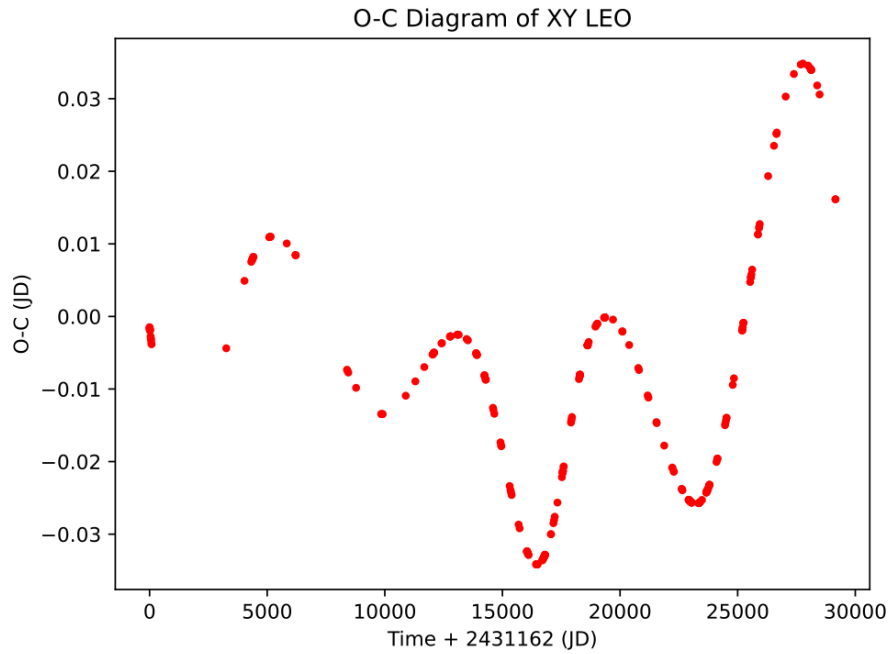


Figure 1. OC diagram generated via `octans`

References

Borucki, W. J., Koch, D. G., Basri, G., et al., Kepler's Planet-Detecting Mission. 2010, *Science*, **327**, 977, DOI:10.1126/science.1185402

Czech Astronomical Society. 2024, VarAstro: A Database of Variable Stars, accessed: 2024-11-05

Kwee, K. K. & van Woerden, H., A method for computing accurately the epoch of minimum of an eclipsing variable. 1956, *Bulletin Astronomical Institute of the Netherlands*, **12**, 327

Pilarčík, L., Jelínek, M., & Hudec, R., Several Methods of Estimating Times of Minima in Cataclysmic Variables And Some Fesults for EX Dra. 2012, in *Proceedings of the WDS 2012* (Matfyzpress), 116–122

Ricker, G. R., Gilbert, H., Larsen, J., et al., Transiting Exoplanet Survey Satellite (TESS). 2015, *Journal of Astronomical Telescopes, Instruments, and Systems*, **1**, 014003, DOI:10.1117/1.JATIS.1.1.014003

Shappee, B. J., Holoien, T. W.-S., Dilday, B., et al., The All-Sky Automated Survey for Supernovae (ASAS-SN). 2014, *The Astrophysical Journal*, **788**, 48, DOI:10.1088/0004-637X/788/1/48

Contrib. Astron. Obs. Skalnaté Pleso **55/3**, 366 – 369, (2025)
https://doi.org/10.31577/caosp.2025.55.3.366

EBOP MAVEN

A machine learning model for predicting eclipsing binary light curve fitting parameters

S. Overall and J. Southworth

Astrophysics Group, Keele University, Staffordshire, ST5 5BG, UK
(E-mail: s.p.overall@keele.ac.uk)

Received: November 16, 2024; Accepted: January 31, 2025

Abstract. Detached eclipsing binary stars (dEBs) are a key source of data on fundamental stellar parameters. While there is a vast source of candidate systems in the light curve databases of survey missions such as *Kepler* and TESS, published catalogues of well-characterised systems fall short of reflecting this abundance. We seek to improve the efficiency of efforts to process these data with the development of a machine learning model to inspect dEB light curves and predict the input parameters for subsequent formal analysis by the JKTEBOP code.

Key words: binaries: eclipsing – methods: data analysis – methods: machine-learning

1. Introduction

Detached eclipsing binary systems are a key source of stellar parameters used in the development and testing of models of stellar evolution. By combining photometric light curve and spectroscopic radial velocity (RV) observations it is possible to measure the components' physical characteristics with great precision (Andersen, 1991; Torres et al., 2010).

Machine learning (ML) approaches are becoming widely used in many areas of science and technology, often as a means to gain new insights into existing datasets or as a way of addressing the vast volumes of data produced by the latest scientific programmes. The key feature of the machine learning approach is that a given program learns to carry out its task through direct experience with the data rather than through a predefined algorithm.

2. Developing the model

EBOP MAVEN is a CNN (Convolutional Neural Network) model implemented in python with the TensorFlow (Abadi et al., 2015) and Keras (Chollet et al., 2015) libraries. CNN models are a type of supervised machine learning model,

one that requires training before use, which are widely used in computer vision scenarios. They typically consist of one or more convolutional layers which with training learn the convolution kernels best able to extract the characteristic features within the input data from which a subsequent neural network can make predictions.

We have developed a regression model which views the 1-D time-series data of a phase-folded dEB light curve to predict the value of six parameters used as the input for subsequent formal analysis with the JKTEBOP code (Southworth, 2008). The predicted parameters are the sum ($r_A + r_B$) and ratio ($k \equiv r_B/r_A$) of the stars' fractional radii, the central surface brightness ratio (J), the orbital eccentricity through the Poincaré elements ($e\cos\omega$ and $e\sin\omega$), and the orbital inclination through the primary impact parameter (b_P).

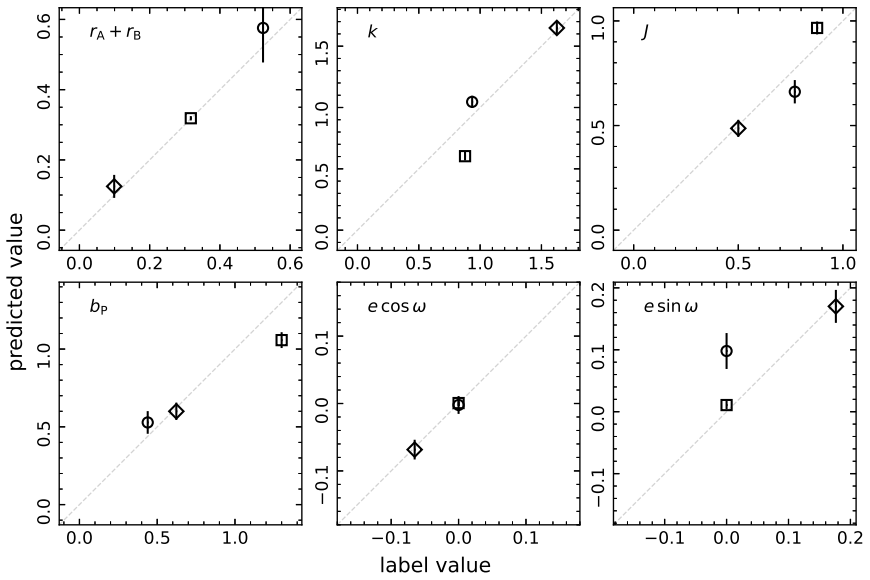
The model was trained on a fully synthetic dataset of 250,000 labelled phase-folded light curves, split 80:20 between training and validation instances. The distribution of the training data was chosen to cover the parameter space supported by JKTEBOP. While training, augmentation steps added random noise and shifts to the data. Dropout layers are included in the model as a regularisation measure to combat overfitting.

3. Testing and results

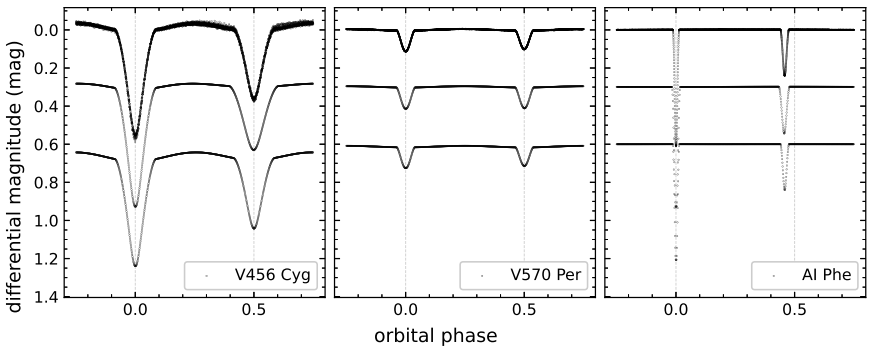
The test dataset consists of synthetic instances representing a population of physically plausible dEB systems. Stellar parameters were taken from MIST (Choi et al., 2016) stellar models with population demographics based on the product of the initial mass function from Chabrier (2003) and the binarity function from Wells & Prša (2021). The treatment of apparent brightness, noise and limb darkening was based on the TESS mission.

A second test dataset of real dEB systems was assembled based on membership of the DEBCat (Southworth, 2015) catalogue of well-characterised detached systems and the availability of TESS timeseries photometry. The test labels were derived from the published works giving the most recent characterisation of each system. A processing pipeline was implemented to prepare and fit light curves from these systems using JKTEBOP, and a set of control fits were made with input parameters based on the test labels. The final set of systems represent a range of targets where it was possible to achieve a stable control fit with results comparable to those published.

The EBOP MAVEN model was used to predict the fitting parameters for the real dEB systems. With the predictions used as the input parameters for the fitting step of the processing pipeline, while all other settings and processes were carried over from the control fits, 22 of the 23 systems yielded a final fitted characterisation in agreement with the equivalent control fit. The exception was AI Phe (see Fig. 1), however this is an especially challenging target where the secondary star is significantly larger than the primary ($k \simeq 1.6$).



(a) The predictions made for V456 Cyg (circles), V570 Per (squares) and AI Phe (diamonds) plotted against the corresponding label values



(b) The phase-folded light curves of V456 Cyg, V570 Per and AI Phe with corresponding generated light curves based on the predicted input parameters (shifted by 0.3 mag) and the fitted characterisation with JKTEBOP (shifted by 0.6 mag)

Figure 1.: The EBOP MAVEN predictions for a subset of the test dataset of real dEB systems below which are the corresponding phase-folded light curves of the input feature, and generated light curves of both the predicted and final fit

4. Conclusion and next steps

We have demonstrated that it is possible to train a machine learning model to predict input parameters for dEB light curve fitting with the JKTEBOP code. When tested with TESS photometry from real systems we achieved a good fit in 22 of 23 targets.

Development of the model is ongoing and a full article is being prepared for publication. The code to build, train and test the version of the model discussed here is publicly available on GitHub[1]. The EBOP MAVEN model will be incorporated into a processing pipeline with which a catalogue of dEB systems will be assembled. This is intended to provide sufficient data for the selection of suitable targets for further observation and formal characterisation.

Acknowledgements. We gratefully acknowledge the support of the Science and Technologies Facilities Council (STFC) in the form of a PhD studentship.

References

Abadi, M., Agarwal, A., Barham, P., et al. 2015, TensorFlow: Large-Scale Machine Learning on Heterogeneous Systems, https://www.tensorflow.org/

Andersen, J., Accurate masses and radii of normal stars. 1991, *Astronomy and Astrophysics Reviews*, **3**, 91, DOI:10.1007/BF00873538

Chabrier, G., Galactic Stellar and Substellar Initial Mass Function. 2003, *Publications of the ASP*, **115**, 763, DOI:10.1086/376392

Choi, J., Dotter, A., Conroy, C., et al., Mesa Isochrones and Stellar Tracks (MIST). I. Solar-scaled Models. 2016, *Astrophysical Journal*, **823**, 102, DOI:10.3847/0004-637X/823/2/102

Chollet, F. et al. 2015, Keras, https://keras.io

Southworth, J., Homogeneous studies of transiting extrasolar planets - I. Light-curve analyses. 2008, *Monthly Notices of the RAS*, **386**, 1644, DOI:10.1111/j.1365-2966.2008.13145.x

Southworth, J., DEBCat: A Catalog of Detached Eclipsing Binary Stars. 2015, in Astronomical Society of the Pacific Conference Series, Vol. **496**, *Living Together: Planets, Host Stars and Binaries*, ed. S. M. Rucinski, G. Torres, & M. Zejda, 164

Torres, G., Andersen, J., & Giménez, A., Accurate masses and radii of normal stars: modern results and applications. 2010, *Astronomy and Astrophysics Reviews*, **18**, 67, DOI:10.1007/s00159-009-0025-1

Wells, M. A. & Prša, A., Building and Calibrating the Binary Star Population Using Kepler Data. 2021, *Astrophys. J., Suppl. Ser.*, **253**, 32, DOI:10.3847/1538-4365/abd5ba

[1] https://github.com/SteveOv/ebop_maven/tree/kopal2024

Contrib. Astron. Obs. Skalnaté Pleso **55/3**, 370 – 373, (2025)
https://doi.org/10.31577/caosp.2025.55.3.370

Prediction of photometric parameters of overcontact eclipsing binaries using deep-learning model

Š. Parimucha[1], P. Gajdoš[1,2], Y. Markus[1] and V. Kudak[3]

[1] *Institute of Physics, Faculty of Science, Šafárik University, Košice, Slovakia*
[2] *Astronomical Institute of the Czech Academy of Sciences 251 65 Ondřejov, The Czech Republic*
[3] *Laboratory of Space Researches, Uzhhorod National University, Uzhhorod, Ukraine*

Received: November 14, 2024; Accepted: December 13, 2024

Abstract. This paper presents a deep-learning model for predicting the photometric parameters of W UMa-type eclipsing binaries without spots. The model assumes that the light curve (LCs) can be described by four parameters: the orbital inclination, photometric mass ratio, temperature ratio, and common potential. The training dataset comprises 500 000 simulated LCs in the Gaia G passband. The best results were obtained using the random forest predictor, achieving a Mean Absolute Percentage Error (MAPE) of 6.1%. The study concluded that the quality of parameter prediction strongly depends on the quality of the analyzed LCs curves, requiring careful data preprocessing.
Key words: eclipsing binaries – machine-learning – deep-learning

1. Introduction

Eclipsing binary stars of the W UMa type (overcontact binaries) are a type of close binary system in which both stars are so close that they share a common envelope of material. Their shapes are strongly distorted by tidal forces and the frame of Roche geometry allows us to describe their common surface by its potential (Prša, 2018). These systems are among the most frequently found variable stars because of their short orbital period (up to 1 d) and typical light-curve (LC) shape. Space and ground-based surveys discovered several tens of thousands of such systems; however, only a small fraction of them determined their photometric parameters. These parameters can be obtained from the solutions of the LCs. However, several software packages dedicated to LCs solutions for eclipsing binaries exist, such as the PHOEBE (Conroy et al., 2020), JKTEBOP (Southworth et al., 2004), and ELISa (Čokina et al., 2021), this procedure is not straightforward. It requires strong interaction with the user and a qualified estimate of the initial parameters. This paper presents a deep-learning model

for predicting the photometric parameters of W UMa-type eclipsing binaries that are unaffected by spots. This prediction model assumes that the LC can be described by four parameters: the orbital inclination i, photometric mass ratio q, the temperature ratio t_1/t_2 and common potential Ω. These parameters determine the shapes of stars, their relative dimensions, and their radiation properties.

2. Training and evaluation dataset

The training dataset was created using the ELISa code (Čokina et al., 2021). The LCs of the overcontact binaries were simulated from parameters covering a wide range of physically correct star values, using a random uniform distribution in the intervals used (Tab. 1). In total, 500 000 LCs were created in the Gaia G passband.

Table 1. Parameters and intervals used for the simulated LCs.

Parameter	Interval
i	40-90°
q	0.05-2.0
Ω	2.0-4.0
t_1/t_2	1.0-1.3

To evaluate our model, we randomly selected 100 LCs of a set of overcontact eclipsing binaries from the Gaia catalogue of eclipsing binaries (Mowlavi et al., 2023), as classified by Parimucha et al. (2024). All LCs were manually fitted using the ELISa code to determine the basic parameters of the systems. The Gaia LCs were preprocessed (outlier removal), rebinned to 100 data points, folded, and normalized to the median flux.

3. Deep learning model and its performance

To train our models, we used all the simulated LCs and the dataset was expanded using Gaussian noise augmentation. The 20% of them were randomly selected for validation of the trained model. We tested several models using different machine-learning algorithms including gradient boosting, random forest, linear, quadratic, and logistic regressions, as well as several convolution networks. The quality of the model was tested on the validation dataset and quantified by the MAPE (Mean Absolute Percentage Error) parameter. The best results were obtained by the random forest predictor, which achieved a MAPE value of 6.1%. Examples of predicted and fitted LCs are shown in Fig. 1.

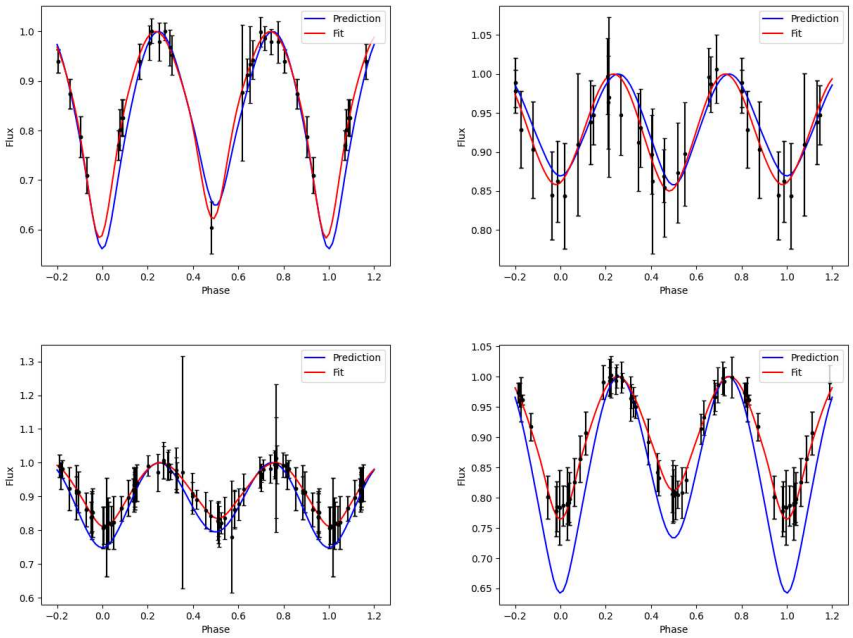


Figure 1. The examples of the predicted and fitted LCs of four overcontact eclipsing binaries from the Gaia catalogue.

4. Discussions

Our study leads to several conclusions. Most importantly, the quality of prediction of the parameters strongly depends on the quality of the analyzed LCs and careful data preprocessing is required. We require good data coverage, remove outliers, and ensure the curve is phase-folded well. The prediction is sensitive mainly to outliers, which is evident for curves with few data points. We also note that the space of the simulated LCs must be sufficiently dense, and a random uniform distribution of parameters appears to be a good solution. The parameters predicted by our model are good starting points for analysis using other methods such as LSQ and/or MCMC fitting to obtain precise results with parameter errors. Subsequent analysis of the residua can reveal bad classifications and/or LC anomalies such as spots and pulsations.

Acknowledgements. This work has made use of data from the European Space Agency (ESA) mission *Gaia* (https://www.cosmos.esa.int/gaia). This research was supported by the Slovak Research and Development Agency under Contract No. APVV-20-0148. P.G. was supported by internal grant No. VVGS-2023-2784 of the

P. J. Šafárik University in Košice and funded by the EU NextGenerationEU through the Recovery and Resilience Plan for Slovakia under the project No. 09I03-03-V05-00008 and The Ministry of Education, Youth and Sports of the Czech Republic by grant LTT-20015. Y.M. was funded by the EU NextGenerationEU through The Recovery and Resilience Plan for Slovakia under project No. 09I03-03-V01-00011 and grant UPJŠ VVGS 2024-3096 V.K. were supported by the Ukrainian national grant 0122U000937.

References

Conroy, K. E., Kochoska, A., Hey, D., et al., Physics of Eclipsing Binaries. V. General Framework for Solving the Inverse Problem. 2020, *Astrophysical Journal, Supplement*, **250**, 34, DOI:10.3847/1538-4365/abb4e2

Mowlavi, N., Holl, B., Lecoeur-Taïbi, I., et al., Gaia Data Release 3. The first Gaia catalogue of eclipsing-binary candidates. 2023, *Astronomy and Astrophysics*, **674**, A16, DOI:10.1051/0004-6361/202245330

Parimucha, Š., Gajdoš, P., Markus, Y., & Kudak, V., Deep-learning classification of eclipsing binaries. 2024, *Contributions of the Astronomical Observatory Skalnaté Pleso*, **54**, 167, DOI:10.31577/caosp.2024.54.2.167

Prša, A. 2018, *Modeling and Analysis of Eclipsing Binary Stars*, 2514-3433 (IOP Publishing), DOI:10.1088/978-0-7503-1287-5, ISBN: 978-0-7503-1287-5

Southworth, J., Maxted, P. F. L., & Smalley, B., Eclipsing binaries in open clusters - II. V453 Cyg in NGC 6871. 2004, *Monthly Notices of the RAS*, **351**, 1277, DOI:10.1111/j.1365-2966.2004.07871.x

Čokina, M., Fedurco, M., & Parimucha, Š., ELISa: A new tool for fast modelling of eclipsing binaries. 2021, *Astronomy and Astrophysics*, **652**, A156, DOI:10.1051/0004-6361/202039171

Contrib. Astron. Obs. Skalnaté Pleso **55/3**, 374 – 376, (2025)
https://doi.org/10.31577/caosp.2025.55.3.374

Classification of light curves of eclipsing binaries using deep-learning models

Š. Parimucha[1], **Y. Markus**[1,2], **P. Gajdoš**[1,3] **and V. Kudak**[4]

[1] *Institute of Physics, Faculty of Science, Pavol Jozef Šafárik University, Košice, Slovakia, stefan.parimucha@upjs.sk*

[2] *International Center of Astronomical, Medical, and Ecological Research, NASU, Kyiv, Ukraine*

[3] *Astronomical Institute of the Czech Academy of Sciences 251 65 Ondřejov, The Czech Republic*

[4] *Laboratory of Space Researches, Uzhhorod National University, Uzhhorod, Ukraine*

Received: November 14, 2024; Accepted: January 20, 2025

Abstract. This paper introduces a hierarchical deep-learning classification model for eclipsing binaries, where the period is also considered. Our classifier provides a tool for categorizing their light curves into four groups: overcontact with/without spots and detached with/without spots. We applied our model to light curves of OGLE eclipsing binaries and showed that it is reliably classified, although the precision of classification depends on the light curve quality.

Key words: stars: binaries: eclipsing – deep-learning

1. Introduction

Eclipsing binaries (EBs) are systems in which the mutual eclipses of components cause typical light curves (LCs). From LCs, we can determine many parameters of the system and stars: their sizes and shapes, potentials, photometric mass ratio, relative temperatures, inclination of the orbital plane, and presence of irregularities caused by spot(s) and/or pulsations. To determine these parameters, it is necessary to know if the components in the binary are inside their Roche lobes (detached system) or if they have a common envelope (overcontact systems). To process large amounts of EBs from ongoing and future surveys, human effort is practically impossible. Therefore, it is necessary to develop other procedures based on deep-learning methods. The first step is the classification of EBs based on their observable properties. For most of them, it is a light curve obtained in one passband and the orbital period.

Parimucha et al. (2024) suggested a scheme based on a deep-learning model that classifies light curves directly into four groups based on their shapes. In this model, they did not consider a period as an input parameter. This has led

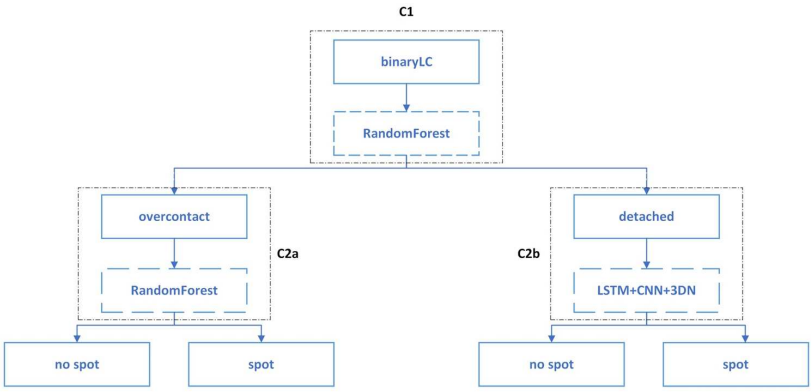


Figure 1. The hierarchical model of the classification scheme and the best models.

to a relatively large amount of misclassification, mainly for binaries with longer orbital periods, which were wrongly classified as overcontact.

This study extended the model for orbital periods to improve the classification precision. This approach allows us to classify all EBs already found in large surveys, such as GAIA, KEPLER, or TESS. It will also be found in prepared surveys like the Vera Rubin Observatory (LSST).

2. Deep-learning model, training and evaluation datasets

The training dataset was created using the ELISa code (Čokina et al., 2021). LCs were simulated for overcontact and detached binary systems with a wide range of realistic stellar, system (including orbital periods), and spot parameters. Each LC has 100 equidistant points and is phase-folded and normalized to the maximum flux. We created a dataset of more than 2.5 million LCs.

For evaluation of our model, the OGLE Eclipsing and Binary Stars Catalog (Soszyński et al., 2016; Pawlak et al., 2016) was used, including EBs from the galactic bulge, LMC, and SMC, classified as contact (C) and non-contact (NC) systems. The LCs in the I passband were folded by catalogue periods, binned into 100 points, and normalized to the maximum flux for consistency with the training dataset.

Our classification scheme enables a hierarchical approach using different models for each group to improve performance and training speed. We selected 100,000 light curves (LCs) per group from the training set and augmented them using Gaussian noise. 20% of the data was reserved for validation.

The classification scheme and best models are shown in Fig 1. The precision of each model on the validation dataset is 97.8%, 95.1%, and 92.7% for C1, C2a, and C2b, respectively.

3. Application to OGLE eclipsing binaries

Our model was applied to the OGLE Eclipsing Binaries Catalog. The key results of our analysis are summarized as follows.

- the model classified nearly all OGLE contact binaries (C) as overcontact, with only a few exceptions,
- many OGLE non-contact (NC) binaries were classified as overcontact, suggesting possible OGLE data misclassification,
- spot detection in LMC and SMC data was challenging and less reliable, due to observational limitations, especially for faint stars with high scatter. More spotted binaries were classified in the bulge, which was likely also underestimated due to light curve (LC) quality.

4. Conclusion

The hierarchical classification approach described in this study demonstrates strong performance when applied to the OGLE dataset, suggesting its suitability for comprehensive analysis of eclipsing binaries in large-scale astronomical surveys. The robustness of the model for differentiating between overcontact and detached systems, even with spot detection limitations, points to its potential for future use in projects such as the Vera Rubin Observatory (LSST).

Acknowledgements. This research was supported by the Slovak Research and Development Agency under Contract No. APVV-20-0148. Y.M. was funded by the EU NextGenerationEU through the Recovery and Resilience Plan for Slovakia under project No. 09I03-03-V01-00011. The research of P.G. was supported by the internal grant No. VVGS-2023-2784 of the P.J. Šafárik University in Košice and funded by the EU NextGenerationEU through the Recovery and Resilience Plan for Slovakia under the project No. 09I03-03-V05-00008. V.K. was supported by Ukrainian National Grant 0122U000937.

References

Parimucha, Š., Gajdoš, P., Markus, Y., & Kudak, V., Deep-learning classification of eclipsing binaries. 2024, *Contributions of the Astronomical Observatory Skalnate Pleso*, **54**, 167, DOI:10.31577/caosp.2024.54.2.167

Pawlak, M., Soszyński, I., Udalski, A., et al., The OGLE Collection of Variable Stars. Eclipsing Binaries in the Magellanic System. 2016, *Acta Astronomica*, **66**, 421, DOI:10.48550/arXiv.1612.06394

Soszyński, I., Pawlak, M., Pietrukowicz, P., et al., The OGLE Collection of Variable Stars. Over 450 000 Eclipsing and Ellipsoidal Binary Systems Toward the Galactic Bulge. 2016, *Acta Astronomica*, **66**, 405, DOI:10.48550/arXiv.1701.03105

Čokina, M., Fedurco, M., & Parimucha, Š., ELISa: A new tool for fast modelling of eclipsing binaries. 2021, *Astronomy and Astrophysics*, **652**, A156, DOI:10.1051/0004-6361/202039171

Contrib. Astron. Obs. Skalnaté Pleso **55/3**, 377 – 381, (2025)
https://doi.org/10.31577/caosp.2025.55.3.377

New "pseudo-rotating" model atmospheres

G. Szász

Dept. of Theoretical Physics and Astrophysics, Masaryk University, Kotlářská 2, 611 37 Brno, Czech Republic (E-mail: gszasz@physics.muni.cz)

Received: November 18, 2024; Accepted: January 18, 2025

Abstract. Regarding model atmospheres, rotation effects are mostly neglected, and, at best, the rotational broadening correction is being applied to a non-rotating synthetic spectrum. However, this approximation does not work for fast rotators ($v_{\rm eq} > 200\,{\rm km\,s^{-1}}$), where the effect of gravity darkening starts to be prominent. The need for this correction starts to be significant for stars hotter than F7. We introduce a new model atmosphere grid covering the region of the main-sequence A- and B-type stars. The model allows more robust follow-up studies, mainly to provide an alternative method to determine the inclination angle of the rotational axis by inversion. Calculating synthetic magnitudes and colors helps constrain the Main Sequence's rotational broadening and determine other biases related to the stellar rotation that influence the parameters determined from CMD. Determining rotational parameters from gravity darkening provides an alternative way of disentangling $v \sin i$ values and leads to a more precise understanding of the distinct populations of rotating stars.

Key words: stars: rotation – stars: atmospheres – stars: fundamental parameters

1. Introduction

The gravity-darkening law, in general form, is given by equation (1), where the exponent β can equal either 1 (von Zeipel law), 0.32 (convective envelope), or other value for the mixed case.

$$F = \sigma T_{\rm eff} \sim C(\tilde{\omega}) g^{\beta} \tag{1}$$

Values of β exponent values were determined by Claret (1998, 2000, 2003). Integrating the surface gravity over Roche surface leads to the equation (2) for the co-latitudinal gradient of effective temperature.

$$T_{\rm eff}(\theta) = \frac{L}{4\pi\sigma R_{\rm pole}^2} t_n^4(\theta) \tag{2}$$

With given $T_{\rm eff}(\theta)$, $g(\theta)$ and a vector towards the line of sight now, we can solve radiative transfer for each (θ, φ) point on the surface to get specific

intensity $I_\nu(\mu)$. Consequently, we can integrate intensity over the surface to get total luminosity radiated in a line of sight (3).

$$\mathcal{L}_\nu(\tilde{\omega}, i) = \int_A I_\nu(\mu)\, \mu\, dA \tag{3}$$

The $\mathcal{L}_\nu(\tilde{\omega}, i)$ is a synthetic spectrum of a rotating star, not yet corrected for rotational broadening.

To achieve more robust results, Espinosa Lara & Rieutord (2011) assumed a generic function (4) that gives the flux of the rotating star.

$$\mathbf{F} = -f(r, \theta)\mathbf{g}_{\text{eff}}, \tag{4}$$

It is safe to assume that the effective surface gravity g_{eff} is very close to the Roche surface and thus defined by (5).

$$\mathbf{g}_{\text{eff}} = \left(-\frac{GM}{r^2} + \Omega^2 r \sin^2\theta\right)\mathbf{e}_r + (\Omega^2 r \sin\theta\cos\theta)\mathbf{e}_\theta \tag{5}$$

With help of the substitution (6) it is possible to derive (7).

$$\cos\vartheta + \ln\tan\frac{\vartheta}{2} = \frac{1}{3}\left(\frac{\Omega}{\Omega_{\text{k}}}\right)^2\left(\frac{r}{R_{\text{e}}}\right)^3\cos^3\theta + \cos\theta + \ln\tan\frac{\theta}{2} \tag{6}$$

$$T_{\text{eff}} = \left(\frac{F}{\sigma}\right)^{1/4} = \left(\frac{L}{4\pi\sigma GM}\right)^{1/4}\sqrt{\frac{\tan\vartheta}{\tan\theta}}\, g_{\text{eff}}^{1/4} \tag{7}$$

The equation (7) represents a more robust gravity darkening law which is not dependent on the free β parameter.

2. Motivation

Compared to non-rotating stars, the spectrum is altered not only in the continuum but also in the shape of the spectral lines as shown already by Maeder & Peytremann (1970). The luminosity of a fast rotator is slightly lower than that of the non-rotating counterpart; however, the mean effective temperature appears to be significantly lower. Fast rotators appear redshifted on an H-R diagram relative to slow rotators with the same composition and mass. At the same time, the apparent effective temperature strongly varies with the inclination of the rotation axis. A rotating star, oriented pole on, appears hotter than the same star oriented perpendicular to the line of sight.

Thanks to CHARA/MIRC, we can perform direct imaging of the rapid rotators (see Fig. 1). On the contrary to what was anticipated, the gravity-darkening exponent β appears to be significantly lower than 1 for A- and B-type stars (Monnier et al., 2014). This suggests that performing follow-up research via indirect methods on a larger sample is vital.

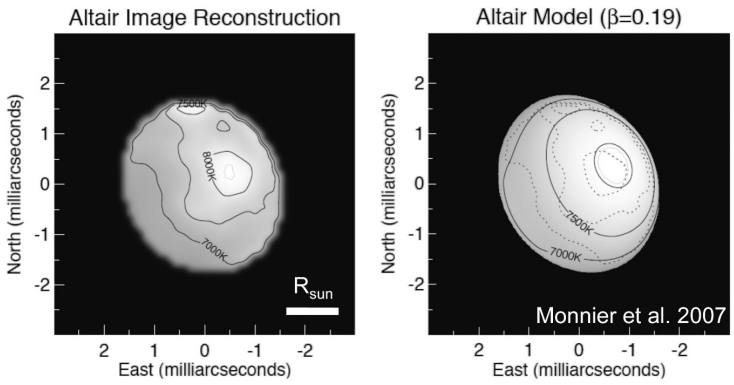


Figure 1. First image of a main-sequence star other than Sun compared to a model (Monnier et al., 2014).

The inclination of the rotational axis of individual stars is mostly unknown. The construction of a model atmosphere grid covering A- and B-type MS stars provides the possibility to perform an inversion to determine the previously unknown inclination of the rotation axis.

Since the position of rotating stars on an H-R diagram depends on rotational velocity and axial tilt, neglecting the population of the fast rotators in a star cluster could undermine the cluster age and distance determination given by isochrone fitting.

3. Method

The equation (7) allows us to calculate the surface grid of the $T_{\rm eff}$ and $\log g$ values. To calculate the specific intensity in the line of sight of the individual surface points, we use ATLAS12 code (Kurucz, 2013) for A-type stars and cooler B-type stars, and TLUSTY code (Hubeny et al., 2021) for hotter B-type stars. Since the resulting spectra result from specific intensity integration, there is no need to do limb darkening correction. Nevertheless, the resulting spectra would still require rotational broadening correction. As explained by Pérez Hernández et al. (1999), rotational broadening does not change equivalent width, so passband convolution can be safely calculated *before* applying the rotational broadening correction; however, to get good high-resolution synthetic spectra, the rotational broadening has to be also calculated implicitly, as the result of the surface synthesis (Montesinos, 2024). The recent versions of our code apply rotational Doppler correction to each individual surface element.

The synthetic spectra are then used to calculate synthetic magnitudes in selected photometric systems (Johnson-Kron-Cousins, Strömgren, Geneva, SDSS,

Table 1. Parameter space of the calculated model atmosphere grid.

Parameter	Range	Step
effective temperature	$10\,000\,\mathrm{K} \leq T_{\mathrm{eff}} \leq 30\,000\,\mathrm{K}$	200 K
surface gravity	$1 \leq \log g \leq 5$	1 dex
metallicity	$+0.5 \leq [\mathrm{M/H}] \leq -2$	0.5 dex
microturbulence	$0\,\mathrm{km\,s^{-1}} \leq \xi \leq 4\,\mathrm{km\,s^{-1}}$	$1\,\mathrm{km\,s^{-1}}$
equatorial velocity	$150\,\mathrm{km\,s^{-1}} \leq v_{\mathrm{eq}} \leq 250\,\mathrm{km\,s^{-1}}$	$50\,\mathrm{km\,s^{-1}}$
inclination	$5^\circ \leq i \leq 90^\circ$	$5^\circ, 10^\circ$

Gaia) to investigate changes in photometric characteristics caused by rotation (as demonstrated by, e.g., Lazzarotto et al., 2023).

4. Challenges

The parameter space of the new model atmosphere grid is constrained by the boundaries defined in Table 1.

This means we have 100 points in effective temperature, 20 points in surface gravity, 5 points in metallicity, 5 points in microturbulence, 6 points in equatorial velocity, and 10 points in inclination. In addition to that, each combination of parameters integrates over approx. 10^4 surface points. As a result, we need to perform 10^{10} model atmosphere calculations to complete the grid. In order to get at least close to this goal we needed to parallelize all computational tasks that are independent. At the same time, we managed to build up and maintain a dedicated computing cluster to fulfill this goal.

5. Conclusion

Construction of model atmospheres for A- and B-type stars incorporating gravity darkening with correction corrected by exponent (Claret, 1998, 2000, 2003) can lead to slightly exaggerated gravity darkening gradient. Comparison with the observing data suggests that the approach used by Espinosa Lara & Rieutord (2011) leads to more realistic results. We are actively working to reach full parameter space coverage, which will open up new possibilities for follow-up studies. Especially in the case of fast rotators, it can give us the more precise position of a star on an H-R diagram, leading to more accurate stellar parameters. The possibility of inverse calculation to determine the axial tilt of individual stars enables us to perform an extensive study of the inclination distribution in the Milky Way Galaxy and the Magellanic Clouds.

Acknowledgements. The project is part of the Open Cluster Working Group[1] collaboration at Masaryk University. This work is supported by the Czech Science Foundation (GAČR 23-07605S), the Specific Research Project of Masaryk University (MUNI/A/1419/2023), and the Europe Research Interest Group of the Red Hat Research initiative[2].

References

Claret, A., Comprehensive Tables for the Interpretation and Modeling of the Light Curves of Eclipsing Binaries. 1998, *Astronomy and Astrophysics Supplement Series*, **131**, 395, DOI:10.1051/aas:1998278

Claret, A., Studies on Stellar Rotation. II. Gravity-darkening: The Effects of the Input Physics and Differential Rotation. New Results for Very Low Mass Stars. 2000, *Astronomy and Astrophysics*, **359**, 289

Claret, A., Studies on Stellar Rotation. III. An Improvement of the Treatment of the Brightening Distribution of Rotating and Tidally Distorted Stars. 2003, *Astronomy and Astrophysics*, **406**, 623, DOI:10.1051/0004-6361:20030690

Espinosa Lara, F. & Rieutord, M., Gravity Darkening in Rotating Stars. 2011, *Astronomy and Astrophysics*, **533**, A43, DOI:10.1051/0004-6361/201117252

Hubeny, I., Allende Prieto, C., Osorio, Y., & Lanz, T. 2021, TLUSTY and SYNSPEC Users's Guide IV: Upgraded Versions 208 and 54

Kurucz, R. L., ATLAS12: Opacity Sampling Model Atmosphere Program. 2013, *Astrophysics Source Code Library*, ascl:1303.024

Lazzarotto, A., Hui-Bon-Hoa, A., & Rieutord, M., Photometric Determination of Rotation Axis Inclination, Rotation Rate, and Mass of Rapidly Rotating Intermediate-Mass Stars. 2023, *Astronomy and Astrophysics*, **676**, A50, DOI:10.1051/0004-6361/202346640

Maeder, A. & Peytremann, E., Stellar Rotation. 1970, *Astronomy and Astrophysics*, **7**, 120

Monnier, J. D., Che, X., Zhao, M., & ten Brummelaar, T., Imaging Rapid Rotators. 2014, **487**, 137

Montesinos, B., Surface Parameterisation and Spectral Synthesis of Rapidly Rotating Stars. Vega as a Testbed. 2024, *Astronomy and Astrophysics*, **688**, A97, DOI:10.1051/0004-6361/202449895

Pérez Hernández, F., Claret, A., Hernández, M. M., & Michel, E., Photometric Parameters for Rotating Models of A- and F-type Stars. 1999, *Astronomy and Astrophysics*, **346**, 586

[1] https://ocwg.physics.muni.cz

[2] https://research.redhat.com/blog/research_project/vega-project/

Contrib. Astron. Obs. Skalnaté Pleso **55/3**, 382 – 384, (2025)
https://doi.org/10.31577/caosp.2025.55.3.382

IGEBC - Interactive Gaia Eclipsing Binary Catalogue

O. Vozyakova, Š. Parimucha and M. Kamenec

Institute of Physics, Faculty of Science, Šafárik University, Košice, Slovakia
(E-mail: olga.vozyakova@student.upjs.sk)

Received: November 12, 2024; Accepted: December 10, 2024

Abstract. We present Interactive Gaia Eclipsing Binary Catalogue (IGEBC) a web service that allows user-friendly access to light curves of eclipsing binaries and parameters from Gaia catalogues. It also aims to consolidate light curves and relevant information from other data sources, making it easier for researchers to access a comprehensive dataset of the studied object. Currently, users can search for eclipsing binaries using coordinates or Simbad-resolved names, view their light curves in different passbands, and access system parameters from the Gaia catalogues, which are also available from ASAS-SN and LAMOST.

Key words: eclipsing binaries – astronomical databases – astronomy web services

1. Introduction

The 3^{rd} Gaia Data Release (GDR3), available from 2022, provides not only an astrometric solution with exceptional precision, but also includes astrophysical parameters of stars, derived from low-resolution BP/RP spectra (Gaia Collaboration et al., 2023). Moreover, this release provides a photometric time series for millions of variable stars spanning approximately 34 months. (Eyer et al., 2023). These light curves were classified into 34 classes including eclipsing binaries. GDR3 contains approximately 2.1 million eclipsing binary stars and candidates. The photometric parameters of these systems were derived from their light curves in the G band (Mowlavi et al., 2023).

2. IGEBC - Interactive Gaia Eclipsing Binary Catalogue

Data from GDR3 are available to the community through the Gaia Archive[1] or VizieR portal[2]. However, retrieving and visualizing these light curves from such services is often challenging and time consuming for users. To make Gaia

[1]https://gea.esac.esa.int/archive/
[2]https://vizier.cds.unistra.fr/viz-bin/VizieR

eclipsing binaries' light curves more accessible to the wider research community, we developed the Interactive Gaia Eclipsing Binary Catalogue - IGEBC. The main goal of these web services is to provide light curves and the basic parameters of Gaia eclipsing binaries from multiple data sources within a single web application.

The current version allows users to manipulate the Gaia and ASAS-SN light curves in the selected band (Jayasinghe et al., 2018). It also provides researchers with Gaia's base parameters, basic astrophysical parameters, and spectra from the LAMOST catalogue (Cui et al., 2012).

2.1. Data storage

To store data on eclipsing binaries from GDR3, we deployed a PostgreSQL database on our university server, where we stored data from the Vizier catalogues `I/358/veb`, together with light curves from `I/355/epphot` and basic parameters from the main catalogue `I/355/gaiadr3`. This local storage accelerates data handling and ensures autonomy from potential fluctuations in remote server availability. In the database, we also store parameters from the LAMOST DR9 catalogue, such as the effective temperature $T_{\rm eff}$, metallicity [Fe/H], and surface gravity $\log g$, together with the link to spectra for approximately 8,000 eclipsing binary systems available in both catalogues.

Data from the ASAS-SN survey were not stored locally because of their ongoing updates. Nevertheless, they are temporarily preserved on the disk cache to improve the retrieval speed and conserve resources. We found that the ASAS-SN database currently contains approximately 140,000 systems from the Gaia catalogue.

2.2. Web application overview

The IGEBC web application provides an interface for searching and exploring the data of eclipsing binaries from the Gaia catalogue. Users can search for objects by name or coordinates, or perform a cone search within a specified radius. The Aladin applet was integrated to identify stars in crowded fields. Once a star is selected, users are directed to the page with detailed information about the system, which includes links to the available light curves and spectra. Light curves can be phase-folded, unwanted points can be removed, and the resulting data can be stored in various commonly used formats.

3. Conclusion

The IGEBC web application provides an intuitive interface for searching and exploring eclipsing binaries in the Gaia catalogue. The web application is available at `https://skvo.science.upjs.sk/igebc`.

In the future, we plan to enhance this application by adding more tools for light-curve manipulation and integration with additional databases, both external and local. In particular, we plan to add a web application for the interactive retrieval of TESS data, with tools for their detrending.

We hope that the new database and web portal will enable researchers to work with light curves more efficiently, thereby saving time in searching and processing data. It may also assist in building training sets for supervised machine learning.

Acknowledgements. This work was supported by the Slovak Research and Development Agency under the contract No. APVV-20-0148. O.V. was supported by the internal grant of UPJS VVGS 2024-3080.

References

Cui, X.-Q., Zhao, Y.-H., Chu, Y.-Q., et al., The Large Sky Area Multi-Object Fiber Spectroscopic Telescope (LAMOST). 2012, *Research in Astronomy and Astrophysics*, **12**, 1197, DOI:10.1088/1674-4527/12/9/003

Eyer, L., Audard, M., Holl, B., et al., Gaia Data Release 3. Summary of the variability processing and analysis. 2023, *Astronomy and Astrophysics*, **674**, A13, DOI:10.1051/0004-6361/202244242

Gaia Collaboration, Vallenari, A., Brown, A. G. A., et al., Gaia Data Release 3. Summary of the content and survey properties. 2023, *Astronomy and Astrophysics*, **674**, A1, DOI:10.1051/0004-6361/202243940

Jayasinghe, T., Kochanek, C. S., Stanek, K. Z., et al., The ASAS-SN catalogue of variable stars I: The Serendipitous Survey. 2018, *Monthly Notices of the RAS*, **477**, 3145, DOI:10.1093/mnras/sty838

Mowlavi, N., Holl, B., Lecoeur-Taïbi, I., et al., Gaia Data Release 3. The first Gaia catalogue of eclipsing-binary candidates. 2023, *Astronomy and Astrophysics*, **674**, A16, DOI:10.1051/0004-6361/202245330

Contrib. Astron. Obs. Skalnaté Pleso **55/3**, 385 – 389, (2025)
https://doi.org/10.31577/caosp.2025.55.3.385

On accuracy of eclipsing binary system parameters determination from light curve modeling

S. Zola, G. Stachowski, K. Jarosik, K. Kasprzak and W. Waniak

Astronomical Observatory of the Jagiellonian University, Orla 171, 30-244 Kraków, Poland (E-mail: szola@oa.uj.edu.pl)

Received: November 19, 2024; Accepted: January 8, 2025

Abstract. Based on multicolour observations of two contact systems with flat bottom minima, we investigate the consistency of derived photometric mass ratio parameters. Applying the Wilson-Devinney code, we derived the best solutions using the Monte Carlo search method for GSC 2723-2376 and GU Ori. We found discrepancies in $q_{\rm phot}$ among our solutions and those previously published for the two systems, reaching more than 10%. This will lead to similar differences in the physical parameters.

Key words: binaries: eclipsing – stars: modelling

1. Introduction

The parameters of contact binaries can be reliably obtained if both spectroscopic and photometric data are available. Surveys such as Kepler and TESS have provided a vast number of binary light curves, however spectroscopic data of sufficient quality to derive mass ratios are only available for a tiny fraction of systems. Terrell & Wilson (2005) showed that the photometric mass ratio ($q_{\rm phot}$) could only be reliably derived for systems showing a flat-bottomed minimum, as for partial eclipses nearly identical fits can be obtained for a wide range of mass ratios. This is especially important for contact binaries since differences in derived $q_{\rm phot}$ lead to inconsistencies in the physical parameters.

We investigated the consistency of light curve solutions by modelling photometric light curves collected during different observing seasons for two contact binaries with flat-bottomed minima: GSC 2723-2376 and GU Ori. These results are compared with previously published ones.

2. Targets and Observations

GSC 2723-2376: the single previous study of this system was by Alton and Stepien in 2018 (Alton & Stepien, 2018), based on BVI data. They derived the

ephemeris $M = 2458051.7941 + 0.28570290E$ and modelled the system using PHOEBE (Prša & Zwitter, 2005). They assumed the primary temperature to be 5430 K based on the system $B-V$ colour and concluded that the system was in a contact configuration, with a fill-out factor of about 14% and $q_{\rm phot} = 0.53$. The model did not include a spot as no asymmetry was seen in the light curve.

GU Ori: this system has a longer history of observations dating back to 1930, when Hoffmeister identified it as an RR Lyr type star. Subsequently, only minima times were published until light curve modelling by Yang et al. (2017), who determined the system spectral type to be G0V and derived the ephemeris $M = 2455581.9658 + 0.47067725E$, and by Zhou et al. (2018). Both groups presented parameters determined using the Wilson-Devinney code.

We observed the two systems photometrically using two 50 cm telescopes located at the Jagiellonian University Astronomical Observatory in Kraków, Poland. The CCD images were calibrated using IRAF for bias, dark and flat field (only sky flats were used). Differential aperture photometry was then performed using CMunipack (Motl, 2011), which is based on DAOPHOT (Stetson, 1987).

GSC 2723-2376 was observed over two seasons. A complete light curve in the *BVRI* bands was collected in 2018, and in *VRI* in 2019. GSC 2327-2128 was used as the comparison star, and GSC 2327-2362 and NOMAD1 1235-0584368 as check stars. GU Ori was observed in the *BVRI* bands in 2017 and 2020. TYC 738-883-1 was used as the comparison, with GSC 00738-00513, 2MASS 06095077+1254152 and TYC 738-2484-1 as the check stars.

3. Light Curve Modelling Using the New Photometric Data

We modelled the light curves separately for each observing season to check consistency of the results. The Wilson-Devinney (Wilson & Devinney, 1973) code was used, extended with a Monte Carlo search to ensure that the fit converged on the global minimum (Zola et al., 1997). Observed differential magnitudes were converted to flux units. The light curve for each filter was normalized to 1 at quadrature and binned into about 200 points.

For GSC 2723-2376, we used the *BVRI* data collected in 2018 to calculate two models with different assumed temperatures for the primary star. One was taken from the Gaia DR2 (Gaia Collaboration et al., 2018) catalogue (5018 K) and the other (5430 K) corresponded to the system $B-V$ colour as derived by Alton and Stepien. We used a model without a spot due to the lack of any noticeable difference in the heights of the maxima of the light curve.

For GU Ori we assumed the primary temperature to be 5920 K based on the system spectral type of G0V and the calibration published by Mamajek (2022). Asymmetries in the light curve required a model with one cool spot. Consistency of the resulting photometric mass ratio was checked by separate modelling of the light curves taken in two observing seasons. The resulting best fits are shown in Fig. 1.

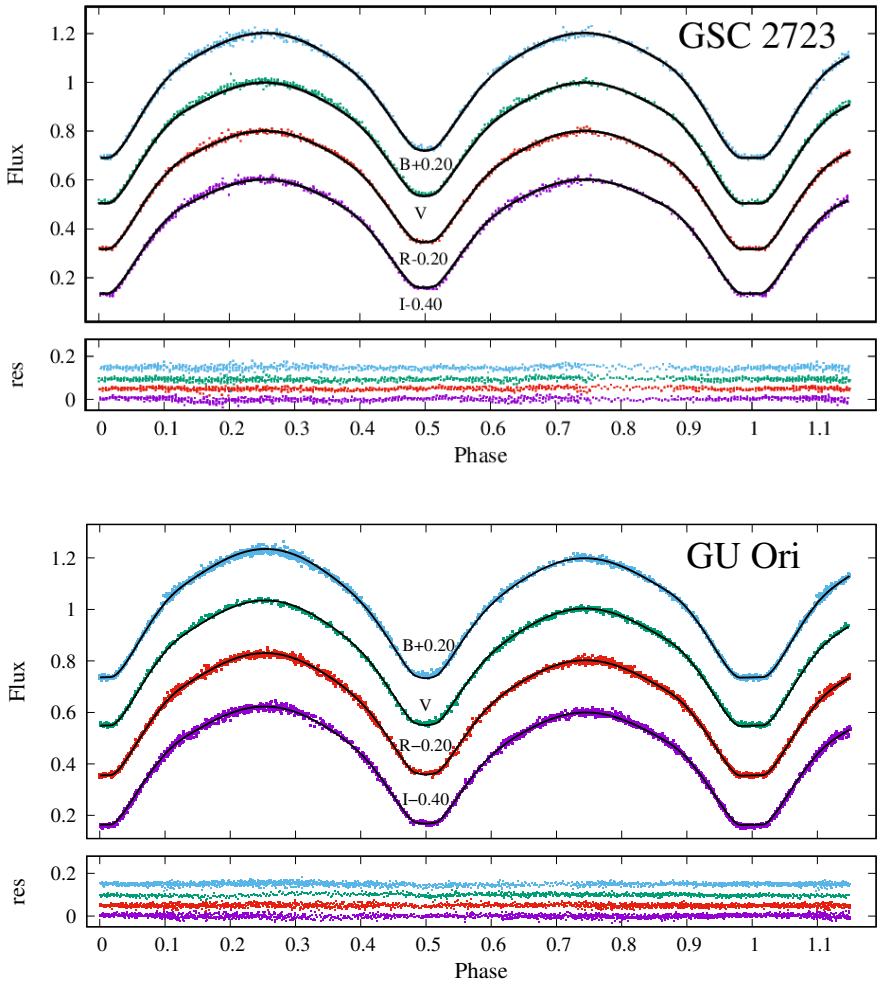


Figure 1. Comparison between data and models for GSC-2723-2376 and GU Ori

4. Results and Conclusions

We investigated the consistency of the determination of the photometric mass ratio $q_{\rm phot}$ based on data from two contact binary systems, considering two possible influences on the models: the assumed fixed temperature of one of the components and the accuracy of the observed light curves. For GSC 2723-2376 we modelled the *BVRI* light curve from 2018 for two assumed values of the primary temperature. For GU Ori, we modelled the *BVRI* light curves observed in 2017 and 2020, and compared our results between seasons and with

those derived by Yang et al. and Zhou et al. The results are shown in Table 1.

Table 1. Results of modelling GSC 2723-2376 and GU Ori

GSC 2723-2376	Alton and Stepien		This work	
assumed T_1	5430 K		5430 K	5018 K
$q_{\rm phot}$	1.894±0.004		2.118±0.010	2.173±0.010
GU Ori	Yang et al.	Zhou et al.	This work	
			2017	2020
assumed T_1	5920 K	6050 K	5920 K	5920 K
$q_{\rm phot}$	0.455±0.020	2.32±0.05	2.207±0.010	2.209±0.013

Looking at the results obtained for GSC 2723-2376, the assumed temperature seems to only have a small impact on $q_{\rm phot}$: an approximately 400 K (∼8%) difference in the temperature of the primary resulted in only a 2% difference in $q_{\rm phot}$ for the same data. On the other hand, despite the same assumed temperature there is a much higher (11%) difference between our result and that of Alton and Stepien, which may be explained by their data, collected with a smaller telescope (28 cm diameter vs. 50 cm). These differences would lead to inconsistencies in the other derived physical parameters in the range of 2–6%.

For GU Ori, we found consistent values for the derived $q_{\rm phot}$ from both two sets of data collected 3 years apart. Our result is about 5% smaller than that of Zhou et al., while Yang et al. obtained the inverse of our value. This appears to be due to poor quality data leading to misidentification of which was the flat minimum (see fig. 2 of Yang et al.). The models included one (Yang et al. and our work) or two dark spots (Zhou at al.) due to the asymmetric light curve.

The presence of spots in models may increase the scatter of the derived values of $q_{\rm phot}$. However, we argue that accuracy of the underlying photometric data has more of an impact on the reliability of the photometric mass ratio. Rucinski (2024) noted that photometrically-determined mass ratios for contact systems tend to have smaller values compared to the spectroscopic determinations. Neither of the two systems presented here has a spectroscopically determined mass ratio as yet, therefore we cannot confirm if they also follow this trend.

Our results and those previously published for these two systems are based on the Roche geometry. Very recently, Rucinski challenged its application in case of two binary systems thought to be in contact configuration: AW UMa and ϵ CrA (Rucinski, 2024), arguing that high resolution spectroscopic observations do not agree with the traditional Lucy (1968a,b) model.

References

Alton, K. B. & Stepien, K., Roche Modeling and Evolutionary History of Mul-

tiple Low Mass Contact Binary Systems. 2018, *Acta Astronomica*, **68**, 449, DOI:10.32023/0001-5237/68.4.7

Gaia Collaboration, Brown, A. G. A., Vallenari, A., et al., Gaia Data Release 2. Summary of the contents and survey properties. 2018, *Astronomy and Astrophysics*, **616**, A1, DOI:10.1051/0004-6361/201833051

Lucy, L. B., The Structure of Contact Binaries. 1968a, *Astrophysical Journal*, **151**, 1123, DOI:10.1086/149510

Lucy, L. B., The Light Curves of W Ursae Majoris Stars. 1968b, *Astrophysical Journal*, **153**, 877, DOI:10.1086/149712

Mamajek, E. 2022, *A Modern Mean Dwarf Stellar Color and Effective Temperature Sequence*, http://www.pas.rochester.edu/~emamajek/EEM_dwarf_UBVIJHK_colors_Teff.txt

Motl, D. 2011, C-Munipack, available from https://c-munipack.sourceforge.net

Prša, A. & Zwitter, T., A Computational Guide to Physics of Eclipsing Binaries. I. Demonstrations and Perspectives. 2005, *Astrophysical Journal*, **628**, 426, DOI:10.1086/430591

Rucinski, S. M., Lessons from the high-resolution spectroscopy of AW UMa and Epsilon CrA: Is the Lucy model valid? 2024, *arXiv e-prints*, arXiv:2406.00155, DOI:10.48550/arXiv.2406.00155

Stetson, P. B., DAOPHOT: A Computer Program for Crowded-Field Stellar Photometry. 1987, *Publications of the ASP*, **99**, 191, DOI:10.1086/131977

Terrell, D. & Wilson, R. E., Photometric Mass Ratios of Eclipsing Binary Stars. 2005, *Astrophysics and Space Science*, **296**, 221, DOI:10.1007/s10509-005-4449-4

Wilson, R. E. & Devinney, E. J., Fundamental data for contact binaries: RZ Comae Berenices, RZ Tauri, and AW Ursae Majoris. 1973, *Astrophysical Journal*, **182**, 539, DOI:10.1086/152162

Yang, Y., Dai, H., Yuan, H., Zhang, X., & Zhang, L., Photometric studies for two contact binaries: V532 Monocerotis and GU Orionis. 2017, *Publications of the ASJ*, **69**, 69, DOI:10.1093/pasj/psx049

Zhou, X., Qian, S., Boonrucksar, S., et al., Photometric investigation of the contact binary GU Orionis with high metallicity. 2018, *Publications of the ASJ*, **70**, 87, DOI:10.1093/pasj/psy084

Zola, S., Kolonko, M., & Szczech, M., Analysis of a photoelectric light curve of the W UMa-type binary ST Ind. 1997, *Astronomy and Astrophysics*, **324**, 1010

Contrib. Astron. Obs. Skalnaté Pleso **55/3**, 390 – 404, (2025)
https://doi.org/10.31577/caosp.2025.55.3.390

Observations of massive contact binaries in the local universe

M. Abdul-Masih[1,2]

[1] *Instituto de Astrofísica de Canarias, C. Vía Láctea, s/n, 38205 La Laguna, Santa Cruz de Tenerife, Spain (E-mail: mabdul@iac.es)*

[2] *Universidad de La Laguna, Dpto. Astrofísica, Av. Astrofísico Francisco Sánchez, 38206 La Laguna, Santa Cruz de Tenerife, Spain*

Received: November 15, 2024; Accepted: January 8, 2025

Abstract. The contact phase represents a crossroad in the evolution of massive binary stars. Depending on the internal physics, the predicted end products can vary greatly including various exotic objects such as Be stars, magnetic massive stars, LBVs and gravitational wave sources. This phase also offers a unique observational laboratory to study binary interaction physics. Here, I review the current state of the field of massive contact binary observations. I summarize the techniques available to identify and characterize these systems as well as the limitations of each and the potential biases that they introduce. I present the sample of known confirmed systems and what the bulk statistics can tell us about their formation and evolution. Next I discuss the challenges that these systems pose from a characterization point of view and how we can overcome these. Finally I discuss the future direction of the field on the observational side.

Key words: comets – cosmogony – celestial mechanics

1. Introduction

Binarity is common in massive stars and ∼70% of all O-type stars are expected to interact with a companion at some point during their lifetime (Sana et al., 2012; Moe & Di Stefano, 2017). Of the systems that interact, 40% (∼25% of all O-type stars) will evolve through a contact phase and eventually merge (Pols, 1994). Population synthesis studies indicate that any given time, approximately 1% of all O-type stars will be found in a contact configuration (Henneco et al., 2024), however, so far very few massive contact systems are known and even fewer have been studied in detail.

The contact phase represents one of the most extreme forms of binary interactions throughout all branches of massive binary evolution. While in a contact configuration, the components share a common envelope through which mass and energy are exchanged and experience a variety of interaction processes including but not limited to tidal locking, mutual illumination, internal mixing, and angular momentum exchange (Wellstein et al., 2001; de Mink et al., 2007).

These binary interactions can fundamentally alter the evolutionary path of a system, affecting the main sequence lifetime, the interior structures of the components, and the positions on the Hertzsprung Russell diagram (Marchant & Bodensteiner, 2024). That said, depending on the treatment of these internal processes and the interaction physics, the theoretically predicted end products of systems that evolve through a contact phase vary widely, including objects such as magnetic massive stars (Schneider et al., 2019; Hubrig et al., 2024), Be stars (Shao & Li, 2014), luminous blue variables (Smith et al., 2018), blue stragglers (Mateo et al., 1990) and double black hole binaries (Marchant et al., 2016; Mandel & de Mink, 2016; de Mink & Mandel, 2016). Without stringent observational constraints during the contact phase, it is impossible to know which of these evolutionary channels will dominate. Over the past few years, there has been a renewed effort to better understand these systems from both the theoretical and observational side. Here, I focus on outlining the current state of the field on the observational side.

2. Detection and characterization

Massive contact binaries are often identified by their short periods ($\sim$ 0.5-3 days) and large amplitude sinusoidal-like light curves. Depending on the mass ratio, fillout factor (see Mochnacki & Doughty, 1972), temperature ratio and inclination, the exact morphology of the light curve can change, but in general contact binaries have smooth light curves without sharp features (except in the case of a total eclipse). The primary and secondary eclipse depths are usually fairly similar (but not necessarily equal) and do not show as strong of variations as other classes of binaries do. Unfortunately, however several other types of objects show similar light curve morphologies making the identification and confirmation of contact systems difficult. Fig. 1 shows the morphology of the light curve and radial velocity curves for a contact system and a semi-detached system generated using the PHOEBE code (Prša et al., 2016; Horvat et al., 2018; Conroy et al., 2020; Jones et al., 2020). In this case, the light curves show almost identical morphologies despite the fact that the binary configurations are quite different. Looking at the radial velocity curves, however, there is a much more significant difference between the semi-amplitudes of each component. Similar comparisons can be made between contact systems and detached ellipsoidal variable systems, however, again in this case, the radial velocity curve can allow one to distinguish between these configurations

The most sure fire way to confirm that a given system is in contact is to directly resolve the stellar surface. This could be done with interferometry, however given the expected angular sizes and magnitudes of the currently known massive contact binary candidates, this is not yet possible. The next best method is performing a simultaneous light curve and radial velocity curve (LC+RV) fit using an appropriate eclipsing binary modelling code. Several such codes exist,

however only the Wilson-Devinney code (Wilson & Devinney, 1971; Wilson, 1979, 2008; Wilson & Van Hamme, 2014) and the PHOEBE code (Prša & Zwitter, 2005; Prša et al., 2016; Horvat et al., 2018; Conroy et al., 2020; Jones et al., 2020) are able to model all binary morphologies ranging from well-detached up to and including contact systems. These different morphologies each require different set-ups within the codes themselves, so, confirming the configuration of a contact binary requires one to model both the light curve and the radial velocity curve assuming a detached, a semi-detached and a contact configuration in order to determine which results in the best fit. For the purposes of this paper, I will consider a system to be a confirmed massive contact binary only if it has been characterized via a combined LC+RV fit. Systems that have been characterized via any other means will be referred to as candidate systems. For the remainder of the paper, unless explicitly stated otherwise, I will be discussing only the confirmed systems.

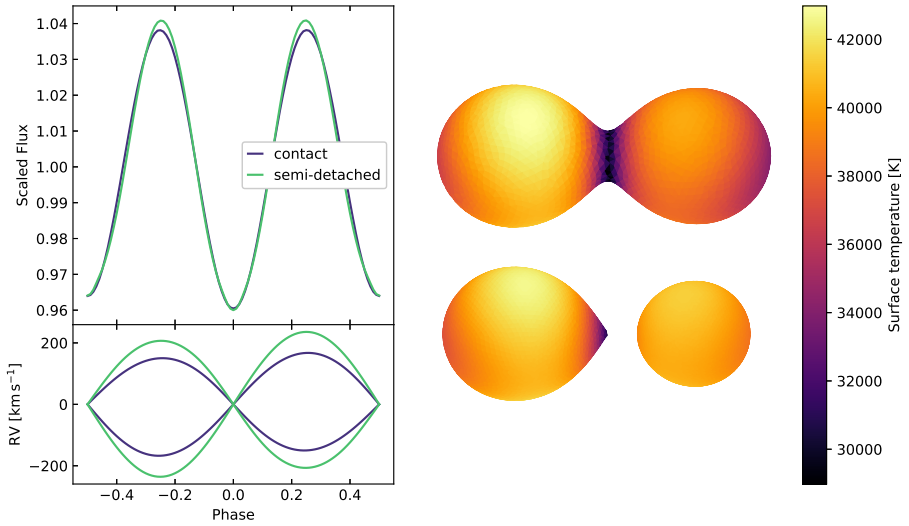


Figure 1. Left: simulated light curve and radial velocity curves for a contact binary (blue) and semi-detached binary (green) using PHOEBE. Right: morphologies of each system simulated on the left panel are displayed with the color representing the surface temperature. Both systems have the same period, semi-major axis, mass ratio and primary temperature, however the secondary temperature, inclination and stellar radii differ.

Table 1. Confirmed massive contact binaries with full LC+RV fits.

Name	Sp. type	V_{mag}	Period [days]	q	f	Multiplicity	Ref.
HD 64315	O+O	9.2	1.019	1.00	1.31	4	1
LSS 3074	O+O	11.7	2.1852	0.86	1.05	2	2
MY Cam	O+O	9.8	1.1755	0.84	1.01	2	3
MY Ser	O+O	7.5	3.3216	0.95	1.99	3	4,5,6
SMC 108086†	O+O	14.9	0.8831	0.85	1.7	2	7
TU Mus	O+O	9.3	1.3873	0.62	1.12	3	8,9
V382 Cyg	O+O	8.7	1.8855	0.73	1.1	3	9,10,11
V729 Cyg	O+O	9.2	6.598	0.29	1.22	6	6,12,13
VFTS 352	O+O	14.5	1.1241	0.99	1.29	2	14
CT Tau	B+B	10.3	0.6668	0.98	1.99	3	15
GU Mon	B+B	11.6	0.8966	0.98	1.72	3	15
V701 Sco	B+B	9.0	0.7619	1.00	1.55	3	15
V745 Cas	B+B	8.1	1.4106	0.57	–	5	16

Notes: † full name: OGLE SMC-SC10 108086
References: (1) Lorenzo et al. (2017), (2) Raucq et al. (2017), (3) Lorenzo et al. (2014), (4) Ibanoglu et al. (2013), (5) Leitherer et al. (1987), (6)Lanthermann et al. (2023), (7) Hilditch et al. (2005), (8) Penny et al. (2008), (9) Qian et al. (2007), (10)Harries et al. (1997), (11) Martins et al. (2017), (12) Yaşarsoy & Yakut (2014), (13) Rauw et al. (2019), (14) Almeida et al. (2015), (15) Yang et al. (2019), (16) Çakırlı et al. (2014)

3. Observational overview

So far only 13 massive contact systems have been confirmed via a combined LC+RV fit in the literature and these are listed in Tab. 1. It should be noted that there are additional objects with LC+RV fits for contact configurations in the literature, however these have later been discarded as contact systems for various reasons and are therefore not included in the sample in Tab. 1.

3.1. Sample statistics

Based on Tab. 1, we can already start to look for trends in the sample to see how these compare with theoretical predictions for this phase. Looking at the sample, all but one object have periods ranging from 0.8-3 days with most concentrating towards the lower end of the period range, however a distinct outlier can be seen in V729 Cyg, which has a period of more than 6 days. This system is classified as a blue supergiant (Sota et al., 2011) and is therefore more evolved than the rest of the sample so it is likely that this system did not originate from Case A mass transfer as is the case for the rest of the systems. That said, binary evolution studies predict that there should be more Case B

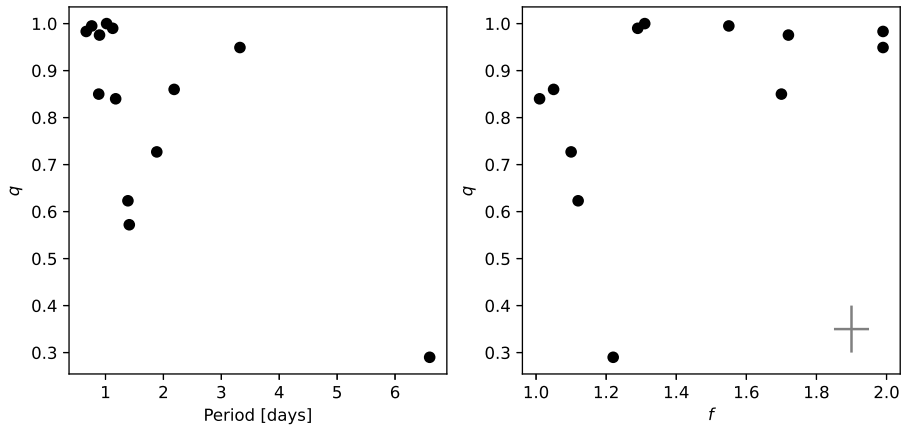


Figure 2. Mass ratio versus orbital period (left) and mass ratio versus fillout factor (right) for the confirmed massive contact systems. Typical error bars for the mass ratio and fillout factor are indicated in grey.

and Case C contact systems formed than Case A contact systems (Henneco et al., 2024), however the shorter lifetimes of these systems may explain why so many more Case A systems are currently known. This could also be due to a selection bias as contact systems with more evolved components are expected to have longer periods, and therefore may not fall within the selection criteria used when searching for contact systems.

The other two important parameters that we can compare with theoretical predictions are the mass ratio and the fillout factor. Both Marchant et al. (2016) and Menon et al. (2021) calculated detailed evolutionary models and performed population synthesis studies focused on contact systems, and both predict that after coming into contact, systems should quickly evolve (on a thermal time scale) towards a mass ratio of unity and then continue to evolve on the nuclear timescale. This would suggest that we would expect to see orders of magnitude more objects with q=1, however observationally, this does not seem to be the case. As is shown in Fig. 2, the mass ratios are fairly well distributed between 0.3 and 1, and while there is certainly an overdensity at q=1, it is not nearly as extreme as theoretical studies predict. Based on the right panel of Fig. 2, which shows the mass ratio as a function of the fillout factor (which can be used as an evolutionary proxy as the fillout factor will increase as the components evolve and expand), there does appear to be a trend towards a mass ratio of 1 as the fillout factor increases, however the scatter is still fairly large. Studies of the rate of period change can provide useful insights in this case as the theoretical predictions state that systems with mass ratios significantly far from 1 should be transferring mass at a higher rate, which in turn will affect

the period accordingly. Observational studies seem to indicate that high mass contact systems show very stable periods that are evolving on the nuclear time scale independent of the mass ratio (Yaşarsoy & Yakut, 2014; Li et al., 2022; Abdul-Masih et al., 2022; Vrancken et al., 2024). This combined with the right panel of Fig. 2 may indicate that either massive contact systems are evolving towards a mass ratio of unity but at a much slower rate than what is expected, or that they may never reach a mass ratio of 1 before merging.

3.2. Stellar properties

Of the 13 confirmed systems, only 4 have been studied in detail spectroscopically to obtain atmosphere parameters and abundances (Raucq et al., 2017; Martins et al., 2017; Abdul-Masih et al., 2019, 2021). A striking result from these works is that in all cases, the abundances of the CNO elements are consistent with the baseline abundances of the regions where the objects are found, indicating little to no CNO processed material on the surface of the stars. Given the extreme rotation rates of these systems ($\geq 300\mathrm{km\,s^{-1}}$) this is surprising as rotational mixing is expected to efficiently mix core processed material to the surface at these rotation rates (Maeder, 2000). The observations also indicate that in general both the primary and secondary components are overluminous and hotter than expected given their masses, which is usually interpreted as a sign of efficient internal mixing. These two observational findings appear to be at odds with one another, and it is still unclear how these fit together (see discussion in Abdul-Masih et al., 2021).

Another important finding from these studies is that the secondary component is always found very close to the primary on the Hertzsprung-Russell diagram, independent of the mass ratio of the system (Raucq et al., 2017; Abdul-Masih et al., 2021). This effect is much too strong to be explained by reflection effects, indicating that there must be a mechanism that efficiently transports energy through the common envelope between the two components. Similar effects have been observed in low mass contact systems and are attributed to sideways convection (Lucy, 1968a,b), however in the case of massive stars the envelopes are radiative so the mechanism is certainly different. Theoretical studies including heat transfer through the radiative envelope have shown that this effect can affect the distribution of mass ratios, however this effect alone is still not enough to rectify the discrepancy between the observed sample and the theoretical predictions (Fabry et al., 2022, 2023, 2024).

3.3. Multiplicity

While no dedicated multiplicity study focused on massive contact systems has been conducted thus far, many confirmed and candidate systems have been discovered to be in higher order multiple systems. The majority of these detections come through eclipse timing variations (ETVs) due to the light travel time effect

(e.g., Qian et al., 2007; Zasche et al., 2017; Yang et al., 2019; Li et al., 2022), however some have been detected as spectroscopic multiples (e.g., Lorenzo et al., 2017; Janssens et al., 2021) or through interferometry (e.g., Lanthermann et al., 2023). Systems with a companion that has been discovered via ETVs show outer orbital periods of between $\sim$ 5-80 years, however companions discovered through spectroscopy and interferometry do not have well constrained orbital periods as of yet. Of the confirmed contact systems, almost 70% of the sample have at least one confirmed companion and about 25% have more than one additional companion. That said, the 4 systems that currently do not have a detected companion have been discovered within the last 10 years and lack sufficient archival data to perform an ETV study, and given the periods of the outer companions discovered with this method, a much longer baseline may be needed to detect any companions. Therefore, this 30% of contact systems without additional companions should be viewed as an upper limit as additional data and time will allow us to probe the parameter space where the companions should be found if they exist.

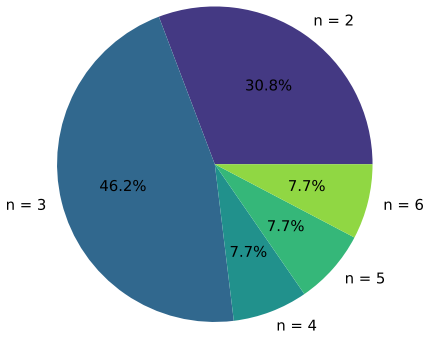


Figure 3. Multiplicity statistics for confirmed massive contact sample

Comparing the multiplicity statistics of the confirmed massive contact sample with those of Offner et al. (2023), the contacts triple fraction is already rather high considering that it contains both B-type and O-type systems. Considering that this is a lower limit on the triple fraction, it is possible that the multiplicity properties of contact systems are fundamentally different from that of other O-type systems, however this is not entirely unexpected due to the compactness of the inner orbit. Given the orbits of the companions, its possible that the companion may play a role in the formation of the contact system, but a deeper investigation is needed to determine the potential evolutionary effects that the companion causes.

4. Challenges

The analysis techniques and tools that we use to characterize contact systems each contain their own set of assumptions and limitations, and it is important to understand how these can affect our understanding of the systems that we apply them to. This applies first and foremost to the techniques that we use to determine the binary configuration for these systems. An underlying assumption for all currently available codes is that of the Lucy model, i.e., that the surface of contact binary coincides with the equipotential, which may not necessarily be viable for all systems. Additionally, while the Wilson-Devinney and PHOEBE 1.0 codes are both able to model contact systems, these codes utilize a trapezoidal meshing that can often lead to gaps in the surface coverage at the bridge. The triangluated meshing used by the PHOEBE 2 code avoids this issue and is able to completely cover the surface, making it a better option for modelling contact systems (Prša et al., 2016). Another important aspect of binary modelling that is often overlooked in codes is the gravity darkening prescription. All of the currently available eclipsing binary modeling codes use the von Zeipel gravity darkening prescription (von Zeipel, 1924) to relate the local surface temperature to the local surface gravity, which while sufficient for well detached binaries, leads to very important systematic biases when applied to highly deformed systems. Improved gravity darkening prescriptions have been developed for rapidly rotating stars and (semi-)detached binaries (Espinosa Lara & Rieutord, 2011, 2012), however so far no such prescription has been developed for contact systems. The von Zeipel gravity darkening prescription leads to more extreme temperatures than is realistic meaning that less deformed systems are needed to reproduce the light curves. By implementing new gravity darkening prescriptions, it is possible that many systems that are currently thought to be semi-detached or ellipsoidal variables may end up becoming contact systems. Until updated gravity darkening prescriptions are developed, however, other clues may help us to determine whether an edge case is actually in contact or not. Vrancken et al. (2024) showed that the period stability may be used to differentiate between contact systems and semi-detached systems which are expected to have higher rates of period change. Additionally, similar component temperatures in unequal mass systems may indicate that a system is in contact.

The spectroscopic analysis techniques that have traditionally been applied to these types of systems also have several important assumptions that are not necessarily valid in the case of contact systems. Usually massive close binaries are analyzed by first disentangling the spectra to obtain the spectral contribution of each component and then fitting each separately using an appropriate radiative transfer code. Spectral disentangling assumes that the morphology of the spectra remains constant over the orbit, and that the only things that vary are the radial velocity and light ratio. This in essence enforces a spherical assumption on the system and does not account for the temperature variations across the surface. This spherical assumption is then reinforced during the fitting process as the

available NLTE radiative transfer codes are almost exclusively one-dimensional. To combat this, new spectroscopic techniques have been developed that patch 1D stellar atmospheres onto a 3D surface, which approximates how the different surface regions contribute to the combined integrated spectrum of the system (see e.g., Palate & Rauw, 2012; Abdul-Masih et al., 2020). Unfortunately, these codes still suffer from the gravity darkening problem discussed above, but overall these codes are more robust and suffer from fewer assumptions and biases than the disentangling methods do.

As demonstrated in Abdul-Masih et al. (2021); Abdul-Masih (2023), accounting for the surface geometry can have an important effect on the derived surface parameters. When comparing the temperatures and abundances obtained using the more traditional disentangling method with those obtained using the spectroscopic patch model SPAMMS (Abdul-Masih et al., 2020), major discrepancies were found that appeared to be dependent on the inclination of the system. This was later confirmed in Abdul-Masih (2023), which focused on single rapidly rotating stars. Here, it was shown that the temperature measured using 1D models could vary by up to 3000K depending on the inclination of the system. Furthermore, failing to account for the surface geometry also heavily biased the abundances, leading to a systematic offset in the helium abundance by more than a factor of 2 in some cases. These studies demonstrate the importance of not only determining the geometry of the system accurately, but accounting for this geometry when measuring atmospheric parameters and surface abundances.

5. Conclusions and future prospects

While the number of confirmed massive contact binaries is far below theoretical expectations, many interesting results have come from these 13 sources already. The sample is well distributed in period, mass ratio and fillout factor, and even though the sample size is rather small, the distribution is already challenging theoretical predictions. The fillout factors, which can be used as a proxy for the time since the initiation of the contact phase, show a loose correlation with the mass ratios suggesting that systems may tend to mass ratios of 1, but on significantly longer time scales than what the theoretical models predict. This is further supported by period stability measurements which show that the systems appear to be stable on the nuclear time scale. Results of spectroscopic analysis also seem to contradict theoretical predictions, as all systems studied so far seem to have baseline abundances, indicating little to no internal mixing. The temperature and luminosities, however, are higher than expected, indicating efficient mixing, presenting an interesting contradiction that has still not been rectified. The sample also shows a high triple fraction of about 70%, however, it is likely that the triple fraction is even higher considering that many systems have been discovered and characterized recently. It is unclear if these companions

have affected the past evolution of these systems, so more dedicated evolutionary modelling is needed to better understand the role of third bodies.

While much progress has been made, there are still many open questions and many avenues for continued investigation. First and foremost, expanding the sample and obtaining a realistic occurrence rate of this phase is of tantamount importance. This includes both searching for new systems and characterizing the systems that have yet to be confirmed. On this front, implementing new gravity darkening prescriptions into our eclipsing binary modelling codes could change the picture somewhat, as this is still one of the largest sources of uncertainty when it comes to determining the configuration of a given system. For the systems that have already been confirmed, spectroscopic analysis of the sample may also reveal useful insights into the evolutionary histories of the systems. Only 4 of the 13 confirmed massive contact systems have been studied in detail spectroscopically, so it is important to analyze the rest of the sample to determine whether the observed abundance and temperature trends hold for the entire sample. This will allow us to better understand when these systems came into contact and whether or not the initial mass transfer leading up to the contact configuration was conservative. On a similar front, characterizing the triple companions around contact systems could also prove to be important to understand their past or future evolution. Overall, we are entering an exciting time in the field of massive contact binaries. We are on the cusp of being able to analyze our sample in a statistical way, which will could lead to some exciting discoveries in the next few years.

Acknowledgements. This project received the support from the "La Caixa" Foundation (ID 100010434) under the fellowship code LCF/BQ/PI23/11970035.

References

Abdul-Masih, M., Effects of rotation on the spectroscopic observables of massive stars. 2023, *Astronomy and Astrophysics*, **669**, L11, DOI:10.1051/0004-6361/202245653

Abdul-Masih, M., Escorza, A., Menon, A., Mahy, L., & Marchant, P., Constraining the overcontact phase in massive binary evolution. II. Period stability of known O+O overcontact systems. 2022, *Astronomy and Astrophysics*, **666**, A18, DOI:10.1051/0004-6361/202244148

Abdul-Masih, M., Sana, H., Conroy, K. E., et al., Spectroscopic patch model for massive stars using PHOEBE II and FASTWIND. 2020, *Astronomy and Astrophysics*, **636**, A59, DOI:10.1051/0004-6361/201937341

Abdul-Masih, M., Sana, H., Hawcroft, C., et al., Constraining the overcontact phase in massive binary evolution. I. Mixing in V382 Cyg, VFTS 352, and OGLE SMC-SC10 108086. 2021, *Astronomy and Astrophysics*, **651**, A96, DOI:10.1051/0004-6361/202040195

Abdul-Masih, M., Sana, H., Sundqvist, J., et al., Clues on the Origin and Evolution of Massive Contact Binaries: Atmosphere Analysis of VFTS 352. 2019, *Astrophysical Journal*, **880**, 115, DOI:10.3847/1538-4357/ab24d4

Almeida, L. A., Sana, H., de Mink, S. E., et al., Discovery of the Massive Overcontact Binary VFTS352: Evidence for Enhanced Internal Mixing. 2015, *Astrophysical Journal*, **812**, 102, DOI:10.1088/0004-637X/812/2/102

Çakırlı, Ö., Ibanoglu, C., & Sipahi, E., V745 Cassiopean interacting young massive binary in a multiple-star system. 2014, *Monthly Notices of the RAS*, **442**, 1560, DOI:10.1093/mnras/stu958

Conroy, K. E., Kochoska, A., Hey, D., et al., Physics of Eclipsing Binaries. V. General Framework for Solving the Inverse Problem. 2020, *Astrophysical Journal, Supplement*, **250**, 34, DOI:10.3847/1538-4365/abb4e2

de Mink, S. E. & Mandel, I., The chemically homogeneous evolutionary channel for binary black hole mergers: rates and properties of gravitational-wave events detectable by advanced LIGO. 2016, *Monthly Notices of the RAS*, **460**, 3545, DOI:10.1093/mnras/stw1219

de Mink, S. E., Pols, O. R., & Hilditch, R. W., Efficiency of mass transfer in massive close binaries. Tests from double-lined eclipsing binaries in the SMC. 2007, *Astronomy and Astrophysics*, **467**, 1181, DOI:10.1051/0004-6361:20067007

Espinosa Lara, F. & Rieutord, M., Gravity darkening in rotating stars. 2011, *Astronomy and Astrophysics*, **533**, A43, DOI:10.1051/0004-6361/201117252

Espinosa Lara, F. & Rieutord, M., Gravity darkening in binary stars. 2012, *Astronomy and Astrophysics*, **547**, A32, DOI:10.1051/0004-6361/201219942

Fabry, M., Marchant, P., Langer, N., & Sana, H., Modeling contact binaries. II. Effects of energy transfer. 2023, *Astronomy and Astrophysics*, **672**, A175, DOI:10.1051/0004-6361/202346277

Fabry, M., Marchant, P., Langer, N., & Sana, H., Modeling contact binaries, III. Properties of a population of close, massive binaries. 2024, *arXiv e-prints*, arXiv:2410.21394, DOI:10.48550/arXiv.2410.21394

Fabry, M., Marchant, P., & Sana, H., Modeling overcontact binaries. I. The effect of tidal deformation. 2022, *Astronomy and Astrophysics*, **661**, A123, DOI:10.1051/0004-6361/202243094

Harries, T. J., Hilditch, R. W., & Hill, G., Interacting O-star binaries: V382 Cyg, V448 CYG and XZ CEP. 1997, *Monthly Notices of the RAS*, **285**, 277, DOI:10.1093/mnras/285.2.277

Henneco, J., Schneider, F. R. N., & Laplace, E., Contact tracing of binary stars: Pathways to stellar mergers. 2024, *Astronomy and Astrophysics*, **682**, A169, DOI:10.1051/0004-6361/202347893

Hilditch, R. W., Howarth, I. D., & Harries, T. J., Forty eclipsing binaries in the Small Magellanic Cloud: fundamental parameters and Cloud distance. 2005, *Monthly Notices of the RAS*, **357**, 304, DOI:10.1111/j.1365-2966.2005.08653.x

Horvat, M., Conroy, K. E., Pablo, H., et al., Physics of Eclipsing Binaries. III. Spin-Orbit Misalignment. 2018, *Astrophysical Journal, Supplement*, **237**, 26, DOI:10.3847/1538-4365/aacd0f

Hubrig, S., Schöller, M., Järvinen, S. P., et al., Detection of extragalactic magnetic massive stars. 2024, *Astronomy and Astrophysics*, **686**, L4, DOI:10.1051/0004-6361/202449793

Ibanoglu, C., Çakırlı, Ö., & Sipahi, E., MY Serpentis: a high-mass triple system in the Ser OB2 association. 2013, *Monthly Notices of the RAS*, **436**, 750, DOI:10.1093/mnras/stt1616

Janssens, S., Shenar, T., Mahy, L., et al., BAT99 126: A multiple Wolf-Rayet system in the Large Magellanic Cloud with a massive near-contact binary. 2021, *Astronomy and Astrophysics*, **646**, A33, DOI:10.1051/0004-6361/202039305

Jones, D., Conroy, K. E., Horvat, M., et al., Physics of Eclipsing Binaries. IV. The Impact of Interstellar Extinction on the Light Curves of Eclipsing Binaries. 2020, *Astrophysical Journal, Supplement*, **247**, 63, DOI:10.3847/1538-4365/ab7927

Lanthermann, C., Le Bouquin, J. B., Sana, H., et al., Multiplicity of northern bright O-type stars with optical long baseline interferometry. Results of the pilot survey. 2023, *Astronomy and Astrophysics*, **672**, A6, DOI:10.1051/0004-6361/202245364

Leitherer, C., Forbes, D., Gilmore, A. C., et al., Photometry and spectroscopy of the O-type variable HD 167971. 1987, *Astronomy and Astrophysics*, **185**, 121

Li, F. X., Liao, W. P., Qian, S. B., et al., V606 Cen: A Newly Formed Massive Contact Binary in a Hierarchical Triple System. 2022, *Astrophysical Journal*, **924**, 30, DOI:10.3847/1538-4357/ac3425

Lorenzo, J., Negueruela, I., Baker, A. K. F. V., et al., MY Camelopardalis, a very massive merger progenitor. 2014, *Astronomy and Astrophysics*, **572**, A110, DOI:10.1051/0004-6361/201424345

Lorenzo, J., Simón-Díaz, S., Negueruela, I., et al., The massive multiple system HD 64315. 2017, *Astronomy and Astrophysics*, **606**, A54, DOI:10.1051/0004-6361/201731352

Lucy, L. B., The Light Curves of W Ursae Majoris Stars. 1968a, *Astrophysical Journal*, **153**, 877, DOI:10.1086/149712

Lucy, L. B., The Structure of Contact Binaries. 1968b, *Astrophysical Journal*, **151**, 1123, DOI:10.1086/149510

Maeder, A., Chemical enrichments by massive stars and the effects of rotation. 2000, *New Astronomy Review*, **44**, 291, DOI:10.1016/S1387-6473(00)00051-8

Mandel, I. & de Mink, S. E., Merging binary black holes formed through chemically homogeneous evolution in short-period stellar binaries. 2016, *Monthly Notices of the RAS*, **458**, 2634, DOI:10.1093/mnras/stw379

Marchant, P. & Bodensteiner, J., The Evolution of Massive Binary Stars. 2024, *Annual Review of Astron and Astrophys*, **62**, 21, DOI:10.1146/annurev-astro-052722-105936

Marchant, P., Langer, N., Podsiadlowski, P., Tauris, T. M., & Moriya, T. J., A new route towards merging massive black holes. 2016, *Astronomy and Astrophysics*, **588**, A50, DOI:10.1051/0004-6361/201628133

Martins, F., Mahy, L., & Hervé, A., Properties of six short-period massive binaries: A study of the effects of binarity on surface chemical abundances. 2017, *Astronomy and Astrophysics*, **607**, A82, DOI:10.1051/0004-6361/201731593

Mateo, M., Harris, H. C., Nemec, J., & Olszewski, E. W., Blue Stragglers as Remnants of Stellar Mergers: The Discovery of Short-Period Eclipsing Binaries in the Globular Cluster NGC 5466. 1990, *Astronomical Journal*, **100**, 469, DOI:10.1086/115530

Menon, A., Langer, N., de Mink, S. E., et al., Detailed evolutionary models of massive contact binaries - I. Model grids and synthetic populations for the Magellanic Clouds. 2021, *Monthly Notices of the RAS*, **507**, 5013, DOI:10.1093/mnras/stab2276

Mochnacki, S. W. & Doughty, N. A., A model for the totally eclipsing W Ursae Majoris system AW UMa. 1972, *Monthly Notices of the RAS*, **156**, 51, DOI:10.1093/mnras/156.1.51

Moe, M. & Di Stefano, R., Mind Your Ps and Qs: The Interrelation between Period (P) and Mass-ratio (Q) Distributions of Binary Stars. 2017, *Astrophysical Journal, Supplement*, **230**, 15, DOI:10.3847/1538-4365/aa6fb6

Offner, S. S. R., Moe, M., Kratter, K. M., et al., The Origin and Evolution of Multiple Star Systems. 2023, in Astronomical Society of the Pacific Conference Series, Vol. **534**, *Protostars and Planets VII*, ed. S. Inutsuka, Y. Aikawa, T. Muto, K. Tomida, & M. Tamura, 275

Palate, M. & Rauw, G., Spectral modelling of circular massive binary systems. Towards an understanding of the Struve-Sahade effect? 2012, *Astronomy and Astrophysics*, **537**, A119, DOI:10.1051/0004-6361/201117520

Penny, L. R., Ouzts, C., & Gies, D. R., Tomographic Separation of Composite Spectra. XI. The Physical Properties of the Massive Close Binary HD 100213 (TU Muscae). 2008, *Astrophysical Journal*, **681**, 554, DOI:10.1086/587509

Pols, O. R., Case A evolution of massive close binaries: formation of contact systems and possible reversal of the supernova order. 1994, *Astronomy and Astrophysics*, **290**, 119

Prša, A., Conroy, K. E., Horvat, M., et al., Physics Of Eclipsing Binaries. II. Toward the Increased Model Fidelity. 2016, *Astrophysical Journal, Supplement*, **227**, 29, DOI:10.3847/1538-4365/227/2/29

Prša, A. & Zwitter, T., A Computational Guide to Physics of Eclipsing Binaries. I. Demonstrations and Perspectives. 2005, *Astrophysical Journal*, **628**, 426, DOI:10.1086/430591

Qian, S. B., Yuan, J. Z., Liu, L., et al., Evolutionary states of the two shortest period O-type overcontact binaries V382 Cyg and TU Mus. 2007, *Monthly Notices of the RAS*, **380**, 1599, DOI:10.1111/j.1365-2966.2007.12184.x

Raucq, F., Gosset, E., Rauw, G., et al., Observational signatures of past mass-exchange episodes in massive binaries: the case of LSS 3074. 2017, *Astronomy and Astrophysics*, **601**, A133, DOI:10.1051/0004-6361/201630330

Rauw, G., Nazé, Y., & Campos, F., Quest for the tertiary component in Cyg OB2 #5. 2019, *Astronomy and Astrophysics*, **627**, A2, DOI:10.1051/0004-6361/201935637

Sana, H., de Mink, S. E., de Koter, A., et al., Binary Interaction Dominates the Evolution of Massive Stars. 2012, *Science*, **337**, 444, DOI:10.1126/science.1223344

Schneider, F. R. N., Ohlmann, S. T., Podsiadlowski, P., et al., Stellar mergers as the origin of magnetic massive stars. 2019, *Nature*, **574**, 211, DOI:10.1038/s41586-019-1621-5

Shao, Y. & Li, X.-D., On the Formation of Be Stars through Binary Interaction. 2014, *Astrophysical Journal*, **796**, 37, DOI:10.1088/0004-637X/796/1/37

Smith, N., Andrews, J. E., Rest, A., et al., Light echoes from the plateau in Eta Carinae's Great Eruption reveal a two-stage shock-powered event. 2018, *Monthly Notices of the RAS*, **480**, 1466, DOI:10.1093/mnras/sty1500

Sota, A., Maíz Apellániz, J., Walborn, N. R., et al., The Galactic O-Star Spectroscopic Survey. I. Classification System and Bright Northern Stars in the Blue-violet at R ~2500. 2011, *Astrophysical Journal, Supplement*, **193**, 24, DOI:10.1088/0067-0049/193/2/24

von Zeipel, H., The radiative equilibrium of a rotating system of gaseous masses. 1924, *Monthly Notices of the RAS*, **84**, 665, DOI:10.1093/mnras/84.9.665

Vrancken, J., Abdul-Masih, M., Escorza, A., et al., Constraining the overcontact phase in massive binary evolution – III. Period stability of known B+B and O+B overcontact systems. 2024, *arXiv e-prints*, arXiv:2410.05084, DOI:10.48550/arXiv.2410.05084

Wellstein, S., Langer, N., & Braun, H., Formation of contact in massive close binaries. 2001, *Astronomy and Astrophysics*, **369**, 939, DOI:10.1051/0004-6361:20010151

Wilson, R. E., Eccentric orbit generalization and simultaneous solution of binary star light and velocity curves. 1979, *Astrophysical Journal*, **234**, 1054, DOI:10.1086/157588

Wilson, R. E., Eclipsing Binary Solutions in Physical Units and Direct Distance Estimation. 2008, *Astrophysical Journal*, **672**, 575, DOI:10.1086/523634

Wilson, R. E. & Devinney, E. J., Realization of Accurate Close-Binary Light Curves: Application to MR Cygni. 1971, *Astrophysical Journal*, **166**, 605, DOI:10.1086/150986

Wilson, R. E. & Van Hamme, W., Unification of Binary Star Ephemeris Solutions. 2014, *Astrophysical Journal*, **780**, 151, DOI:10.1088/0004-637X/780/2/151

Yaşarsoy, B. & Yakut, K., An interacting O + O supergiant close binary system: Cygnus OB2-5 (V729 Cyg). 2014, *New Astronomy*, **31**, 32, DOI:10.1016/j.newast.2014.02.005

Yang, Y., Yuan, H., & Dai, H., A Comprehensive Study of Three Early-type Contact Twin Binaries: CT Tau, GU Mon, and V701 Sco. 2019, *Astronomical Journal*, **157**, 111, DOI:10.3847/1538-3881/aafee1

Zasche, P., Wolf, M., & Vraštil, J., The first study of the light-traveltime effect in bright eclipsing binaries in the Small Magellanic Cloud. 2017, *Monthly Notices of the RAS*, **472**, 2241, DOI:10.1093/mnras/stx2026

Contrib. Astron. Obs. Skalnaté Pleso **55/3**, 405 – 411, (2025)
https://doi.org/10.31577/caosp.2025.55.3.405

Spectroscopic binaries in *Gaia*-ESO, *Gaia* and 4MOST surveys

T. Merle[1,2], G. Traven[3], M. Van der Swaelmen[1,4], S. Van Eck[1], A. Jorissen[1], J. Desuter[1], M. Dorsch[5] and G. Van de Steene[2]

[1] *BLU-ULB, Institut d'Astronomie et d'Astrophysique, Université Libre de Bruxelles, CP 226, Bvd du Triomphe, 1050 Brussels, Belgium (E-mail: tmerle@ulb.ac.be)*

[2] *Royal Observatory of Belgium, Avenue Circulaire 3, 1180 Brussels, Belgium*

[3] *Faculty of Mathematics & Physics, University of Ljubljana, Jadranska 19, 1000 Ljubljana, Slovenia*

[4] *INAF – Osservatorio Astrofisico di Arcetri, Largo E. Fermi 5, 50125 Firenze, Italy*

[5] *Institut für Physik und Astronomie, Universität Potsdam, Karl-Liebknecht-Str. 24/25, 14476 Potsdam, Germany*

Received: November 1, 2024; Accepted: January 7, 2025

Abstract. The properties of binary stars are fundamental for understanding star formation and evolution. Spectroscopic binaries (SB) are genuine binaries that probe short to intermediate orbital periods, shedding light on various stellar evolution pathways. We share recent findings from the *Gaia*-ESO Survey regarding stellar multiplicity from a statistical point of view. Additionally, we present the binary content of *Gaia* DR3 and compare *Gaia* NSS SB with the SB9 reference catalogue of spectroscopic orbits. Finally, we provide insights into the detectability of SB within the context of other large spectroscopic surveys, such as 4MOST, which is set to begin operations next year.

Key words: binaries: spectroscopic – techniques: radial velocities – methods: data analysis – methods: statistical

1. Introduction

Why is spectroscopy of binary stars so important? The first argument is related to the fact that the method to detect spectroscopic binaries (SB) is insensitive to the geometrical distance between the system and the observer, as long as the instrument catches sufficient flux; as opposed to visual and astrometric binaries (AB) that can be detected up to 2 kpc (see Fig. 14 of Van der Swaelmen et al. 2023) with the *Gaia* space mission (Gaia Collaboration et al., 2016, 2023b). Similarly, eclipsing binaries (EB) can only be detected if the orbital plane is almost perpendicular to the sky plane. The second argument is related to the

fact that SB cover a wide range of periods. Indeed, EB cover periods ranging from 0.1 to some tens day, and AB from 100 to 1 000 days, this latter value being an inherent limitation of the amount of data analysed in *Gaia* DR3. SB nicely bridge the gap from the shortest EB periods to the largest AB periods.

The first historical catalogue of spectroscopic orbits was setup at the beginning of the last century at the Lick Observatory (Campbell & Curtis, 1905). This first version include about 140 SB, but most of them were just detections. The following decades were dedicated to monitoring them and to computing their orbital solutions. The catalogue was continuously updated at the Dominion Astronomical Observatory until its version eight, reaching about 1 500 SB (Batten et al., 1989). Since 2 000, an IAU initiative endorsed the update towards an electronic version of the catalogue managed by Pourbaix et al. (2004). After his last update, the SB9 catalogue contained 5 000 orbits for 4 000 SB, because some systems have several orbital solutions published in literature. The era of large ground-based spectroscopic surveys allow the detection of many new SB. Here we report their detections in three (past, present, and future) large surveys: *Gaia*-ESO, *Gaia* and 4MOST. The reader can refer to Merle (2024) for more details on recent photometric and spectroscopic surveys.

2. The past: *Gaia*-ESO

The *Gaia*-ESO Survey (GES) targeted about 100 000 stars in all stellar populations of the Galaxy (Gilmore et al., 2022; Randich et al., 2022). The final release (GES DR5.1) is publicly available since July 2023. The observing strategy was not tailored for the detection of binaries, but it was possible to detect about 1000 SB1, 430 SB2, a dozen of SB3 and one SB4 (Merle et al., 2017, 2020; Van der Swaelmen et al., 2023). Figure 1 shows the identified SB1 against the GES parent population (left), whereas the right figure shows the SB2, forming a main sequence of twin stars, shifted compared to the main sequence of single stars, because photometrically unresolved, appearing brighter than their single counterpart. The GES SB frequency, after correction for selection biases, is about 12%: 10% for SB1 and 2% for SB2, well in line with the close binary fraction of 15 ± 3 % determined by Moe & Di Stefano (2017). For the sample of SB1, statistical inference of the period distribution was derived, as well as the metallicity-dependence of the binary fraction, which increases at a rate of $\sim$ 10% per dex of decreasing metallicity. The higher rate in low-metallicity environments is caused by lower gas opacities that favour efficient cooling and fragmentation even on scales lower than 10 au (Bate, 2005). Finally one interesting spectroscopic quadruple has popped up in the GES dataset. Combining archival data (GIRAFFE, UVES) to the data from a new spectroscopic follow-up (HRS/SALT, HERCULES/UCMJO), it was possible to characterise this compact hierarchical 2+2 system. Some of the evolutionary scenarios lead to

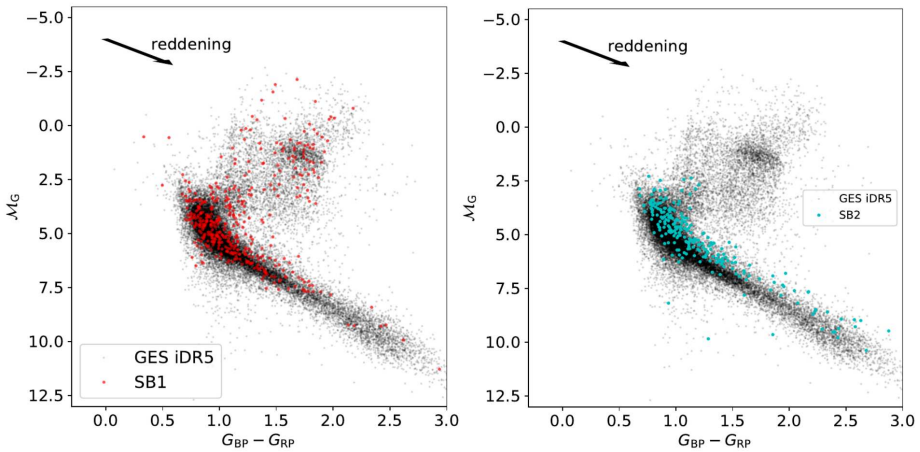


Figure 1. Colour-absolute magnitude diagram of stars in the *Gaia*-ESO Survey with detected SB1 (left panel) and detected SB2 (right panel), using *Gaia* parallaxes and photometry.

the formation of type Ia supernova through a sequence of merger events (Merle et al., 2022).

3. The present: *Gaia*

The ESA *Gaia* mission (Gaia Collaboration et al., 2016, 2023b) started operations in 2013. The 3rd data release (DR3) provided an unprecedented large and homogeneous sample of binary stars, making a quantitative leap in the datasets and orbital parameters for binaries. In *Gaia* DR3, there are 3 sources to explore in term of binarity: (i) the Non-Single Star (NSS) catalogue (Gaia Collaboration et al., 2023a) that contains about 800k binaries, see Fig. 2, (ii) the catalogue of variables that contains about 2 million of eclipsing binaries and more than 6 300 ellipsoidal variables (Eyer et al., 2023), (iii) the Multiple Star Classifier (Creevey et al., 2023) with about 480 million *Gaia* unresolved photometric binaries. The latest should be used with caution, since no validation was performed, but it constitutes an interesting starting point for having rough estimates of effective temperature, gravity and metallicity of individual components.

In brief in NSS, there are about 450k astrometric binaries (AB), 219k SB and 86k eclipsing binaries (EB) as illustrated in Fig. 2. There is a sample of about 58k AB+SB; while the numbers of SB+EB, AB+EB and AB+SB+EB are more anecdotic, still providing an effective number of candidates that will probably serve as a benchmark binary sample.

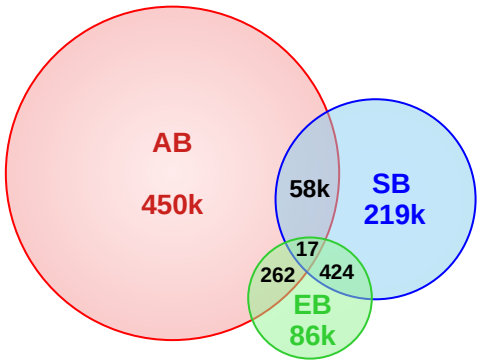


Figure 2. *Gaia* Non-Single Star catalogue content. AB, SB and EB mean Astrometric, Spectroscopic and Eclipsing Binaries. The intersection between AB and SB allows to derive accurate masses for about 20k binaries, reported in the *Gaia* table `binary_masses`.

A careful cross-match of the SB9 with *Gaia* NSS allows to find about 800 common binaries only. This is mainly explained by two reasons: first, the limiting magnitude of the *Gaia* spectrograph for SB is about $G \sim 13$ mag, while reaching ~ 19 mag in SB9; second, the measured orbital periods is limited to about 1 000 d, while reaching 10^5 d in SB9. When comparing the periods, we identified a number of outliers (about 10%) which are investigated in detail in a forthcoming paper (Merle et al., in prep). We can also mention Gosset et al. (2024) who used the SB9 catalogue to validate the *Gaia* NSS SB pipeline.

4. The future: 4MOST

The 4-m Multi-Object Spectrograph Telescope (4MOST, de Jong et al. 2019) is a large ground-based spectroscopic survey on the 4 m VISTA/ESO telescope. The first light is scheduled for 2025. With 2 400 fibres (1 600 in low resolution, $R \sim 6\,000$; and 800 in high resolution, $R \sim 20\,000$) the probing magnitudes will reach 20 (S/N$\sim$ 10 Å^{-1}) and 16 (S/N$\sim$ 100 Å^{-1}) in G band, respectively, in low and high resolution. The accessible range of declinations is $[-80, +20]^\circ$. Such facility will roughly provide about a million spectra a month to analyse, which is considerable and will require automated processes. In this context, the Multiplicity Working Group has developed a cadence strategy for some of the

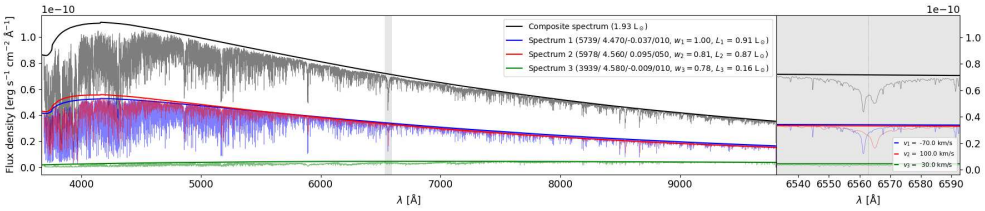


Figure 3. Synthetic composite spectrum of a spectroscopic triple stellar system (grey line)to test the SB detection module implemented in the 4MOST Galactic Pipeline. The primary (blue) and the secondary (red) have similar atmospheric parameters while the third component (green) is almost 2000 K cooler. The panel on the right is a zoom around Hα.

sub-samples to optimise the number of repeated observations. On the one hand, we want a maximum possible time span between required repeats to boost SB1 detection efficiency and, on the other hand, we will follow-up some of the *Gaia* and OGLE (Soszyński et al., 2016) EB and ellipsoidal variables to derive precise stellar masses and radii. In addition, the Detection Of Extrema code (DOE, Merle et al. 2017) is implemented in the 4MOST Galactic Pipeline to ease the detection of SB with two components and more. To test it, we simulate synthetic composite spectra (see the spectroscopic triple star in Fig. 3 as an example), to determine detection efficiency and threshold, as well as precision and accuracy on measured radial velocities. For SB2, the minimum separation between components are about 23 km s^{-1} in high resolution mode and 64 km s^{-1} in low resolution mode. Finally an implementation of a module that will characterise composite spectra with n components is undergoing, following the methodology of El-Badry et al. (2018) and using machine learning approach based on *The Payne* (Ting et al., 2019).

5. Conclusion

In the era of large spectroscopic surveys, many SB candidates are identified, most of them being new discoveries. Nevertheless, follow-up of these candidates is necessary to confirm their multiple nature and characterise their orbital parameters. However, often smaller facilities can follow only the brightest and the most interesting candidates. With the rise of *Gaia*, and new large multi-object spectrographs like 4MOST, we enter a new *industrial* scale where machine learning will be fully exploited to detect and characterise SB, including the most numerous ones having orbital periods beyond a hundred years.

Acknowledgements. T.M. is granted by the BELSPO Belgian federal research program FED-tWIN under the research profile Prf-2020-033_BISTRO. G.T. acknowl-

edges financial support of the Slovenian Research Agency (research core funding No. P1-0188) and the European Space Agency (PRODEX Experiment Arrangement No. 4000143450).

References

Bate, M. R., The dependence of the initial mass function on metallicity and the opacity limit for fragmentation. 2005, *Monthly Notices of the RAS*, **363**, 363, DOI:10.1111/j.1365-2966.2005.09476.x

Batten, A. H., Fletcher, J. M., & MacCarthy, D. G., Catalogue of the orbital elements of spectroscopic binary systems : 8 : 1989. 1989, *Publications of the Dominion Astrophysical Observatory Victoria*, **17**, 1

Campbell, W. W. & Curtis, H. D., First catalogue of spectroscopic binaries. 1905, *Lick Observatory Bulletin*, **79**, 136, DOI:10.5479/ADS/bib/1905LicOB.3.136C

Creevey, O. L., Sordo, R., Pailler, F., et al., Gaia Data Release 3. Astrophysical parameters inference system (Apsis). I. Methods and content overview. 2023, *Astronomy and Astrophysics*, **674**, A26, DOI:10.1051/0004-6361/202243688

de Jong, R. S., Agertz, O., Berbel, A. A., et al., 4MOST: Project overview and information for the First Call for Proposals. 2019, *The Messenger*, **175**, 3, DOI:10.18727/0722-6691/5117

El-Badry, K., Rix, H.-W., Ting, Y.-S., et al., Signatures of unresolved binaries in stellar spectra: implications for spectral fitting. 2018, *Monthly Notices of the RAS*, **473**, 5043, DOI:10.1093/mnras/stx2758

Eyer, L., Audard, M., Holl, B., et al., Gaia Data Release 3. Summary of the variability processing and analysis. 2023, *Astronomy and Astrophysics*, **674**, A13, DOI:10.1051/0004-6361/202244242

Gaia Collaboration, Arenou, F., Babusiaux, C., et al., Gaia Data Release 3. Stellar multiplicity, a teaser for the hidden treasure. 2023a, *Astronomy and Astrophysics*, **674**, A34, DOI:10.1051/0004-6361/202243782

Gaia Collaboration, Prusti, T., de Bruijne, J. H. J., et al., The Gaia mission. 2016, *Astronomy and Astrophysics*, **595**, A1, DOI:10.1051/0004-6361/201629272

Gaia Collaboration, Vallenari, A., Brown, A. G. A., et al., Gaia Data Release 3. Summary of the content and survey properties. 2023b, *Astronomy and Astrophysics*, **674**, A1, DOI:10.1051/0004-6361/202243940

Gilmore, G., Randich, S., Worley, C. C., et al., The Gaia-ESO Public Spectroscopic Survey: Motivation, implementation, GIRAFFE data processing, analysis, and final data products. 2022, *Astronomy and Astrophysics*, **666**, A120, DOI:10.1051/0004-6361/202243134

Gosset, E., Damerdji, Y., Morel, T., et al., Gaia Data Release 3: spectroscopic binary-star orbital solutions and the SB1 processing chain. 2024, *arXiv e-prints*, arXiv:2410.14372, DOI:10.48550/arXiv.2410.14372

Merle, T., Dancing with the Stars: a Review on Stellar Multiplicity. 2024, *Bulletin de la Societe Royale des Sciences de Liege*, **93**, 170, DOI:10.25518/0037-9565.11641

Merle, T., Hamers, A. S., Van Eck, S., et al., A spectroscopic quadruple as a possible progenitor of sub-Chandrasekhar type Ia supernovae. 2022, *Nature Astronomy*, **6**, 681, DOI:10.1038/s41550-022-01664-5

Merle, T., Van der Swaelmen, M., Van Eck, S., et al., The Gaia-ESO Survey: detection and characterisation of single-line spectroscopic binaries. 2020, *Astronomy and Astrophysics*, **635**, A155, DOI:10.1051/0004-6361/201935819

Merle, T., Van Eck, S., Jorissen, A., et al., The Gaia-ESO Survey: double-, triple-, and quadruple-line spectroscopic binary candidates. 2017, *Astronomy and Astrophysics*, **608**, A95, DOI:10.1051/0004-6361/201730442

Moe, M. & Di Stefano, R., Mind Your Ps and Qs: The Interrelation between Period (P) and Mass-ratio (Q) Distributions of Binary Stars. 2017, *Astrophysical Journal, Supplement*, **230**, 15, DOI:10.3847/1538-4365/aa6fb6

Pourbaix, D., Tokovinin, A. A., Batten, A. H., et al., S_{B^9}: The ninth catalogue of spectroscopic binary orbits. 2004, *Astronomy and Astrophysics*, **424**, 727, DOI:10.1051/0004-6361:20041213

Randich, S., Gilmore, G., Magrini, L., et al., The Gaia-ESO Public Spectroscopic Survey: Implementation, data products, open cluster survey, science, and legacy. 2022, *Astronomy and Astrophysics*, **666**, A121, DOI:10.1051/0004-6361/202243141

Soszyński, I., Pawlak, M., Pietrukowicz, P., et al., The OGLE Collection of Variable Stars. Over 450 000 Eclipsing and Ellipsoidal Binary Systems Toward the Galactic Bulge. 2016, *Acta Astronomica*, **66**, 405, DOI:10.48550/arXiv.1701.03105

Ting, Y.-S., Conroy, C., Rix, H.-W., & Cargile, P., The Payne: Self-consistent ab initio Fitting of Stellar Spectra. 2019, *Astrophysical Journal*, **879**, 69, DOI:10.3847/1538-4357/ab2331

Van der Swaelmen, M., Merle, T., Van Eck, S., et al., The Gaia-ESO Survey: new spectroscopic binaries in the Milky Way. 2023, *arXiv e-prints*, arXiv:2312.04721, DOI:10.48550/arXiv.2312.04721

Contrib. Astron. Obs. Skalnaté Pleso **55/3**, 412 – 420, (2025)
https://doi.org/10.31577/caosp.2025.55.3.412

Accurate dynamical masses from binaries with extreme brightness ratios

D. Sebastian[1], **A.H.M.J. Triaud**[1], **P.F.L. Maxted**[2] **and M. Brogi**[3,4]

[1] *School of Physics and Astronomy, University of Birmingham, Edgbaston, Birmingham B15 2TT, UK (E-mail: D.Sebastian.1@bham.ac.uk)*

[2] *Astrophysics group, Keele University, Staffordshire, ST5 5BG, UK*

[3] *Department of Physics, University of Turin, Via Pietro Giuria 1, I-10125, Turin, Italy*

[4] *INAF – Osservatorio Astrofisico di Torino, Via Osservatorio 20, 10025, Pino Torinese, Italy*

Received: November 15, 2024; Accepted: February 5, 2025

Abstract. High-resolution cross-correlation techniques are a powerful tool to explore exoplanet atmospheres. We introduce their application to binary stars from the EBLM project. In particular, we focus on eclipsing, high-contrast binaries consisting of a solar-type star and a low mass M-dwarf companion. These binary systems have typical brightness ratios $\sim 0.1\%$ at optical wavelengths and appear as single-lined binaries in optical high-resolution spectra. Since the spectral features of low-mass stars are well known, we can recover the signal of the M-dwarf companion from what otherwise appears as noise, and accurately measure the masses of both stars, turning the system into a double-lined binary. We show that this application is a powerful new tool to not only derive accurate and precise dynamical masses for fully convective stars, but also to extract phase-dependent information. We will furthermore discuss the application to high-resolution infrared spectroscopy to characterise stars at the very bottom of the main-sequence.

Key words: binaries: spectroscopic – stars: fundamental parameters – planets and satellites: atmospheres – stars: low-mass – binaries: eclipsing – techniques: spectroscopic

1. Introduction

Accurate masses and radii of main-sequence stars are crucial to calibrate stellar evolution models which is essential not only to characterise binaries, but also planetary systems as well as their atmospheres. Very low mass main-sequence ($M < 0.35\,\mathrm{M}_\odot$) stars play a special role. A very long standing issue has been the 'radius inflation problem' (e.g. Casagrande et al., 2008; Torres et al., 2010; Spada et al., 2013; Kesseli et al., 2018). Stellar radii from evolutionary models

appear to be under-predicted by a few percent. This has also implications for the characterisation of exoplanets of such very low-mass stars. Their parameters crucially depend on the stellar parameters of isolated M-dwarfs which are inferred from stellar models (Dotter et al., 2008; Baraffe et al., 2015).

Eclipsing binaries with F,G, & K-type primaries and very low-mass stellar companions, which we denote as EBLM (eclipsing binary - low mass) are perfect laboratories to characterise the stellar parameters of the low-mass companion. The main goal of the EBLM project (e.g. Triaud et al., 2013; Maxted et al., 2023) is to create an empirical mass-radius-luminosity-metalicity diagram for very low-mass main-sequence stars. While the program targets were initially detected as false positives from surveys for transiting planets such as the WASP survey (Pollacco et al., 2006), the advent of space based photometry as well as an intensive spectroscopic follow up using high-precision spectrographs (Triaud et al., 2017; Martin et al., 2019) led to a large sample of well characterised M-dwarfs with reliable stellar parameters (e.g. von Boetticher et al., 2019; Swayne et al., 2021; Sebastian et al., 2023; Swayne et al., 2024). Due to the high contrast of the binary components, these appear as single-lined binaries, which allows to not only achieve extreme precise measurements of the binary mass function, but also to measure the reflex motion of circumbinary planets (Triaud et al., 2022; Standing et al., 2023).

These high contrast ratios also mean that the masses for the M-dwarf secondaries are derived from stellar parameters of the solar-like primary, which in turn depend on stellar evolution models. Inaccuracies in the parameters of the primary lead to systematic biases for the M-dwarf (Duck et al., 2023). In order to minimise such systematic biases in the EBLM project, Freckelton et al. (2024) presented a homogenous spectroscopic analysis of 179 EBLM primary stars, based on more than 4500 high-resolution spectra. The stellar parameters inferred from this analysis depends on stellar evolution models of F,G, & K-type stars. To verify these we can use the eclipsing configuration of EBLM binaries. Thanks to precision light curves from space and accurate stellar radii from Gaia, the mass of the primary star can be derived directly. This has been shown to be a powerful method to directly verify the accuracy of the primary stellar parameters (Davis et al., 2024). A fully model independent method to verify the accuracy of the EBLM primary parameters are dynamical mass measurements, which are difficult due to the intrinsic contrast of both binary components.

2. Dynamical masses

To measure dynamical masses of these systems, we have to transform high-contrast binaries (single lined) to double-lined binaries. In order to increase the contrast and thus to derive dynamical masses from optical high-resolution spectra, we apply the High-Resolution Cross-Correlation Spectroscopy method (HRCCS; Snellen et al., 2010). This method has been used successfully to detect

cross-correlation signals as faint as 10^{-5} and measure atomic and molecular species in exoplanet atmospheres for more than a decade.

This method involves a two step process. First the spectra are detrended to remove telluric or stellar contributions from the host-star. Second the detrended spectra are cross-correlated and combined in the rest-frame of the M-dwarf. The detrending makes use of the fact that a planet signal (i) is buried in the noise of its host star and (ii) is moving significantly (by several $\mathrm{km\,s^{-1}}$) during the observation, which leaves the spectral lines of the exoplanet atmosphere basically unaffected. Both of these requirements are fulfilled for high-contrast binaries.

2.1. Application to optical spectroscopy

We, thus, applied the HRCCS method to measure the dynamical masses of the binary EBLM J0608−59, using optical high-resolution spectra obtained with ESPRESSO at the VLT (Pepe et al., 2021). The binary is composed of a solar-type primary component with M-dwarf companion and features an average contrast ratio 0.2 per cent at optical wavelengths. In the following we lay-out the method while the details of this study are described in Sebastian et al. (2024b).

Optical spectra are dominated by the absorption spectrum of the primary star. Telluric contributions can be avoided in the cross-correlation thanks to the wide spectral range of these data. We thus detrend the spectra to effectively remove the absorption spectrum of the primary. This has been achieved by applying a singular value decomposition ((SVD, Kalman, 1996)) to the spectra, which are aligned into the primary's rest-frame. The SVD decomposes the spectra into a sum of components, which are correlated to the primary's rest-frame as well. In this way, the SVD components with largest eigenvectors, contain basically the primary spectral lines and can simply be subtracted. We define the optimal number of components to be removed by the "effective rank", which is based on the entropy of the eigenvectors (Roy & Vetterli, 2007). This estimates the significant number of components needed to describe the correlated signal. In other words, if this number of SVD components are removed, the correlation of the remaining data in the primary's rest-frame is not distinguishable from white noise. In contrast to typical exoplanet applications, which define the optimal number of removed components by optimising the detected cross-correlation peak returned from the planets atmosphere (e.g. Cheverall et al., 2023), this definition is basically based on the noise of the data. A typical spectral Frame before and after the application of the SVD detrending is shown in Fig. 1.

The detection was made by enhancing the M-dwarfs signal (i) by a combination of all detrended spectra in the rest-frame of the M-dwarf and (ii) by performing a cross-correlation with a M-dwarf line list. Such a combination requires the orbital velocity of the M-dwarf, and thus the knowledge of its orbital parameters. In case of EBLM binaries these can be inferred precisely from the orbit of the primary star. The only unknown parameter is the semi-amplitude

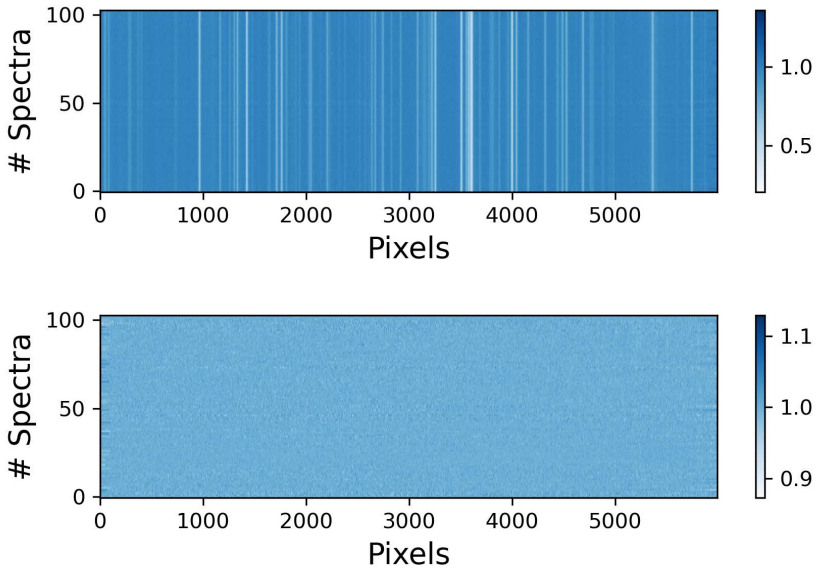


Figure 1. Spectral segment from 103 ESPRESSO spectra of EBLM J0608−59 in the rest-frame of the primary. Upper panel: normalised spectra, Lower panel: Spectra after SVD detrending.

of the M-dwarf. By sampling such combinations over a range of different semi-amplitudes, the M-dwarfs signal gets amplified, once all spectra are combined in the rest-frame of the M-dwarf. In practice, the M-dwarfs semi-amplitude can now be inferred from the maximum amplification of the cross-correlation peak. This method can also be referred to as "K-focusing" (e.g. Sebastian et al., 2024a). Fig. 2 left panel shows the cross correlation to the combined and detrended ESPRESSO spectra sampled for different semi-amplitudes (K_2), as well as the systemic velocity ($V_{\rm rest}$) of the M-dwarf. We used the publicly available *Saltire* model (Sebastian et al., 2024a) to measured the semi-amplitude of the M-dwarf with an uncertainty better than $\sim 500\,{\rm ms}^{-1}$, which allowed us to determine the dynamical masses of both companions with accuracies better than 2 per cent for the primary and better than 1 per cent for the M-dwarf. The well detected CCF signal, as well as the known orbit parameters of the secondary, both allow us to extract the CCF signal in the time domain. We can, thus, measure the phase-dependent CCF contrast, which is a function of the used line list, the individual absorption lines of the M-dwarf, and the contrast of the binary components. Such phase dependent CCF contrast variations do carry information about e.g. reflected light for close in binaries at optical wavelengths. Since the ESPRESSO spectra do cover the full orbital phase of EBLM J0608−59, we

can -within the uncertainties- confirm a constant CCF contrast for the M-dwarf (Sebastian et al., 2024b).

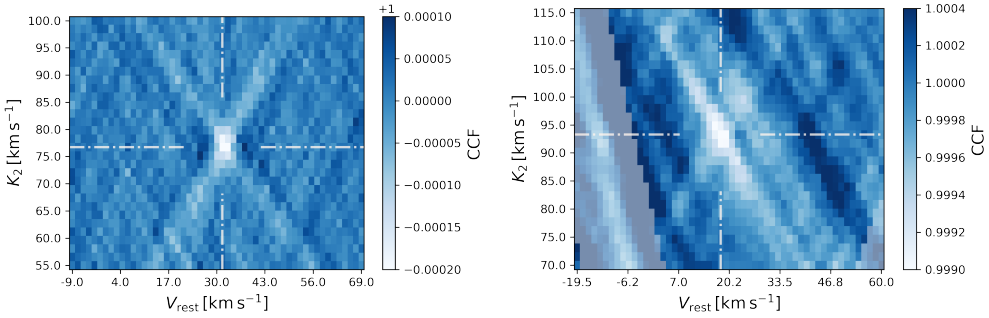


Figure 2. $K_2 - V_{\rm rest}$ mapping as a result from the K-focusing. Left panel: EBLM J0608−59 ($M_2 \sim 0.3\,M_\odot$), using 103 optical ESPRESSO spectra, Right panel: EBLM J0040+01 ($M_2 \sim 0.1\,M_\odot$), using 15 infrared CRIRES$^+$ spectra. Dashed lines mark the expected semi-amplitude and rest velocities of the M-dwarf. Shaded areas: Positions of artefacts from SVD detrending.

2.2. Application to infrared spectroscopy

We showed the power of the HRCCS method to derive dynamical masses from high-contrast binaries. Nevertheless, the majority of the targets from the EBLM project have been observed with optical spectrographs. The contrast ratios of these allow us to derive dynamical masses with the HRCCS method for M-dwarfs down to $\sim 0.2\,M_\odot$.

To allow the dynamical mass measurement of M-dwarfs at the bottom of the main-sequence, we can make use of the decreased contrast ratio at near infrared wavelengths due to the late-type secondary star. This has successfully been shown for EBLM J0113+31 ($M_2 \sim 0.2\,M_\odot$) using high-resolution near infrared SPIRou spectra (Maxted et al., 2022).

In an ongoing survey, we focus on EBLM binaries with M-dwarf companions $\sim 0.1\,M_\odot$ which are observed in the K-band using CRIRES$^+$ on the ESO 8.2-m VLT (Kaeufl et al., 2004). We adopt the full HRCCS frame work, to these infrared observations, including SVD detrending and fitting the M-dwarfs semi-amplitude using the *Saltire* model. In a first part of this survey, we observed the binaries EBLM J0040+01 (15 spectra) and EBLM J1219−39 (9 spectra). Both have orbital periods ~ 7 d. As opposed to the situation in the optical, these data are now dominated not only by the primary's absorption spectrum, but also by significant telluric contributions. Before SVD detrending, we thus fit and clean the spectra from telluric features using the ESO molecfit pipeline (Smette et al.,

2015). For both binaries, we successfully detect the M-dwarf components and estimate their dynamical masses. Due to the relatively small number of spectra, the detrended data show residuals of the primary star. We use the *Saltire* model to estimate the areas of the CCF map, affected by artefacts from the primary component. These are finally masked, when we measure the M-dwarfs signal position. The right panel of Fig. 2 shows the detection of the M-dwarf of EBLM J0040+01 on a 3 sigma level with only 15 infrared spectra. In a preliminary analysis, we achieved a precision on the M-dwarf masses (both ~ 0.1 $M_{\odot}$) of better than 3 per cent for EBLM J0040+01 and better than 7 per cent for EBLM J1219−39.

This demonstrates the power of the HRCCS method, for high-precision infrared spectra, to measure dynamical masses at the very bottom of the main-sequence. Since these binaries are transiting, their radii are well determined and metallicities are well known from the primary star. The full analysis from this survey will be published in Sebastian et al. (2025). We expect to improve the accuracy on the dynamical masses by including more spectra, as well an improved removal of telluric contributions.

3. Summary

In this contribution, we introduced the HRCCS method as a powerful tool to derive precise dynamical masses for high-contrast binaries. Although this method has been in use to detect and analyse exoplanet atmospheres for more than a decade, this is the first time it is applied to spectra of high-contrast binaries. It's application to optical spectra allows us to validate previous, model dependent mass-measurements from the EBLM project and to turn them into benchmark targets for a precise mass-radius diagram for fully convective low-mass stars. We introduce our survey to extend our abilities to measure dynamical masses of EBLM binaries down to the lowest mass star on the main-sequence.

Acknowledgements. Based on observations collected at the European Southern Observatory under ESO programmes 103.2024, 106.216B, 111.2523.001 and 111.2523.002. This research is supported work funded from the European Research Council (ERC) the European Union's Horizon 2020 research and innovation programme (grant agreement no803193/BEBOP). This research was supported by UK Science and Technology Facilities Council (STFC) research grant number ST/Y002563/1.

References

Baraffe, I., Homeier, D., Allard, F., & Chabrier, G., New evolutionary models for pre-main sequence and main sequence low-mass stars down to the hydrogen-burning limit. 2015, *Astronomy and Astrophysics*, **577**, A42, DOI:10.1051/0004-6361/201425481

Casagrande, L., Flynn, C., & Bessell, M., M dwarfs: effective temperatures, radii and metallicities. 2008, *Monthly Notices of the RAS*, **389**, 585, DOI:10.1111/j.1365-2966.2008.13573.x

Cheverall, C. J., Madhusudhan, N., & Holmberg, M., Robustness measures for molecular detections using high-resolution transmission spectroscopy of exoplanets. 2023, *Monthly Notices of the RAS*, **522**, 661, DOI:10.1093/mnras/stad648

Davis, Y. T., Triaud, A. H. M. J., Freckelton, A. V., et al., The EBLM Project XII. An eccentric, long-period eclipsing binary with a companion near the hydrogen-burning limit. 2024, *Monthly Notices of the RAS*, **530**, 2565, DOI:10.1093/mnras/stae842

Dotter, A., Chaboyer, B., Jevremović, D., et al., The Dartmouth Stellar Evolution Database. 2008, *Astrophysical Journal, Supplement*, **178**, 89, DOI:10.1086/589654

Duck, A., Martin, D. V., Gill, S., et al., The EBLM project X. Benchmark masses, radii, and temperatures for two fully convective M-dwarfs using K2. 2023, *Monthly Notices of the RAS*, **521**, 6305, DOI:10.1093/mnras/stad452

Freckelton, A. V., Sebastian, D., Mortier, A., et al., BEBOP V. Homogeneous stellar analysis of potential circumbinary planet hosts. 2024, *Monthly Notices of the RAS*, **531**, 4085, DOI:10.1093/mnras/stae1405

Kaeufl, H.-U., Ballester, P., Biereichel, P., et al., CRIRES: a high-resolution infrared spectrograph for ESO's VLT. 2004, in Society of Photo-Optical Instrumentation Engineers (SPIE) Conference Series, Vol. **5492**, *Ground-based Instrumentation for Astronomy*, ed. A. F. M. Moorwood & M. Iye, 1218–1227

Kalman, D., A Singularly Valuable Decomposition: The SVD of a Matrix. 1996, *The College Mathematics Journal*, **27**, 2

Kesseli, A. Y., Muirhead, P. S., Mann, A. W., & Mace, G., Magnetic Inflation and Stellar Mass. II. On the Radii of Single, Rapidly Rotating, Fully Convective M-Dwarf Stars. 2018, *Astronomical Journal*, **155**, 225, DOI:10.3847/1538-3881/aabccb

Martin, D. V., Triaud, A. H. M. J., Udry, S., et al., The BEBOP radial-velocity survey for circumbinary planets. I. Eight years of CORALIE observations of 47 single-line eclipsing binaries and abundance constraints on the masses of circumbinary planets. 2019, *Astronomy and Astrophysics*, **624**, A68, DOI:10.1051/0004-6361/201833669

Maxted, P. F. L., Miller, N. J., Hoyer, S., et al., Fundamental effective temperature measurements for eclipsing binary stars - III. SPIRou near-infrared spectroscopy and CHEOPS photometry of the benchmark G0V star EBLM J0113+31. 2022, *Monthly Notices of the RAS*, **513**, 6042, DOI:10.1093/mnras/stac1270

Maxted, P. F. L., Triaud, A. H. M. J., & Martin, D. V., The EBLM Project—From False Positives to Benchmark Stars and Circumbinary Exoplanets. 2023, *Universe*, **9**, 498, DOI:10.3390/universe9120498

Pepe, F., Cristiani, S., Rebolo, R., et al., ESPRESSO at VLT. On-sky performance and first results. 2021, *Astronomy and Astrophysics*, **645**, A96, DOI:10.1051/0004-6361/202038306

Pollacco, D. L., Skillen, I., Collier Cameron, A., et al., The WASP Project and the SuperWASP Cameras. 2006, *Publications of the ASP*, **118**, 1407, DOI:10.1086/508556

Roy, O. & Vetterli, M., The effective rank: A measure of effective dimensionality. 2007, in *2007 15th European Signal Processing Conference*, 606–610

Sebastian, D., Swayne, M. I., Maxted, P. F. L., et al., The EBLM project - IX. Five fully convective M-dwarfs, precisely measured with CHEOPS and TESS light curves. 2023, *Monthly Notices of the RAS*, **519**, 3546, DOI:10.1093/mnras/stac2565

Sebastian, D., Triaud, A. H. M. J., & Brogi, M., Saltire: a model to measure dynamical masses for high-contrast binaries and exoplanets with high-resolution spectroscopy. 2024a, *Monthly Notices of the RAS*, **527**, 10921, DOI:10.1093/mnras/stad3765

Sebastian, D., Triaud, A. H. M. J., Brogi, M., et al., The EBLM project - XIII. The absolute dynamical masses of the circumbinary planet host TOI-1338/BEBOP-1, and applications to the study of exoplanet atmospheres. 2024b, *Monthly Notices of the RAS*, **530**, 2572, DOI:10.1093/mnras/stae459

Sebastian, D., Triaud, A. H. M. J., Maxted, P. F. L., & Brogi, M. 2025, in prep.

Smette, A., Sana, H., Noll, S., et al., Molecfit: A general tool for telluric absorption correction. I. Method and application to ESO instruments. 2015, *Astronomy and Astrophysics*, **576**, A77, DOI:10.1051/0004-6361/201423932

Snellen, I. A. G., de Kok, R. J., de Mooij, E. J. W., & Albrecht, S., The orbital motion, absolute mass and high-altitude winds of exoplanet HD209458b. 2010, *Nature*, **465**, 1049, DOI:10.1038/nature09111

Spada, F., Demarque, P., Kim, Y. C., & Sills, A., The Radius Discrepancy in Low-mass Stars: Single versus Binaries. 2013, *Astrophysical Journal*, **776**, 87, DOI:10.1088/0004-637X/776/2/87

Standing, M. R., Sairam, L., Martin, D. V., et al., Radial-velocity discovery of a second planet in the TOI-1338/BEBOP-1 circumbinary system. 2023, *Nature Astronomy*, **7**, 702, DOI:10.1038/s41550-023-01948-4

Swayne, M. I., Maxted, P. F. L., Triaud, A. H. M. J., et al., The EBLM project - VIII. First results for M-dwarf mass, radius, and effective temperature measurements using CHEOPS light curves. 2021, *Monthly Notices of the RAS*, **506**, 306, DOI:10.1093/mnras/stab1687

Swayne, M. I., Maxted, P. F. L., Triaud, A. H. M. J., et al., The EBLM Project- XI. Mass, radius, and effective temperature measurements for 23 M-dwarf companions to solar-type stars observed with CHEOPS. 2024, *Monthly Notices of the RAS*, **528**, 5703, DOI:10.1093/mnras/stad3866

Torres, G., Andersen, J., & Giménez, A., Accurate masses and radii of normal stars: modern results and applications. 2010, *Astronomy and Astrophysics Reviews*, **18**, 67, DOI:10.1007/s00159-009-0025-1

Triaud, A. H. M. J., Hebb, L., Anderson, D. R., et al., The EBLM project. I. Physical and orbital parameters, including spin-orbit angles, of two low-mass eclipsing binaries on opposite sides of the brown dwarf limit. 2013, *Astronomy and Astrophysics*, **549**, A18, DOI:10.1051/0004-6361/201219643

Triaud, A. H. M. J., Martin, D. V., Ségransan, D., et al., The EBLM Project. IV. Spectroscopic orbits of over 100 eclipsing M dwarfs masquerading as transiting hot

Jupiters. 2017, *Astronomy and Astrophysics*, **608**, A129, DOI:10.1051/0004-6361/201730993

Triaud, A. H. M. J., Standing, M. R., Heidari, N., et al., BEBOP III. Observations and an independent mass measurement of Kepler-16 (AB) b - the first circumbinary planet detected with radial velocities. 2022, *Monthly Notices of the RAS*, **511**, 3561, DOI:10.1093/mnras/stab3712

von Boetticher, A., Triaud, A. H. M. J., Queloz, D., et al., The EBLM Project. V. Physical properties of ten fully convective, very-low-mass stars. 2019, *Astronomy and Astrophysics*, **625**, A150, DOI:10.1051/0004-6361/201834539

Contrib. Astron. Obs. Skalnaté Pleso **55/3**, 421 – 424, (2025)
https://doi.org/10.31577/caosp.2025.55.3.421

The multiplicity properties of early-type stars from LAMOST DR8

Y. Guo[1], C. Liu[2], L. Wang[1], J. Wang[1], B. Zhang[2], K. Ji[1], Z. Han[1] and X. Chen[1]

[1] *Yunnan observatories, Chinese Academy of Sciences, P.O. Box 110, Kunming, 650011, China (E-mail: cxf@ynao.ac.cn)*

[2] *School of Astronomy and Space Science, University of Chinese Academy of Sciences, Beijing, 100049, China*

Received: May 1, 2020; Accepted: July 28, 2020

Abstract. Massive binary stars are key to understanding stellar formation and evolution. To explore the intrinsic binary fraction ($f_{\rm b}^{\rm in}$), mass ratio distribution ($f(q)$), and orbital period distribution ($f(P)$) of early-type stars (O/B/A-types), we analyze a homogeneous spectroscopic sample of 886 stars from LAMOST DR8, each with more than six observations. These stars are classified based on effective temperature ($T_{\rm eff}$), metallicity ([M/H]), and projected rotational velocity ($v \sin i$). Monte Carlo simulations were applied to correct for observational biases. Results show that the intrinsic binary fraction increases with $T_{\rm eff}$ and metallicity, while remaining relatively constant across $v \sin i$. For stars in groups of B8-A, B4-B7, O-B3, the binary fractions are $f_{\rm b}^{\rm in} = 48\% \pm 10\%$, $60\% \pm 10\%$, and $76\% \pm 10\%$, respectively.

Key words: Statistical-catalogs-surveys-early-type-binaries-rotation

1. Introduction

Most stars are part of binary systems, with early-type stars showing particularly high binary fractions (Heintz, 1969; Abt & Levy, 1976; Duquennoy & Mayor, 1991). Statistical analyses of binary systems, including the binary fraction, orbital period, and mass ratio distributions, are crucial for understanding stellar formation and compact object evolution (Sana et al., 2012; Liu, 2019; Han et al., 2020). These properties help explain the formation of double black holes, neutron stars, and other gravitational wave sources (Chen et al., 2018; Han et al., 2020; Langer et al., 2020). Among the statistical properties, the binary fraction, f_b, is one of the most critical parameters and has been widely explored over the past few decades. However, previous studies on massive binaries have reported binary fractions ranging from 51% to 69% for O-type stars, and there are ongoing debates over whether metallicity correlates with the binary fraction (Raghavan et al., 2010; Kobulnicky et al., 2014; Guo et al., 2022; Liu, 2019).

Many of these studies have been based on small or heterogeneous samples. Large spectroscopic surveys like LAMOST offer a chance to improve this anal-

ysis with more homogeneous data. Recent LAMOST studies have reported binary fractions of early-type stars, though some aspects, such as the impact of metallicity, remain unexplored due to limited observations. With the release of LAMOST DR8, we aim to improve upon previous work by analyzing a larger sample of 886 early-type stars with higher observational cadence, focusing on the binary fraction's dependency on metallicity and other stellar parameters.

2. Data

In this study, we adopt the 9,382 early-type stars from Guo et al. (2022) to investigate their statistical properties, in which the atmospheric parameters from Guo et al. (2021) and the radial velocity from Zhang et al. (2021). We then selected 886 stars from the LAMOST MRS database with more than six observations to minimize uncertainties in binary fraction, mass ratio, and orbital period distributions. The sample is divided into groups based on effective temperature ($T_{\rm eff}$), metallicity ([M/H]), and projected rotational velocity ($v \sin i$). The stars were classified into three spectral type groups: B8-A, B4-B7, and O-B3. For metallicity ([M/H]), the stars were divided into three categories: [M/H] $<$ -0.55, -0.55 $\leq$ [M/H] $<$ -0.1, and [M/H] $\geq$ -0.1. Additionally, based on projected rotational velocity ($v \sin i$), we classified the stars into three groups: $v \sin i$ $<$ 35 km/s, 35 $\leq$ $v \sin i$ $<$ 70 km/s, and $v \sin i \geq$ 70 km/s.

3. Method

We adopt the Monte-Carlo (MC) simulation approach from Sana (2013) to estimate the intrinsic binary fraction ($f_{\rm b}^{\rm in}$) based on the observed binary fraction ($f_{\rm b}^{\rm obs}$). Two synthetic cumulative distribution functions (CDFs) are constructed for the radial velocity variation (ΔRV) and the minimum time interval between exposures (ΔMJD), assuming orbital configurations. The distributions for the orbital period (P) and mass ratio (q) are modeled using power laws, $f(P) \propto P^{\pi}$ and $f(q) \propto q^{\gamma}$. Using the assumptions of two-body Keplerian systems, we simulate radial velocity (RV) variations and construct cumulative distribution functions (CDFs) for both ΔRV and ΔMJD. The simulated CDFs are compared to the observed data using the Kolmogorov-Smirnov (KS) test, and the simulated binary fraction ($f_{\rm b}^{\rm sim}$) is compared to the observed binary fraction ($f_{\rm b}^{\rm obs}$) using a Binomial distribution. The final results are obtained by optimizing a global merit function (GMF), which combines KS probabilities for ΔRV and ΔMJD distributions, as well as the Binomial probability.

4. Results

We found that $f_{\rm b}^{\rm in}$ increases with increasing $T_{\rm eff}$. For stars in groups of B8-A, B4-B7, O-B3, the binary fractions are $f_{\rm b}^{\rm in} = 48\% \pm 10\%$, $60\% \pm 10\%$, and $76\% \pm 10\%$,

respectively. The binary fraction is positively correlated with metallicity for spectra in the sample, with derived values of $f_{\rm b}^{\rm in} = 44\% \pm 10\%$, $60\% \pm 10\%$ and $72\% \pm 10\%$ for spectra with metallicity spanning from [M/H]<-0.55, -0.55 $\leq$ [M/H]¡-0.1, to [M/H] $\geq$ -0.1. Over all the $v \sin i$ values we have considered, the $f_{\rm b}^{\rm in}$ have constant values as $\sim$50%. It seems that the binary population is relatively evenly distributed over a wide range of $v \sin i$ values, while the whole sample shows that most of the stars are concentrated in low values of $v \sin i$ (probably from strong wind and magnetic braking of single massive stars), and in high values of $v \sin i$ (likely from the merge of binary stars) in cases. Stellar evolution and binary interaction may be partly responsible for this. In case of observations with more than six observations, we have derived $\pi = -0.9 \pm 0.35$, -0.9 ± 0.35, and -0.9 ± 0.35, and $\gamma = -1.9 \pm 0.9$, -1.1 ± 0.9 and -2 ± 0.9 for O-B3, B4-B7, B8-A type stars, respectively. There are no correlations being found between $\pi(\gamma)$ and $T_{\rm eff}$, and neither for $\pi(\gamma)$ and [M/H]. The uncertainties of the distribution decrease towards a larger sample size with higher observational cadence.

Acknowledgements. The authors are extremely thankful to everyone who provided their help. This work is supported by the Natural Science Foundation of China (Nos. 2021YFA1600403/1, 12125303, 11733008, 12090040/3).

References

Abt, H. A. & Levy, S. G., Multiplicity among solar-type stars. 1976, *Astrophysical Journal, Supplement*, **30**, 273, DOI:10.1086/190363

Chen, X., Li, Y., & Han, Z., The formation of double compact objects as gravitational wave sources. 2018, *Scientia Sinica Physica, Mechanica & Astronomica*, **48**, 079803, DOI:10.1360/SSPMA2018-00097

Duquennoy, A. & Mayor, M., Multiplicity among solar-type stars in the solar neighbourhood. II - Distribution of the orbital elements in an unbiased sample. 1991, *Astronomy and Astrophysics*, **500**, 337

Guo, Y., Li, J., Xiong, J., et al., The Binarity of Early-type Stars from LAMOST medium-resolution Spectroscopic Survey. 2022, *Research in Astronomy and Astrophysics*, **22**, 025009, DOI:10.1088/1674-4527/ac3e5a

Guo, Y., Zhang, B., Liu, C., et al., The Early-type Stars from the LAMOST Survey: Atmospheric Parameters. 2021, *Astrophysical Journal, Supplement*, **257**, 54, DOI:10.3847/1538-4365/ac2ded

Han, Z.-W., Ge, H.-W., Chen, X.-F., & Chen, H.-L., Binary Population Synthesis. 2020, *Research in Astronomy and Astrophysics*, **20**, 161, DOI:10.1088/1674-4527/20/10/161

Heintz, W. D., Parallaxes and masses of the visual binary stars ADS 3475, 8862, 9617, and 16326. 1969, *Astronomical Journal*, **74**, 768, DOI:10.1086/110855

Kobulnicky, H. A., Kiminki, D. C., Lundquist, M. J., et al., Toward Complete Statistics of Massive Binary Stars: Penultimate Results from the Cygnus OB2 Radial Velocity Survey. 2014, *Astrophysical Journal, Supplement*, **213**, 34, DOI:10.1088/0067-0049/213/2/34

Langer, N., Schürmann, C., Stoll, K., et al., Properties of OB star-black hole systems derived from detailed binary evolution models. 2020, *Astronomy and Astrophysics*, **638**, A39, DOI:10.1051/0004-6361/201937375

Liu, C., Smoking gun of the dynamical processing of solar-type field binary stars. 2019, *Monthly Notices of the RAS*, **490**, 550, DOI:10.1093/mnras/stz2274

Raghavan, D., McAlister, H. A., Henry, T. J., et al., A Survey of Stellar Families: Multiplicity of Solar-type Stars. 2010, *Astrophysical Journal, Supplement*, **190**, 1, DOI:10.1088/0067-0049/190/1/1

Sana, H., de Mink, S. E., de Koter, A., et al., Binary Interaction Dominates the Evolution of Massive Stars. 2012, *Science*, **337**, 444, DOI:10.1126/science.1223344

Zhang, B., Li, J., Yang, F., et al., Self-consistent Stellar Radial Velocities from LAMOST Medium-resolution Survey DR7. 2021, *Astrophysical Journal, Supplement*, **256**, 14, DOI:10.3847/1538-4365/ac0834

Contrib. Astron. Obs. Skalnaté Pleso **55/3**, 425 – 430, (2025)
https://doi.org/10.31577/caosp.2025.55.3.425

Physical stellar properties of red giant ellipsoidal binaries in Gaia DR3

C. Navarrete[1], A. Recio-Blanco[1], P. de Laverny[1] and A. Escorza[2,3]

[1] *Université Côte d'Azur, Observatoire de la Côte d'Azur, CNRS, Laboratoire Lagrange, Bd de l'Observatoire, CS 34229, 06304, Nice Cedex 4, France (E-mail: camila.navarrete@oca.eu)*

[2] *Instituto de Astrofísica de Canarias, C. Vía Láctea, s/n, 38205 La Laguna, Santa Cruz de Tenerife, Spain*

[3] *Universidad de La Laguna, Dpto. Astrofísica, Av. Astrofísico Francisco Sánchez, 38206 La Laguna, Santa Cruz de Tenerife, Spain.*

Received: November 1, 2024; Accepted: February 5, 2025

Abstract. Ellipsoidal red giant binaries are a particular class of binary stars where the primary gets tidally deformed by the interaction with the companion. They are the prelude stage before binary interactions, and the study of their population properties is therefore of great relevance to understanding the effects of tidal circularization and the binary evolution of these systems. Combining various *Gaia* data sets, including astrometry, photometry and spectroscopy, as well as variability information, we derived the physical parameters of more than 300 ellipsoidal red giant binary candidates. An estimate for the mass of the secondary star was also recovered. This unprecedentedly large sample allows us to compare its physical properties (mass, luminosity, radius), orbital parameters (mass-ration, filling factor, eccentricity) and chemical information (metallicity, [α/Fe] abundances), to better understand this stage in binary evolution.

Key words: binaries: general – binaries: spectroscopic – binaries: close

1. Introduction

The *Gaia* mission has produced a revolution in the fields of Galactic and stellar astronomy, providing an unprecedentedly large sample of stars having precise astrometry, photometry and spectroscopy. In particular, the third data release (DR3; Gaia Collaboration et al., 2023c) presented for the first time the analysis of binary stars in the non-single star catalogue (see Gaia Collaboration et al., 2023a). More than 800 000 binary systems with orbital solutions are included, among which more than 180 000 are spectroscopic binaries. This is the largest sample of single-line spectroscopic binaries collected so far (see the review of El-Badry, 2024, for a detailed comparison of the *Gaia* binary star sample and

previous compilations in the literature), offering a unique dataset to study binary stars in a holistic approach, having homogeneous and high-quality *Gaia* data available for all the sources.

Ellipsoidal binaries are systems in which the primary star gets tidally deformed, adopting an ellipsoidal shape. This geometric deformation produces that, during one orbital period, the photometric light curve shows two maxima and two minima. Hence, the photometric period results in being half of the orbital period. The study of the population of ellipsoidal variables can therefore provide useful constraints to (i) the expected tidal effects in binary systems (Nie et al., 2017); and (ii) population studies of asymmetric planetary nebulae, as they are considered their immediate precursors (see e.g., Jones & Boffin, 2017). Having *Gaia* data, both photometric and spectroscopic, provides us with the opportunity to characterize this population in terms of its physical parameters (luminosities, mass and radii) and, thereby, better understand the effects of tidal circularization and binary evolution.

2. Ellipsoidal red giant binaries in Gaia FPR

The Gaia Focused Product Release (FPR; Gaia Collaboration et al., 2023b) produced an additional catalogue of variability information, both in terms of photometric G, $G_{\rm BP}$, $G_{\rm RP}$ magnitudes and spectroscopic, radial velocity (RV) time series, for thousands of long-period, $>$ 40 days, variable stars. Among this sample, pulsating variable stars such as Mira and semi-regular variables are included, as well as long-secondary period variables and a subpopulation of non-pulsating sources, mainly composed of ellipsoidal variables. Based on their variability amplitudes, non-pulsating variables in this sample can be isolated as

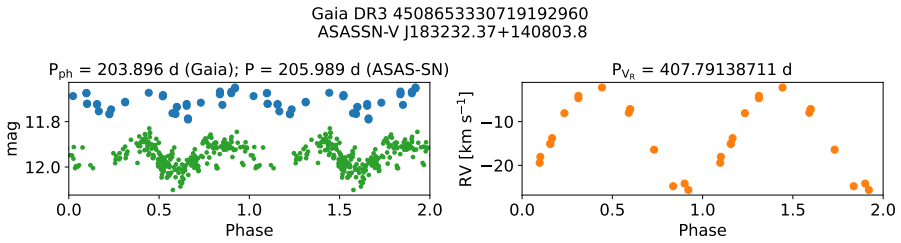


Figure 1. Photometric light curve (left panel) and RV time series (right panel) for one of the ellipsoidal candidates in our sample. The V-band light curve, in green, comes from the ASAS-SN, while the G-band (blue points, left panel) and RV (orange points, right panel) time series are from Gaia. The periods derived in each survey are shown in the title of each panel.

$$A_G < 0.3\,\mathrm{mag} \quad \text{and} \quad \frac{A_G}{\mathrm{mag}} < 2.5 \cdot 10^{-3} \cdot \left(\frac{A_{V_R}}{\mathrm{km\,s^{-1}}} \right)^2 . \tag{1}$$

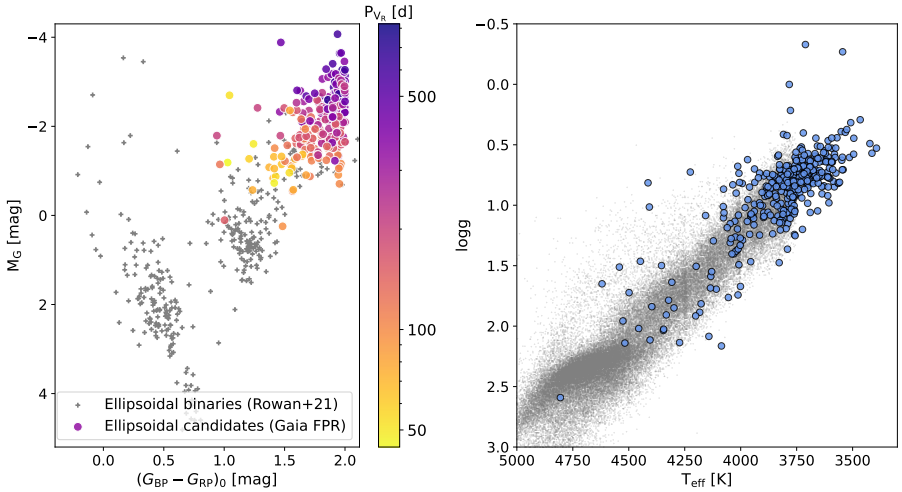


Figure 2. Left panel: Color-Magnitude diagram for the ellipsoidal candidates and those detected based on the photometric ASAS-SN by Rowan et al. (2021) (shown as grey crosses). The ellipsoidal binary candidates in *Gaia* are colored based on the orbital period, P_{V_R}. Right panel: Kiel diagram for the spectroscopic effective temperature and surface gravity of the ellipsoidal red giant binary sample. The grey points in the background are a comparison sample of stars having accurate atmospheric parameters from *Gaia* DR3.

This selection boundary separates pulsating, high-amplitude variables from those having relatively small G-amplitudes ($A_G \lesssim 0.2$ mag) and large RV variations ($A_{V_R} \gtrsim 5$ km s^{-1}, see Section 3 in Gaia Collaboration et al. 2023b). Figure 1 shows the G-band light curves and the RV time series of one of the ellipsoidal variables in the *Gaia* FPR. The V-band light curve from the All-Sky Automated Survey for Supernovae (ASAS-SN; Jayasinghe et al., 2018), where the source is classified as a semi-regular variable, is included as green dots. The photometric periods based on *Gaia* and ASAS-SN are compatible and correspond to half the RV (orbital) period. This example shows the advantage of *Gaia* data: despite having a smaller number of epochs, the cadence is enough to recover the variability while the epoch spectroscopy is complementary to the photometry to identify this kind of binaries.

The initial sample of ellipsoidal binaries is therefore composed of variable sources satisfying the condition in Eq. 1, as well as having compatible periods for the G, G_{BP} and G_{RP} photometric time series. Moreover, we restricted the sample to those sources having low parallax uncertainty ($\epsilon_\varpi/\varpi < 0.15$). From this sample, those having available atmospheric parameters (T_{eff}, log g, [M/H]) from Gaia spectra (either from the Gaia Radial Velocity Spectrometer, RVS, or the BP/RP spectra, see Recio-Blanco et al., 2023; Andrae et al., 2023, respectively). We recovered more than 400 systems having atmospheric parameters, as well

as photo-geometric distance estimates based on Gaia early DR3 parallaxes and photometry derived by Bailer-Jones et al. (2021). This unprecedented dataset, in terms both of the number of sources as well as the homogenous photometric and variability observations, allows us to derive luminosities, radii and masses of this population. Figure 2 shows the Color-Magnitude diagram (left panel) and Kiel diagram (right panel) for the ellipsoidal variable sample. For reference, the CMD includes the sample of ellipsoidal variables from the ASAS-SN in Rowan et al. (2021), while the Kiel diagram includes a sample of *Gaia* sources having precise atmospheric parameters from the *GSP-Spec* module (see Recio-Blanco et al., 2023). The extinction of the sources was obtained based on the observed (G_{BP} - G_{RP}) color and the expected intrinsic color for the effective temperature, using the color-T_{eff} relations for *Gaia* DR3 bandpasses[1]. Our sample of ellipsoidal binaries is located at the same position as the giant ellipsoidal variables from Rowan et al. (2021), as expected given the minimum orbital period considered in *Gaia* FPR being 35 days. In the Kiel diagram, our sample is consistent with cool K and M giants.

3. Physical parameters

Combining the *Gaia* measurements for the distance, spectroscopic T_{eff} and the apparent mean G magnitude with the derived extinction, the bolometric magnitude and luminosity of the primary star were derived. The radii and masses were derived by combining the luminosity and the spectroscopic atmospheric parameters (T_{eff}, $\log g$, see de Laverny et al. 2025, in preparation). The masses and radii obtained through these measurements were compared to the values obtained using asteroseismology observations for single stars in *Gaia* (Recio-Blanco et al., 2024), and red giant binaries from Beck et al. (2024). We found an excellent agreement in the measured radii, while the masses have a good agreement with a median bias difference in the spectroscopic estimates of 0.1 $M_\odot$, with a dispersion of 0.8 $M_\odot$.

Figure 3 shows the spectroscopic mass for the primary star derived in this work versus the minimum mass for the secondary component, obtained by solving the mass function of the system at a maximum inclination (i.e, $\sin i = 1$). The equivalent measurements for red giant ellipsoidal binaries in the Large Magellanic Cloud (LMC) from Nie et al. (2017) are shown as pink points. The distribution of masses in our sample is consistent with low and intermediate-mass primary stars, from $\simeq 0.45$ up to 5 $M_\odot$, slightly less massive than the distribution of ellipsoidals in the LMC. The masses of the secondaries are predominantly below 1.0 $M_\odot$, indicating low-mass companions (a main sequence or a compact object).

[1] https://github.com/casaluca/colte

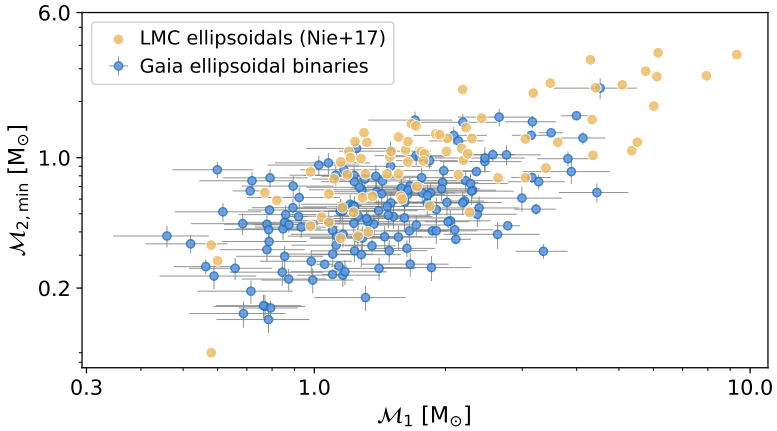


Figure 3. Mass of the primary star, $\mathcal{M}_1$ and minimum mass for the secondary star, $\mathcal{M}_{2,\mathrm{min}}$ for our sample of Galactic ellipsoidal red giant binary candidates, and the primary and secondary masses of ellipsoidal red giant binaries in the LMC, derived based on the modeling of the photometric and RV time series in Nie et al. (2017).

4. Conclusions

Previous measurements for this kind of stars were done based on the modelling of the photometric light curve, particularly for ellipsoidal binaries in which the primary star is a main-sequence (see e.g., Rowan et al., 2021), or using both photometry and spectroscopy for a limited sample, such as the 81 ellipsoidal red giant binaries in the LMC analyzed in Nie et al. (2017). Our sample is composed of more than 300 ellipsoidal red giant binaries, which allows us to analyse the physical and orbital (eccentricities, mass of the companion, tidal circularization) properties of this population for the first time in the Milky Way. The detailed analysis of this population, as well as a subsample of rotational variables, is published Navarrete et al. (2025).

Acknowledgements. This work has made use of data from the European Space Agency (ESA) mission Gaia (https://www.cosmos.esa.int/gaia), processed by the Gaia Data Processing and Analysis Consortium (DPAC). Funding for the DPAC has been provided by national institutions, in particular the institutions participating in the Gaia Multilateral Agreement.

References

Andrae, R., Rix, H.-W., & Chandra, V., Robust Data-driven Metallicities for 175 Million Stars from Gaia XP Spectra. 2023, *Astrophysical Journal, Supplement*, **267**, 8, DOI:10.3847/1538-4365/acd53e

Bailer-Jones, C. A. L., Rybizki, J., Fouesneau, M., Demleitner, M., & Andrae, R., Estimating Distances from Parallaxes. V. Geometric and Photogeometric Distances to 1.47 Billion Stars in Gaia Early Data Release 3. 2021, *Astronomical Journal*, **161**, 147, DOI:10.3847/1538-3881/abd806

Beck, P. G., Grossmann, D. H., Steinwender, L., et al., Constraining stellar and orbital co-evolution through ensemble seismology of solar-like oscillators in binary systems. A census of oscillating red giants and dwarf stars in Gaia DR3 binaries. 2024, *Astronomy and Astrophysics*, **682**, A7, DOI:10.1051/0004-6361/202346810

El-Badry, K., Gaia's binary star renaissance. 2024, *arXiv e-prints*, arXiv:2403.12146, DOI:10.48550/arXiv.2403.12146

Gaia Collaboration, Arenou, F., Babusiaux, C., et al., Gaia Data Release 3. Stellar multiplicity, a teaser for the hidden treasure. 2023a, *Astronomy and Astrophysics*, **674**, A34, DOI:10.1051/0004-6361/202243782

Gaia Collaboration, Gaia Collaboration, Trabucchi, M., et al., Gaia Focused Product Release: Radial velocity time series of long-period variables. 2023b, *arXiv e-prints*, arXiv:2310.06051, DOI:10.48550/arXiv.2310.06051

Gaia Collaboration, Vallenari, A., Brown, A. G. A., et al., Gaia Data Release 3. Summary of the content and survey properties. 2023c, *Astronomy and Astrophysics*, **674**, A1, DOI:10.1051/0004-6361/202243940

Jayasinghe, T., Kochanek, C. S., Stanek, K. Z., et al., The ASAS-SN catalogue of variable stars I: The Serendipitous Survey. 2018, *Monthly Notices of the RAS*, **477**, 3145, DOI:10.1093/mnras/sty838

Jones, D. & Boffin, H. M. J., Binary stars as the key to understanding planetary nebulae. 2017, *Nature Astronomy*, **1**, 0117, DOI:10.1038/s41550-017-0117

Navarrete, C., Recio-Blanco, A., de Laverny, P., & Escorza, A., A comprehensive Gaia view of ellipsoidal and rotational red giant binaries. 2025, *Astronomy and Astrophysics*, **696**, A82, DOI:10.1051/0004-6361/202453394

Nie, J. D., Wood, P. R., & Nicholls, C. P., The Orbital Nature of 81 Ellipsoidal Red Giant Binaries in the Large Magellanic Cloud. 2017, *Astrophysical Journal*, **835**, 209, DOI:10.3847/1538-4357/835/2/209

Recio-Blanco, A., de Laverny, P., Palicio, P. A., et al., Double red giant branch and red clump features of Galactic disc stellar populations with Gaia GSP-Spec. 2024, *Astronomy and Astrophysics*, **692**, A235, DOI:10.1051/0004-6361/202449443

Recio-Blanco, A., de Laverny, P., Palicio, P. A., et al., Gaia Data Release 3. Analysis of RVS spectra using the General Stellar Parametriser from spectroscopy. 2023, *Astronomy and Astrophysics*, **674**, A29, DOI:10.1051/0004-6361/202243750

Rowan, D. M., Stanek, K. Z., Jayasinghe, T., et al., High tide: a systematic search for ellipsoidal variables in ASAS-SN. 2021, *Monthly Notices of the RAS*, **507**, 104, DOI:10.1093/mnras/stab2126

Contrib. Astron. Obs. Skalnaté Pleso **55/3**, 431 – 437, (2025)
https://doi.org/10.31577/caosp.2025.55.3.431

Non-evolutionary effects on period change in Magellanic Cepheids

R.S. Rathour[1], R. Smolec[1], G. Hajdu[1], P. Karczmarek[2], V. Hocdé[1], O. Ziółkowska[1], I. Soszyński[3] and A. Udalski[3]

[1] *Nicolaus Copernicus Astronomical Centre, Polish Academy of Sciences, Bartycka 18, 00-716 Warszawa, Poland (E-mail: rajeevsr@camk.edu.pl)*

[2] *Departamento de Astronomía, Universidad de Concepción, Casilla 160-C, Concepción, Chile*

[3] *Astronomical Observatory, University of Warsaw, Aleje Ujazdowskie 4, Warsaw, 00-478, Poland*

Received: November 15, 2024; Accepted: January 8, 2025

Abstract. Classical Cepheids are a cornerstone class of pulsators, fundamental to testing stellar evolution and pulsation theories. Their secular period changes, characterized through $O-C$ (Observed minus Calculated) diagrams, offer valuable insights into their evolution. While evolutionary period changes are well understood from both observational and theoretical perspectives, shorter timescale period changes (on the order of ($\sim 10^2$-10^4 days) - known as non-evolutionary period changes are yet to be systematically explored.

In this work, we present a detailed and comprehensive search for non-evolutionary period changes using $O-C$ analysis of Magellanic Cloud (MC) Cepheids, based on 20+ years of OGLE photometry data. Our sample includes both the Large Magellanic Cloud (LMC) and the Small Magellanic Cloud (SMC) Cepheids, focusing on single radial mode Cepheids (both fundamental (FU) and first overtone (FO) modes). The results are grouped into two phenomena: (a) Cepheids in binary systems (b) Non-linear period changes.
Key words: stars – variable – Cepheids

1. Introduction

Classical Cepheids (hereafter Cepheids) are intermediate- to high-mass ($3-13\,M_\odot$) supergiant stars undergoing core-helium burning. These variable stars are known for their large-amplitude radial pulsations and are found within a narrow region in the Hertzsprung-Russell diagram known as the classical instability strip (IS). Cepheids hold a pivotal role as standard candles due to their well-defined period-luminosity (P-L) relation, also referred to as the Leavitt law (Leavitt & Pickering, 1912). As these stars evolve across the IS, Cepheids experience changes in their pulsation periods as a consequence of change in their internal structure. The $O-C$ diagram technique provides a valuable perspective

on both the evolutionary and non-evolutionary aspects affecting these pulsating stars.

Extensive investigations have been conducted on evolutionary period changes in Cepheids (e.g., Pietrukowicz, 2001, 2002; Turner et al., 2006; Karczmarek et al., 2011; Rodríguez-Segovia et al., 2022). In contrast, shorter-timescale period changes ($\sim 10^2$-10^4 days) arising from non-evolutionary origins remain largely unexplored (e.g., Poleski, 2008). Notably, the Cepheid V1154 Cygni is studied in detail for cycle-to-cycle period fluctuations changes using *Kepler* data, revealing light curve modulation and granulation signatures (Derekas et al., 2012, 2017). Among these non-secular period changes, a fraction of them which are periodic in nature are due to light-travel time effect (LTTE; Irwin, 1952, 1959), suggesting that these Cepheids may belong to binary systems. In the Milky Way (MW), a high binary fraction among Cepheids (up to 80%) is expected (Szabados, 2003a; Evans, 1992; Evans et al., 2013), and out of ∼15,000 known MW Cepheids (Pietrukowicz et al., 2021), only ∼200-300 have been spectroscopically confirmed as binaries (see Szabados, 2003b; Anderson et al., 2024). In the Magellanic Clouds, the numbers are even lower, with only ∼14 confirmed in the SMC and ∼27 in the LMC (Szabados, 1983; Pilecki et al., 2021, 2024). This gap highlights the need for a comprehensive study of period changes in MC Cepheids.

We use of OGLE photometry data spanning over 20 years, specifically the I-band MC data from the OGLE-III and OGLE-IV phases (Soszyński et al., 2019, and OGLE references therein) of the survey. To construct $O-C$ diagrams, we employ the modified Hertzsprung method (e.g., Hajdu et al., 2021). These $O-C$ diagrams are then categorized by shape into three primary groups: linear, parabolic, and others. The third group, consisting of non-linear period change candidates, are further divided into periodic and aperiodic (irregular) $O-C$ groups.

2. Periodic $O-C$: binary candidates

The analysis of $O-C$ diagrams followed by filtering candidates with periodic signatures were subjected to our Bayesian binary fitting routine. In total this resulted in 197 Cepheids candidates (52 in LMC and 145 in SMC) which show non-evolutionary period changes associated with binarity. In Fig. 1 some example $O-C$ diagrams are shown. For all final candidates, we determined a total of five orbital parameters: orbital period ($P_{\rm orb}$), time of periastron passage (T_0), eccentricity (e), argument of the periastron (ω), projected semi-major axis ($a \sin i$). Using these, we also calculate three more derived parameters, period change rate (β), radial velocity semi-amplitude (K) and mass function ($f(m)$). The distribution of important binary parameters are presented in Fig. 2.

Cepheids that are systematically brighter than the Period-Luminosity relation were investigated by Pilecki et al. (2021) to search for binarity. Their work

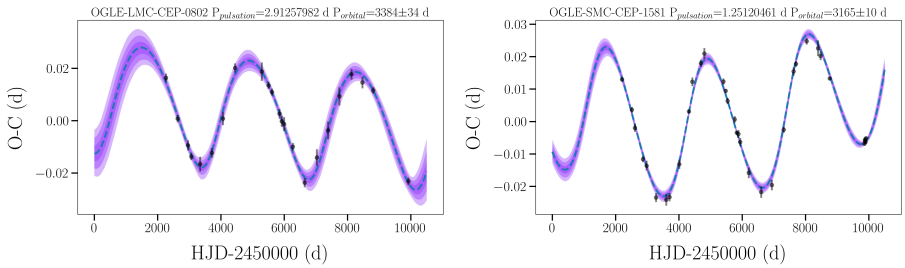


Figure 1. Example $O - C$ diagram of FU mode candidates in LMC (*left*) and SMC (*right*). The dashed blue line depicts the median MCMC binary fit solution along with shaded regions showing uncertainty the fit. The header shows its OGLE-ID, pulsation period (in days) and orbital period (in days)

hypothesizes that such Cepheids are brighter because of the additional light contribution from the companion likely to be in a giant phase. We searched for such '*overbright*' Cepheids in our sample and obtained four such candidates (two in each Magellanic Cloud). The LMC candidates OGLE-LMC-CEP-0837 and OGLE-LMC-CEP-0889 were previously identified by Pilecki et al. (2021) as SB2-type systems. Whereas the SMC candidates OGLE-SMC-CEP-3061 and OGLE-SMC-CEP-4365 are new detections and are yet to be confirmed spectroscopically. For details of the work refer to Rathour et al. (2024).

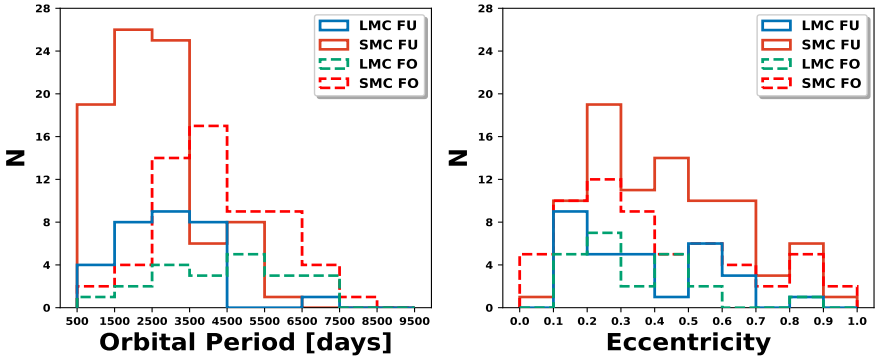


Figure 2. Distribution of orbital periods (*left*) and eccentricities (*right*) for binary Cepheid candidates.

3. Irregular $O-C$: non-linear period change candidates

In a sample of 1,585 Cepheids, we identified non-linear period changes exhibiting varied behaviors, ranging from quasi-periodic to abrupt and complex $O-C$ patterns, as illustrated by examples in Fig. 3. The origin of these irregular period changes remains unknown, and no definitive mechanism has been proposed to explain them. To characterize these candidates, we employ several techniques, including the Eddington–Plakidis test (Eddington & Plakidis, 1929), time-frequency analysis, instantaneous period method, and the Stetson L index (Stetson, 1996).

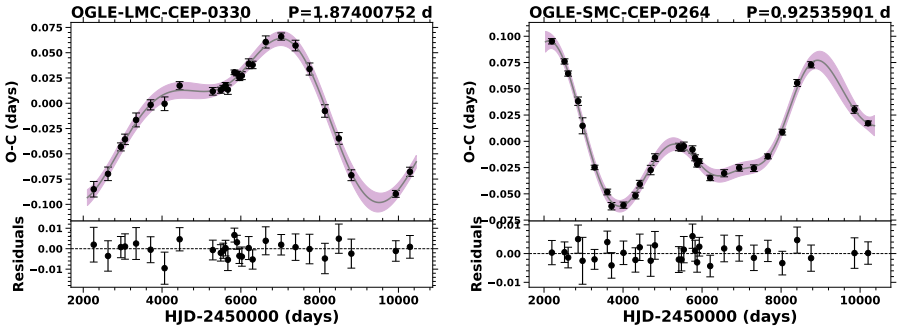


Figure 3. Example $O-C$ diagrams of FO mode irregular period change candidates in LMC (*left*) and the SMC (*right*) candidates. The header shows the OGLE-ID and pulsation period (in days).

The distribution of these irregular period change candidates as a function of pulsation period is shown in Fig. 4. Detailed incidence rates including characterization of their amplitudes and timescales, will be presented in our upcoming work (Rathour et al. *in prep.*).

4. Conclusions

Our comprehensive search for non-evolutionary period changes using $O-C$ analysis of Cepheids from OGLE photometry has resulted in a compilation of two classes of candidates. The first category contains 197 candidates showing light travel time effect signature meaning they are Cepheid candidates likely of binarity nature: (LMC: 30 (FU) and 22 (FO); SMC: 85 (FU) and 60 (FO)). Theses candidates indicate a detection fraction of binary Cepheid candidates: LMC: 1.7 % (FU); 1.8 % (FO); SMC: 3.3 % (FU); SMC 3.7 % (FO). The second class consists of a sample of 1585 Cepheids candidates exhibiting irregularities in their $O-C$ diagrams corresponding to non-evolutionary period changes of

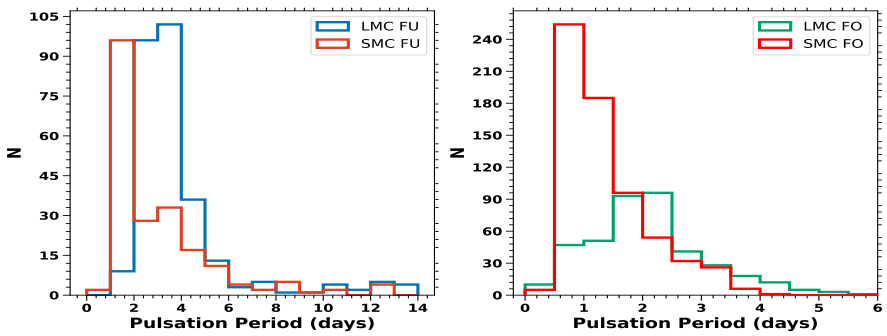


Figure 4. Pulsation period distribution of irregular period change candidates.

unknown origin. The inventory contains 695 LMC Cepheids (FU: 290 and FO: 405) and 890 SMC Cepheids (FU: 231 and FO: 659). With FO mode Cepheids exhibiting irregular period changes in systematically larger fraction of the sample than FU mode ones, we conclude that FO mode is more susceptible to period change, which in agreement with previous findings by Poleski (2008).

Acknowledgements. RSR, RS, and OZ are supported by the National Science Center, Poland, Sonata BIS project 2018/30/E/ST9/00598. GH, VH and PK acknowledges grant support from European Research Council (ERC) under the European Union's Horizon 2020 research and innovation program (grant agreement No. 695099). IS and AU are funded by the National Science Centre, Poland, grant no. 2022/45/B/ST9/00243.

References

Anderson, R. I., Viviani, G., Shetye, S. S., et al., VELOcities of CEpheids (VELOCE). I. High-precision radial velocities of Cepheids. 2024, *Astronomy and Astrophysics*, **686**, A177, DOI:10.1051/0004-6361/202348400

Derekas, A., Plachy, E., Molnár, L., et al., The Kepler Cepheid V1154 Cyg revisited: light curve modulation and detection of granulation. 2017, *Monthly Notices of the RAS*, **464**, 1553, DOI:10.1093/mnras/stw2399

Derekas, A., Szabó, G. M., Berdnikov, L., et al., Period and light-curve fluctuations of the Kepler Cepheid V1154 Cygni. 2012, *Monthly Notices of the RAS*, **425**, 1312, DOI:10.1111/j.1365-2966.2012.21538.x

Eddington, A. S. & Plakidis, S., Irregularities of period of long-period variable stars. 1929, *Monthly Notices of the RAS*, **90**, 65, DOI:10.1093/mnras/90.1.65

Evans, N. E., Bond, H. E., Schaefer, G. H., et al., Binary Cepheids: Separations and Mass Ratios in 5 $M_\odot$ Binaries. 2013, *Astronomical Journal*, **146**, 93, DOI:10.1088/0004-6256/146/4/93

Evans, N. R., A Magnitude-limited Survey of Cepheid Companions in the Ultraviolet. 1992, *Astrophysical Journal*, **384**, 220, DOI:10.1086/170865

Hajdu, G., Pietrzyński, G., Jurcsik, J., et al., Studies of RR Lyrae Variables in Binary Systems. I. Evidence of a Trimodal Companion Mass Distribution. 2021, *Astrophysical Journal*, **915**, 50, DOI:10.3847/1538-4357/abff4b

Irwin, J. B., The Determination of a Light-Time Orbit. 1952, *Astrophysical Journal*, **116**, 211, DOI:10.1086/145604

Irwin, J. B., Standard light-time curves. 1959, *Astronomical Journal*, **64**, 149, DOI:10.1086/107913

Karczmarek, P., Dziembowski, W. A., Lenz, P., Pietrukowicz, P., & Pojmański, G., Large Magellanic Cloud Cepheids in the ASAS Data. 2011, *Acta Astronomica*, **61**, 303

Leavitt, H. S. & Pickering, E. C., Periods of 25 Variable Stars in the Small Magellanic Cloud. 1912, *Harvard College Observatory Circular*, **173**, 1

Pietrukowicz, P., Period Changes of the LMC Cepheids Determined from the Harvard, OGLE and ASAS Data. 2001, *Acta Astronomica*, **51**, 247

Pietrukowicz, P., Period Changes of the SMC Cepheids from the Harvard, OGLE and ASAS Data. 2002, *Acta Astronomica*, **52**, 177

Pietrukowicz, P., Soszyński, I., & Udalski, A., Classical Cepheids in the Milky Way. 2021, *Acta Astronomica*, **71**, 205, DOI:10.32023/0001-5237/71.3.2

Pilecki, B., Pietrzyński, G., Anderson, R. I., et al., Cepheids with Giant Companions. I. Revealing a Numerous Population of Double-lined Binary Cepheids. 2021, *Astrophysical Journal*, **910**, 118, DOI:10.3847/1538-4357/abe7e9

Pilecki, B., Thompson, I. B., Espinoza-Arancibia, F., et al., Cepheids with giant companions. II. Spectroscopic confirmation of nine new double-lined binary systems composed of two Cepheids. 2024, *Astronomy and Astrophysics*, **686**, A263, DOI:10.1051/0004-6361/202349138

Poleski, R., Period Changes of LMC Cepheids in the OGLE and MACHO Data. 2008, *Acta Astronomica*, **58**, 313

Rathour, R. S., Hajdu, G., Smolec, R., et al., Non-evolutionary effects on period change in Magellanic Cepheids. I. New binary systems revealed from light travel time effect. 2024, *Astronomy and Astrophysics*, **686**, A268, DOI:10.1051/0004-6361/202349117

Rodríguez-Segovia, N., Hajdu, G., Catelan, M., et al., Period-change rates in Large Magellanic Cloud Cepheids revisited. 2022, *Monthly Notices of the RAS*, **509**, 2885, DOI:10.1093/mnras/stab3246

Soszyński, I., Udalski, A., Szymański, M. K., et al., Final Release of the OGLE Collection of Cepheids and RR Lyrae Stars in the Magellanic System. The Outer Regions. 2019, *Acta Astronomica*, **69**, 87, DOI:10.32023/0001-5237/69.2.1

Stetson, P. B., On the Automatic Determination of Light-Curve Parameters for Cepheid Variables. 1996, *Publications of the ASP*, **108**, 851, DOI:10.1086/133808

Szabados, L., Period Changes of Cepheid Variables - Part One - Secular Period Changes. 1983, *Astrophysics and Space Science*, **96**, 185, DOI:10.1007/BF00661952

Szabados, L., Cepheids: observational properties, binarity and GAIA. 2003a, in Astronomical Society of the Pacific Conference Series, Vol. **298**, *GAIA Spectroscopy: Science and Technology*, ed. U. Munari, 237

Szabados, L., Database on Binaries among Galactic Classical Cepheids. 2003b, *Information Bulletin on Variable Stars*, **5394**, 1

Turner, D. G., Abdel-Sabour Abdel-Latif, M., & Berdnikov, L. N., Rate of Period Change as a Diagnostic of Cepheid Properties. 2006, *Publications of the ASP*, **118**, 410, DOI:10.1086/499501

Contrib. Astron. Obs. Skalnaté Pleso **55/3**, 438 – 443, (2025)
https://doi.org/10.31577/caosp.2025.55.3.438

Adding TESS to CRÉME

Light curves and masses of 300+ eclipsing binaries

K.G. Hełminiak[1], **A. Moharana**[1,2], **T.B. Pawar**[1] **and G. Pawar**[1]

[1] *Nicolaus Copernicus Astronomical Center, Polish Academy of Sciences, ul. Rabiańska 8, 87-100 Toruń, Poland (E-mail: xysiek@ncac.torun.pl)*

[2] *Astrophysics Group, Keele University, Staffordshire, ST5 5BG, UK*

Received: November 22, 2024; Accepted: January 10, 2025

Abstract. The Comprehensive Research with Echelles on the Most interesting Eclipsing binaries (CRÉME) projects was aimed to collect high-resolutions spectra of about 380 detached eclipsing binaries (DEBs), which mostly do not have literature RV data. From this vast observational material we were able to estimate masses of components of 325 double-lined system. Since the launch of the TESS mission we have been collecting 2-min cadence photometry for the CRÉME targets through successful GI proposals. As by Sector 85, we obtained data for >330 of them. We are thus now in the process of comprehensively analysing our targets. This paper presents the recent status of the CRÉME project and its space photometry counterpart, and describes several sub-projects within CRÉME that focus on specific classes of targets.

Key words: binaries: eclipsing – binaries: spectroscopic – stars: fundamental parameters

1. Introduction

Detached eclipsing binaries (DEBs), especially those that are also double-lined spectroscopic (SB2) pairs, are one of the most useful objects in astrophysics. Their importance can not be overestimated, as they are used, for example to: test models of stellar structure and evolution, derive observational calibrations, test stellar formation theories, provide high-precision distances, characterise extrasolar planet hosts, etc. Many crucial stellar parameters, like mass, radius, effective temperature, age, or metallicity, can be derived simultaneously and accurately only from DEBs. So far, fewer than 350 DEBs have the desired level of uncertainty in masses or radii (<2%), and a large fraction still does not have reliable information about the age and metallicity (Southworth, 2015). Furthermore, many interesting classes of stars, and many areas of the H-R diagram, are underrepresented among the best-measured stars. For this reason, a large observational survey, dedicated for searching and characterising interesting stars in DEBs, has been started.

2. The CRÉME status

2.1. Spectroscopy

The *Comprehensive Research with Échelles on the Most interesting Eclipsing binaries* (CRÉME) is an observational project of high-resolution spectroscopic observations, intended to derive precise radial velocity (RV) measurements and atmospheric parameters. The main goals of the project are:

1. Identification of new examples of rare, poorly studied, or otherwise interesting DEBs.
2. Precise characterisation of the studied systems i.e. determination of masses, radii, temperatures, distances, metallicities, and ages of stars.

Table 1. Statistics of telescope time granted for the CRÉME project.

Telesc./Spectr.	Time	Telesc./Spectr.	Time
OAO-188cm/HIDES	87.5 n	Subaru/HDS+IRCS	9 n
SMARTS 1.5m/CHIRON	753 h	ESO 3.6m/HARPS	10 n
Euler/CORALIE	40 n	Magellan-Clay/PSF	4 n
MPG-2.2m/FEROS	30 n	NOT/FIES	4 n
TNG/HARPS-N	16 n	OHP 1.9m/SOPHIE	3 n
SALT/HRS	116 h	VLT/UVES	3.5 h

Note: With additional data from AAT/UCLES, Radcliffe/GIRAFFE, Keck I/HIRES, TNG/SARG, Hamilton/HamSpec (all pre-2011), OUC-50cm/PUCHEROS; and archives: ESO, SOPHIE, ELODIE, KOA, APOGEE.

The CRÉME project was a successor of a previous search for low-mass stars (2005-2010), and a small-scale survey of F- and G-type DEBs (2008-2009) made with iodine cell spectrographs. The project goals were defined and the observations started in 2011. Initially, the target sample was made of DEBs from the southern hemisphere, identified by the All-Sky Automated Survey (ASAS; Pojmanski, 2002). In 2013 CRÉME has been extended to the northern hemisphere, with a significant portion of targets coming from the main field of the *Kepler* mission. The intensive spectroscopic campaign lasted till 2017, but since then additional data have been taken for selected objects, if needed.

At the moment (November 2024) the CRÉME target sample consists of 386 DEBs (Figure 1). A total of >7000 spectra has been gathered with 19 spectrographs attached to 17 telescopes (from 0.5 to 10-m apertures), or were found in public archives. The total telescope time granted to the project exceeded 300 nights (Table 1).

The project intended to observe relatively bright ($V < 12.5$ mag) and "red" ($V-K > 1.1$ mag) systems, so a sufficient precision of RVs would be possible to obtain. However, several early-type objects with large $E(B-V)$ were included

and later kept in the sample. Out of the 386 systems observed within CRÉME, 32 were marked as not qualified for further studies, 22 were found to be single-lined (SB1), 3 early-type systems pose difficulties in RV determination and require an individual approach, and 4 systems do not have enough sufficient RV measurements ($N < 4$). Therefore, we currently have 325 systems with a sufficient number of good-quality data to estimate orbital parameters and masses of the components[1].

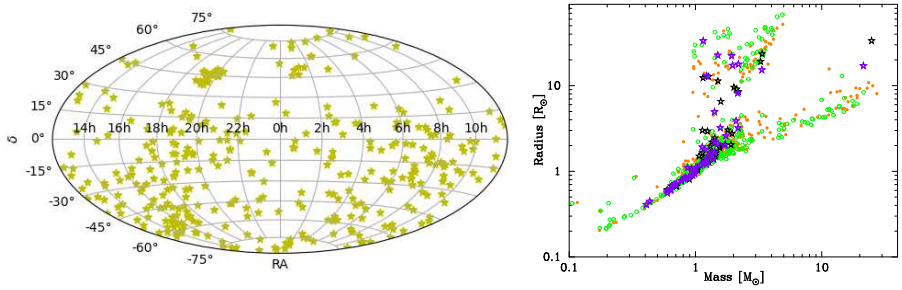


Figure 1. Left: On-sky distribution of CRÉME targets. Right: Masses and radii of binary components from the DEBCat catalogue (orange and green for primaries and secondaries, respectively) and CRÉME DEBs published so far (black and purple for primaries and secondaries, respectively).

Masses alone, or even the orbital solutions, can already point towards some of the interesting properties, such as: location on the cool (<0.9 $M_\odot$) or hot (>3 $M_\odot$) parts of the main sequence; location inside the instability strips (γ Dor, δ Sct), or multiplicity (especially in hierarchical triple SB+3, or quadruple SB+SB configurations). In CRÉME we have so far 76 individual low-mass and 19 high-mass stars, 14 confirmed and 8 candidates for pulsating stars in DEBs, or 80 multiples of various architectures, including compact hierarchical triples (outer period $P_3 < 1000$ d; CHTs) and SB+SB quadruples.

2.2. TESS, *Kepler*, and ground-based photometry

To obtain the required precision in parameters, especially radii, one needs photometric measurements taken with high enough precision, sufficient cadence, and phase coverage. It quickly became clear that the publicly available data from such projects as ASAS or SuperWASP are not enough for the purposes of CRÉME, so additional dedicated observations had to be taken. This turned out to be very time-consuming and ineffective, especially when comes to the orbital phase coverage. Only the objects from the *Kepler/K2* fields had sufficient data available. Therefore, after the launch TESS, we started applying for

[1]Technically only the lower mass limits $M \sin^3(i)$, but in DEBs $\sin^3(i) \simeq 1$, therefore they are good proxies of true stellar masses.

2-minute-cadence photometry of the CRÉME targets through the TESS Guest Investigator (GI) programs. These programs allow to dedicate part of the mission's resources to scientific research outside of the main mission goals. We have been successful during all seven cycles of the mission.

At the moment of writing this article, the TESS satellite is observing in Sector 85 during its seventh cycle of operations. A total of 329 CRÉME targets have their 2-minute cadence photometry, including: 66 in just one sector, 117 in two sectors, 49 in three, 34 in four, 50 in 5 to 12 sectors, and 13 in at least 13 sectors. Additionally, 6 more targets were in the satellite's field of view, thus the longer cadence data (30 or 10 minutes) are available, and another 13 systems are expected to be observed by the end of Cycle 7. Since TESS has by now covered almost the entire sky, including the Ecliptic, we were able to gather data for systems previously observed with *Kepler* and K2. Only 3 CRÉME targets have K2 photometry, but no TESS.

3. CRÉME + TESS (+ *Kepler*/K2) results

In Figure 1 we present masses and radii of components of 348 binaries collected in the DEBCat catalogue, together with 50 systems with published[2] orbital and physical parameters based on CRÉME data. One can note on the mass-radius panel that the CRÉME targets appear in regions poorly populated by the DEBCat objects, which shows that the goals of the project are possible to achieve. Notably, about 30 CRÉME targets are now listed in DEBCat, thus some points may overlap. For most of them the solutions utilise TESS photometry from our GI programmes, or *Kepler*/K2 data. Currently, about 100 DEBs have been modelled with the use of CRÉME data. This includes results presented in 35 publications, as well as unpublished ones (in preparation).

3.1. Projects dedicated to specific classes of systems

A number of studies dedicated to specific scientific cases have been conducted by the team. Two of them were described in other contributions in these proceedings: by A. Moharana (see also: Moharana et al., 2023, 2024) and G. Pawar. Other projects include but are not limited to:

Masses of 650 stars. Using spectroscopic data alone we were able to estimate absolute masses of components of 325 binaries (650 individual stars). From them we selected 78 long-period ($P_{\rm orb} > 4$ d) pairs to determine realistic mass precision, unaffected by stellar rotation or activity. We found mass uncertainty lower than 1.0% in 90% cases, and for ∼60% of stars was better than 0.5%. In the best case we reached 0.051+0.058%.

[2]Including preliminary solutions presented on conferences, and results based on pre-2011 observations.

Low-mass stars. The CRÉME survey partially evolved from the search for new DEBs composed of low-mass stars (K- and M-type dwarfs, e.g. Hełminiak et al., 2011). This topic has been continued, and with the mass estimates of the 650 individual stars we were able to identify a total 19 cases DEBs with both components $M < 0.9\,\mathrm{M}_\odot$ (Hełminiak et al., in prep.), 29 more cases of pairs with a more massive (F/G-type) primary and low-mass secondary, and 9 more systems that seemingly underwent a mass transfer, where the secondary low-mass component was stripped of its outer layers (Pawar et al., in prep.).

Giants and sub-giants. This was a topic of high interest in the earlier stages of the project, since before 2010 the DEBCat listed only a few cases. Our publications include both multi-object (Ratajczak et al., 2013, 2016, 2021) and single-object (Hełminiak et al., 2015). The latter includes HD 187669, the first Galactic double-giant DEB with high-precision stellar parameters. Several other cases were included in various publications. There are at least 5 more unpublished double-giant systems in CRÉME and numerous others with a sub-giant component.

δ Sct and γ Dor pulsators. Both kinds of pulsators are main sequence stars of a particular range of masses. By focusing on stars with those mass ranges we selected a number of candidate DEBs and inspected their light curves in search for pulsations. This way we identified and studied 12 systems with δ Sct-type pulsations (e.g. Pawar et al., 2024), some of which are pending publication (in prep.), as well as 6 with γ Dor-type components (Pawar et al. in prep).

Systems with total eclipses. The totally-eclipsing DEBs are pairs with a fortunate geometry, when during one of the minima the eclipsed component hides completely behind the other one. For a brief moment we may record light from only one star of the system. This provides several advantages: strong bonds on the flux ratio, individual color indices, or spectroscopic analysis of one of the components without disentangling. These have been utilised in CRÉME studies several times, most recently in Hełminiak et al. (2024), where we presented results of a dedicated UVES campaign, aimed for spectra taken during total eclipses of 11 DEBs. We showed that by adding spectroscopic information about just one component, we can drastically reduce the uncertainty in age and distance determination.

Acknowledgements. CRÉME is a collaborative project that involved a large number of people, therefore we'd like to thank: R. Brahm, J. Coronado, N. Espinoza, D. Graczyk, M. Hempel, A. Jordán, E. Kambe, M. Konacki, S. Kozłowski, H. Maehara, F. Marcadon, D. Minniti, E. Niemczura, J. Olszewska, B. Pilecki, M. Rabus, M. Ratajczak, P. Sybilski, A. Tajitsu, M. Tamura, A. Tokovinin, N. Ukita, and L. Vanzi for their various valuable contributions. We'd also like to thank the staff of La Silla-Paranal, CTIO, Okayama, Las Campanas, Subaru, NOT, TNG, OHP, SALT, and AAO telescopes/observatories for their support during many years.

We acknowledge the support provided by the Polish National Science Center through grants no. 2021/41/N/ST9/02746 and 2023/49/B/ST9/01671. A.M. acknowl-

edges support from the UK Science and Technology Facilities Council (STFC) under grant number ST/Y002563/1. Polish participation in SALT is funded by grant No. MEiN nr 2021/WK/01.

References

Hełminiak, K. G., Graczyk, D., Konacki, M., et al., Orbital and physical parameters of eclipsing binaries from the ASAS catalogue - VIII. The totally eclipsing double-giant system HD 187669. 2015, *Monthly Notices of the RAS*, **448**, 1945, DOI:10.1093/mnras/stu2680

Hełminiak, K. G., Konacki, M., Złoczewski, K., et al., Orbital and physical parameters of eclipsing binaries from the All-Sky Automated Survey catalogue. III. Two new low-mass systems with rapidly evolving spots. 2011, *Astronomy and Astrophysics*, **527**, A14, DOI:10.1051/0004-6361/201015127

Hełminiak, K. G., Olszewska, J. M., Puciata-Mroczynska, M., & Pawar, T. B., High-resolution spectroscopy of detached eclipsing binaries during total eclipses. 2024, *Astronomy and Astrophysics*, **691**, A170, DOI:10.1051/0004-6361/202450607

Moharana, A., Hełminiak, K. G., Marcadon, F., et al., Spectroscopy of eclipsing compact hierarchical triples: I. Low-mass double-lined and triple-lined systems. 2024, *Astronomy and Astrophysics*, **690**, A153, DOI:10.1051/0004-6361/202450797

Moharana, A., Hełminiak, K. G., Marcadon, F., et al., Detached eclipsing binaries in compact hierarchical triples: triple-lined systems BD+442258 and KIC 06525196. 2023, *Monthly Notices of the RAS*, **521**, 1908, DOI:10.1093/mnras/stad622

Pawar, T. B., Hełminiak, K. G., Moharana, A., et al., A comprehensive study of five candidate δ Scuti-type pulsators in detached eclipsing binaries. 2024, *Astronomy and Astrophysics*, **691**, A101, DOI:10.1051/0004-6361/202451126

Pojmanski, G., The All Sky Automated Survey. Catalog of Variable Stars. I. 0 h - 6 h Quarter of the Southern Hemisphere. 2002, *Acta Astronomica*, **52**, 397, DOI:10.48550/arXiv.astro-ph/0210283

Ratajczak, M., Hełminiak, K. G., Konacki, M., & Jordán, A., Orbital and physical parameters of eclipsing binaries from the ASAS catalogue - V. Investigation of sub-giants and giants: the case of ASAS J010538-8003.7, ASAS J182510-2435.5 and V1980 Sgr. 2013, *Monthly Notices of the RAS*, **433**, 2357, DOI:10.1093/mnras/stt906

Ratajczak, M., Hełminiak, K. G., Konacki, M., et al., Orbital and physical parameters of eclipsing binaries from the ASAS catalogue - IX. Spotted pairs with red giants. 2016, *Monthly Notices of the RAS*, **461**, 2234, DOI:10.1093/mnras/stw1448

Ratajczak, M., Pawłaszek, R. K., Hełminiak, K. G., et al., Orbital and physical parameters of eclipsing binaries from the ASAS catalogue - XI. CHIRON investigation of long-period binaries. 2021, *Monthly Notices of the RAS*, **500**, 4972, DOI:10.1093/mnras/staa3488

Southworth, J., DEBCat: A Catalog of Detached Eclipsing Binary Stars. 2015, in Astronomical Society of the Pacific Conference Series, Vol. **496**, *Living Together: Planets, Host Stars and Binaries*, ed. S. M. Rucinski, G. Torres, & M. Zejda, 164

Contrib. Astron. Obs. Skalnaté Pleso **55/3**, 444 – 451, (2025)
https://doi.org/10.31577/caosp.2025.55.3.444

Determining the physical parameters of eclipsing binaries from the B-Type Binaries Characterization programme (BBC) with PHOEBE

H. Willems

Max Planck Institute for Astronomy, Königstuhl 17, 69117 Heidelberg, Germany (E-mail: willems@mpia.de)

Received: November 15, 2024; Accepted: January 9, 2025

Abstract. Most massive stars, especially eclipsing binaries, offer a great opportunity to study their physical properties, yet they remain poorly understood. The objective of this work is to understand better the evolution and configuration of massive binaries. This is done by constraining the physical parameters of the eclipsing B-type binaries with the help of the `PHOEBE`, which have been observed spectroscopically and photometrically. From these values, the configuration of these systems is inferred, giving insight to the current state and past and future evolution.

Key words: eclipsing binaries – massive stars – 30 Doradus

1. Introduction

Most B-type stars are located in binaries or even multiple stellar systems (Offner et al., 2023). However, the evolution of massive stars, especially in binaries, has remained elusive. To enhance the understanding of these type of stars, they are studied in this work. The sample is located in the most active star-forming region of the local group, 30 Doradus (Fahrion & De Marchi, 2024), a nebula, where many massive stars are found, inside the Large Magellanic Cloud (LMC). The B-type Binaries Characterization programme (BBC; Villaseñor et al., 2021) is a multi-epoch spectroscopic campaign that followed 88 early B-type binaries inside 30 Doradus. With a radial velocity analysis, orbital solutions for 84 out of these systems were obtained - the largest homogeneous sample as of 2021. They included the semi-amplitude K_1 of the primary, the orbital eccentricity e, the period P and for double-lined spectroscopic binaries, the mass ratio q and the semi-amplitude of the secondary K_2. However, the inclination i remains an unknown parameter for determining the masses and the semi-major axis. This unknown can be measured by photometric observations of eclipsing binaries that have been carried out with the Optical Gravitational Lensing Experiment (OGLE; Pawlak et al., 2016).

Photometry also allows to get constraints of the effective temperatures $T_{\rm eff}$,

the equivalent radii $R_{\rm eq}$. The period and eccentricity can be inferred from both types of observations.
With the combination of the existing spectroscopic analysis and the photometric analysis being carried out by this work, the aim is to accurately compute the physical parameters of the binaries and determine the orbital configuration of the system (i.e., detached, semi-detached or contact) can be found. This will allow us to strongly constrain the evolutionary history of the system as well as the probable future evolution.

2. OGLE data

OGLE is a multidecade photometric survey that became operational in its first phase (OGLE-I) in 1992 (Udalski et al., 1992) with a 1 m telescope, continuing with the second phase (OGLE-II) in 1996 when a 1.3 m telescope - both situated at Las Campanas observatory in Chile - dedicated to OGLE was used. The third phase with more technological upgrades started in 2003 (Udalski, 2003) (OGLE-III) and the current fourth phase (OGLE-IV) was initialized in 2010. In this work, data from OGLE-III and OGLE-IV is used to perform the analysis, making a total used baseline of 13 years with the two most recent phases until the paper Pawlak et al. (2016) was published.
OGLE was primarily inaugurated to detect gravitational micro-lensing events when exoplanets pass in front of their parent star. It can also detect exoplanets via transiting events.
OGLE-IV observed in the I band (from 700 to 900 nm) and the V band (from 500 to 600 nm) at a cadence of 1 to 3 days in the Magellanic systems (Udalski et al., 2015). 48605 systems in the Magellanic Clouds have been classified as eclipsing binaries, of which 40204 are inside the LMC (Pawlak et al., 2016).

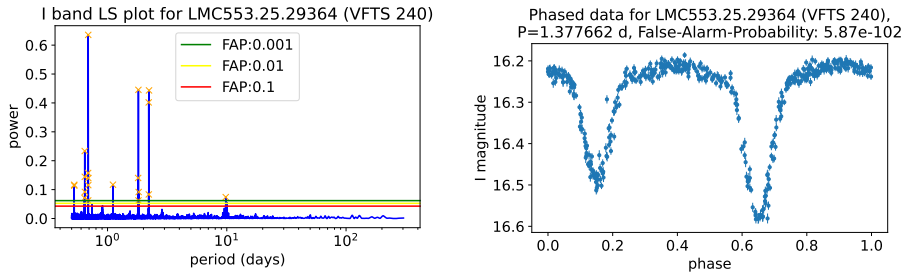
3. Methodology

The following procedure was applied for the analysis: The photometric period is determined first in order to phase-fold the data accordingly to make the eclipses visible. In order to achieve this, the OGLE data, which was available for 85 of them, was analysed through a Lomb-Scargle periodogram. The highest peaks were investigated to see the phase-folded data according to the period found. Eclipsing binaries can be identified using the phase-folded light curve, where `PHOEBE` v. 2.4.14 (Conroy et al., 2020) is used. Using initial values that are set to get close to the light curve, the `Nelder-Mead` is used to optimize the parameters, finding the best set that matches the light curve. Nelder-Mead is opted to find the point of minimal χ^2 in a multi-parameter space, resulting in the best fit to the light curve observations. Finally, `EMCEE` is used to get estimates of the parameter uncertainties. `EMCEE` is a sampler using the Markov Chain Monte

Carlo (MCMC) algorithm, sampling around the optimized values and returning their likelihoods.

3.1. Period determination

The first step in the analysis is to find the photometric period of the system. For that, a Lomb-Scargle (LS) periodogram (Lomb, 1976), (Scargle, 1982) is used. LS fits a set of sine curves to unevenly spaced data and finds the frequencies that reduce the χ^2 the most to find possible periodicities. The likelihood of a frequency matching the data is given by the power of the LS periodogram. In this work, the periods between 0.5 and 300 days with an oversampling factor of 2000 were analysed by the LS periodogram. For a few systems, the analysis was run again with a minimum frequency of 0.0002 (5000 days) to a maximum of 0.1 (10 days) because they showed periodicities from hundreds of days to a few years.



(a) Lomb-Scargle periodogram for VFTS240

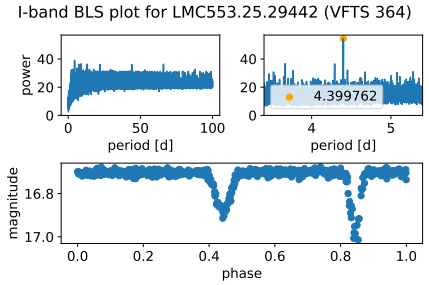
(b) Corresponding plot for the period of the eclipsing binary

Figure 1.: Lomb-Scargle periodogram for VFTS 240 with phased data to the best period

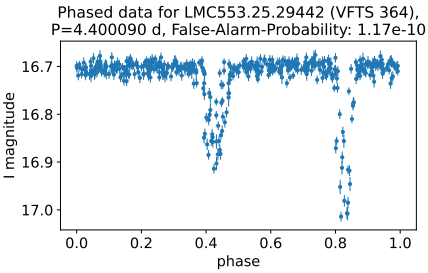
It can happen that the best period is not the one with the highest peak in the periodogram, making it necessary to check several periods. In most cases, the best period was twice the period of the highest LS power, as it can be seen in Fig. 1. This happens because at the highest LS power, the eclipses were positioned at the same phase and they have to be disentangled by multiplying the period by 2.

In a few other cases, when the eclipses are exceptionally sharp and narrow and have a non-sinusoidal shape, a different period-finding mechanism, the so called Box-Least-Squares (BLS; Collier Cameron et al., 2006), was applied to find the correct period. Box-Least Squares is mainly used in exoplanet transit detections, but it can also be used for eclipsing binaries. Contrary to Lomb-Scargle, the Box-Least Squares fits rectangular boxes to the light curve. VFTS

364 is a perfect example when it turned out to find the correct period. The top panels in Fig. 2a show the power at different periods where the top-right plot shows a refined search around the initial highest peak. Both searches were done with 50000 different periods within 0.1-100 days for the top left plot and 1 day around the highest peak for the top right plot.



(a) BLS plot for VFTS364 top panels described in text



(b) Corresponding object with LS

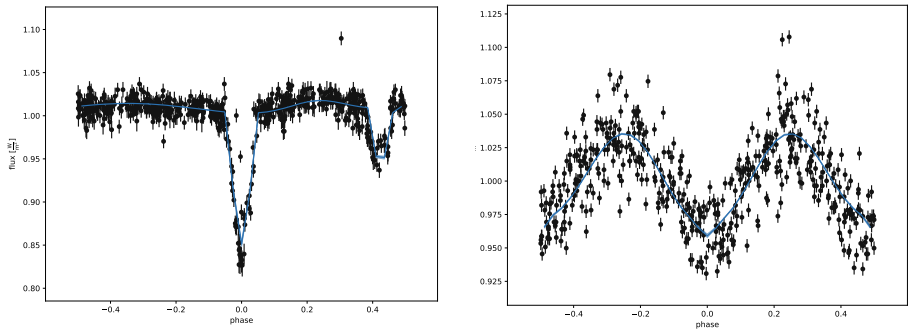
Figure 2.: Comparison between BLS and LS for VFTS364

A good period is defined as that the eclipses are well-defined and the data does not scatter in the eclipses. For example, the BLS plot for VFTS 364 in Fig. 2a shows a good period, while the period found through LS (Fig. 2b) is not good because the eclipses are not clearly enough resolved.
During the analysis of the light curves, 9 of them showed clear eclipses, 4 of them were ellipsoidal variables with higher amplitudes; 10 more showed low variations of the order of 0.02 magnitudes. 6 systems have long periodicities of longer than 100 days and one heartbeat star was in the sample. And 59 systems did not have good periods because for 50 of them, the light curve was fairly constant. 6 out of the 9 systems with no period showed no LS peak with a false-alarm probability of less than 0.1%. The remaining 3 objects did not have OGLE data available.

3.2. Modelling with PHOEBE

When a good period is found, `PHOEBE` can be used to get a model of the light curve of eclipsing binaries for its reproduction and the period becomes a fixed parameter. `PHOEBE` takes a set of orbital and stellar parameters as an input and it returns the light curve model, which can be overlaid with the observational data for comparison. While changing them, the impact of the parameters can be studied until a close agreement between the observations and the model is found. The initial temperatures were set to typical values of early B-type stars (around 20000 K).

When a good point in the parameter space is found, the values of the effective temperatures, radii, the orbital inclination and for single-lined spectroscopic binaries, the mass ratio are further optimized with the help of `Nelder-Mead`. This fitting mechanism works with a χ^2 minimization of the model with the observational data and returns a set of optimized values. After about 150 to 250 iterations, the mechanism converges and the final set of values is the base to estimate the uncertainties with `emcee`. Emcee samples around a point in the parameter space and with trying the values, it obtains parameter uncertainties. In this analysis, the starting point are the parameters that are fitted through Nelder-Mead (effective temperatures, equivalent radii, the inclination; and for single-lined spectroscopic binaries, the mass ratio) and Gaussians around them were set for the sampler to investigate (e.g. 3000 K for the temperatures).
Figure 3 shows the final fits (blue lines) of an eclipsing system and an ellipsoidal system.



(a) VFTS 248 **(b)** VFTS 430

Figure 3.: `EMCEE` results for an eclipsing binary and an ellipsoidal variable

4. Looking for mass-transferring systems

The results from fitting the parameters via `Nelder-Mead` and `emcee` are used to plot them in an HRD with added isochrones to find out if both components are located on the same isochrone. Because the effective temperatures and the radii of the components were fitted, the result can be plotted on the HRD. With isochrones [1] plotted on the same HRD, the age of the systems can be estimated. From that plot, it can be referred to if the system has undergone a phase of mass transfer if the components are not located on the same isochrone. That is because mass transfer has happened and the change of mass heavily impacts the main sequence lifetime of stars. If the stars have evolved separately and have formed at the same time, they should be located on the same isochrone. An example

[1] http://stev.oapd.inaf.it/cgi-bin/cmd

for two systems can be found in Fig. 4 with two different isochrones. Both of

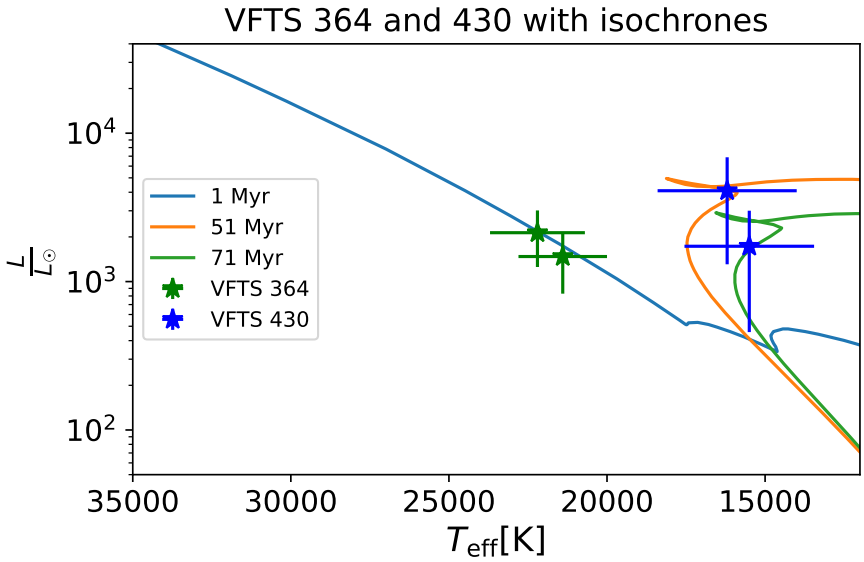


Figure 4.: VFTS 364 and 430 with two isochrones

the components of VFTS 364 are located close to the 10^6 year isochrone (Fig. 4), meaning that they have likely been evolving independently of each other. It can be seen that the components of VFTS 364 lie on the 1 Myr isochrone. And for VFTS 430, the isochrone for the primary (51 Myr) does not lie on the secondary component. VFTS430's light curve shows no eclipses but ellipsoidal variability. This concludes that VFTS 430 is likely a mass-transferring system unlike VFTS 364 where both stars have evolved independently of each other.

5. Summary

The photometric analysis of 85 stars with OGLE data that also have spectroscopy available through BBC showed that 9 stars are eclipsing and 4 ellipsoidal variables were found. A more detailed analysis has been carried out for these systems except for the peculiar star VFTS 698 (Dunstall et al., 2012). Most of them are located on the same isochrone or close to it, making them evolve separately. For two of these twelve systems (VFTS 27, 430), a contact phase is likely because their components deviate more from the same isochrone. The periods for the eclipsing binaries ranged from 1.378 days for VFTS 240 to 12.945 days for VFTS 157.

6. Future work

In the future, this analysis should be carried out for more eclipsing binary systems, particularly in other regions of the sky. This is especially interesting in finding out a spatial dependency of the proportion of binary systems that have undergone a phase of mass transfer.

References

Collier Cameron, A., Pollacco, D., Street, R. A., et al., A fast hybrid algorithm for exoplanetary transit searches. 2006, *Monthly Notices of the Royal Astronomical Society*, **373**, 799, DOI:10.1111/j.1365-2966.2006.11074.x

Conroy, K. E., Kochoska, A., Hey, D., et al., Physics of Eclipsing Binaries. V. General Framework for Solving the Inverse Problem. 2020, *The Astrophysical Journal Supplement*, **250**, 34, DOI:10.3847/1538-4365/abb4e2

Dunstall, P. R., Fraser, M., Clark, J. S., et al., The VLT-FLAMES Tarantula Survey V: The peculiar B[e]-like supergiant, VFTS698, in 30 Doradus. 2012, *Astronomy & Astrophysics*, **542**, 1, DOI:10.1051/0004-6361/201218872

Fahrion, K. & De Marchi, G., The hierarchical formation of 30 Doradus as seen by JWST. 2024, *Astronomy & Astrophysics*, **681**, A20, DOI:10.1051/0004-6361/202348097

Lomb, N. R., Least-Squares Frequency Analysis of Unequally Spaced Data. 1976, *Astrophysics and Space Science*, **39**, 447, DOI:10.1007/BF00648343

Offner, S. S. R., Moe, M., Kratter, K. M., et al., The Origin and Evolution of Multiple Star Systems. 2023, in Astronomical Society of the Pacific Conference Series, Vol. **534**, *Protostars and Planets VII*, ed. S. Inutsuka, Y. Aikawa, T. Muto, K. Tomida, & M. Tamura, 275, DOI:10.48550/arXiv.2203.10066

Pawlak, M., Soszyński, I., Udalski, A., et al., The OGLE Collection of Variable Stars. Eclipsing Binaries in the Magellanic System. 2016, *Acta Astronomica*, **66**, 421, DOI:10.48550/arXiv.1612.06394

Scargle, J. D., Studies in astronomical time series analysis. II. Statistical aspects of spectral analysis of unevenly spaced data. 1982, *The Astrophysical Journal*, **263**, 835, DOI:10.1086/160554

Udalski, A., The Optical Gravitational Lensing Experiment. Real Time Data Analysis Systems in the OGLE-III Survey. 2003, *Acta Astronomica*, **53**, 291, DOI:10.48550/arXiv.astro-ph/0401123

Udalski, A., Szymanski, M., Kaluzny, J., Kubiak, M., & Mateo, M., The Optical Gravitational Lensing Experiment. 1992, *Acta Astronomica*, **42**, 253

Udalski, A., Szymański, M. K., & Szymański, G., OGLE-IV: Fourth Phase of the Optical Gravitational Lensing Experiment. 2015, *Acta Astronomica*, **65**, 1, DOI:10.48550/arXiv.1504.05966

Villaseñor, J. I., Taylor, W. D., Evans, C. J., et al., The B-type binaries characterization programme I. Orbital solutions for the 30 Doradus population. 2021, *Monthly Notices of the Royal Astronomical Society*, **507**, 5348, DOI:10.1093/mnras/stab2197

Contrib. Astron. Obs. Skalnaté Pleso **55/3**, 452 – 461, (2025)
https://doi.org/10.31577/caosp.2025.55.3.452

Characterizing the variability of a sample of massive stars in eclipsing binaries

C.I. Eze[1,2], **G. Handler**[1], **F. Kahraman Aliçavuş**[3], **T. Pawar**[4] **and A. Miszuda**[1]

[1] *Nicolaus Copernicus Astronomical Center, Bartycka 18, 00-716 Warsaw, Poland (E-mail: cheze@camk.edu.pl)*

[2] *Department of Physics and Astronomy, University of Nigeria, Nsukka, Nigeria*

[3] *Çanakkale Onsekiz Mart University, Faculty of Sciences, Physics Department, 17100, Çanakkale, Türkiye*

[4] *Nicolaus Copernicus Astronomical Center, Polish Academy of Sciences, ul. Rabiańska 8, 87-100 Toruń, Poland*

Received: October 29, 2024; Accepted: February 5, 2025

Abstract. Massive stars exhibit a perplexing mismatch between their inferred masses from different observational techniques, posing a significant challenge to our understanding of stellar evolution and structure. This discrepancy is believed to be caused by the underestimation of the convective core masses. The efficiency of such measurement is usually impaired by a lot of processes at work in the interior of the stars such as convective core overshooting and interior rotation. By integrating the precision of asteroseismology which provides insights into the internal structure and dynamics of stars, with the detailed observational constraints offered by eclipsing binary systems, this study aims to precisely characterize a sample of massive stars in eclipsing binaries to infer their properties and evolutionary state. In this paper, the sample, observed photometrically with TESS and spectroscopically with SALT HRS, CHIRON, HERMES and a spectrograph at Skalnate Pleso Observatory between 2021 and 2024, are analyzed. The orbital elements as well as the basic stellar parameters of the targets in the sample are fitted to derive the geometry of their orbits as well as their absolute parameters. The asteroseismic properties of the targets are also obtained, which unravel their core dynamics and profiles. This is a precursor work that provides detailed characterization of the targets in the sample for future theoretical modeling.

Key words: Asteroseismology, binaries, massive stars, stellar evolution, pulsations, rotation

1. Introduction

There has been a perennial problem in the estimation of the masses of massive stars. The problem manifests in the mismatch between the masses inferred from model-independent observational techniques and those obtained from stellar evolution models. This was first observed by Herrero et al. (1992), who pointed out that masses they obtained from spectroscopy were discrepant with masses obtained from evolutionary models. This has since been dubbed the mass discrepancy problem in massive stars and adjudged to be caused by the underestimation of the convective core mass.

Massive stars have convective cores, a radiative envelope, and a convective boundary layer between the core and the envelope. The mixing at the boundary layer transports chemical elements and, in some cases, heat to the core, thereby increasing the thermonuclear fuel in the core of the star. This, in turn, leads to an increase in the temperature and mass of the stellar core. This convective boundary mixing impairs the estimation of the convective core mass leading to the observed mass discrepancy. The boundary layer and the mixing have unfortunately proven quite difficult to calibrate. Several authors have investigated different mixing prescriptions (e.g Pedersen et al., 2021; Anders & Pedersen, 2023)

Several attempts have been made by several researchers to calibrate the mixing at the boundary layer and solve the mass discrepancy problem. Whereas some researchers (e.g. Tkachenko et al., 2020) applied eclipsing binary modeling, several other researchers (e.g. Burssens et al., 2023) applied asteroseismic modeling on apparently single stars. The effects of different convective boundary mixing (CBM) mechanisms on various stellar parameters such as luminosity, radius, helium core mass e.t.c. have also been investigated Johnston et al. (e.g. 2024). While these efforts have improved the results obtained and our knowledge of what is happening at the boundary layer, it appears that the problem still persists. To solve this problem by leveraging on the combined strengths of eclipsing binary modeling and asteroseismology, Eze & Handler (2024a,b) searched for and discovered dozens of new β Cephei pulsators in eclipsing binaries. To be able to use the stars in the catalog of these targets for the said purpose, their stellar parameters and properties are expected to be first determined. The paper seeks to characterize a few stars from the catalogs. It is a prerequisite work, which aims to determine the properties of the stars. These estimated parameters would serve as the input priors for the detailed modeling of the systems aimed at resolving the mass discrepancy problem.

2. Spectroscopic analysis

Targets in Eze & Handler (2024a), which are relatively bright (brighter than V=11) with both primary and secondary eclipses visible in their photomet-

ric light curves and their pulsation spectra having several significant pulsations that appear promising for asteroseismic analysis are selected for immediate spectroscopic follow-up. This amounts to 25 targets in the sample in this work (The details are contained in our upcoming paper (Eze et al., in prep)). Their spectra were obtained using SALT HRS (Buckley et al., 2006; Bramall et al., 2010, 2012; Crause et al., 2014; Crawford et al., 2010), CHIRON spectrograph in SMARTS 1.5-m telescope operated by the SMARTS Consortium (Tokovinin et al., 2013; Paredes et al., 2021), HERMES spectrograph (Raskin et al., 2011) and the MUSICOS-type spectrograph at 1.3-m telescope of Skalnate Pleso observatory (SPO) (Baudrand & Bohm, 1992; Pribulla et al., 2024) using appropriate exposure time, resolution, signal-to-noise ratio and under suitable sky conditions. The observed spectra were normalized and the radial velocities (RV) as well as the atmospheric solutions of the targets were determined. The RVs were extracted using the IRAF/PYRAF FXCOR task (Tody, 1986; Science

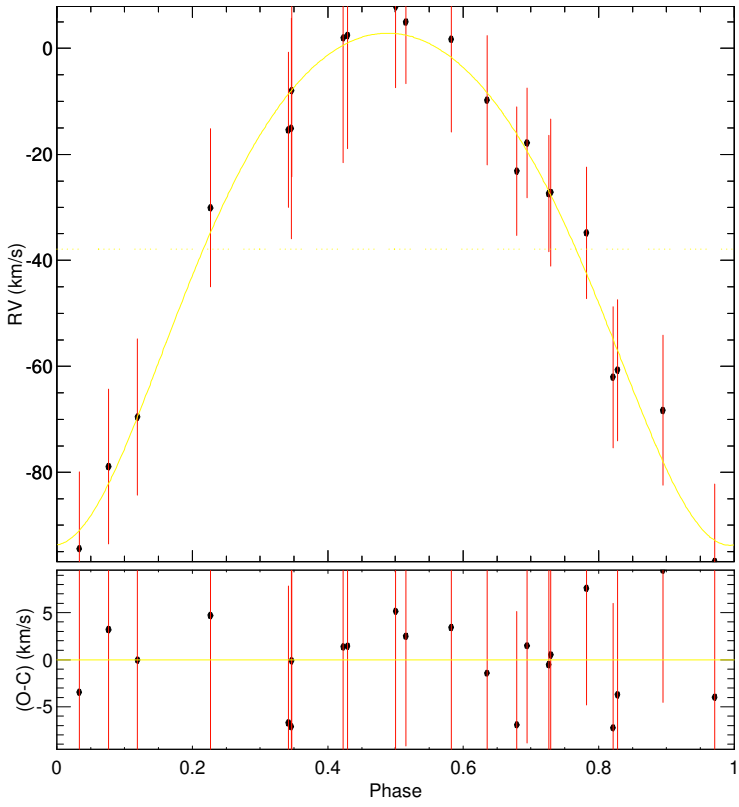


Figure 1. The fit to the RV curve of V1166 Cen.

Software Branch at STScI, 2012) in cross-correlation with synthetic spectra obtained with the Spectrum code (Gray, 1999) using ATLAS model atmospheres (Castelli & Kurucz, 2003). Appropriate values of $T_{\rm eff}$, $\log g$ and $v \sin i$ used for the synthetic spectra of each target were inferred from preliminary fits to the spectra using HANDY[1]. The RV curves were fitted using rvfit (Iglesias Marzoa et al., 2015) to obtain the orbital elements/parameters of the systems. Figure 1 shows the fitted RV curve and Table 1 gives the fitted parameters of one of the targets (V1166 Cen) in the sample. V1166 Cen is used as an example target in this paper to demonstrate the analysis where applicable.

In the case of V1166 Cen, all the orbital parameters are fitted as free parameters. It has an eccentric orbit with eccentricity of 0.2(1), and a radial velocity semi-amplitude (K) of 48(5) $\mathrm{km\,s^{-1}}$. The mass function of the system is 0.15(8) $\mathrm{M_\odot}$. The period agrees with the photometric period reported in Eze & Handler (2024a) up to 1 decimal places.

Table 1. The fitted parameters of V1166 Cen.

Parameter	Value
Adjusted Quantities	
P (d)	13.6(2)
T_p (HJD)	2459956(1)
e	0.2(1)
ω (deg)	183(34)
γ (km/s)	-37(3)
K_1 (km/s)	48(5)
Derived Quantities	
$a_1 \sin i$ (10^6 km)	9(1)
$f(m_1, m_2)$ ($\mathrm{M_\odot}$)	0.15(8)
Other Quantities	
χ^2	2.39
N_{obs} (primary)	22
Time span (days)	73.06
rms_1 (km/s)	4.64

The atmospheric parameters (T_{eff}, logg and vsini) were also obtained by cross-matching the normalized observed spectrum with a synthetic model atmosphere template obtained using the Non-Local Thermodynamic Equilibrium (NLTE) Tlusty BSTAR2006 grids (Hubeny & Lanz, 2017). For the T_{eff} and

[1]https://github.com/RozanskiT/HANDY)

$\log g$, H_β or H_γ was used whereas HeI 4387 and/or HeI 5878 lines were used for $v \sin i$. The errors obtained are at 1-sigma (1σ) tolerance in the goodness of fit parameter. For example, the T_{eff}, $\log g$ and $v \sin i$ of V1166 Cen are 27000(1000) K, 3.8(1) dex and 252(10) km s^{-1} respectively. The details of the analysis are contained in our upcoming paper (Eze et al., in prep), which discusses the spectroscopic follow-up on a sample of β Cephei pulsators in eclipsing binaries.

For double-lined spectroscopic binaries in our sample, the spectra are first disentangled using the FD3 program ((Ilijic et al., 2004) and the atmospheric parameters of each of the individual components estimated from the disentangled spectra. FD3 is a C-based program, which performs the separation of the spectra of double-lined spectroscopic binaries in the Fourier space. An example of the double-lined spectroscopic binaries in our sample is V1216 Sco. The orbital and atmospheric solutions of this system, for instance, are used as priors for the detailed binary modeling (Miszuda et al., submitted to $A\&A$).

3. Pulsation analysis

The preliminary pulsation analyses were done as described in detail, in Eze & Handler (2024a). Additionally, at this time, all significant β Cephei pulsations in the systems are extracted instead of a few dominant pulsations. Figure 2 (left panel) and Table 2 show the Fourier spectrum and pulsation frequencies respectively of V1166 Cen. Figure 2 (left panel) shows a possible rotationally split quadrupole mode of l=2. There is an observed asymmetry in the split mode. Asymmetries in rotationally split mode multiplets were recently comprehensively discussed by Guo et al. (2024) who examined the effects of perturbations from rotational non-spherical distortions, intrinsic magnetic fields, resonant mode coupling, and binarity on the observed frequency splittings. V1166 Cen is a fast rotator as suggested by its $v \sin i = 252(10)$ km s^{-1} and the asymmetry is most likely to originate from the rotationally induced non-spherical distortions.

Further pulsation analysis was also conducted by plotting the échelle diagrams of the targets using all significant frequencies found in the data. Figure 2 (right panel) shows the échelle diagram of V1166 Cen. There are observed curved patterns in the échelle diagram, which likely arise from the effects of rotation. The exact mode characteristics (ℓ, m, n) of the systems in our sample are yet to be confirmed. The modes are inferred via rotational splitting or the use of ground-based multicolor photometric data. For systems where the ground-based multicolor photometric follow-up are feasible, the multicolor photometric observations have been conducted with SHOC in the 1.0 m SAAO telescope (Coppejans et al., 2013) and are currently being reduced. For systems like V1166 Cen where the amplitude of even its strongest mode is too small to reliably conduct actual mode identification with ground-based multicolor photomeric data with-

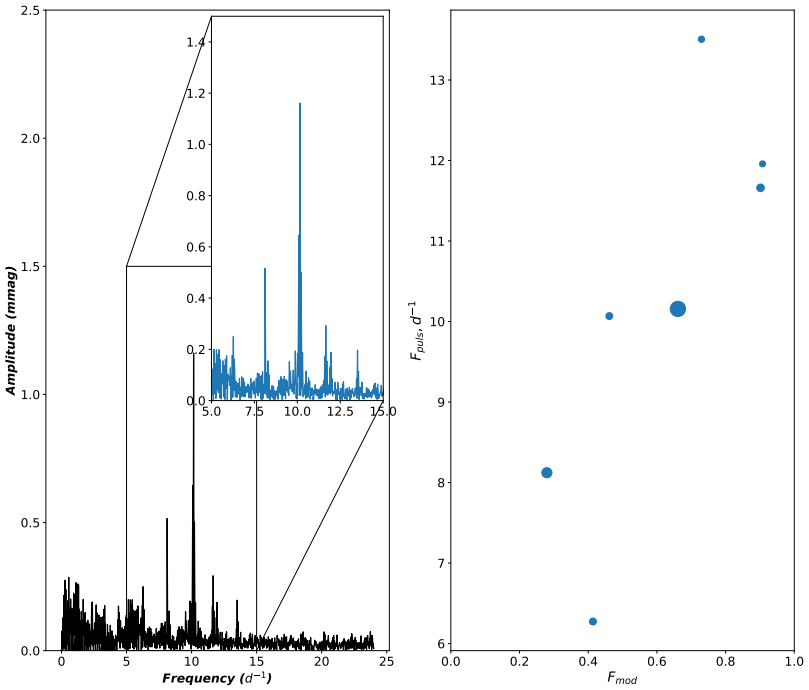


Figure 2. Fourier spectra of V1166 Cen with the neighborhood of the dominant pulsation zoomed into (left panel) and échelle diagram of V1166 Cen (right panel).

out excessive usage of telescope time, only the rotational splitting method has been used and no ground-based multicolor photometric follow up is planned.

4. Ensemble pulsational characteristics

With the now considerably larger sample of β Cephei stars in eclipsing binaries (see Eze & Handler, 2024a), the ensemble pulsational characteristics of β Cephei pulsators in eclipsing binaries are investigated. We plotted different pulsational and orbital parameters obtained in Eze & Handler (2024a) for the sample reported in Eze & Handler (2024a). The plot of amplitude against the dominant pulsation frequency in Figure 3 (left panel) shows that the amplitude of p-mode pulsations decays exponentially with an increase in pulsation frequency. One outlier with pulsation amplitude of 116.99(9) mmag was removed from the plots to avoid its undue driving force to the trends. This appears to be in line with Fritzewski et al. (2024), who observed a similar decay in the amplitude of β Cephei pulsations.

Table 2. The Pulsation Frequencies of V1166 Cen. 'F' is the frequency and 'A' is the amplitude of the frequency.

	F (d^{-1})	A (mmag)
F1	10.157(1)	1.17(6)
F2	8.122(3)	0.52(6)
F3	11.661(5)	0.29(6)
F4	6.274(6)	0.24(6)
F5	10.068(6)	0.24(6)
F6	11.959(8)	0.18(6)
F7	13.506(7)	0.20(6)

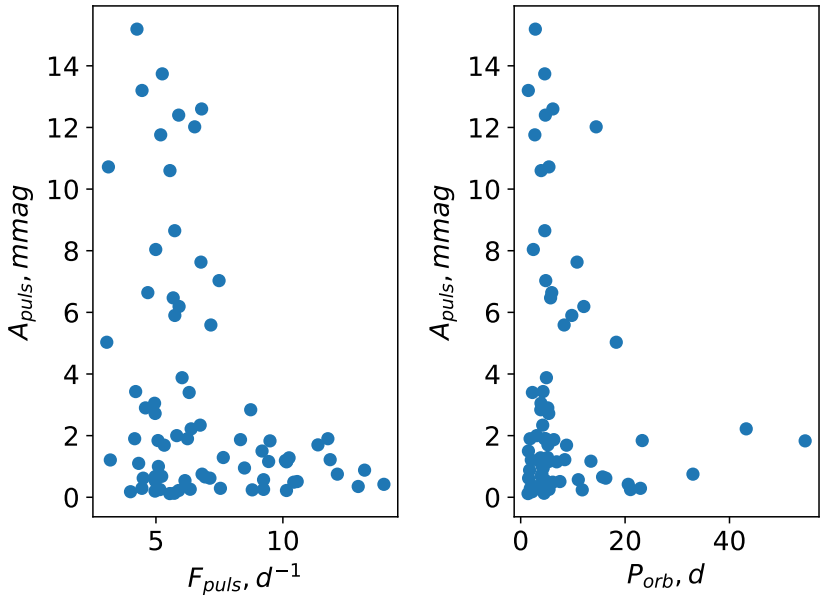


Figure 3. Frequency-amplitude relation for β Cep p modes (left panel) and Period-pulsation amplitude relation for our sample of β Cep pulsators in eclipsing binaries (right panel).

To check the impact of the orbit or possible tidal interactions of the systems on the amplitude of pulsations in eclipsing binaries, the amplitude of the pulsation is plotted against the orbital period as shown in Figure 3 (right panel). The preliminary result shows an exponential decay. It is not yet clear whether the closeness or possible tidal interactions as a result, enhance or dampen the am-

plitude of the pulsations. This is owing to the fact that the sample was treated, at this point, as a perfectly homogeneous sample without distinction between systems where tidal interactions are possible and where they are not. A possible selection effect is not ruled out as there are much less systems with long orbital periods. A detailed ensemble analysis is underway to explore the possible orbital period-pulsation frequency and orbital period-pulsation amplitude relations, among others, in β Cephei stars in eclipsing binary systems. Such a detailed study has been conducted for δ Scuti stars in eclipsing binaries by Liakos & Niarchos (2017), who observed a linear $\log P_{pul} - \log P_{orb}$ relation for stars with orbital period < 13 d. However, preliminary results do not show such a relation in β Cephei stars in eclipsing binaries.

5. Conclusion

A sample of β Cephei stars in eclipsing binaries is characterized to obtain their stellar properties. Their orbital as well as their atmospheric solutions are determined. The T_{eff}, $\log g$ and $v \sin i$ of V1166 Cen, for instance, are 27000(1000) K, 3.8(1) dex and 252(10) km s^{-1} respectively. The pulsational mode characteristics that are visible in the Fourier spectra and échelle diagrams of the stars in our sample are investigated. The ensemble pulsational characteristics are also reported. Multicolor photometry for direct mode identification is currently being reduced.

Acknowledgements. The work is supported by the Polish National Science Foundation (NCN) under grant nr 2021/43/B/ST9/02972. C.I. Eze is grateful for the support received from the staff of the Stellar Department, Astronomical Institute of the Slovak Academy of Sciences during his observation runs at the Skalnaté Pleso Observatory.

References

Anders, E. H. & Pedersen, M. G., Convective Boundary Mixing in Main-Sequence Stars: Theory and Empirical Constraints. 2023, *Galaxies*, **11**, 56, DOI:10.3390/galaxies11020056

Baudrand, J. & Bohm, T., MUSICOS : a fiber-fed spectrograph for multi-site observations. 1992, *Astronomy and Astrophysics*, **259**, 711

Bramall, D. G., Schmoll, J., Tyas, L. M. G., et al., The SALT HRS spectrograph: instrument integration and laboratory test results. 2012, in Society of Photo-Optical Instrumentation Engineers (SPIE) Conference Series, Vol. **8446**, *Ground-based and Airborne Instrumentation for Astronomy IV*, ed. I. S. McLean, S. K. Ramsay, & H. Takami, 84460A

Bramall, D. G., Sharples, R., Tyas, L., et al., The SALT HRS spectrograph: final design, instrument capabilities, and operational modes. 2010, in Society of Photo-Optical Instrumentation Engineers (SPIE) Conference Series, Vol. **7735**, *Ground-*

based and Airborne Instrumentation for Astronomy III, ed. I. S. McLean, S. K. Ramsay, & H. Takami, 77354F

Buckley, D. A. H., Swart, G. P., & Meiring, J. G., Completion and commissioning of the Southern African Large Telescope. 2006, in Society of Photo-Optical Instrumentation Engineers (SPIE) Conference Series, Vol. **6267**, *Ground-based and Airborne Telescopes*, ed. L. M. Stepp, 62670Z

Burssens, S., Bowman, D. M., Michielsen, M., et al., A calibration point for stellar evolution from massive star asteroseismology. 2023, *Nature Astronomy*, **7**, 913, DOI:10.1038/s41550-023-01978-y

Castelli, F. & Kurucz, R. L., New Grids of ATLAS9 Model Atmospheres. 2003, in IAU Symposium, Vol. **210**, *Modelling of Stellar Atmospheres*, ed. N. Piskunov, W. W. Weiss, & D. F. Gray, A20

Coppejans, R., Gulbis, A. A. S., Kotze, M. M., et al., Characterizing and Commissioning the Sutherland High-Speed Optical Cameras (SHOC). 2013, *Publications of the ASP*, **125**, 976, DOI:10.1086/672156

Crause, L. A., Sharples, R. M., Bramall, D. G., et al., Performance of the Southern African Large Telescope (SALT) High Resolution Spectrograph (HRS). 2014, in Society of Photo-Optical Instrumentation Engineers (SPIE) Conference Series, Vol. **9147**, *Ground-based and Airborne Instrumentation for Astronomy V*, ed. S. K. Ramsay, I. S. McLean, & H. Takami, 91476T

Crawford, S. M., Still, M., Schellart, P., et al., PySALT: the SALT science pipeline. 2010, in Society of Photo-Optical Instrumentation Engineers (SPIE) Conference Series, Vol. **7737**, *Observatory Operations: Strategies, Processes, and Systems III*, ed. D. R. Silva, A. B. Peck, & B. T. Soifer, 773725

Eze, C. I. & Handler, G., β Cephei Pulsators in Eclipsing Binaries Observed with TESS. 2024a, *Astrophysical Journal, Supplement*, **272**, 25, DOI:10.3847/1538-4365/ad39c5

Eze, C. I. & Handler, G., Photometric sample of early B-type pulsators in eclipsing binaries observed with TESS. 2024b, *Contributions of the Astronomical Observatory Skalnate Pleso*, **54**, 70, DOI:10.31577/caosp.2024.54.2.70

Fritzewski, D. J., Vanrespaille, M., Aerts, C., Hey, D., & De Ridder, J., Mode identification and ensemble asteroseismology of 164 beta Cep stars discovered from Gaia light curves and monitored by TESS. 2024, *arXiv e-prints*, arXiv:2408.06097, DOI:10.48550/arXiv.2408.06097

Gray, R. O. 1999, SPECTRUM: A stellar spectral synthesis program, Astrophysics Source Code Library, record ascl:9910.002

Guo, Z., Bedding, T. R., Pamyatnykh, A. A., et al., Oscillation Frequencies of Moderately Rotating Delta Scuti Stars: Asymmetric Mode Splittings Due to Non-spherical Distortion. 2024, *arXiv e-prints*, arXiv:2406.15678, DOI:10.48550/arXiv.2406.15678

Herrero, A., Kudritzki, R. P., Vilchez, J. M., et al., Intrinsic parameters of galactic luminous OB stars. 1992, *Astronomy and Astrophysics*, **261**, 209

Hubeny, I. & Lanz, T., TLUSTY User's Guide III: Operational Manual. 2017, *arXiv e-prints*, arXiv:1706.01937, DOI:10.48550/arXiv.1706.01937

Iglesias Marzoa, R., Lopez-Morales, M., & Morales, M., The rvfit Code: A Detailed Adaptive Simulated Annealing Code for Fitting Binaries and Exoplanets Radial Velocities. 2015, *Publications of the Astronomical Society of the Pacific*, **127**, DOI:10.1086/682056

Ilijic, S., Hensberge, H., Pavlovski, K., & Freyhammer, L. M., Obtaining normalised component spectra with FDBinary. 2004, in Astronomical Society of the Pacific Conference Series, Vol. **318**, *Spectroscopically and Spatially Resolving the Components of the Close Binary Stars*, ed. R. W. Hilditch, H. Hensberge, & K. Pavlovski, 111–113

Johnston, C., Michielsen, M., Anders, E. H., et al., Modelling Time-dependent Convective Penetration in 1D Stellar Evolution. 2024, *Astrophysical Journal*, **964**, 170, DOI:10.3847/1538-4357/ad2343

Liakos, A. & Niarchos, P., Catalogue and properties of δ Scuti stars in binaries. 2017, *Monthly Notices of the RAS*, **465**, 1181, DOI:10.1093/mnras/stw2756

Paredes, L. A., Henry, T. J., Quinn, S. N., et al., The Solar Neighborhood XLVIII: Nine Giant Planets Orbiting Nearby K Dwarfs, and the CHIRON Spectrograph's Radial Velocity Performance. 2021, *Astronomical Journal*, **162**, 176, DOI:10.3847/1538-3881/ac082a

Pedersen, M. G., Aerts, C., Pápics, P. I., et al., Internal mixing of rotating stars inferred from dipole gravity modes. 2021, *Nature Astronomy*, **5**, 715, DOI:10.1038/s41550-021-01351-x

Pribulla, T., Vaňko, M., Komžík, R., & Sivanič, P., High-resolution échelle spectrograph at Skalnaté Pleso Observatory. 2024, *Contributions of the Astronomical Observatory Skalnate Pleso*, **54**, 43, DOI:10.31577/caosp.2024.54.2.43

Raskin, G., van Winckel, H., Hensberge, H., et al., HERMES: a high-resolution fibre-fed spectrograph for the Mercator telescope. 2011, *Astronomy and Astrophysics*, **526**, A69, DOI:10.1051/0004-6361/201015435

Science Software Branch at STScI. 2012, PyRAF: Python alternative for IRAF, Astrophysics Source Code Library, record ascl:1207.011

Tkachenko, A., Pavlovski, K., Johnston, C., et al., The mass discrepancy in intermediate- and high-mass eclipsing binaries: The need for higher convective core masses. 2020, *Astronomy and Astrophysics*, **637**, A60, DOI:10.1051/0004-6361/202037452

Tody, D., The IRAF Data Reduction and Analysis System. 1986, in Society of Photo-Optical Instrumentation Engineers (SPIE) Conference Series, Vol. **627**, *Instrumentation in astronomy VI*, ed. D. L. Crawford, 733

Tokovinin, A., Fischer, D. A., Bonati, M., et al., CHIRON—A Fiber Fed Spectrometer for Precise Radial Velocities. 2013, *Publications of the ASP*, **125**, 1336, DOI:10.1086/674012

Contrib. Astron. Obs. Skalnaté Pleso **55/3**, 462 – 465, (2025)
https://doi.org/10.31577/caosp.2025.55.3.462

Spectroscopic monitoring of eclipsing binaries at Ondřejov observatory

P. Gajdoš[1,2] **and Š. Parimucha**[2]

[1] *Astronomical Institute of the Czech Academy of Sciences*
251 65 Ondřejov, The Czech Republic

[2] *Institute of Physics, Faculty of Science, Šafárik University, Košice, Slovakia*

Received: November 11, 2024; Accepted: December 11, 2024

Abstract. To date, a large number of variable stars have been classified as eclipsing binaries. Large photometric surveys such as Kepler, TESS or Plato are finding thousands of new candidates. However, only a few have been studied in detail. Moreover, photometric data provide no information about the masses of stars, which is the key information about the system. Spectroscopic observations and radial-velocity measurements are required for this purpose. Therefore, ground-based spectroscopy is a useful supplementary source of data for large photometric surveys. Additionally, a few interesting phenomena can be discovered using radial velocity curves, which are hardly detectable on the light curve. Binary orbits could be significantly eccentric, the system could have an unusually low mass ratio, or it would not have to be binary at all. Here, we present some interesting systems observed using the OES spectrograph attached at the Perek 2-meter telescope in Ondřejov together with their light curves obtained by the TESS mission.

Key words: eclipsing binaries – spectroscopy – radial velocities

1. Introduction

We used the Perek telescope at the Ondřejov observatory for spectroscopic monitoring of eclipsing binaries (EBs). We selected systems with orbital periods of less than 5 days, brighter than approximately 10 mag, and without any systematic spectroscopic observations and radial velocity (RV) measurements. Data from the *TESS* space mission were used to analyze the light curves (LCs) of the individual binaries. The main goal of this project is to use both sources of data (photometry and spectroscopy) to precisely determine the absolute physical parameters of the studied systems and their components.

This paper presents some initial results of a few systems in which spectroscopy and RV measurements reveal interesting features hidden for photometry-only analysis.

2. Ground-based spectroscopy

For the ground-based spectroscopic observations, we used a fibre-fed echelle spectrograph OES installed on a 2-m Perek telescope at the Ondřejov observatory (Kabáth et al., 2020). The spectral resolution was $R = 50\,000$ in the wavelength range 3600 − 9500 Å. A ThAr lamp was used for the spectral calibration.

The spectra were processed using the standard tools in IRAF. We used the spectrum with the highest SNR as the template spectrum to measure the RVs. For HD 247917, which is an SB2 binary, we created synthetic spectra as a template. The RVs were obtained using the cross-correlation function in ISPEC (Blanco-Cuaresma et al., 2014). It was impossible to correctly measure the RVs of HD 247917 for phases close to 0.0 and 0.5. Therefore, we adopted the KOREL code (Hadrava, 2004) to disentangle the spectra of both the components and precisely determine the RVs in these phases.

3. Discussions

KIC 7023917 is a short-period EB (0.7728 days). The depth and shape of the primary and secondary minima on the LC are very similar (see left panel of Fig. 1), suggesting comparable temperatures and radii of the stars. However, we could only detect the spectral lines of one component, and the amplitude of the RVs was surprisingly small. Further analysis (Gajdoš et al., 2024) showed that the mass ratio is only 0.1, which is unusual for stars with close spectral types (A7 & F6) and radii of 2 and 1 $R_\odot$.

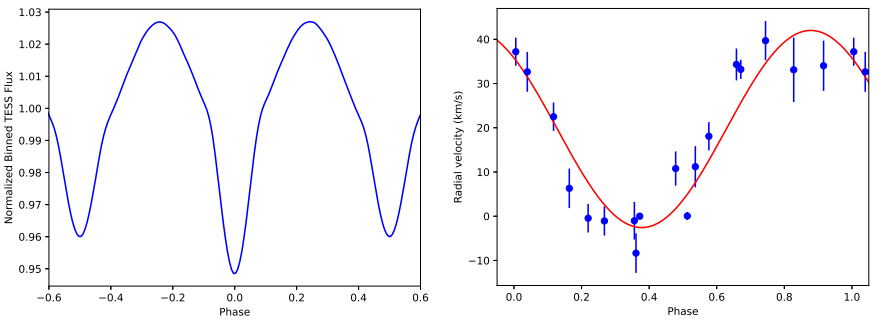


Figure 1. Normalized binned *TESS* LC (*left*) and measured RVs (*right*) of KIC 7023917.

Detached EB HD 247917 consists of two A-type stars with an orbital period of about 2.69 days. The LC looks similar to a normal Algol-type EB without any interesting features. However, the RV measurements classified it as an SB2

binary with a significantly eccentric orbit (upper right panel of Fig. 2). The eccentricity determined was 0.202 ± 0.014. However, the argument of the pericenter ($\omega = 93.2 \pm 0.9°$) causes the phase shift of the secondary minima to be 0.006. Both components have nearly the same masses - the mass ratio is about 0.94. Preliminary LC analysis suggests that they are both main-sequence stars of the later part of spectral type A (probably A8 or A9).

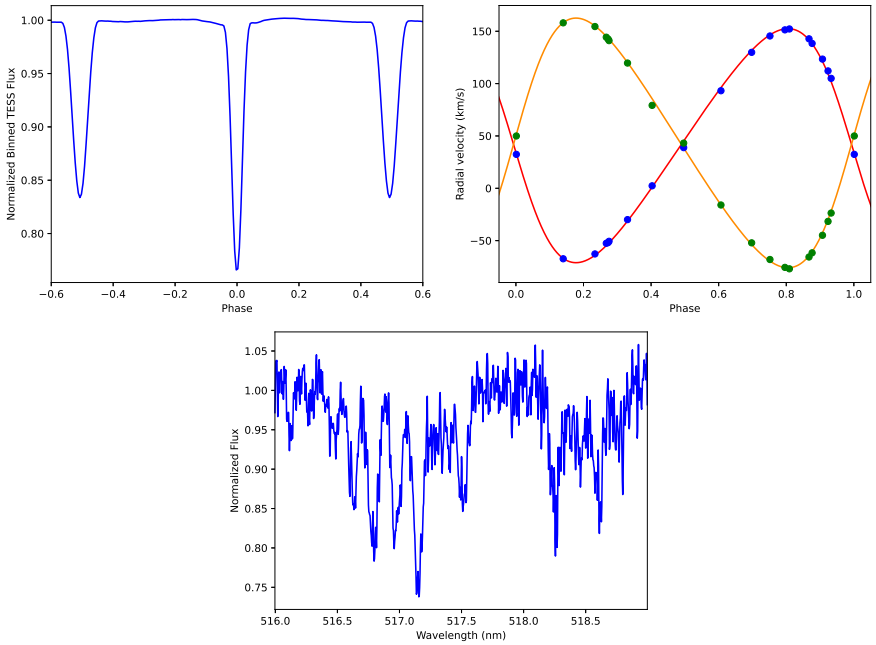


Figure 2. *TESS* LC (*left*) and obtained RVs (*right*) of HD 247917. Example of spectra of HD 247917 for the region of magnesium triplet, close to photometric phase 0.75 (*bottom*).

Star η UMi is classified as an Algol-type EB of spectral type F in the VSX catalogue with a period of 2.2 days. The classification was based on data from *TESS* sector 14 (Shi et al., 2022, highlighted in bold in the *left* panel of Fig. 3)). However, the LCs from the following sectors look weird and definitely differ from the LCs of any kind of EB. Moreover, we could not measure any changes in RVs (larger than 1km/s). Therefore, the system is not binary at all. The spectral lines of this target are extremely broad. We hypothesize that the star is the rotational variable.

A more detailed analysis of systems HD 247917 and η UMi is in preparation.

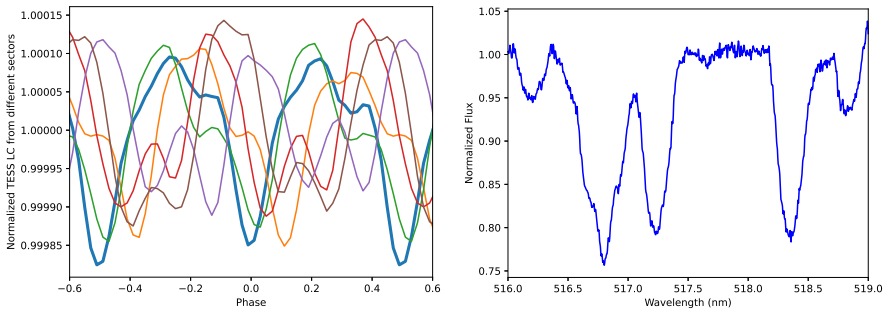


Figure 3. LCs from different *TESS* sectors (*left*) and example of spectra of η UMi (*right*).

Acknowledgements. This study is based on data collected using Perek's 2-m telescope. This work has been supported by the grant of the Slovak Research and Development Agency with number APVV-20-0148 and The Ministry of Education, Youth and Sports of the Czech Republic by grant LTT-20015. The research of P.G. was supported by the internal grant No. VVGS-2023-2784 of the P. J. Šafárik University in Košice and funded by the EU NextGenerationEU through the Recovery and Resilience Plan for Slovakia under the project No. 09I03-03-V05-00008.

References

Blanco-Cuaresma, S., Soubiran, C., Heiter, U., & Jofré, P., Determining stellar atmospheric parameters and chemical abundances of FGK stars with iSpec. 2014, *Astronomy and Astrophysics*, **569**, A111, DOI:10.1051/0004-6361/201423945

Gajdoš, P., Parimucha, Š., Skarka, M., et al., Analysis of KIC 7023917: Spotted Low-mass Ratio Eclipsing Binary with δ Scuti Pulsations. 2024, *Astronomical Journal*, **168**, 171, DOI:10.3847/1538-3881/ad6dd3

Hadrava, P., KOREL - User's guide. 2004, *Publ. Astron. Inst. Czechosl. Acad. Sci.*, **92**, 15

Kabáth, P., Skarka, M., Sabotta, S., et al., Ondřejov Echelle Spectrograph, Ground Based Support Facility for Exoplanet Missions. 2020, *Publications of the ASP*, **132**, 035002, DOI:10.1088/1538-3873/ab6752

Shi, X.-D., Qian, S.-B., & Li, L.-J., New Pulsating Stars Detected in EA-type Eclipsing-binary Systems Based on TESS Data. 2022, *The Astrophysical Journal Supplement Series*, **259**, 50, DOI:10.3847/1538-4365/ac59b9

Contrib. Astron. Obs. Skalnaté Pleso **55/3**, 466 – 469, (2025)
https://doi.org/10.31577/caosp.2025.55.3.466

ObserPy: A tool for efficient observation planning in astronomy

B. Güler[1,2], **Ö. Baştürk**[2,3], **E.M. Esmer**[2,4], **E. Sertkan**[1,2] and **F. Akar**[1,2]

[1] *Ankara University, Graduate School of Natural & Applied Sciences, Astronomy & Space Sciences Department, Ankara, Türkiye*

[2] *Ankara University, Faculty of Science, Astronomy & Space Sciences Department, Ankara, Türkiye*

[3] *Ankara University, Astronomy & Space Sciences Research & Application Center, Kreiken Observatory, Incek Blvd., Ankara, Türkiye*

[4] *Department of Physics and McDonnell Center for the Space Sciences, Washington University, St. Louis, USA*

Received: November 15, 2024; Accepted: January 12, 2025

Abstract. ObserPy is an observation planning program developed in Python. It assists astronomers in selecting the most viable systems to observe based on specific criteria and time intervals, providing detailed information on optimal observation dates, scheduling, and log creation for each target.

Key words: python – observation planning

1. Introduction

Selecting a system for observing extrema in the light curves of variable stars can be challenging, especially when observers have numerous options but limited time. To address this, we developed ObserPy[1]—a Python-based application that helps observers identify the best systems to observe at any given time. It suggests optimal dates for observing a specific system within a set time frame and allows users to create detailed logs documenting each observation.

2. Key features of ObserPy

2.1. Sorting and altitude tracking

ObserPy lets users sort systems by observability, helping astronomers quickly identify which objects will be the "best" targets for the observations of extremum light levels at a given time. It provides altitude data so that users

[1] https://github.com/baris-guler/ObserPy

can track how the position of each object changes over time and the important timings such as light level minima. Additionally, ObserPy calculates the Moon's phase and altitude, which is useful for observers concerned about lunar conditions.

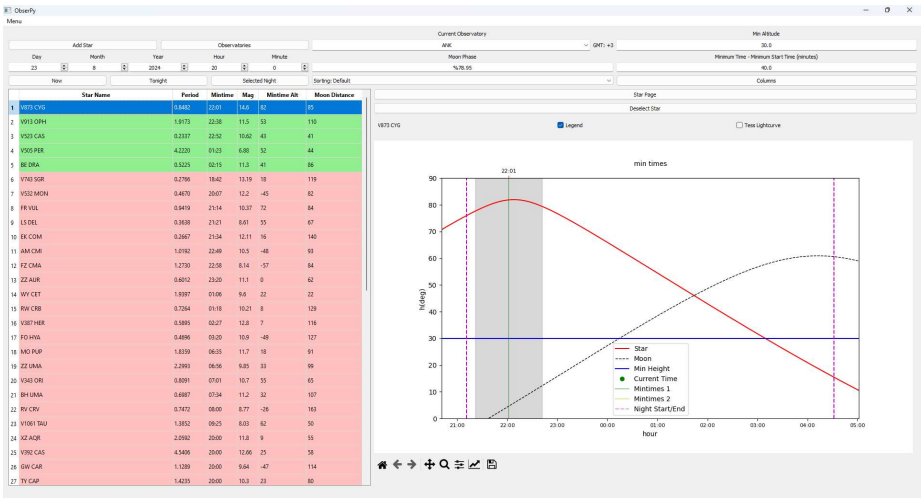


Figure 1. Sorting and altitude tracking in ObserPy

2.2. Custom scheduling and system-specific planning

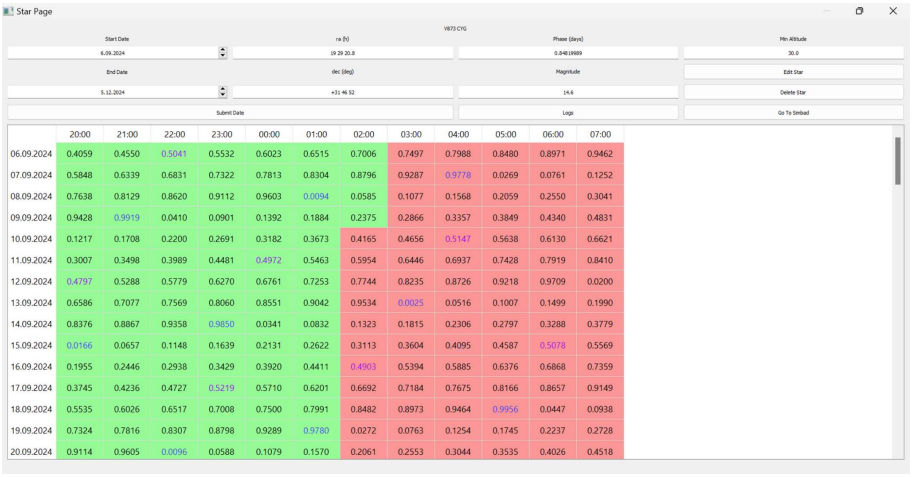
The program is ideal for building observing schedules for research proposals. It calculates observability and minima times within specific intervals, making it adaptable to various observation needs. It provides the data table as output, primarily in graphical format, making it unsuitable for automated or robotic observations unless the user specifically customizes it. Quick access to system data via the SIMBAD database is also provided.

2.3. Log creation for easy record-keeping

ObserPy makes it easy to save logs for each observation, with options to add details and up to two images that can be any .jpg or .png image related to the observation per entry. This feature supports consistent, organized record-keeping for future reference.

2.4. Open-source and customizable

As an open-source tool, ObserPy can be adjusted to suit individual research needs. Users can easily add new systems and observatories. Additionally, the



	20:00	21:00	22:00	23:00	00:00	01:00	02:00	03:00	04:00	05:00	06:00	07:00
06.09.2024	0.4059	0.4550	0.5041	0.5532	0.6023	0.6515	0.7006	0.7497	0.7988	0.8480	0.8971	0.9462
07.09.2024	0.5848	0.6339	0.6831	0.7322	0.7813	0.8304	0.8796	0.9287	0.9778	0.0269	0.0761	0.1252
08.09.2024	0.7638	0.8129	0.8620	0.9112	0.9603	0.0094	0.0585	0.1077	0.1568	0.2059	0.2550	0.3041
09.09.2024	0.9428	0.9919	0.0410	0.0901	0.1392	0.1884	0.2375	0.2866	0.3357	0.3849	0.4340	0.4831
10.09.2024	0.1217	0.1708	0.2200	0.2691	0.3182	0.3673	0.4165	0.4656	0.5147	0.5638	0.6130	0.6621
11.09.2024	0.3007	0.3498	0.3989	0.4481	0.4972	0.5463	0.5954	0.6446	0.6937	0.7428	0.7919	0.8410
12.09.2024	0.4797	0.5288	0.5779	0.6270	0.6761	0.7253	0.7744	0.8235	0.8726	0.9218	0.9709	0.0200
13.09.2024	0.6586	0.7077	0.7569	0.8060	0.8551	0.9042	0.9534	0.0025	0.0516	0.1007	0.1499	0.1990
14.09.2024	0.8376	0.8867	0.9358	0.9850	0.0341	0.0832	0.1323	0.1815	0.2306	0.2797	0.3288	0.3779
15.09.2024	0.0166	0.0657	0.1148	0.1639	0.2131	0.2622	0.3113	0.3604	0.4095	0.4587	0.5078	0.5569
16.09.2024	0.1955	0.2446	0.2938	0.3429	0.3920	0.4411	0.4903	0.5394	0.5885	0.6376	0.6868	0.7359
17.09.2024	0.3745	0.4236	0.4727	0.5219	0.5710	0.6201	0.6692	0.7184	0.7675	0.8166	0.8657	0.9149
18.09.2024	0.5535	0.6026	0.6517	0.7008	0.7500	0.7991	0.8482	0.8973	0.9464	0.9956	0.0447	0.0938
19.09.2024	0.7324	0.7816	0.8307	0.8798	0.9289	0.9780	0.0272	0.0763	0.1254	0.1745	0.2237	0.2728
20.09.2024	0.9114	0.9605	0.0096	0.0588	0.1079	0.1570	0.2061	0.2553	0.3044	0.3535	0.4026	0.4518

Figure 2. Altitude table for single system planning in ObserPy

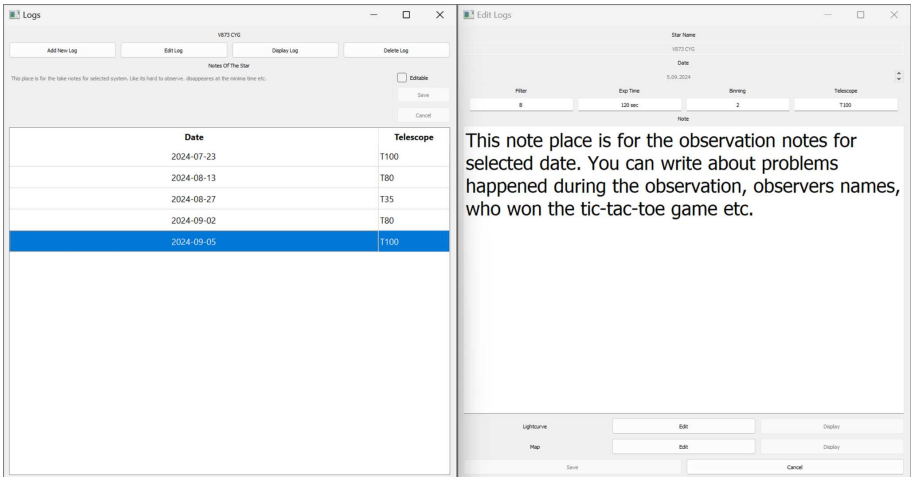


Figure 3. Log creation and management in ObserPy

code can be customized as needed, making ObserPy a flexible choice for astronomers.

2.5. Simple documentation

ObserPy includes straightforward documentation available through github, making it easy for new users to get started and explore its full capabilities.

3. Comparison with existing tools

Several observation planning tools, such as the Isaac Newton Group of Telescopes' Visibility Tool[2] and `Astroplan`[3], offer helpful features for planning. ObserPy, however, focuses on a simple design and easy use as well as the needs of variable star observers, making it a useful for them, who would like to know when and at which altitude their variable stars will be in extremum light levels.

Acknowledgements. The team gratefully acknowledge the support of TÜBİTAK under the research project 122F358, which made the development of ObserPy possible.

[2] https://astro.ing.iac.es/staralt/

[3] https://github.com/astropy/astroplan

Contrib. Astron. Obs. Skalnaté Pleso **55/3**, 470 – 473, (2025)
https://doi.org/10.31577/caosp.2025.55.3.470

Spectral variations of Be/shell star Pleione connected with its 218^d binary period

L. Iliev[1] **and A. Miroshnichenko**[2,3]

[1] *Institute of Astronomy, Bulgarian Academy of Sciences, Bulgaria (E-mail: liliev@astro.bas.bg, iliev_lubomir@yahoo.com)*

[2] *University of North Carolina, Greensboro, USA*

[3] *Fesenkov Astrophysical Institute, Almaty, Kazakhstan*

Received: November 15, 2024; Accepted: January 18, 2025

Abstract. Pleione is a prototype of a group of Be/shell stars that represent cyclic changes in their spectral appearance. The star was suspected to be a binary or multiple system . In the present study we are trying to obtain more precise picture of going on spectral changes of Pleione by data-mining in existing archives of Be stars spectral observations. New results reveal unknown before details about developments in the circumstellar envelope of Pleione, connected with the interactions in the system.

Key words: emission line stars – binary stars – Be stars – shell stars – circumstellar disks

1. Introduction

Pleione was proved as a binary system with 218.023^d period (see Nemravová et al., 2010, and references therein). Spectral variations of Pleione connected with it's binarity were reported by Pollmann (2018) and Iliev (2019). Iliev et al. (2023) described outburst of Hα emission based on observations from ESO-VLT. It was found that this outburst coincides with a periastron passage in Pleione's binary system. Here we report detailed study of a set of parameters of Hα emission line in the spectrum of the star during 4 other periastron passages in the binary system. Observations, used in the present study were retrieved from the archives of BeSS database (Neiner, 2018; Neiner et al., 2011), and Three College Observatory (North Caroline University, Greensboro, USA).

2. Results

1. There is obvious connection between episodes of increase of strength of Hα emission and binary solution with 218.023^d period of Pleione's.
2. Level of the central absorption core of Hα in such activity episodes significantly exceeds the continuum level in all of the measured observational sets.
3. As seen from Fig 1 and Fig 2, significant variations of the examined elements

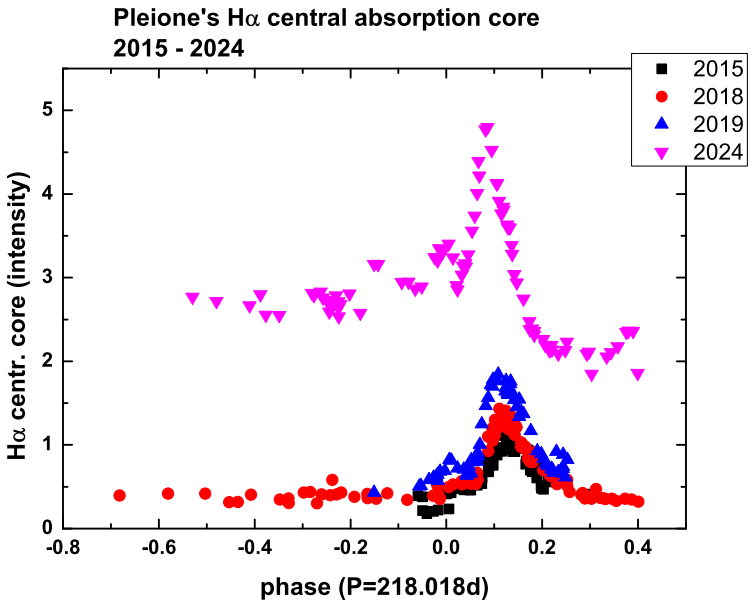


Figure 1. Variations of central absorption core of Hα emission in the spectrum of Pleione during periastron passages in 2015, 2018, 2019 and 2024.

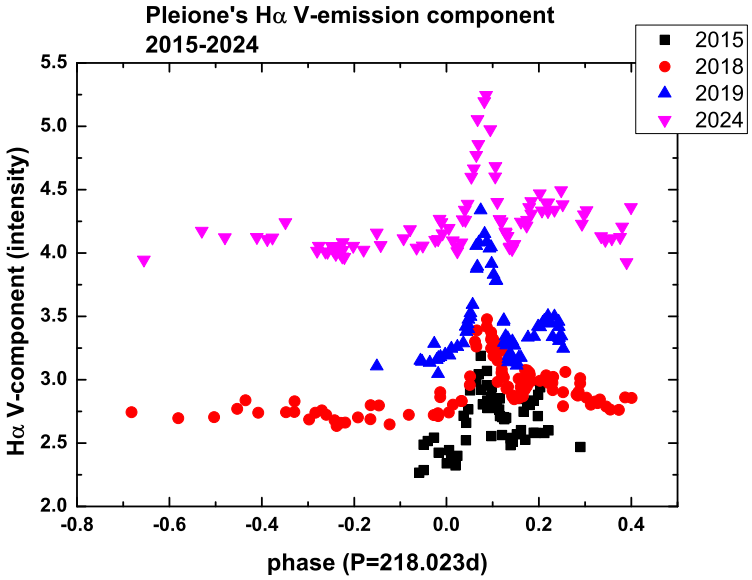


Figure 2. Variations of V-emission component of Hα in the spectrum of Pleione during periastron passages in 2015, 2018, 2019 and 2024.

of the Hα emission profile reach maximum approximately 20 days (at phase 0.1) after the periastron passage (which is at phase 0.0) and last until about phase 0.22. The overall increase of emission level in 2024 is connected with spectral-phase transition of Pleione, registered in 2022.
4. V-emission component passes through a secondary maximum on some of the cycles (Fig. 2) due to possible existence of structure in the emitting envelope around Pleione.
5. In a contrast, significant variations of the V/R ratio of Hα start immediately after the periastron passage (Fig. 3).

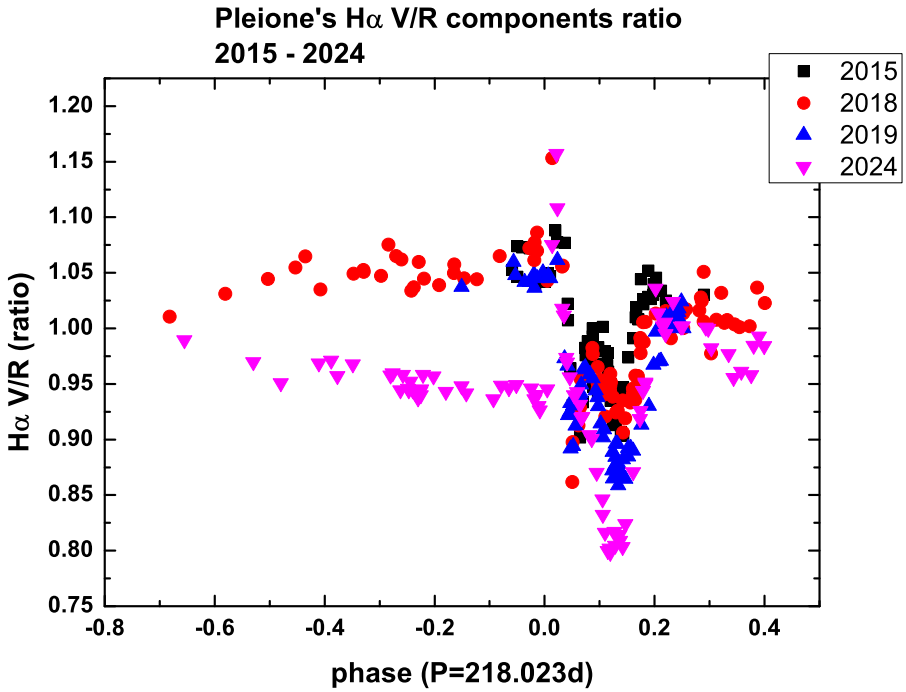


Figure 3. Variations of V/R ratio of Hα emission components in the spectrum of Pleione during periastron passages in 2015, 2018, 2019 and 2024.

Acknowledgements. The authors are extremely thankful to dozens of amateur astronomers that contributed to the Database of Be Star Spectra (BeSS) and to the organizers of the information in it for the excellent and very useful work. This work made intensive use of International Virtual Observatory tools and facilities.

References

Iliev, L., Binarity of Pleione and its influence on the circumstellar disk. 2019, in IAU Symposium, Vol. **346**, *High-mass X-ray Binaries: Illuminating the Passage from Massive Binaries to Merging Compact Objects*, ed. L. M. Oskinova, E. Bozzo, T. Bulik, & D. R. Gies, 149–151

Iliev, L., Kubat, J., Kubatova, B., & Dankova, L., Spectral activity episode of the Be-shell star Pleione in 2013-2018. 2023, *Bulgarian Astronomical Journal*, **39**, 3

Neiner, C., The BeSS database: a fruitful professional-amateur collaboration. 2018, in *SF2A-2018: Proceedings of the Annual meeting of the French Society of Astronomy and Astrophysics*, ed. P. Di Matteo, F. Billebaud, F. Herpin, N. Lagarde, J. B. Marquette, A. Robin, & O. Venot, Di

Neiner, C., de Batz, B., Cochard, F., et al., The Be Star Spectra (BeSS) Database. 2011, *Astronomical Journal*, **142**, 149, DOI:10.1088/0004-6256/142/5/149

Nemravová, J., Harmanec, P., Kubát, J., et al., Properties and nature of Be stars. 27. Orbital and recent long-term variations of the Pleiades Be star Pleione = BU Tauri. 2010, *Astronomy and Astrophysics*, **516**, A80, DOI:10.1051/0004-6361/200913885

Pollmann, E., Precession of the Disk in Pleione Study of the Halpha Line Profile. 2018, *Information Bulletin on Variable Stars*, **6239**, 1, DOI:10.22444/IBVS.6239

Contrib. Astron. Obs. Skalnaté Pleso **55/3**, 474 – 477, (2025)
https://doi.org/10.31577/caosp.2025.55.3.474

BD+48 873b - a brown dwarf companion candidate

R. Jaros[1], **A. Niedzielski**[1], **A. Wolszczan**[2] **and E. Villaver**[3,4]

[1] *Institute of Astronomy, Nicolaus Copernicus University, ul. Gagarina 11, 87-100 Toruń, Poland (E-mail: jaros@doktorant.umk.pl)*

[2] *Department of Astronomy and Astrophysics, Pennsylvania State University, 525 Davey Laboratory, University Park, PA 16802, USA*

[3] *Instituto de Astrofísica de Canarias, 38205 La Laguna, Tenerife, Spain*

[4] *Agencia Espacial Española (AEE), 41015 Sevilla, Spain*

Received: October 19, 2024; Accepted: January 7, 2025

Abstract. We report the discovery of a brown dwarf candidate around evolved star BD +48 873. Companion is located in eccentric orbit at around 5 AU semi-major axis, which places it in an exciting location at the edge of the theorized brown dwarf desert. We present the radial velocity data analysis results of brown dwarf parameters and the host star's characteristics.

Key words: brown dwarfs – binary – planets

1. Introduction

Pennsylvania-Torun Planet Search (PTPS) project monitored about 1000 objects in the northern hemisphere. Focused mostly on evolved stars, the sample contains a wide range of stars at various evolutionary stages. Here, we present one of the detected potential brown dwarf (BD) candidates orbiting BD+48 873, a giant star in a 5 AU orbit, placing it at the edge of the brown dwarf desert. Brown dwarfs are defined as objects between planets and stars in mass region of 13 - ∼75 M_J (Burrows et al. (2001)). Brown dwarf desert is a noticeable lack of those objects in region for orbits < 5 AU(Grether & Lineweaver (2006)). Radial velocity (RV) observations were mostly collected within the PTPS project, using the High-Resolution Spectrograph (HRS, Tull (1998)) at the Hobby-Eberly Telescope (HET, Ramsey et al. (1998)) with later additional follow-up with HARPS-N spectrograph at Telescopio Nazionale Galileo. Keplerian orbital fit parameters were modeled and posterior parameters determined with the RadVel PYTHON package (Fulton et al. (2018)).

2. The star, observations, and the keplerian model

BD+48 873 is a $T_{\rm eff}$= 4830± 10 K and $\log g$ = 2.70±0.03 cms^{-2} [Fe/H]=-0.12±0.06 intermediate-mass giant star with $logL/L_\odot$ = 1.81±0.16 and M=

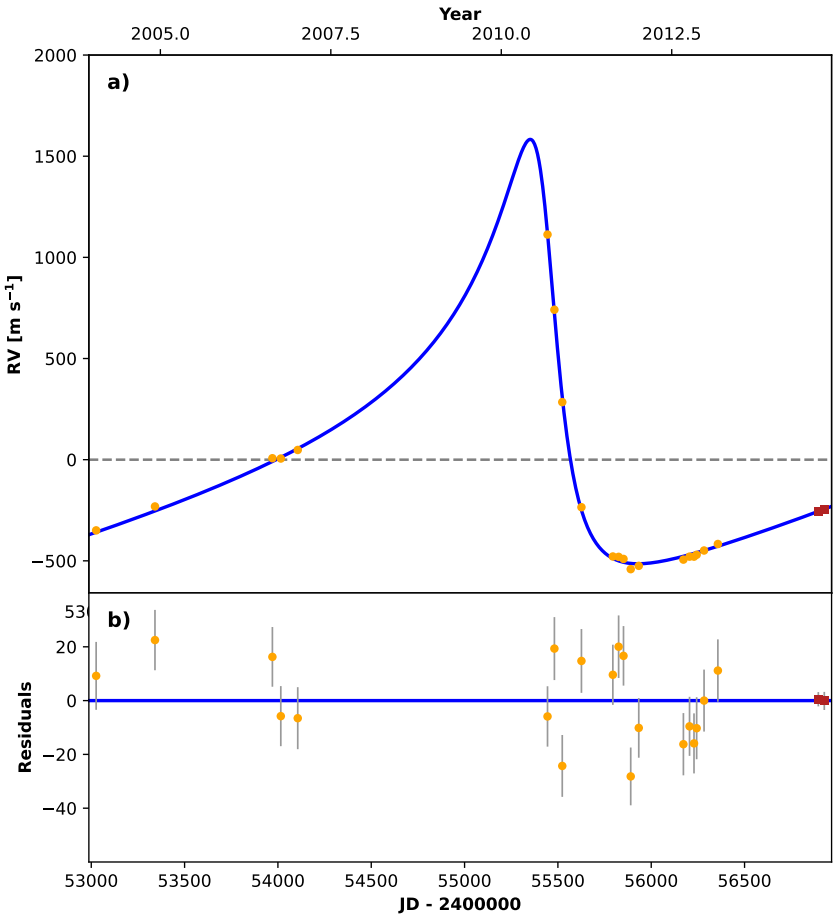


Figure 1. Timeseries with residuals of fitted RV signal for BD+48 873 star.

1.65±0.21 $M_\odot$ with brightness of V=8.31 mag. It belongs to the sample of twelve BD candidates with minimum masses of $m \sin i < 100$ M_J that have been identified in the PTPS sample (Niedzielski et al. (2013)).

Through almost 9 years of spectroscopic observations, 22 epochs have been gathered in total with HET/HRS and two additional epochs with HARPS-N/TNG. Typical uncertainty of HET/HRS data is ∼6 ms^{-1} and ∼3 ms^{-1} in the case of HARPS-N/TNG.

These data show the difference between the highest and lowest points leads

to conclusion that real radial velocity amplitude is higher than 1650 ms^{-1}, which is >250 times the HET/HRS uncertainty and a long-term variation.

We modeled these combined data with RadVel and obtained a keplerian orbit of 3686±83 days with a large eccentricity of 0.67±0.01 and semi-amplitude of 1052±43 ms^{-1}. The results are presented in the figure above. The upper panel (a) presents the timeseries of the collected data with modeled keplerian orbit. Yellow dots represent observations made by Hobby-Eberly Telescope. Red squares represent the follow-up observations made with HARPS-N. The lower panel (b) presents the radial velocity post-fit residuals showing the model fit quality. The uncertainties change is caused by stellar jitter fitting, making it bigger to adjust for that possible star effect.

3. Discussion

Table 1. Spectroscopic elements of BD+48 873.

Parameter	Value
P [d]	3686±83
T_c [d]	55498.7±5.3
e	0.67±0.01
ω [rad]	0.86±0.03
K [ms^{-1}]	1052±43
$m \sin i$ [$\mathrm{M_J}$]	83±10
a [AU]	5.52±0.32
σ_{jitter} [ms^{-1}]	16.8±4.3

Presented posterior value results were acquired in the first stage by using the Keplerian model fitting through the likelihood function. The fit was optimized with *scipy* package function *optimize.minimize* for finding the local minimum using Powell's method. For second stage of analysis to extract posterior values and uncertainties, *emcee* package's Affine Invariant Markov chain Monte Carlo (MCMC) Ensemble sampler algorithm was used (Goodman & Weare (2010)).

Within the estimated mass uncertainties, the object could appear to be a brown dwarf as it sits near the maximum of the BD mass region. However, it is highly uncertain about object classification, given the lack of known inclination, naming it instead as a very low mass (VLM) object. From the current estimate of parameters, we can conclude that this object can be categorized as sitting at the outer edge of a BD desert ($\sim$ 5AU). The Keplerian model presented is obviously based on a limited set of data points, not covering evenly the postulated orbit. This adds uncertainty to our detection. It is, therefore, important to

collect more observation epochs, specifically around the peak of the RV signal, to straighten the case.

Acknowledgements. This research was partly supported by "Excellence Initiative – Research University" programme through the Nicolaus Copernicus University in Torun. The HET is a joint project of the University of Texas at Austin, the Pennsylvania State University, Stanford University, Ludwig-Maximilians-Universität München, and Georg-August-Universität Göttingen. The HET is named in honor of its principal benefactors, William P. Hobby and Robert E. Eberly.

References

Burrows, A., Hubbard, W. B., Lunine, J. I., & Liebert, J., The theory of brown dwarfs and extrasolar giant planets. 2001, *Reviews of Modern Physics*, **73**, 719, DOI:10.1103/RevModPhys.73.719

Fulton, B. J., Petigura, E. A., Blunt, S., & Sinukoff, E., RadVel: The Radial Velocity Modeling Toolkit. 2018, *Publications of the ASP*, **130**, 044504, DOI:10.1088/1538-3873/aaaaa8

Goodman, J. & Weare, J., Ensemble samplers with affine invariance. 2010, *Communications in Applied Mathematics and Computational Science*, **5**, 65, DOI:10.2140/camcos.2010.5.65

Grether, D. & Lineweaver, C. H., How Dry is the Brown Dwarf Desert? Quantifying the Relative Number of Planets, Brown Dwarfs, and Stellar Companions around Nearby Sun-like Stars. 2006, *Astrophysical Journal*, **640**, 1051, DOI:10.1086/500161

Niedzielski, A., Wolszczan, A., Adamów, M., et al., Brown dwarf candidates from the PennState-Toruń Planet Search with the Hobby-Eberly Telescope . 2013, *Mem. Societa Astronomica Italiana*, **84**, 1035

Ramsey, L. W., Adams, M. T., Barnes, T. G., et al., Early performance and present status of the Hobby-Eberly Telescope. 1998, in Society of Photo-Optical Instrumentation Engineers (SPIE) Conference Series, Vol. **3352**, *Advanced Technology Optical/IR Telescopes VI*, ed. L. M. Stepp, 34–42

Tull, R. G., High-resolution fiber-coupled spectrograph of the Hobby-Eberly Telescope. in , *Optical Astronomical Instrumentation*, Vol. **3355**, SPIE, 387–398

Contrib. Astron. Obs. Skalnaté Pleso **55/3**, 478 – 480, (2025)
https://doi.org/10.31577/caosp.2025.55.3.478

The first orbital period investigation of low mass ratio systems from Catalina Sky Survey

L. Lantzi and P.-E. Christopoulou

Department of Physics, University of Patras, 26500, Patra, Greece
(E-mail: up1066348@ac.upatras.gr)

Received: November 18, 2024; Accepted: February 6, 2025

Abstract. We present the first results of our project to analyze the orbital period variations of 5 newly discovered low-mass ratio (LMR) eclipsing binaries from the Catalina survey. We collected data from CRTS, LINEAR, SUPERWASP, ASSASN, ZTF, and ATLAS, covering a time of $10 - 15$ years, and determined the mid-eclipse times by fitting our CSS light curve model and varying the conjunction times. Analyzing the ETVs the highest rate of period variation was found in the order of 10^{-6} days/year and only in one case, we derive an additional light-time effect and a period of a possible third body of 12.8 yr.

Key words: contact binaries- eclipsing binaries - period variation

1. Introduction

In the era of large surveys contact binaries remain one of the most interesting research fields of astrophysics as they provide unique insights into the study of binary evolution, including mass and energy transfer in the common envelope. The low mass ratio (LMR) contact binaries present particular interest as they can lead to mergers and appear as peculiar stars such as blue stragglers and fast-rotating FK Com stars (Rasio, 1995; Wadhwa et al., 2021). A well-known technique for investigating period variations in eclipsing binaries is the analysis of eclipse time variations (ETVs) via O-C. Here we present the first results of our project to analyze the orbital period variations of the newly discovered LMRs (Christopoulou et al., 2022) from the Catalina Sky Survey (CSS; Drake et al., 2014): Obj 1($q = 0.080 \pm 0.015$), Obj 2 ($q = 0.110 \pm 0020$), Obj 3 ($q = 0.110 \pm 0015$), Obj 4 ($q = 0.120 \pm 0025$), and Obj 5 ($q = 0.220 \pm 0015$).

1.1. O-C diagram analysis

We constructed O-C diagrams with archival data from ATLAS, CRTS, ASSAS-SN, LINEAR, NSVS, and ZTF covering a period of 15-25 years. We used the ephemeris (HJD_0, P_{bin}) and the CSS light curve model from (Christopoulou et al., 2022) to determine the mid-eclipse times by fitting the phased light curve from every survey. We used PHOEBE-0.31 (Prsa & Zwitter, 2005) to fit the light curve model using the parameters of Christopoulou et al. (2022). Limb-darkening coefficients were interpolated from van Hamme (1993) tables for the

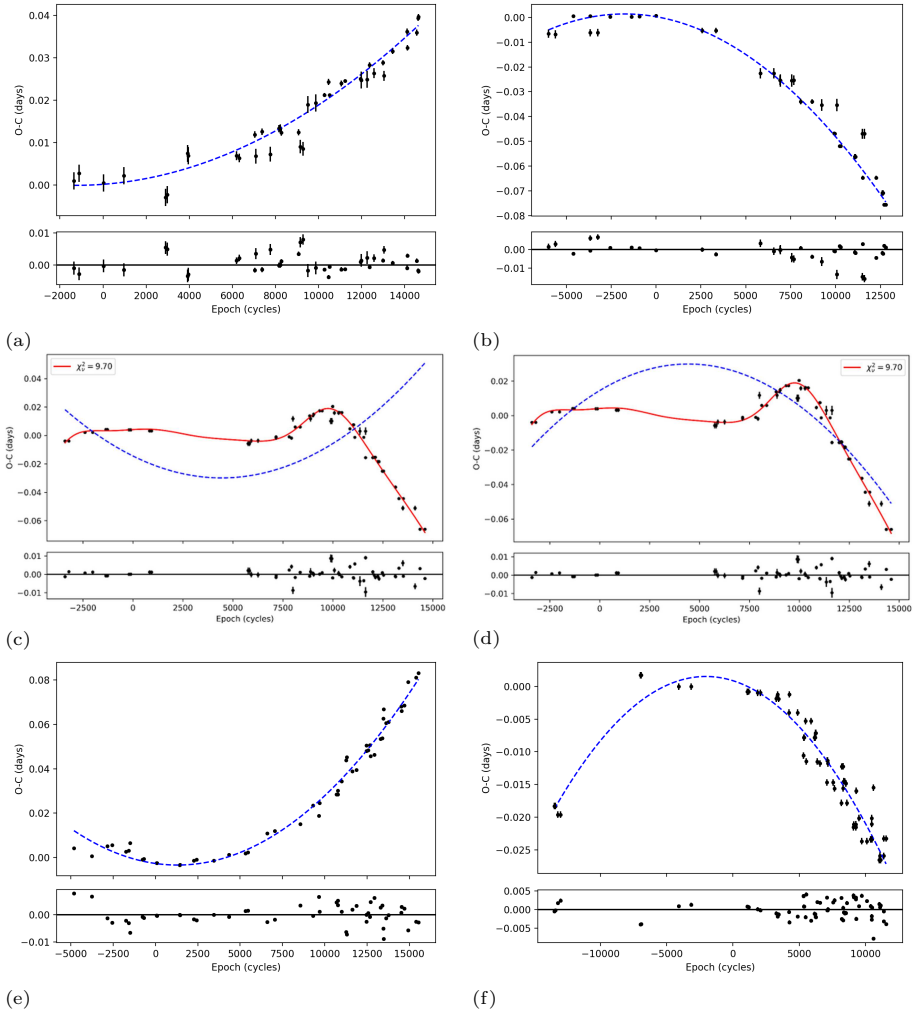


Figure 1. The O-C versus epoch of the five LMRs: (a) Obj 1, (b) Obj 2, (c) and (d) Obj 3, (e) Obj 4 and (f) Obj 5. Upper panel: the dashed line represents the quadratic curve and the solid line the cyclic curve. Lower panel: the residuals.

given temperatures while gravity-darkening coefficients g and surface albedos A were accordingly assumed for convective ($g = 0.32$, $A = 0.5$) envelopes as all objects have $T < 7200$ K. The (O-C) curves are plotted in Fig.1 together with the residuals in the lower panel. The following equation is applied to fit the O-C curves

$$O - C = \Delta HJD_0 + \Delta P + (dP/dE) \times E^2 + \tau. \quad (1)$$

where ΔHJD_0 is the modification value of the initial epoch, ΔP the correction of the orbital period, dP/dE the rate of orbital period variation in the long term, and τ is related to more complex periodic variations such as the third body light time orbital effect (LTTE) or periodic magnetic activity.

2. Preliminary results and conclusions

Our preliminary analysis of five new LMRs shows that the general trend of objects 1 and 4 O-C curves is an upward parabola, which means that the period is slowly increasing. For objects 2 and 5, it is downward, which means that the period is decreasing. An alternative description is that the parabolic line may be a segment of a cyclic variation. The O-C curve of object 3 is a more complex one and reveals the possible existence of a third body or the action of a magnetically active primary (Applegate mechanism), therefore, future monitoring of the system is required. The results of dP/dt and dM/dt rates are in agreement with other investigations of low mass ratio systems (Liu et al., 2023).

References

Christopoulou, P.-E., Lalounta, E., Papageorgiou, A., et al., New low mass ratio contact binaries in the Catalina Sky Survey. 2022, *Monthly Notices of the RAS*, **512**, 1244, DOI:10.1093/mnras/stac534

Drake, A. J., Graham, M. J., Djorgovski, S. G., et al., VizieR Online Data Catalog: Catalina Surveys periodic variable stars (Drake+, 2014). 2014, *VizieR Online Data Catalog*, J/ApJS/213/9

Liu, X.-Y., Li, K., Michel, R., et al., The study of 11 contact binaries with mass ratios less than 0.1. 2023, *Monthly Notices of the RAS*, **519**, 5760, DOI:10.1093/mnras/stad026

Prsa, A. & Zwitter, T., Introducing Adapted Nelder & Mead's Downhill Simplex Method to a Fully Automated Analysis of Eclipsing Binaries. 2005, in ESA Special Publication, Vol. **576**, *The Three-Dimensional Universe with Gaia*, ed. C. Turon, K. S. O'Flaherty, & M. A. C. Perryman, 611

Rasio, F. A., The Minimum Mass Ratio of W Ursae Majoris Binaries. 1995, *Astrophysical Journal, Letters*, **444**, L41, DOI:10.1086/187855

van Hamme, W., New Limb-Darkening Coefficients for Modeling Binary Star Light Curves. 1993, *Astronomical Journal*, **106**, 2096, DOI:10.1086/116788

Wadhwa, S. S., De Horta, A., Filipović, M. D., et al., ZZ Piscis Austrinus (ZZ PsA): a bright red nova progenitor and the instability mass ratio of contact binary stars. 2021, *Monthly Notices of the RAS*, **501**, 229, DOI:10.1093/mnras/staa3637

Contrib. Astron. Obs. Skalnaté Pleso **55/3**, 481 – 483, (2025)
https://doi.org/10.31577/caosp.2025.55.3.481

The double star catalogs of the USNO

B.D. Mason and R.A. Matson

U.S. Naval Observatory, 3450 Massachusetts Ave., Washington, DC, USA
(E-mail: brian.d.mason.civ@us.navy.mil)

Received: October 29, 2024; Accepted: December 30, 2024

Abstract. Since 1964 the US Naval Observatory (USNO) has been charged with maintaining and distributing double star catalogs. Beginning later in 2025 all four of our catalogs will be available online for the first time. These include:

1. The Washington Double Star (WDS) Catalog contains the epochs, position angles, separations, magnitudes, spectral types, proper motions and precise positions of classic double and multiple stars.
2. The WDS Supplement (WDSS) is a database for large duplicity surveys.
3. The Sixth Catalog of Orbits of Visual Binary Stars (ORB6) contains 3,655 orbits of 3,539 systems from a master file database of 10,685 orbits.
4. The Second Catalog of Rectilinear Elements (LIN2) contains 1,288 linear fits for systems whose motions do not appear to be Keplerian.

These last two catalogs are not discussed here.

Key words: binary stars – multiple stars

1. Washington Double Star (WDS) catalog

The Washington Double Star (WDS) Catalog (Mason et al., 2001) currently consists of 156,861 systems based on 2,216,034 measures. It includes a summary of relative positions, precise position, proper motions, cross reference identifier, spectral types, and notes to other data sets or catalogs. The WDS is successor to the Index Catalog of Double Stars (Jeffers et al., 1963) which was codified at the Commission 26 (Double & Multiple Stars) meeting at the 1964 International Astronomical Union General Assembly (van de Kamp, 1966). The summary catalog is available online or as a VizieR overlay and is updated regularly.

While perusal of literature for double star measures from classic techniques has always been fruitful, the WDS has been matched with astrometric catalogs, primarily those used for the determination of proper motion for other astrometric catalogs produced at the USNO. These catalogs have significantly improved the identification of pairs with their precise position such that 97% of them have at least arcsecond-precise positions. Also the proper motion of the secondary is now provided for 38% of all pairs, aiding in the identification of common proper motion binaries and optical doubles. Pairs having common or mutually exclusive parallaxes are also indicated. The average number of measures per system

has increased from 6.7 in 2001 to over 14 measures per system today. Many identified binaries from Gaia DR2 and DR3 have been matched with previously known WDS pairs and added to the catalog.

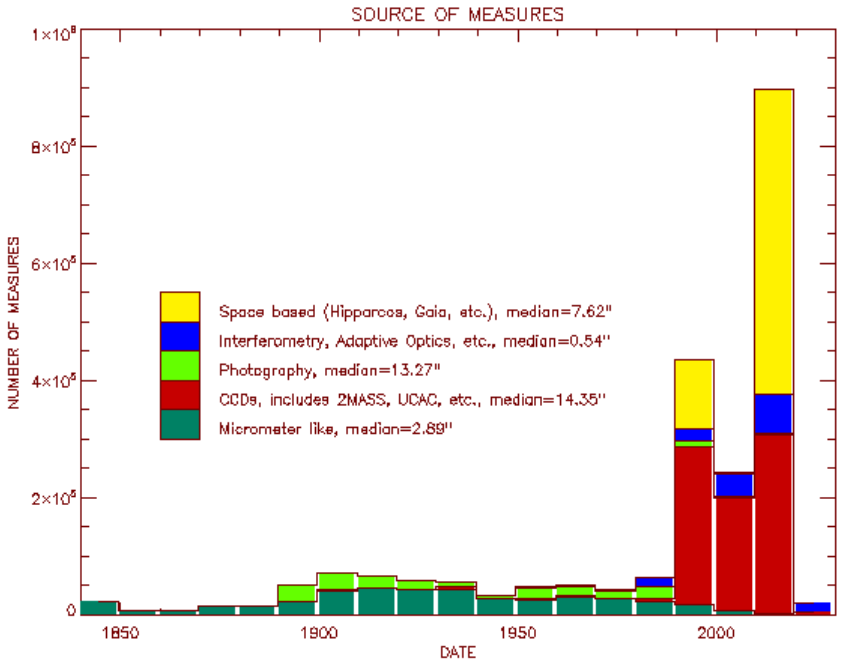


Figure 1. Observation types in WDS vs. time

The source of WDS measures versus time is shown in Figure 1. The median separation of each broad data-type is given as well. The majority of the data classified as CCD is from matching like that described above.

Historically, only the summary version of the WDS was available online with all measures of individual systems delivered on demand. However, we anticipate making the entire measurements database accessible in mid 2025.

2. Washington Double Star Supplemental (WDSS) catalog

With the advent of these new discoveries in the Era of Big Sky Surveys, the historical 10-digit WDS designation was of insufficient precision for the number of new pairs. However, as a Designation it could not be changed. Also, the vast number of these new pairs created difficulties in searching for these well-observed historical pairs. The Washington Double Star Supplemental Catalog (WDSS) is a database created for these large, faint duplicity surveys. It currently consists of 2,428,631 systems based on 11,245,028 measures. The WDSS has

shown significant and rapid growth since the mid 2017 initial release, primarily due to Gaia. Figure 2 indicates the number of measures compared with the WDS: it currently has 5× as many measures and 15× as many systems.

The entire WDSS is available online.

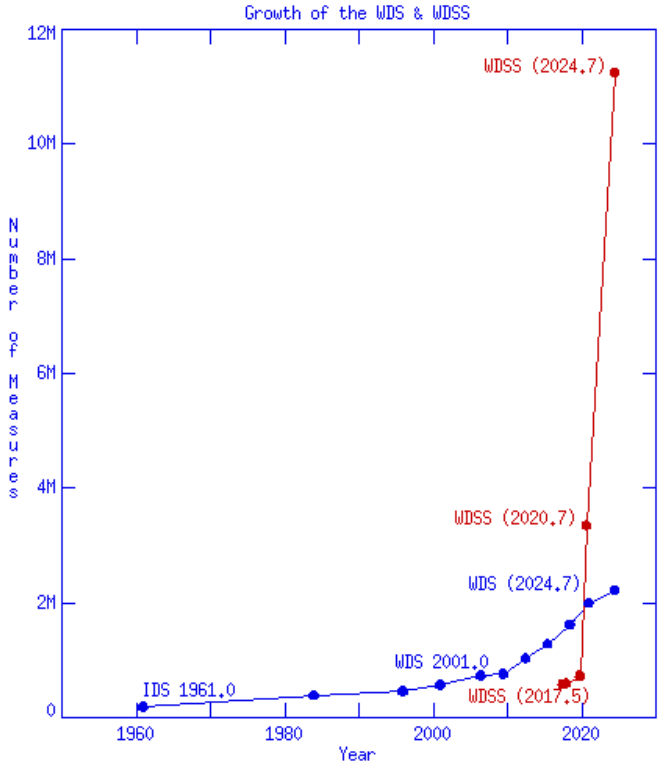


Figure 2. In the plot above the number of WDS measures (blue) is shown with the number of WDSS measures, keyed to the left axis.

References

Jeffers, H. M., van den Bos, W. H., & Greeby, F. M. 1963, *Index Catalogue of Visual Double Stars, 1961.0*

Mason, B. D., Wycoff, G. L., Hartkopf, W. I., Douglass, G. G., & Worley, C. E., The 2001 US Naval Observatory Double Star CD-ROM. I. The Washington Double Star Catalog. 2001, *Astronomical Journal*, **122**, 3466, DOI:10.1086/323920

van de Kamp, P., Etoiles Doubles (Double Stars). 1966, *Transactions of the International Astronomical Union, Series B*, **12B**, 267

Contrib. Astron. Obs. Skalnaté Pleso **55/3**, 484 – 486, (2025)
https://doi.org/10.31577/caosp.2025.55.3.484

Kinematic solutions in the Washington Double Star catalog: adding 169,000 orbits to the Visual Orbit catalog

R.A. Matson[1], **B.D. Mason**[1] **and S. Stepanoff**[1,2]

[1] *U.S. Naval Observatory, 3450 Massachusetts Avenue NW, Washington, D.C. 20392, USA (E-mail: rachel.a.matson2.civ@us.navy.mil)*

[2] *Georgia Institute of Technology, North Avenue, Atlanta, GA 30332, USA*

Received: November 15, 2024; Accepted: January 3, 2025

Abstract. The Washington Double Star catalogs, maintained by the US Naval Observatory, are the world's principal database of astrometric double and multiple star information. Double stars showing significant relative motion are catalogued in the Sixth Catalog of Orbits of Visual Binary Stars (ORB6), a compilation of visual and astrometric orbits of more than 3500 binaries, and the Second Catalog of Rectilinear Elements (LIN2). The current status of each catalog and ongoing work to produce a new orbit catalog incorporating the ∼160,000 astrometric obits from Gaia DR3 are presented.

Key words: binary stars – multiple stars

1. Introduction

The US Naval Observatory (USNO) double star catalogs include kinematic solutions for stars showing significant relative motion. The Sixth Catalog of Orbits of Visual Binary stars[1] (ORB6; Hartkopf et al., 2001) is part of a series of compilations of visual binary star orbits begun in the 1930's. The Second Catalog of Rectilinear Elements[2] (LIN2) provides linear fits for pairs of stars whose motion does not appear to be Keplerian. LIN2 was most recently updated in July 2024 and contains linear fits for 1,288 pairs.

2. The Sixth Catalog of Orbits of visual binary stars

ORB6 currently contains 3,655 orbits of 3,539 systems and is updated regularly using orbits published in the literature. The catalog provides the J2000 coordinates, Washington Double Star (WDS; Mason et al., 2001) designation, orbital elements, grades, notes, and references, as well as additional parameters

[1]https://crf.usno.navy.mil/wds-orb6
[2]https://crf.usno.navy.mil/wds-lin2

and ephemerides for each system. Each orbit is graded from 1 (definitive) to 5 (tentative) based on the orbital coverage, weighted rms residuals, and number of revolutions observed. While primarily made up of visual orbits, the catalog also contains ∼40 incomplete (grade 7), ∼20 interferometric (grade 8), and ∼500 astrometric (grade 9) orbits.

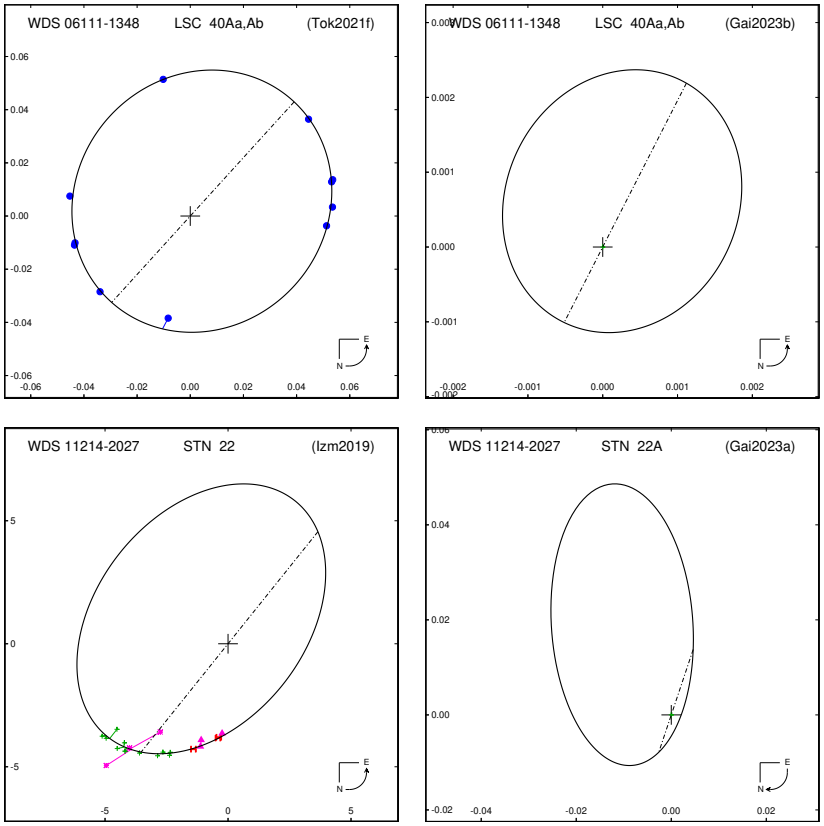


Figure 1. Examples of common (top) and hierarchical (bottom) systems from ORB6 (left) and Gaia DR3 (right). Visual observations are color-coded by technique (blue = speckle, green = micrometry, pink = space-based, red = CCD).

3. The Seventh Catalog of Orbits of visual binary stars

Gaia DR3 (Gaia Collaboration et al., 2023) includes a catalog of non-single-stars with astrometric orbital solutions for approximately 169,000 binary stars (Halbwachs et al., 2023; Holl et al., 2023). As a majority of the DR3 astrometric orbits have periods less than 1000 days, ORB6 serves as an overlapping and

complementary sample. We are therefore working on a new version of the orbit catalog (ORB7) that will include DR3 astrometric orbits, enabling comparisons between orbits and the identification of hierarchical systems.

We performed a crossmatch between ORB6+WDS and the DR3 astrometric orbits, then split the existing orbit catalog by visual vs. astrometric orbits. Preliminary grades were determined for DR3 astrometric orbits (9.1 – 9.9) based on the orbit significance, efficiency, and number of observations. Verification of the 34 (1800) tentative matches between ORB6 (WDS) and DR3 astrometric orbits is currently underway. The names and Campbell orbital elements for an example common (WDS 06111-1348) and possible hierarchical system (WDS 11214-2027) are provided in Table 1 and the orbits are shown in Figure 1.

Table 1. Orbital elements of common systems in ORB6 and Gaia DR3

Name	P (y)	a ($''$)	i ($^\circ$)	Ω ($^\circ$)	T (y)	e	ω ($^\circ$)	Grade
WDS 06111-1348 Aa,Ab	2.5	0.051	21.1	137.7	2020.0	0.14	184.6	2.2
DR3 2994437527894182272	2.2	0.002	21.6	152.9	2015.2	0.37	184.4	9.5
WDS 11214-2027 AB	1028.1	6.532	49.3	141.3	2072.5	0.35	267.2	5.4
DR3 3545469496823737856	13.4	0.054	110.2	161.5	2016.6	0.90	107.7	9.5

For Gaia DR3 orbits, a$''$ is the semi-major axis of the photocentric orbit (a_0).

References

Gaia Collaboration, Vallenari, A., Brown, A. G. A., et al., Gaia Data Release 3. Summary of the content and survey properties. 2023, *Astronomy and Astrophysics*, **674**, A1, DOI:10.1051/0004-6361/202243940

Halbwachs, J.-L., Pourbaix, D., Arenou, F., et al., Gaia Data Release 3. Astrometric binary star processing. 2023, *Astronomy and Astrophysics*, **674**, A9, DOI:10.1051/0004-6361/202243969

Hartkopf, W. I., Mason, B. D., & Worley, C. E., The 2001 US Naval Observatory Double Star CD-ROM. II. The Fifth Catalog of Orbits of Visual Binary Stars. 2001, *Astronomical Journal*, **122**, 3472, DOI:10.1086/323921

Holl, B., Sozzetti, A., Sahlmann, J., et al., Gaia Data Release 3. Astrometric orbit determination with Markov chain Monte Carlo and genetic algorithms: Systems with stellar, sub-stellar, and planetary mass companions. 2023, *Astronomy and Astrophysics*, **674**, A10, DOI:10.1051/0004-6361/202244161

Mason, B. D., Wycoff, G. L., Hartkopf, W. I., Douglass, G. G., & Worley, C. E., The 2001 US Naval Observatory Double Star CD-ROM. I. The Washington Double Star Catalog. 2001, *Astronomical Journal*, **122**, 3466, DOI:10.1086/323920

Contrib. Astron. Obs. Skalnaté Pleso **55/3**, 487 – 489, (2025)
https://doi.org/10.31577/caosp.2025.55.3.487

Revisiting the unique qWR – B7V composite binary HD 45166

P. Németh[1], O. Maryeva[2], E.S.G. de Almeida[3], J.P. Sánchez Arias[2], M. Kraus[2], J. Vos[2], J. Kubát[2], M. Vučković[3] and B. Doležalová[2]

[1] *Astroserver.org, Fő tér 1, 8533 Malomsok, Hungary*
(E-mail: peter.nemeth@astroserver.org)

[2] *Astronomical Institute of the Czech Academy of Sciences*
251 65 Ondřejov, The Czech Republic

[3] *Instituto de Física y Astronomía, Universidad de Valparaíso. Av. Gran Bretaña 1111, 2360102 Valparaíso, Chile*

Received: November 14, 2024; Accepted: January 13, 2025

Abstract. We applied wavelength space binary spectral disentangling for a FEROS observation of HD 45166 and derived the atmospheric parameters of the binary components. Our results suggest a B7V-type companion in the system and prefer a lower mass solution for the quasi-WR primary than previous analyses, resembling a He-rich sdO star.

Key words: massive stars – composite spectrum binaries

1. Introduction

The one-of-a-kind composite spectrum binary HD 45166 astonished spectroscopists for decades. The emission line component resembles a Wolf-Rayet (WR) star and the companion is proposed to be a late B-type star. Comprehensive studies for precise stellar and wind parameters have been performed. Groh et al. (2008) found wind asymmetries in the quasi-WR (qWR) star and Shenar et al. (2023) found pulsations in the B star and a strong magnetic field in the qWR, which is believed to be the precursor of a magnetar. Although these comprehensive studies recognized the composite nature of the object, they did not resolve or analyze the members of the system.

Here we apply the latest version of XTGRID to address the composite spectrum. We modeled the binary members in parallel and coadded the individual models to fit a FEROS observation with the linear combination of two synthetic spectra. We took the best of two worlds and modeled the B7V component with TLUSTY v208 and the qWR component with the 2017 version of CMFGEN. This is the first time the two codes are connected to model the components of a physical binary.

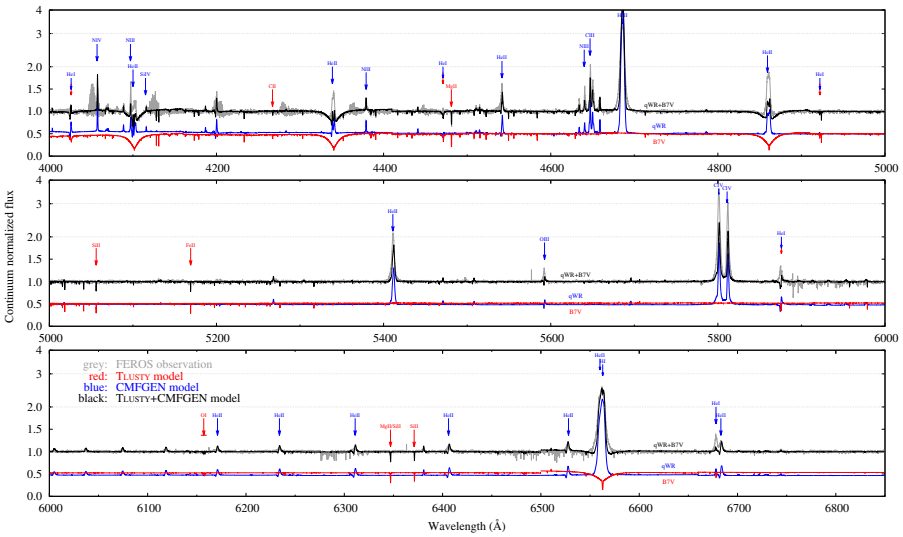


Figure 1. Our near-best-fit XTGRID / TLUSTY+CMFGEN composite model for HD 45166 shown in *black*. The FEROS observation is in *grey*, the CMFGEN model is in *blue*, and the TLUSTY model is shown in *red*. Line identifications for the B7V star are in *red* and for the qWR component in *blue*. The model parameters are available on request.

2. Spectral modeling with TLUSTY and CMFGEN

We processed one FEROS spectrum to show that non-LTE radiative transfer models calculated with TLUSTY and CMFGEN are perfectly adequate to derive the stellar and wind parameters. Our iterative, data-driven spectral analysis pipeline XTGRID determines the surface properties of the stars by managing 36 free parameters and using a robust chemical composition including heavy elements such as Fe and Ni. Along the spectral modeling of the observation as in Figure 1, the actual CMFGEN+TLUSTY model was used to predict the binary spectral energy distribution (SED), which is compared to observed broad-band photometric data from VizieR in Figure 2.

3. Results

Our main result is the reclassification of the qWR component as a He-dominated hot subdwarf (sdO) star, which is based on the SED contributions of the binary members and the resulting lower mass of the primary. This suggests a recent merger event in an initially triple system, where the B-star was the distant tertiary component. The disrupted lower-mass companion formed a hot

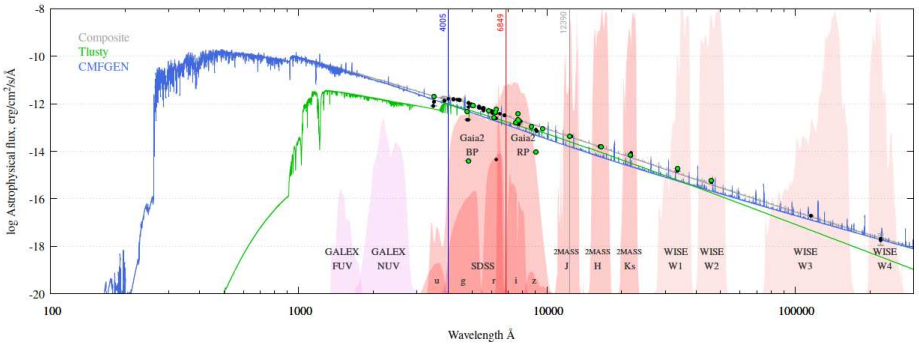


Figure 2. SED of HD 45166. All data points were taken from the VizieR Photometry Viewer service. The photometric data were de-reddened using $E(B-V) = 0.16$ mag (stilism.obspm.fr). The green points were used to match the slope of the passband convolved combined CMFGEN and TLUSTY fluxes to the observations and the model was normalized to the observed SED in the 2MASS/J band.

corona around the more massive star in the inner binary, potentially exhibiting a magnetic field.

Although based on a single spectrum, our findings highlight the importance of binary disentangling in exploring the system properties. With appropriately stacked models, one can reproduce the members' surface properties. The orbital parameters will become available once all spectra are processed. That will allow us to determine the dynamic mass ratio from radial velocity measurements, and reconcile the spectral and photometric variability of the system. Our results demonstrate that wavelength space decomposition, using the right combination of hydrostatic plane-parallel and spherical wind models, is effective for modeling HD 45166, and similar systems.

Acknowledgements. This project has received funding from the European Union's Framework Programme for Research and Innovation Horizon 2020 (2014-2020) under the Marie Skłodowska-Curie Grant Agreement No. 823734. The research which led to the results was supported by the Grant Agency of the Czech Republic (GAČR 22-34467S).

References

Groh, J. H., Oliveira, A. S., & Steiner, J. E., The qWR star HD 45166. II. Fundamental stellar parameters and evidence of a latitude-dependent wind. 2008, *Astronomy and Astrophysics*, **485**, 245, DOI:10.1051/0004-6361:200809511

Shenar, T., Wade, G. A., Marchant, P., et al., A massive helium star with a sufficiently strong magnetic field to form a magnetar. 2023, *Science*, **381**, 761, DOI:10.1126/science.ade3293

Contrib. Astron. Obs. Skalnaté Pleso **55/3**, 490 – 492, (2025)
https://doi.org/10.31577/caosp.2025.55.3.490

Binary stars in Pennsylvania-Toruń Planet Search

A. Niedzielski[1], **A. Wolszczan**[2,3], **R. Jaros**[1] and **B. Deka-Szymankiewicz**[1]

[1] *Institute of Astronomy, Nicolaus Copernicus University in Toruń, Gagarina 11, 87-100 Toruń, Poland (E-mail: Andrzej.Niedzielski@umk.pl)*

[2] *Department of Astronomy and Astrophysics, Pennsylvania State University, 525 Davey Laboratory, University Park, PA 16802, USA*

[3] *Center for Exoplanets and Habitable Worlds, Pennsylvania State University, 525 Davey Laboratory, University Park, PA 16802, USA*

Received: December 16, 2024; Accepted: January 13, 2025

Abstract. We present preliminary results of binary star frequency study within the Pennsylvania-Toruń Planet Search sample.

Key words: stares: late type – stars:binary

1. Introduction

The Pennsylvania-Toruń Planet Search (PTPS) is one of the most extensive RV searches for exoplanets around evolved stars. The project was designed to use the Hobby-Eberly Telescope (HET; Tull 1998) and its High-Resolution Spectrograph (HRS; Ramsey et al. 1998). It has surveyed a sample of stars distributed across the northern sky, with the typical, apparent V magnitudes between 7.5 and 10.5 mag, and the B–V colour indices between 0.6 and 1.3. On the Hertzsprung-Russell diagram, these stars occupy an area delimited by the MS, the instability strip, and the coronal dividing line Linsky & Haisch (1979). In total, the program sample of 885 stars contains 515 giants, 238 subgiants, and 132 dwarfs Deka-Szymankiewicz et al. (2018). A detailed description of this sample, including their atmospheric and integrated parameters (masses, luminosities, and radii), is presented in a series of papers: Zieliński et al. (2012); Adamów et al. (2014); Niedzielski et al. (2016); Adamczyk et al. (2016); Deka-Szymankiewicz et al. (2018). The first detection of a gas giant orbiting a red giant star by the PTPS project was reported by Niedzielski et al. (2007). The project is continued within the TAPAS (Tracking Advanced Planetary Systems) project with Harps-N Niedzielski et al. (2015), and over 30 exoplanets were detected so far.

2. The sample and the data

This research project is based on existing, unpublished high precision (typical uncertainty of 6-9 m s^{-1}) radial velocity (RV) measurements collected between 2004 and 2014 with HET/HRS.

After acquiring multiple epochs of RV, many of these stars were found to be unsuitable for further observations aiming at planetary-mass companions detection. They either presented RV variations of up to 50 m s^{-1} and, were rejected as potentially single stars, or were found to be RV variables at a level above 2000 m s^{-1} and were rejected as potentially stellar binaries.

Altogether, several thousands of precise multi-epoch RVs will be used in this study of 517 stars. The sample contains 83 dwarfs, 162 subgiants, and 272 giants from the entire PTPS sample. The main goal is to present results for the new spectroscopic binaries identified in the sample. Our coarse analysis of the data shows that our sample contains 51 new SBs with enough data to present orbital solutions, 45 systems with not enough data for orbital solutions, for which only preliminary system parameters can be presented based on HET/HRS data alone.

3. Binary and multiple stars in PTPS

First (preliminary) estimates of binary frequency in our sample show that: among dwarfs 11±5% stars are spectroscopic binaries, 59±8% appear to be single and 30±7% stars are potentially hosts of low-mass companions; 18±5% of subgiants are spectroscopic binaries, 55±6% are single stars, and 27±5% are potentially hosts of low-mass companions; 14±3% of giants appear binary, 43±4% are single, and 43±4% represent potential planetary/BD-mass companions and/or active stars.

We note that our estimates of single stars fractions among dwarfs 57±4% and subgiants 53±3% are consistent with results of Raghavan et al. (2010) 54±2%. Also our estimate of spectroscopic binaries fraction among (K) giants 15±2% is in agreement with results of Famaey et al. (2005) - 13.7%.

Acknowledgements. The HET is a joint project of the University of Texas at Austin, the Pennsylvania State University, Stanford University, Ludwig-Maximilians-Universität München, and Georg-August-Universität Göttingen. The HET is named in honor of its principal benefactors, William P. Hobby and Robert E. Eberly. This research was partly supported by "Excellence Initiative – Research University" programme through the Nicolaus Copernicus University in Toruń.

References

Adamczyk, M., Deka-Szymankiewicz, B., & Niedzielski, A., Masses and luminosities for 342 stars from the PennState-Toruń Centre for Astronomy Planet Search. 2016, *Astronomy and Astrophysics*, **587**, A119, DOI:10.1051/0004-6361/201526628

Adamów, M., Niedzielski, A., Villaver, E., Wolszczan, A., & Nowak, G., The Penn State - Toruń Centre for Astronomy Planet Search stars. II. Lithium abundance analysis of the red giant clump sample. 2014, *Astronomy and Astrophysics*, **569**, A55, DOI:10.1051/0004-6361/201423400

Deka-Szymankiewicz, B., Niedzielski, A., Adamczyk, M., et al., The Penn State - Toruń Centre for Astronomy Planet Search stars. IV. Dwarfs and the complete sample. 2018, *Astronomy and Astrophysics*, **615**, A31, DOI:10.1051/0004-6361/201731696

Famaey, B., Jorissen, A., Luri, X., et al., Local kinematics of K and M giants from CORAVEL/Hipparcos/Tycho-2 data. Revisiting the concept of superclusters. 2005, *Astronomy and Astrophysics*, **430**, 165, DOI:10.1051/0004-6361:20041272

Linsky, J. L. & Haisch, B. M., Outer atmospheres of cool stars. I. The sharp division into solar-type and non-solar-type stars. 1979, *Astrophysical Journal, Letters*, **229**, L27, DOI:10.1086/182924

Niedzielski, A., Deka-Szymankiewicz, B., Adamczyk, M., et al., The Penn State - Toruń Centre for Astronomy Planet Search stars. 2016, *Astronomy and Astrophysics*, **585**, A73, DOI:10.1051/0004-6361/201527362

Niedzielski, A., Konacki, M., Wolszczan, A., et al., A Planetary-Mass Companion to the K0 Giant HD 17092. 2007, *Astrophysical Journal*, **669**, 1354, DOI:10.1086/521784

Niedzielski, A., Villaver, E., Wolszczan, A., et al., Tracking Advanced Planetary Systems (TAPAS) with HARPS-N . I. A multiple planetary system around the red giant star TYC 1422-614-1. 2015, *Astronomy and Astrophysics*, **573**, A36, DOI:10.1051/0004-6361/201424399

Raghavan, D., McAlister, H. A., Henry, T. J., et al., A Survey of Stellar Families: Multiplicity of Solar-type Stars. 2010, *Astrophysical Journal, Supplement*, **190**, 1, DOI:10.1088/0067-0049/190/1/1

Ramsey, L. W., Adams, M. T., Barnes, T. G., et al., Early performance and present status of the Hobby-Eberly Telescope. 1998, in SPIE Conference Series, Vol. **3352**, *SPIE Conference Series*, ed. L. M. Stepp, 34–42

Tull, R. G., High-resolution fiber-coupled spectrograph of the Hobby-Eberly Telescope. 1998, in SPIE Conference Series, Vol. **3355**, *SPIE Conference Series*, ed. S. D'Odorico, 387–398

Zieliński, P., Niedzielski, A., Wolszczan, A., Adamów, M., & Nowak, G., The Penn State-Toruń Centre for Astronomy Planet Search stars. I. Spectroscopic analysis of 348 red giants. 2012, *Astronomy and Astrophysics*, **547**, A91, DOI:10.1051/0004-6361/201117775

Contrib. Astron. Obs. Skalnaté Pleso **55/3**, 493 – 497, (2025)
https://doi.org/10.31577/caosp.2025.55.3.493

The first light curve analysis of marginally eclipsed binary KZ Vir using TESS data

İ. Özavcı[1,2], E. Bahar[1,2], M. Yılmaz[1,2], H.V. Şenavcı[1,2] and E.B. Yorulmaz[1,2]

[1] *Department of Astronomy and Space Sciences, Faculty of Science, Ankara University, Tandoğan 06100 Ankara, Türkiye*
(E-mail: iozavci@ankara.edu.tr)

[2] *Ankara University, Astronomy and Space Sciences Research and Application Center (Kreiken Observatory), İncek Blvd., TR-06837, Ahlatlıbel, Ankara, Türkiye*

Received: September 24, 2024; Accepted: January 27, 2025

Abstract. In this study, we present the first analysis of the light curve of the eclipsing binary KZ Vir. The light curve of KZ Vir were obtained from the TESS database, while radial velocity measurements were taken from the literature. By utilizing simultaneous light and radial velocity curve analysis, we determined the absolute parameters of the system and discussed the evolutionary status of its components. Our analysis revealed that the orbital inclination of the KZ Vir system is $i \sim 57^{\circ}$, and it exhibits marginal eclipses.

Key words: binaries: close – binaries: eclipsing – stars: individual (KZ Vir) – stars: fundamental parameters

1. Introduction

Binary stars play a crucial role in stellar astrophysics. Through simultaneous analysis of light and radial velocity curves, key parameters (e.g., orbital inclination, masses, radii, and temperatures of the component stars) can be determined. These parameters are essential for providing reliable data for statistical studies of both single and binary stars, enabling more accurate predictions about stellar structure and evolution.

KZ Vir (HD 114726) was first noticed by Bond (1976) to exhibit light variation; however, due to its low light variation amplitude ($0^m.05$), its period and light curve could not be determined. The spectral type of the system was identified as F3V (Houk & Swift, 1999), and it was classified as a suspected eclipsing binary based on `HIPPARCOS` observations Kazarovets et al. (1999). The first radial velocity study in the literature was performed by Rucinski et al. (2001) and the spectroscopic mass ratio of the system was determined as 0.848(8). This study also emphasized that the system is unlikely to be a contact binary and that both components may be distorted detached stars. They attributed the low

light variation amplitude to the system's low orbital inclination. Although light curves of KZ Vir obtained from various survey missions such as `HIPPARCOS` (ESA, 1997), `ASAS` (Pojmanski, 2002), `ASAS-SN` (Jayasinghe et al., 2018) and `MASCARA` (Burggraaff et al., 2018) exist in the literature, the nature of its variability has not been fully understood due to the low amplitude of brightness variation. However, thanks to the high-precision data provided by the TESS space telescope, a detailed light curve analysis can be performed.

2. Data and analyses

The TESS light curves used in this study were obtained from the MAST database, and the radial velocity data were taken from Rucinski et al. (2001). We conducted a simultaneous analysis of KZ Vir's light and radial velocity curves using the PyWD2015 code (Güzel & Özdarcan, 2020), which was developed in Python and is based on the 2015 version of the Wilson-Devinney (WD) code (Wilson & Devinney, 1971) with a graphical user interface (GUI).

During the analyses with PyWD2015, Mode-2 for detached systems was used, as suggested by Rucinski et al. (2001) and Avvakumova & Malkov (2014). The effective temperature of the primary component was fixed to $T_1 = 6436$ K, as provided by Schofield et al. (2019), which was derived from color-temperature relationships using dereddened (B-V) colors and validated against spectroscopic temperatures from the PASTEL catalog (Soubiran et al., 2016), as well as interferometric and asteroseismic data. The gravity darkening and the albedo coefficients were set to 0.32 and 0.5, respectively. The limb darkening coefficients were interpolated automatically from the van Hamme (1993) tables under the linear-cosine law assumption. We adjusted the effective temperature of the secondary component (T_2), orbital inclination (i), surface potential of components (Ω_1, Ω_2), the system mass ratio (q), the luminosity of the primary component (L_1), semi-major axis (a), and the gamma velocity (V_γ) during the simultaneous analysis. Due to the time difference between the radial velocity data and the light curve data, both datasets were phased using different ephemeris, as given in Rucinski et al. (2001) and Prša et al. (2022), respectively.

3. Results and discussion

The radial velocity and light curve analyses are presented in Fig. 1, illustrates the Roche geometry of the system and the graphic representation of the model in Fig. 2, illustrates the evolutionary status of the components in Fig. 3. The obtained parameters are listed in Table 1.

Both components are slightly evolved, but the primary component is more evolved. This situation explains the low light variation outside of eclipses, which is attributed to the distortion of the primary component (see Fig. 2 left panel.

Also, as can be seen in the right panel of Fig. 2, a marginal eclipse occurs with only a slight occultation of the primary component.

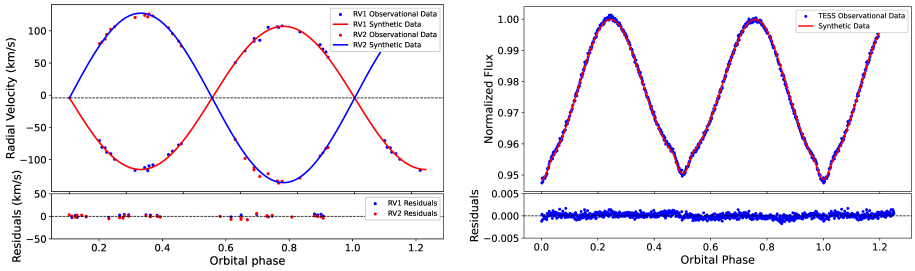


Figure 1. The left panel shows RV curves of the KZ Vir system (red and blue dots) and RV fits with PyWD2015 (red and blue lines), right panel shows LC curves from TESS of the KZ Vir system (blue dots) and LC fits with PyWD2015 (red line).

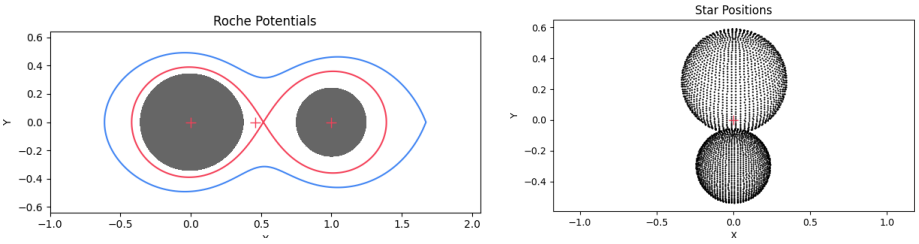


Figure 2. The left panel illustrates the Roche geometry of the system, and the right panel presents a 3D visualization of the stellar components at phase 0.0.

Table 1. Results from the light curve analysis (with formal errors from the WD code) and the absolute parameters of KZ Vir.

Parameter	Value	Parameter	Value
i [°]	56.69 ± 0.78	M_1 [$M_\odot$]	1.59 ± 0.03
a [$R_\odot$]	6.537 ± 0.028	M_2 [$M_\odot$]	1.35 ± 0.04
V_γ [km/s]	-4.18 ± 0.41	R_1 [$R_\odot$]	2.24 ± 0.01
$q = M_2/M_1$	0.850 ± 0.003	R_2 [$R_\odot$]	1.58 ± 0.02
T_1 [K]	6436	L_1 [$L_\odot$]	7.72 ± 0.09
T_2 [K]	6471 ± 10	L_2 [$L_\odot$]	3.94 ± 0.11
Ω_1	3.840 ± 0.006	$\log g_1$ [cgs]	3.938 ± 0.003
Ω_2	4.620 ± 0.017	$\log g_2$ [cgs]	4.168 ± 0.004

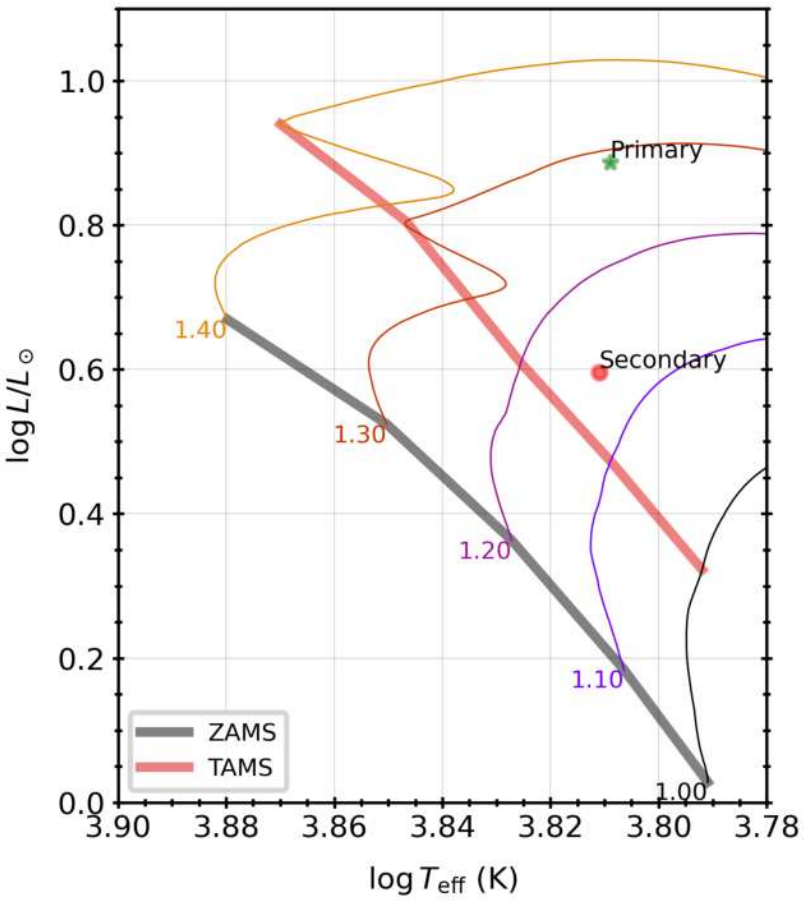


Figure 3. The positions of the components of KZ Vir on H–R diagram ($\log T_{\rm eff}$ - $\log L/L_\odot$). The green star shape and red dot represent the primary and secondary components, respectively.

References

Avvakumova, E. A. & Malkov, O. Y., Assessment of evolutionary status of eclipsing binaries using light-curve parameters and spectral classification. 2014, *Monthly Notices of the RAS*, **444**, 1982, DOI:10.1093/mnras/stu1572

Bond, H. E., Eclipsing Binaries Found Spectroscopically III. HD 199497. 1976, *Information Bulletin on Variable Stars*, **1214**, 1

Burggraaff, O., Talens, G. J. J., Spronck, J., et al., Studying bright variable stars with the Multi-site All-Sky CAmeRA (MASCARA). 2018, *Astronomy and Astrophysics*, **617**, A32, DOI:10.1051/0004-6361/201833142

ESA, ed. 1997, ESA Special Publication, Vol. **1200**, *The HIPPARCOS and TYCHO catalogues. Astrometric and photometric star catalogues derived from the ESA HIPPARCOS Space Astrometry Mission*

Güzel, O. & Özdarcan, O., PyWD2015 - A new GUI for the Wilson-Devinney code. 2020, *Contributions of the Astronomical Observatory Skalnate Pleso*, **50**, 535, DOI:10.31577/caosp.2020.50.2.535

Houk, N. & Swift, C., Michigan catalogue of two-dimensional spectral types for the HD Stars, Vol. 5. 1999, *Michigan Spectral Survey*, **5**, 0

Jayasinghe, T., Kochanek, C. S., Stanek, K. Z., et al., The ASAS-SN catalogue of variable stars I: The Serendipitous Survey. 2018, *Monthly Notices of the RAS*, **477**, 3145, DOI:10.1093/mnras/sty838

Kazarovets, E. V., Samus, N. N., Durlevich, O. V., et al., The 74th Special Name-list of Variable Stars. 1999, *Information Bulletin on Variable Stars*, **4659**, 1

Pojmanski, G., The All Sky Automated Survey. Catalog of Variable Stars. I. 0 h - 6 hQuarter of the Southern Hemisphere. 2002, *Acta Astronomica*, **52**, 397, DOI:10.48550/arXiv.astro-ph/0210283

Prša, A., Kochoska, A., Conroy, K. E., et al., TESS Eclipsing Binary Stars. I. Short-cadence Observations of 4584 Eclipsing Binaries in Sectors 1-26. 2022, *Astrophysical Journal, Supplement*, **258**, 16, DOI:10.3847/1538-4365/ac324a

Rucinski, S. M., Lu, W., Mochnacki, S. W., Ogłoza, W., & Stachowski, G., Radial Velocity Studies of Close Binary Stars. V. 2001, *Astronomical Journal*, **122**, 1974, DOI:10.1086/323106

Schofield, M., Chaplin, W. J., Huber, D., et al., The Asteroseismic Target List for Solar-like Oscillators Observed in 2 minute Cadence with the Transiting Exoplanet Survey Satellite. 2019, *Astrophysical Journal, Supplement*, **241**, 12, DOI:10.3847/1538-4365/ab04f5

Soubiran, C., Le Campion, J.-F., Brouillet, N., & Chemin, L., The PASTEL catalogue: 2016 version. 2016, *Astronomy and Astrophysics*, **591**, A118, DOI:10.1051/0004-6361/201628497

van Hamme, W., New Limb-Darkening Coefficients for Modeling Binary Star Light Curves. 1993, *Astronomical Journal*, **106**, 2096, DOI:10.1086/116788

Wilson, R. E. & Devinney, E. J., Realization of Accurate Close-Binary Light Curves: Application to MR Cygni. 1971, *Astrophysical Journal*, **166**, 605, DOI:10.1086/150986

Contrib. Astron. Obs. Skalnaté Pleso **55/3**, 498 – 501, (2025)
https://doi.org/10.31577/caosp.2025.55.3.498

New spectroscopic observations of the semidetached binary V375 Cas

B. Özkardeş[1,2] **and H. Bakış**[3]

[1] *Department of Space Sciences and Technologies, Faculty of Sciences, Çanakkale Onsekiz Mart University, Terzioğlu Kampüsü, TR-17020, Çanakkale, Türkiye (E-mail: burcu@comu.edu.tr)*

[2] *Çanakkale Onsekiz Mart University, Astrophysics Research Center and Ulupınar Observatory, TR-17100, Çanakkale, Türkiye*

[3] *Department of Space Sciences and Technologies, Faculty of Sciences, Akdeniz University, Konyaaltı Kampüsü, TR-07058, Antalya, Türkiye*

Received: November 28, 2024; Accepted: January 18, 2025

Abstract. We present the low resolution (R∼5099) spectroscopy of the eclipsing binary V375 Cas (TIC 326630342) in this study. The low resolution spectroscopic observations of the system were made at the TUBITAK National Observatory using a TFOSC spectrograph in 2020 and 2021. For measuring the radial velocities of both components of the eclipsing binary Gaussian fitting method was used. According to Keplerian orbital solution the spectroscopic mass ratio of the close binary was determined as 0.626 ± 0.098. The best fitting orbital elements are $a_1 \sin i = 0.0243 \pm 0.0018$ au, $a_2 \sin i = 0.0351 \pm 0.0018$ au, $M_1 \sin^3 i = 7.06 \pm 0.87$ $M_\odot$ and $M_2 \sin^3 i = 4.42 \pm 0.75$ $M_\odot$.

Key words: binary stars – spectrocopic observations – V375 Cas

1. Introduction

V375 Cas (= GSC 04285 00577; TIC 326630342) is a relatively faint (V∼ 10.1 mag) massive semidetached B2V type binary. It was first discovered by Weber (1958). Brancewicz & Dworak (1980) listed some parameters of V375 Cas such as its spectral type B3; $T_1 = 14\,220$ K; $T_2 = 11\,450$ K; $M_1 = 9.25$ $M_\odot$, mass ratio q = 0.61, and classified it as a β Lyrae type binary. Li et al. (2022) observed the system on 2021 February 7 with the 2.16 m telescope at Xinglong Station of National Astronomical Observatories (Chinese Academy of Sciences) and gave the spectral type of V375 Cas to be B2. In this study we aimed to present the preliminary results obtained from new spectroscopic observations of V375 Cas.

2. Spectroscopic observations

Spectroscopic observations of V375 Cas were made at the TUBITAK National Observatory in 2020 and 2021 using TFOSC (TUG Faint Object Spectrograph

and Camera) and a 2048 x 2048 Andor iKon-L 936 CCD camera attached to the 1.5 m telescope (RTT 150). Grism number 9 with a slit width of 10.68 arcsec which has a spectral coverage of 335 – 940 nm was used. The exposure time was 2400 s.

A total of 12 spectra of V375 Cas have been collected during observing programme. For all observations an iron–argon lamp was used for wavelength calibration. Halogen lamp spectra for flat fielding were also taken every night. We used the IRAF[1] package to reduce the spectroscopic images and to extract the spectrum.

3. Radial velocities and orbital solution

Radial velocities (RVs) of both components of V375 Cas were measured using Gaussian fitting of selected spectral line. According to the B2 V spectral type of the system there should be strong neutral He lines in the observed spectra. But we used H alpha line (656.28 nm) because the secondary star's spectral lines could be clearly detected (see Fig. 1).

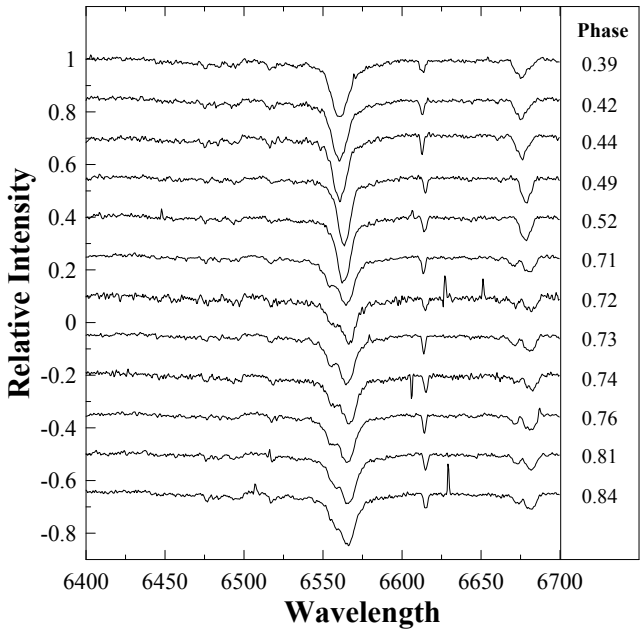


Figure 1. Hydrogen alpha lines of primary and secondary components of V375 Cas.

[1]IRAF is distributed by the National Optical Astronomical Observatories, operated by the Association of the Universities for Research in Astronomy, Inc under coop erative agreement with the National Science Foundation.

Using the least square method for best curve fitting the orbital parameters were obtained. The best fitted orbital elements we derived are given in Table 1. Fig. 2 shows the best theoretical fit to the radial velocity curves of the system

Table 1. Spectroscopic orbital parameters of V375 Cas.

Parameter	Value
P (days)	1.47344 (constant)
T_0 (HJD+2452501)	0.1930 ± 0.0192
e	0.0 (assumed)
K_1 (km/s)	162.9 ± 11.1
K_2 (km/s)	260.3 ± 44.2
q	0.626 ± 0.098
V_γ (km/s)	-19.3 ± 8.6
$M_1 \sin^3 i$	7.06 ± 0.87
$M_2 \sin^3 i$	4.42 ± 0.75
$a_1 \sin i$	0.0243 ± 0.0018
$a_2 \sin i$	0.0351 ± 0.0025

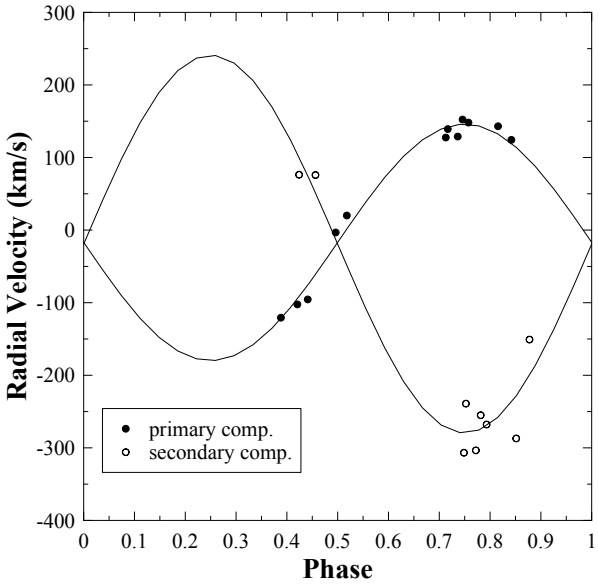


Figure 2. Best theoretical fit to the radial velocity curves of V375 Cas with a Keplerian orbit (continuous line).

Acknowledgements. We thank to TUBITAK for a partial support in using RTT 150 (Russian–Turkish 1.5 m telescope in Antalya) with project number 1361. The authors thank Ö. Hilal for her help with IRAF procedures and the RTT 150 officers for their assistance in the observations.

References

Brancewicz, H. K. & Dworak, T. Z., A catalogue of parameters for eclipsing binaries. 1980, *Acta Astronomica*, **30**, 501

Li, F. X., Qian, S. B., Zhang, J., et al., The massive system V375 Cassiopeia is a semidetached mass-transfer binary with a massive stellar companion. 2022, *Monthly Notices of the RAS*, **514**, 1206, DOI:10.1093/mnras/stac1327

Weber, R., Catalogue d'étoiles variables nouvelles. 1958, *Journal des Observateurs*, **41**, 74

Contrib. Astron. Obs. Skalnaté Pleso **55/3**, 502 – 505, (2025)
https://doi.org/10.31577/caosp.2025.55.3.502

The PLATO Multiple Star Working Group (MSWG)

J. Southworth and P.F.L. Maxted

Astrophysics Group, Keele University, Staffordshire, ST5 5BG, UK
(E-mail: taylorsouthworth@gmail.com)

Received: November 15, 2024; Accepted: February 4, 2025

Abstract. The PLATO mission is scheduled for launch in December 2026. It is an ESA M-class mission designed to find small planets around bright stars via the transit technique. The light curves it obtains will be wonderful for other science goals, among which is the study of binary and multiple stars. We are creating the Multiple Star Working Group (MSWG) to bring together the community to best exploit this unique opportunity. We will assemble the many science cases, create target lists, and co-ordinate applications for PLATO observations. We include instructions on how to register your interest.

Key words: stars: fundamental parameters – stars: binaries: eclipsing

1. The PLATO mission

PLATO (Planetary Transits and Oscillations of Stars) was selected by the European Space Agency (ESA) in 2014 as a mission to search for small transiting extrasolar planets (Rauer et al., 2024). Its baseline aim is to to detect a $1\,R_\oplus$ planet orbiting in the habitable zone of a G0 V star of magnitude $V = 10$, and to determine the planetary radius to 3% and system age to 10%. The planet detection and characterisation will be performed using the transits, and the age determination will be obtained from asteroseismology.

PLATO will consist of one spacecraft hosting 26 cameras, of two types. The main scientific instruments are 24 "normal" cameras (N-CAM), each of which will have a 12 cm entrance pupil and a 4510×4510-pixel CCD. Each will have a field of view of $1037\,\mathrm{deg}^2$ with a sampling of $15''$ per pixel, and will observe in a red passband (500-1000 nm). The other cameras are two fast cameras (F-CAM) which will be used for fine-pointing of the satellite and may also be available for high-speed observations. They have smaller fields of view ($610\,\mathrm{deg}^2$) and different passbands to the science instruments (505–700 nm for the blue and 665–1000 nm for the red camera).

PLATO is scheduled for launch in December 2026, and will take approximately 90 days to move to the second Lagrangian point in the Earth–Sun system. Its observations will be divided into 90-day segments between which the satellite will rotate by 90° to keep its solar panels illuminated by the Sun. The baseline

duration of the mission is four years, of which at least the first two years will be used to observe the LOPS2 (the second Long-duration Observation Phase South) field in the southern hemisphere (Nascimbeni et al., 2022). The spacecraft will hold consumables to last 8.5 years and the strategy for the remainder of the mission will be decided after observations of LOPS2 have commenced (Rauer et al., 2024).

2. Complementary science

A set of PLATO Complementary Science Work Packages[1] have been formed to aid the organisation of all scientific areas which will benefit from the availability of PLATO data but do not contribute to the core science goals. The Complementary Science Work Packages include binary and multiple stars, stellar pulsation and rotation, mass loss, debris discs, galactic structure and transient phenomena, and are co-ordinated by Conny Aerts and Andrew Tkachenko.

The Complementary Science teams will submit applications for PLATO data using the same Guest Observer (GO) mechanism as other scientists, and will have no influence on the observing strategy for PLATO. The GO programme has been allocated 8% of the PLATO data rate, and the call for proposals is expected nine months before launch.

3. WP 161 000: Binary and Multiple Stars

Complementary Science Work Package 161 000 (PI Southworth) deals with binary and multiple stars. Our task is to co-ordinate target selection, GO applications and scientific work within the community. This will be done by forming a PLATO Multiple Star Working Group (MSWG) which all members of the scientific community with suitable research interests can join. Our first goal will be to compile a White Paper detailing the work of the Working Group and thoroughly discussing the science cases which we can address. This will naturally lead into the second goal: to co-ordinate the GO applications.

A catalogue of variable stars will be made available prior to the GO deadline. Work at Keele University will lead to an automated pipeline to estimate the physical properties of eclipsing systems based on data from the NASA Transiting Exoplanet Survey Satellite (TESS; Ricker et al., 2015) and *Gaia* missions (see Overall & Southworth, these proceedings). The PLATO MSWG will then co-ordinate applications for GO observations. We will be able to select as targets anything within the PLATO Input Catalogue (PIC; Montalto et al. 2021) and outside the PLATO prime sample. Some targets are already in the process of being selected via the PLATO scvPIC (Science Calibration and Validation PIC; Zwintz, 2024) and WP 125 500 (PLATO Benchmark stars) activities.

[1] `https://fys.kuleuven.be/ster/research-projects/plato-cs/work_packages`

PLATO is expected to produce light curves of extremely high quality, thus continuing the revolution within the field of binary and multiple stars triggered by the previous *CoRoT*, *Kepler* and TESS missions (Southworth, 2021). The combined differential photometric precision (CDPP) over two hours is less than 100 ppm for stars brighter than TESS magnitude 12 (Börner et al., 2024). This is substantially better than TESS (Eschen et al., 2024) – and comparable to *Kepler* (Borucki, 2016) but over a much larger field of view – in order to satisfy the scientific requirements. These data will be useful for a huge range of science cases including, but not limited to:

- determination of the properties of massive stars;
- the study of pulsating stars in eclipsing binary systems;
- the study of binary systems in stellar clusters and associations;
- analysis of giant and subgiant stars in eclipsing binaries;
- investigation of the radius discrepancy in low-mass stars;
- the study of mass exchange and loss in interacting binaries;
- assessing magnetic activity in binary stars via detection of starspot and flare activity;
- the detection of multiplicity through additional sets of eclipses and/or eclipse timing and duration variations;
- the population of binary and multiple star systems.

Many of these activities, in turn, are valuable for furthering the knowledge of the structure and evolution of stars, by constraining phenomena such as convective mixing, tidal effects, angular momentum transport and magnetic activity.

4. How to get involved

Anyone interested in joining the PLATO MSWG and helping with this work can contact the PLATO MSWG at the email address `platomswg@gmail.com` – please provide a brief statement of your science interests and how you would like to contribute. The MSWG is formally launched with this conference proceedings and will be organised via a webpage, teleconferences, in-person meetings, and the production of a white paper on multiple-star science to aid the forthcoming applications for PLATO GO time. We look forward to hearing from you!

Acknowledgements. JS and PFLM acknowledge support from the Science and Technology Facilities Council (STFC) under grant number ST/Y002563/1. We are grateful for extensive discussions about PLATO with many colleagues.

References

Börner, A., Paproth, C., Cabrera, J., et al., PLATO's signal and noise budget. 2024, *Experimental Astronomy*, **58**, 1

Borucki, W. J., Kepler mission: development and overview. 2016, *Reports on Progress in Physics*, **79**, 036901

Eschen, Y. N. E., Bayliss, D., Wilson, T. G., et al., Viewing the PLATO LOPS2 field through the lenses of TESS. 2024, *MNRAS*, **535**, 1778

Montalto, M., Piotto, G., Marrese, P. M., et al., The all-sky PLATO input catalogue. 2021, *A&A*, **653**, A98

Nascimbeni, V., Piotto, G., Börner, A., et al., The PLATO field selection process. I. Identification and content of the long-pointing fields. 2022, *A&A*, **658**, A31

Rauer, H., Aerts, C., Cabrera, J., et al., The PLATO Mission. 2024, *arXiv.2406.05447*

Ricker, G. R., Winn, J. N., Vanderspek, R., et al., Transiting Exoplanet Survey Satellite (TESS). 2015, *Journal of Astronomical Telescopes, Instruments, and Systems*, **1**, 014003

Southworth, J., Space-based photometry of binary stars: from Voyager to TESS. 2021, *Universe*, **7**, 369

Zwintz, K., The PLATO Science Calibration and Validation Targets (scvPIC). 2024, in *EAS2024*, 1836

Contrib. Astron. Obs. Skalnaté Pleso **55/3**, 506 – 511, (2025)
https://doi.org/10.31577/caosp.2025.55.3.506

A detailed analysis of close binary OCs

S. Taşdemir and D.C. Çınar

Istanbul University, Institute of Graduate Studies in Science, Programme of Astronomy and Space Sciences, 34116, Beyazıt, Istanbul, Türkiye
(E-mail: tasdemirr.seval@gmail.com)

Received: October 13, 2024; Accepted: January 28, 2025

Abstract. In this study, we analysed the close binary open clusters CWNU2666 and HSC224. They are in close spatial proximity, using photometric and astrometric data from the *Gaia* DR3. Most likely member stars were used with a membership probability ($P \geq 0.5$) were identified 106 and 146, the mean proper motion components ($\mu_\alpha \cos\delta$, μ_δ) obtained as (0.646±0.155, -0.769±0.124) and (0.665±0.131, -0.728±0.107) mas yr^{-1}, isochrone distances ($d_{\rm iso}$) as 1885±44 and 1866±29 pc, and ages (t) as 160±15 and 140±15 Myr, for CWNU 2666 and HSC 224, respectively.

Key words: Open clusters: individual (CWNU 2666, HSC 224)

1. Introduction

Open clusters (OCs) are stellar groups of hundreds or thousands of young stars that are bound together by the weak gravitational forces. Formed from the same gas and dust cloud, OCs typically share age and chemical properties, making them valuable tools for studying stellar evolution and Galactic structure and dynamics (Friel, 1995). Recent observations have shown that some OCs are located quite close to each other and can interact gravitationally (Song et al., 2022; Li & Zhu, 2024; Haroon et al., 2024; Palma et al., 2024). Such clusters are called close binary open clusters (CBOCs). CBOCs provide unique opportunities to study their dynamical evolution and star formation in the Milky Way, serving as valuable laboratories for investigating both astrophysical processes and cluster interactions with the Galactic structure.

2. Astrometric and photometric data

Tha photometric and astrometric anaylses of CWNU 2666 and HSC 224 utilized data from the *Gaia* DR3 catalogued (DR3; Gaia Collaboration et al., 2023). The data were generated based on the equatorial coordinates provided by Hunt & Reffert (2024) (α, δ) = ($18^{\rm h}44^{\rm m}05^{\rm s}.33$, -11°54′21″.78). Figure 1a presents the star field for CWNU 2666 and HSC 224 in the 120′ × 120′ area.

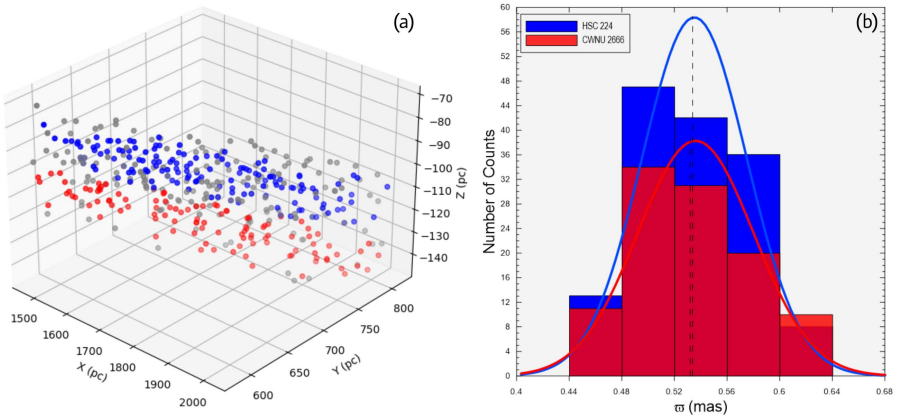


Figure 1. Left panel (a) shows the 3D distribution of most likely stars ($P \geq 0.5$) of HSC 224 (blue) and CWNU 2666 (red). Also grey circles represent the stars that are out of the limit radii of CBOCs. Right panel (b) illustrates the *Gaia* DR3-based trigonometric parallax histogram. The black dashed lines represent the median of the Gaussian curves fitted to the parallax histograms for both clusters.

3. Analyses and results

This study provides a photometric and astrometric analysis of the CBOCs CWNU 2666 and HSC 224, as catalogued by Hunt & Reffert (2024). Using *Gaia* DR3 data, we identified and differentiated member stars to determine their fundamental astrophysical and astrometric parameters (Yontan et al., 2022; Dursun et al., 2024).

3.1. Spatial distribution

In this study, a spatial separation was performed by considering the central coordinates of the CBOCs. To accurately identify the most probable members of the cluster from field stars, we employed the Unsupervised Photometric Membership Assignment in Stellar Clusters (UPMASK) method (Krone-Martins & Moitinho, 2014), which utilizes astrometric parameters from *Gaia* DR3 (Taşdemir & Yontan, 2023). This machine-learning approach, based on k-means clustering, resulting in the classification of 146 and 106 stars as probable ($P \geq 0.5$) members of CWNU 2666 and HSC 224, respectively and shown Figure 1a. A histogram of the most probable members's trigonometric parallaxes was fitted with a Gaussian to estimate the mean, as shown in Figure 1b.

The 3D spatial positions of member stars in the open clusters CWNU 2666 and HSC 224 are analysed in heliocentric Cartesian coordinates (X, Y, Z) using

the following transformations:

$$\begin{aligned} X &= d\ \cos\delta\ \cos\alpha - R_{\odot}, \\ Y &= d\ \cos\delta\ \sin\alpha, \\ Z &= d\ \sin\delta. \end{aligned} \tag{1}$$

where $R_{\odot} = 8$ kpc is the distance of Sun to the Galactic centre (Majewski, 1993), d is the distance, α and δ represent the equatorial coordinates, and the calculations are performed using data from high-probability member stars identified in the *Gaia* DR3 catalogue.

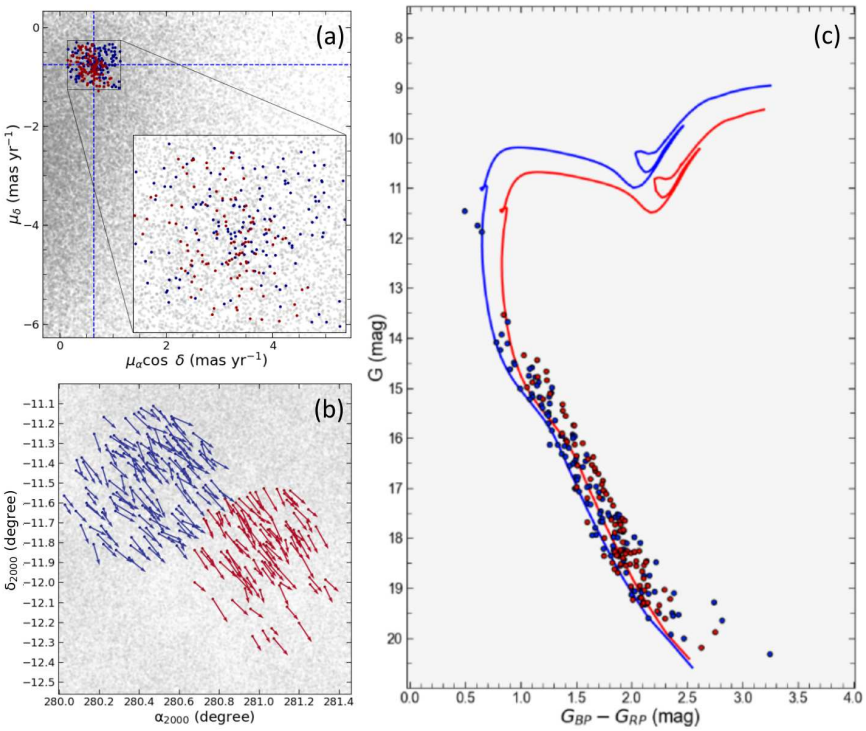


Figure 2. Left-upper panel (a) the zoomed-box reveal regions with a high concentration member stars in the VPDs, left-bottom panel (b) proper-motion velocity vectors, and right panel (c) for the CWNU 2666 and HSC 224 in CMD.

3.2. Astrometric and astrophysical parameters

To determine the mean proper-motion components of the clusters, we created the vector point diagram (VPD) from the most likely members and shown Fig-

ures 2a and 2b. UPMASK method was employed for the membership analyses of the open clusters CWNU 2666 and HSC 224. This method utilised astrometric parameters, including proper motion components ($\mu_\alpha \cos\delta$, μ_δ) and trigonometric parallaxes (ϖ), along with their associated uncertainties, obtained from the *Gaia* DR3 catalogue. Consequently, the mean trigonometric parallaxes (ϖ) were obtained and via the linear equation, $d(\mathrm{pc}) = 1000/\varpi$ (mas), converted to the distance (d_ϖ). The results are in a good agreement with Li & Zhu (2024).

For each of the two open clusters under study, we determined their astrophysical parameters using the isochrone-fitting method applied to high-probability member stars. This approach simultaneously estimates the colour excess, distance, and age of the clusters by fitting PARSEC isochrones to observational data on *Gaia*-based colour-magnitude diagrams. These results are compatible with Hunt & Reffert (2024) listed in Table 1. We utilized a classical technique for determining the fundamental astrophysical parameters of CBOCs called the main-sequence fitting method as shown in Figure 2c (Yontan, 2023; Yontan & Canbay, 2023; Elsanhoury et al., 2024).

Table 1. Astrometric and Astrophysical Parameters of CWNU 2666 and HSC 224 with comparisons to other published values.

	This Study		Hunt & Reffert (2024)	
Parameter	CWNU 2666	HSC 224	CWNU 2666	HSC 224
Astrometric Parameters				
$(\alpha, \delta)_{J2000}$ (Decimal)		(281.02, -11.90)	(280.23, -11.80)	
$(l, b)_{J2000}$ (Decimal)		(21.49, -03.79)	(21.23, -03.06)	
Members ($P \geq 0.5$)	106	146	51	61
$\mu_\alpha \cos\delta$ (mas yr^{-1})	0.646 ± 0.155	0.665 ± 0.131	0.607±0.067	0.662±0.150
μ_δ (mas yr^{-1})	-0.769 ± 0.124	-0.728 ± 0.107	-0.803±0.100	-0.761±0.126
ϖ (mas)	0.537 ± 0.006	0.530 ± 0.005	0.563 ±0.004	0.552±0.004
d_ϖ (pc)	1863 ± 102	1857 ± 169	1776±142	1811±138
X, Y, Z (pc)	1730, 681, -123	1729, 671, -99	-6560, 614, -94	-6547, 611, -73
R_{gc} (kpc)	6.71	6.71	–	–
k-means	25	34	–	–
Astrophysical Parameters				
$E(G_{\mathrm{BP}}$-$G_{\mathrm{RP}})$ (mag)	0.975 ± 0.025	0.807 ± 0.016	1.159±0.085	0.884±0.085
A_{G} (mag)	1.816 ± 0.047	1.503 ± 0.030	2.159±0.158	1.647±0.158
[Fe/H] (dex)	0.010 ± 0.05	0.010 ± 0.05	–	–
Age (Myr)	160 ± 15	140 ± 15	98±43	63±27
G - M_{G} (mag)	13.192 ± 0.051	12.857 ± 0.034	–	–
d_{iso} (pc)	1885 ± 44	1866 ± 29	1682±11	1691±11

4. Future works

Future research will involve conducting spectral energy distribution (SED) analyses for the most probable member stars of each cluster, followed by a comparison with model atmosphere parameters from existing spectral studies in the literature. Additionally, the total masses of the clusters will be calculated for comparative purposes. These analyses aim to enhance our understanding of the previous interactions and formation processes of the clusters in relation to one another.

Acknowledgements. We are indebted to the referees for their invaluable feedback, which served to enhance the quality of the paper. We made use of NASA's Astrophysics Data System as well as the VizieR and Simbad databases at CDS, Strasbourg, France and data from the European Space Agency (ESA) mission *Gaia*[1], processed by the *Gaia* Data Processing and Analysis Consortium (DPAC)[2]. Funding for DPAC has been provided by national institutions, in particular, the institutions participating in the *Gaia* Multilateral Agreement.

References

Dursun, D. C., Tasdemir, S., Koc, S., & Iyer, S., SED Analysis of the Old Open Cluster NGC 188. 2024, *Physics and Astronomy Reports*, **2**, 1, DOI:10.26650/PAR.2024.00002

Elsanhoury, W. H., Haroon, A. A., Elkholy, E. A., & Çınar, D. C. 2024, Deeply Comprehensive Astrometric, Photometric, and Kinematic Studies of the Three OCSN Open Clusters with Gaia DR3

Friel, E. D., The Old Open Clusters Of The Milky Way. 1995, *Annual Review of Astron and Astrophys*, **33**, 381, DOI:10.1146/annurev.aa.33.090195.002121

Gaia Collaboration, Vallenari, A., Brown, A. G. A., et al., Gaia Data Release 3. Summary of the content and survey properties. 2023, *Astronomy and Astrophysics*, **674**, A1, DOI:10.1051/0004-6361/202243940

Haroon, A. A., Elsanhoury, W. H., Saad, A. S., & Elkholy, E. A., Deep investigation of a pair of open clusters NGC 7031 and NGC 7086 utilizing Gaia DR3. 2024, *Contributions of the Astronomical Observatory Skalnate Pleso*, **54**, 22, DOI:10.31577/caosp.2024.54.3.22

Hunt, E. L. & Reffert, S., Improving the open cluster census. III. Using cluster masses, radii, and dynamics to create a cleaned open cluster catalogue. 2024, *Astronomy and Astrophysics*, **686**, A42, DOI:10.1051/0004-6361/202348662

Krone-Martins, A. & Moitinho, A., UPMASK: unsupervised photometric membership assignment in stellar clusters. 2014, *Astronomy and Astrophysics*, **561**, A57, DOI:10.1051/0004-6361/201321143

[1]https://www.cosmos.esa.int/gaia

[2]https://www.cosmos.esa.int/web/gaia/dpac/consortium

Li, Z. & Zhu, Z., A catalog of newly discovered close binary open clusters in the Milky Way from Gaia DR3. 2024, *arXiv e-prints*, arXiv:2405.02530, DOI:10.48550/arXiv.2405.02530

Majewski, S. R., Galactic structure surveys and the evolution of the Milky Way. 1993, *Annual Review of Astron and Astrophys*, **31**, 575, DOI:10.1146/annurev.aa.31.090193.003043

Palma, T., Coenda, V., Baume, G., & Feinstein, C., Binary and Grouped Open Clusters: A New Catalogue. 2024, *arXiv e-prints*, arXiv:2412.05376

Song, F., Esamdin, A., Hu, Q., & Zhang, M., Binary open clusters in the Gaia data. 2022, *Astronomy and Astrophysics*, **666**, A75, DOI:10.1051/0004-6361/202243524

Taşdemir, S. & Yontan, T., Analysis of the Young Open Cluster Trumpler 2 Using Gaia DR3 Data. 2023, *Physics and Astronomy Reports*, **1**, 1, DOI:10.26650/PAR.2023.00001

Yontan, T., An Investigation of Open Clusters Berkeley 68 and Stock 20 Using CCD UBV and Gaia DR3 Data. 2023, *Astronomical Journal*, **165**, 79, DOI:10.3847/1538-3881/aca6f0

Yontan, T. & Canbay, R., Comprehensive Analysis of the Open Cluster Collinder 74. 2023, *Physics and Astronomy Reports*, **1**, 65, DOI:10.48550/arXiv.2310.13582

Yontan, T., Çakmak, T., Bilir, S., et al., A Study of the NGC 1193 and NGC 1798 Open Clusters Using CCD UBV Photometric and Gaia EDR3 Data. 2022, *The Revista Mexicana de Astronomía y Astrofísica*, **58**, 333, DOI:10.22201/ia.01851101p.2022.58.02.14

Contrib. Astron. Obs. Skalnaté Pleso **55/3**, 512 – 516, (2025)
https://doi.org/10.31577/caosp.2025.55.3.512

Direct imaging potential of outer companions of eclipsing binary stars with 4-meter telescope of the Eastern Anatolia Observatory (DAG)

F. Tezcan[1], **Ö. Baştürk**[2], **C. Yeşilyaprak**[3,4] **and S. Aliş**[5]

[1] *Atatürk University, Graduate School of Natural and Applied Sciences, Astronomy and Astrophysics, Erzurum, Türkiye*
(E-mail: fatosuyanik9@gmail.com)

[2] *Ankara University Faculty of Science, Astronomy and Space Sciences, Ankara, Türkiye*

[3] *Atatürk University Faculty of Science, Astronomy and Space Sciences, Erzurum, Türkiye*

[4] *Türkiye National Observatories, DAG, Erzurum, Türkiye*

[5] *İstanbul University, Faculty of Science, Astronomy and Space Sciences, İstanbul, Türkiye*

Received: November 14, 2024; Accepted: December 19, 2024

Abstract. Investigation of gravitationally bound objects to the binary star systems is crucial for understanding binary star formation and their orbital evolution. They also provide significant advantages in the empirical determination of the observational limits of a direct imaging system thanks to the wide range of spectral type and magnitude differences (contrast), and angular separations between binary components and their additional companions. In this study, the potential of direct imaging of these additional bodies proposed by various methods around binary stars with the brand-new 4-meter DAG telescope will be discussed. DAG Direct Imaging System (DGS) is composed of an active and adaptive optics system, a coronagraph, and an infrared imager to be operated in the near infrared wavelengths (<3 microns), for which the first light is expected to be acquired in 2025.

Key words: direct imaging – binary stars – multistellar systems – infrared observations

1. Introduction

Close binary star systems are often observed to have additional components gravitationally bound to the system. If the systems are hierarchical, the third body can maintain a stable orbit for an extended period. Hierarchical triples consist of an "inner" binary star and a third star orbiting a common center of mass with the binary (Borkovits et al., 2015).

Formation of tertiaries in such systems can be explained by captures, in-situ or ex-situ formation followed by subsequent migration theories. First- and second-generation formation theories are also considered for objects in the sub-stellar mass regime, with formation timing classified as either simultaneous with or occurring after the common envelope ejection in post-common-envelope systems (Zorotovic & Schreiber, 2013). These tertiaries also affect the orbital evolution of the binary through mechanisms such as von Zepel-Kozai-Lidov cycles (von Zeipel, 1910; Kozai, 1962; Lidov, 1962).

In order to characterize a direct imaging system empirically, one needs the observations of objects spanning a wide range of spectral types, magnitudes, and angular separations. Hence, hierarchical triplets become the ideal objects for the task. In addition to the known hierarchicals, many additional bodies have been suggested around eclipsing binaries with different techniques, primarily with the Eclipse Timing Variations (ETVs) such bodies induce through the Light-Time Effect (LiTE). Eclipsing binaries are also advantageous because they are fainter during the eclipses enhancing the contrast. We are planning an observational project with DAG 4m telescope and its imaging system composed of an active coronograph (PLACID) to contribute to the 1) determination of its limits, 2) confirmation of suggested bodies and determination of their physical and orbital parameters, 3) statistical studies on the frequency of occurrence of such systems.

2. DAG direct imaging system

A limited number of additional components of binary star systems can be identified with the high-precision astrometric observations of the Gaia Space Telescope. Due to the limited angular resolution of Gaia, it is known that components with an angular distance below 2 arcseconds cannot be identified in a wide contrast range (Mugrauer, 2019). Most other direct imaging systems concentrate either on planet discovery programs and / or follow-up observations of Transiting Exoplanet Survey Satellite (TESS) to determine potential contamination sources. Therefore, systems that may have additional components around them need to be investigated with high contrast and angular resolution using direct imaging techniques.

The Eastern Anatolia Observatory (DAG) Telescope is being built in Türkiye (3170 m elevation), on the Karakaya peaks of Erzurum province. The DAG Telescope is also the largest telescope in the country with a 4-meter primary mirror diameter and 56-meter focal length (F/14.2) Ritchey-Chretien design (Yesilyaprak et al., 2022). The DAG Telescope has two selectable focal points called Nasmyth platforms. High-resolution photometric images will be obtained with the sensitive Infrared camera (¡ 3 microns - DIRAC (Zhelem et al., 2022)), Coronagraph (PLACID - (Kühn et al., 2021)) and Pyramid Adaptive Optics system (TROIA - (Keskin et al., 2022)) to be located on one of these platforms.

The coronagraph system planned to be used at the DAG Telescope will have an adaptively programmable liquid crystal structure (Programmable Liquid-crystal Active Coronographic Imager for the DAG Telescope - PLACID - Kühn et al. (2021)). It will be able to acquire images in a $7''x\ 7''$field at 1.6 microns (H band) and up to 2.15 microns (Ks). When used with adaptive optics, it will be able to obtain diffraction-limited, high-contrast images and will be used for direct imaging of exoplanets, interstellar matter, and multiple star systems. Some laboratory results listed in Table 1.

Table 1. The Programmable Liquid-crystal Active Coronagraphic Imager for the DAG Telescope PLACID

Observing Bands	H-Band: 1.63 μm, Ks-Band: 2.15 μm
SLM Specification	1920x1152 pixels, 8 bits
Field of View	$16''$x $9.6''$
λ/D at H-Band	85 mas
Optical Throughput	22 %
Raw Contrast at 2λ/D	$< 5.3x10^{-2}$
Raw Contrast at 5λ/D	$< 5.3x10^{-4}$

3. Potential observations of outer companions of eclipsing binaries

In its first years of operation of DAG, a significant time will be devoted to high contrast direct imaging. Hence, binary and multiple star systems with resolvable faint components can be targeted in such an extended observation window. With that in mind, a list of systems around which additional objects have been suggested primarily based on ETVs, the third light contribution observed in light curve solutions, and signals related to the third component in radial velocity profiles, has been compiled from the literature for the detection and confirmation of unseen additional components with the DAG DGS. The list is not final and objects may be added or removed during the study. We listed first 5 stars and their information in Table 2

We will first compile and / or derive the J, H, and K magnitudes for the binary systems and their additional components allowing us to have estimates on the expected contrast values. Based on the previous literature, ETV solutions, databases, and archives such as Gaia, HIPPARCOS, and Washington Double Star Catalogue (WDS), we are going to determine the expected positions (position angle and angular separation at a given time) of the additional objects in our list. The most promising systems will be selected from this list spanning a wide range of spectral types, contrasts, and angular separations to determine the limits of the DAG DGS.

Table 2. Five examples from our list of potential candidate systems, compiled based on their compatibility with DAG-DGS observations.

Object	Type	Ang.Sep.	Mag G	G Flux Ratio	Mag R	R Flux Ratio
GSC 1387-0475	Double or Multiple Star	0.70	10.45	5.97×10^{-1}	9.36	6.77×10^{-1}
LV Vir	Spectroscopic Binary	0.89	8.96	6.96×10^{-1}	8.02	9.86×10^{-1}
V829 Her	Spectroscopic Binary	1.19	13.12	6.47×10^{-2}	-	-
NSVS 12277727	Eclipsing Binary	1.55	15.38	1.31×10^{-1}	-	-
V508 Oph	Spectroscopic Binary	1.66	16.24	4.39×10^{-3}	-	-

Acknowledgements. We thank the Council of Higher Education in Türkiye (YÖK) for their support with the ADEP projects carried out in Ankara University (FBA-2023-2698) and in İstanbul University (FBA-2022-39121). We thank the Türkiye National Observatories for the infrastructure provided for this study.

References

Borkovits, T., Rappaport, S., Hajdu, T., & Sztakovics, J., Eclipse timing variation analyses of eccentric binaries with close tertiaries in the Kepler field. 2015, *Monthly Notices of the RAS*, **448**, 946, DOI:10.1093/mnras/stv015

Keskin, O., Jolissaint, L., Bouxin, A., & Yesilyaprak, C., TROIA adaptive optics system for DAG telescope: assembly and laboratory performance prior to on-sky assessment. 2022, in Society of Photo-Optical Instrumentation Engineers (SPIE) Conference Series, Vol. **12185**, *Adaptive Optics Systems VIII*, ed. L. Schreiber, D. Schmidt, & E. Vernet, 121851W

Kozai, Y., Secular perturbations of asteroids with high inclination and eccentricity. 1962, *Astronomical Journal*, **67**, 591, DOI:10.1086/108790

Kühn, J. G., Jolissaint, L., Bouxin, A., & Patapis, P., SLM-based Active Focal-Plane Coronagraphy: Status and future on-sky prospects. 2021, *arXiv e-prints*, arXiv:2102.03201, DOI:10.48550/arXiv.2102.03201

Lidov, M. L., The evolution of orbits of artificial satellites of planets under the action of gravitational perturbations of external bodies. 1962, *Planetary Space Science*, **9**, 719, DOI:10.1016/0032-0633(62)90129-0

Mugrauer, M., Search for stellar companions of exoplanet host stars by exploring the second ESA-Gaia data release. 2019, *Monthly Notices of the RAS*, **490**, 5088, DOI:10.1093/mnras/stz2673

von Zeipel, H., Sur l'application des séries de M. Lindstedt à l'étude du mouvement des comètes périodiques. 1910, *Astronomische Nachrichten*, **183**, 345, DOI:10.1002/asna.19091832202

Yesilyaprak, C., Keskin, O., & Jolissaint, L., Eastern Anatolia Observatory (DAG): the status in 2022, towards the first light. 2022, in Society of Photo-Optical Instrumentation Engineers (SPIE) Conference Series, Vol. **12182**, *Ground-based and Airborne Telescopes IX*, ed. H. K. Marshall, J. Spyromilio, & T. Usuda, 121820X

Zhelem, R., Content, R., Churilov, V., et al., Design of the near infrared camera DIRAC for East Anatolia Observatory. 2022, in Society of Photo-Optical Instrumentation Engineers (SPIE) Conference Series, Vol. **12184**, *Ground-based and Airborne Instrumentation for Astronomy IX*, ed. C. J. Evans, J. J. Bryant, & K. Motohara, 1218440

Zorotovic, M. & Schreiber, M. R., Origin of apparent period variations in eclipsing post-common-envelope binaries. 2013, *Astronomy and Astrophysics*, **549**, A95, DOI:10.1051/0004-6361/201220321

Contrib. Astron. Obs. Skalnaté Pleso **55/3**, 517 – 520, (2025)
https://doi.org/10.31577/caosp.2025.55.3.517

Photometric and spectroscopic analysis of the eccentric eclipsing binary BD+72 780

M. Yılmaz[1,2], **İ. Özavcı**[1], **E. Bahar**[1], **H.V. Şenavcı**[1] **and B.S. Azizoglu**[2]

[1] *Ankara University, Department of Astronomy and Space Sciences, TR-06100, Tandogan, Ankara, Türkiye (E-mail: mesutyilmaz@ankara.edu.tr)*

[2] *Ankara University, Astronomy and Space Sciences Research and Application Center (Kreiken Observatory), TR-06837, Ahlatlıbel, Ankara, Türkiye*

Received: October 18, 2024; Accepted: January 9, 2025

Abstract. In this study, we present the first radial velocity measurements of the eclipsing binary BD+72 780. We simultaneously modeled TESS light curves with our radial velocity data to derive the orbital and absolute parameters of the system. The analysis shows that the system is a detached binary with two different spectral types of components, and the orbit is slightly eccentric ($e \sim 0.07$).

Key words: stars – eclipsing binary – radial velocity

1. Introduction

Close binary stars allow us to accurately determine stellar masses through simultaneous spectroscopic and photometric analyses. These analyses also provide other fundamental parameters such as orbital inclination, eccentricity, semi major-axis, radii and luminosity, which help us better understand binary star evolution. These parameters are also essential for providing reliable data for statistical studies of both single and binary stars.

The literature on the BD+72 780 system (TIC 441739153, α: 17h 17m 42.16s, δ: +72° 06′ 09.72″) is quite sparse and limited. The orbital period is obtained to be 3.21 days (Shi et al., 2022) and the spectral type is derived as A2 (Cannon & Pickering, 1993). The first light curve characteristic was determined by Prša et al. (2022) based on morphological classification of the light curves. According to these results, this system reported as detached eclipsing binary.

In this context, we investigate the spectroscopic and photometric properties of the eclipsing binary systems BD+72 780 to derive physical and orbital characteristics.

2. Observations

We collected the TESS data of BD+72 780 from the MAST Portal. The system was observed from sectors 14 to 26 of the TESS observations in short cadence (2-min) mode. During the light curve analysis we used the data from sector 15. Photometry was performed by SPOC pipeline (Jenkins et al., 2016) and we used PDCSAP-FLUX data during the simultaneous light and radial velocity curve analysis. We also checked photometric apertures for light/background contamination if exists or not.

Spectroscopic observations of the system were performed using the Whoppshel echelle spectrograph attached to the T80 telescope at the Ankara University Kreiken Observatory (AUKR). We obtained 13 spectra of BD+72 780 between March 25 and December 10, 2023, using the exposure time of 1800 s. Our spectra cover a wavelength range from 3950 Å to 7400 Å with a mean spectral resolution of R ˜ 14000. The average SNR values of the data vary between 50 and 80, which is sufficient to obtain the radial velocities of both components of BD+72 780. The radial velocity measurements of the system were carried out by broadening functions routine (Rucinski, 1992).

3. Analysis and Results

We simultaneously analysed the light and radial velocity curves of the eclipsing binary BD+72 780 using the PyWD2015 code (Güzel & Özdarcan, 2020), which is a graphical user interface (GUI) that is based on the 2015 version of the Wilson–Devinney (WD) code (Wilson & Devinney, 1971). We assumed the system as an detached binary and therefore selected Mode-2 in PyWD2015. We adjusted the orbital inclination (i), semi-major axis (a), eccentricity (e), mass ratio (q), center of mass velocity (V_γ), temperature of the secondary component (T_2), surface potentials (Ω_1, Ω_2), and luminosity of the primary (L_1); while fixing the temperatures of the primary component (T_1) as constant values according to their spectral types. We also fixed the albedo and the gravity brightening parameters to based on the assumed natures of the system. Since there is a slight difference between the maxima levels on phases 0.25 and 0.75 of the light curve of BD+72 780, we assumed one stellar cool spot available on the secondary component during the iterations.The observed light and radial data, and best model fits as well as their residuals are given in Figs. 1. The geometric representations of BD+72 780 are also illustrated bottom in Figs. 1. The parameters obtained from the simultaneous light and radial velocity curve modelling as well as the absolute parameters are summarized in Table 1.

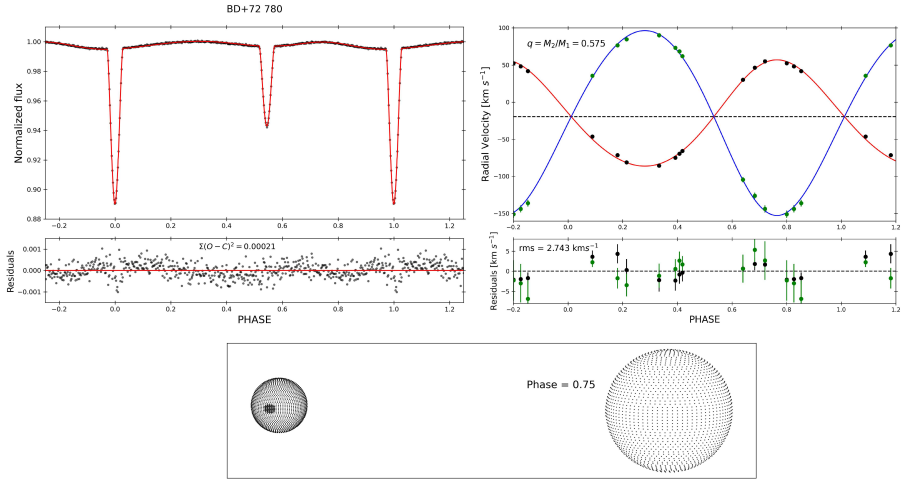


Figure 1. Phase-folded TESS light from Sector 15 and radial velocity curve of BD+72 780 as well as the best model fits (solid lines) obtained using Mode-2. The panels below shows the residuals from the theoretical models and bellow the geometric model of the system is given for phase 0.75.

Table 1. Results from the light and radial curve analysis.

Parameter	**Value**	**Parameter**	**Value**
i [°]	81.75 ± 0.04	M_1 $[M_\odot]$	2.02 ± 0.02
a $[R_\odot]$	13.325 ± 0.136	M_2 $[M_\odot]$	1.05 ± 0.07
e	0.074 ± 0.001	R_1 $[R_\odot]$	2.06 ± 0.05
ω [°]	10.47 ± 0.02	R_2 $[R_\odot]$	0.94 ± 0.05
V_γ [km/s]	-21.77 ± 0.80	L_1 $[L_\odot]$	11.651 ± 0.008
$q = M_2/M_1$	0.515 ± 0.005	L_2 $[L_\odot]$	0.925 ± 0.009
T_1 [K]	7894	ϕ [°]	90.0
T_2 [K]	5522 ± 124	λ [°]	255.88 ± 0.58
Ω_1	7.006 ± 0.023	θ [°]	14.18 ± 0.57
Ω_2	8.858 ± 0.036	T_{sp}/T_2	0.676 ± 0.008

4. Conclusions

In this study, TESS light curves and first ground based spectroscopic observation of the eclipsing binary BD+72 780 were simultaneously analysed using the WD code. The orbital and absolute parameters of the system first time obtained in this study. According to the Mode 2 solutions, the system is detached, and each component has not yet filled its inner Roche lobe. The absolute parameters

obtained in the study are given in Table 1. The present analysis showed that one spot located on the secondary component is needed to fit light curves. The effective temperature of the secondary significantly lower than that of the primary. Therefore, its contribution to the total system light is less than 1%. Hence, spotted area on the secondary leads to comparatively small photometric effect. The solution also shows that the system has an orbit with a slightly low eccentricity ($e \sim 0.07$).

Acknowledgements. The data in this study were obtained with the T80 telescope at the Ankara University Astronomy and Space Sciences Research and Application Center (Kreiken Observatory) with project number of 23A.T80.01. The TESS data presented in this paper were obtained from the Mikulski Archive for Space Telescopes (MAST) at the Space Telescope Science Institute (STScI). This paper includes data collected by the TESS mission. Funding for the TESS mission is provided by the NASA's Science Mission Directorate.

References

Cannon, A. J. & Pickering, E. C. 1993, VizieR Online Data Catalog: Henry Draper Catalogue and Extension (Cannon+ 1918-1924; ADC 1989), VizieR On-line Data Catalog: III/135A. Originally published in: Harv. Ann. 91-100 (1918-1924)

Güzel, O. & Özdarcan, O., PyWD2015 - A new GUI for the Wilson-Devinney code. 2020, *Contributions of the Astronomical Observatory Skalnate Pleso*, **50**, 535, DOI:10.31577/caosp.2020.50.2.535

Jenkins, J. M., Twicken, J. D., McCauliff, S., et al., The TESS science processing operations center. 2016, **9913**, 99133E, DOI:10.1117/12.2233418

Prša, A., Kochoska, A., Conroy, K. E., et al., TESS Eclipsing Binary Stars. I. Short-cadence Observations of 4584 Eclipsing Binaries in Sectors 1-26. 2022, *Astrophysical Journal, Supplement*, **258**, 16, DOI:10.3847/1538-4365/ac324a

Rucinski, S. M., Spectral-Line Broadening Functions of WUMa-Type Binaries. I. AW UMa. 1992, *Astronomical Journal*, **104**, 1968, DOI:10.1086/116372

Shi, X.-d., Qian, S.-b., & Li, L.-J., New Pulsating Stars Detected in EA-type Eclipsing-binary Systems Based on TESS Data. 2022, *Astrophysical Journal, Supplement*, **259**, 50, DOI:10.3847/1538-4365/ac59b9

Wilson, R. E. & Devinney, E. J., Realization of Accurate Close-Binary Light Curves: Application to MR Cygni. 1971, *Astrophysical Journal*, **166**, 605, DOI:10.1086/150986

PRÁCE ASTRONOMICKÉHO OBSERVATÓRIA
NA SKALNATOM PLESE
LV, číslo 3

Zostavovatelia:	RNDr. Theodor Pribulla, CSc. Doc. RNDr. Miloslav Zejda, PhD.
Výkonný redaktor:	RNDr. Richard Komžík, CSc.
Vedecký redaktor:	RNDr. Augustín Skopal, DrSc.
Vydal:	Astronomický ústav SAV, Tatranská Lomnica
IČO vydavateľa:	00 166 529
Periodicita:	3-krát ročne
ISSN (on-line verzia):	1336-0337
CODEN:	CAOPF8
Rok vydania:	2025
Počet strán:	522

Contributions of the Astronomical Observatory Skalnaté Pleso are processed using
LaTeX 2ε CAOSP DocumentClass file 3.10 ver. 2024.